Beta Writer

Lithium-Ion Batteries

A Machine-Generated Summary of Current Research

Springer

Lithium-Ion Batteries

Beta Writer

Lithium-Ion Batteries

A Machine-Generated Summary of Current Research

Springer

Beta Writer
Heidelberg, Germany

ISBN 978-3-030-16799-8 ISBN 978-3-030-16800-1 (eBook)
https://doi.org/10.1007/978-3-030-16800-1

Library of Congress Control Number: 2019936280

This book was machine-generated.

Scientific Advisor: Steffen Pauly

This Springer imprint is published by the registered company Springer Nature Switzerland AG
The registered company address is: Gewerbestrasse 11, 6330 Cham, Switzerland

Preface

1 Introduction

Henning Schoenenberger

Advances in technology around Natural Language Processing and Machine Learning have brought us to the point of being able to publish automatically generated meaningful research text.

We have seen the rise of automated text generation in popular fiction (with quite diverse and fascinating results), automated journalism such as in sports, stock market reports or auto-produced weather forecast (data-to-text), automated medical reviews and not to forget the remarkable progress in dialog systems (chat bots, smart speakers).

As far as it concerns scholarly publishing, many attempts in this area up to now have had a negative perception, and the outcome has fallen short of expectations. Often such texts have been however quite successful in demonstrating flaws in the scientific reviewing processes, clearly serving as an important corrective.

1.1 The First Machine-Generated Research Book

What you read here on your mobile device or on your computer screen or even hold in your hand as a printed book is of a different kind. In fact it is the first machine-generated research book. This book about *Lithium-Ion Batteries* has the potential to start a new era in scientific publishing. With the exception of this preface it has been created by an algorithm on the basis of a re-combined accumulation and summarization of relevant content in the area of Chemistry and Materials Science.

The book is a cross-corpora auto-summarization of current texts from Springer Nature's content platform "SpringerLink", organized by means of a similarity-based clustering routine in coherent chapters and sections. It automatically condenses a

large set of papers into a reasonably short book. This method allows for readers to speed up the literature digestion process of a given field of research instead of reading through hundreds of published articles. At the same time, if needed, readers are always able to identify and click through to the underlying original source in order to dig deeper and further explore the subject. It can assist anyone who, for example, has to write a literature survey or requires a quick start into the topic. This book proposes one solution (out of many others) to the problem of managing information overload efficiently.

As it involves a number of experimental aspects, the *Beta Writer* was developed in a joint effort and in collaboration between Springer Nature and researchers from Goethe University Frankfurt, Germany. The current implementation will be subject to ongoing refinement, with the machine-generated book on Lithium-Ion Batteries providing the basis to explore strategic improvements of the technology, its integration into production and consumption workflows of scientific literature, the merits it provides and the limitations that it currently faces.

1.2 Why Lithium-Ion Batteries

More than 53,000 articles were published in the last three years, presenting research results on lithium-ion batteries. Rechargeable batteries are a crucial part of our daily life, energizing smartphones, tablets, laptops, alarm clocks, screwdrivers and many other devices. They will become even more important as energy storage systems for electric and hybrid vehicles as well as photovoltaic systems. Therefore, they are a key technology for limiting carbon-dioxide emissions and slowing down climate change. The future of mankind depends on progress in research on lithium-ion batteries, and we need to think of innovative ways to enable researchers to achieve this progress. This is where the potential of natural language processing and artificial intelligence (AI) comes in that might help researchers stay on top of the vast and growing amount of literature.

This first machine-generated book on the topic of lithium-ion batteries is a prototype which shows what is possible today if a researcher wants to get a summarized overview of the existing literature.

Next to Chemistry we are planning to publish prototypes in other subject areas as well, including the Humanities and Social Sciences, with special emphasis on an interdisciplinary approach, acknowledging how difficult it often is to keep an overview across the disciplines.

1.3 A Technological and Publishing Challenge

From the very beginning of developing this prototype we have considered our assignment equally as a technological as well as a publishing challenge. It was evident to us that numerous questions would arise from machine-generated content and from the generation process itself.

Many of these questions, related to machine-generated research content, remain open, and some of them we may not even be aware of yet. Hence we will use this preface as starting point to raise a number of questions which all stakeholders of the scientific community have to answer in a responsible and also collaborative manner. This prototype about Lithium-Ion Batteries is meant to commence an important and necessary discussion that the scholarly community will need to have much sooner than later.

We aim to explore the opportunities and limits of machine-generated research content and simultaneously suggest answers to a number of questions related to the impact of Artificial Intelligence on the scholarly publishing industry and its potential implications.

These questions focus on the crucial elements of scientific publishing:

Who is the originator of machine-generated content? Can developers of the algorithms be seen as authors? Or is it the person who starts with the initial input (such as "Lithium-Ion Batteries" as a term) and tunes the various parameters? Is there a designated originator at all? Who decides what a machine is supposed to generate in the first place? Who is accountable for machine-generated content from an ethical point of view?

We have held extensive discussions on these topics, and we have come to the preliminary conclusion that one possible answer is that there may be a joint accountability which is shared by the developers and the involved publishing editors. However, this is far from being finally decided. And there might be quite some different and equally valid answers.

1.4 Why Transparency Is Important

Full transparency is essential for us to discover both the opportunities of machine-generated content and the current limitations that technology still confronts us with.

But it was also an ethical decision that if we start this journey, we want to do so in a correct and responsible manner, in order to enable a discussion in the research communities that is as open-minded as possible.

During the entire process—from the idea to produce the first machine-generated research book to its realization—there has always been a large consensus that full transparency is one of the key elements of this project.

We also hope that the publication of this book encourages as much feedback as possible to help up learn and improve.

1.5 Continuous Improvement

We are genuinely convinced that exposing the way we work—step by step—failure as integral part of the progress—continuous feedback loop into the development—iterative approach to continuously improve—encourage criticism and learn from it—will help us turning this into a successful prototype and in the long run, shape a product that will be suitable for a large variety of use cases, increasing efficiency and allowing researchers to spend their time more effectively. That is also the reason why we decided to outline the technological side of the implementation of this book in this very preface (see below). Truly, we have succeeded in developing a first prototype which also shows that there is still a long way to go: the extractive summarization of large text corpora is still imperfect, and paraphrased texts, syntax and phrase association still seem clunky at times. However, we clearly decided not to manually polish or copy-edit any of the texts due to the fact that we want to highlight the current status and remaining boundaries of machine-generated content. We have experimented on quite a number of components, and we developed alternative implementations for most of them. Some of the more advanced modules we implemented did not find their way into the final pipeline, and we were following the preferences of the subject matter experts consulted during the development process for their selection. For example, this includes neural techniques, which will improve with additional training data and development time. While we expect them to eventually yield better results, for now they will be held in reserve as we move forward upon the solid foundation of this initial publication.

How will the publication of machine-generated content impact our role as a research publisher? As a global publisher it is our responsibility to take potential implications into consideration and therefore start providing a framework for machine-generated research content. As with many technological innovations we also acknowledge that machine-generated research text may become an entirely new kind of content with specific features not yet fully foreseeable. It would be highly presumptuous to claim we knew exactly where this journey would take us in the future.

1.6 The Role of Peer-Review

It was already pointed out that the technology is still facing a variety of shortcomings which we plan to deal with in a transparent way. We do expect that continuous improvement is necessary to constantly increase the level of quality to be delivered by machine-generated content. On the other hand, we know that the quality of machine-generated text can only be as good as the underlying sources

which have been used to generate it. At Springer Nature, we publish research which stands up to scientific scrutiny. In consequence, machine-generated content makes it even more necessary to re-emphasize the crucial role of peer-review itself. Though peer-review is also in the course of being continuously re-defined (and in the future we expect to see substantial progress in machine-support also in this regard) we still think that for the foreseeable future we will need a robust human review process for machine-generated text.

Especially in the area of Deep Learning it becomes increasingly difficult to understand how a result has been actually derived. While concepts such as Explainable Artificial Intelligence (XAI) become more and more crucial, also the review process on machine-generated research content needs refinement, if not a complete re-definition. The term peer itself indicates a certain inadequacy for machine-generated research content. Who are the peers in this context? Would you as a human reader consider yourself as peer to a machine? And should an expert in a specific research field become an expert of neural networks and Natural Language Processing as well in order to be able to evaluate the quality of a text and the related research? In the field of machine-summarization of texts this might not be an issue yet, especially since the underlying sources are peer-reviewed. However, soon enough we will see machine-generated texts from unstructured knowledge bases that will lead to more complex evaluation processes. Also in this area, we have to work together to find answers and define common standards related to machine-generated content. Once more we would like to consider this book as an opportunity to initiate the discussion—as early and anticipatory as possible.

1.7 The Role of the Scientific Author

Finally, what does all this mean for the role of the scientific author? We foresee that in future there will be a wide range of options to create content—from entirely human-created content to a variety of blended man-machine text generation to entirely machine-generated text. We do not expect that authors will be replaced by algorithms. On the contrary, we expect that the role of researchers and authors will remain important, but will substantially change as more and more research content is created by algorithms. To a degree, this development is not that different from automation in manufacturing over the past centuries which has often resulted in a decrease of manufacturers and an increase of designers at the same time. Perhaps the future of scientific content creation will show a similar decrease of writers and an increase of text designers or, as Ross Goodwin puts it, writers of writers:

"When we teach computers to write, the computers don't replace us any more than pianos replace pianists—in a certain way, they become our pens, and we become more than writers. We become writers of writers."[1]

[1] https://medium.com/artists-and-machine-intelligence/adventures-in-narrated-reality-6516ff395ba3.

We do join Zackaray Thoutt's enthusiasm who indicates that "technology is finally on the cusp of breaking through the barrier between interesting toy projects and legitimate software that can dramatically increase the efficiency of humankind."[2]

We have started this exciting journey to explore this area, to find answers to the manifold questions this fascinating field offers, and to initiate a broad discussion about future challenges and limitations, together with the research communities and with technology experts. As a research publisher with a strong legacy, expertise and reputation we feel committed to push the boundaries in a pioneering and responsible way and in continuous partnership with researchers.

2 Book Generation System Pipeline

Christian Chiarcos, Niko Schenk

Automatically generating a structured book from a largely unstructured collection of scientific publications poses a great challenge to a computer which we approach with state-of-the-art *Natural Language Processing* (NLP) and Machine Learning techniques. Book generation involves numerous problems that have been addressed as separate research problems before, and solved to a great extent, but the challenge in its entirety has not found a satisfying solution thus far. The present volume aims to demonstrate what can be achieved in this regard if expertise in scientific publishing and natural language processing meet.

We aim to demonstrate both possible merits and possible limitations of the approach, and to put it to the test under real-world conditions, in order to achieve a better understanding of what techniques work and which techniques do not. In addition, we wish to better understand the demands and expectations of creators, editors, publishers and consumers towards such a product including their reactions to its limitations, and their assessment of its prospective value, both economically and scientifically.

2.1 Choosing a Methodology

As mentioned above, the development process involved both computer scientists and engineers, and editorial subject matter experts who both formulated possible topics and evaluated generated manuscripts and their shortcomings. A key insight from the development process is that different strands of science (and possibly, different personalities) formulate different constraints and preferences regarding the balance between 'creative' automated writing and a mere collation of existing publications. While it is possible to emulate the style and phrasing of prose

[2] https://blog.udacity.com/2017/08/neural-network-game-of-thrones.html.

descriptions rather accurately (e.g., from plain key words, as in Feng et al. [1], or by mean of state-of-the-art language models as reported in the recent work of Radford et al. [2]), the factual accuracy of such 'more creative' reformulations remains questionable. As creators and consumers of scientific publications tend to value correctness over style, we eventually decided for a relatively conservative approach, a workflow based on

1. document clustering and ordering,
2. extractive summarization, and
3. paraphrasing of the generated extracts.

A requirement was to produce novel content, with novelty provided by the organization of sources into a coherent work, and in the generation of chapter introductions and related work sections. We initially considered two thematic domains, chemistry and social sciences, and in both areas, subject matter experts urged us to stay as close to the original text as possible. In other areas of application, where better training and test data for developing advanced summarization workflows may exist, many technical preferences would have been different, but for these branches of research, we designed a workflow according to the premise to preserve as much as possible from the original text—while still producing readable, factually correct, compact, and, of course, novel descriptions. The interested reader may decide to what extent we achieved this goal, but more importantly, let us know where we failed, as it is human feedback—and human feedback only—that can improve the advance of artificial authoring.

2.2 System Architecture

We implement book generation as a modular pipeline architecture, where the output of one module serves as input to the next. Input to the system is a collection of publications that define the scope of the book—typically in the range of several hundred documents. For the present volume, this collection consisted of 1086 initial publications which were identified by keywords and further restricted by year of publication (cf. the next section for details). Output of the system is a manuscript in an XML format which can be rendered in HTML or further processed in the regular publishing workflow.

Main components of the pipeline are illustrated in Fig. 1 and include:

1. **Preprocessing** of input documents, i.e., conversion into the internal format, bibliography analysis, detection of chemical entities, linguistic annotation for parts of speech, lemmatization, dependency parsing, semantic roles, coreference, etc., and re-formulation of context-sensitive phrases such as pronominal anaphora, and normalization of discourse connectives.

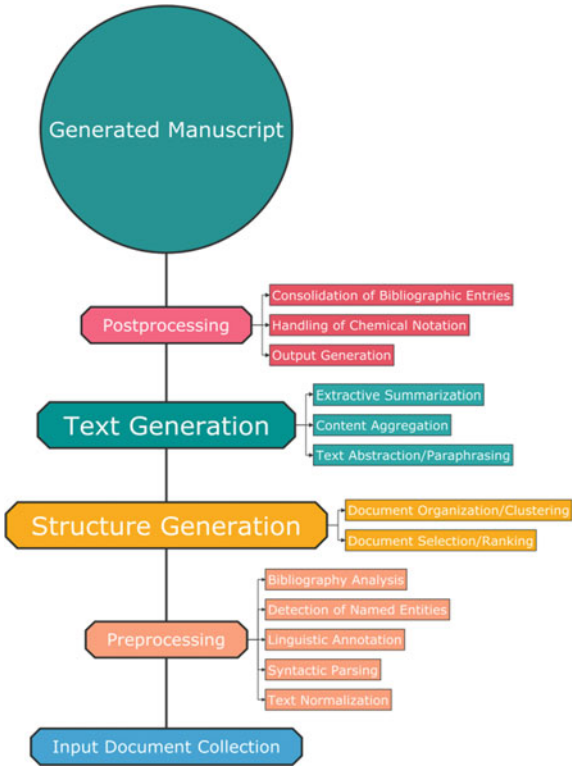

Fig. 1 Book generation system pipeline and NLP components

2. **Structure Generation**
   a. **Document organization** in order to identify the specific contribution and scope of individual input documents, to use this information to group them into chapter- and section-level clusters. As a result, we obtain a preliminary table of contents, a list of associated publications, and keywords that characterize chapters and sections.
   b. **Document selection** is a subsequent processing step during which we identify and arrange the most representative publications per section-level cluster.
3. **Text Generation**
   a. **Extractive summarization** creates excerpts of the selected documents which serve as a basis for subsections.
   b. **Content aggregation** techniques are applied to create sections with introductions and related research from multiple individual documents. Unlike document-level extractive summarization, these are composed of re-arranged

fragments of different input documents, such that information is presented in a novel fashion.

c. **Abstraction** is implemented in a conservative fashion as a postprocessing step to extraction (resp., aggregation). Here, we take single sentences into consideration and employ syntactic and semantic paraphrasing.

4. **Postprocessing** includes the consolidation of bibliographical references, chemical entities, and conversion into an output format that is suitable for generating HTML as well as a manuscript to be handed over to the publishing editor.

For every single component (resp., modules within a component), we provide alternative implementations, and eventually select among these possibilities or combine their predictions according to the preferences of the subject matter experts.

We focus on functionality, less on design. We do not provide a graphical user interface, but the feedback we obtained from subject matter experts during their qualitative evaluation of our system, resp., the generated candidate manuscripts represent invaluable input for the requirement specification of user interfaces to the book generation pipeline.

The pipeline itself is implemented as a chain of command-line tools, each configured individually according to the preferences of the subject matter experts. One premise has been to design an end-to-end system that generates manuscripts from input documents, so the scientific contribution is the overall framework and architecture, not so much the implementation of elementary components for basic machine learning or fundamental NLP tasks. For these, we build on existing open source software (e.g., Manning et al. [3], Clark and Manning [4], Cheng and Lapata [5], Barrios et al. [6]) wherever possible. It should be noted, however, that we do not depend on any specific third-party contribution, but that these are generic components for which various alternatives exist (and have been tested).

2.3 Implementational Details

In **preparation** for generating a book, we identify a seed set of source documents as a thematic data basis for the final book, which serve as input to the pipeline. These documents are obtained by searching for keywords in publication titles or by means of meta data annotations.[3] The document types can be of various kinds: complete books, single chapters, or journal articles.

For **structure generation**, we provide two alternative clustering methods operating on two alternative similarity metrics. As for the latter, we explored bibliography overlap and document-level textual similarity. As bibliography

[3] In the present volume this includes, e.g., any realization of “li-ion battery”, “lithium-ion batteries”, etc. and all occurrences containing “anode” and/or “cathode” as found in either article, chapter, book titles or document meta data.

overlap comes with a considerable bias against publications with a large number of references, we eventually settled on textual similarity as a more robust and more generic metric.

As for clustering methods, *hierarchical clustering* creates a tree structure over the entire set of documents. Clusters can be mapped to chapters and sections according to preferences with respect to size and number. However, we found that the greedy mapping algorithm we implemented for this purpose produces clusters of varying degrees of homogeneity. For the current volume, we thus performed *recursive non-hierarchical clustering* instead: (i) over the set of all documents, core thematic topics are automatically detected (*chapter generation*), and (ii) subtopics are identified within these (*section generation*). If a restriction on the number of input documents per section is defined, the *n* most representative publications per cluster (closest to the center) are chosen, and ordered within the manuscript according to their prototypicality for the cluster (i.e., distance from the cluster center). More advanced selection and ordering mechanisms are possible, but will be subject for future refinements. Figure 2 shows a graphical illustration of the cluster analysis of this book. Each color represents the membership to one of four chapters, bigger labeled dots represent chapters and sections, respectively, small dots show documents.

Interestingly, due to their proximity in the 2-D visualization the graphics shows that Chaps. 1 and 2 are thematically much more closely related (anode versus cathode materials) than Chaps. 3 and 4 (model properties and battery behaviour).

Even though the structure generation for the manuscript is fully automated, here, a number of parameter values can be set and tuned by the human expert who uses the program, such as the desired number of chapters (i.e., cluster prototypes) and

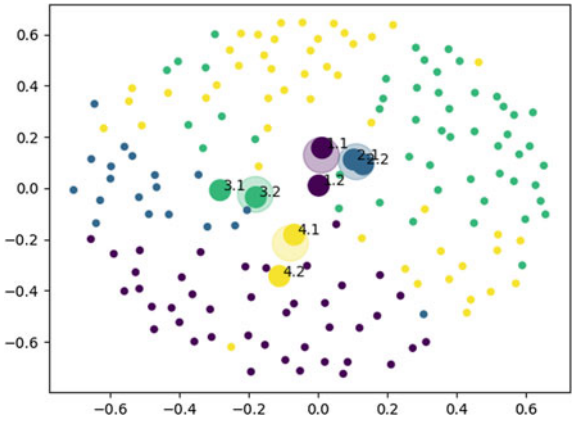

Fig. 2 Two-dimensional projection (PCA) of the cluster analysis with 4 chapters and 2 subsections, and a maximum of 25 documents per section

sections, as well as the number of document assignments per section.[4] The result of this process is a structured table of content, i.e., a manuscript skeleton in which pointers to single publications serve as placeholder for the subsequent text.

At this level, subject matter experts requested the possibility for manual refinement of the automatically generated structure. We permit publications to be moved or exchanged between chapters or sections, or even removed if necessary, for example, if they seem thematically unrelated according to the domain expertise of the editor.[5] We consider the resulting publication nevertheless to be machine-generated, as such measures to refine an existing structure are comparable to interactions between editors of collected volumes and contributing authors, e.g., during the creation of reference works.

Chapter and section headings are represented as a list of automatically generated keywords. Technically, these keywords are the most distinctive linguistic phrases (*n-gram* features) as obtained as a side-product of the clustering process and are characteristic for a particular chapter/section. Again, human intervention is possible at this stage, for instance, in order to select the most meaningful phrases for the final book. In the present volume, the keywords remained unchanged. More advanced techniques include the generation of headlines from keywords using neural sequence-to-sequence methods, and while we provide an implementation for this purpose, we found it hard to ensure a consistent level of quality, so that we eventually stayed with plain keywords for the time being.

Text generation is the task to fill the chapter stubs with descriptive content. In the present volume, this is based on *extractive, reformulated summaries*. Every chapter consists of an introduction, a predefined number of sections as determined in the previous step, a related work section, a conclusion, and a bibliography. We elaborate on each of them in the following.

Every *chapter introduction* contains a paragraph-wise concatenation of extractive summaries of all individual document introductions which have been assigned to the chapter.[6] Since all documents of a chapter have been identified to belong to the same topic, the motivation here is to combine the content of individual introductions from the publication level and merge them into a global one on the book

[4] For the present volume, the number of chapters, sections, and the maximum number of documents per section have been initially set to 4, 2, and 25, respectively. The document clusters, i.e. document to chapter assignments, are produced by k-means clustering on the term-document matrix with different weighting schemes, e.g. TF-IDF. Additional, advanced parameters to be set include the minimum/maximum document frequency of a term, the total number of features (*n-grams*) used, or whether to use stemming or other types of text normalization.

[5] For the present volume, 9 documents have been moved between chapters, and 8 documents were excluded from the final book. Overall, the generated book is based on 151 distinct publications.

[6] We elaborate on extractive summarization below.

level. The summary length (in words and as a proportion of the original text length) is parameterizable by the human editor who uses the system.[7] The conclusion of the book is built in the same way. The introduction produced in this way is conservative in that it reflects the introductions of the input documents selected for the chapter—both in order and content. As an alternative, we also implemented an approach for *reordering and combining sentences* obtained from *different* publications in single paragraphs, based on an arrangement of semantically similar sentences closer to each other and the elimination of near-duplicates. For the present volume, however, the more simplistic implementation was eventually selected, as subject matter experts found that the coherence of the resulting text suffered from the heterogeneity of the underlying documents. For future generation experiments, it would be desirable to allow an expert trying to produce a book with this technology to compare the conservative and the aggregated introductions for each chapter. For more homogeneous chapters, the latter approach may be favorable.

On the *section level*, following the introduction, publication stubs are filled with extractive summaries obtained according to different technologies:

- *Unsupervised extractive summarization*: A classical baseline for extractive summarization is the application of the page rank algorithm to the text itself, respectively, the graph of linguistic annotations obtained from it. As a result, both important phrases and relevant sentences are augmented with relevance scores, and a ranking according to these, and extractive summarization boils down to retrieving the x most relevant sentences until a certain length threshold is met. The method has the great advantage of being simple, mature and well-tested. It is, however, context-insensitive, in that essential information may be lost, or that sentence and keyword relevance in the context of a book project diverts from their relevance within the original publication in isolation.
- *Supervised extractive summarization*: An alternative approach to produce a ranking of sentences is to train a regressor to approximate a pre-defined score, e.g., the extraction probability of a sentence. Unfortunately, such training data is not available for our domain and cannot be created without massive investments. As a shorthand for such data, we measure the textual similarity of each body sentence with the sentences of the abstract of the same publication. We then trained a regressor to reproduce these scores, given the sentences (resp., their embeddings) in isolation. This regressor was trained for all publications from the Chemistry and Material Science, as well as Engineering domains, and it assigns every sentence a score, and thus, all sentences from a document a domain-specific rank, which then serves as a basis for extraction.
- *Extended abstracts:* An extended abstract is a reformulated and compressed version of the original abstract of a document, potentially enriched with sentences from the body of the publication as useful additional information can be retrieved

[7] The summary length has been set to either 270 words or 60% of the original text length—depending on which one was shorter. This combined metric handles the trade-off between too lengthy summaries on the one hand, and summaries which contain almost every sentence of the source, on the other.

from the document itself. For the current volume, we append sentences from the body to any sentence in the original abstract by a similarity metric (provided they exist). Similarity is measured by customizable n-gram overlap. An alternative, and slightly more aggressive implementation, is to replace sentences from the original abstract with the most similar sentences from the body.

- *Weighted combined ranking:* Each of the aforementioned methods assign sentences a score (or a classification, which can be interpreted as a binary score), from which a rank can be calculated. We provide a re-ranker that uses the weighted sum of ranks produced by different components to produce an average rank, so that more conservative approaches (extended abstracts) can be combined with context-sensitive, machine-learning based rankers (supervised extraction) and with context-insensitive, graph-based methods (unsupervised extraction) according to the relative weights the user of the system assigns to each component.

Subject matter experts from the chemistry domain found that the first two methods (and their combination) are prone to factual errors, if applied to original sections on methodology and experimental setup, so that such sections (which constitute the majority of text in this domain) must not be summarized but either dropped or quoted. This may be a characteristic of the chemistry domain, where instructions on replicating a particular experiment must be followed carefully and any omission of a step in the procedure or an ingredient is potentially harmful. For the present volume, we thus operate with extended abstracts only.

Conclusions are aggregated in the same way as introductions. It is followed by a related work section which is compiled from the citations of the input documents.

The *related work section* is typically short and organized around pivotal publications. A pivotal publication is defined as a DOI that is referred to within different publications from a chapter, and we take the number of documents referring to this publication as an indicator of its relevance. The user of the system defines a threshold n for the number of documents that define a pivotal publication. For instance, if n is set to 4, at least four different documents within a chapter need to cite the same publication DOI. From each document, we retrieve the citation context, i.e., the sentences that contain the reference, and arrange them according to their textual similarity. We thus obtain 4 sentences, at least. The frequency threshold n needs to be set by the user of the system.[8] It should increase in proportion with a greater number documents per chapter. Ideally, the most frequently referred to publications by distinct sources have global importance within a chapter.

The final component of text generation is **text abstraction**, i.e., here the linguistic reformulation of the original sentences, respectively. In order to create text which is not only novel with respect to its arrangement, but also with respect to its formulation, and in order to circumvent issues related to copyright of the original texts, we attempt to reformulate a majority of the sentences as part of the generated book, while trying to preserve their original meaning as best as possible. At the

[8] For the present volume, $n = 2$.

same time, subject matter experts urged us to stay as close to the original formulation as possible. Although we do perform deep parsing, this is used to inform reformulation rules only, but not as a basis for the summarization itself: The original text is preserved and reformulated, rather than being reduced to a graph and then re-generated from scratch. In this more conservative approach, we provide annotation-based reformulation components for which integrated different NLP modules have been integrated in a preprocessing step, as outlined above: identification of word boundaries,[9] part-of-speech label assignment for words (i.e. word categories, such as noun, verb, etc.), and the application of syntactic and semantic parses to each sentence in order to obtain a linguistic analysis in terms of dependency structure and semantic roles. Furthermore, coreference resolution is employed in order to detect mentions in the text and associated referential expressions (e.g., personal or possessive pronouns in subsequent sentences).

We provide the following modules:

- *Rule-based simplification*: Sentence-initial adverbials, discourse markers and conjunctions are removed as they would otherwise appear out of context after text summarization.
- *Sentence compression*: Using relevance scores such as created during keyword extraction above, and a reduction threshold of, e.g., 90%, eliminate the least relevant parts of the sentence until the reduction threshold is met. An alternative implementation shortens a sentence by removing omittable modification information, e.g., non-core, local/temporal cues, or discourse modification.
- *Sentence restructuring*: A range of syntactic transformation rules were implemented which operate on the automatically produced structure, for instance, to turn an active utterance into its passive variant.
- *Semantic reformulation*: In a final step, we substitute single words as well as longer phrases if we find synonymous expressions that exceed a predefined similarity threshold.[10] What constitutes a phrase is automatically detected by high pointwise mutual information of word co-occurrences. Note that all synonyms are automatically learned from large amounts of raw unlabeled texts using state-of-the-art methods for unsupervised learning of word representations with neural networks.

Along with these reformulation components, a module for anaphora resolution is applied to replace intersentential pronominal anaphora with the respective last nominal representation: We replace pronouns (e.g., sentence-initial *"It"*) by interpretable mentions of the same coreferential chain that are found in the prior context (e.g., full noun phrases such as *"the first study in this field"*) in order to prevent the rendering of sentences in which single pronouns appear without context after text

[9] Specifically, we developed special analyzers on the sentence level to detect, normalize and later on reinsert chemical notations, textual content in brackets (such as references and supplementary information) and other entities which need to be treated holistically and must not be parsed or split into parts.

[10] When more than one word exceeds the threshold, we select one synonym randomly.

summarization. Note, however, that this is applied during preprocessing already, in order to guarantee that extractive summarization does not create unresolvable anaphoric references.

Apart from the fully automated text generation module, the human user still has influence on the quality of the text, for example by specifying a list of prohibitive synonym replacements, or by setting the thresholds for the replacements. For compiling this volume, we selected among the aforementioned modules and adjusted their respective threshold in accordance with the feedback from subject matter experts. It is to be noted, however, that users would apparently like to scale freely between different degrees of reduction and reformulation, ranging from literal quotes to complete paraphrases. Our implementation does not provide such an interface, but developing such a tool may be a direction for future extensions.

As an example of two reformulated sentences compared to their original source sentences, involving preposing of temporal information and most of the NLP techniques described above, consider the following sentences (synonym replacements in bold, syntactic changes and coreference replacements underlined).

Source[11]:

Lithium-ion batteries have played a major role in the development of vehicle electrification since the 2000s. They are currently considered to be the most efficient technology in this market.

Automatically reformulated:

Since the 2000s, lithium-ion batteries have played a ***main*** *role in the development of vehicle electrification.* ***Lithium-ion batteries*** *are* ***presently regarded*** *to be the most* ***effective*** *technology in this market.*

Advanced syntactic reformulation, e.g., turning active into passive voice is illustrated in the next example.

Source:[12]

Finally, these results can develop a test methodology to determine the management of lithium batteries pack that experiences a potential heating threat.

Automatically reformulated:

A test ***approach*** *to* ***specify*** *the management of* ***Li-ion*** *batteries pack that experiences a potential heating threat* ***could be devised by these*** *results*.

In total, for the present volume, approximately ¾ of all sentences were syntactically reformulated, i.e. for 74% at least one transformation rule triggered. Semantic replacements (unigram, bigram, or trigrams substituted) were made to 14.7% of all tokens. More than 96% of all sentences were modified by at least one semantic substitution. Sentence compression was kept in a very conservative mode and removed only a small portion of 0.9% of the tokens. In order to acknowledge the original source, every sentence is coupled with the DOI of its source document. In addition, sentences which were not affected by reformulation, synonym replacements, or sentence compression are marked as literal quotes (1.2% of all sentences).

[11] Sabatier et al. [7] https://link.springer.com/chapter/10.1007%2F978-3-319-55011-4_3.

[12] Chen et al. [8] https://link.springer.com/article/10.1007/s10973-017-6158-y.

2.4 Challenges and Future Directions

Our book generation pipeline has been designed to not only compile extractive summaries, but also to rephrase and make creative modifications to the original text wherever possible. At the same time, however, it is forced to be conservative enough to preserve the original meaning of the sentences. Besides selecting the most important sentences in extractive summaries, this tradeoff can be seen as the most difficult challenge in the design and implementation of the system.

The system in its current version is a minimalist implementation of core components of a book generation workflow and can be refined and extended in many ways. This preliminary state is also indicated by the name of the virtual author, *Beta Writer*. Aside from creating a scalable end-to-end system for the generation of books from large bodies of scientific publications, we see our main contribution as the first successful attempt to push a machine-generated book beyond mere technical challenges through an established publication workflow up to the level of a printed book. At the same time, the name entails a commitment for future extensions and refinements, for which manifold possibilities exist, including the following:

- *Improving linguistic quality*: Current limitations of the system are mainly due to error propagation in the NLP pipeline. For instance, the very basic preprocessing steps, word and sentence identification, are both non-trivial tasks, especially for texts containing various chemical notations, numbers, or abbreviations in which punctuation symbols do not necessarily indicate a sentence or word boundary. Wrongly detected words and sentences lead to faulty linguistic annotations by the part-of-speech taggers, ultimately to wrong parses, and finally to restructured sentences which are meaningless.
- *Improving paraphrasing*: Issues regarding legibility, grammaticality, and correctness, are also partly due to the component which replaces words by synonyms: This component is not yet sensitive to aspect, or context and, thus, in some cases a substitution of a word is acceptable (*revealed* good performance -> *showed* good performance), in others not (it is *revealed* -> it is *showed*). Even more problematic in this regard is a well-known disadvantage associated to word embeddings, namely that antonyms have very similar distributions compared to synonyms. Replacing a word by its antonym, however, changes the meaning and is prohibitive in sentence reformulation. We have tried to overcome these issues as well as in any way possible using conservative similarity thresholds.
- *Headline generation*: The generation of suitable, narrative headlines (for chapters and sections) is yet another highly complex task which we did not approach in the current version of the system, but rather prompted us to stick to the keywords that we obtained as a result of text clustering. Note that the keywords themselves are not necessarily the most interpretable and meaningful phrases to a human reader, even though technically they are in fact the most distinctive n-gram features. Future research will address their combination into syntactically more appealing descriptions.

- *Improving coherence*: In this current version, we have not addressed any discourse properties of the texts. Typically, sentences do not occur in isolation. Instead, they are part of a well-formed and coherent text structure which is signaled either explicitly (e.g., using discourse markers but, next, if, etc.) or sometimes even implicitly. In fact, our extractive summaries break up and remove parts from the discourse structure of the original source documents and, in future versions of the system, special focus needs to be taken to ensure that the reformulated extractive summaries adhere to the original discourse structure and its associated global meaning. This would also entail fusing sentences and reintroducing discourse markers where applicable. We want to point out, however, that such a feature is not only non-trivial to implement but also extremely hard to evaluate.
- *Reordering*: A related challenge is the sequential order of sentences—and, similarly, the sequential ordering of sections within a chapter. Here, we have implemented different simplifications that either preserve the original order of sentences or perform re-ordering in a way that maximizes similarity between adjacent sentences. More advanced implementations could build on formal representations of discourse structure as also necessary for improving coherence.
- *Abstraction via graph representations*: A book generation pipeline based on full-fledged abstractive summarization requires the decomposition of texts and sentences into their logical parts, their representation as a graph, and the re-generation of natural language from the abstract graphs. At the moment, this is an area of intense research, and several experimental prototypes already do exist, but we estimate that a production-ready implementation will not be available for another, 3–5 years. For the academic partners in this enterprise, this is of course one of the aspects of the book generation challenge that we are particularly interested in.
- *Neural abstraction*: Another way of abstraction is the application of neural sequence-to-sequence models to translate full sentences into their paraphrases. Again, this would be a strategic goal, but we currently lack training data for our domain, and where training data is synthesized (e.g., by means of a neural noisy channel model), it is virtually impossible to guarantee a consistent level of quality in the generated output. Our own experiments show that the output that can be produced is superficially readable, but often has severe flaws when it comes to its meaning and factual correctness. For the present system, and the eventual pipeline we developed, we thus went for a conservative, extraction-based architecture. Nevertheless, this is an area of intense research.
- *Creative writing*: Another scientific challenge is the production of novel text fragments *from contextual cues* rather than from a given input sentence. While on a technical level, this is similar to neural headline generation, such apparent simulation of creative behaviour is probably the most fascinating aspect of modern-day AI. In fact, it is fairly easy to build and train a model to re-generate sentences given the previous and the next sentence. However, the quality of the generated output is even less controllable than the results we achieved by neural abstraction. Again, this remains an area of research.

- *Including structured data sources*: At the moment, the *Beta Writer* builds on three pillars: Established NLP techniques, word embeddings for the target domain, and vast amounts of scientific publications to optimize both and to create summaries from. There is another possible component that we did not take into account so far: Structured knowledge graphs can provide additional background information, e.g., about chemical entities and relations between them. In fact, such information is already available, and Springer Nature can build on the Springer Nature SciGraph in this regard. For the creation of this publication, however, we focused on core functionalities of a generic book generation pipeline, which will permit domain-specific knowledge base integration in future iterations.
- *The nasty little details*: Last but not least, we have to mention that a great deal of the errors that we are currently facing are due to specifics of the domain and the data. The interested reader will immediately spot such apparently obvious errors—with rather obvious solutions. This includes, for example, the occasional use of *us*, *ourselves*, *this paper* etc. which refers back to the original publication but is clearly misplaced in the generated book. The solution to these is a simple replacement rule, the challenge in this solution is the sheer number and the distribution of errors that require a domain-specific solution each, sometimes referred to as 'the long tail'. While we made some efforts to cover such obvious cases, continuous control and refinement of an increasingly elaborate set of repair rules is necessary, and will accompany the subsequent use and development of the *Beta Writer*.
- *Getting the human in the loop*: Error correction can potentially also be covered by a human expert—or, in a book production workflow, as part of copyediting. But even beyond this level of manual meddling with the machine-generated manuscript, a clear, and somewhat unexpected result of our internal discussions with subject matter experts on chemistry and social sciences was that editors would like to maintain a certain level of control. At the moment, the system remains a blackbox to its users, and we manually adjust parameters or (de)select modules according to the feedback we get about the generated text, then re-generate, etc. At the same time, it is impossible to optimize against a gold standard—because such data does not exist. One solution is to provide a user interface that allows a user to switch parameters on the fly and see and evaluate the modifications obtained by this and thus optimize the machine-generated text according to personal preferences, and—also depending on the feedback we elicit on this volume—developing such an interface is a priority for the immediate future.

We are well aware of experimental approaches that improve upon the current state of our implementation. With a publication that links every generated sentence with its original form in the original publication, we aim to establish a reference point for evaluation by the scientific community and a baseline for future systems to meet. Yet, at the core of this challenge is not so much scientific originality, but the balance of having an automated system performing autonomous and 'creative' operations and the degree to which the factual accuracy of the underlying text can

be preserved. Guided by subject matter experts on chemistry and social sciences, we eventually went for a conservative approach to book generation, in that as much information is preserved from the original as possible. We are aware of the expectations in trustworthiness and verifiability in scientific publications which—for the time being—, a more radical, abstraction-based approach on book generation would be impossible to meet. We expect this to change in the immediate future, and we are working towards it, but at the same time as Artificial Intelligence—or, for that matter, neural Natural Language Processing—is about to reach the fringes of creativity, we still need to learn how to restrict its creativity to producing content that remains factually true to the data its predictions are generated from.

Another technical challenge that we identified during the creation of this book was that human users aim to remain in control. While an automatically generated book may be a dream come true for providers and consumers of scientific publications (and a nightmare to peer review), advanced interfaces to help users to guide the algorithm, to adjust parameters and to compare their outcomes seem to be necessary to ensure both standards of scientific quality and correctness. Advanced interfaces will also help to identify areas where it is possible to deviate from the cautious, conservative approach on text generation applied for producing the present volume, and to include more experimental aspects of AI.

References

1. Feng X, Liu M, Liu J, Qin B, Sun Y, Liu T (2018) Topic-to-essay generation with neural networks. In: Proceedings of the twenty-seventh international joint conference on artificial intelligence (IJCAI-18), pp 4078–4084
2. Radford A, Wu J, Child R, Luan D, Amodei D, Sutskever I (2019) Language models are unsupervised multitask learners. https://blog.openai.com/better-language-models/
3. Manning CD, Surdeanu M, Bauer J, Finkel J, Bethard SJ, McClosky D (2014) The stanford coreNLP natural language Processing Toolkit. In: Proceedings of the 52nd annual meeting of the association for computational linguistics: system demonstrations. pp 55–60
4. Clark K, Manning CD (2016) Deep reinforcement learning for mention-ranking coreference models. In: Proceedings of EMNLP
5. Cheng J, Lapata M (2016) Neural summarization by extracting sentences and words. In: Proceedings of the 54th annual meeting of the association for computational linguistics (Volume 1: Long Papers) pp 484–494. https://doi.org/10.18653/v1/P16-1046
6. Barrios F, López F, Argerich L, Wachenchauzer R (2015) Variations of the similarity function of textRank for automated summarization. Anales de las 44JAIIO. Jornadas Argentinas de Informática. In: Argentine Symposium on Artificial Intelligence
7. Sabatier J, Guillemard F, Lavigne L, Noury A, Merveillaut M, Francico JM (2018) Fractional models of lithium-ion batteries with application to state of charge and ageing estimation. In: Madani K, Peaucelle D, Gusikhin O (eds) Informatics in control, automation and robotics. Lecture notes in electrical engineering, vol 430. Springer, Cham
8. Chen M, Yuen R, Wang JJ (2017) Therm Anal Calorim 129:181. https://doi.org/10.1007/s10973-017-6158-y

Contents

Chapter 1
Anode Materials, SEI, Carbon, Graphite, Conductivity, Graphene, Reversible, Formation

1.1 Introduction

Lithium-ion batteries (Li-ion batteries) have been commonly used as power sources in consumer electronics including laptops, cellular phones, and full and hybrid electric vehicles because of their long cycling life, high energy capacity, and eco-friendliness [1, 47–49]. Considerable efforts have been devised to examine useful electrode materials for Li-ion batteries with long cycle life and high capacity [1]. Due to its high theoretical capacity (718 mAh g^{-1}), low cost, relative abundance [50–52], and environmental benignity, NiO has attracted considerable attention among multiple TMOs for Li-ion batteries [1]. Through solid-state thermolysis of Ni-MOF, porous NiO had been fabricated for Li-ion batteries and showed a high initial capacity of ∼800 mAh g^{-1} at 100 mA g^{-1} [1, 53]. That NiO nanoflowers utilized as anodes for Li-ion batteries displayed a reversible capacity of 551.8 mAh g^{-1} at a current density of 100 mA g^{-1} after 50 cycles [54] had been indicated by Mollamahale and others [1]. Porous Co_3O_4/CNT composites were synthesized through the decomposition of ZIF-67/CNTs and revealed an excellent specific capacity of 813 mAh g^{-1} at a current density of 100 mA g^{-1} after 100 cycles, whilst that of pure Co_3O_4 had been just 118 mAh g^{-1} [1, 55]. Porous ZnO/CNT composites derived from Zn-MOFs/CNT precursors showed superior lithium-ion storage performance with a high reversible capacity of 419.8 mAh g^{-1} after 100 cycles at 200 mA g^{-1}, whilst the pure ZnO subsample had been ultimately stabilized with a capacity of less than 200 mAh g^{-1} [1, 56]. Introducing 1D CNTs into MOF-based NiO must be an efficient way to improve the lithium-ion transport and storage performance for Li-ion batteries [1].

The current commercial graphite carbon electrodes with a low theoretical capacity (372 mAh g^{-1}) indicate inferior rate performance and restricted energy capacity, particularly in the high-energy consuming applications [2]. That sort of research's

This book was machine-generated

Beta Writer, *Lithium-Ion Batteries*,
https://doi.org/10.1007/978-3-030-16800-1_1

principal aim is to attain the materials with superior properties such as high capacity, fast Li-ion diffusion rate, easy to operate, and stable structure [2]. Materials, a number of metal oxides with high theoretical capacity have aroused more and more attention including SnO_2, Fe_3O_4, Co_3O_4, and MoO_2 [2]. Due to safe lithiation potential (Zhang and others [57, 58]) and its high theoretical capacity (782 mAh g^{-1}), SnO_2 is treated as one of the most extensively investigated anode materials for Li-ion batteries [2]. Jiang and others [59] have utilized the graphene/TiO_2–SnO_2 composites as the anode; this anode deliver the enhanced cycling performance (537 mAh g^{-1} at 50 mA g^{-1} accompanied by columbic efficiency of 97% after 50 cycles) and satisfactory reversible capacity (250 mAh g^{-1} even at the current density 1000 mA g^{-1}) [2]. "Han and others [60] have prepared TiO_2–SnO_2–graphene aerogels with a high reversible capacity of 750 mAh g^{-1} at 100 mA g^{-1} for 100 cycles" [2]. Through Tang and others [61], mesoporous graphene-based TiO_2/SnO_2 nanosheet is synthesized and it can deliver a huge reversible capacity of 600 mAh g^{-1} at current density of 160 mA g^{-1} [2]. The prepared commodities indicate a distinctive nanostructure, a huge BET surface area of 274.5 m^2 g^{-1}, and high chemical purities [2]. An outstanding electrochemical performance is shown by the SnO_2–TiO_2@graphene composites, and the discharge capacity can arrive at high as 1276 mAh g^{-1} after 200 cycles at the current density 200 mA g^{-1} [2]. It is still maintained the huge capacity of 611 mAh g^{-1} at an ultra-high current density of 2000 mA g^{-1}, when utilized as an anode for Li-ion batteries [2].

The ionic and electronic electrical conductivity of TiO_2 (anatase) is comparatively inferior, leading to the low electronic transfer and ion diffusion efficiency, which might severely decline the electrochemical properties for Li-ion batteries as a semiconductor material [3]. Various carbon-added TiO_2 composites [62–65] were indicated and employed as the anode materials of Li-ion batteries, and those carbon-added composites did display an enhanced cycle retention and rate performance; this retention demonstrated that the addition of carbon actually fosters the electrical conductivity of the entire architecture [3]. Carbon can safeguard TiO_2 from the direct contact with electrolyte; this electrolyte additional enhances the structure resistance to electrode material invalidation and pulverization [3]. Molybdenum disulphide (MoS_2), characteristic layered transition metal dichalcogenides (TMDs), has aroused considerable attention as a fruitful electrode material because of its high theoretical specific capacity and distinctive 2D layered structure where hexagonal layers of Mo are stuck in two S layers and held together by strong covalent forces, whilst the MoS_2 lamella is bonded by weak van der Waals relationships [3, 66]. Once assessed as the anode material for Li-ion batteries, the bulk MoS_2 might suffer tremendous volume expansion, which results in unanticipated pulverization and serious systemic deformation, which triggers a fairly meager cycling performance, whilst the few-layer MoS_2 configuration can keep the few-layer MoS_2's original structure and become more stable during the discharge/charge cycles because of the ultra-thin 2D flexible nanostructure [3]. Apart from, few-layer MoS_2 nanosheets enhance a fast insertion/extraction of lithium ions and provide more active sites to enhance the specific capacity [3]. Once assessed as the anode material of lithium-ion batteries, the synthesized MoS_2-C@TiO_2 nano-composites display excellent cyclic performance and high specific capacity [3].

Based on transition metal oxides (TMOs) including TiO_2 [67], ZnO [68], CuO [69], Fe_3O_4 [70], NiO [71], CoO_x [72–75] as anode materials for Li-ion batteries, and MnO [76], has made considerable progress among the wide range of efforts [4]. Co_3O_4 materials with multiple structures have been efficiently prepared, including lamellar [77, 78], nanorods [79], hollow spheres [80], nanoparticles [81, 82], and cubes [4, 83]. High lithium storage Co_3O_4 electrodes could be obtained by the indicators of designing hollow structures [4]. There is still a challenge to enhance the electric conductivity and agglomeration issue of Co_3O_4, which are the contextual factors impeding the development of Co_3O_4 electrodes for use in Li-ion batteries [4]. Carbonaceous materials have functioned as the most optimum conductive materials to enhance the electric conductivity of Li-ion batteries' electrodes [4]. Two-dimensional (2D) graphene (GR) with an excellent electric conductivity, systemic flexibility [84], and rich surface area, is another influential carbon material [4]. A hybrid of these two types of materials which formed a new 3-D (3D) layered structure is the most efficient technique in order to harness the advantages of the 1D CNTs and 2D GR [4]. The 3D graphene/carbon nanotubes (GR/CNTs) network can not just maintain the excellent properties of CNTs and GR though enhance the inferior electric conductivity between graphene sheets [4, 85]. Co_3O_4 hollow microsphere/graphene/carbon nanotube (Co_3O_4/GR/CNT) flexible film is prepared through a two-stage technique; this technique comprises a subsequent thermal decrease process and a straightforward filtration route [4]. That the film electrode showed better lithium storage capacities in rate and cycling performances than hollow Co_3O_4 materials is revealed by the results [4].

Numerous researches on CuO/graphene composites utilized as Li-ion batteries anode have been indicated; for instance, Rai and others [86] have synthesized CuO/rGO nanocomposite through a spex-milling technique [5]. The first discharge capacity of 1043.3 mAh g^{-1} had been delivered by the CuO/rGO composite, and the charge capacity can be maintained at 516.4 mAh g^{-1} after 45 cycles at 0.1 mA cm^{-2} [5]. Enhanced anodic performance, which is compared to the pure CuO nanoparticles, had been shown by this CuO/rGO composite [5]. A novel kind of CuO nanosheets/rGO composite paper, which revealed better cyclic retention than that of the pure CuO nanosheets had been indicated by Liu and others [5, 87]. Improved electrochemical performance than pure CuO had been demonstrated by the composites [5]. Porous CuO nanorods/rGO had been synthesizeded by Zhang and others [88] composite through hydrothermal reaction [5]. Improved electrochemical properties than the pristine CuO nanorods were shown by the composite electrode [5]. A facile refluxing approach had been utilized to synthesize ultra-short rice-like CuO-NRs/rGO composite [5]. Cu^{2+} ions absorbed into $Cu(OH)_2$ and then rapidly dehydrated into CuO-NRs under high temperature, with homogeneous distribution on the rGO nanosheets after the addition of NaOH [5]. The as-prepared CuO-NRs/rGO composite anode indicates enhanced electrochemical performance in Li-ion batteries due to the synergetic effect between the high electrical conductivity of rGO nanosheets and the well-dispersed CuO-NRs [5]. The rGO nanosheets offer a substrate for the anchoring of CuO-NRs and an electrical

network to preserve the electrical contacts between the active material and current collector [5]. A huge reversible capacity, satisfactory rate property of CuO-NRs/rGO composite, and advantageous cyclic performance, could be attained [5].

Throughout the overcharge process, the current marketed graphite anode with a low operating voltage versus Li/Li^+, which results in the generation of lithium dendrite, leading to serious safety issue (Zhou and others [89]), [6]. The development of a practical TiO_2 material for commercialization is still restricted because of its low theoretical capacity (336 mAh g^{-1}), inferior electric conductivity ($\sim 10^{-13}$ S cm^{-1}), and low lithium diffusion coefficient ($\sim 10^{-9}$ to 10^{-13} cm^2 s^{-1}) (Wagemaker and others [90]; Kamata and others [91]), [6]. It is still a considerable challenge to employ TiO_2 nanostructures as anode in Li-ion batteries to settle the instinct low electronic electrical conductivity (Chu and others [92]) and the aggregation issue [6]. Owing to the high electrical conductivity of carbonaceous materials, considerable efforts have been made to construct multiple TiO_2/C nanostructures, the aggregation of TiO_2 nanostructures is reasonably well tackled and in which carbon serves as conceptual framework to foster the electron transport ability [6]. The electrical conductivity of carbon matrix is still inadequate due to the low pyrolysis temperature, which substantially affects the electric and reactivity transfer ability and consequently, the lithium storage capacity even though enhanced electrochemical properties of TiO_2/C nano-composites have been shown [6]. Carbon, which is Dual-doped, can drastically enhance the electric conductivity performance and the lithium storage performance because of the greater electronegativity and the systemic defects (Wang and others [93, 94]; Xing and others [95]; Zhuang and others [96]), [6]. The incorporation of heteroatoms in carbon matrix and the rational design of TiO_2/C nano-composites are both of considerable significant for obtaining high electrochemical property as anode in Li-ion batteries [6]. Nano-TiO_2 anchored on N/S dual-doped carbon conceptual framework (NSC@TiO_2) had been accomplished through a facile technique as high performance anode material for Li-ion batteries [6].

Co_3O_4 had been a fascinating Li-ion batteries' anode material due to its high theoretical specific capacity (890 mAh g^{-1}), low cost, eco-friendliness, and relative abundance, among multiple TMOs [7]. The extensive application of Co_3O_4-based anodes had been restricted because of its tremendous volume expansion effect in the process of charge/discharge [7]. An efficient strategy had been to fabricate mesoporous Co_3O_4-based nanomaterials as potential electrode materials to solve the issue [7]. The mesoporous Co_3O_4-based nanomaterials normally showed satisfactory performance because of some distinctive mesoporous Co_3O_4-based nanomaterials' huge specific surface area, a huge number of holes efficiently impeding the systemic disintegration and potential hazards triggered by volume expansion in the process of charge/discharge, and rapid mass transfer between the electrolyte and the active material [7]. At a current density of 0.1, a high reversible capacity of 1067 mAh had been delivered by Cluster-like Co_3O_4 g^{-1} Ah g^{-1} after 100 cycles [7, 97]. Upon 30 cycles at a current density of 0.1 Ah g^{-1} [98], a stable specific discharge/charge capacity of 765 and 749 mAh g^{-1} had been shown by

Mesoporous Co_3O_4 microdisks [7]. The designation and synthesis of mesoporous Co_3O_4-based nanomaterials owning special distribution of particle and pore sizes were still quite required for additional amelioration of performance [7]. A novel mesoporous dandelion-like Co_3O_4 nanomaterial had been synthesized [7]. "The as-prepared dandelion-like mesoporous Co_3O_4 consisted of well-distributed nanoneedles which were about 50 nm in width and about 5 μm in length" [7]. The as-prepared Co_3O_4 mesoporous dandelion-like Co_3O_4 nanomaterial reveals superior electrochemical performance of Li-ion batteries when assessed as anode materials [7].

Transition metal oxides (TMOs), including Co_3O_4 [99], MnO_2 [100], V_2O_5 [101], and Fe_3O_4 [102], have been researched as fruitful anode materials for Li-ion batteries because of natural relative abundance [103, 104] and their high theoretical capacities [8]. MCo_2O_4 (M = Ni, Zn, Fe, Mn) have been commonly used as anode materials to substitute graphite, which owes to their high theoretical capacities [105–108], as a kind of ternary TMOs [8]. More substantially, high specific capacity, which is usually two times greater than that of traditional graphite-based materials is shown by $CuCo_2O_4$ [8]. "Yuan's group [109] synthesized $CuCo_2O_4$, the discharge capacity of which still remained 740 mAh g^{-1} at 0.1 C (1 C = 1000 mA g^{-1}) after 50 cycles" [8]. In contrast with the same-sized solid nanomaterials, porous hollow spheres can offer huge active area, abundant buffer space, and short ion diffusion pathways, to ameliorate the volume change during repeated Li^+ insertion/extraction mechanisms; these mechanisms can efficiently foster the electrochemical reaction [8, 110, 111]. A facile and general hydrothermal technique to synthesize porous $CuCo_2O_4$ hollow spheres (PHS-$CuCo_2O_4$) is indicated by us without employing any templates [8]. The crucial step is one-pot to form porous $CuCo_2O_4$ hollow precursor spheres [8]. The porous $CuCo_2O_4$ hollow precursor spheres reshape into well-retained PHS-$CuCo_2O_4$ via a thermal annealing process in air [8]. Full cells were assembled employing the as-prepared PHS-$CuCo_2O_4$ and $LiCoO_2$ as the cathode as the anode; this anode indicate a comparatively high capacity of 660 mAh g^{-1} after 50 cycles [8].

A critical factor for overall electrochemical performance; huge pore volumes, the porous structure of carbon material with high surface zones, and homogeneous pore sizes normally display greater lithiation capability and better cycling stability, which can shorten the Li^+ ions transport path, accommodate the huge volume change, improve the electrode/electrolyte interface, and decide the contact between electrode and electrolyte solution, and enhance the interfacial lithium ion diffusion [112, 113] is the porosity of electrode materials [9]. The carbon material with spherical structure have been shown to be competent for employing as anode materials for Li-ion batteries, since spherical materials enjoy a high packing density, a low surface to maximal systemic stability, volume ratio, and ease to preparing electrode films [9, 114]. Developing new, which is carbon-based anode materials with porous and spherical structure as the host of the lithium insertion and transport, is imperative to enhance the performance of Li-ion batteries [9]. Studying a sustainable and cheap synthetic technique to prepare micropores spherical structure of carbon sphere as anode material for Li-ion batteries will enormously

enhanced lithium ion storage, which is crucial to the structure design and modifier of carbon anode material application in Li-ion batteries in the future [9]. We report a carbon microsphere with highly prepared micropores by green and straightforward technique, which had been utilized to anode material of Li-ion batteries and indicate high discharge capacity and long cycle life at various current density in this work [9]. NCM and the RF-C were utilized to anode materials of Li-ion batteries, respectively, compared with RF-C; the lithium-ion storage capacity of NCM had been enormously enhanced because of their microporous structure; this structure indicates a high discharge capacity and excellent cycle performance at various current [9].

Fe_3O_4 has been viewed as an advanced alternative anode material for Li-ion batteries because of low cost and its high theoretical capacity among all the reports for M_xO_y [10]. There are many reports on that the quantum dots display enhanced electrochemical performance [10, 115]. The distinctive quantum dots have multiple merits for excellent cycling stability and high-rate capability in terms of electronic/ionic electrical conductivity, volume effect, specific surface area, and grain boundary defects [10, 116]. Much work till date has revolved around that the quantum dots dispersed on graphene display enhanced electrochemical performance [10]. Highly distributed Fe_3O_4 quantum dots on commercially readily available graphite nanoplates, which revealed high-rate capability (530 mAh g^{-1} at 5 A g^{-1}) including a high cycling performance (960 mAh g^{-1} at 200 mA g^{-1} after 147 cycles) had been efficiently prepared by Su and others [10, 116]. The ultrafine Fe_3O_4 quantum dots on hybrid carbon nanosheets indicated by Liu showed an enhanced electrochemical performance [10, 117]. There are handful reports about combining 3D graphene aerogel and 0D quantum dots, the distinctive structure shown the efficacy of the synergetic effect between 3D GA to the lithium storage properties and the 0D Fe_3O_4 quantum dots [10]. It is a particular challenge to build a facile technique to prepare single-phase Fe_3O_4 quantum dots reasonably well dispersed on graphene foam matrix [10]. Fe_3O_4 quantum dots/graphene composite showed cycling stability (312 mAh g^{-1} after 200 cycles at 50 mA g^{-1}) [118] and satisfactory sodium storage capacity (525 mAh g^{-1} at 30 mA g^{-1}) in our group [10]. Benefitting from the Fe_3O_4 quantum size of 2–5 nm, the obtained Fe_3O_4 QDs/GA performs satisfactory behaviour properties on cyclic stability and rate capability [10].

Decades, transition metal oxides (TMOs) have been extensively examined as fruitful anodes for Li-ion batteries due to low cost and their high theoretical capacities [11]. Much attention has been paid to Fe-based ternary metal oxides as fruitful anodes for Li-ion batteries to enhance their cycleability [11]. It is anticipated that Fe-based ternary metal oxides as fruitful anodes for Li-ion batteries can efficiently circumvent the shortcomings of pure iron oxide anode; then bigger reversible capacity, better rate performance, and better cycleability, could be accomplished by the useful combination of various metal species (Yuan and others [119]), [11]. The use of $ZnFe_2O_4$ as anodes in Li-ion batteries for the first time (Li and others [120]) had been indicated by Li and others, and the initial reversible capacity had been 556 mAh g^{-1} and 78% of the capacity (434 mAh g^{-1}) had been

still preserved after 100 cycles [11]. An efficient way to enhance rate performance and the battery cycling by both improving the nanomaterial surface electronic electrical conductivity and minimizing the electrode/electrolyte interfacial side reaction (Zhang and others [121]; Lee and others [122]) is surface coating on TMO nanoparticles [11]. A new-generation carbon material, which not just possesses high electrical conductivity and the high surface area though can serve as a reliable matrix to load multiple metal oxides is Graphene [11]. It is supposed that the 3D network graphene composites as anode material can efficiently ameliorate the aggregation of metal oxides [11]. The enhancement of electrochemical performances could be attributable to the synergetic role of graphene and homogeneous carbon layer, which can hinder the volume expansion, enhance the electron transfer of the composites, and deter the pulverization/aggregation upon prolonged cycling [11].

In the variety 670–893 mAh g^{-1} have been indicated (Xiong and others [123]; Qi and others [124]; Huang and others [125]), CoO has received particular attention because of specific capacities and its high theoretical capacity (716 mAh g^{-1}) [12]. Numerous efforts were made toward the synthesis of CoO that comprises octahedral nanocages (Guan and others [126]) and nanodisks (Sun and others [127, 128]) with enhanced capacities of 893 and 1118 mAh g^{-1}, respectively since morphologically tailored nanostructured materials can provide distinctive properties [12]. Superior performance with specific capacities of 1592 mAh g^{-1} at 50 mA g^{-1} (Peng and others [129]) and $\sim$1018 mAh g^{-1} at 500 mA g^{-1} (Sun and others [127, 128]) is demonstrated by CoO-graphene composites [12]. Zhou and others [130] have indicated specific capacity of 2223 F g^{-1} at a current density of 1 mA cm^{-2} from 3D CoO@polypyrrole nanowires (in 3 M NaOH electrolyte), while Wang and others [131] have detected a high specific capacity of 3282.2 F g^{-1} at 1 mA cm^{-2} (in 6 M KOH electrolyte) for a hybrid composite of conductive carbon and CoO [12]. Some researches are concentrated on mixed metal oxide composites including CoO@NiO and specific capacities in the variety of 145–840 F g^{-1} can be obtained (Gao and others [132]; Yang and others [133]) in order to solve the electrical conductivity issue of CoO and enhance capacitance [12]. Based on carbon-based composite materials, although gives rise to an enhancement of gravimetric capacitance of metal oxide supercapacitors, normally results in lower areal capacitance because of high volume to mass ratio of carbon (e.g., CNT, graphene, etc.) [12]. That by synthesizing 1D materials with useful morphology, high capacitance values could be derived from CoO (1167 F g^{-1} after 10,000 cycles at 5 A g^{-1} and areal capacitance of 728 mF cm^{-2}) without the need to form with carbon or other metal oxides any composite and hence, enhancing both gravimetric and volumetric capacitance is demonstrated here by us [12].

Porous carbon materials have been devised as a fruitful electrode material for lithium batteries because of physicochemical properties [134–138] and the distinctive systemic elements among all carbon-based materials [13]. Template technique and activation technique were usually introduced to synthesize high surface area porous carbon materials [13, 139–141]. Lithium batteries delivered the electrochemical performance with specific charge capacities of 445 mAh g^{-1} at 0.1 C

and 370 mAh g^{-1} at 1 C [142] had been material-based by the carbon [13]. Porous carbon particles based on peanut shells, which shown reversible capacity of 480 mAh g^{-1} with high columbic efficiency of 98.9% after 20 cycles [143] were prepared by Cao and others [13]. One practical approach to additional enhance the electrochemical performance of the porous carbon-based anode is by controlling structure [46, 144–146] and morphology [13]. That the obtained porous carbon reaches the high reversible capacity of 660 mAh g^{-1} after 70 cycles at a current density of 100 mA g^{-1} [147] had been shown by Guo and others [13]. Nanostructured porous carbon materials with structure and characteristic morphology shown the enhanced electrochemical properties [13, 148–150]. The FPCMs highlight rate performance (378 mAh g^{-1} at 1 A g^{-1}) and the optimal cycle capacity (643 mAh g^{-1} at 100 mA g^{-1}) whilst employing as anode materials of lithium batteries [13]. The link between morphology and structure of porous carbon and electrochemical performance of lithium batteries had been examined [13]. Possibilities of enhancing the lithium storage capacity of porous carbon materials by controlling both morphology and structure are provided by the results [13].

A wide range of materials have been exploited as anode materials for Li-ion batteries in the past decades, including silicon-based [151–153] or tin-based [154–156] materials, and transition-metal oxides [157–159]; these decades have ultra-high theoretical capacity [14]. Silver is an attractive option for anode materials, due to its comparatively high specific capacity; this capacity is attributable to the formation of numerous Ag–Li alloys (up to $AgLi_{12}$) within a quite low voltage variety (0.25–0 V) [14, 160]. A common matrix for silver is carbon [14]. Shilpa and others utilized hollow carbon nanofibres as a buffer matrix and enmeshed silver nanoparticles in them via the coaxial electrospinning technique [14, 161]. Metal organic approaches (MOFs) have been attracting increased attention as carbon sources for anode materials because multiple kinds of MOF precursors can consequence in deduced carbon with allow innate doping of heteroatoms [162–164] and a homogeneous, controllable, porous structure [14]. A cage-like carbon/nano-Si composite as anode materials by the template technique to incorporate Si nanoparticles into ZIF-8 had been prepared by Song and others [14]. Porous nitrogen-doped carbon (PNCs@Gr) via the pyrolysis of zeolitic imidazolate conceptual framework nanoparticles grown in situ on GO (ZIF-8@GO), which showed outstanding electrochemical performance among carbonaceous materials utilized as anode materials [165], a sandwich-like had been fabricated by Xie and others, graphene-based [14]. Carbon, which is ZIF-8-derived, had been utilized by us as a matrix for silver nanoparticles (Ag nanoparticles); these nanoparticles can offer not just rigid matrices with nanopores, though also a comparatively high nitrogen content [14]. Once utilized as the anode material for the lithium ion battery, the Ag-NPC revealed excellent electrochemical performance over bare NPC; this NPC had been attributable to the carbon matrix and the synergetic effect of Ag nanoparticles [14].

Several carbon-doped anode materials with multiple structures have been devised to improve the electric conductivity [166–170] and to ameliorate tremendous volume variability during the process of Li^+ insertion/extraction in recent

decades [15]. Since they are quite environment-friendly and renewable, though offer a novel approach to prepare anode materials with distinctive nanostructures for improving performances [171–176], sustainability could be not just maintained by such materials [15]. Upon 60 cycles at the current density of 0.2 and 2 A g^{-1}, which had been considerably greater than the theoretical capacity of graphite (372 mAh g^{-1}), the lithium storage capacity of MnO/C nano-composites showed 610 and 350 mAh g^{-1} [15]. Through the approach of biotemplating method, which is based on Zhang, microalgaes and others, prepared MnO/C nano-composites; these nano-composites the enhanced lithium storage performance may be attributed to the porous hollow microsphere architecture [177] and released a relative high capacity of 700 at 100 mA g^{-1} after 50 cycles [15]. Through utilizing bacillus subtilis as templates, Kim and others synthesized Co_3O_4 nanorods with porous hollow nanostructure and it revealed high reversible capacity of 903 mAh g^{-1} after 20 cycles under the current density of 240 mA g^{-1} [15, 178]. A cheap and environment-friendly approach to prepare graphene (G)-Co/CoO shaddock, which is peel-derived carbon foam (SPDCF) hybrid as anode materials for Li-ion batteries, had been devised by us [15]. The carbonized porous shaddock peels can act as the supporting skeleton to accommodate the mechanical strain and keep elastic for Li^+ insertion/extraction, which might enhance the cycle stability of the G-Co/CoO SPDCF substantially [15]. The devised approach to prepare the G-Co/CoO SPDCF with nanoflakes nanostructure based upon biological materials could be extended to the synthesis of other comparable materials for Li-ion batteries, supercapacitor, catalysis, etc. [15].

Nickel oxide (NiO) as an alternative anode material for Li-ion batteries has been extensively researched because of its high theoretical capacity (718 mAh g^{-1}), non-toxicity and low cost [16]. Design and synthesis of nanoscaled NiO with distinctive structure, e.g., porous and hollow structures, in which free space can accommodate enhance Li-ion diffusion and the tremendous volume change including swiftly throughout the whole electrode during the lithiation/delithiation process is one efficient approach [16]. Owing to the distinctive porous architecture, enhanced electrochemical performance with good cycleability and high lithium storage capacity is shown by the porous NiO hollow microspheres [16]. Nanosphere electrode delivers a high capacity of 393 mAh g^{-1} after 50 cycles of charge-discharge at a rate of 0.3 C are hollowed by the NiO [16]. The satisfactory electrochemical behaviour of the NiO electrode, which is attributed to the nano-size effect coupled with the hollow void space of NiO nanospheres that can accommodate the volume transformations occurring during the conversion reactions and enhance faster Li-ion intercalation/deintercalation kinetics, is noted by they [16]. Previous studies have clearly suggested that controlled synthesis of NiO anode materials with porous hollow structures for Li-ion batteries had been the pursuing aim [16]. The controlled and facile synthesis of porous hollow NiO electrode materials based on nanoscaled Ni-MOF still encounters many issues and might have considerable interest in the field of materials science [16]. We report on synthesis of porous NiO hollow quasi-nanospheres employing a MOF as both the precursor and the self-sacrificing template [16]. The NiO electrode prepared from

the porous NiO hollow quasi-nanospheres displays high reversible capacity, rate performance and satisfactory cycling stability when assessed as an anode material for Li-ion batteries [16].

The specific energy of traditional Li-ion batteries is not sufficient for these applications because of the restricted specific capacity of the traditional graphite anode (372 mAh g^{-1}) [17]. Exploration of novel anode materials with greater capacity is one of the main research directions for Li-ion batteries (Poizot and others [179]; Ji and others [109]; Wang and others [180]; Manthiram and others [181]; Cheng and others [182]), [17]. Transition metal carbonates (TMCs) have been hot research concentrates in recent decades because of their facile synthesis, satisfactory electrochemical durabilities (Zhao and others [183]) and high specific capacities as a novel sort of readily available anode lithium storage materials [17]. That porous $ZnCO_3$ nanoparticles (NPs) revealed an initial capacity of satisfactory rate ability and 735 mAh g^{-1} had been indicated by Zhang and others [17, 184]. There are handful reports about multi-metal carbonates utilized as anode materials for Li-ion batteries till now [17]. The TMCs could be as precursors of the synthesis of transition metal oxides (TMOs); to the optimal of our knowledge, the TMOs are emerging as fruitful anode materials because of their high capacities usually two or three times greater than those of traditional graphite-based electrodes (Poizot and others [179]; Reddy and others [185]), [17]. TMOs, Co_3O_4 indicates comparatively high capacity and is regarded as most potential candidate for Li-ion batteries (Wu and others [186]), [17]. Due to its satisfactory electronic electrical conductivity, easy electrolyte penetration (Cui and others [187]; Wei and others [188]) and low diffusion resistance to protons/cations, TMOs, $ZnCo_2O_4$ is regarded as one of the most fruitful electrode materials for Li-ion batteries application [17]. The as-prepared ZCO and ZCCO microspheres display satisfactory electrochemical performance as anode materials for LIB applications, suggesting that the electrochemical properties of ZCO might be linked to the electrochemical performance of ZCCO [17].

Owing to theoretical capacities [189] (>600 mAh g^{-1}) and the high natural relative abundance, metal oxides (Co_3O_4 [190], Mn_2O_3 [191], ZnO [192], SnO_2 [193], NiO [194]), are supposed to be the possible anode candidates for high-performance Li-ion batteries [18]. Zn_2SnO_4 (ZTO) retains distinctive properties of high theoretical irreversible capacity of 1231 mAh g^{-1}, a wide band disparity of 3.6 eV and superior electron mobility of 10–15 $cm^2\ V^{-1}\ s^{-1}$ [18]. Upon 200 cycles at 100 mA g^{-1}, where monodispersed SnO_2 nanoparticles existed within 3D linked carbon networks, by dexterously employing the porous structures and adsorption properties of MOFs [195], SnO_2@CNT had been devised by Wang and others with a reversible capacity of 880 mAh g^{-1} [18]. A two-step calcining process to efficiently synthesize Sn@graphene-based nanosheets integrating of optimized nitrogen species had been devised by Zhong and others, and this anode delivered the discharge capacity of 890 mAh g^{-1} after continuous tests from 0.1 to 1 A^{-1} cycle at 100 mA g^{-1} [18, 196]. A greater capacity of 520 mAh, which is compared g^{-1} with the SnO_2 nanoparticles failing totally after 100 cycles [197], had been shown by a SnO_2–graphene nanocomposite [18]. Upon 50 cycles, the RGO/C/

ZnO anode materials showed the reversible capacity of 600 mAh g^{-1}, and this value had been much more than bare ZnO aggregates [18, 198]. Graphene-MWCNT demonstrates a specific capacity of 768 mAh g^{-1} at the current density of 100 mA g^{-1} after 100 cycles, which is 2.5 times superior to that of pure graphene [18, 199]. At the current density of 100 mA g^{-1}, Ge/RGO establishes a specific capacity of 863.8 mAh g^{-1} after 100 cycles, though displays an inferior cycle life performance compared with Ge/RGO/CNT [200] without adding CNT [18].

A restricted theory capacity of 372 mAh g^{-1} [173, 201, 202], which substantially restricted the additional development had been demonstrated by Li-ion batteries with the commercial graphite as the anode material [20]. ZnO is a fascinating Li-ion batteries' anode material among multiple anode materials, for its high theoretical capacity of 978 mAh g^{-1} [20, 203]. Recent work [204] synthesized the ZnO/graphene composites and utilized to prepare Li-ion batteries anode, which indicates a striking specific capacity of 870 mAh g^{-1} after 100 cycles at the current density of 1 A g^{-1} and 713 mAh g^{-1} after the sequential 100 cycles at the current density of 2 A g^{-1} [20]. On the surface of ZnO nanoparticles with an mean diameter of $\sim$50 nm [205], which indicates specific capacity of $\sim$975 mAh g^{-1} at the current density of 40 mA g^{-1}, an amorphous coating of carbon had been created [20]. Sucrose had been utilized as carbon precursor grants to improve the electrochemical performance of ZnO [206], displaying an initial discharge capacity of 1440 mAh g^{-1} with a reversible (charge) capacity of 1050 mAh g^{-1} at the current density of 50 mA g^{-1} [20]. ZIF-8 nanocrystals were pyrolyzed to prepare the anode material of Li-ion batteries demonstrating discharge capacity of 600 mAh g^{-1} after 50 cycles [20, 207]. That structure, which is dispersed not just reasonably well nano-ZnO though also enhanced the capacity of ZIF-8 [20]. Spherical ZnO@C nano-composites is poroused by the hybrid as anode materials for Li-ion batteries possessed superior electrochemical properties, including high specific capacity, fine cycle performance, and satisfactory rate capability; these properties have been validated in previous report [20, 208–212].

Rechargeable lithium-ion batteries (Li-ion batteries) have been intensively studied to satisfy the expanding power-supply requirements for a wide range of applications in mobile and portable communication tools, electric/hybrid vehicles due to the high energy density, durable power output [213–216], and stable cycle life [21]. Titanium dioxide (TiO_2) has been acknowledged as an alternative material to substitute the graphite electrodes in lithium batteries because of its high safety performance, low volume change, eco-friendliness [217, 218], and natural relative abundance [21]. Through the inferior Li ions and the aggregation tendency nanoparticles, electron transport, and the inherent low electrical conductivity, the practical electrochemical performance is still restricted [21]. It is an efficient strategy to improve the electrochemical performance by controlling the unidimensional morphologies, including nanofibres, nanowires, and nanotubes; these morphologies have the huge surface to volume ratio, excellent ion and electron electrical conductivity [219–221], and high surface area [21]. Low electronic electrical conductivity and the slow lithium-ion diffusion are still the principal obstacles for its practical application [21, 222]. Graphene (G) has aroused intensive

attention due to its superior mechanical, electrical, chemical, and thermal, properties and is regarded as an optimal support for metal oxides (MO) as lithium ion battery electrodes [223–226] as is known to all [21]. Some literatures have been indicated on graphene/TiO_2 composite materials with excellent electrochemical performance as anodes for lithium-ion batteries because of the influential synergetic impacts [21, 227–229]. Upon the decrease of graphene oxide, the G/TiO_2 composite nanofibres were finally obtained and utilized as an anode for lithium batteries with excellent high rate performance and the excellent rechargeable stability [21].

Transition metal cobalt-based compounds ($Co(OH)_2$, Co_3O_4, CoN, CoS, CoP), etc. $NiCo_2O_4$, are an crucial class of fruitful materials due to their high theoretical capacity, adequate cycleability [230–236] and rich redox reaction among the wide range of anode materials examined [22]. The redox mechanism of the cobalt-based compounds versus lithium is based upon conversion reactions rather than intercalation reactions unlike traditional carbon negative electrodes [22]. The low electronic electrical conductivity of most of cobalt-based compounds is another inherent drawback [22]. Several indicators have been taken to ameliorate the two difficulties by designing nanostructured cobalt-based electrodes with heterogeneous morphologies (including nanoparticles [233], nanowires (NWs) [123], hollow spheres [237], nanoboxes [238], nanorods [239], nanosheets [240] and nanoplates [241], etc.) or by preparing them on high electric conductivity substrates (including graphene [242, 243], lowered graphene oxide [244, 245], carbon cloth [246], nitrogen-doped carbon nanotubes [247] and Ni foam [248], etc.) [22]. It is the fact that the conversion reaction-based electrodes exhibit low initial columbic efficiency because of the incomplete conversion reaction, the irreversible stage transitions and the irreversible lithium deterioration, which is based on the formation of a solid electrolyte interphase (SEI) layer [22, 186, 230]. There is a need for reviewing the recent progress in multiple cobalt-based compounds as anode materials [22]. That review focuses on the synthetic methodologies and the nanostructures of cobalt-based compounds and their corresponding performances in Li-ion batteries, and expects to give readers the guideline on how to circumvent the issues of huge volume change and inferior electric conductivity for these cobalt-based compounds [22].

Commercial anodes for Li-ion batteries are still graphite-based materials their restricted specific capacities are not sufficient for greater energy density with the rapid development of the modern society, and whose theoretical capacity is as low as 372 mAh g^{-1} [23]. Novel anode materials with greater capacity for LIB applications (Huang and others [249]; Manthiram and others [181]; Wang and others [180]; Ji and others [109]; Cheng and others [182]) must be examined by us [23]. That special S–Mo–S layered structure is favourable for Li-ion insertion/extraction during the discharge/charge process, whilst the previous reports show that MoS_2 has many drawbacks (Xie and others [250]; Liao and others [251]), [23]. To solve this issue, the most efficient one is to combine MoS_2 with materials which have satisfactory electrical conductivity, and fairly plenty of tactics are put forth [23]. Some conductive metals including Cu, Sn, and Co, are doped in MoS_2 to help engender rapid electron transport and enhance the electrical conductivity of active

materials [23]. A high theoretical capacity of 991 mAh g^{-1} is possessed by metallic tin (Sn) and has been regarded as the most fruitful anode materials for high-performance Li-ion batteries (Hou and others [252]), [23]. Previous studies have discovered lately that MoS_2 doped with Sn can substantially enhance the cycling performance during the lithiation/delithiation process (Li and others [253]), [23]. Once evaluated as anode material for Li-ion batteries, all the as-prepared Sn/MoS_2 composites display both greater reversible capacity and better cycling performance, which is compared with the pure MoS_2 [23]. That the doping of metal Sn can substantially enhance the electrochemical properties of MoS_2 is revealed by the results [23].

There has been a greater requirement for lithium-ion batteries about energy density, the safety of the electrode materials [254, 255], and rate performance, with the development of multiple electronic mobile tools and the hybrid electric vehicles [24]. Graphite, as a prevailing commercial anode material for lithium-ion batteries, delivers a gravimetric capacity of 372 mAh g^{-1} and a volumetric capacity of 840 mAh cm^{-3}, much from meeting the increased requirement of consumers [24, 256]. Bismuth's layered crystal structure is facile to Li^+ insertion/extraction during delithiation and lithiation process, making bismuth readily available as an anode material for lithium-ion batteries [24, 257–260]. The astonishing volume transformations, which gives rise to expansion and pulverization of subsequently a serious capacity fade [261] and materials is the principal challenge of the metals and alloys directly utilized as anode materials for lithium-ion batteries [24]. With regard to the preceding accomplishments, heterogeneous graphene-based nano-composites, extensively examined as anode materials for lithium-ion batteries, have showed enhanced electrochemical performance [24, 186, 262–266]. Co-workers and Yang showed Bi@C as anode materials for sodium/lithium-ion batteries, obtaining almost similar capacities [24, 260]. Graphene, comparable to other pure carbon materials, suffers from a huge irreversible capacity and rapid capacity fade during cycling, though nitrogen-doped graphene can circumvent these demerits and present enhanced electrochemical performance than the pristine graphene, which is because of the enhanced electric conductivity, more defects, intensive electrode/electrolyte wettability, and active sites for Li^+ adsorption from nitrogen, which is incorporated [267–273], to the optimal of our knowledge [24]. It is quite possible to derive high performance electrode materials via combining the bismuth with the nitrogen-doped graphene [24]. We synthesized N-doped graphene/Bi nanocomposite as an anode material for lithium-ion batteries through a two-stage technique, combining the gas/liquid interface reaction with the rapid heat treatment technique [24].

The traditional graphite materials are much from being able to which additional hinder its applications in electric vehicles (EVs), fulfil the market requirement due to the inferior rate performance and its restricted theoretical capacity (372 mAh g^{-1}) and hybrid electric vehicles (HEVs) with the extensive application of Li-ion batteries [25]. Spinel $NiCo_2O_4$ has been attracted considerable attention because of its high theoretical capacity (890 mAh g^{-1}), low cost, eco-friendliness, abound resources [274–276], and high electronic electrical conductivity, among those of potential alternative anode materials [25]. The meager capacity retention and rate

performance of the spinel $NiCo_2O_4$ inhibit spinel $NiCo_2O_4$'s practical application [25, 277, 278]. That the $NiCo_2O_4$ hollow microspheres with the distinctive high and porous specific surface can offer a short path for lithium ions and electrons in comparison with bulk materials, whose microstructure can give rise to satisfactory electrical conductivity and high ion diffusion rate had been shown by coworkers and Yu [25, 279]. Urchin-like $NiCo_2O_4$ nanostructures [280] have been followed by annealing, suggesting satisfactory cycleability and better rate property and synthesized through a solvothermal technique, which employs hexadecyl trimethyl ammonium bromide (CTAB) as a soft template [25]. A facile microemulsion-assisted solvothermal route with the assistance of employing a mixture of cosurfactant (n-heptanol and n-heptane) as soft template and sodium dodecyl sulfate (SDS) to derive Ni-Co precursor, which are followed by annealing at 400 °C for 4 h to prepare urchin-like $NiCo_2O_4$ microspheres had been indicated by us [25]. That the $NiCo_2O_4$ microspheres will display better cycling stability and greater specific capacity is hoped by us [25].

The field of Li-ion batteries [281, 282] can offer a novel approach to solve the shortcomings existing in anode materials, including the huge volume change, meager cycling performance, and low electrical conductivity, by coating polymer film or the carbon layer on the surface of nanoparticles [27]. Several researches on the carbon-coated anode materials have been indicated in the scientific literature, and the reasons for the amelioration of the electrochemical performance of Li-ion batteries have been described from the point of view of the SEI film [27, 283, 284]. That the carbon coating can buffer the volume change, improve the stability of the electrode, enhance the electronic electrical conductivity, and deter the SEI layer from breaking during cycling even at a high rate is shown by all the results [27]. Choi and others coated a thin layer of polymer film efficiently on the lithium electrode surface by ultraviolet radiation technology and observed that the SEI film on lithium electrode surface with a protective film is considerably denser than that without one; the battery with a protective film has a greater discharge capacity and better cycling performance [27, 285]. On the impacts of polymer shell on the SEI film and the mechanism of how the polymer shell can enhance the electrochemical performance of Li-ion batteries and the stability of SEI films is lack of understanding, handful researches indicated even though the electrochemical performance of anode materials is can efficiently enhanced by the polymer shell [27]. The examination of the role of the polymer shell in the formation of SEI film is of paramount importance for additional amelioration of the performance of Li-ion batteries, which comprises high energy density, safety, cycle performance, and so on [27].

In voltage areas exceeded the stability window of the electrolytes, most kinds of lithium-ion batteries are operated, and they present a potential safety hazard; this hazard limits the voltage variety [28]. Through the formation of a homogenous and stable electron-insulating solid electrolyte interphase (SEI) on the anode, additional electrolyte break-down and critical degradation processes could be precluded [28]. The composition and structure of SEIs formed on the anode material, i.e., graphite, which is utilized most frequently, have previously been researched intensively [28,

286–293]. Several alternative anode materials were outlined to satisfy the requirement for safety [294], which is increasing, and greater capacities [28]. It is indispensable to better comprehend SEI formation to enhance capacity retention and longevity and to maximize alloy anodes [28]. Lithium titanate (LTO) anodes still indicate serious gassing when they come into titanium oxides (TiO_2, $Li_4Ti_5O_{12}$) particularly with the electrolyte, which results in film formation and battery swelling on the anode surface [28]. Stable SEI layers are replied to be efficient in suppressing additional electrolyte decomposition [295] to lessen gassing of LTO-based batteries [28]. Upon the first cycle, the formation of SEI layers, which is formed on LTO and silicon anodes, had been examined by us [28]. That the overall resistance of the silicon anodes substantially declined in the second cycle, suggesting the formation of a stable SEI had been founded by us [28]. That is in contrast to the LTO anodes, where the overall resistance increasing by a factor of two under comparable conditions, implying that SEI formation would not have been full after the first cycle [28].

Through ultimately results in the inferior cycling performance and a volume increase of 300% [296], which gives rise to the pulverization of electrode material, the silicon alloy electrode, which is lithiated completely, is accompanied [29]. Carbon-based composites could be utilized as buffer matrix material to enhance the electrode cycle performance [29, 297, 298]. The decrease of electrolyte caused in the surface film formation as a solid electrolyte intermediate stage (SEI) on the anode surface [299, 300] in the case of silicon-carbon composite at lower anodic potential [29]. "The stability of the SEI film is critical to the long cycle life of the silicon-carbon anode" [29]. Some film-forming additives [301, 302] could be utilized to lessen the irreversible capacity deterioration and enhance the cycle life by changing the surface film composition [29]. The participation of additives can change at electrode surface to enhance the stability of SEI film [29]. Numbers of work have been indicated that the cycle performance of silicon anodes is increasing by introducing the FEC into the electrolyte solution [29]. The FEC can form a common SEI on the silicon electrode to restrain the occurrence of huge fissures to enhance the cycle performance [29, 303]. That surface analysis of FTIR demonstrates and silicon electrodes by XPS that an electrolyte containing LiF, Li_xSiO_y in the SEI, and an insoluble polymeric species, had been indicated by Nie and others [29, 304]. There is no thorough comparative investigation of the quantity of the FEC as an additive, which is utilized for silicon-carbon composite anodes [29]. A thorough investigation of the impacts of SEI composition of silicon-carbon anodes and various quantity of FEC on cycling performance is indicated by us [29].

"Part of electrolyte will decompose to form a solid electrolyte interface (SEI) film on graphite electrode during the first intercalation of lithium ions into the graphite electrode" [30]. The formation of the SEI film gives rise to an irreversible capacity deterioration of the first discharge/charge cycle of the lithium-ion batteries and capacity fading might progressively take place with the thickening of SEI film in the subsequent cycles [30, 289]. In the electrolyte, adding additives is one of the most effective techniques to affect the properties of the SEI films and then to enhance the performance of lithium-ion batteries [30, 305–309]. The SEI film,

which is formed before the intercalation of lithium ions, is rich in inorganic elements and unstable [30]. The reduction-type additives, with greater reductive potentials than that of the electrolyte solvents, are lowered to form an insoluble solid film before the electrolyte solvents decomposes [30]. We indicated the use of tea polyphenols (TP) as a reaction-type additive in electrolyte for lithium-ion batteries [30]. The aim of this research had been to examine the effect and reaction mechanism of TP employing as an electrolyte additive for lithium-ion batteries [30]. Electrochemical impedance spectroscopic (EIS), which is one of the most potent devices to examine electrochemical mechanisms taking place at electrode/electrolyte interfaces [310–313], had been utilized to elaborate the film-forming properties of graphite electrode in the TP-containing electrolyte [30]. That the introduction of TP can efficiently enhance the capacity and cyclic stability of the graphite electrode by forming a thin, compact and smooth SEI film and scavenging less stable radical anions had been demonstrated by the results [30].

Tin, a comparatively inexpensive and plentiful material with high theoretical capacity is one alternative anode material [31]. Several researches have been concentrated on high-capacity oxide, which is Sn-based, materials such as SnO_2, their composites and SnO, particularly with carbon [31, 314, 315]. The enhanced cycleability of the tin oxide-based materials could be described via their lithiation mechanism [31]. Composites with carbon-based materials [316], particularly with graphene [317], are commonly used for enhancing the cycleability of the tin oxide-based anodes [31]. It is required to employ high potentials (20–40 V) and thereafter the formed tin oxide powders should be annealed in air at 700 °C for obtaining the crystalline structure of the [318] oxide in order to derive tin oxide under direct current conditions [31]. The use of sinusoidal alternating current can substantially accelerate the process of tin oxide formation [31]. Pulse alternating currents, on the other hand, offer novel opportunities for the synthesis of highly dispersed metal oxides because of the non-equilibrium conditions of electrolysis [31]. The rate of oxidation and dispersion of the metal under the impact of an alternating current is greater than the rate of anodic oxidation under direct current [31, 319]. The technique of pulsed alternating current for the synthesis of electrochemically active nanomaterials had been efficiently utilized in our previous researches [31, 320–322]. The technique of alternating current had been utilized for the synthesis of NiO nanoparticles; these nanoparticles were evaluated as active materials for hybrid supercapacitors [31, 322]. Under alternating pulse current as a new strategy for the synthesis of SnO_2 nanoparticles, we utilized the technique of dispersion of tin and electrochemical oxidation [31].

Owing to its advantages including flat and low potentials (<0.25 V vs. Li^+/Li), stable cycling performance, and low expenses, graphite has been utilized as the overwhelming vast majority of negative electrodes since the commercialization of lithium-ion batteries [32]. Traditional carbonate-based electrolytes comprising of ethylene carbonate (1,3-dioxa-cyclopentan-2-one, EC), lithium hexafluorophosphate ($LiPF_6$), and other linear carbonate mixed solvents are usually introduced as lithium-ion conductor between anode and cathode to match graphite-based lithium-ion batteries [32]. Due to its high melting point, low ionic electrical

conductivity at low temperature [323], and high viscosity, utilization of EC is accompanied with numerous shortcomings to the low-temperature performance of Li-ion batteries [32]. At low temperature, which limits the power and capacity of the batteries [324–326], the SEI film, which is formed with EC, indicates low Li^+ electrical conductivity [32]. Adding low melting point cosolvent is one of the most efficient methodologies to improve the low-temperature performance of the lithium-ion batteries with traditional carbonate-based electrolytes [32, 327]. Jet Propulsion Laboratory (JPL) previously indicated that numerous battery models employing their Gen 3 low-temperature electrolyte, which is the mixture of ester cosolvents and traditional carbonate-based electrolytes, revealed outstanding low-temperature performances [32, 328–330]. His coworkers and K. A. Smith asserted that fluorinated aliphatic carboxylate is one of the most fruitful cosolvent for low-temperature electrolyte [329] in these reports [32]. K. A. Smith and his co-workers' results indicated that these cosolvents are contributing to the enhanced performance of batteries and engaged to formation and properties of the SEI on graphite electrode [32]. The SEI on graphite electrode in numerous traditional carbonate-based electrolytes has been researched by numerous scholars during the 1990s [32, 331–336]. Through mixing traditional carbonate-based electrolyte and the three $RCOOCH_2CF_3$ cosolvents, three modified electrolytes are obtained, respectively [32].

In lithium-ion batteries, carbon materials of morphologies and various types are utilized as anodes, primarily because of satisfactory cycling performance [337] and their plausible theoretical capacity (372 mAh g^{-1}) [33]. Research towards a more effective material in regard to storage capacity is still on-going [33]. There is a need to come up with a more stable and cheaper anode material [33, 185]. Silicon, because of its high theoretical capacity of about 4200 mAh g^{-1} is regarded as a replacement for graphite anodes in energy storage tools [33]. That pulverization process gives rise to contact deterioration of anode materials, resulting in capacity fading [33]. The silicon oxide nanostructures were evaluated as an alternative anode material for Li-ion batteries [33, 338–341]. A high theoretical capacity of about 1965 mAh g^{-1} is shown by Silica as an anode material and is known to undergo faradaic mechanisms in the presence of lithium ions at an enough high cathodic potential [33]. A various mechanism with parallel lithium oxide creation [342] and irreversible silicate formation: Above electrochemical reactions of SiO_2 could be the source of a high theoretical capacity, substantially greater than the capacity of LiC_6 [341] had been devised by Guo, [33]. We revealed that under lithiation reversible, reactions took place on an anode material, which is derived from high temperature reconfiguration of sea water diatoms [33]. The evaluated material had been a composite of silica and the carbonaceous part [33]. All material from red algae had been chemically discarded and just the part, which comes from diatoms, has been utilized for anode preparation [33]. Electrochemical performance of silica anodes, of diatomic origin, has been investigated by means of electrochemical impedance spectroscopy (EIS) [33].

In contrast with nickel-hydrogen and nickel-cadmium batteries, lithium-ion battery has more advantages, including high voltage, high specific energy, security, no pollution, no memory effect, long cycle life [343] and little self-discharge rate [34]. It is difficult for graphite anode to satisfy the need of high energy storage tools [34]. Silicon is regarded as fruitful alternative anode material because of its high capacity (4200 mAh g^{-1}) [34, 344]. The research of silicon-based anode materials is primarily concentrated on increased electrical conductivity [345] and reducing volume effect [34]. The rational design of a wide range of composite electrodes, including Si/carbon [346] and Si/metal [347] composite electrodes can accommodate the serious volume expansion [34]. In environment-friendly energy storage and light-weight tools [348, 349], electronically conducting polymers are commonly used [34]. The theoretical capacity of conducting polymer ranges from roughly 100 to 140 mAh g^{-1} [350, 351], and the thin layers of these materials could be oxidized and lowered with a quite high rate [34, 352, 353]. Since the polyaniline shell accommodates the huge volume expansion and shrinkage of Si core during the extraction and lithium intercalation process, which fosters the contact of electrode materials [354], the Si/polyaniline core/shell composite anode exhibits reasonably well cycling stability [34]. The polypyrrole nanofiber is favourable for gathering and facile charge delivery, whilst the porosity of the electrode can effectively cushion the volume expansion of Si [34]. Polythiophene-coated nano-silicon (Si/PTh), which employs composite in situ oxidation polymerization technique, had been prepared by us [34]. The Si/PTh composite electrode revealed satisfactory cycling performance and high capacity [34].

Graphite is the most frequent anode material for lithium-ion batteries because of next-generation electric vehicles' low cost, durability, and availability, though the practical capacity of graphite has a theoretical restrict of 372 mAh g^{-1} [35]. Tin in particular has a theoretical capacity of 994 mAh g^{-1} and has been examined as one of the most fruitful prospective next-generation anode materials [35, 355]. The research and development of electrodeposited tin materials have been the principal focus since tin layers could be formed on copper current collectors by plating [35]. The dealloying and alloying reactions consequence in a tremendous volume change and eventual pulverization of the active tin material, leading to isolation of the tin from the copper current collector during charge-discharge cycling, which generates inferior cycleability [35]. Additionally improvements of both the practical specific capacity and the cycleability of tin-based anodes, including the development of practical fabrication mechanisms, are still needed [35]. Li and others have indicated that a Sn/CNTs composite film, which electrodeposition displays formed, enhanced first charge and discharge capacities compared with a tin film, even though the capacity decreases with increased cycle number [35, 356]. Through fibrous objects including the CNTs might potentially be efficient, an anode structure in which the adhesion strength between the copper layer and the tin layer are bolstered in order to improve the cycleability of tin active material layers [35]. A CNT-reinforced noble tin anode structure in which the CNTs fasten the copper underlayer and the tin active material layer had been generated employing a plating method, and the electrochemical attributes of the resulting noble anode were assessed [35].

Due to its outstanding capacity performance, excellent safety performance, and cost advantage, the requirement for lithium-ion batteries with power density and a high energy density in electric vehicle (EVs) and hybrid electric vehicle (HEVs) is roaring up [36]. Much attention has been paid on the search for high capacity, safe, and price-competitive, electrode materials [357–360] since the holistic advantage of lithium-ion batteries primarily rests on its electrode materials [36]. The studies on anode materials are centred whilst the examination on cathode materials focuses on Li–M–O (M = Co, Ni, Mn), $LiMPO_4$ (M = Co, Fe), and ASP materials [361–366], etc. on carbon materials, alloy materials and transition-metal oxides, in recent decades [36]. The spinel $LiMn_2O_4$, as lithium-ion battery cathode material, has difficulties including serious capacity decay and meager cycling, particularly at temperature [367–370], which is elevated [36]. The principal approach for the novel stable $LiMn_2O_4$ materials is to restrain Mn break-up [36]. TiN coating can improve the performance of silicon nanoparticles as a lithium-ion battery anode [371], TiN had been observed to be helpful for enhancing the rate capability and long cycle stability of $Li_4Ti_5O_{12}$ [372] and lithium iron phosphate thin films [373], and TiO_2@TiN composite nanowires on carbon cloth revealed striking rate capability for flexible lithium-ion batteries [36, 374]. TiN had been utilized as an additive to enhance the performance of $LiMn_2O_4$/Li battery with 1 M $LiPF_6$ in EC/DMC (1:1, v/v) [36]. In contrast to pristine $LiMn_2O_4$, $LiMn_2O_4$ with TiN additive revealed also better rate capability and excellent cycling stability though not just greater specific capacity [36]. The impacts of TiN on the amelioration of cycle life of the $LiMn_2O_4$/Li battery were examined [36].

Advances have been made on multiple facets of the cathode materials, including a drive towards bigger working potential (spinel-type $LiNi_{0.5}Mn_{1.5}O_4$ [375, 376] and $LiCoMnO_4$ [377], olivine-type $LiNiPO_4$ [378]), including cathode capacity (Li-S [379–382], Li-Air [383–385] batteries), which is increasing substantially [38]. Notwithstanding some advantages, the use of graphite electrode has proven difficult due to its low specific capacity (theoretical 372 mAh g^{-1}), low lithiation potential that can give rise to lithium dendrite growth, and low rate capability, on the anode side [38]. Materials with greater lithium storage capability, lower cost are required, and safer operation, were anoded by Novel [38]. Tin oxides (SnO, SnO_2) and Tin (Sn) are a family of potential high-capacity anode materials [314, 386–388], which is investigated extensively [38]. Sn has a volumetric capacity (2020 mAh cm^{-3}) similar to that of Si (2400 mAh cm^{-3}) [38, 389]. Capacity retention is still one of the largest hurdles; these hurdles impedes the commercialization of Sn-based materials [38]. A tire-derived carbon (TC) anode has been shown as a fruitful application for a recycled tire product, which haves greater capacity and considerably lower cost than those of commercial graphite [38, 390–392]. Larger capacity is required from this kind of anode material to be more appealing [38]. An easy process for a cheap is indicated by us, high-capacity LIB anode made employing tin oxide (TC/SnO) and a TC composite [38]. The carbon, which is based on waste tires, functioned as the absorbing matrix; this matrix efficiently mitigated the degradation of the electrode and the volume change [38]. Upon 300 cycles at a current density of 40 mA g^{-1}, this TC/SnO anode kept a capacity of 690 mAh g^{-1} [38].

In roll-to-roll mechanisms where a slurry of active material, binder, and conductive additives, are cast onto a conductive substrate, including copper, and dried, Standard LIB anodes are fabricated [39]. The majority of LIB anodes nowadays employ multiple modes of carbon as an active material, most frequently graphitic carbon; these modes have a theoretical capacity of 372 mAh g^{-1} [39]. A new technique that employs a facile in situ infiltration method with an aqueous infiltration solution, which includes silicon and binder nanoparticles, is examined by the present study to fabricate silicon anodes [39]. The anodes fabricated through this method might provide similar cycling performance compared to other silicon-containing anodes if refined and enhanced [39]. The through-plane electrical conductivity of the CNT mat is on the identical order as that of carbon black [393] and this winding process has been the object of numerous researches; these researches infiltrate or coat the CNTs with multiple active materials [394–399] or resin [39]. A new binder for the anode, hydroxypropyl guar gum (HPG) is examined by the current study [39]. Prior work [400–402] on native guar gum observed that it is an efficient binder in LIB anodes whilst its cost is on the present study identical order of magnitude, if not less this study's, of traditional binders including carboxymethylcellulose and polyvinylidene difluoride [39]. Several researches have demonstrated that native guar gum is also capable of conducting lithium ions with a maximal electrical conductivity of 2.2×10^{-3} S cm^{-1} at 303 K [39, 403].

Si-premised materials have been extensively viewed as fruitful negative electrodes for their high specific capacity, low cost [345, 404, 405] and proper lithiation/delithiation voltage [40]. Reports, constructing stable structure for Si particles had been considered to accommodate the tremendous volume expansion and shrinkage during the charge-discharge process [40]. A convenient and straightforward technique to construct systemic stable Si-premised anode materials with high performance is quite required [40]. Powders prepared by spray-drying can display more stable structure, which provides numerous advantages, including a better electrochemical performance [406, 407] with the other techniques [40]. A new spray, which drys-technology to prepare Si/CNTs@C composite, is devised by us [40]. Both carbon and CNTs were utilized to sustain the structure and make up for the low electronic electrical conductivity of silicon [40]. The obtained composite Si/CNTs@C had been preliminarily researched in regard of systemic, electrochemical, and morphological, properties [40].

Organosilane-based compounds have been indicated as electrolyte solvents for lithium-ion batteries due to their distinctive properties, including nonflammable, biocompatible, nonvolatile, and thermally and electrochemically stable [41, 408–410]. $Li_{1.2}Ni_{0.2}Mn_{0.6}O_2/Li_4Ti_5O_{12}$ complete cell are incompatible with graphite anode even with VC as a solid electrolyte interphase (SEI) film-forming additive, resulting in a continuing decomposition reaction of the electrolyte solvent on graphite anode [41]. The commercial electrolyte solvents include esters and organic

carbonates, among which ethylene carbonate (EC) is an essential element due to its SEI film-forming capability on graphite anode [41, 411]. The utilization of organosilane compounds as SEI film-forming additive, including polyether-functionalized disiloxanes [412], vinyl tris-2-methoxyethoxysilane [413], phenyl tris-2-methoxydiethoxysilane [414], for the PC-based electrolyte has been shown [415], where PC is utilized as the principal electrolyte solvent for graphite anode [41]. That the compatibility issue of the TMSM2 electrolyte solvent with graphite anode could be resolved by employing PC as an additive/co-solvent had been indicated by us [41]. A highly effective performance of graphite/Li cells in enhancing the discharge capacity retention and in increased the initial columbic efficiency have been obtained in the electrolyte of 1 M $LiPF_6$ in the dichotomous solvent of PC (TMSM2: PC = 9:1, by vol) and TMSM2 [41].

That a PC-based electrolyte solution with a high lithium salt content showed reversible lithium-ion intercalation/de-intercalation because of the decline in the PC-solvation number of the lithium ions [416, 417] had been indicated by us [43]. That the solvation structure of PC-solvated lithium ions is inhibition of co-intercalation reactions and a significant factor in the formation of an efficient SEI had been revealed by this consequence [43]. That the addition of calcium ions as a Lewis acid to a PC-based electrolyte solution fostered the intercalation/de-intercalation of lithium ions [418, 419] had been indicated by us [43]. Influenced by these results, we turned our focus to employing a Lewis base in the electrolyte solution as a means to control the solvation structure of PC-solvated lithium ions [43]. Counter anion and the cosolvent are regarded as the Lewis bases in the PC-based electrolyte solution [43]. "Lithium ions form aggregates with counter anions in electrolyte solutions [43, 420–423]." It is possible that the formation of an efficient SEI between electrolyte solution and the graphite negative electrode might be fostered by exploiting the Lewis basicity of the counter and cosolvent anion in the system [43]. We concentrated on the Lewis basicity of the counter and cosolvent anion in a PC-based electrolyte solution [43]. We have previously indicated that reversible intercalation and de-intercalation of lithium ions occurs in PC-based electrolyte solutions upon addition of diethylene glycol dimethyl ether (diglyme); this place displays stronger Lewis basicity than PC [43, 424]. Through adding various glymes, the effect of the Lewis basicity of the solvent in a PC-based electrolyte solution had been examined, and the effect of the Lewis basicity of the counter anion had been examined employing various lithium salts [43].

Due to the enormous volume change of Si during repeated charge-discharge cycles [425–427], the cycle lives of Si anodes do not normally satisfy the commercial standards [44]. A wide range of nanostructured Si materials have been introduced, as the nanometre facets can efficiently release the strain constructed during the volume expansion of Si in an effort to tackle the above-mentioned problems linked to the volume expansion [44]. They suffer from low tap densities and are more liable to undesired surface reactions because of the huge

surface-to-volume ratios [152, 428] even though these nanostructured Si shown enhanced cycling performance to considerable extents [44]. It is desired to build Si microparticles in which internal nanostructures are enmeshed [44]. Since their particle sizes are in the micrometer variety whilst the wall thicknesses of pores are in the nanometre variety, microporous or meso-Si materials are well-aligned to this design consideration [44]. Has been lately shown as an excellent LIB anode material, exclusive use of Si_{RH} leaves a disparity before immediate commercial adoption while mesoporous Si originating from rice husk SiO_2, namely Si_{RH} [44]. Since unavoidable volume expansion of Si_{RH} is still huge in such a way that the electrode swelling and charge-discharge reversibility are not as controllable as those of current graphite counterparts [44]. The current study is supposed to serve as a helpful ground in developing high capacity LIB anodes incorporating Si materials, with considerable potential towards commercialization from the perspectives of resource scalability and volumetric energy density [44].

Relatively high energy density, long lifespan, light design, and low environmental influence in comparison with other battery systems including nickel-cadmium (NiCd), nickel-metal hydride (NiMH) could be provided by lithium-ion batteries [45]. The issue with carbonaceous electrode materials is that they are not useful for next-generation lithium-ion batteries, electric vehicles [429] and that is, smart electrical grid systems [45]. These a lithium ion battery is constructed from a transition metal oxide cathode material and graphite anode material [45]. In the first step, which lithium-tin alloy in the second step followed, the electrochemical reaction of lithium and tin ions offers metallic lithium and tin oxide: Metallic tin formation in reaction triggers volume transformations for tin oxide-based electrodes as it is detected for pure metallic tin [45]. Through modification of the tin oxide electrode material in terms of structure and morphology, this issue might be circumvented [45]. The hydrothermal process is commonly used, particularly when tin oxide nanoparticles are attached to carbon materials [317, 430–434] among those techniques [45]. It exemplified and revealed that a porous carbon matrix acts as a buffer for volume expansion/shrinkage for tin and tin oxide-based electrode materials [45, 435]. Carbon is quite important in terms of employing carbon as a buffer in preventing electric contact deterioration of the tin negative electrode with the current collector [45, 284]. That review is revolved around the modification of tin oxide-carbon negative electrode materials in lithium-ion batteries [45]. I wished to indicate the tactics utilized to enhance battery performance by incorporation of tin oxide into the carbonaceous matrix as a negative electrode in energy conversion applications and energy storage [45].

1.2 Graphene, Anode Materials, Lithium Storage, Current Density, Reversible Capacity, Pore, Nanoparticles

1.2.1 NiO/CNTs Derived from Metal-Organic Frameworks as Superior Anode Material for Lithium-Ion Batteries [1]

That the introduction of CNTs can enhance the lithium-ion storage performance of NiO/CNT composites is demonstrated by the results [1]. That NiO/CNT composites are appealing as potential anodes for Li-ion batteries is demonstrated by the results [1]. At 100 mA g^{-1}, NiO/CNTs-10 shows the highest reversible capacity of 812 mAh g^{-1} after 100 cycles [1]. The excellent electrochemical performance of NiO/CNT composites must be attributable to the formation of 3D conductive network structure with porous NiO microspheres connected by CNTs; this CNTs benefits the buffering of the volume expansion during the cycling process and the electron transfer ability [1]. Reveal performance, which is satisfied, is based on MOFs always by the TMOs and have been extensively utilized in catalysis [436, 437], biomedicine [438], supercapacitors [439, 440], etc. Li-ion batteries [441, 442], because of high surface zones and their hierarchical structures [1]. That NiO/CNT composites display excellent cycling stability and high specific capacity primarily because of the synergetic effect between NiO and CNTs including the 3D network porous structure is confirmed by the results [1].

1.2.2 Intergrown SnO_2–TiO_2@Graphene Ternary Composite as High-Performance Lithium-Ion Battery Anodes [2]

The obtained composite reveals a distinctive structure and high surface zones, in which both TiO_2 and SnO_2 nanoparticles are reasonably well grown on the surface of graphene [2]. The electrochemical tests suggest that as-prepared SnO_2–TiO_2@graphene composite displays a high capacity of 1276 mAh g^{-1} after 200 cycles at the current density of 200 mA g^{-1} [2]. The specific capacity of 611 mAh g^{-1} at an ultra-high current density of 2000 mA g^{-1}, which is superior to those of the indicated SnO_2/graphene and SnO_2 hybrids is kept by the composite [2]. The striking electrochemical performance of ternary SnO_2–TiO_2@graphene composites is primarily attributable to high surface zones, their distinctive nanostructure, and the synergetic effect not just between graphene and metal oxides though also between the intergrown SnO_2 and TiO_2 nanoparticles [2].

1.2.3 Carbon and Few-Layer MoS_2 Nanosheets Co-modified TiO_2 Nanosheets with Enhanced Electrochemical Properties for Lithium Storage [3]

Few-layer and carbon MoS_2 nanosheets co-modified TiO_2 nano-composites (conceptualized as MoS_2-C@TiO_2) were prepared via a facile single-step pyrolysis reaction method [3]. The TiO_2 nanosheets with stable structure serve as the backbones, and carbon coating and few-layer MoS_2 tightly conform onto the surface of the TiO_2 in this distinctive nanostructure [3]. The TiO_2 needs to be noted that the carbon coating enhances the overall electronic electrical conductivity and the few-layer MoS_2 fosters the diffusion of lithium ions and provides more active sites for lithium-ion storage [3].

1.2.4 Preparation of Co_3O_4 Hollow Microsphere/Graphene/Carbon Nanotube Flexible Film as a Binder-Free Anode Material for Lithium-Ion Batteries [4]

Following a subsequent process, which is treated thermally, and a facile filtration approach, a flexible Co_3O_4 hollow microsphere/graphene/carbon nanotube hybrid film is efficiently prepared [4]. Following the morphology characterizations on the hybrid film, the Co_3O_4 hollow microspheres are homogeneously and closely attached on 3-D (3D) graphene/carbon nanotubes (GR/CNTs) network; this network decreases the agglomeration of Co_3O_4 microspheres efficiently [4]. Following the CV results, the electrochemical reaction between Co_3O_4 and Li^+ could be expressed as follows [55]: in the CV curves, it is notable that after the first cycle, the CV curves of the subsequent 4 cycles were not coincident [4]. The 3D GR/CNT network which improves prevents aggregation including conductance is a profit to help Co_3O_4 to exert its lithium storage capacities enough in this hybrid film [4].

1.2.5 In Situ Growth of Ultrashort Rice-Like CuO Nanorods Supported on Reduced Graphene Oxide Nanosheets and Their Lithium Storage Performance [5]

A facile refluxing approach in aqueous solution had been involved to synthesize ultra-short rice-like CuO nanorods/reduced graphene oxide (CuO-NRs/rGO) composite [5]. A facile refluxing approach had been utilized to synthesize ultra-short rice-like CuO-NRs/rGO composite [5]. The consequence of the high-resolution transmission electron microscopy indicates that the as-synthesized rice-like CuO nanorods have a homogeneous size of about 8 nm in width and 28 nm in length and

are homogeneously dispersed on rGO nanosheets [5]. Through the graphene nanosheets lowered from GO, the CuO nanorods are homogeneously dispersed and immobilized [5].

1.2.6 A Facile Synthesis of Heteroatom-Doped Carbon Framework Anchored with TiO_2 Nanoparticles for High Performance Lithium-Ion Battery Anodes [6]

We present a facile approach to synthesize N/S dual-doping carbon conceptual framework, which is anchored with TiO_2 nanoparticles (NSC@TiO_2) as Li-ion batteries anode, to circumvent these shortcomings [6]. The as-obtained NSC@TiO_2 electrode displays a high specific capacity of 250 mAh g^{-1} with a columbic efficiency of 99% after 500 cycles at excellent rate performance and 200 mA g^{-1}, suggesting its fruitful as anode material for Li-ion batteries [6]. At 1350 and 1580 cm^{-1}, two distinctive peaks could be detected, corresponding to the D and G band, respectively [6]. The plateaus still could be observed, representing a reasonably well partial reversibility of the reaction after 200 cycles [6].

1.2.7 Dandelion-Like Mesoporous Co_3O_4 as Anode Materials for Lithium-Ion Batteries [7]

A dandelion-like mesoporous Co_3O_4 had been fabricated and utilized as anode materials of Li-ion batteries (Li-ion batteries) [7]. Electrochemical experiments exemplified that the as-prepared dandelion-like mesoporous Co_3O_4 as anode materials of Li-ion batteries showed high reversible specific capacity of 1013.4 mAh g^{-1} and 1430.0 mAh g^{-1} at the current density of 0.2 A g^{-1} for the 100th and first cycle, respectively [7]. Its high-rate capability including the enhanced capacity made the as-prepared dandelion-like mesoporous Co_3O_4 to be a satisfactory candidate as a high-performance anode material for Li-ion batteries [7]. It could be detected that the precursor looked like dandelion and consisted of several irregular nanoneedles with length and diameter, which ranges from 2 to 10 μm, ranging from 30 to 50 nm [7]. The discharge capacities of 1st of 1427.9 mAh g^{-1}, 2nd of 1025.5 mAh g^{-1}, and 100th of 1013.4 mAh g^{-1} were all greater than the theoretical capacity of Co_3O_4 (890 mAh g^{-1}) as can be detected [7]. A high charge specific capacity of 1013.4 mAh g^{-1} at 0.2 A g^{-1} with considerable capacity retention can be detected after 100 cycles, as reasonably well [7]. At 2.13 V, an oxidation peak can be detected, arising from the reversible oxidation reaction of Co to Co_3O_4 [7, 137].

1.2.8 Template-Free Fabrication of Porous $CuCo_2O_4$ Hollow Spheres and Their Application in Lithium-Ion Batteries [8]

Once utilized in Li-ion batteries, the porous $CuCo_2O_4$ hollow spheres indicate excellent lithium storage performance; this performance can deliver a high specific capacity of 930 mAh g^{-1} after 150 cycles for 660 mAh g^{-1} and half-cell after 50 cycles for complete cell [8]. The satisfactory electrochemical properties of the as-synthesized porous $CuCo_2O_4$ hollow spheres could be attributable to their distinctive porous structure, which is beneficial for alleviating the systemic stress of volume change and shorting lithium ion-electron transmission path [8]. Full cells and the better electrochemical performance in both half suggest that the PHS-$CuCo_2O_4$ might have a potential application as electrode for Li-ion batteries in the future [8]. Both the TEM and SEM results suggest that the as-synthesized PHS-$CuCo_2O_4$ have a hierarchical porous hollow nanostructure [8]. It could be observed from the curve that the octahedral Cu^{2+} at 933.6 eV is evidently predominant because this structure is more energetically stable [8, 446, 447]. In the subsample [448, 449], the consequence suggests the existence of Co^{3+} and mixed Co^{2+} [8]. The consequence suggests the stable cycling performance of PHS-$CuCo_2O_4$ [8]. It could be detected that the cycling performance of the two electrodes displayed differently [8]. That the PHS-$CuCo_2O_4$ could be utilized as a fruitful anode material for Li-ion batteries is thought by us [8].

1.2.9 Nanoporous Carbon Microspheres as Anode Material for Enhanced Capacity of Lithium-Ion Batteries [9]

In contrast with the NCMs with porous structure, RFs carbon microspheres (RF-C), after activating with hot CO_2 and high BET surface area of 2798.8 m^2 g^{-1}; this g^{-1} offers plentiful lithium-ion storage site including stable lithium-ion transport channel [9]. The porous spherical structure of NCM retains markedly lithium-ion storage capability; this capability displays high discharge capacity and excellent cycling stability at various current density [9]. The CO_2 activating carbonaceous materials utilized in anode materials can enormously improve the capacity storage; this storage offers a fruitful modification approach to enhance the storage capacity and cyclic stability of carbonaceous anode materials for Li-ion batteries [9]. Studying a sustainable and cheap synthetic technique to prepare micropores spherical structure of carbon sphere as anode material for Li-ion batteries will enormously enhanced lithium ion storage, which is crucial to the structure design and modifier of carbon anode material application in Li-ion batteries in the future [9]. More and more carbonized materials are utilized to Li-ion batteries, it will be viewed as a fruitful stratagem to enhance the electrochemical performance of carbonaceous anode material application in Li-ion batteries in the future [9].

1.2.10 Fe_3O_4 Quantum Dots on 3D-Framed Graphene Aerogel as an Advanced Anode Material in Lithium-Ion Batteries [10]

Fe_3O_4 quantum dots/graphene aerogel materials (Fe_3O_4 QDs/GA) were derived from a facile hydrothermal approach, followed by a subsequently heat treatment process were fabricated by 3-D [10]. The Fe_3O_4 QDs (2–5 nm) are anchored tightly and dispersed homogeneously on the surface of 3-D GA [10]. On the 3D graphene pore structure, the Fe_3O_4 QDs (2–5 nm) are homogeneously anchored [10]. The enhanced electrochemical performance is attributable to that the GA not just acts as a 3-D electronic conductive matrix for electrons and the fast transportation of Li^+, though also offers with pulverization of Fe_3O_4 QDs during cycling and double protection against the aggregation [10]. The Fe_3O_4 QDs/GA composites are fruitful materials as advanced anode materials for Li-ion batteries [10]. "The Fe_3O_4 QDs/GA has an excellent reversible capacity of 1078 mAh g^{-1} after 70 cycles at a current density of 100 mA g^{-1}" [10].

1.2.11 Facial Synthesis of Carbon-Coated $ZnFe_2O_4$/Graphene and Their Enhanced Lithium Storage Properties [11]

Carbon-coated $ZnFe_2O_4$ spheres with sizes of ~110–180 nm anchored on graphene nanosheets (ZF@C/G) are efficiently prepared and utilized as anode materials for Li-ion batteries (Li-ion batteries) [11]. The obtained ZF@C/G introduces an initial discharge capacity of 1235 mAh g^{-1} and establishes a reversible capacity of 775 mAh g^{-1} after 150 cycles at a current density of 500 mA g^{-1} [11]. The enhanced electrochemical performances could be attributable to the synergetic role of graphene and homogeneous carbon coating (~3–6 nm), which can hinder the volume expansion, enhance the electron transfer between carbon-coated $ZnFe_2O_4$ spheres, and deter the pulverization/aggregation upon prolonged cycling [11].

1.2.12 High Electrochemical Energy Storage in Self-assembled Nest-Like CoO Nanofibers with Long Cycle Life [12]

The electrochemical properties of hydrothermally synthesized CoO nanofibres of diameter 30–80 nm, which is assembled in a nest-like morphology which revealed a quite high reversible lithium storage capacity of 2000 mAh g^{-1} after 600 cycles at

0.1 mA cm^{-2} as lithium-ion battery anode, are indicated by us [12]. Once investigated as a supercapacitor electrode in 1.0 M KOH, a capacitance of 1167 F g^{-1} is accomplished from these 1D CoO nanofibres after 10,000 charge discharge cycles at a high current density of 5, which reveals A g^{-1} satisfactory application potential [12]. Upon 600 cycles, Nest-like CoO nanofibres revealed a reversible lithium storage capacity of 2000 mAh g^{-1} as LIB anode and a capacitance of 1167 F g^{-1} after 10,000 cycles as electrochemical supercapacitor [12]. The Raman, and XRD, FTIR, spectroscopy results suggest successful synthesis of phase-pure CoO by this straightforward hydrothermal process inside an autoclave where areal oxidation to impurity stages like Co_3O_4 can be avoided [12]. In the discharge state and in the charged state, remarkable difference in morphologies can be detected [12].

1.2.13 *Shape-Controlled Porous Carbon from Calcium Citrate Precursor and Their Intriguing Application in Lithium-Ion Batteries [13]*

The as-prepared commodities indicate homogeneous morphologies, in which the FPCMs are self-assembled from PCNSs [13]. Upon 50 cycles at 100 mA g^{-1}, these carbon materials deliver a stable reversible capacity above 515 mAh g^{-1} as anodes of lithium-ion (lithium ion) batteries [13]. That the new shape-controlled porous carbon materials have potential applications as electrode materials in electronic tools is revealed by the investigation [13]. It could be detected that the microspheres are comprised of nanosheets via a characteristic self-assembly process from a broken microsphere [13].

1.2.14 *Novel Ag@Nitrogen-Doped Porous Carbon Composite with High Electrochemical Performance as Anode Materials for Lithium-Ion Batteries [14]*

Upon 200 cycles at a current density of 0.1 A g^{-1}, the reversible capacity of Ag-NPC remained at 852 mAh g^{-1}, demonstrating its striking cycling stability [14]. The reversible capacity for both materials progressively declined with the current rate [14]. The enhancement of the electrochemical properties including reversible capacity, cycling performance and rate performance of Ag-NPC, which is compared to the NPC, led to the synergetic impacts between NPC and Ag nanoparticles [14]. At 0.35 and 0.12 V, the peaks linked to the dealloying process of Li–Ag could be detected in the anodic scan [14]. It had been notable that for the charge-discharge profile of the Ag-NPC, numerous small plateaus could be detected apart from the one at 0.75 V [14].

1.2.15 Graphene-Co/CoO Shaddock Peel-Derived Carbon Foam Hybrid as Anode Materials for Lithium-Ion Batteries [15]

The preparation of G-Co/CoO SPDCF had been according to the following two steps [15]. That graphene had been homogeneously dispersed into the SPDCF and the carbonized shaddock peels had hierarchical porous nanoflakes structures had been demonstrated by the results [15]. The nano-sized Co/CoO had been formed on the G-SPDCF [15]. The caused G-Co/CoO SPDCF hybrid can retain a high capacity of 600 mAh g^{-1} at 0.2 A g^{-1} after 80 cycles, which had been considerably greater than that of commercial graphite (372 mAh g^{-1}) [15].

1.2.16 Porous NiO Hollow Quasi-nanospheres Derived from a New Metal-Organic Framework Template as High-Performance Anode Materials for Lithium-Ion Batteries [16]

Once assessed as an anode material for Li-ion batteries, the MOF deduced NiO electrode displays high capacity, rate performance (760 mAh g^{-1} at 200 mA g^{-1} after 100 cycles, 392 mAh g^{-1} at 3200 mA g^{-1}) and satisfactory cycling stability [16]. That superior lithium storage performance is primarily attributable to the distinctive hollow and porous nanostructure of the as-synthesized NiO; this hollow provide sufficiently space to accommodate the dramstic volume change and ameliorate the pulverization issue during the repeated lithiation/delithiation mechanisms, and offer more electro-active sites for fast electrochemical reactions including foster lithium ions and electrons transfer at the electrolyte/electrode interface [16]. Between 300 and 500 °C, which is attributable to the combustion of adsorbed PVP, a final slight weight deterioration could be detected [16].

1.2.17 Synthesis of $ZnCo_2O_4$ Microspheres with $Zn_{0.33}Co_{0.67}CO_3$ Precursor and Their Electrochemical Performance [17]

Through a facile solvothermal technique, $Zn_{0.33}Co_{0.67}CO_3$ (ZCCO) microspheres are fabricated at various temperatures, and $ZnCo_2O_4$ (ZCO) microspheres were additional obtained by pyrolysis of the relative ZCCO precursors at 450 °C [17]. Upon 70 cycles under the voltage variety of 0.01–3.0 V at the current density of 100 mA g^{-1}, compared with the synthesized of 180 °C, the synthesized of 200

(ZCCO-200) °C showed greater (1530 mAh g^{-1}) discharge capacity and better rate performance with the reversible capacity of 876 mAh g^{-1} [17]. In contrast with the first cycle, the principal decrease peak in the following cycles had been shifted to 0.95 V, which is indicative of the various electrochemical reactions during the two mechanisms (Wang and others [443]), [17]. In contrast with the ZCCO-180, the as-prepared ZCCO-200 microspheres showed greater discharge capacity (1530 mAh g^{-1}) and better rate performance with the reversible capacity of 876 mAh g^{-1} after 70 cycles [17]. The as-obtained ZCO microspheres from the pyrolysis of ZCCO-200 showed better cycling stability (741 mAh g^{-1} after 70 cycles) than that for the microspheres from the pyrolysis of ZCO-180 and greater discharge capacity of 1416 mAh g^{-1}, suggesting that the electrochemical properties of ZCO might be linked to the electrochemical performance of ZCCO [17]. Our present work indicated that both the ZCO and ZCCO microspheres could be fruitful candidates as new anode materials for lithium-ion battery applications [17].

1.2.18 *Carbon Nanotubes Cross-Linked Zn_2SnO_4 Nanoparticles/Graphene Networks as High Capacities, Long Life Anode Materials for Lithium-Ion Batteries [18]*

Acting as bridge and the strut to open the graphene sheets, 3D RGO/MWCNT nets not just deal with the issue of the aggregation of ZTO nanoparticles and volume expansion, though retain the integration of anode materials for high electrochemical performance in the designed hybrid nanostructure [18]. Material indicates high reversible capacity, long-running cycle performance for Li-ion batteries (Li-ion batteries) and superior rate capacity were anoded by the resultant [18]. Our investigation reveals significant potential of ZTO/RGO/MWCNTs as anode materials for Li-ion batteries [18]. A restricted capacity of 372 mAh g^{-1} [444, 445] could be just showed by graphitic carbon at complete lithiation [18].

1.2.19 *Environmental-Friendly and Facile Synthesis of Co_3O_4 Nanowires and Their Promising Application with Graphene in Lithium-Ion Batteries [19]*

The 1D nanowire structure with a high facet ratio had been readily accomplished through a magnetic-field-assisted self-assembly of cobalt ion complexes during decrease [19]. In huge scale, the Co_3O_4 nanowires were prepared and willing to be utilized as the anode material for lithium-ion batteries after air-calcinations [19]. The Co_3O_4 nanowires possessed a length, which ranges from 3 to 8 μm with the

dimension ratio more than 15, and showed a reversible lithium storage capacity up to ~790 mAh/g when employing a small quantity of defect-free graphene flakes as conductive additives [19]. The Co_3O_4 nanowire/graphene composite holds fruitful application for lithium-ion batteries [19].

1.2.20 Porous ZnO@C Core-Shell Nanocomposites as High Performance Electrode Materials for Rechargeable Lithium-Ion Batteries [20]

A new porous spherical ZnO@carbon (C) nanocomposite, which is based upon zeolitic imidazolate approaches (ZIFs-8)-directed technique, had been prepared for lithium-ion batteries (Li-ion batteries) [20]. Via pyrolyzing the corresponding ZnO@ZIF-8, the new porous spherical ZnO@C nano-composites were obtained [20]. The new porous spherical ZnO@C nano-composites were typified with various analysis methods including scanning electron microscopy, X-ray powder diffraction and transmission electron microscopy [20].

1.2.21 Synthesis of One-Dimensional Graphene-Encapsulated TiO_2 Nanofibers with Enhanced Lithium Storage Capacity for Lithium-Ion Batteries [21]

The unidimensional graphene/TiO_2 composite nanofibres with the distinctive microstructures have been efficiently synthesized through an effective technique and revealed excellent high rate performances as anode materials for lithium-ion batteries and the enhanced rate capacity [21]. The existence of graphene not just enhances the electronic electrical conductivity for serving as the further transport channel though avoids the agglomeration of anatase TiO_2 nanofibres, hence keeping their high active surface area [21].

1.2.22 Recent Progress in Cobalt-Based Compounds as High-Performance Anode Materials for Lithium-Ion Batteries [22]

A number of cobalt-based compounds ($Co(OH)_2$, Co_3O_4, CoN, CoS, CoP, $NiCo_2O_4$, etc.) have been devised over the past years as fruitful anode materials for Li-ion batteries (Li-ion batteries) because of their high theoretical capacity,

adequate cycleability and rich redox reaction [22]. The Li-ion batteries performances of the cobalt-based compounds have been substantially enhanced in recent decades, and it is anticipated that these materials will become a tangible reality for practical applications in the near future [22]. That review briefly investigates recent progress in this field, particularly highlights the synthetic methodologies and their corresponding performances in Li-ion batteries and the prepared nanostructures of the heterogeneous cobalt-based compounds, such as the storage capacity, cycling stability, rate capability and so on [22]. That cobalt oxides can be a satisfactory choice for the practical application in Li-ion batteries is revealed by the above results [22]. It is anticipated that the Li-ion batteries performance of the cobalt-based compounds will make significant progress and become a tangible reality for practical applications in the near future [22].

1.2.23 Synthesis and Electrochemical Properties of Tin-Doped MoS_2 (Sn/MoS_2) Composites for Lithium-Ion Battery Applications [23]

Through employing $SnCl_2{\cdot}2H_2O$ and $(NH_4)_6Mo_7O_{24}{\cdot}4H_2O$ as raw materials via a straightforward solvothermal technique, which pyrolysis followed, SnO_2–MoO_3 composites were synthesized [23]. "SnO_2–MoO_3 composites were formed on the basis of Ostwald ripening mechanism (Li and others [253]), [23]." Tin-doped MoS_2 (Sn/MoS_2) flowers have been synthesized by a solvothermal technique followed with annealing in Ar(H_2) atmosphere, with SnO_2–MoO_3, urea as starting materials, and thioacetamide (TAA) [23]. Both greater reversible capacity and better cycling performance at current density of 200 mA g^{-1}, compared with MoS_2 without Sn doping is shown by all Sn/MoS_2 composites as anode materials for Li-ion battery (LIB) [23]. Both high reversible capacity and satisfactory cycling performance is shown by nearly all Sn/MoS_2 composites as anode materials for Li-ion batteries [23]. That the Sn/MoS_2 composite can be a fruitful candidate as a new anode material for LIB application is demonstrated by the satisfactory electrochemical performance [23]. That the Sn/MoS_2 composites can be fruitful anode materials for LIB applications is demonstrated by the satisfactory electrochemical performance, and our present work offers a novel strategy to the LIB and fabrication applications of MoS_2 [23].

1.2.24 N-Doped Graphene/Bi Nanocomposite with Excellent Electrochemical Properties for Lithium-Ion Batteries [24]

N-doped graphene/Bi nanocomposite had been prepared through a two-stage technique, combining the gas/liquid interface reaction with the rapid heat treatment technique [24]. "The prepared N-doped graphene/Bi nanocomposite as an anode material for lithium-ion batteries delivers excellent electrochemical performance" [24]. The N-doped graphene/Bi nanocomposite can still deliver a specific capacity of 218 mAh g^{-1} even at the high current density of 1000 mA g^{-1} [24]. The excellent electrochemical performance of the N-doped graphene/Bi nanocomposite is supposed to profit from the synergetic effect of bismuth nanoparticles and nitrogen-doped graphene and the high electronic electrical conductivity of nitrogen-doped graphene [24]. It could be detected that the lumpish $Bi_2O_2CO_3$ are distributed on the surface of sheet-like graphene, though the size of the lump is not homogeneous [24]. Various from the first discharge curve, one plateau could be detected because of the overlapping in the subsequent discharge cycles [24]. It could be detected the superior capacity retention could be obtained [24].

1.2.25 Fabrication of Urchin-Like $NiCo_2O_4$ Microspheres Assembled by Using SDS as Soft Template for Anode Materials of Lithium-Ion Batteries [25]

Through a facile protocol, which comprises microemulsion-solvothermal reaction and subsequent calcining at 400 °C for 4 h, the urchin-like $NiCo_2O_4$ microspheres assembled by employing sodium dodecyl sulfate (SDS) as soft template are efficiently fabricated fabricated [25]. It has been clearly confirmed that the prepared 3-D urchin-like $NiCo_2O_4$ microspheres are represented by one-dimension nanowires [25]. The high reversible specific capacity, rate performance, and perfect cycleability, are attributable to the distinctive urchin-like $NiCo_2O_4$ microspheres; these microspheres can ameliorate the volume expansion and shorten the diffusion path of ions and electrons during lithiation/delithiation process [25]. The self-standing urchin-like $NiCo_2O_4$ microspheres might be a quite fruitful candidate in place of the commercial graphite-based anode materials for high-performance Li-ion batteries [25]. It could be observed that there is an apparent long discharge plateau in the initial discharge curve, which is congruent with the consequence of CV [25]. It could be observed that the urchin-like $NiCo_2O_4$ microspheres anode offers a greater reversible capacity of 1034.2 mAh/g at 100 mA/g even after 40 cycles, which is more superior to other $NiCo_2O_4$ electrodes [25].

1.2.26 *Synthesis of Spherical Silver-Coated $Li_4Ti_5O_{12}$ Anode Material by a Sol-Gel-Assisted Hydrothermal Method [26]*

Ag-coated spherical $Li_4Ti_5O_{12}$ composite had been efficiently synthesized through a sol-gel-assisted hydrothermal technique, which employs silver and an ethylene glycol nitrate mixture as the precursor, and the impact of the Ag coating contents on the electrochemical properties of its had been intensively examined [26]. The electrochemical impedance spectroscopy (EIS) analyses shown that the excellent electric conductivity of the $Li_4Ti_5O_{12}$/Ag caused from the presence of the silver coating layer, which conducts highly [26]. The nano-thick silver layer had been homogeneously coated on the particles and substantially enhanced the rate capability of this material [26]. The silver-coated micro-sized spherial $Li_4Ti_5O_{12}$ showed excellent electrochemical performance [26].

1.3 Silicon, SEI, Tin, Graphite, CNTs, Carbon, Anodes, Film

1.3.1 *Effects of Solid Polymer Electrolyte Coating on the Composition and Morphology of the Solid Electrolyte Interphase on Sn Anodes [27]*

The composition and morphology of the solid electrolyte interphase (SEI) film on the surface of Sn@PEO and Sn anode materials have been examined in order to explore the effect of polymer coating layer on the Sn anode [27]. In contrast with the bare cycled Sn electrode, the SEI on the surface of cycled Sn@PEO electrode is thinner, more stable, and smoother [27]. Obtained from X-ray photoelectron spectroscopy (XPS), the SEI formed on the Sn@PEO electrode is typified by inorganic elements (Li_2CO_3)-rich outer layer and organic components-rich inner which can make the SEI more stable and hinder the electrolyte, which immerges into the active materials [27]. Notably better capacity retention than bare Sn electrodes is demonstrated by the Sn@PEO electrodes [27].

1.3.2 *Insights into Solid Electrolyte Interphase Formation on Alternative Anode Materials in Lithium-Ion Batteries [28]*

Through electrochemical impedance spectroscopy (EIS), SEI formation on lithium and silicon titanate (LTO) anodes had been researched and ex situ X-ray

photoelectron spectroscopy (XPS) measurements to gain novel insight into the formation of the solid electrolyte interphase (SEI) as a basis for the effective and safe use of novel anode materials [28]. A decrease of the resistance in the second cycle had been detected, which indicates the formation of a stable SEI with SiO_2, Li_4SiO_4, various carbonates as its principal elements, and LiF, on the silicon anodes [28]. The resistance increasing by a factor of two, suggesting incomplete SEI formation on the LTO anodes [28].

1.3.3 Effect of Fluoroethylene Carbonate as an Electrolyte Additive on the Cycle Performance of Silicon-Carbon Composite Anode in Lithium-Ion Battery [29]

The cycling performance of silicon-carbon anodes in the electrolyte with various content (0, 2, 5, 10 wt%) fluorinated ethylene carbonate (FEC) had been researched [29]. Based on 54.81–83.82%, the retention capacity of silicon carbon anode enhanced after 50 cycles among all the electrolytes the injection of 2 wt% FEC into carbonate electrolyte [29].

1.3.4 Tea Polyphenols as a Novel Reaction-Type Electrolyte Additive in Lithium-Ion Batteries [30]

Tea polyphenols (TP) enhanced the electrochemical performance of the graphite electrode including reversible capacity and cyclic stability by cyclic voltammetry (CV), and electrochemical impedance microscope (EIS), which scans electron microscope (SEM), discharge/charge test, and electrochemical impedance microscope (EIS) to a certain extent [30]. "The first charge capacities of the graphite electrodes in electrolytes without and with TP were 327.1 and 349.1 mAh g^{-1}, respectively" [30]. The amelioration had been benefited from the efficient scavenging the less stable radical anions and amelioration the oxidation stability of EC and formation of a thin and compact, stable solid electrolyte interface (SEI) film with lower resistance [30].

1.3.5 Electrochemical Dispersion Method for the Synthesis of SnO_2 as Anode Material for Lithium-Ion Batteries [31]

A technique of electrochemical oxidation and dispersion of tin electrodes under alternating pulse current had been devised as a new strategy for the synthesis of SnO_2 nanoparticles useful as an alternative anode for Li-ion batteries [31].

1.3.6 Identification of Solid Electrolyte Interphase Formed on Graphite Electrode Cycled in Trifluoroethyl Aliphatic Carboxylate-Based Electrolytes for Low-Temperature Lithium-Ion Batteries [32]

Trifluoroethyl aliphatic carboxylates with various length of carbon-chain in acyl groups have been introduced into carbonate-based electrolyte as cosolvents to enhance the low-temperature performance of lithium-ion batteries, both lowering polarization of graphite electrode and in capacity retention [32]. The elements and properties of the surface film on graphite electrode, which is cycled in, various electrolytes are examined employing Fourier reshape infra-red spectroscopy (FTIR), electrochemical measurements, and X-ray photoelectron spectroscopy (XPS), to pinpoint the additional impact of trifluoroethyl aliphatic carboxylates on graphite electrode [32]. XPS results and the IR indicate that the chemical species of the solid electrolyte interphase (SEI) on graphite electrode strongly rely on the selection of cosolvent [32].

1.3.7 Biosilica from Sea Water Diatoms Algae—Electrochemical Impedance Spectroscopy Study [33]

We report on an electrochemical impedance investigation of silica of organic origin as an active electrode material [33]. The electrode is electrochemically stable during subsequent cyclic voltammetry measurements taken in the potential variety from 0.005 up to 3.0 V versus Li/Li^+ [33]. Electrochemical impedance spectroscopy, which is carried out at an equilibrated potential E = 0.1 V in the temperature variety 288–294 K, discloses low diffusional impedance and low charge transfer resistivity [33]. Crushing is supposed to increase the active surface area, which is needed for a sufficient current outcome [33]. That the relaxation time in SEI films diminishes with temperature increase and is lower for T = 294 K and the fastest for T = 286 K and equal to 0.00796 and 0.017 s, respectively is demonstrated by the

results [33]. That naturally taking place, renewable source of nanoporous silica from sea water diatoms are observed to be useful as the anode material for lithium-ion battery applications with comparable time constants for the lithiation process and a greater specific charge capacity than graphite is demonstrated by the results [33].

1.3.8 Polythiophene-Coated Nano-silicon Composite Anodes with Enhanced Performance for Lithium-Ion Batteries [34]

Through in situ chemical oxidation polymerization technique, a novel polythiophene-coated silicon composite anode material had been prepared [34]. The better electric contact between silicon particles could be offered by the polythiophene [34]. The as-prepared Si/polythiophene composite electrodes attain better cycling performance than the bare Si anode [34].

1.3.9 A Carbon Nanotube-Reinforced Noble Tin Anode Structure for Lithium-Ion Batteries [35]

A carbon noble tin anode structure in which CNTs fasten the tin layer to a copper underlayer, which is bolstered nanotube (CNT)-, has been fabricated employing plating methods so as to enhance the cycleability of lithium-ion batteries [35]. Through a substitution-type electroless plating method, the surface of this composite layer is subsequently coated with a tin layer, resulting in the CNT-reinforced noble tin anode structure [35]. The electrochemical attributes of this noble tin anode structure have been assessed and compared to those of a tin anode structure without CNTs [35].

1.3.10 An Approach to Improve the Electrochemical Performance of $LiMn_2O_4$ at High Temperature [36]

The XPS and XRD test results suggest that the TiN can efficiently deter Mn from dissolving in electrolyte; galvanostatic discharge/charge test indicates that $LiMn_2O_4$ electrode with TiN displays capacity retention at high temperature with capacity of 105.1 mAh g^{-1} at 1 C in the first cycle at 55 °C, which is enhanced remarkably, and the capacity establishes 88.9% retention after 150 cycles [36]. That TiN, as an addictive, made apparent contribution to the electrochemical cycling

performance of $LiMn_2O_4$, which is enhanced substantially, could be concluded by us [36]. Upon the discharge/charge had been collapsed [450], the crystal lattice in the electrodes is revealed by these results [36].

1.3.11 *Effect of Different Binders on the Electrochemical Performance of Metal Oxide Anode for Lithium-Ion Batteries [37]*

Once testing the electrochemical performance of metal oxide anode for lithium-ion batteries (Li-ion batteries), binder played crucial role on the electrochemical performance [37]. Which binder had been more useful for preparing transition metal oxides anodes of Li-ion batteries has not been systematically studied [37]. SBR +CMC binder had been more useful for making transition metal oxides anodes of Li-ion batteries [37]. Test results indicate that active material had been easy to fall off from the current collector if use PVDF for binder [37]. It could be detected that fabricated with SBR+CMC binder, particularly when the slurry ratio had been 80:10:10, the electrode shown an outstanding electric conductivity, excellent charge transfer, influential binding capability, satisfactory rate performance, and striking cycling performance, and ultimately consequence in the brilliant electrochemical performance [37].

1.3.12 *Carbon/Tin Oxide Composite Electrodes for Improved Lithium-Ion Batteries [38]*

Tin and Tin oxide-based electrodes are fruitful high-capacity anodes for lithium-ion batteries [38]. A technique to prepare scalable carbon, a cheap and tin (II) oxide composite anode is indicated [38]. Through ball milling of carbon, which is recovered from utilized tire powders with 25 wt% tin (II) oxide to form lithium-ion battery anode, the composite material had been prepared [38]. Inside the pores of carbon, which is waste-tire-derived, tin oxide powders were evenly distributed with the influence of energy from the ball milling [38]. A technique to prepare cheap carbon/tin (II) oxide (SnO) composite by ball milling is indicated [38].

1.3.13 *A Silicon-Impregnated Carbon Nanotube Mat as a Lithium-Ion Cell Anode [39]*

A material for the anodes of lithium-ion batteries because of its high practical charge capacity of 3600 mAh g^{-1}, which is $\sim$10 times the specific capacity of

traditional graphitic materials, which is studied extensively, is silicon [39]. Silicon is a meager conductor so silicon should be coupled with conductive additives, usually carbonaceous in character, to enhance electron conduction from the silicon to the current collector [39]. We report a new silicon anode fabrication method; this method entails winding an congruent carbon nanotube (CNT) sheet and commensurately infiltrating it in situ silicon an aqueous solution, which includes silicon nanoparticles and hydroxypropyl guar binder [39]. The resulting infiltrated felts were assessed, processed, and compared to traditional silicon-carbon black anodes with the identical carbon, silicon, and binder content as a proof of notion investigation [39]. Through a drawing operation from a CNT vertical assortment, a new fabrication technique is explained for the negative electrode for a lithium-ion battery: a CNT mat is formed whilst simultaneously being impregnated with a solution, which includes hydroxypropyl guar gum binder and silicon nanoparticles [39]. The resulting CNT-Si anode structure indicates enhanced life-time cycling performance, which is compared to conventional slurry-based silicon anodes [39].

1.3.14 High Cycling Performance Si/CNTs@C Composite Material Prepared by Spray-Drying Method [40]

Through a spray, the anode material Si/CNTs@C composite is prepared-drying combined pyrolysis technology [40]. Excellent electrochemical performance is demonstrated by the composite as anode for LIB [40]. AC impedance analysis and the CV suggest that the prepared composite individually indicates low charge-transfer impedance R ct and satisfactory electrode stability [40]. That the Si/CNTs@C composite is a potential alternative to graphite for high energy-density lithium-ion batteries is revealed by the results [40]. It could be observed that, as the current density increases from 50 to 1000 mA g^{-1}, the reversible specific capacity is 633.4, 626, 617.3, 591.4, and 551.7 mAh g^{-1} at the current density of 50, 100, 200, 500, and 1000 mA g^{-1}, respectively [40]. It could be observed that the charge transfer resistance had been substantially declined after adding CNTs [40].

1.3.15 Synergistic Film-Forming Effect of Oligo(Ethylene Oxide)-Functionalized Trimethoxysilane and Propylene Carbonate Electrolytes on Graphite Anode [41]

In graphite/Li cells employing the electrolyte of 1 M $LiPF_6$ in the dichotomous solvent of PC and TMSM2, with the PC content in the variety of 10–30 vol.%, good SEI film-forming cycling and capability performance had been detected [41]. The graphite/Li cells delivered greater specific capacity and better capacity

retention in the electrolyte of 1 M $LiPF_6$ in TMSM2 and PC (TMSM2: PC = 9:1, by vol), compared with those in the electrolyte of 1 M $LiPF_6$ in TMSM2 and EC (TMSM2: EC = 9:1, by vol) [41]. Through electrolyte solution structure analysis, the synergetic SEI film-forming properties of PC and TMSM2 on the surface of graphite anode had been typified via Raman surface and spectroscopy analysis, which is observed by scanning electron microscopy (SEM), energy dispersive spectroscopy (EDS), and Fourier reshape infra-red spectroscopy (FT-IR) analysis [41].

1.3.16 *Effect of Tungsten Nanolayer Coating on Si Electrode in Lithium-Ion Battery [42]*

The first charge capacities of uncoated electrode cells and the W-coated were 2558 mAh g^{-1} and 1912 mAh g^{-1}, respectively with the electrochemical property analysis [42]. Morphology transformations in the W-coated Si anode during cycling electrochemical attributes were investigated via impedance analysis, and were detected employing TEM and SEM [42]. Due to W-coated Si's mechanical and electrical conductivity properties from the atomic W layer coating via PVD, the electrode enhanced the electrode's cycleability and preserved the electrode's structure from volumetric demolition [42].

1.3.17 *Solid Electrolyte Interphase Formation in Propylene Carbonate-Based Electrolyte Solutions for Lithium-Ion Batteries Based on the Lewis Basicity of the Co-solvent and Counter Anion [43]*

In PC-based electrolyte solutions and reversible intercalation and de-intercalation of the lithium ions at the graphite negative electrode do not proceed, an efficient solid electrolyte interphase (SEI) is not formed [43]. Another solution to this issue is to control the structure of the solvated lithium ions [43]. We concentrated on the Lewis basicity of the counter and cosolvent anion in the lithium salt to form an efficient SEI and control the solvation in a PC-based electrolyte solution [43]. Tetraglyme and triglyme were utilized as the cosolvents, and lithium trifluoromethanesulfonate and lithium bis (fluorosulfonyl) amide were utilized as the anion sources [43].

1.3.18 Rice Husk-Originating Silicon–Graphite Composites for Advanced Lithium-Ion Battery Anodes [44]

Nearly 20 wt% of mesoporous SiO_2 is contained by rice husk [44]. Through reducing the rice husk-originating SiO_2 employing a magnesio-milling process, we yield mesoporous silicon (Si) [44]. Taking advantage of huge readily available amount and meso-porosity, we employ rice, which husk-originates Si, to Li-ion battery anodes in a composite form with commercial graphite [44]. The series of electrochemical results indicate that rice, which husk-originates Si graphite composites are fruitful candidates for high capacity Li-ion battery anodes, with the influential advantages in scalability and battery performance [44].

1.3.19 Composites of Tin Oxide and Different Carbonaceous Materials as Negative Electrodes in Lithium-Ion Batteries [45]

Tin oxide and Tin have been regarded as useful materials with a high theoretical capacity for Li-ion batteries [45]. The issue to circumvent with tin oxide, including with other metallic materials, is high volume transformations during alloying/dealloying, subsequent pulverization, delamination from current collectors, which follows continuous degradation of the anode [45]. Much attention had been paid to integrate carbonaceous materials [45]. Summarized results concerning utilization of the tin oxide-carbonaceous negative electrode material are summarized [45]. These an strategy caused in attaining a discharge capacity of over 140 mAh g^{-1} at a current density equal to 400 mA g^{-1} for the Sn/SnO_2/PC composite in a sodium-ion battery [45].

1.4 Conclusion

That NiO/CNT composites display excellent cycling stability and high specific capacity primarily because of the synergetic effect between NiO and CNTs including the 3D network porous structure is confirmed by the results [1]. A maximal capacity of 812 mAh g^{-1} after 100 cycles at 100 mA g^{-1} is accomplished for NiO/CNTs-10 [1]. That NiO/CNT composites are appealing as potential anodes for Li-ion batteries is demonstrated by the results [1].

A facile, one-pot, and easy, hydrothermal strategy has been summarized for producing a new kind of SnO_2–TiO_2@graphene ternary composite with high surface zones and distinctive structure [2]. Benefitting from the products' distinctive structure, the product displays outstanding cycle ability, high reversible specific capacity, and satisfactory rate capability as an anode material for Li-ion batteries,

which owes to the synergetic relationships between graphene and metal oxides [2]. Upon 200 cycles at a current density of 200 mA g^{-1}, the as-prepared SnO_2–TiO_2@graphene hybrid delivers a reversible discharge capacity as high as 1276 mAh g^{-1} [2]. The SnO_2–TiO_2@graphene composite could be utilized as a fruitful anode material for next-generation Li-ion batteries in view of the superior electrochemical properties [2].

A facile single-step pyrolysis reaction technique had been efficiently devised to prepare carbon and few-layer MoS_2 nanosheets co-modified TiO_2 nano-composites; these nano-composites are regarded to be of considerable profit to enhance both the electronic electrical conductivity and ionic electrical conductivity of TiO_2 [3]. Once assessed as a LIB anode, the nano-composites display cycle stability and enhanced specific capacity [3]. The specific capacity decreases slightly from 180 to 160 mAh g^{-1} at the current density of 1.0 C after 300 cycles, demonstrating a superior cycle stability [3].

Via a facile filtration approach, a flexible Co_3O_4/GR/CNT hybrid film had been efficiently synthesized and thermally treated process [4]. In contrast with the GR/CNT and Co_3O_4 films, the hybrid film showed an enhanced electrochemical performance, which comprises an enhanced cycling stability of 863 mAh g^{-1} at a current density of 100 mA g^{-1} after 55 cycles and excellent rate performances of 1195, 916, 707, 457, and 185 mAh g^{-1} at current densities of 100, 200, 400, 800, and 1600 mA g^{-1}, respectively [4].

In aqueous solution, a composite comprising of ultra-short rice-like CuO-NRs supported on rGO nanosheets had been synthesized through a straightforward refluxing approach [5]. Once the CuO-NRs had been functioned as anode active material for Li-ion batteries, the CuO-NRs/rGO composite indicates substantially enhanced satisfactory rate capability and cyclic stability compared to rGO nanosheets and the pure CuO-NRs [5].

The utilization of N/S dual-doped carbon as conceptual framework for the homogenous anchoring of TiO_2 nanoparticles had been devised by us [6]. TiO_2 nanoparticles are anchored into the porous graphene-based sheets with N, S dual doping characteristic; this N is generated by KOH activation process and carbonization [6]. Superior rate capacity and the excellent cycling performance might correspond to the effect of the N/S heteroatoms doping of the well-defined structure and carbon matrix [6].

The mesoporous dandelion-like Co_3O_4 material had been synthesized through a facile hydrothermal technique, which calcining at 400 °C in air followed [7]. A greater first reversible charge capacity of 1430.0 mAh g^{-1} had been shown by the electrode material [7]. The super electrochemical properties and the simplicity of the preparation technique make the mesoporous dandelion-like Co_3O_4 material a candidate for the next generation of anode materials for Li-ion batteries [7].

We have devised a facile template-free technique for the fabrication of PHS-$CuCo_2O_4$ as a high-performance anode material for Li-ion batteries [8]. The lithium storage property tests on half-cell system showed that the PHS-$CuCo_2O_4$ electrode showed greater specific capacity, rate performance, and better cycling stability, compared with SS-$CuCo_2O_4$ electrode [8]. Rate

performance and excellent cycling performance had been also showed by PHS-$CuCo_2O_4$ electrode for complete cell [8]. The excellent electrochemical performance of the as-prepared PHS-$CuCo_2O_4$ is attributable to its distinctive porous hollow structure [8].

Once NCM and RF-C are utilized to anode material for Li-ion batteries, at the identical current density of 210 mA g^{-1}, the retain capacity are 429.379 and 926.654 mAh g^{-1}, respectively, and the initial specific discharge capacity are 482.4 and 2575.992 mAh g^{-1}, respectively, after 50 cycles [9]. Upon activation with CO_2 atmosphere, the nanopores are formed on the carbon spheres; NCM as anode material indicate stable specific discharge capacity at various current density in continue cycling, and the performance of anode materials are enormously enhanced; the NCM as anode material of Li-ion batteries displays greater discharge capacity than RF-C [9]. The material still kept 780.744 mAh g^{-1} specific discharge capacity at current density of 400 mA g^{-1} after continuous 250 cycles charge-discharge testing at various current density [9].

Through subsequent annealing and a hydrothermal treatment, we have devised a facile strategy to preparing Fe_3O_4 QDs/GA [10]. "The Fe_3O_4 QDs/GA has an excellent reversible capacity of 1078 mAh g^{-1} after 70 cycles at a current density of 100 mA g^{-1}" [10]. The bigger reversible capacity might be attributable to a short Li^+ transfer distance of Fe_3O_4 QDs and the quantum size impacts [10].

The electrochemical tests indicate that the fabricated ZF@C/G electrode displays high capacity and satisfactory cycling performance, with an initial discharge capacity of 1235 mAh g^{-1} that is kept over 770 mAh g^{-1} after 150 cycles [11]. A satisfactory rate capacity with a high current density of 2.5 A g^{-1}, a reversible specific capacity is 410 mAh g^{-1} is shown by the ZF@C/G electrode [11]. A potential alternative anode to high-performance Li-ion batteries is ZF@C/G [11].

It is shown that a scalable and straightforward low-temperature solvothermal technique could be utilized to synthesize cubic brucite stage of CoO nanofibres with a nest-like morphology [12]. Through the enhancement of $Co^{2+} \leftrightarrow Co^{x+}$ ($2 < x \leq 3$) redox process in addition to formation of polymer like gel and the morphological evolution, the mechanism of Li storage is described [12].

The FPCMs present the highest specific surface area ($\sim$1489 m^2 g^{-1}) due to their distinctive structure that well-organized assembling FPCMs' nanosheets [13]. The highest discharge/charge capacities during the first cycle are shown by the FPCMs [13]. The rate capacity of FPCMs (378 mAh g^{-1} at 1 A g^{-1}) is also greater than that of PCNFs (364 mAh g^{-1} at 1 A g^{-1}) and PCNSs (311 mAh g^{-1} at 1 A g^{-1}), suggesting a superior specific capacity compared with the graphite [13]. The three kinds of porous carbon display significant improvements in cycling performance and reversible capacities particularly for FPCMs [13].

In cycling performance including the reversible capacity (852 mAh g^{-1} after 200 cycles), striking enhancement had been demonstrated by the Ag-NPC composite, compared to NPC without incorporated Ag nanoparticles [14]. That had been attributable to the synergetic effect of N-doped and Ag nanoparticles porous carbon [14]. The N-doped porous carbon functioned as a reliable matrix for Ag nanoparticles; this NPs can deter particle aggregation and ameliorate the volumetric

expansion [14]. The Ag nanoparticles that showed superior electrical conductivity including a comparatively high specific capacity can effectively raise its reversible capacity and improve cycling performance by enhancing the quality of SEI films in return [14].

Convenient technique and a new had been devised to fabricate G-Co/CoO SPDCF hybrid [15]. Due to the tremendous specific surface area of G-SPDCF, a huge number of Co/CoO nanoparticles were homogeneously dispersed on the surface of G-SPDCF and reasonably well immobilized [15]. Once utilized as anode materials for Li-ion batteries, the G-Co/CoO SPDCF showed satisfactory Li^+ storage capacity ($\sim$600 mAh g^{-1} at 0.2 A g^{-1}), long-cycling stability and enhanced rate performance (405 mAh g^{-1} at high current density of 2 A g^{-1}) [15]. The enhanced electrochemical performances of G-Co/CoO SPDCF hybrid were attributable to the nanoflakes structures to increase the surface area of the target materials and the satisfactory dispersion of a huge number of Co/CoO nanoparticles [15].

The hollow porous structure of the MOF-derived NiO anode materials can increase the electrode/electrolyte contact, shorten the diffusion length of both Li ions and electrons, and efficiently accommodate the dramstic volume change and ameliorate the pulverization issue during the repeated lithiation/delithiation mechanisms [16]. In high-capacity anode materials for next-generation Li-ion batteries, taken into consideration the straightforward preparation process, satisfactory electrochemical performances and mass production, the MOF-derived NiO indicates considerable potentials [16].

In contrast with the ZCCO-180, the as-prepared ZCCO-200 microspheres showed greater discharge capacity (1530 mAh g^{-1}) and better rate performance with the reversible capacity of 876 mAh g^{-1} after 70 cycles [17]. The as-obtained ZCO-200 microspheres showed better cycling stability (741 mAh g^{-1} after 70 cycles) than that for the ZCO-180 and greater reversible discharge capacity of 1416 mAh g^{-1} [17]. The electrochemical properties of ZCO might be linked to the electrochemical performance of ZCCO [17]. Our present work indicated that both the ZCO and ZCCO microspheres could be fruitful candidates as new anode materials for Li-ion batteries [17].

Through anchoring ZTO nanoparticles on the surface of entwined MWCNTs and wrinkled graphene, to form an advanced electrode materials for Li-ion batteries, we have devised a new ZTO/RGO/MWCNTs architectures [18]. That the introduction of MWCNTs and GO efficiently ameliorate the capacity fading and maximize the ZTO electrodes with new porous structure and high specific surface area, tremendous electronic carry out is confirmed by the results [18].

SAED results and the XRD suggested that the as-obtained Co_3O_4NW samples displayed satisfactory quality in stage and chemical composition [19]. Through TEM and SEM, the Co_3O_4NWs with the mean diameter roughly nm 180 and the length, which ranges from 3 to 8 μm, were detected [19]. Such nanowires display satisfactory electrochemical performance, volume-change-accommodating character of the distinctive 1D-2D hybrid nanostructure in conjunction with 2D

graphene and attaining lithium storage capacity greater than 700 mAh/g, as a consequence of the fast electron transport [19].

The potent buffer capability of the porous carbon shell, which is beneficial to enhance electrochemical performance and the superior capacity of the ZnO core is combined by this unusual configuration [20]. In contrast with the commercial and ZnO ZnO and other indicated ZnO-based materials, the nanocomposite with porous core/shell structure of ZnO@C display high specific capacity (750 mAh g^{-1} at 100 mA g^{-1}) and striking rate performance (351 mAh g^{-1} at 2000 mA g^{-1}) [20]. Remarkable electrochemical performance of hollow porous ZnO@C composites and the facile synthesis make it be a fruitful anode material for high performance Li-ion batteries [20].

The G/TiO_2 nanofibres revealed excellent rate performance, the high reversible capacity, and superior cycle stability which were attributable to the complementary and synergetic effect between anatase TiO_2 nanofibres and graphene [21].

Various from traditional carbon negative electrodes, the redox operation of the cobalt-based compounds versus lithium is based upon conversion reactions rather than intercalation reactions [22]. It appears that the most fruitful one is the cobalt-based ternary oxides because of the greater electrochemical activity with various oxidation states, their cheaper and more environmentally friendly doped elements and better electric conductivity than that of single element metal oxides among the examined cobalt-based compounds [22]. Through combining the cobalt-based compounds with highly conductive substrates or by designing the heterogeneous structures of cobalt-based electrodes, the lithium ion storage of the cobalt-based compounds could be substantially enhanced [22]. It is anticipated that the Li-ion batteries performance of the cobalt-based compounds will make significant progress and become a tangible reality for practical applications in the near future [22].

That the doping of Sn in MoS_2 can help to enhance the electrical conductivity of pure MoS_2, enhancing the cycling performance of MoS_2 is demonstrated by the results [23]. Both high reversible capacity and satisfactory cycling performance is shown by nearly all Sn/MoS_2 composites as anode materials for Li-ion batteries [23]. That the Sn/MoS_2 composites can be fruitful anode materials for LIB applications is demonstrated by the satisfactory electrochemical performance, and our present work offers a novel strategy to the LIB and fabrication applications of MoS_2 [23].

The synthesized nanocomposite delivers more superior electrochemical performance in comparison with the other bismuth-based materials indicated previously when utilized as an anode material for lithium-ion batteries; this material is attributed to the high electronic electrical conductivity of N-doped graphene and the synergetic effect of both bismuth nanoparticles and nitrogen-doped graphene [24]. The excellent electrochemical performance consequence makes it readily available as a potential anode material for lithium-ion batteries, which might be positive and encouraged to build more high-performance bismuth-based composites electrode for lithium-ion batteries [24].

The $NiCo_2O_4$ electrode displays an excellent cycling stability and rate performance, which is attributable to its distinctive urchin-like $NiCo_2O_4$ microspheres with more active sites, high lithium-ion diffusion coefficient, and satisfactory electrical conductivity, as it is utilized to anode material for Li-ion batteries [25].

Through a sol-gel-assisted hydrothermal technique, anode materials spherical $Li_4Ti_5O_{12}$/Ag composites with a high tap density were prepared [26]. The excessive silver content will cause the electrochemical properties of material poorer [26]. Appropriate Ag-coated spherical $Li_4Ti_5O_{12}$ composite is a superior lithium storage material with excellent safety and a high capacity, and it has real potential as a fruitful material in power Li-ion batteries [26].

The morphologies and compositions of SEI layers formed on Sn@PEO and the Sn anode material surfaces have been examined through a distinctive combination of XPS, and SEM, TEM [27]. We have detected that the passivation layer on the surface of the bare Sn electrode modes just when the first contact with the electrolyte, various from the Sn@PEO electrode before cycling [27]. Based on TEM measurement and the SEM, the Sn@PEO electrode indicates better film-forming feature than bare Sn electrode, which has better capacity retention and clearer separation of the Sn nanoparticles and a thinner SEI after cycling [27]. Reveal clear variations between the bare Sn@PEO and Sn electrodes concerning the thickness and composition of the SEI is spectraed by XPS [27]. Whereas the SEI formed on the Sn@PEO is quite thin and Sn@PEO's fluctuation extent upon cycling is less than that on Sn [27]. The Sn@PEO electrode is favourable to form a stable and compact SEI layer since the Sn@PEO electrode includes high insoluble passivating actors including Li_2CO_3 in the outer part of SEI [27].

SEM, XPS, DRT analyses for silicon and LTO, and EIS, had been carried out by us to investigation SEI growth in half-cells during the first cycle [28]. The combined techniques revealed that a surface layer formed on both the LTO and silicon anodes [28]. Surface layer formation on the lithium counter electrode can not be overlooked as it relates substantially to the overall surface resistance, R Surf particularly in the case of LTO [28].

The cycling performance of silicon-carbon anodes with various concentrations of FEC had been compared [29]. Cycle performance had been anoded by the silicon-carbon and capacity retention rate has been substantially enhanced with the FEC addition [29]. The excellent electrochemical performance of the silicon-carbon anode in FEC-containing electrolytes is because of the stable SEI film [29].

TP had been shown as a stable and novel reaction-type additive for Li-ion batteries in this work by FTIR, discharge/charge, CV, EIS measurements, and SEM [30].

We have efficiently prepared for the first time SnO_2 powder by employing electrochemical oxidation-dispersion of tin under ac pulse operation [31]. The mean grain size of crystallites of the as-prepared tin oxide had been 11–16 nm and it had 82.5 $m^2\ g^{-1}$ specific surface [31]. The reversible capacity in the first cycle had been around 680 mAh g^{-1} close to the theoretical capacity [31]. The columbic efficiency in the first cycle had been 44% similar with that supposed for SnO_2 anodes [31].

Capacity retention of about 66% over 60 cycles had been demonstrated by the material [31].

Carbonate-based electrolytes with trifluoroethyl aliphatic carboxylate as cosolvent were systematically examined for low-temperature lithium-ion batteries [32]. That the cells employing these cosolvents deliver greater Li^+ intercalation capacities than baseline electrolyte at low temperature without compromise to the performance at room temperature had been founded by us [32]. TFENH might be the most useful cosolvent for low-temperature carbonate-based electrolyte [32].

The material, which pyrolysis of marine algae obtained, includes porous silica [33]. The presence of distressed semicircles, in the form of constant stage elements instead of pure capacitors in the electric equivalent circuit, suggests that the surface is rough and that the material is porous, inhomogeneous [33]. In the SEI film, Electrochemical mechanisms taking place and between SEI interface/silica particles have been identified [33]. The time constant of SEI film impedance is 10^4 lower in comparison with the time constant originating from modified Randles circuit values linked to the charge transfer process between silica particles and the SEI interface [33]. The slowest process is lithium-ion diffusion in the bulk film [33]. The pseudocapacitance of the SEI film is constant and affects the charge transfer capacitance though is not temperature-dependent [33]. We are cognizant that the presence of crystobalite, quartz, traces of magnetite and albite would vary if one goes from batch to batch [33]. That naturally taking place, renewable source of nanoporous silica from sea water diatoms are observed to be useful as the anode material for lithium-ion battery applications with comparable time constants for the lithiation process and a greater specific charge capacity than graphite is demonstrated by the results [33].

Improved electric contact between silicon particles could be offered by the polythiophene [33]. "The electrochemical cycling performance of Si/PTh composite anodes is better than the bare Si anode" [33]. Upon 50 cycles, the specific capacity of Si/30% PTh composite electrode possesses 478 mAh g^{-1} [34].

A novel tin anode structure for lithium-ion batteries, in which CNTs fasten tin active material layer and the copper underlayer, has been fabricated employing plating methods [35]. CV measurements indicate that the lithiation rate is enhanced by the presence of CNTs and that the lithiation mechanism of the novel tin anode is various from that of a standard tin anode in the first cycle [35].

TiN is utilized as an active material additive to decline the practical capacity decay of $LiMn_2O_4$ at high temperature [36]. Galvanostatic discharge/charge test indicates that $LiMn_2O_4$ electrode with TiN displays enhanced cyclic stability at high temperature with 93.4 mAh g^{-1} and capacity of 105.1 mAh g^{-1} at the first cycle after 150 cycles at 1 C at 55 °C [36]. TiN can be an efficient addictive for enhancing the cycling performance of $LiMn_2O_4$ and the application prospect of TiN is fairly appealing [36].

That investigation has examined the electrochemical performance of CuO electrodes deal with with various binders and studied the adhesive properties of the organic PVDF binders or aqueous binders of SBR+CMC and LA133 could be varied over the weight ratio of conductive slurry [37]. It could be detected that

fabricated with SBR+CMC binder, particularly when the slurry ratio had been 80:10:10, the electrode shown an outstanding electric conductivity, excellent charge transfer, influential binding capability, satisfactory rate performance, and striking cycling performance, and ultimately consequence in the brilliant electrochemical performance [37]. The experimental feasibility and theoretical proof of manufacturing Li-ion batteries anode materials employing inexpensive aqueous SBR+CMC binder instead of poisonous solvent like costly PVDF and NMP had been offered by this work [37].

We have shown a cheap electrode composite for Li-ion batteries by ball milling of waste-tire-derived oxide (SnO) and tin (II) carbon (TC) powders [38]. The influence energy of Ball milling fosters satisfactory bonding between the SnO and TC matrix particles; this bonding has a positive synergetic effect on the composite [38]. That TC/SnO composite indicates potential as a low cost, ecologically benign, and performance-improved anode material for energy storage applications [38].

A novel technique of fabricating silicon-containing LIB anodes through a straightforward infiltration-based process had been summarized by the present study [39]. The resulting infiltrated CNT-Si anodes were typified and compared to CB-Si control samples containing carbon black as a conductive additive instead of CNTs [39]. The CNT-Si samples outperformed the CB-Si anodes in life-time cycling and matched the CB-Si anodes in rate capability [39]. The focus of the present study had been to examine a new silicon anode fabrication method, and follow-up work is planned to maximize the infiltration process to enhance performance and correlate anode structure with device performance [39].

The Si/CNTs@C particles have a homogenous morphology, CNTs is distributed throughout the surface and the interior of the composite, and the surface of the composite is coated with the carbon layer [40]. The Si/CNTs@C composites not just indicate better dynamic performance compared with Si/C composite, though display satisfactory electrochemical performance [40]. The amelioration on electrochemical performance offered the possibility to build as a Si/CNTs@C fruitful high-performance anode material for lithium, which demands power, and greater energy density-ion batteries [40].

Based on the electrolyte of 1 M $LiPF_6$ in the dichotomous solvent of PC and TMSM2, the graphite/Li half cells can deliver an excellent specific discharge capacity of 359.9 mAh g^{-1} after 60 cycles, which is even better than that with EC as the cosolvent [41]. It could be inferred that there is a synergetic SEI film-forming effect between PC and TMSM2 on graphite electrode to restrain the decomposition of TMSM2 and limit the co-intercalation of PC from the electrolyte surface and solution structure measurement analysis [41].

W had been coated onto a Si electrode employing the PVD protocol to enhance the electrochemical performance of the electrode [42]. The capacity retention of the W-coated electrode shown cycleability, which is enhanced, and had been sustained at 61.1% via 50 cycles, while the retention of the uncoated electrode had been just 25.5% [42]. The W-coated layer reduced the resistivity of the electrode and enhanced the electric conductivity of the cell [42].

In PC-based electrolyte solutions, the co-intercalation of PC-solvated lithium ions at about 0.5 V had been not adequately repressed [43]. In a mixed tetraglyme and PC electrolyte solution, which includes LiOTf compared with the one containing LiFSA, the co-intercalation of PC-solvated lithium ions had been more substantially repressed [43]. Through the OTf anion, the Lewis basicity of the OTf anion is bigger than that of the FSA anion; PC-solvated lithium ions were stabilized [43]. The stability of the PC-solvated lithium ions had been observed to be an crucial factor in the formation of an efficient SEI, and this stability is shaped by the counter anion [43].

We have evaluated c-Si_{RH}–graphite and c-Si_{RH} alone composites with multiple compositions as LIB anodes, in order to exploit of Si_{RH} in both manufacturing and systemic facets [44]. The electrochemical performance of c-Si_{RH}–graphite composites with multiple compositions showed a comparable tradeoff phenomenon, impairing the charge-discharge reversibility with increased the c-Si_{RH} fraction [44]. Additionally enhancement in the reversibility is an crucial 'must-solve' task for these composites to be integrated into practical cells [44].

The practical specific capacity of a graphite electrode of 350 mAh g^{-1} is not appealing anymore for next-generation lithium-ion batteries [45]. Materials demonstrated were oxide-based by all tin all those materials included usage of the carbonaceous matrix, and showed capacities greater than 430 mAh g^{-1} [45]. That indicates that environmental benignity and the low cost make tin oxides able to substitute graphite anodes [45]. That the main issue with tremendous volume transformations of the tin oxide electrode might be efficiently circumvent by utilization of the carbonaceous matrix as a stress-accommodating stage, which is coupled with reducing the size of tin oxide particles, had been demonstrated by the results [45]. That even though the size of tin oxide-based electrode material could be lowered, it still itself undergoes volume transformations must be taken into consideration by one [45]. There are still two principal difficulties to be resolved: (1) transferring material preparation from the laboratory scale into the industrial scale even though the engineering requirements and expectations concerning the capacity level were fulfilled [45]. The point at which 80% of the initial capacity is reached is the end of battery life [45]. A considerably lower capacity fade is needed in a battery, which is utilized virtually [45]. The crucial parameter for usage of such materials in next-generation lithium-ion batteries is the application of high capacity and high cycleability tin oxide-carbonaceous-based materials manufactured by a cost-efficient, industrial-scalable process [45].

1.5 Related Work

Ji L, Lin Z, Alcoutlabi M, Zhang X (2011) Recent developments in nanostructured anode materials for rechargeable lithium-ion batteries. Energy Environ Sci 4:2682–2699 [https://doi.org/10.1039/c0ee00699h**]**

"Yuan's group [109] synthesized $CuCo_2O_4$, the discharge capacity of which still remained 740 mA g^{-1} at 0.1 C (1 C = 1000 mA g^{-1}) after 50 cycles" [8]. Exploration of novel anode materials with greater capacity is one of the main research directions for Li-ion batteries (Poizot and others [179]; Ji and others [109]; Wang and others [180]; Manthiram and others [181]; Cheng and others [182]), [17]. Novel anode materials with greater capacity for LIB applications (Huang and others [249]; Manthiram and others [181]; Wang and others [180]; Ji and others [109]; Cheng and others [182]) must be examined by us [23].

Park CM, Kim JH, Kim H, Sohn HJ (2010) Li-alloy based anode materials for Li secondary batteries. Chem Soc Rev 39:3115 [https://doi.org/10.1039/b919877f**]**

Several researches have been revolved around high-capacity oxide, which is Sn-based, materials such as SnO_2, their composites and SnO, particularly with carbon [31, 314, 315]. Tin oxides (SnO, SnO_2) and Tin (Sn) are a family of potential high-capacity anode materials [314, 386–388], which is researched widely [38].

Wu ZS, Ren WC, Wen L, Gao LB, Zhao JP, Chen ZP, Zhou GM, Li F, Cheng HM (2010) Graphene anchored with Co_3O_4 nanoparticles as anode of lithium ion batteries with enhanced reversible capacity and cyclic performance. ASC Nano 4:3187–3194 [https://doi.org/10.1021/nn100740x**]**

TMOs, Co_3O_4 indicates comparatively high capacity and is regarded as most potential candidate for Li-ion batteries (Wu and others [186]), [17]. It is the fact that the conversion reaction-based electrodes exhibit low initial columbic efficiency because of the incomplete conversion reaction, the irreversible stage transitions and the irreversible lithium loss, which is based on the formation of a solid electrolyte interphase (SEI) layer [22, 186, 230]. With regard to the preceding achievements, heterogeneous graphene-based nanocomposites, extensively examined as anode materials for lithium-ion batteries, have showed enhanced electrochemical performance [24, 186, 262–266].

References

Main Document References

1. Xu Y, Hou S, Yang G et al (2018) J Solid State Electrochem 22:785. https://doi.org/10.1007/s10008-017-3811-0
2. Jiao Z, Gao R, Tao H et al (2016) J Nanopart Res 18:307. https://doi.org/10.1007/s11051-016-3617-5
3. Lu HH, Shi CS, Zhao NQ et al (2018) Rare Met 37:107. https://doi.org/10.1007/s12598-017-0983-9
4. Li F, Zhai G, Ren H et al (2018) Ionics 24:111. https://doi.org/10.1007/s11581-017-2173-z

5. Li G, He B, Zhou M et al (2017) Ionics 23:607. https://doi.org/10.1007/s11581-016-1822-y
6. Long B, Chen S, Wang B et al (2018) J Nanopart Res 20:164. https://doi.org/10.1007/s11051-018-4263-x
7. Zhou R, Chen Y, Fu Y et al (2018) Ionics 24:1595. https://doi.org/10.1007/s11581-017-2329-x
8. Cai S, Wang G, Jiang M et al (2017) J Solid State Electrochem 21:1129. https://doi.org/10.1007/s10008-016-3414-1
9. Xu S, Zhang Z, Wu T et al (2018) Ionics 24:99. https://doi.org/10.1007/s11581-017-2191-x
10. Wang Y, Jin Y, Duan Y et al (2017) Ionics 23:2005. https://doi.org/10.1007/s11581-017-2044-7
11. Yao L, Su Q, Xiao Y et al (2017) J Nanopart Res 19:261. https://doi.org/10.1007/s11051-017-3935-2
12. Pramanik A, Maiti S, Sreemany M et al (2016) J Nanopart Res 18:93. https://doi.org/10.1007/s11051-016-3401-6
13. Gao Y, Li J, Liu Y et al (2017) Ionics 23:2301. https://doi.org/10.1007/s11581-017-2089-7
14. Chen Y, Li J, Yue G et al (2017) Nano-Micro Lett 9:32. https://doi.org/10.1007/s40820-017-0131-y
15. Zhou R, Chen Y, Fu Y et al (2018) Ionics 24:1321. https://doi.org/10.1007/s11581-017-2294-4
16. Xu J, Tang H, Xu T et al (2017) Ionics 23:3273. https://doi.org/10.1007/s11581-017-2160-4
17. Lu L, Xu S, Luo Z et al (2016) J Nanopart Res 18:183. https://doi.org/10.1007/s11051-016-3492-0
18. Shan H, Zhao Y, Li X et al (2016) J Appl Electrochem 46:851. https://doi.org/10.1007/s10800-016-0961-1
19. Xu Z, Liu W, Yang Y et al (2017) Nanoscale Res Lett 12:615. https://doi.org/10.1186/s11671-017-2382-4
20. Fu Y, Zhong B, Chen Y et al (2017) J Porous Mater 24:613. https://doi.org/10.1007/s10934-016-0297-6
21. Li D, Guo E, Lu Q et al (2017) J Solid State Electrochem 21:2313. https://doi.org/10.1007/s10008-017-3579-2
22. Wu J, Lau WM, Geng DS (2017) Rare Met 36:307. https://doi.org/10.1007/s12598-017-0904-y
23. Lu L, Min F, Luo Z et al (2016) J Nanopart Res 18:357. https://doi.org/10.1007/s11051-016-3677-6
24. Zhang Y, Wang Q, Wang B et al (2017) Ionics 23:1407. https://doi.org/10.1007/s11581-017-1975-3
25. Li Y, Wu X (2018) Ionics 24:1329. https://doi.org/10.1007/s11581-017-2291-7
26. Li J, Huang S, Xu S, Lan L, Lu L, Li S (2017) Nanoscale Res Lett 12(1):576. https://doi.org/10.1186/s11671-017-2342-z
27. Cao Z, Meng H, Dou P et al (2017) J Solid State Electrochem 21:955. https://doi.org/10.1007/s10008-016-3440-z
28. Steinhauer M, Diemant T, Heim C et al (2017) J Appl Electrochem 47:249. https://doi.org/10.1007/s10800-016-1032-3
29. Tang WJ, Peng WJ, Yan GC et al (2017) Ionics 23:3281. https://doi.org/10.1007/s11581-017-2143-5
30. Bian S, Liu M, Shi Y et al (2018) Ionics 24:1919. https://doi.org/10.1007/s11581-018-2445-2
31. Kuriganova AB, Vlaic CA, Ivanov S et al (2016) J Appl Electrochem 46:527. https://doi.org/10.1007/s10800-016-0936-2
32. Lu W, Xiong S, Xie K et al (2016) Ionics 22:2095. https://doi.org/10.1007/s11581-016-1743-9
33. Nowak AP, Lisowska-Oleksiak A, Wicikowska B et al (2017) J Solid State Electrochem 21:2251. https://doi.org/10.1007/s10008-017-3561-z
34. Wang QT, Li RR, Zhou XZ et al (2016) J Solid State Electrochem 20:1331. https://doi.org/10.1007/s10008-016-3127-5

35. Arai S, Fukuoka R (2016) J Appl Electrochem 46:331. https://doi.org/10.1007/s10800-016-0933-5
36. Tian J, Zhao F, Xue P et al (2017) Ionics 23:1357. https://doi.org/10.1007/s11581-016-1947-z
37. Wang R, Feng L, Yang W, Zhang Y, Zhang Y, Bai W, Liu B, Zhang W, Chuan Y, Zheng Z, Guan H (2017) Nanoscale Res Lett 12:575. https://doi.org/10.1186/s11671-017-2348-6
38. Li Y, Levine AM, Zhang J et al (2018) J Appl Electrochem 48:811. https://doi.org/10.1007/s10800-018-1205-3
39. Ho DN, Yildiz O, Bradford P et al (2018) J Appl Electrochem 48:127. https://doi.org/10.1007/s10800-017-1140-8
40. Su M, Liu Y, Wan H et al (2017) Ionics 23:405. https://doi.org/10.1007/s11581-016-1867-y
41. Wang J, Qin X, Yan X et al (2017) Ionics 23:1131. https://doi.org/10.1007/s11581-016-1909-5
42. Son BD, Lee JK, Yoon WY (2018) Nanoscale Res Lett 13(1):58. https://doi.org/10.1186/s11671-018-2460-2
43. Song HY, Fukutsuka T, Miyazaki K et al (2016) J Appl Electrochem 46:1099. https://doi.org/10.1007/s10800-016-0996-3
44. Kim HJ, Choi JH, Choi JW (2017) Nano Converg 4(1):24. https://doi.org/10.1186/s40580-017-0118-x
45. Nowak AP (2018) J Solid State Electrochem 22:2297. https://doi.org/10.1007/s10008-018-3942-y

Other Bibliographic References

46. Pan QM, Qin LM, Liu J, Wang HB (2010) Flower-like ZnO–NiO–C films with high reversible capacity and rate capability for lithium-ion batteries. Electrochim Acta 55:5780–5785
47. Lu J, Chen ZH, Ma ZF, Pan F, Curtiss LA, Amine K (2010) The role of nanotechnology in the development of battery materials for electric vehicles. Nat Nanotech 11:1031–1038
48. Hameer S, Niekerk JL (2015) A review of large-scale electrical energy storage. Int J Energy Res 39:1179–1195
49. Peters JF, Baumann M, Zimmermann B, Braun J, Weil M (2017) The environmental impact of Li-ion batteries and the role of key parameters—a review. Renew Sust Energ Rev 67:491–506
50. Wang BB, Wang G, Cheng XM, Wang H (2016) Synthesis and electrochemical investigation of core-shell ultrathin NiO nanosheets grown on hollow carbon microspheres composite for high performance lithium and sodium ion batteries. Chem Eng J 306:1193–1202
51. Xu X, Tan H, Xi K, Ding SJ, Yu DM, Cheng SD, Yang G, Peng XY, Fakeeh A, Kumar RV (2015) Bamboo-like amorphous carbon nanotubes clad in ultrathin nickel oxide nanosheets for lithium-ion battery electrodes with long cycle life. Carbon 84:491–499
52. Zou F, Chen YM, Liu KW, Yu ZT, Liang WF, Bhaway SM, Gao M, Zhu Y (2016) Metal organic frameworks derived hierarchical hollow NiO/Ni/graphene composites for lithium and sodium storage. ACS Nano 10:377–386
53. Zhang F, Jiang DG, Zhang XG (2016) Porous NiO materials prepared by solid-state thermolysis of a Ni-MOF crystal for lithium-ion battery anode. Nano-Struct Nano-Objects 5:1–6
54. Mollamahale YB, Liu Z, Zhen YD, Tian ZQ, Hosseini D, Chen LW, Shen PK (2016) Simple fabrication of porous NiO nanoflowers: growth mechanism, shape evolution and their application into Li-ion batteries. Int J Hydrog Energy 42:7202–7211

55. Huang G, Zhang FF, Du XC, Qin YL, Yin DG, Wang LM (2015) Metal organic frameworks route to in situ insertion of multiwalled carbon nanotubes in Co_3O_4 polyhedra as anode materials for lithium-ion batteries. ACS Nano 9:1592–1599
56. Zou YL, Qi ZG, Ma ZS, Jiang WJ, Hu RW, Duan JL (2017) MOF-derived porous ZnO/MWCNTs nanocomposite as anode materials for lithium-ion batteries. J Electroanal Chem 788:184–191
57. Zhang H, Tao H, Jiang Y, Jiao Z, Minghong Wu, Zhao B (2010) Ordered nanostructure CoO/CMK-3 nanocomposites as the anode materials for lithium-ion batteries. J Power Sources 195:2950–2955
58. Zhang LS, Jiang LY, Yan HJ, Wang WD, Wang W, Song WG, Guo YG, Wan LJ (2010) Mono dispersed SnO_2 nanoparticles on both sides of single layer graphene sheets as anode materials in Li-ion batteries. J Mater Chem 20:5462–5467
59. Jiang X, Yang X, Zhu Y, Fan K, Zhao P, Li C (2013) Designed synthesis of graphene–TiO_2–SnO_2 ternary nanocomposites as lithium-ion anode materials. New J Chem 37:3671–3678
60. Han S, Jiang J, Huang Y, Tang Y, Cao J, Wu D, Feng X (2015) Hierarchical TiO_2–SnO_2–graphene aerogels for enhanced lithium storage. Phys Chem Chem Phys 17:1580–1584
61. Tang Y, Wu D, Chen S, Zhang F, Jia J, Feng X (2013) Highly reversible and ultra-fast lithium storage in mesoporous graphene-based TiO_2/SnO_2 hybrid nanosheets. Energy Environ Sci 6:2447–2451
62. Xia T, Zhang W, Wang ZH, Zhang YL, Song XY, Murowchick J, Battaglia V, Liu G, Chen X (2014) Amorphous carbon-coated TiO_2 nanocrystals for improved lithium-ion battery and photocatalytic performance. Nano Energy 6:109
63. Xing Z, Asiri AM, Obaid AY, Sun X, Ge X (2014) Carbon nanofiber-templated mesoporous TiO_2 nanotubes as a high-capacity anode material for lithium-ion batteries. RSC Adv 4 (18):9061
64. Liu L, Fan Q, Sun C, Gu X, Li H, Gao F, Chen Y, Dong L (2013) Synthesis of sandwich-like TiO_2@C composite hollow spheres with high rate capability and stability for lithium-ion batteries. J Power Sources 221:141
65. Moitzheim S, Nimisha CS, Deng S, Cott DJ, Detavernier C, Vereecken PM (2014) Nanostructured TiO_2/carbon nanosheet hybrid electrode for high-rate thin-film lithium-ion batteries. Nanotechnology 25(50):504008
66. Ramakrishna Matte HSS, Gomathi A, Manna AK, Late DJ, Datta R, Pati SK, Rao CNR (2010) MoS_2 and WS_2 analogues of graphene. Angew Chem Int Ed 122(24):4153
67. Bai L, Fang F, Zhao YY, Liu YG, Li JP, Huang GY, Sun HY (2014) A sandwich structure of mesoporous anatase TiO_2 sheets and reduced graphene oxide and its application as lithium-ion battery electrodes. RSC Adv 4:43039–43046
68. Xiao CL, Zhang SC, Wang SB, Xing YL, Lin RX, Wei X, Wang WX (2016) ZnO nanoparticles encapsulated in a 3D hierarchical carbon framework as anode for lithium ion battery. Electrochim Acta 189:245–251
69. Xiao SN, Pan DL, Wang LJ, Zhang ZZ, Lyu ZY, Dong WH, Chen XL, Zhang DQ, Chen W, Li HX (2016) Porous CuO nanotubes/graphene with sandwich architecture as high-performance anodes for lithium-ion batteries. NANO 8:19343–19351
70. Wang BB, Wang G, Zheng ZZ, Wang H, Bai JT, Bai JB (2013) Carbon coated Fe_3O_4 hybrid material prepared by chemical vapor deposition for high performance lithium-ion batteries. Electrochim Acta 106:235–243
71. Huang GY, Xu SM, Cheng YB, Zhang WJ, Li J, Kang XH (2015) NiO nanosheets with large specific surface area for lithium-ion batteries and supercapacitors. Int J Electrochem Sci 10:2594–2601
72. Huang GY, Xu SM, Yang Y, Sun HY, Li ZB, Chen Q, Lu SS (2014) Micro-spherical $CoCO_3$ anode for lithium-ion batteries. Mater Lett 131:236–239
73. Huang GY, Xu SM, Yang Y, Chen YB, Li ZB (2015) Rapid-rate capability of micro-/nano-structured CoO anodes with different morphologies for lithium-ion batteries. Int J Electrochem Sci 10:10587–10596

74. Yan CS, Chen G, Zhou X, Sun JX, Lv C (2016) Template-based engineering of carbon-doped Co_3O_4 hollow nanofibers as anode materials for lithium-ion batteries. Adv Funct Mater 26:1428–1436
75. Wang YQ, Geng FS, Yue XB, Yuan AB, Xu JQ (2016) Enhanced lithium storage performance of a self-assembled hierarchical porous Co_3O_4/VGCF hybrid high-capacity anode material for lithium-ion batteries. Ionics 1–8
76. Liu CF, Zhang CK, Song HQ, Zhang CP, Liu YG, Nan XH, Cao GZ (2016) Mesocrystal MnO cubes as anode for Li-ion capacitors. Nano Energy 22:290–300
77. Huang GY, Xu SM, Li LY, Wang XJ, Lu SS (2014) Synthesis and modification of a lamellar Co_3O_4 anode for lithium-ion batteries. Acta Phys Chim Sin 30:1121–1126
78. Huang GY, Xu SM, Lu SS, Li LY, Sun HY (2014) Porous polyhedral and fusiform Co_3O_4 anode materials for high-performance lithium-ion batteries. Electrochim Acta 135:420–427
79. Zhang DW, Qian A, Chen JJ, Wen JW, Wang L, Chen CH (2012) Electrochemical performances of nano-Co_3O_4 with different morphologies as anode materials for Li-ion batteries. Ionics 18:591–597
80. Ma JM, Manthiram A (2012) Precursor-directed formation of hollow Co_3O_4 nanospheres exhibiting superior lithium storage properties. RSC Adv 2:3187
81. Fan S, Liu XJ, Li YF, Yan E, Wang CH, Liu JH, Zhang Y (2013) Non-aqueous synthesis of crystalline Co_3O_4 nanoparticles for lithium-ion batteries. Mater Lett 91:291–293
82. Wang DL, Yu YC, He H, Wang J, Zhou WD, Abruña HD (2015) Template-free synthesis of hollow-structured Co_3O_4 nanoparticles as high-performance anodes for lithium-ion batteries. ACS Nano 9:1775–1781
83. Huang GY, Xu SM, Lu SS, Li LY, Sun HY (2014) Micro-/nanostructured Co_3O_4 anode with enhanced rate capability for lithium-ion batteries. ACS Appl Mater Interfaces 6:7236–7243
84. Ye MH, Li CX, Zhao Y, Qu LT (2016) Graphene decorated with bimodal size of carbon polyhedrons for enhanced lithium storage. Carbon 106:9–19
85. Shen LF, Zhang XG, Li HS, Yuan CZ, Cao GZ (2011) Design and tailoring of a three-dimensional TiO_2–graphene–carbon nanotube nanocomposite for fast lithium storage. J Phys Chem Lett 2:3096–3101
86. Rai AK, Anh LT, Gim J, Mathew V, Kang J, Paul BJ, Singh NK, Song JJ, Kim J (2013) Facile approach to synthesize CuO/reduced graphene oxide nanocomposite as anode materials for lithium-ion battery. J Power Sources 244:435–441
87. Liu Y, Wang W, Gu L, Wang YW, Ying YL, Mao YY, Sun LW, Peng XS (2013) Flexible CuO nanosheets/reduced-graphene oxide composite paper: binder-free anode for high-performance lithium-ion batteries. ACS Appl Mater Interfaces 5:9850–9855
88. Zhang X, Hu YG, Zhu DZ, Xie AJ, Shen YH (2016) A novel porous CuO nanorod/rGO composite as a high stability anode material for lithium-ion batteries. Ceram Int 42:1833–1839
89. Zhou X, Xi L, Chen F, Bai T, Wang B, Yang J (2016) In situ growth of SnO_2, nanoparticles in heteroatoms doped cross-linked carbon frameworks for lithium ion batteries anodes. Electrochim Acta 213:633–640
90. Wagemaker M, van Eck ERH, Kentgens APM, Mulder FM (2009) Li-ion diffusion in the equilibrium nanomorphology of spinel $Li_{4+x}Ti_5O_{12}$. J Phys Chem B 113:224–230
91. Kamata M, Fujine S, Yoneda K, Kanda K, Esaka T (1999) Diffusion coefficient measurement of lithium ion in sintered $Li_{1.33}Ti_{1.67}O_4$ by means of neutron radiography. Solid State Ionics 123(1):165
92. Chu S, Zhong Y, Cai R, Zhang Z, Wei S, Shao Z (2016) Mesoporous and nanostructured TiO_2 layer with ultra-high loading on nitrogen-doped carbon foams as flexible and free standing electrodes for lithium-ion batteries. Small 12(48):6724–6734
93. Wang X, Sun G, Routh P, Kim DH, Huang W, Chen P (2014) Heteroatom-doped graphene materials: syntheses, properties and applications. Chem Soc Rev 43(20):7067–7098

94. Wang X, Weng Q, Liu X, Wang X, Tang DM, Tian W, Zhang C, Yi W, Liu D, Bando Y, Golberg D (2014) Atomistic origins of high rate capability and capacity of n-doped graphene for lithium storage. Nano Lett 14(3):1164–1171
95. Xing LB, Hou SF, Zhang JL, Zhou J, Li Z, Si W, Zhuo S (2015) A facile preparation of three dimensional N, S co-doped graphene hydrogels with thiocarbohydrazide for electrode materials in supercapacitor. Mater Lett 147:97–100
96. Zhuang GL, Bai J, Tao X, Luo JM, Wang X, Gao Y, Zhong X, Li XN, Wang JG (2015) Synergistic effect of S, N-co-doped mesoporous carbon materials with high performance for oxygen-reduction reaction and li-ion batteries. J Mater Chem A 3(40):20244–20253
97. Wu S, Xia T, Wang J, Lu F, Xu C, Zhang X, Huo L, Zhao H (2017) Ultrathin mesoporous Co_3O_4 nanosheets-constructed hierarchical clusters as high rate capability and long life anode materials for lithium-ion batteries. Appl Surf Sci 406:46–55
98. Jin Y, Wang L, Shang Y, Gao J, Li J, He X (2014) Facile synthesis of monodisperse Co_3O_4 mesoporous microdisks as an anode material for lithium ion batteries. Electrochim Acta 151:109–117
99. Wang Y, Ding PS, Wang C (2016) J Alloys Compd 654:273–279
100. Yang Q, Wu J, Huang K, Lei M, Wang WJ, Tang SS, Lu PJ, Lu YK, Li J (2016) J Alloys Compd 667:29–35
101. Glushenkov AM, Hassan MF, Stukachev VI, Guo Z, Liu HK, Kuvshinov GG, Chen Y (2010) J Solid State Electrochem 14:1841–1846
102. Zhou ZY, Xie WH, Li SY, Jiang XY, He DY, Peng SL, Ma F (2015) J Solid State Electrochem 19:1211–1215
103. Niu CJ, Meng JS, Han CH, Zhao KN, Yan MY, Mai LQ (2014) Nano Lett 14:2873–2878
104. Wang Z, Su F, Madhavi S, Lou XW (2011) Nanoscale 3:1618–1623
105. Mo YD, Ru Q, Song X, Hu SJ, Guo LY, Chen XQ (2015) Electrochim Acta 176:575–585
106. Chen H, Zhang Q, Wang J, Wang Q, Zhou X, Li X, Yang Y, Zhang K (2014) Nano Energy 10:245–258
107. Mohamed SG, Chen CJ, Chen CK, Hu SF, Liu RS (2014) ACS Appl Mater Interfaces 6:22701–22708
108. Fu C, Li G, Luo D, Huang X, Zheng J, Li L (2014) ACS Appl Mater Interfaces 6:2439–2449
109. Ji L, Lin Z, Alcoutlabi M, Zhang X (2011) Recent developments in nanostructured anode materials for rechargeable lithium-ion batteries. Energy Environ Sci 4:2682–2699
110. Zhang GQ, Lou XW (2014) Angew Chem Int Ed 53:9041–9044
111. Liang J, Yu XY, Zhou H, Wu HB, Ding SJ, Lou XW (2014) Angew Chem Int Ed 53:12803–12807
112. Wang HG, Yuan S, Ma DL, Zhang XB, Yan JM (2015) Electrospun materials for rechargeable batteries: from structure evolution to electrochemical performance. Energy Environ Sci 8:1660–1681
113. Guo R, Zhao L, Yue W (2015) Assembly of core–shell structured porous carbon–graphene composites as anode materials for lithium-ion batteries. Electrochim Acta 152:338–344
114. Chen T, Pan L, Loh TAJ, Chua DHC, Yao Y, Chen Q, Li D, Qin W, Sun Z (2014) Porous nitrogen-doped carbon microspheres as anode materials for lithium ion batteries. Dalton Trans 43:14931–14935
115. Yang SJ, Nam S, Kim T, Im JH, Jung H, Kang JH, Wi S, Park B, Park CR (2013) Preparation and exceptional lithium anodic performance of porous carbon-coated ZnO quantum dots derived from a metal-organic framework. J Am Chem Soc 135:7394
116. Su LW, Wu XB, Zheng LH, Zheng TL, Hei JP, Wang LB, Wang YH, Ren MM (2016) Excellent lithium storage materials consisting of highly distributed Fe_3O_4 quantum dots on commercially available graphite nanoplates. Part Part Syst Charact 33:597
117. Liu SH, Wang YW, Dong YF, Zhao ZB, Wang ZY, Qiu JS (2015) Ultrafine Fe_3O_4 quantum dots on hybrid carbon nanosheets for long-life. High-Rate Alkali-Metal Storage 3:38
118. Liu H, Jia MQ, Zhu QZ, Cao B, Chen RJ, Wang Y, Wu F, Xu B (2016) 3D-0D graphene-Fe_3O_4 quantum dot hybrids as high-PerformanceAnode materials for sodium-ion batteries. ACS Appl Mater Interfaces 8:26878

119. Yuan C, Wu HB, Xie Y, Lou XW (2014) Mixed transition-metal oxides: design, synthesis, and energy-related applications. Angew Chem Int Ed 53:1488–1504
120. Li YN, Chu YQ, Qin QZ (2004) Nanocrystalline $ZnFe_2O_4$ and Ag-doped $ZnFe_2O_4$ films used as new anode materials for Li-ion batteries. J Electrochem Soc 151:A1077–A1083
121. Zhang WM, Wu XL, Hu JS, Guo YG, Wan LJ (2008) Carbon coated Fe_3O_4 nanospindles as a superior anode material for lithium-ion batteries. Adv Funct Mater 18:3941–3946
122. Lee S, Cho Y, Song HK, Lee KT, Cho J (2012) Carbon-coated single-crystal $LiMn_2O_4$ nanoparticle clusters as cathode material for high-energy and high-power lithium-ion batteries. Angew Chem Int Ed 51:8748–8752
123. Xiong T, Chen JS, Lou XW, Zeng HC (2012) Mesoporous Co_3O_4 and CoO@C Topotactically transformed from chrysanthemum-like $Co(CO_3)_{0.5}(OH)\cdot 0.11H_2O$ and their lithium-storage properties. Adv Funct Mater 22(4):861
124. Qi Y, Zhang H, Du N, Yang D (2013) Highly loaded CoO/graphene nanocomposites as lithium-ion anodes with superior reversible capacity. J Mater Chem A 1:2337–2342
125. Huang X, Wang R, Xu D, Wang Z, Wang H, Xu J, Wu Z, Liu Q, Zhang Y, Zhang X (2013) Homogeneous CoO on graphene for binder-free and ultralong-life lithium ion batteries. Adv Funct Mater 23:4345–4353
126. Guan H, Wang X, Li H, Zhi C, Zhai T, Bando Y, Golberg D (2012) CoO octahedral nanocages for high-performance lithium ion batteries. Chem Commun 48:4878–4880
127. Sun Y, Hu X, Luo W, Huang Y (2012) Ultrathin CoO/graphene hybrid nanosheets: a highly stable anode material for lithium-ion batteries. J Phys Chem C 116:20794
128. Sun Y, Hu X, Luo W, Huang Y (2012) Self-assembled mesoporous CoO nanodisks as a long-life anode material for lithium-ion batteries. J Mater Chem 22:13826
129. Peng C, Chen B, Qin Y, Yang S, Li C, Zuo Y, Liu S, Yang J (2012) Facile ultrasonic synthesis of CoO quantum dot/graphene nanosheet composites with high lithium storage capacity. ACS Nano 6:1074
130. Zhou C, Zhang Y, Li Y, Liu J (2013) Construction of high-capacitance 3D CoO@polypyrrole nanowire array electrode for aqueous asymmetric supercapacitor. Nano Lett 13:2078
131. Wang H, Qing C, Guo J, Aref AA, Sun D, Wang B, Tang Y (2014) Highly conductive carbon–CoO hybrid nanostructure arrays with enhanced electrochemical performance for asymmetric supercapacitors. J Mater Chem A 2:11776
132. Gao Z, Song N, Li X (2015) Microstructural design of hybrid CoO@NiO and graphene nano-architectures for flexible high performance supercapacitors. J Mater Chem A 3:14833
133. Yang M, Lv F, Wang Z, Xiong Y, Li M, Wang W, Zhang L, Wu S, Liu H, Gu Y, Lu Z (2015) Binder-free hydrogenated NiO–CoO hybrid electrodes for high performance supercapacitors. RSC Adv 5:31725
134. Zhou YQ, Wang HG, Zeng Y, Li C, Shen Y, Chang JJ, Duan Q (2015) Nitrogen-doped porous carbon/Sn composites as high capacity and long life anode materials for lithium-ion batteries. Mater Lett 155:18–22
135. Li WH, Li MS, Wang M, Zeng LC, Yu Y (2015) Electrospinning with partially carbonization in air: highly porous carbon nanofibers optimized for high-performance flexible lithium-ion batteries. Nano Energy 13:693–701
136. Ji LW, Yao YF, Toprakci O, Lin Z, Liang YZ, Shi Q, Medford AJ, Millns CR, Zhang XW (2010) Fabrication of carbon nanofiber-driven electrodes from electrospun polyacrylonitrile/polypyrrole bicomponents for high-performance rechargeable lithium-ion batteries. J Power Sources 195:2050–2056
137. Wu J, Zuo L, Song Y, Chen Y, Zhou R, Chen S, Wang L (2016) Preparation of biomass-derived hierarchically porous carbon/Co_3O_4 nanocomposites as anode materials for lithium-ion batteries. J Alloy Compd 656:745–752
138. Mei T, Zhang L, Wang XB, Qian YT (2014) One-pot synthesis of carbon nanoribbons and their enhanced lithium storage performance. J Mater Chem 2:11974–11979

139. Zhang F, Wang KX, Li GD, Chen JS (2009) Hierarchical porous carbon derived from rice straw for lithium ion batteries with high-rate performance. Electrochem Commun 11:130–133
140. Chang JL, Gao ZY, Wang XR, Wu DP, Xu F, Wang X, Guo YM, Jiang K (2015) Activated porous carbon prepared from paulownia flower for high performance supercapacitor electrodes. Electrochim Acta 157:290–298
141. Fey GTK, Chen CL (2001) High-capacity carbons for lithium-ion batteries prepared from rice husk. J Power Sources 97:47–51
142. Ru HH, Bai NB, Xiang KX, Zhou W, Chen H, Zhao XS (2016) Porous carbons derived from microalgae with enhanced electrochemical performance for lithium-ion batteries. Electrochim Acta 194:10–16
143. Cao XY, Chen SQ, Wang GX (2014) Porous carbon particles derived from natural peanut shells as lithium ion battery anode and its electrochemical properties. Mater Lett 4:819–826
144. Ou J, Zhang YZ, Chen L, Guo Y, Xiao D (2015) Hierarchical porous carbons fabricated from silica via flame synthesis as anode materials for high-performance lithium-ion batteries. Ionics 21(7):1881–1891
145. Yuan GH, Wang G, Wang H, Bai T (2015) Synthesis and electrochemical investigation of radial ZnO microparticles as anode materials for lithium-ion batteries. Ionics 21(2):365–371
146. Wang W, Sun Y, Liu B, Wang SG, Cao MH (2015) Porous carbon nanofiber webs derived from bacterial cellulose as an anode for high performance lithium ion batteries. Carbon 91:56–65
147. Guo DC, Han F, Lu AH (2015) Porous carbon anodes for a high capacity lithium-ion battery obtained by incorporating silica into benzoxazine during polymerization. Chem Eur J 21:1520–1525
148. Peng YT, Lo CT (2015) Electrospun porous carbon nanofibers as lithium ion battery anodes. J Solid State Electrochem 19:3401–3410
149. Li DD, Chen HB, Wei M, Ding LX, Wang SQ, Wang HH (2015) Porous nitrogen doped carbon sphere as high performance anode of sodium-ion battery. Carbon 94:888–894
150. Liu P, Hao QL, Xia XF, Lu L, Lei W, Wang X (2015) 3D hierarchical mesoporous flowerlike cobalt oxide nanomaterials: controllable synthesis and electrochemical properties. J Phys Chem 119:8537–8546
151. Du FH, Wang KX, Fu W, Gao PF, Wang JF, Yang J, Chen JS (2013) A graphene-wrapped silver-porous silicon composite with enhanced electrochemical performance for lithium-ion batteries. J Mater Chem A 1(43):13648–13654. https://doi.org/10.1039/c3ta13092d
152. Song JX, Chen SR, Zhou MJ, Xu T, Lv DP et al (2014) Micro-sized silicon-carbon composites composed of carbon-coated sub-10 nm Si primary particles as high-performance anode materials for lithium-ion batteries. J Mater Chem A 2(5):1257–1262. https://doi.org/10.1039/c3ta14100d
153. Wang CD, Chui YS, Ma RG, Wong TL, Ren JG, Wu QH, Chen XF, Zhang WJ (2013) A three-dimensional graphene scaffold supported thin film silicon anode for lithium-ion batteries. J Mater Chem A 1(35):10092–10098. https://doi.org/10.1039/c3ta11740e
154. Shiva K, Jayaramulu K, Rajendra HB, Maji T, Bhattacharyya AJ (2014) In-situ stabilization of tin nanoparticles in porous carbon matrix derived from metal organic framework: high capacity and high rate capability anodes for lithium-ion batteries. Z Anorg Allg Chem 640 (6):1115–1118. https://doi.org/10.1002/zaac.201300621
155. Wang YX, Lim YG, Park MS, Chou SL, Kim JH, Liu HK, Dou SX, Kim YJ (2014) Ultrafine SnO_2 nanoparticle loading onto reduced graphene oxide as anodes for sodium-ion batteries with superior rate and cycling performances. J Mater Chem A 2(2):529–534. https://doi.org/10.1039/c3ta13592f
156. Yin JF, Cao HQ, Zhou ZF, Zhang JX, Qu MZ (2012) SnS_2@reduced graphene oxide nanocomposites as anode materials with high capacity for rechargeable lithium ion batteries. J Mater Chem 22(45):23963–23970. https://doi.org/10.1039/c2jm35137d

157. Liu X, Zhao C, Zhang H, Shen Q (2015) Facile synthesis of porous $ZnMnO_3$ spherulites with a high lithium storage capability. Electrochim Acta 151:56–62. https://doi.org/10.1016/j.electacta.2014.11.020
158. Zhao S, Wang Y, Liu R, Yu Y, Wei S, Yu F, Shen Q (2015) Full-molar-ratio synthesis and enhanced lithium storage properties of $Co_xFe_{1-x}CO_3$ composites with an integrated lattice structure and an atomic-scale synergistic effect. J Mater Chem A 3(33):17181–17189. https://doi.org/10.1039/c5ta03785a
159. Feng F, Kang W, Yu F, Zhang H, Shen Q (2015) High-rate lithium storage capability of cupric-cobaltous oxalate induced by unavoidable crystal water and functionalized graphene oxide. J Power Sources 282:109–117. https://doi.org/10.1016/j.jpowsour.2015.02.043
160. Taillades G, Sarradin J (2004) Silver: high performance anode for thin film lithium ion batteries. J Power Sources 125(2):199–205. https://doi.org/10.1016/j.jpowsour.2003.07.004
161. Shilpa A (2015) Sharma, Enhanced electrochemical performance of electrospun Ag/hollow glassy carbon nanofibers as free-standing Li-ion battery anode. Electrochim Acta 176:1266–1271. https://doi.org/10.1016/j.electacta.2015.07.093
162. Li ZQ, Yin LW (2015) Sandwich-like reduced graphene oxide wrapped MOF-derived $ZnCo_2O_4$-ZnO-C on nickel foam as anodes for high performance lithium ion batteries. J Mater Chem A 3(43):21569–21577. https://doi.org/10.1039/c5ta05733g
163. Li C, Chen T, Xu W, Lou X, Pan L, Chen Q, Hu B (2015) Mesoporous nanostructured Co_3O_4 derived from MOF template: a high-performance anode material for lithium-ion batteries. J Mater Chem A 3(10):5585–5591. https://doi.org/10.1039/c4ta06914e
164. Ma JJ, Wang HJ, Yang X, Chai YQ, Yuan R (2015) Porous carbon-coated $CuCo_2O_4$ concave polyhedrons derived from metal-organic frameworks as anodes for lithium-ion batteries. J Mater Chem A 3(22):12038–12043. https://doi.org/10.1039/c5ta00890e
165. Xie Z, He Z, Feng X, Xu W, Cui X et al (2016) Hierarchical sandwich-like structure of ultrafine n-rich porous carbon nanospheres grown on graphene sheets as superior lithium-ion battery anodes. ACS Appl Mater Interfaces 8(16):10324–10333. https://doi.org/10.1021/acsami.6b01430
166. Su P, Xiao H, Zhao J, Yao Y, Shao Z, Li C, Yang Q (2013) Nitrogen-doped carbon nanotubes derived from Zn-Fe-ZIF nanospheres and their application as efficient oxygen reduction electrocatalysts with in situ generated iron species. Chem Sci 4:2941–2946
167. Zhou G, Wang DW, Li F, Zhang L, Li N, Wu ZS, Wen L, Lu GQ, Cheng HM (2010) Graphene-wrapped Fe_3O_4 anode material with improved reversible capacity and cyclic stability for lithium ion batteries. Chem Mater 22:5306–5313
168. Song Y, Zuo L, Chen S, Wu J, Hou H, Wang L (2015) Porous nano-Si/carbon derived from zeolitic imidazolate frameworks@ nano-Si as anode materials for lithium-ion batteries. Electrochim Acta 173:588–594
169. Tan Y, Zhu K, Li D, Bai F, Wei Y, Zhang P (2014) N-doped graphene/Fe–Fe_3C nano-composite synthesized by a Fe-based metal organic framework and its anode performance in lithium ion batteries. Chem Eng J 258:93–100
170. Liu H, Li W, Shen D, Zhao D, Wang G (2015) Graphitic carbon conformal coating of mesoporous TiO_2 hollow spheres for high-performance lithium ion battery anodes. J Am Chem Soc 137:13161–13166
171. Jiang C, Lin X (2009) Electrochemical synthesis of Fe_3O_4-PB nanoparticles with core-shell structure and its electrocatalytic reduction toward H_2O_2. J Solid State Electrochem 13:1273–1278
172. Chen T, Hu Y, Cheng B, Chen R, Lv H, Ma L, Zhu G, Wang Y, Yan C, Tie Z, Jin Z, Liu J (2016) Multi-yolk-shell copper oxide@ carbon octahedra as high-stability anodes for lithium-ion batteries. Nano Energy 20:305–314
173. Wang L, Zheng Y, Wang X, Chen S, Xu F, Zuo L, Wu J, Sun L, Li Z, Hou H, Song Y (2014) ACS Appl Mater Interfaces 6:7117

174. Wang L, Zheng Y, Zhang Q, Zuo L, Chen S, Chen S, Hou H, Song Y (2014) Template-free synthesis of hierarchical porous carbon derived from low-cost biomass for high-performance supercapacitors. RSC Adv 4:51072–51079
175. Zhou X, Shi J, Liu Y, Su Q, Zhang J, Du G (2014) Microwave-assisted synthesis of hollow CuO–Cu_2O nanosphere/graphene composite as anode for lithium-ion battery. J Alloy Compd 615:390–394
176. Wang X, Yang Z, Sun X, Li X, Wang D, Wang P, He D (2011) NiO nanocone array electrode with high capacity and rate capability for Li-ion batteries. J Mater Chem 21:9988–9990
177. Xia Y, Xiao Z, Dou X, Huang H, Lu X, Yan R, Gan Y, Zhu W, Tu J, Zhang W, Tao X (2013) Green and facile fabrication of hollow porous MnO/C microspheres from microalgaes for lithium-ion batteries. ACS Nano 7:7083–7092
178. Shim HW, Jin YH, Seo SD, Lee SH, Kim DW (2011) Highly reversible lithium storage in bacillus subtilis-directed porous Co_3O_4 nanostructures. ACS Nano 5:443–449
179. Poizot P, Laruelle S, Grugeon S, Dupont L, Tarascon JM (2000) Nano-sized transition-metal oxides as negative-electrode materials for lithium-ion batteries. Nature 407:496–499
180. Wang Y, Li H, He P, Hosono E, Zhou H (2010) Nano active materials for lithium-ion batteries. Nanoscale 2:1294–1305
181. Manthiram A, Murugan AV, Sarkar A, Muraliganth T (2008) Nanostructured electrode materials for electrochemical energy storage and conversion. Energy Environ Sci 1:621–638
182. Cheng F, Liang J, Tao Z, Chen J (2011) Functional materials for rechargeable batteries. Adv Mater 23:1695–1715
183. Zhao SQ, Wei SS, Liu R, Wang YX, Yu Y, Shen Q (2015) Cobalt carbonate dumbbells for high-capacity lithium storage: a slight doping of ascorbic acid and an enhancement in electrochemical performances. J Power Sources 284:154–161
184. Zhang RH, Zhang F, Feng JK, Qian YT (2014) Green and facile synthesis of porous $ZnCO_3$ as a novel anode material for advanced lithium-ion batteries. Mater Lett 118:5–7
185. Reddy MV, Subba Rao GV, Chowdari BVR (2013) Metal oxides and oxysalts as anode materials for Li ion batteries. Chem Rev 113:5364–5457
186. Wu ZS, Ren W, Wen L, Gao L, Zhao J, Chen Z, Zhou G, Li F, Cheng H-M (2010) Graphene anchored with Co_3O_4 nanoparticles as anode of lithium ion batteries with enhanced reversible capacity and cyclic performance. ACS Nano 4(6):3187
187. Cui B, Lin H, Li JB, Li X, Yang J, Tao J (2008) Core–ring structured $NiCo_2O_4$ nanoplatelets: synthesis, characterization, and electrocatalytic applications. Adv Funct Mater 18:1440–1447
188. Wei TY, Chen CH, Chien HC, Lu SY, Hu CC (2010) A cost-effective supercapacitor material of ultrahigh specific capacitances: spinel nickel cobaltite aerogels from an epoxide-driven sol–gel process. Adv Mater 22:347
189. Su Y, Li S, Wu D, Zhang F, Liang H, Gao P, Cheng C, Feng X (2012) Two-dimensional carbon-coated graphene/metal oxide hybrids for enhanced lithium storage. ACS Nano 6:8349–8356
190. Huang G, Xu S, Lu S, Li L, Sun H (2014) Micro-/nanostructured Co_3O_4 anode with enhanced rate capability for lithium-ion batteries. ACS Appl Mater Interfaces 6:7236–7243
191. Su H, Xu YF, Feng SC, Wu ZG, Sun XP, Shen CH et al (2015) Hierarchical Mn_2O_3 hollow microspheres as anode material of lithium ion battery and its conversion reaction mechanism investigated by XANES. ACS Appl Mater Interfaces 7:8488–8494
192. Köse H, Karaal Ş, Aydın AO, Akbulut H (2015) A facile synthesis of zinc oxide/multiwalled carbon nanotube nanocomposite lithium ion battery anodes by sol–gel method. J Power Sources 295:235–245
193. Zhou X, Wan LJ, Guo YG (2013) Binding SnO_2 nanocrystals in nitrogen-doped graphene sheets as anode materials for lithium-ion batteries. Adv Mater 25:2152–2157
194. Yan B, Li M, Li X, Bai Z, Dong L, Li D (2015) Electrochemical impedance spectroscopy illuminating performance evolution of porous core-shell structured nickel/nickel oxide anode materials. Electrochim Acta 164:55–61

195. Wang M, Yang H, Zhou X, Shi W, Zhou Z, Cheng P (2015) Rational design of SnO_2@C nanocomposites for lithium ion batteries by utilizing adsorption properties of MOFs. Chem Commun (Camb) 52:717–720
196. Zhong Y, Yang M, Zhou X, Zhou Z (2015) Structural design for anodes of lithium-ion batteries: emerging horizons from materials to electrodes. Mater Horiz 2:553–566
197. Yao J, Shen X, Wang B, Liu H, Wang G (2009) In situ chemical synthesis of SnO_2–graphene nanocomposite as anode materials for lithium-ion batteries. Electrochem Commun 11:1849–1852
198. Wi S, Woo H, Lee S, Kang J, Kim J, An S et al (2015) Reduced graphene oxide/carbon double-coated 3-D porous ZnO aggregates as high-performance Li-ion anode materials. Nanoscale Res Lett 10:204
199. Vinayan BP, Nagar R, Raman V, Rajalakshmi N, Dhathathreyan KS, Ramaprabhu S (2012) Synthesis of graphene-multiwalled carbon nanotubes hybrid nanostructure by strengthened electrostatic interaction and its lithium ion battery application. J Mater Chem 22:9949
200. Fang S, Shen L, Zheng H, Zhang X (2015) Ge–graphene–carbon nanotube composite anode for high performance lithium-ion batteries. J Mater Chem A 3:1498–1503
201. Jiang B, Han C, Li B, He Y, Lin Z (2016) ACS Nano 10:2728
202. Wu J, Song Y, Zhou R, Chen S, Zuo L, Hou H, Wang L (2015) J Mater Chem A 3:7793
203. Wang X, Huang L, Zhao Y (2016) Nanoscale Res Lett 11:37
204. Yao X, Kong J, Zhou D, Zhao C, Zhou R, Lu X (2014) Carbon 79:493
205. Bresser D, Paillard E, Kloepsch R, Krueger S, Fiedler M, Schmitz R, Baither D, Winter M, Passerini S (2013) Adv Energy Mater 3:513
206. Mueller F, Bresser D, Paillard E, Winter M, Passerini S (2013) J Power Sources 236:87
207. Han Y, Qi P, Li S, Feng X, Zhou J, Li H, Su S, Li X, Wang B (2014) Chem Commun 50:8057
208. Chen K, Song S, Xue D (2015) J Mater Chem A 3:2441
209. Liu J, Xia H, Lu L, Xue D (2010) J Mater Chem 20:1506
210. Wu J, Xue D (2011) Nanosci Nanotech Lett 3:371
211. Liu J, Xue D (2010) Electrochim Acta 56:243
212. Liu J, Liu F, Gao K, Wua J, Xue D (2009) J Mater Chem 19:6073
213. Yin YX, Xin S, Guo YG, Wan LJ (2013) Angew Chem Int Ed 52(50):13186–13200
214. Liu J, Zhang JG, Yang ZG, Lemmon JP, Imhoff C, Graff GL, Li LY, Hu JZ, Wang CM, Xiao J, Xia GD, Viswanathan VV, Baskaran S, Sprenkle V, Li XL, Shao YY, Schwenzer B (2013) Adv Funct Mater 23(8):929–946
215. Bhattab MD, Dwyer CÓ (2015) Phys Chem Chem Phys 17(7):4799–4844
216. Goodenough JB, Park KS (2013) J Am Chem Soc 135(4):1167–1176
217. Chen ZH, Belharouak I, Sun YK, Amine K (2013) Adv Funct Mater 23(8):959–969
218. Li HB, Zhou QY, Gao YT (2015) Nano Res 8(3):900–906
219. Peng YT, Lo CT (2015) J Solid State Electrochem 19(11):3401–3410
220. Yu CY, Bai Y, Yan D, Li XG, Zhang WF (2014) J Solid State Electrochem 18(7):1933–1940
221. Li XD, Li W, Li MC, Cui P, Chen DH, Gengenbach T, Chu LH, Liu HY, Song GS (2015) J Mater Chem A 3(6):2762–2769
222. Wang ZY, Sha JW, Liu EZ, He CN, Shi CS, Li JJ, Zhao NQ (2014) J Mater Chem A 2(23):8893–8901
223. Novoselov KS, Geim AK, Morozov SV Jiang D, Zhang Y, Dubonos SV, Grigorieva IV, Firsov AA (2004) Science 306(5696):666–669
224. Geim AK, Novoselov KS (2007) Nat Mater 6(3):183–191
225. Zhu YW, Murali S, Cai WW, Li XS, Suk JW, Potts JR, Ruoff RS (2010) Adv Mater 22(35):3906–3924
226. Loh KP, Bao QL, Ang PK, Yang JX (2010) J Mater Chem 20(12):2277–2289
227. Zheng CC, He CH, Zhang HY, Wang WG, Lei XL (2015) Ionics 21(1):51–58
228. Yang SL, Cao CY, Huang PP, Peng L, Sun YB, Wei F, Song WG (2015) J Mater Chem A 3(16):8701–8705

229. Fu XX, Shi L, Fan CY, Yu SQ, Qian GD, Zhiyu Wang ZY (2015) Electrochim Acta 190:25–32
230. Cabana J, Monconduit L, Larcher D, Palacin MR (2010) Beyond intercalation-based Li-ion batteries: the state of the art and challenges of electrode materials reacting through conversion reactions. Adv Mater 22(35):E170
231. He YS, Bai DW, Yang X, Chen J, Liao XZ, Ma ZF (2010) A $Co(OH)_2$−graphene nanosheets composite as a high performance anode material for rechargeable lithium batteries. Electrochem Commun 12(4):570
232. Zhou Y, Yan D, Xu H, Feng J, Jiang X, Yue J, Yang J, Qian Y (2015) Hollow nanospheres of mesoporous Co_9S_8 as a high-capacity and long-life anode for advanced lithium ion batteries. Nano Energy 12:528
233. Das B, Reddy MV, Rao GVS, Chowdari BVR (2012) Synthesis of porous-CoN nanoparticles and their application as a high capacity anode for lithium-ion batteries. J Mater Chem 22(34):17505
234. Li J, Xiong S, Liu Y, Ju Z, Qian Y (2013) High electrochemical performance of monodisperse $NiCo_2O_4$ mesoporous microspheres as an anode material for Li-ion batteries. ACS Appl Mater Interfaces 5(3):981
235. Xie J, Cao GS, Zhao XB (2005) $CoSb_3$-graphite composite anode material for lithium ion batteries. Rare Met 24(1):42
236. Yan N, Hu L, Li Y, Wang Y, Zhong H, Hu X, Kong X, Chen Q (2012) Co_3O_4 nanocages for high-performance anode material in lithium-ion batteries. J Phys Chem C 116(12):7227
237. Wang Q, Jiao L, Han Y, Du H, Peng W, Huan Q, Song D, Si Y, Wang Y, Yuan H (2011) CoS_2 hollow spheres: fabrication and their application in lithium-ion batteries. J Phys Chem C 115(16):8300
238. Wang Z, Wang Z, Liu W, Xiao W, Lou XW (2013) Amorphous $CoSnO_3$@C nanoboxes with superior lithium storage capability. Energy Environ Sci 6(1):87
239. Chen X, Cheng M, Chen D, Wang R (2016) Shape-controlled synthesis of Co_2P nanostructures and their application in supercapacitors. ACS Appl Mater Interfaces 8 (6):3892
240. Wu J, Liu WW, Wu YX, Wei TC, Geng D, Mei J, Liu H, Lau WM, Liu LM (2016) Three-dimensional hierarchical interwoven nitrogen-doped carbon nanotubes/Co_xNi_{1-x}-layered double hydroxides ultrathin nanosheets for high-performance supercapacitors. Electrochim Acta 203:21
241. Su X, Xu Y, Liu J, Wang R (2015) Controlled synthesis of $Ni_{0.25}Co_{0.75}(OH)_2$ nanoplates and their electrochemical properties. Cryst Eng Commun 17(26):4859
242. Lu A, Zhang X, Chen Y, Xie Q, Qi Q, Ma Y, Peng DL (2015) Synthesis of Co_2P/graphene nanocomposites and their enhanced properties as anode materials for lithium ion batteries. J Power Sources 295:329
243. Xie J, Liu S, Cao G, Zhu T, Zhao X (2013) Self-assembly of CoS_2/graphene nanoarchitecture by a facile one-pot route and its improved electrochemical Li-storage properties. Nano Energy 2(1):49
244. Li Z, Xue H, Wang J, Tang Y, Lee CS, Yang S (2015) Reduced graphene oxide/marcasite-type cobalt selenide nanocrystals as an anode for lithium-ion batteries with excellent cyclic performance. ChemElectroChem 2(11):1682
245. Yang T, Zhang H, Luo Y, Mei L, Guo D, Li Q, Wang T (2015) Enhanced electrochemical performance of $CoMoO_4$ nanorods/reduced graphene oxide as anode material for lithium-ion batteries. Electrochim Acta 158:327
246. Zou R, Zhang Z, Yuen MF, Sun M, Hu J, Lee CS, Zhang W (2015) Three-dimensional-networked $NiCo_2S_4$ nanosheet array/carbon cloth anodes for high-performance lithium-ion batteries. NPG Asia Mater 7(6):e195
247. Wu J, Guo P, Mi R, Liu X, Zhang H, Mei J, Liu H, Lau WM, Liu LM (2015) Ultrathin $NiCo_2O_4$ nanosheets grown on three-dimensional interwoven nitrogen-doped carbon nanotubes as binder-free electrodes for high-performance supercapacitors. J Mater Chem A 3(29):15331

248. Wang JG, Jin D, Zhou R, Shen C, Xie K, Wei B (2016) One-step synthesis of $NiCo_2S_4$ ultrathin nanosheets on conductive substrates as advanced electrodes for high-efficient energy storage. J Power Sources 306:100
249. Huang XK, Cui SM, Chang JB, Hallac PB, Fell CR, Luo YT, Metz B, Jiang JW, Hurley PT, Chen JH (2015) A hierarchical tin/carbon composite as an anode for lithium-ion batteries with a long cycle life. Angew Chem Int Edit 54:1490–1493
250. Xie J, Zhang J, Li S, Grote F, Zhang X, Zhang H, Wang R, Lei Y, Pan B, Xie Y (2013) Controllable disorder engineering in oxygen-incorporated MoS_2 ultrathin nanosheets for efficient hydrogen evolution. J Am Chem Soc 135:17881–17888
251. Liao L, Zhu J, Bian X, Zhu L, Scanlon MD, Girault HH, Liu B (2013) MoS_2 formed on mesoporous graphene as a highly active catalyst for hydrogen evolution. Adv Funct Mater 23:5326–5333
252. Hou HS, Tang XN, Guo MQ, Shi YQ, Dou P, Xu XH (2014) Facile preparation of Sn hollow nanospheres anodes for lithium-ion batteries by galvanic replacement. Mater Lett 128:408–411
253. Li QY, Pan QC, Yang GH, Lin XL, Yan ZX, Wang HQ, Huang YG (2015) Synthesis of Sn/MoS_2/C composites as high-performance anodes for lithium-ion batteries. J Chem Mater A 3:20375–20381
254. Tarascon JM, Armand M (2001) Issues and challenges facing rechargeable lithium batteries. Nature 414:359–367
255. Manthiram A (2011) Materials challenges and opportunities of lithium ion batteries. J Phys Chem Lett 2:176–184
256. Zhu Z, Wang S, Du J, Jin Q, Zhang T, Cheng F, Chen J (2014) Ultrasmall Sn nanoparticles embedded in nitrogen-doped porous carbon as high-performance anode for lithium-ion batteries. Nano Lett 14:153–157
257. Dai R, Wang Y, Da P, Wu H, Xu M, Zheng G (2014) Indirect growth of mesoporous Bi@C core-shell nanowires for enhanced lithium-ion storage. Nanoscale 6:13236–13241
258. Shao Y, Gu M, Li X, Nie Z, Zuo P, Li G, Liu T, Xiao J, Cheng Y, Wang C (2014) Highly reversible Mg insertion in nanostructured Bi for Mg ion batteries. Nano Lett 14:255–260
259. Su D, Dou SX, Wang GX (2015) Bismuth: a new anode for the Na-ion battery. Nano Energy 12:88–95
260. Yang FH, Yu F, Zhang ZA, Zhang K, Lai YQ, Li J (2016) Bismuth nanoparticles embedded in carbon spheres as anode materials for sodium/lithium-ion batteries. Chemistry 22:2333–2338
261. Crosnier O, Devaux X, Brousse T, Fragnaud P, Schleich DM (2001) Influence of particle size and matrix in "metal" anodes for Li-ion cells. J Power Sources 97:188–190
262. Beck FR, Epur R, Hong D, Manivannan A, Kumta PN (2014) Microwave derived facile approach to Sn/graphene composite anodes for lithium-ion batteries. Electrochim Acta 127:299–306
263. Du YJ, Zhu GN, Wang K, Wang YG, Wang CX, Xia YY (2013) Si/graphene composite prepared by magnesium thermal reduction of SiO_2 as anode material for lithium-ion batteries. Electrochem Commun 36:107–110
264. Lian PC, Zhu XF, Liang SZ, Li Z, Yang WS, Wang HH (2011) High reversible capacity of SnO_2/graphene nanocomposite as an anode material for lithium-ion batteries. Electrochim Acta 56:4532–4539
265. Liu X, Du YC, Hu LY, Zhou XS, Li YF, Dai ZH, Bao JC (2015) Understanding the effect of different polymeric surfactants on enhancing the silicon/reduced graphene oxide anode performance. J Phys Chem C 119:5848–5854
266. Wang HT, He DW, Wang YS, Wu HP, Wang JG (2012) SnO_2/graphene nanocomposite as an enhanced anode material for lithium ion batteries. Adv Mater Res 465:108–111
267. Fu CJ, Li S, Wang Q (2015) High reversible capacity of nitrogen-doped graphene as an anode material for lithium-ion batteries. Adv Mater Res 1070–1072:459–464

268. Li XF, Geng DS, Zhang Y, Meng XB, Li RY, Sun XL (2011) Superior cycle stability of nitrogen-doped graphene nanosheets as anodes for lithium ion batteries. Electrochem Commun 13:822–825
269. Liu XW, Wu Y, Yang ZZ, Pan FS, Zhong XW, Wang JQ, Gu L, Yu Y (2015) Nitrogen-doped 3d macroporous graphene frameworks as anode for high performance lithium-ion batteries. J Power Sources 293:799–805
270. Xu Y, Zhu XS, Zhou XS, Liu X, Liu YX, Dai ZH, Bao JC (2014) Ge nanoparticles encapsulated in nitrogen-doped reduced graphene oxide as an advanced anode material for lithium-ion batteries. J Phys Chem C 118:28502–28508
271. Park SK, Jin AH, Yu SH, Ha J, Jang B, Bong SY, Woo S, Sung YE, Piao YZ (2013) In situ hydrothermal synthesis of Mn_3O_4 nanoparticles on nitrogen-doped graphene as high-performance anode materials for lithium ion batteries. Electrochim Acta 120:452–459
272. Wu ZS, Ren WC, Xu L, Li F, Cheng HM (2011) Doped graphene sheets as anode materials with superhigh rate and large capacity for lithium ion batteries. ACS Nano 5:5463–5471
273. Cai DD, Wang SQ, Lian PC, Zhu XF, Li DD, Yang WS, Wang HH (2013) Superhigh capacity and rate capability of high-level nitrogen-doped graphene sheets as anode materials for lithium-ion batteries. Electrochim Acta 90:492–497
274. Li T, Li XH, Wang ZX, Guo HJ, Li Y (2015) A novel $NiCo_2O_4$ anode morphology for lithium-ion batteries. J Mater Chem A 3:11970–11975
275. Shen L, Yu L, Yu XY, Zhang X, Lou XW (2015) Self-templated formation of uniform $NiCo_2O_4$ hollow spheres with complex interior structures for lithium-ion batteries and supercapacitors. Angew Chem Int Ed 54(6):1868–1874
276. Shen L, Che Q, Li HS, Zhang XG (2014) Mesoporous $NiCo_2O_4$ nanowire arrays grown on carbon textiles as binder-free flexible electrodes for energy storage. Adv Funct Mater 24(18):2630–2637
277. Chen YJ, Zhu J, Qu BH, Graphene ZX (2014) Improving lithium-ion battery performance by construction of $NiCo_2O_4$/graphene hybrid nanosheet arrays. Nano Energy 3:88–94
278. Ju ZC, Ma GY, Zhao YL, Xing Z, Qiang YH, Qian YT (2015) A facile method for synthesis of porous $NiCo_2O_4$ nanorods as a high-performance anode material for Li-ion batteries. Part Part Syst Charact 32(11):1012–1019
279. Umeshbabu E, Rajeshkhanna G, Rao GR (2014) Urchin and sheaf-like $NiCo_2O_4$ nanostructures: synthesis and electrochemical energy storage application. Int J Hydrog Energy 39(28):15627–15638
280. Yu XY, Yao XZ, Luo T, Jia Y, Liu JH, Huang XJ (2014) Facile synthesis of urchin-like $NiCo_2O_4$ hollow microspheres with enhanced electrochemical properties in energy and environmentally related applications. ACS Appl Mater Interfaces 6(5):3689–3695
281. Huang X, Chen J, Yu H, Peng S, Cai R, Yan Q, Hng HH (2013) Immobilization of plant polyphenol stabilized-Sn nanoparticles onto carbon nanotubes and their application in rechargeable lithium ion batteries. RSC Adv 3:5310–5313
282. Mukherjee R, Krishnan R, Lu TM, Koratkar N (2012) Nanostructured electrodes for high-power lithium ion batteries. Nano Energy 1:518–533
283. Zhong Y, Zhang Y, Cai M, Balogh MP, Li R, Sun X (2013) Core-shell heterostructures of SnM (M = (Fe, Ni, and Cr) or Cu) alloy nanowires@CNTs on metallic substrates. Appl Surf Sci 270:722–727
284. Li X, Zhong Y, Cai M, Balogh MP, Wang D, Zhang Y, Li R, Sun X (2013) Tin-alloy heterostructures encapsulated in amorphous carbon nanotubes as hybrid anodes in rechargeable lithium ion batteries. Electrochim Acta 89:387–393
285. Choi NS, Lee YM, Park JH, Park JK (2003) Interfacial enhancement between lithium electrode and polymer electrolytes. J Power Sources 119:610–616
286. Peled E, Tow DB, Merson A, Gladkich A, Burstein L, Golodnitsky D (2001) Composition, depth profiles and lateral distribution of materials in the SEI built on HOPG-TOF SIMS and XPS studies. J Power Sources 98:52–57. https://doi.org/10.1016/S0378-7753(01)00505-5

287. Zhuang GV, Xu K, Jow TR, Ross PN (2004) Study of SEI layer formed on graphite anodes in PC/LiBOB electrolyte using IR spectroscopy. Electrochem Solid State Lett 7:A224. https://doi.org/10.1149/1.1756855
288. Eshkenazi V, Peled E, Burstein L, Golodnitsky D (2004) XPS analysis of the SEI formed on carbonaceous materials. Solid State Ion 170:83–91. https://doi.org/10.1016/S0167-2738(03)00107-3
289. Buqa H, Würsig A, Vetter J, Spahr ME, Krumeich F, Novák P (2006) SEI film formation on highly crystalline graphitic materials in lithium-ion batteries. J Power Sources 153(2):385–390. https://doi.org/10.1016/j.jpowsour.2005.05.036
290. Bryngelsson H, Stjerndahl M, Gustafsson T, Edström K (2007) How dynamic is the SEI? J Power Sources 174:970–975. https://doi.org/10.1016/j.jpowsour.2007.06.050
291. Leroy S, Blanchard F, Dedryvère R, Martinez H, Carré B, Lemordant D et al (2005) Surface film formation on a graphite electrode in Li-ion batteries: AFM and XPS study. Surf Interface Anal 37:773–781. https://doi.org/10.1002/sia.2072
292. Xiao A, Yang L, Lucht BL, Kang S-H, Abraham DP (2009) Examining the solid electrolyte interphase on binder-free graphite electrodes. J Electrochem Soc 156:A318–A327. https://doi.org/10.1149/1.3078020
293. Hirasawa KA, Sato T, Asahina H, Yamaguchi S, Mori S (1997) In situ electrochemical atomic force microscope study on graphite electrodes. J Electrochem Soc 144:L81–L84. https://doi.org/10.1149/1.1837560
294. Goriparti S, Miele E, De Angelis F, Di Fabrizio E, Proietti Zaccaria R, Capiglia C (2014) Review on recent progress of nanostructured anode materials for Li-ion batteries. J Power Sources 257:421–443. https://doi.org/10.1016/j.jpowsour.2013.11.103
295. He Y-B, Li B, Liu M, Zhang C, Lv W, Yang C et al (2012) Gassing in Li(4)Ti(5)O(12)-based batteries and its remedy. Nat Sci Rep 2:913. https://doi.org/10.1038/srep00913
296. Zhou Y, Guo H, Yong Y, Wang Z, Li X, Zhou R (2017) Introducing reduced graphene oxide to improve the electrochemical performance of silicon-based materials encapsulated by carbonized polydopamine layer for lithium ion batteries. Mater Lett 195:164–167
297. Yang J, Wang BF, Wang K, Liu Y, Xie JY, Wen ZS (2003) Si/C composites for high capacity lithium storage materials. Electrochem Solid State Lett 6:A154–A156
298. Lee HY, Lee SM (2004) Carbon-coated nano-Si dispersed oxides/graphite composites as anode material for lithium ion batteries. Electrochem Commun 6:465–469
299. Wang J, Liu Z, Yan G, Li H, Peng W, Li X, Song L, Shih K (2016) Improving the electrochemical performance of lithium vanadium fluorophosphate cathode material: focus on interfacial stability. J Power Sources 329:553–557
300. Liu YJ, Lv J, Fei Y, Huo XD, Zhu YZ (2013) Improvement of storage performance of $LiMn_2O_4$/graphite battery with AlF_3-coated $LiMn_2O_4$. Ionics 19:1241–1246
301. Wang RH, Li XH, Wang ZX, Guo HJ, Hou T, Yan GC, Huang B (2015) Lithium carbonate as an electrolyte additive for enhancing the high-temperature performance of lithium manganese oxide spinel cathode. J Alloys Compd 618:349–356
302. Wang RH, Li XH, Wang ZX, Guo HJ, Wang JX, Hou T (2015) Impacts of vinyl ethylene carbonate and vinylene carbonate on lithium manganese oxide spinel cathode at elevated temperature. J Alloys Compd 632:435–444
303. Xu C, Lindgren F, Philippe B, Gorgoi M, Bjorefors F, Edstrom K, Gustafsson T (2015) Improved performance of the silicon anode for Li-ion batteries: understanding the surface modification mechanism of fluoroethylene carbonate as an effective electrolyte additive. Chem Mater 27:2591–2599
304. Nie M, Abraham DP, Chen Y, Bose A, Lucht BL (2013) Silicon solid electrolyte interphase (SEI) of lithium ion battery characterized by microscopy and spectroscopy. J Phys Chem C 117:13403–13412
305. Zhao M, Zuo X, Ma X, Xiao X, Yu L, Nan J (2016) Diphenyl disulfide as a new bifunctional film-forming additive for high-voltage $LiCoO_2$/graphite battery charged to 4.4 V. J Power Sources 323:29–36. https://doi.org/10.1016/j.jpowsour.2016.05.052

306. Wagner R, Brox S, Kasnatscheew J, Gallus DR, Amereller M, Cekic-Laskovic I, Winter M (2014) Vinyl sulfones as SEI-forming additives in propylene carbonate based electrolytes for lithium-ion batteries. Electrochem Commun 40:80–83. https://doi.org/10.1016/j.elecom.2014.01.004
307. Wang R, Li X, Wang Z, Zhang H (2017) Electrochemical analysis graphite/electrolyte interface in lithium-ion batteries: p-Toluenesulfonyl isocyanate as electrolyte additive. Nano Energy 34:131–140. https://doi.org/10.1016/j.nanoen.2017.02.037
308. Jurng S et al (2016) Low-temperature characteristics and film-forming mechanism of elemental sulfur additive on graphite negative electrode. J Electrochem Soc 163:A223–A228
309. Abe K, Yoshitake H, Kitakura T, Hattori T, Wang H, Yoshio M (2004) Additives-containing functional electrolytes for suppressing electrolyte decomposition in lithium-ion batteries. Electrochim Acta 49(26):4613–4622. https://doi.org/10.1016/j.electacta.2004.05.016
310. Dimov N, Fukuda K, Umeno T, Kugino S, Yoshio M (2003) Characterization of carbon-coated silicon: structural evolution and possible limitations. J Power Sources 114(1):88–95. https://doi.org/10.1016/S0378-7753(02)00533-5
311. Zhang XW, Patil PK, Wang C, Appleby AJ, Little FE, Cocke DL (2004) Electrochemical performance of lithium ion battery, nano-silicon-based, disordered carbon composite anodes with different microstructures. J Power Sources 125(2):206–213. https://doi.org/10.1016/j.jpowsour.2003.07.019
312. Chu YQ, Fu ZW, Qin QZ (2004) Cobalt ferrite thin films as anode material for lithium ion batteries. Electrochim Acta 49(27):4915–4921. https://doi.org/10.1016/j.electacta.2004.06.012
313. Choi WC, Byun D, Lee JK, Cho B (2004) Electrochemical characteristics of silver- and nickel-coated synthetic graphite prepared by a gas suspension spray coating method for the anode of lithium secondary batteries. Electrochim Acta 50(2–3):523–529. https://doi.org/10.1016/j.electacta.2003.12.070
314. Park C-M, Kim J-H, Kim H, Sohn H-J (2010) Li-alloy based anode materials for Li secondary batteries. Chem Soc Rev 39:3115–3141
315. Chen JS, Lou XWD (2013) SnO_2-based nanomaterials: synthesis and application in lithium-ion batteries. Small 9:1877–1893
316. Wu HB, Chen JS, Hng HH, Lou XWD (2012) Nanostructured metal oxide-based materials as advanced anodes for lithium-ion batteries. Nanoscale 4:2526–2542
317. Ding S, Luan D, Boey FYC, Chen JS, Lou XW (2011) SnO_2 nanosheets grown on graphene sheets with enhanced lithium storage properties. Chem Commun 47:7155–7157
318. Chen W, Ghosh D, Chen S (2008) Large-scale electrochemical synthesis of SnO_2 nanoparticles. J Mater Sci 43:5291–5299
319. Yanson AI, Rodriguez P, Garcia-Araez N, Mom RV, Tichelaar FD, Koper MTM (2011) Cathodic corrosion: a quick, clean, and versatile method for the synthesis of metallic nanoparticles. Angew Chem Int Ed 50:6346–6350
320. Leontyev I, Kuriganova A, Kudryavtsev Yu, Dkhil B, Smirnova N (2012) New life of a forgotten method: electrochemical route toward highly efficient Pt/C catalysts for low-temperature fuel cells. Appl Catal A 431:120–125
321. Smirnova NV, Kuriganova AB, Leontyeva DV, Leontyev IN, Mikheikin AS (2013) Structural and electrocatalytic properties of Pt/C and Pt-Ni/C catalysts prepared by electrochemical dispersion. Kinet Catal 54:255–262
322. Leontyeva DV, Leontyev IN, Avramenko MV, Yuzyuk YuI, Kukushkina YuA, Smirnova NV (2013) Electrochemical dispersion as a simple and effective technique toward preparation of NiO based nanocomposite for supercapacitor application. Electrochim Acta 114:356–362
323. Smart MC, Ratnakumar BV, Surampudi S (1999) J Electrochem Soc 146:486
324. Huang CK, Sakamoto JS, Wolfenstine J, Surampudi S (2000) J Electrochem Soc 147:2893
325. Contestabile M, Morselli M, Paraventi R, Neat RJ (2003) J Power Sources 119–121:943
326. Zhang SS (2006) J Power Sources 162:1379

327. Herreyre S, Huchet O, Barusseau S, Perton F, Bodet JM, Biensan P (2001) J Power Sources 97–98:576
328. Smart MC, Ratnakumar BV, Ryan-Mowrey VS, Surampudi S, Prakash GKS, Hu J, Cheung I (2003) J Power Sources 119–121:359
329. Smith KA, Smart MC, Prakash GKS, Ratnakumar BV (2008) ECS Trans 11:91
330. Smart MC, Whitacre JF, Ratnakumar BV, Amine K (2007) J Power Sources 168:501
331. Aurbach D, Markovsky B, Weissman I, Levi E, Ein-Eli Y (1999) Electrochim Acta 45:67
332. Aurbach D, Zaban A, Gofer Y, Ely YE, Weissman I, Chusid O, Abramson O (1995) J Power Sources 54:76
333. Aurbach D, Zaban A, Ein-Eli Y, Weissman I, Chusid B, Markovsky M, Levi E, Levi A, Schechter E, Granot Y (1997) J Power Sources 68:91
334. Peled E, Golodnitsky D, Menachem C, BarTow D (1998) J Electrochem Soc 145:3482
335. Aurbach D, Gamolsky K, Markovsky B, Gofer Y, Schmidt M, Heider U (2002) Electrochim Acta 47:1423
336. Sasaki T, Abe T, Iriyama Y, Inaba M, Ogumi Z (2005) J Electrochem Soc 152:A2046
337. Winter BM, Besenhard JO, Spahr ME, Novak P (1998) Insertion electrode materials for rechargeable lithium batteries. Adv Mater 10:725–763
338. Chang WS, Park CM, Kim JH, Kim YU, Jeong G, Sohn HJ (2012) Quartz (SiO_2): a new energy storage anode material for Li-ion batteries. Energy Environ Sci 5(5):6895–6899
339. Doh CH, Veluchamy A, Lee DJ, Lee JH, Jin BS, Moon SI, Park CW, Kim DW (2010) Comparative study on performances of composite anodes of SiO, Si and Graphite for lithium rechargeable batteries. Bull Korean Chem Soc 31(5):1257–1261
340. Seong IW, Kim KT, Yoon WY (2009) Electrochemical behavior of a lithium-pre-doped carbon-coated silicon monoxide anode cell. J Power Sources 189(1):511–514
341. Yan N, Wang F, Zhong H, Li Y, Wang Y, Hu L, Chen Q (2013) Hollow porous SiO_2 nanocubes towards high-performance anodes for lithium-ion batteries. Sci Rep 3:1568–1574
342. Guo B, Shu J, Wang Z, Yang H, Shi L, Liu Y, Chen L (2008) Electrochemical reduction of nano-SiO_2 in hard carbon as anode material for lithium ion batteries. Electrochem Commun 10:1876–1878
343. Gao P, Yang J (2011) Si-based composite anode materials for Li-ion batteries. Prog Chem 23(0203):264–274
344. Bruce PG, Scrosati B, Tarascon JM (2008) Nanomaterials for rechargeable lithium batteries. Angew Chem Int Ed 47(16):2930–2946
345. Szczech JR, Jin S (2011) Energy Environ Sci 4:56
346. Li H, Zhou H (2012) Enhancing the performances of Li-ion batteries by carbon-coating: present and future. Chem Commun 48(9):1201–1217
347. Guo S, Li H, Bai H, Tao Z, Chen J (2014) Ti/Si/Ti sandwich-like thin film as the anode of lithium-ion batteries. J Power Sources 248:1141–1148
348. Nishide H, Oyaizu K (2008) Toward flexible batteries. Science (New York, NY) 319(5864):737–738
349. Rogers JA, Someya T, Huang Y (2010) Materials and mechanics for stretchable electronics. Science (New York, NY) 327(5973):1603–1607
350. Naoi K, Morita M (2008) Advanced polymers as active materials and electrolytes for electrochemical capacitors and hybrid capacitor systems. Electrochem Soc Interface 17(1):44–48
351. Snook GA, Kao P, Best AS (2011) Conducting-polymer-based supercapacitor devices and electrodes. J Power Sources 196(1):1–12
352. Laforgue A, Robitaille L (2010) Deposition of ultrathin coatings of polypyrrole and poly (3,4-ethylenedioxythiophene) onto electrospun nanofibers using a vapor-phase polymerization method. Chem Mater 22(8):2474–2480
353. Nyström G, Razaq A, Strømme M, Nyholm L, Mihranyan A (2009) Ultrafast all-polymer paper-based batteries. Nano Lett 9(10):3635–3639

354. Tu J, Hu L, Wang W, Hou J, Zhu H, Jiao S (2013) In-situ synthesis of silicon/polyaniline core/shell and its electrochemical performance for lithium-ion batteries. J Electrochem Soc 160(10):A1916–A1921
355. Winter M, Besenhard JO (1999) Electrochemical lithiation of tin and tin-based intermetallics and composites. Electrochim Acta 45:31–50
356. Li CM, Zhang RY, Li WS, Zhao LZ, Hu SJ, Rao MM, Xu JX (2007) Ultrasonic-electrodeposited Sn-CNTs composite used as anode material for lithium ion battery. Trans Nonferr Met Soc China 17:s934–s936
357. Zhang L, Xiang H, Li Z, Wang H (2012) Porous $Li_3V_2(PO_4)_3$/C cathode with extremely high-rate capacity prepared by a sol–gel-combustion method for fast charging and discharging. J Power Sources 203:121–125
358. Lian P, Zhu X, Xiang H, Li Z, Yang W, Wang H (2010) Enhanced cycling performance of Fe_3O_4–graphene nanocomposite as an anode material for lithium-ion batteries. Electrochim Acta 56:834–840
359. Wu D, Cheng Y (2012) Enhanced high-rate performance of sub-micro $Li_4Ti_{4.95}Zn_{0.05}O_{12}$ as anode material for lithium-ion batteries. Ionics 19:395–399
360. Wang L, Yang C, Dou S, Wang S, Zhang J, Gao X, Ma J, Yu Y (2016) Nitrogen-doped hierarchically porous carbon networks: synthesis and applications in lithium-ion battery, sodium-ion battery and zinc-air battery. Electrochim Acta 219:592–603
361. Wu Y, Wen Z, Li J (2011) Hierarchical carbon-coated $LiFePO_4$ nanoplate microspheres with high electrochemical performance for Li-ion batteries. Adv Mater 23:1126–1129
362. Wu Y, Wen Z, Feng H, Li J (2012) Hollow porous $LiMn_2O_4$ microcubes as rechargeable lithium battery cathode with high electrochemical performance. Small 8:858–862
363. Wang H, Liang Q, Wang W, An Y, Li J, Guo L (2011) Preparation of flower-like SnO_2 nanostructures and their applications in gas-sensing and lithium storage. Cryst Growth Des 11:2942–2947
364. Zhou W, Lin L, Wang W, Zhang L, Wu Q, Li J, Guo L (2011) Hierarchial mesoporous hematite with "electron-transport channels" and its improved performances in photocatalysis and lithium ion batteries. J Phys Chem C 115:7126–7133
365. Cao K, Jiao L, Xu H, Liu H, Kang H, Zhao Y, Liu Y, Wang Y, Yuan H (2016) Reconstruction of mini-hollow polyhedron Mn_2O_3 derived from MOFs as a high-performance lithium anode material. Adv Sci (Weinh) 3:1500185
366. Cao K, Jiao L, Liu H, Liu Y, Wang Y, Guo Z, Yuan H (2015) 3D hierarchical porous α-Fe_2O_3 nanosheets for high-performance lithium-ion batteries. Adv Energy Mater 5:1401421
367. Zhang L, Zhang Y, Yuan X (2014) Enhanced high-temperature performances of $LiMn_2O_4$ cathode by $LiMnPO_4$ coating. Ionics 21:37–41
368. Li X, Yang R, Cheng B, Hao Q, Xu H, Yang J, Qian Y (2012) Enhanced electrochemical properties of nano-Li_3PO_4 coated on the $LiMn_2O_4$ cathode material for lithium ion battery at 55 C. Mater Lett 66:168–171
369. Yuan G, Bai J, Doan TNL, Chen P (2014) Synthesis and electrochemical investigation of nanosized $LiMn_2O_4$ as cathode material for rechargeable hybrid aqueous batteries. Mater Lett 137:311–314
370. Tang W, Liu LL, Tian S, Li L, Li LL, Yue YB, Bai Y, Wu YP, Zhu K, Holze R (2011) $LiMn_2O_4$ nanorods as a super-fast cathode material for aqueous rechargeable lithium batteries. Electrochem Commun 13:1159–1162
371. Tang D, Yi R, Gordin ML, Melnyk M, Dai F, Chen S, Song J, Wang D (2014) Titanium nitride coating to enhance the performance of silicon nanoparticles as a lithium-ion battery anode. J Mater Chem A 2:10375–10378
372. Zhang J, Zhang J, Peng Z, Cai W, Yu L, Wu Z, Zhang Z (2014) Outstanding rate capability and long cycle stability induced by homogeneous distribution of nitrogen doped carbon and titanium nitride on the surface and in the bulk of spinel lithium titanate. Electrochim Acta 132:230–238

373. Bünting A, Uhlenbruck S, Dellen C, Finsterbusch M, Tsai CL, Sebold D, Buchkremer HP, Vaßen R (2015) Influence of titanium nitride interlayer on the morphology, structure and electrochemical performance of magnetron-sputtered lithium iron phosphate thin films. J Power Sources 281:326–333
374. Balogun M-S, Li C, Zeng Y, Yu M, Wu Q, Wu M, Lu X, Tong Y (2014) Titanium dioxide@titanium nitride nanowires on carbon cloth with remarkable rate capability for flexible lithium-ion batteries. J Power Sources 272:946–953
375. Kraytsberg A, Ein-Eli Y (2012) Higher, stronger, better… A review of 5 Volt cathode materials for advanced lithium-ion batteries. Adv Energy Mater 2:922
376. Song J, Shin DW, Lu YH et al (2012) Role of oxygen vacancies on the performance of Li $[Ni_{0.5-x}Mn_{1.5+x}]O_4$ (x = 0, 0.05, and 0.08) spinel cathodes for lithium-ion batteries. Chem Mater 24:3101
377. Kawai H, Nagata M, Tukamoto H, West AR (1998) A new lithium cathode $LiCoMnO_4$: toward practical 5 V lithium batteries. Electrochem Solid State Lett 1:212
378. Dimesso L, Forster C, Jaegermann W et al (2012) Developments in nanostructured $LiMPO_4$ (M = Fe, Co, Ni, Mn) composites based on three dimensional carbon architecture. Chem Soc Rev 41:5068
379. Ji X, Lee KT, Nazar LF (2009) A highly ordered nanostructured carbon-sulphur cathode for lithium-sulphur batteries. Nat Mater 8:500
380. Yang Y, Zheng G, Misra S et al (2012) High-capacity micrometer-sized Li_2S particles as cathode materials for advanced rechargeable lithium-ion batteries. J Am Chem Soc 134:15387
381. Wang H, Yang Y, Liang Y et al (2011) Graphene-wrapped sulfur particles as a rechargeable lithium–sulfur battery cathode material with high capacity and cycling stability. Nano Lett 11:2644
382. Manthiram A, Fu Y, Chung SH et al (2014) Rechargeable lithium-sulfur batteries. Chem Rev 114:11751
383. Girishkumar G, McCloskey B, Luntz AC et al (2010) Lithium–air battery: promise and challenges. J Phys Chem Lett 1:2193
384. Hu Y-Y, Liu Z, Nam K-W et al (2013) Origin of additional capacities in metal oxide lithium-ion battery electrodes. Nat Mater 12:1130
385. Luntz AC, McCloskey BD (2014) Nonaqueous Li-air batteries: a status report. Chem Rev 114:11721
386. Derrien G, Hassoun J, Panero S, Scrosati B (2007) Nanostructured Sn–C composite as an advanced anode material in high-performance lithium-ion batteries. Adv Mater 19:2336
387. Park M-S, Kang Y-M, Wang G-X et al (2008) The effect of morphological modification on the electrochemical properties of SnO_2 nanomaterials. Adv Funct Mater 18:455
388. Chen XT, Wang KX, Zhai YB et al (2014) A facile one-pot reduction method for the preparation of a SnO/SnO_2/GNS composite for high performance lithium ion batteries. Dalton Trans 43:3137
389. Liu L, Xie F, Lyu J et al (2016) Tin-based anode materials with well-designed architectures for next-generation lithium-ion batteries. J Power Sources 321:11
390. Naskar AK, Bi Z, Li Y et al (2014) Tailored recovery of carbons from waste tires for enhanced performance as anodes in lithium-ion batteries. RSC Adv 4:38213
391. Li Y, Adams RA, Arora A et al (2017) Sustainable potassium-ion battery anodes derived from waste-tire rubber. J Electrochem Soc 164:A1234
392. Li Y, Paranthaman MP, Akato K et al (2016) Tire-derived carbon composite anodes for sodium-ion batteries. J Power Sour 316:232
393. Bradford PD et al (2010) A novel approach to fabricate high volume fraction nanocomposites with long aligned carbon nanotubes. Compos Sci Technol 70:1980–1985
394. Zhang L et al (2015) Strong and conductive dry carbon nanotube films by microcombing. Small 11:3830–3836
395. Zhang X et al (2007) Strong carbon-nanotube fibers spun from long carbon-nanotube arrays. Small 3:244–248

396. Wang X et al (2011) Mechanical and electrical property improvement in CNT/Nylon composites through drawing and stretching. Compos Sci Technol 71:1677–1683
397. Wang X et al (2012) Ultrastrong, stiff and multifunctional carbon nanotube composites. Mater Res Lett 1:1–7
398. Fu K et al (2013) Aligned carbon nanotube-silicon sheets: a novel nano-architecture for flexible lithium ion battery electrodes. Adv Mater 25:5109–5114
399. Faraji S et al (2014) Structural annealing of carbon coated aligned multi-walled carbon nanotube sheets. Carbon N Y 79:113–122
400. Dufficy MK, Khan SA, Fedkiw PS (2015) Galactomannan binding agents for silicon anodes in Li-ion batteries. J Mater Chem A 3:12023–12030
401. Cuesta N, Ramos A, Cameán I, Antuña C, García AB (2015) Hydrocolloids as binders for graphite anodes of lithium-ion batteries. Electrochim Acta 155:140–147
402. Liu J et al (2015) A robust ion-conductive biopolymer as a binder for Si anodes of lithium-ion batteries. Adv Funct Mater 25:3599–3605
403. Sudhakar YN, Selvakumar M, Bhat DK (2014) Tubular array, dielectric, conductivity and electrochemical properties of biodegradable gel polymer electrolyte. Mater Sci Eng B 180:12–19
404. Wang J, Chen Y, Qi L (2011) Open Mater Sci J 5:228
405. Kasavajjula U, Wang CS, Appleby AJ (2007) J Power Sources 163:1003
406. Chen LB, Xie XH, Wang BF, Wang K, Xie JY (2006) Mater Sci Eng B 131:186
407. Ng SH, Wang J, Konstantinov K, Wexler D, Chew SY, Guo ZP, Liu HK (2007) J Power Sources 174:823
408. Amine K, Wang QZ, Vissers DR, Zhang ZC, Rossi NAA, West R (2006) Novel silane compounds as electrolyte solvents for Li-ion batteries. Electrochem Commun 8:429–433
409. Rossi NAA, West R (2009) Silicon-containing liquid polymer electrolytes for application in lithium ion batteries. Polym Int 58:267–272
410. Zhang LZ, Zhang ZC, Harring S, Straughan M, Butorac R, Chen ZH, Lyons L, Amine K, West R (2008) Highly conductive trimethylsilyl oligo(ethylene oxide) electrolytes for energy storage applications. J Mater Chem 18:3713–3717
411. Xu K (2004) Nonaqueous liquid electrolytes for lithium-based rechargeable batteries. Chem Rev 104:4303–4417
412. Walkowiak M, Waszak D, Schroeder G, Gierczyk B (2008) Polyether-functionalized disiloxanes as new film-forming electrolyte additive for Li-ion cells with graphitic anodes. Electrochem Commun 10:1676–1679
413. Schroeder G, Gierczyk B, Waszak D, Kopczyk M, Walkowiak M (2006) Vinyl tris-2-methoxyethoxy silane—a new class of film-forming electrolyte components for Li-ion cells with graphite anodes. Electrochem Commun 8:523–527
414. Xia Q, Wang B, Wu YP, Luo HJ, Zhao SY, van Ree T (2008) Phenyl tris-2-methoxydiethoxy silane as an additive to PC-based electrolytes for lithium-ion batteries. J Power Sources 180:602–606
415. Qin XY, Wang JL, Zhang LZ (2012) Progress of organosilicon based electrolytes for lithium-ion batteries. Prog Chem 24(5):155–167
416. Jeong SK, Inaba M, Iriyama Y, Abe T, Ogumi Z (2003) Electrochemical intercalation of lithium ion within graphite from propylene carbonate solutions. Electrochem Solid-State Lett 6:A13–A15
417. Jeong SK, Inaba M, Iriyama Y, Abe T, Ogumi Z (2008) Interfacial reactions between graphite electrodes and propylene carbonate-based solution: electrolyte-concentration dependence of electrochemical lithium intercalation reaction. J Power Sources 175:540–546
418. Takeuchi S, Miyazaki K, Sagane F, Fukutsuka T, Jeong SK, Abe T (2011) Electrochemical properties of graphite electrode in propylene carbonate-based electrolytes containing lithium and calcium ions. Electrochim Acta 56:10450–10453
419. Takeuchi S, Fukutsuka T, Miyazaki K, Abe T (2013) Electrochemical lithium ion intercalation into graphite electrode in propylene carbonate-based electrolytes with dimethyl carbonate and calcium salt. J Power Sources 238:65–68

420. Henderson WA (2006) Glyme-lithium salt phase behavior. J Phys Chem B 110:13177–13183
421. Seo DM, Borodin O, Han SD, Boyle PD, Henderson WA (2012) Electrolyte solvation and ionic association II acetonitrile-lithium salt mixtures: highly dissociated salts. J Electrochem Soc 159:A1489–A1500
422. Yamada Y, Yaegashi M, Abe T, Yamada A (2013) A superconcentrated ether electrolyte for fast-charging li-ion batteries. Chem Commun 49:11194–11196
423. Yamada Y, Furukawa K, Sodeyama K, Kikuchi K, Yaegashi M, Tateyama Y, Yamada A (2014) Unusual stability of acetonitrile-based superconcentrated electrolytes for fast-charging lithium-ion batteries. J Am Chem Soc 136:5039–5046
424. Song HY, Fukutsuka T, Miyazaki K, Abe T (in press) suppression of co-intercalation reaction of propylene carbonate and lithium ion into graphite negative electrode by addition of diglyme. J Electrochem Soc
425. Liu XH, Zheng H, Zhong L, Huang S, Karki K, Zhang LQ, Liu Y, Kushima A, Liang WT, Wang JW (2011) Nano Lett 11:3312–3318
426. Lee SW, McDowell MT, Berla LA, Nix WD, Cui Y (2012) Proc Natl Acad Sci USA 109:4080–4085
427. Wu H, Cui Y (2012) Nano Today 7:414–429
428. Yi R, Dai F, Gordin ML, Chen S, Wang D (2013) Adv Energy Mater 3:295–300
429. Abraham KM (2015) Prospects and limits of energy storage in batteries. J Phys Chem Lett 6:830–844
430. Demir-Cakan R, Hu YS, Antonietti M, Maier J, Titirici MM (2008) Facile one-pot synthesis of mesoporous SnO_2 microspheres via nanoparticles assembly and lithium storage properties. Chem Mater 20:1227–1229
431. Chen JS, Cheah YL, Chen YT, Jayaprakash N, Madhavi S, Yang YH, Lou XW (2009) SnO_2 nanoparticles with controlled carbon nanocoating as high capacity anode materials for lithium-ion batteries. J Phys Chem C 113:20504–20508
432. Wen Z, Cui Kim H, Mao S, Yu K, Lu G, Pu H, Mao O, Chen J (2012) Binding Sn based nanoparticles on graphene as the anode of rechargeable lithium-ion batteries. J Mater Chem 22:3300–3306
433. Wang D, Yang J, Li X, Geng D, Li R, Cai M, Sham TK, Sun X (2013) Layer by layer assembly of sandwiched graphene/SnO_2 nanorod/carbon nanostructures with ultrahigh lithium ion storage properties. Energy Environ Sci 6:2900–2906
434. Wang J, Song W-L, Wang Z, Fan L-Z, Zhang Y (2015) Facile fabrication of binder free metallic tin nanoparticle/carbon nanofiber hybrid electrodes for lithium-ion batteries. Electrochim Acta 153:468–475
435. Li X, Li X, Fan L, Yu Z, Yan B, Xiong D, Song X, Li S, Adair KR, Li D, Sun X (2017) Rational design of Sn/SnO_2/porous carbon nanocomposites as anode materials for sodium-ion batteries. Appl Surf Sci 412:170–176
436. Guo ZG, Cheng JK, Hu ZG, Zhang M, Xu Q, Kang ZX, Zhao D (2014) Metal-organic frameworks (MOFs) as precursors towards TiO_x/C composites for photodegradation of organic dye. RSC Adv 4:34221–34225
437. DeKrafft KE, Wang C, Lin WB (2012) Metal-organic framework templated synthesis of Fe_2O_3/TiO_2 nanocomposite for hydrogen production. Adv Mater 24:2014–2018
438. Liu JJ, Yang Y, Zhu WW, Yi X, Dong ZL, Xu XN, Chen MW, Yang K, Lu G, Jiang LX, Liu Z (2016) Nanoscale metal-organic frameworks for combined photodynamic & radiation therapy in cancer treatment. Biomaterials 97:1–9
439. Meng WJ, Chen W, Zhao L, Huang Y, Zhu MS, Huang Y, Fu YQ, Geng FX, Yu J, Chen XF, Zhi CY (2014) Porous Fe_3O_4/carbon composite electrode material prepared from metal-organic framework template and effect of temperature on its capacitance. Nano Energy 8:133–140
440. Li GC, Liu PF, Liu R, Liu M, Tao K, Zhu SR, Wu MK, Yi FY, Han L (2016) MOF-derived hierarchical double-shelled NiO/ZnO hollow spheres for high-performance supercapacitors. Dalton Trans 45:13311–13316

441. Yue HY, Shi ZP, Wang QX, Cao ZX, Dong HY, Qiao Y, Yin YH, Yang ST (2014) MOF-derived cobalt-doped ZnO@C composites as a high-performance anode material for lithium-ion batteries. ACS Appl Mater Interfaces 6:17067–17074
442. Guo WX, Sun WW, Lv LP, Kong SF, Wang Y (2017) Microwave-assisted morphology evolution of Fe-based metal-organic frameworks and their derived Fe_2O_3 nanostructures for Li-ion storage. ACS Nano 11:4198–4205
443. Wang W, Yang Y, Yang SJ, Guo ZP, Feng CQ, Tang XC (2015) Synthesis and electrochemical performance of $ZnCo_2O_4$ for lithium-ion battery application. Electrochim Acta 155:297–304
444. Huang B, Yang J, Zou Y, Ma L, Zhou X (2014) Sonochemical synthesis of SnO_2/carbon nanotubes encapsulated in graphene sheets composites for lithium ion batteries with superior electrochemical performance. Electrochim Acta 143:63–69
445. Zhang B, Zheng QB, Huang ZD, Oh SW, Kim JK (2011) SnO_2–graphene–carbon nanotube mixture for anode material with improved rate capacities. Carbon 49:4524–4534
446. Koninck MD, Poirier SC, Marsan B (2006) J Electrochem Soc 153:A2103–A2110
447. Rosa-Toro AL, Berenguer R, Quijada C, Montilla F, Morallon E, Vazquez JL (2006) J Phys Chem B 110:24021–24029
448. Feng Y, Liu JH, Wu DL, Zhou ZY, Deng Y, Zhang T, Shih K (2015) Chem Eng J 280:514–524
449. Shi YQ, Yu B, Zhou KQ, Yuen RKK, Gui Z, Hu Y, Jiang SH (2015) J Hazard Mater 293:87–96
450. Yunjian L, Xinhai L, Huajun G, Zhixing W, Qiyang H, Wenjie P, Yong Y (2009) Electrochemical performance and capacity fading reason of $LiMn_2O_4$/graphite batteries stored at room temperature. J Power Sources 189:721–725

Chapter 2
Cathode Materials, Samples, Pristine, Layered, Doping, Discharge Capacity

2.1 Introduction

$LiCoO_2$ has been commonly used in Li-ion batteries (Li-ion batteries) designed for portable electronics [57, 58] as one of the earliest-emerged cathode materials [1]. The inherent shortcomings with toxicity, low capacity of $LiCoO_2$, and high cost, severely deter its widespread application in lithium-ion batteries (Li-ion batteries) [1]. It remains a considerable challenge to simultaneously avoid the formation of undesired metal ion impurities in the commodities and synthesize materials with homogeneous cation distribution even though a wide range of progresses have been obtained in the fabrication process [1]. At molecular level, molten-salt routes [59] can attain homogeneous, which mixes of raw materials, though certain quantities of metal ion impurities are formed in the commodities, which might worsen the electrochemical performances [60] among the traditional preparation techniques [1]. Li^+ can not be coprecipitated together with other transition metal ions even though many scholars can fabricate material without impurities formed in the final commodities by employing special precipitant to substitute Na_2CO_3 [61] or NaOH [1]. It is highly advantageous to examine a new path; this path can simultaneously precipitate Li^+ with transition metal ions [1]. Synthesis of LNMO cathode material is summarized by the investigation through a modified oxalate coprecipitation technique, which is combined with high-temperature solid-state reaction [1]. The insoluble property of lithium oxalate, nickel oxalate in ethanol solution, and manganese oxalate, assures the coprecipitation of all metal ions [1]. Lithium ions are coprecipitated with transition metal ions, forming a precursor with homogeneous cation distribution at molecular level during the process [1]. Due to the homogeneous cation distribution inside the material, the LNMO cathode, which the modified oxalate coprecipitation technique prepared, displays high capacity, superior rate capability, and excellent cycle performance [1].

This book was machine-generated

Beta Writer, *Lithium-Ion Batteries*,
https://doi.org/10.1007/978-3-030-16800-1_2

High-voltage $LiNi_{0.5}Mn_{1.5}O_4$ (LNMO), as a derivative of the spinel $LiMn_2O_4$, has been regarded as one of the hottest cathode candidates, because of the theoretical capacity of 146.7 mAh g^{-1}, cubic spinel structure, satisfactory electrochemical performance, environment-friendly properties [56, 62–65], and low cost of raw material [2]. Carbonate coprecipitation is viewed as one of the most efficient ways to prepare excellent electrochemical performance of materials [56] and multiple morphologies [2]. In recent decades [55, 66–68], hollow structures with well-defined morphology, interior, and composition, have aroused intense attention among the multiple structured electrode materials [2]. Hollowing the electrode materials with well-defined nano-architectures might lead to the enhanced electrochemical performance [2]. The hollow structure, which is made of nanoparticles, frequently has a lowered efficient diffusion distance for Li^+ and a bigger surface area, leading to enhanced rate capability [2]. Throughout the lithium insertion/extraction cycling, the void space in the hollow sphere might buffer against the local volume change, fostering the systemic stability of the electrode material and enhancing the cycleability [2, 55, 67–70]. Given the particular advantages of hollow structures, LNMO hollow structures might be a quite appealing cathode material for Li-ion batteries [2]. A cheap and straightforward technique for synthesis of LNMO hollow structures is required [2]. A facile coprecipitation approach to fabricate hollow LNMO microspheres for LIB applications is summarized by the investigation [2]. The $(Ni_{0.25}Mn_{0.75})CO_3$ precursors directly blend with a stoichiometric quantity of Li_2CO_3, and calcine in air to derive the final commodities; these commodities indicate satisfactory electrochemical performances including rate capability, specific capacity, and cycling stability [2].

$LiMn_2O_4$ has been reasonably well indicated [71, 72]. Various cation-substituted and it has been noted that co-doping of metal ions has a synergetic effect on the amelioration of the cycle life [3]. Our earlier results [73] revealed that dual doping of Zn and La into the $LiMn_2O_4$ cathode material substantially enhanced the electrochemical performance including charge capacity and cycling stability at high current [3]. Spinel $LiMn_2O_4$ material doped with single metal ions provides a high initial capacity though with restricted cyclability upon prolonged charge/discharge cycling [3]. Through an impurity $Li_xNi_{1-x}O$ stage because of oxygen deficiency, synthesis of heavily Ni-doped spinel $LiMn_2O_4$ is normally accompanied and partial Ni ions seem to occupy the Li (8a) sites in the spinel matrix which results in inferior stability and lower capacity during charge/discharge cycling [3, 74]. Especially in the handful initial cycles [75], an attempt has been made in the past to co-dope vanadium ions (V^{5+}) along with Cr^{3+}; a serious capacity fading had been noticed around 4.0 V [3]. Between 0.1 and 0.5, two things which are common to both reports are (i) employing high-content dopants (Ni and/or Cr) x to substitute Mn and (ii) charge/discharge researches at low current rates it is of paramount importance to examine the affects of variability in dopant quantities particularly at low content on the electrochemical performance of the material including the cycling performance at greater rates, i.e. 0.15 C. Therefore, and the identical is the aim of this quite report [3]. Given the indicated scientific literature, many strong synergetic effect of Cr and Ni co-doping is supposed to manifest substantially the enhanced electrochemical performance of spinel $LiMn_2O_4$ [3].

Since it can provide a high operating voltage of ~4.7 V (vs. Li/Li^+), which emerges from fast 3D lithium-ion diffusion channels and Ni^{2+}/Ni^{4+} redox couple, within the cubic lattice [76–78], $LiNi_{0.5}Mn_{1.5}O_4$ spinel has received significant interest among the cathode materials [4]. For example, solid-state technique, the Mn^{3+} content could be enforced by synthesis conditions (such as the kinds and quantities of raw materials, calcining temperature and time, etc.), which have critical relevance on the crystalline structure, then on the electrochemical performance if the synthesis technique is fixed [4]. There have been various conclusions about the effect of lithium excess quantities on electrochemical properties and the crystalline to the optimal of our knowledge [4]. Porous $MnCO_3$ microsphere had been utilized by Chen and others [79] as precursor, and the lithium excess quantity had been selected at 0, 2, 5, and 8%, respectively [4]. That the $Li_xNi_{1-x}O$ impurity stage is progressively increasing with lithium excess quantity increased had been founded by Chen and others [4, 79]. Octahedral $LiNi_{0.5}Mn_{1.5}O_4$ cathode materials were synthesizeded by Deng and others [80] via a single-step nonaqueous coprecipitation technique, and the lithium excess quantity had been selected at 0, 1, 3, and 5% [4]. The subsample with 5% lithium excess quantity has the smallest lattice parameter and Mn^{3+} content, which is just contrary to the results of Ref. [4]. Through a facile solid-state technique, $LiNi_{0.5}Mn_{1.5}O_4$ cathode material had been synthesized, and the impacts of various lithium excess quantities (0, 2, 6, and 10%) on electrochemical properties including the physicochemical properties were systematically examined [4].

Throughout the first charging process, the huge initial ICL and fast capacity fading primarily emerge from the activation reaction of Li_2MnO_3 element [5]. Some methodologies have been taken to enhance the electrochemical performance of LMNC materials, such as surface modification [81, 82], mild acidic treatment [83, 84], cation doping [85–87], and structure and morphology controlling [5, 88, 89]. Some metal cations (e.g., Mg [90], Zn [91], Al [92], and Cr [93]) have been efficiently doped into the structure of Li-rich cathode materials [5]. That the Li $(Li_{0.19}Mn_{0.54}Ni_{0.13}Co_{0.12}Ru_{0.01})O_2$ cathode indicates a high discharge capacity of 182 mAh g^{-1} at 5 C with a capacity fade of 0.06% per cycle in 700 cycles because the suitable Ru-doping can foster the stage transition from layered $Li(Li_{1/3}Mn_{2/3})O_2$ to certain spinel-like stages [94] and enhance the Li^+ diffusion in LMNC had been indicated by B. Song and others [5]. Via a sol-gel technique, X. Jin and others efficiently synthesized Mg-doped LMNC, and the Mg-doping can expand the inter-slap distance of lattices to enhance the Li^+ insertion/extraction and enhance rate performance (160.5 mAh g^{-1} at 1000 mA g^{-1} and remains 127.5 mAh g^{-1} after 50 cycles) of cathode materials [95] and the cycle stability [5]. That Zr dopant can enhance the Li^+ diffusion, which efficiently improves the cycle stability and rate performance of LMNC [96] and sustain the crystal structure of Li-rich cathode had been founded by X. Jin and others [5]. Through improving the systemic stability [97], the Sn^{4+} dopant can distinctively enhance the electrochemical performance of cathodes [5]. There has no report on the amelioration in the electrochemical performance of Li-rich $Li_{1.2}Mn_{0.54}Ni_{0.13}Co_{0.13}O_2$ cathode materials by the doping of

Sn ions [5]. Sn^{4+} ions were introduced into the crystal structure of LMNC materials to partially substitute Mn^{4+} through a sol-gel technique [5].

The comparatively low electrical conductivity of $LiNi_{0.5}Mn_{1.5}O_4$ results in meager high-rate performance and inevitably limits its practical applications [6, 98]. A surface coating treatment and a solid-state process are usually utilized to synthesize and sustain $LiNi_{0.5}Mn_{1.5}O_4$ with high electrochemical performance [99, 100] as a common technique [6]. The coating modification not just prevents the direct contact of the electrolyte with the inner elements though also enhances the reversible capacity, rate capability of $LiNi_{0.5}Mn_{1.5}O_4$, and cycle performance [6]. The disproportionation reaction of Mn^{3+} and the oxidation decomposition of the electrolyte could be lowered, and subsequently, the systemic stability of $LiNi_{0.5}Mn_{1.5}O_4$ will be increasing [6]. In surface modification due to its high electronic electrical conductivity, excellent systemic stability [101], and huge surface area, Graphene has attracted much attention [6]. Designing a $LiNi_{0.5}Mn_{1.5}O_4$-graphene composite structure has been shown as an effective way to enhance electrochemical performance by offering a highly conductive matrix [6, 102]. The distinctive nanostructure, enhanced electrocatalytic activity of the CNF, and graphitic structure, extend their potential application in the electronic, electrochemical, and electrocatalytic, energy-storage fields [6]. We synthesized $LiNi_{0.5}Mn_{1.5}O_4$ cathode materials with nano-micro structures by a process, which spray-drys coprecipitation and calcining, and efficiently introduced the CNF into the $LiNi_{0.5}Mn_{1.5}O_4$ spheres during the coprecipitation spray-drying period [6]. CNF not just increases the bulk electrical conductivity of $LiNi_{0.5}Mn_{1.5}O_4$ powders though also protects the surface of sub-particles [6].

It is required to break the bottleneck of high capacity density, long cycle life, excellent rate capability for lithium-ion batteries [103–105], and satisfactory security, with the increased development of the portable electronic tools, hybrid electrical vehicles (HEVs) and electric vehicles (EVs) [7]. $Li(Ni_xM_{1-x})O_2$ cathode materials were layered by Nickel-rich with high discharge specific capacity, comparatively low cost and considerable rate capability are becoming one of the most fruitful cathode materials for lithium-ion battery [7]. $LiNi_{0.8}Co_{0.15}Al_{0.05}O_2$ with a high tap density, cycling stability and an excellent rate capability is regarded to be the next generation cathode materials for green lithium-ion battery [106] as the isomorphous solid solution of $LiAlO_2$, and $LiNiO_2$, $LiCoO_2$ [7]. Cathode materials have been devised in the direction of high tap density with the increased requirements of high volume capacity density had been layered by Nickel-rich [7]. An suitable quantity of Ti, which dopes in Nickel-rich, layered materials can improve thermostability and systemic integrity because the Ti^{4+} ions deter impurity Ni^{2+} migration into the lithium sites [107–109] among the doping elements [7]. The $LiNi_{0.8}Co_{0.15}Ti_{0.05}O_2$ cathode materials with a high tap density and a satisfactory spherical morphology have been prepared efficiently by employing the spherical $Ni_{0.8}Co_{0.15}(OH)_{1.9}$ as precursor; this precursor had been synthesized through a co-oxidation-controlled crystallization technique [7].

Two crucial improvements could be made to increase the electrochemical performance of Li_2FeSiO_4, such as coating it with carbon materials [110, 111] and

declining the Li_2FeSiO_4 particle size to circumvent these hurdles [8]. Through tedious calcinations, employing a solid-state reaction technique, micro-sized Li_2FeSiO_4 particles were prepared at high temperature although the huge particle size had a negative effect on electrochemical performance [8, 112]. Based on iron, soluble lithium, and silicon sources and hydrothermal-assisted or microwave-solvothermal sol-gel techniques, Li_2FeSiO_4/C commodities can attain satisfactory rate performance [8, 113, 114]. Both the carbon-coating method and carbon source wide range can affect the electrochemical performance of Li_2FeSiO_4/C [8]. One efficient strategy to enhance the electrochemical performance of Li_2FeSiO_4/C is cation doping [8]. Hitherto, zinc-, copper-, nickel-, chromium-, vanadium-, magnesium-doped Li_2FeSiO_4/C cathodes, and cobalt-, have been prepared by the sol-gel technique [8, 115–120]. Our group indicated that the capacity retention had been substantially enhanced by 10 proportion points after magnesium doping, and doping with magnesium cation had been beneficial for enhancing the cycle performance of Li_2FeSiO_4/C [8]. It might be supposed that strontium cation doping can improve the electrochemical performance of Li_2FeSiO_4/C compared with magnesium cation doping [8]. Through the sol-gel technique, we efficiently synthesized strontium-doped Li_2FeSiO_4/C for the first time [8]. It had been proven that rate performance and the special discharge capacity were enhanced after strontium cation doping because of the Li^+ diffusion capability, which is enhanced substantially, via examining electrochemical impedance spectra of the undoped and strontium-doped Li_2FeSiO_4/C cathodes for the cells [8].

$LiCoO_2$ had been the cathode material since lithium-ion batteries (Li-ion batteries) had been marketed by Sony in 1991 [121], which is utilized most extensively [9]. Ni^{2+} is the just electrochemically active element to lead the high capacity whilst Mn^{4+} plays as the stable octahedral ion to assure the stability of the layered structure during the intercalation/de-intercalation of Li ions in this material [9]. That material suffers from inherent low electronic electrical conductivity and meager lithium-ion diffusivity that drastically lessen this material's discharge capacity at high current density even though the $LiNi_{0.5}Mn_{0.5}O_2$ cathode material has many advantages [9]. Kiziltas-Yavuz and others [122] synthesized $LiNi_{0.4}Ru_{0.05}Mn_{1.5}O_4$ material employing the citric acid-assisted sol-gel technique which delivered the enhanced electrochemical performances [9]. The Ru-doped $LiNi_{0.5}Mn_{1.5}O_4$ cathodes, which summarized high-rate capability, which is enhanced pronouncedly, because of the enhanced ionic and electronic electrical conductivity were indicated by Wang and others [9, 123]. Through doping the Ru element, Wang and others [124] indicated the amelioration of the electrochemical properties of $LiFePO_4$ cathode materials [9]. We prepared $LiNi_{0.5}Mn_{0.45}Ru_{0.05}O_2$ employing a moist chemical technique, and the structure and electrochemical property of the as-synthesized material were examined for the first time [9].

The cathode material is a crucial material in lithium-ion batteries, and research and development into high-potential cathode materials is one of the principal ways to enhance the energy density of lithium-ion batteries [10]. At roughly 4.7 V, Spinel $LiNi_{0.5}Mn_{1.5}O_4$ has the advantage of discharge voltage plateaus: low cost, heat stability, and excellent systemic stability, and is regarded one of the most

fruitful cathode materials for lithium-ion batteries [10]. The cycling stability of $LiNi_{0.5}Mn_{1.5}O_4$ is meager, and cycling of this material results in the Jahn-Teller effect and Mn break-up [10, 125–128]. Modification of the material by coating and doping has been utilized to restrain the Jahn-Teller effect and to lessen Mn deterioration in order to enhance the electrochemical properties of the material [10]. Through employing a small quantity of and doping, surface coating and, doping can enhance the rate capability and cycling performance of the material [129–131], the volume change in the material during the insertion/extraction process of Li ions could be efficiently repressed [10].

Since an mean 4.0 V ($\sim$0.6 V greater than $LiFePO_4$) extraction/reinsertion voltage could be obtained between 3.0 and 4.8 V and the greater theoretical capacity of 197 mAh g^{-1} for full removal of three lithium ions, NASICON conceptual framework monoclinic $Li_3V_2(PO_4)_3$ (LVP) had been regarded as a prospective candidate for employing as the cathode in lithium-ion battery [11]. LVP undergoes serious capacity, which fades whilst charging up to 4.8 V for the extraction of more than two lithium ions [11, 132]. One efficient strategy is aliovalent or isovalent doping at the transition metal sites, for example, in $Li_3V_2(PO_4)_3$, V^{3+} has been partly replaced with W^{5+} [133], Ti^{4+} [134], Zr^{4+} [135], Fe^{3+} [136], Al^{3+} [137–140], Cr^{3+} [141], Sc^{3+} [142], Y^{3+} [143], Mn^{2+} [144], Mg^{2+} [145, 146], and Co^{2+} [147] to enhance the electrochemical performance by stabilizing the structure during high voltage charging [11, 137]. That $Li_3V_{2-x}W_x(PO_4)_3/C$ (x = 0.10) showed better cycle stability than the pure one and greater discharge capacity had been indicated by Xia and others [11]. The initial discharge capacity had been 160.3 mAh g^{-1} and 95.5% capacity retention had been detected after 50 cycles at 0.5 C rate [133] for the optimum composition of $Li_3V_{1.93}W_{0.07}(PO_4)_3/C$ [11]. It is required to research metal or LVP/C ions doping LVP/C as cathode material for Li-ion batteries [11]. LVP displays greater capacity and better cycle stability than that of undoped LVP had been carbon-coateded by the Y-doped and [11].

The high specific energy and power readily available from lithium-ion batteries and the possibility to charge and discharge them hundreds of times are the reason for their crucial relevance in electronic portable tools and future development of hybrid vehicles [12, 148]. Once a battery is operative, the redox reactions affect the electrode materials molecular/crystalline structure, influencing their stability, and consequently necessitate frequent replacement after numerous cycles [12]. In the electrodes that eventually give rise to performance degradation [149], the high rate exchange of lithium ions requiring produces and more power faster charging strains and significant emphasizes [12]. The issues rise from the effort to increase the cycle life and stability of the cathode materials in standard commercial LIB's [12, 150]. That work on AuPt alloy transition metal alloy-surface modified spinel $LiMn_2O_4$ cathode materials can offer a network for electron diffusion because of a shortened transportation path, i.e., highly crystalline nanostructures [151], enhanced stage transition kinetics of Li-ion intercalation/deintercalation and high rate discharge capacities [152], which connects better [12].

Traditional cathode materials including $LiFePO_4$, $LiCoO_2$ suffer from high cost, inferior cycle stability [153, 154], and huge capacity deterioration [13]. Traditional cathode materials including $LiFePO_4$, $LiCoO_2$'s derivatives and Layered $LiNiO_2$ are fruitful cathode materials for lithium-ion batteries due to low cost [155] and Traditional cathode materials including $LiFePO_4$, $LiCoO_2$'s high theoretical capacity [13]. $LiNiO_2$ is difficult to synthesize, and its structure is unstable during cycling due to the cation mixing, which results from the comparable ion radius of Li^+ (0.76 Å) and Ni^{2+} (0.69 Å) ions [13]. Ni relates to increase the specific capacity, though the increase content of Ni results in irreversible initial capacities and more cation mixing [13, 156, 157]. Ni-rich layered oxides $LiNi_{1-y-z}Mn_yCo_zO_2$ has been extensively researched because of low cost and co's high discharge capacity in recent decades [158], including $LiNi_{0.8}Co_{0.15}Al_{0.05}O_2$ [159] and $LiNi_{0.5}Co_{0.2}Mn_{0.3}O_2$ [13, 160]. To circumvent the shortcomings of Ni-rich oxides $LiNi_{1-y-z}Mn_yCo_zO_2$ materials by doping with cations [161, 162] and coating with an suitable material [163, 164] are primary techniques till date, doping cations such as Cr^{3+} [165], Al^{3+} [166], Mg^{2+} [167], and so on [13]. We designed a novel composite material with the nominal compositions of 0 in order to build alternatives of traditional cathode materials and $LiNiO_2$ [13]. The novel composite materials were among the medium-high nickel class with low content of cobalt ($0.1 \leq \times \leq 0.19$); this class had a comprehensive advantage in the facets of cost control, capacity, and sintering technology compared with Ni-poor or Ni-rich materials [13]. Four various compositions of cathode materials $Li(Ni_{0.56}Co_{0.19}Mn_{0.24}Al_{0.01})_{1-y}Al_yO_2$ (y = 0, 0.02, 0.04, 0.06) were undertaken the researches on electrochemical behaviour [13]. The results were compared with that of the traditional $LiNi_{0.8}Co_{0.15}Al_{0.05}O_2$ and $LiNi_xCo_yMn_{1-x-y}O_2$ materials [13].

Due to its low cost, relative abundance, eco-friendliness, stability [168–170], and high columbic efficiency, $LiMn_2O_4$ with a 3-D tunnel structure for the migration of lithium ions appears to be one of the most fruitful cathode materials for Li-ion batteries among the multiple cathode materials [14]. $LiMn_2O_4$ has satisfactory cycle performance and high capacity, while lithium ions' rate performance needs to be enhanced compared with the other cathode materials [14]. Another of the tactics to enhance the lithium-ion intercalation capacity and rate capability of electrodes is to prepare and use materials with nano-size [14, 171–173]. The preparation of nano materials normally entails some various mechanisms, such as sol-gel technique [174], hydrothermal techniques [175–177], and coprecipitation [178], though these techniques are normally expensive, complex, and time-consuming [14]. We have synthesized nano-sized $LiMn_2O_4$ materials employing a comparatively straightforward single-step solid-state reaction technique [14]. Is utilized as a functional material to lose volatile gases during the process of calcining in order to change the particle size of materials [179–181] and control the morphology had been acided by Oxalic [14]. The suitable crystallinity needs to be reasonably well controlled for obtaining the surface area of the particles including satisfactory electrochemical performance at high C-rates [14]. Through adjusting the content of oxalic acid, the crystallite structure, capacity, powder properties, and power capability of obtained $LiMn_2O_4$ with various morphologies and particle sizes have been assessed and compared [14].

High capacity cathode materials with long-lasting cycle life is one of the hottest topics in lithium-ion battery research in recent decades [15]. The marketed cathode materials for lithium-ion batteries including $LiCoO_2$, $LiMn_2O_4$, $LiNi_{1/3}Co_{1/3}Mn_{1/3}O_2$ and $LiFePO_4$ indicate discharge capacities of below 200 mAh g^{-1} with the operating voltage variety of 2.8–4.4 V [15, 182]. More and more scholars have concentrated on the series of Li-rich layered composite $xLi_2MnO_3{\cdot}(1-x)LiMO_2$ (M = Ni, Co, Mn, $Ni_{1/2}Mn_{1/2}$, $Ni_{1/3}Co_{1/3}Mn_{1/3}$…) as cathode materials for their high reversible capacities (200–300 mAh g^{-1}) [15, 138, 183–188]. Li_2MnO_3 is the crucial element because it can offer further high capacity when electrochemically activated above 4.4 V [189–192] and sustain the crystal structure for the composite in this material [15]. The diffusion of lithium ions from octahedral sites in the Li_2MnO_3 element to tetrahedral sites in the lithium-depleted layer, considerably stabilizing the composite structure during the cycling process [15, 193]. Complete extraction of Li_2O from the inactive Li_2MnO_3 element yields electrochemically active layered MnO_2 stage, improving the discharge capacity of the material [15, 194, 195]. In the preparation of the Li-rich layered composites, by which the starting materials could be mixed on molecular level, coprecipitation technique is commonly used [15]. Throughout the washing process, employing coprecipitation technique, many of the transition metal ions in the raw materials will be lost [15]. Materials have been synthesized by hydrothermal technique [196–198] had been layered by Li-rich [15]. There are handful reports about Li-rich layered material preparation by a combined technique of hydrothermal process and template [15]. We first report the use of carbon nanotubes (CNTs) as template actor during hydrothermal process to synthesize nanosized Li-rich layered material 0 [15].

Lithium-ion batteries with $LiNi_{0.5}Mn_{1.5}O_4$ as the cathode material are regarded to be the most fruitful rechargeable energy storage systems due to the advantageous properties of $LiNi_{0.5}Mn_{1.5}O_4$, including its low production cost, long cycle life, environmental compatibility, in particular, and satisfactory thermal stability, high energy density of 630 Wh kg^{-1} [199–201] and its high discharge voltage of 4.7 V [16]. The electrochemical performance of cathode materials is dependent upon both academia and industry's composition not just though also on both academia and industry's morphology and particle size [16, 202, 203]. Some scholars have sought synthesizing $LiNi_{0.5}Mn_{1.5}O_4$ with nanoparticles because small size and its huge specific surface area favour fast electrode kinetics, shortening pathways for Li^+ and, nanoparticles aggregate readily electronic transportation, which can improve the rate capability of the cathode material [56, 204, 205]; and have a small tap density, which are disadvantageous to the other electrochemical properties of the material [16]. Spherical secondary microparticles, formed via aggregation of nanosized primary particles, are complementary to the insufficiency of the nanoparticles and enhance the electrochemical performance of the cathode materials [16]. Some spherical secondary $LiNi_{0.5}Mn_{1.5}O_4$ particles have been synthesized [16, 206–210]. The principal techniques of preparing these spherical secondary particles are the spray, which drys granulation [206, 207], and template techniques [16, 208–210]. Materials that are synthesized by this reaction display inferior electrochemical and

physical properties due to huge particle sizes [211], and their block-like, irregular morphology [16]. Micrometer-sized, spherical secondary $LiNi_{0.5}Mn_{1.5}O_4$ particles, comprised of nano-and/or sub-micrometer-sized particles, were efficiently prepared employing this technique [16]. We synthesized two $LiNi_{0.5}Mn_{1.5}O_4$ samples employing the enhanced and conventional (LNMO-A) solid-state techniques (LNMO-B) to examine the electrochemical properties [16].

Lithium-ion batteries (Li-ion batteries) have been extensively employed as the storage of renewables and power vehicles, in view of their several virtues associate with high-energy-density, environmental benignity, and long cycle life [17]. That fosters the development of high-power cathode and high-energy materials (Goodenough and Kim [138]; Tarascon and Armand [212]), [17]. Such lithium-rich high-capacity materials suffer from meager cycle stability and inferior rate property; this stability hinder their successful commercialization in high-energy-density lithium-ion batteries (Boulineau and others [213]; Thackeray and others [194]; Xu and others [214]), [17]. Under consequence in inferior cycling performance (Guo and others [215]) and high operating potentials, these nanoscaled materials with high surface activity might arouse undesired electrode-electrolyte reactions [17]. It is reasonably well recognized that the morphology of the cathode materials has a significant effect on the electrochemical performance [17]. Nano-sized hierarchical hollow structures and Micro have been indicated as optimal architectures for cathode materials to attain long cycling stability and high rate capability because they present the advantages of both nano-sized building blocks and microsized assemblies (Li and others [216, 217]; Wu and others [218]; Lin and others [219]; He and others [220]), [17]. Throughout electrochemical process, which ows to the short diffusion pathways of electrons and an suitable contact area between electrode and electrolyte, lithium ions, and stable structure, these hollow structure electrode materials might exhibit excellent electrochemical performances [17]. An efficient technique to prepare hollow sphere materials in microsize (Abdelaal and Harbrecht [221]) is employing cetyltrimethylammonium bromide (CTAB) and Sucrose as a combined template [17]. We employ sucrose and CTAB as a soft template, which is combined with hydrothermal assisted homogenous precipitation technique to fabricate hollow sphere cathode material, to improve the electrochemical performance of the $Li_{1.2}Mn_{0.54}Ni_{0.13}Co_{0.13}O_2$ material [17]. That technique indicates a route to synthesize the hollow microspheres assembled by nano-sized primary particles and provides a strategic strategy to enhance electrochemical performances for lithium-ion batteries [17].

The layered structure series material $LiNi_{1-x-y}Co_xMn_yO_2$ (NCM) has received increased attention [18, 222]. $LiNi_{1/3}Co_{1/3}Mn_{1/3}O_2$ compound, which Makimura [223] and Ohzuku devised, has been regarded as a fruitful candidate of next-generation cathode materials to substitute $LiCoO_2$ for rechargeable Li-ion batteries [18]. Since the combination of nickel, cobalt, and manganese, can offer advantages including greater theoretical capacity, milder thermal stability, and lower material cost, this material has aroused significant interest [18]. $LiNi_{1/3}Co_{1/3}Mn_{1/3}O_2$ suffers from two shortcomings of the toxicity and high cost of cobalt; in addition, thermal stability, the actual capacity, and rate capacity of $LiNi_{1/3}Co_{1/}$

$_3Mn_{1/3}O_2$ needs to be enhanced [18, 224]. The development of alternative cheap cathode materials with satisfactory thermal stability and high-specific capacity becomes the unavoidable trend [18, 225]. That Co^{3+} is just oxidized to Co^{4+} at rather high voltage in this material [226] had been revealed by principles computation [18], Some scholars have attempted to cost decrease and enhanced the capacity and thermal stability by employing other element to substitute of Co [18]. It has been shown that Al or Ti substitute of Coon $LiNi_{1/3}Co_{1/3}Mn_{1/3}O_2$ compound enhanced the thermal stability [18, 227]. Fe^{3+} has variable valence; this valence means ferrum additive on $Li[Ni_{1/3}Co_{1/3}Mn_{1/3}]O_2$ will have greater discharge capacity in theory [18]. Preliminary discharge specific capacity of $Li[Ni_{1/3}Co_{0.67/3}Mn_{1/3}Fe_{0.33/3}]O_2$ had been 122.24 mAh/g with a charge and discharge rate of 36 mAh/g in 3.0–4.5 V, which had been similar to the specific capacity of the state-of-art $LiCoO_2$ cathode material of LIB [18, 228]. $Li[Ni_{1/3}Co_{1/6}Mn_{1/3}Fe_{1/6}]O_2$ compound has been revealed that Fe substitution gives rise to a lower potential at the end of charge synthesized [18].

The spinel-type $LiNi_{0.5}Mn_{1.5}O_4$ with a high operating-voltage ($\sim$5 V) retains the readily available 3-D channels for the fast diffusion of Li^+ ions, providing a high energy density of 640 Wh kg^{-1} and a theoretical specific capacity of 147 mAh g^{-1} [229–232] with the previously marketed positive electrode materials including $LiCoO_2$, $LiFePO_4$, etc. [19]. That material $LiNi_{0.5}Mn_{1.5}O_4$ still suffers from numerous difficulties that should be circumvented, including comparatively low first-cycle columbic efficiency (75–85%) because of the electrolyte decomposition at high operating voltage, dissatisfied rate performance [230, 233] and meager cycling performance at high temperatures (50–60 °C) [19]. Some tactics including surface coating, lattice doping, and high-voltage-tolerant electrolytes, are devised to additional enhance its electrochemical properties to fulfil the commercial demands [19]. Some articles have indicated various coating materials for $LiNi_{0.5}Mn_{1.5}O_4$, including $Li_4Ti_5O_{12}$ [234], Li_3PO_4 [235], Al_2O_3 [236], carbon [237–239], ZnO [240], and so on, which can safeguard the particle surface against the electrolyte erosion at a high temperature or at a high voltage [19]. Zhong and others have prepared lattice-doped $LiNi_{0.5}Mn_{1.5}O_4$ materials employing trivalent Fe, Cr, Co, and Al to substitute Mn or Ni in $LiNi_{0.5}Mn_{1.5}O_4$ [19, 241, 242]. They have barely accomplished considerably amelioration on their electrochemical properties compared with the trivalent metal-doped $LiNi_{0.5}Mn_{1.5}O_4$ and the pristine [19]. It is reasonable to say that the lattice, which dops with high valence (>+2) metal ions, has been quite mature, though the effect of divalent doping for the $LiNi_{0.5}Mn_{1.5}O_4$ is not good [19]. Especially at a high temperature (55 °C), the $LiNi_{0.45}Cu_{0.05}Mn_{1.5}O_4$ subsample indicates satisfactory cycling stability [19].

Hereinto, the tavorite-like $LiMPO_4F$ (M = V, Mn, Fe, Co, Ni.) cathode materials are composed of 1D chains of metal octahedral interlinked by phosphate tetrahedral; this tetrahedral enable electron transport [20, 243]. It has been examined as cathode materials for Li-ion batteries since $LiFePO_4F$ indicated by Barker and others without electrochemical performance [20, 244]. $LiFePO_4F$ has been synthesized efficiently through multiple techniques, including solid-state [245–248], sol-gel [249], ionothermal [250] technique, solvothermal [251, 252], and others

Recham and others highlight the efficacy of ionothermal synthesis in the preparation of irregular morphology $LiFePO_4F$ with the particle size of 2–5 μm, and the as-prepared $LiFePO_4F$ displays ∼130 mAh g^{-1} at C/15 after ten cycles [20, 250]. A cheap and environmental friendly solvothermal process to prepare matchstick-like $LiFePO_4F$ with lengths up to 1 μm, which exhibits a discharge capacity of ∼123 mAh g^{-1} at C/50 [251] is indicated by Ellis and others [20]. Through Choudhury and others utilizing a low melting flux route, Plate-like $LiFePO_4F$ with numerous hundred nanometers is prepared, and the synthesized subsample retains the discharge capacity of 146 mAh g^{-1} (97% of theoretical capacity) at C/50 [20, 253]. There are seldom indicated about almost monodisperse $LiFePO_4F$ nanospheres [20]. It is highly advantageous to build an approach to synthesize homogeneous $LiFePO_4F$ nanospheres [20]. We build an approach to synthesize almost monodisperse $LiFePO_4F$ nanospheres through solid-state route, which is correlated with precipitation technique [20]. The $FePO_4$ had been subsequently mixed with LiF, and had been sintered to derive almost monodisperse $LiFePO_4F$ nanospheres [20]. The structure and electrochemical performance of almost monodisperse $LiFePO_4F$ nanospheres are examined [20].

Oxides $xLi_2MnO_3{\cdot}(1-x)LiMO_2$ (M frequently relates to Ni, Co, Cr, and Mn) are regarded to be alternative cathode materials because of greater capacity (>250 mAh g^{-1}), winder voltage variety (2.0–4.8 V), better security [254–259], and lower cost, were layered by the lithium-rich [21]. Some efforts have been indicated to enhance the electrochemical performance by many techniques including surface modification, doping [260–262], and nanoparticle, in order to satisfy requirement commercialization [21]. Cations doping has been demonstrated as an efficient technique to enhance the systemic stability of cycle stability [263] and cathode materials [21]. Partial substitutions of the transition metal in $xLi_2MnO_3{\cdot}(1-x)LiMO_2$ with Cr [264], Zr [96], V [265], Mg [266], Al [267], or Na [268], have been indicated for improving the longer-term cycle performance by enhancing the systemic stability [21]. As one of the most efficient doping elements, Cr has been intensively utilized by scholars to improve the electrochemical performance of lithium-rich layered oxides over the past numerous years [21, 264, 269–272]. Some of the advantages of Cr doping can be outlined as (i) Cr doping can improve the activation of Li_2MnO_3 below room temperature [271] and (ii) the following: (i) Cr^{3+}/Cr^{6+} redox is electrochemically active in contributing capacity in Li-rich layered cathodes [21, 269]. The samples $Li_{1.2}Ni_{0.16}Mn_{0.56}Cr_{0.08}O_2$ and $Li_{1.2}Ni_{0.2}Mn_{0.6}O_2$ were selected as a representative material of the Mn-based layered oxides to highlight the Cr-doping processes by the application of electron and lithium-ion diffusion X-ray and coefficient diffraction (XRD) and XPS (before and after cycling) [21].

Previous studies were concentrated on understanding and tailoring either the chemical composition or physical structure of the material (Ding and others [273]; Pampal and others [274]) for additional improving the comprehensive performances of $Li(Ni_{0.5}Co_{0.2}Mn_{0.3})O_2$ [22]. The physical structures, including particle size, particle morphology and its distribution, stage purity, and crystallinity in addition to Li^+/Ni^{2+} cation mixing (Ding and others [273]; Kuriyama and others [275]; Yuan and others [276]), which substantially impacted the electrochemical properties of

the cathodes, were optimized, as reasonably well [22]. The crystallite size is as crucial as crystalline stage, the elemental composition, and morphology because of its feature systemic elements in between the isolated atoms and the bulk macroscopic material (Waje and others [277]) in a nanometer-sized crystalline material [22]. Several relationship between crystallite sizes for multiple materials and the properties have been examined (Pukazhselvan [278]; Mguni and others [279]; Iqbal and others [280]; Upadhyay and others [281]; Zhao and others [282]; Tlili and others [283]), [22]. It could be observed that the natures of the material could be substantially dependent upon crystallite size (Burton and others [284]; Uvarov and Popov [285, 286]; Yashpal and others [287]; Sikora and others [288]), [22]. XRD is a method for crystallite size determination of nanocrystalline materials, which is utilized potent and frequently, in the present time [22]. The impacts of the calcining temperatures on the morphology, electrochemical performances of Li $(Ni_{0.5}Co_{0.2}Mn_{0.3})O_2$, and structure, have been deeply examined (Kong and others [289, 290]) [22]. Calcination temperature had been observed to specify the microstructure (particularly the crystallite size) of the material in the process of preparing $Li(Ni_{0.5}Co_{0.2}Mn_{0.3})O_2$ by a high-temperature solid-state technique [22]. In the thermal and electrochemical stability performances of the material, the crystallite size plays a distinctive role [22]. No or handful researches have been carried out systematically on insights into the correlation between crystallite size and the performance of the $Li(Ni_{0.5}Co_{0.2}Mn_{0.3})O_2$ active material up to now [22].

$LiCoO_2$, $LiNiO_2$, $LiFePO_4$, $LiMn_2O_4$ and $LiNi_xCo_yMn_{1-x-y}O_2$ are the most frequent cathode materials utilized in Li-ion batteries [23, 291–293]. Spinel $LiMn_2O_4$ has been intensively studied as cathode material for nontoxicity [294, 295] and its low cost among the several transition metal oxides [23]. The development of hybrid electric vehicles (HEVs) and plugin hybrid electric vehicles (PHEVs) demands for lithium-ion batteries with high power and safety stability, though the conventional $LiMn_2O_4$ material can not satisfy the technical requirements [23]. Some studies have concentrated on the substitution of Mn with other transition metal elements to form novel spinel cathode material [296, 297] to enhance the cycle performance of $LiMn_2O_4$ [23]. $LiNi_{0.5}Mn_{1.5}O_4$ cathode material has been observed as one of the most prospective lithium-ion battery materials because of high discharge platform [298, 299] and its high theoretical capacity (147 mAh g^{-1}) among multiple doped materials [23]. Carbonate and oxalate are utilized as precipitants for preparing $LiNi_{0.5}Mn_{1.5}O_4$ cathode material by coprecipitation technique [23]. Through hydroxide coprecipitation technique [300, 301], compared with oxalate precipitation technique or carbonate, some spherical cathode materials ($LiCoO_2$, $LiNiO_2$, $LiCo_{1/3}Ni_{1/3}Mn_{1/3}O_2$) with high tap density, better thermal stability and homogeneous particle size can be synthesized [23]. The high content of OH^- and Mn^{2+} is easy to form fine hydroxide precipitant nucleation [302], and the pure $LiNi_{0.5}Mn_{1.5}O_4$ cathode material with regular spherical morphology is hard to be prepared by hydroxide coprecipitation technique [23]. Spherical $LiNi_{0.5}Mn_{1.5}O_4$ cathode material had been efficiently synthesized through coprecipitation technique with the help of sodium hydroxide as ammonia as complexing

actor and precipitant [23]. Excellent electrochemical properties were shown by the prepared pure $LiNi_{0.5}Mn_{1.5}O_4$ cathode material with spherical morphology [23].

$LiFePO_4$ has low electrical conductivity ($\sim 10^{-11}$ S cm^{-1}) and low lithium ion diffusion dynamics ($\sim 1.8 \times 10^{-14}$ cm^2 s^{-1}) at room temperature (RT) [24, 303]. Two properties-small-sized cathode and homogeneous conductive coating-are thought to substantially improve the ionic and electric kinetics of $LiFePO_4$ under low temperature and foster −20 °C's low-temperature performance among multiple techniques to solve this issue [24]. The nano-scale size of $LiFePO_4$ and homogeneous carbon coating of 6.7 wt% by oleylamine medium and post-heat treatment for 4 h; this composite material, which is delivered excellent low-temperature performance, had been accomplished by Fan [24, 304]. Wu [305] devised a polyol route to fabricate two layers of carbon-coated nano-$LiFePO_4$ cathodes with mean primary particle size of ca 90 nm, which a later calcining process for 8 h to attain satisfactory low-temperature performances followed [24]. Uniform carbon coating and these nanosized commodities are responsible for the excellent low-temperature performance [24]. The production expenses of these mechanisms are fairly high because not just are the raw materials including Fe $(Cl)_2$ costly and Fe $(Ac)_2$, though also these soluble raw materials might give rise to low crystallinity of the commodities after liquid-phase decrease [24]. Such fine-sized particles below 100 nm might decline the tap density and give rise to inferior processing performance, which is utilized when commercially as cathodes for lithium batteries [24]. We have observed that $LiFePO_4$/C prepared by a polyol route retains a high capacity retention after 300 cycles [306] and an excellent room temperature performance with a high rate capability [24]. The low-temperature performance (0, −10, and −20 °C) of as-prepared $LiFePO_4$/C will be examined [24].

Since organic electronic tools are based upon thin films, flexibility, light weight, large-area application [307–310] including semitransparency, such materials showed their low processing and cost advantages [25]. CNTs have been intensively studied for their distinctive properties including 1D tubular structure, high thermal and electrical conductivities, exceedingly huge surface area and mechanical, optical properties since discovery in 1991 [25, 311]. The development of novel electrodes having a huge surface area, high electric/thermal conductions and a short diffusion is required to circumvent the drawbacks of traditional materials [25]. Shao et al. [312] has indicated the synthesis of SnO_2-based composite coaxial nanocables with multi-walled CNTs and polypyrrole (PPy), SnO_2@CNTs@SnO_2@PPy; these nanocables display a reversible capacity as high as 600 mAh g^{-1} and a columbic efficiency close to 100%, which is potential for practical application in lithium-ion batteries [25]. Zhao et al. [313] indicated the synthesis of a new CNTs@SnO_2@PPy coaxial nanocable as superior anode material with SnO_2 particle size of 2–3 nm, furthermore this composite showed a high capacity of 823 mAh g^{-1} after 100 cycles [25]. The combination of P3HT and CNTs might be interest materials for potential cathode materials in Li-ion batteries [25]. The approach to increase the dispersion of P3HT-g-CNTs in solution to form the nannocomposite, which additional utilized to combine with doped spinel $LiNi_{0.5}Mn_{1.5}O_4$ (LNMO) for fabrication of cathode materials as LNMO/P3HT-g-CNTs nano-composites in Li-ion batteries had been

summarized by us [25]. Through electrochemical impedance spectroscopy (EIS) and cyclic voltammetry (CV), the efficiency of the electrode materials employing LNMO/P3HT-g-CNTs nano-composites had been assessed [25].

Lithium-sulphur accumulators are one of the fruitful potential ways of commercial accumulators' development [26]. Practical use of lithium-sulphur accumulators is quite tempting due to the quite high theoretical capacity of sulfur-1675 mAh/g; this mAh/g, in combination with the potential around 2.1 V against lithium, means that its gravimetric energy density reaches about 3000 Wh/kg [26, 314, 315]. The theoretical capacity of sulfur is considerably greater than the capacity of currently readily available cathode materials as $LiMn_2O_4$ (148 mAh/g) [316], $LiNi_{1/3}Mn_{1/3}Co_{1/3}O_2$ (280 mAh/g) [151, 316, 317] or $LiFePO_4$ (170 mAh/g) [26, 318]. The fact that there is no intercalation process of lithium ions during conversion of materials though cycling happens during cycling is one of the largest difficulties of this accumulator kind [26]. A compound of sulfur and lithium-Li_2S (lithium sulfide) is the consequence of this conversion [26]. The resulting polysulphides, Li_2S_8 to Li_2S_4, are soluble in the electrolyte and they deposit on the anode surface of metal lithium during cycling which gives rise to a quite steep drop of the capacity during cycling [26, 319]. Its low electrical conductivity ($5 \cdot 10^{-30}$ S/cm), which results from the fact that sulfur is an insulator [320, 321], is an further drawback of the material [26]. Another possibility is to encapsulate sulfur with carbon; this carbon prevents the release of polysulphides into the electrolyte and increases electrical conductivity of the sulfur particles [26, 322, 323]. Such polymers are conductive and deter the break-up of polysulphides into the electrolyte and these materials have their own capacity [26, 324]. The creation of a special 3D cathode structure into which sulfur is enclosed, which prevents thereby the deposition of polysulphides at the anode side [325–327], is another possibility [26].

The olivine $LiFePO_4$ (LFP) has aroused more substantial attentions because of its stable performance, high capacity retention, excellent thermal stability, environment-friendly, and cheap since the first introduction to science community in 1997 [27]. Some synthesis procedures (e.g., ball-mill combination with solvothermal/hydrothermal) were indicated to give the practical capacity closely to theoretical value as 170 mAh/g [328] among various methodologies for improving the electrochemical performance of LPF material; these methodologies were previously indicated [27]. A detailed review of advancements of issues of $LiFePO_4$ and lithium-ion batteries as one fruitful cathode material had been carried out by Li and others [27, 329]. That significant progress was made in enhancing the electrochemical performance of $LiFePO_4$ cathode material by coating, doping supervalent cation, and minimization of particle size, had been concluded by previous reports [27]. The exact mechanism for increasing electronic electrical conductivity to comprehend the kinetic behaviour of $LiFePO_4$ synthesis is required [27, 330, 331]. Based on carbon coating appears to be efficient strategy to improve electrochemical performance of $LiFePO_4$, particularly at high charge-discharge rate [27]. The results were because of the wrapping of highly conductive thin rGO sheets; these sheets increasing the electronic electrical conductivity of the $LiFePO_4$ [27]. Several

researches which examined the electrochemical performance of $LiFePO_4$ composite by use of graphene are observed in [27, 332–335]. The transport properties should be greater, which depends additional on the mixing/coating of substances on molecular level [332] in order to derive the satisfactory electrochemical performance of cathode materials [27]. The principal issue is to synthesize the homogenous mixture of $LiFePO_4$ and C, and consequently, in situ techniques are required which motivated authors to examine its electrochemical performance and build a novel cathode material (nanocomposite) of $LiFePO_4$/C [27].

Lithium-ion batteries (Li-ion batteries) continue to power consumer electronics and are increasingly utilized in defense, aerospace, and automotive, applications due to their high energy density (Larcher and Tarascon [336]; Thackeray and others [337]) as a state-of-art energy storage system [28]. It is hard for sodium-ion batteries (SIBs) to compete with Li-ion batteries in compact applications because of lowered energy density, SIBs are considered as the most fruitful complements to Li-ion batteries for large-scale electrical storage applications (Palomares and others [338]), [28]. Mn-based cathodes for Li-ion batteries and a critical criterion for the development of future Fe-is to attain similar or even greater energy densities [28]. Through discharge potential and its Li storage capacity, the energy density of cathode material is dictated collectively [28]. Taking advantage of plentiful Na sources, SIBs hold the promise to support large-scale energy storage applications, which is critical in harnessing intermittent renewable energies including wind and solar power [28]. The research advancements on Fe- and Mn-based cathode materials for Li-ion batteries and SIBs, respectively, which are grouped into polyanion compounds, oxides, and hexacyanometalates (for SIBs) are presented by this review [28]. We additional put forth many insight into the opportunity of Fe- and Mn-based cathode materials and explore the impendent issues and prospects in this field with a grasp of the inherent properties and up-to-date accomplishments of these candidates, particularly highly stable SIB cathodes and high-energy LIB cathode candidates [28]. That this review can inform Mn-based cathode materials and readers of the rationality and priority of Fe-as candidates for future Li-ion batteries and SIBs, and call for additional efforts to satisfy this aim is hoped by us [28].

$LiNi_{0.5}Mn_{1.5}O_4$ has been acknowledged as one of the most tremendous high-voltage cathode materials for Li-ion batteries [29, 339, 340]. The electrolyte becomes instable and easy to be broken down at high voltage (4.7 V), leading to the formation of a deleterious solid electrolyte interface (SEI) film that inhibits the Li^+ ion migration and induces the capacity fading [341, 342] the practical application of the $LiNi_{0.5}Mn_{1.5}O_4$ material is restricted because $LiNi_{0.5}Mn_{1.5}O_4$ suffers from serious drawbacks: (1) and (2) the break-up of Mn ion degrades the quality of $LiNi_{0.5}Mn_{1.5}O_4$ cathode during cycling, resulting in the irreversible capacity deterioration [343, 344, 29]. A series of tactics have been undertaken to circumvent these shortcomings, such as surface modification and cation substitution in order to improve electrochemical properties of the $LiNi_{0.5}Mn_{1.5}O_4$ material [29]. Surface coating materials can deter the immediate contact between electrolyte and the spinel

$LiNi_{0.5}Mn_{1.5}O_4$ material so as to safeguard the active material from HF corrosion [29]. Some compounds, including metal oxides (e.g., ZnO [240, 345], Bi_2O_3 [346], Al_2O_3 [236]), metal phosphates (e.g., $FePO_4$ [347], $LiFePO_4$ [344]), and metal fluorides (e.g., AlF_3 [348], MgF_2 [349], BiOF [350]), have been utilized as a coating film of $LiNi_{0.5}Mn_{1.5}O_4$, leading to the amelioration in cyclic stability of the $LiNi_{0.5}Mn_{1.5}O_4$ materials and the rate performance [29]. An optimal electrode material for Li-ion batteries because of its high reversible capacity, huge theoretical Li-storage capacity of 770 mAh g^{-1} (9 mol Li could be stored in 1 mol $BiFeO_3$) [351, 352], and excellent capacity retention, is $BiFeO_3$ [29]. Given the semiconductor character of $BiFeO_3$ and the excellent electrochemical properties, it could be reasonably anticipated that the surface coating of $BiFeO_3$ might enhance the electrochemical properties of $LiNi_{0.5}Mn_{1.5}O_4$ cathode material [29]. Through a $BiFeO_3$ coating on the spinel $LiNi_{0.5}Mn_{1.5}O_4$ through moist chemical technique and a combined coprecipitation, the cathode materials were obtained [29]. It had been demonstrated that the coating of $BiFeO_3$ can improve the electrochemical performance of coated materials [29].

The layered lithium transition metal oxides have been intensively examined as the cathode materials in the next generation of the rechargeable lithium-ion battery (LIB) [30, 223, 353]. In contrast with the commonly used layered ternary or $LiCoO_2$ cathode materials with α-$NaFeO_2$ structure, layered Li-rich Mn-based ones constituted as $yLi_2MnO_3{\cdot}(1–y)LiMO_2$ (M = Co, Ni, Mn, etc.) or $Li[Li_{(1/3–2x/3)}M_xMn_{(2/3–x/3)}]O_2$ have many advantages including lower cost, safer on overcharge [194, 354, 355], and less toxic [30]. They have high capacities about 250 mAh g^{-1} at high voltage, which can play a key role in stabilizing the electrode structure [189, 194] and supply the excess lithium to the layered structure [30]. Such coatings are usually unfavourable for both lithium ion conduction and interfacial charge transfer of the electrode, because above insulative coatings can increase the Li^+ diffusion length, which results in the deterioration of electrochemical performance [30, 356, 357]. Nano-sized monoclinic Li_2TiO_3 has a high AC electrical conductivity of 10^{-3} S cm^{-1} [358], considerably greater than that (10^{-6} S cm^{-1}) of the layered Li-excess Mn-based oxides [30, 359]. 2.5×10^{-7} S cm^{-1} [360], considerably greater than that (10^{-16}–10^{-12} S cm^{-1}) of the layered Li-rich Mn-based ones [361, 362] because of the meager lattice and electrical conductivity disorder of Li_2MnO_3 domain is the Li^+ ion electrical conductivity of Li_2TiO_3 [30]. Li_2TiO_3 has a 3-D diffusion path for lithium ion diffusion, where the Li^+ migration can occur along c-direction [357, 363] as a layered material [30]. The impact of the Li_2TiO_3 loading on the rate capability and cyclability of the Li-rich layered oxide had been especially tackled [30].

Nickel-rich layered $Li(Ni_{1–x–y}Mn_xCo_y)O_2$, whereby the composition of Ni is hegemonic over Mn and Co, is a fruitful material due to its lower cost, lesser toxicity, enhanced thermal stability, safety [364–367], and sound cycling stability [31]. High capacity is provided by Ni, Mn establishes an excellent cycling stability, because of co's sound chemical and electrochemical stabilities when electrolyte contact happens, and Co offers an increasing electrical conductivity that affects rate performance, in these materials [31]. The electrochemical performance of Ni-rich

materials still needs to be additional enhanced [31]. The serious capacity fading of Ni-rich materials during cycling, particularly those materials with high cut-off voltage, is because of the comparatively meager low diffusion and electronic electrical conductivity rate of Li^+ within the structure [31, 368]. A handful studies on Na-doped layered Li-rich materials have been carried out [31]. Ni-rich cathode materials have not yet been examined whilst both of these groups indicated that Na doping had been efficient for improving the rate capability, systemic properties of Na-doped, layered and the impacts of Na^+ on the cycling performances [31]. We examined the impacts of Na doping on the structure, electrochemical performances of the Ni-rich cathode material, and morphology, and explore the details [31].

Layered $LiMO_2$ (M = Mn, Co, Ni), $LiNi_{0.3}Mn_{0.3}Co_{0.3}O_2$, olivine-type $LiFePO_4$, spinel-type $LiMn_2O_4$, lithium-rich material $xLi_2MnO_3{\cdot}(1{-}x)LiMO_2$ (M = Co, Fe, $Ni_{1/2}Mn_{1/2}$), etc. are the principal cathode materials for rechargeable lithium-ion batteries [32]. Throughout the cycling process [369–373], coating the cathode material with multiple particles or films such as SiO_2, ZnO, CeO_2, LaF_3, $FePO_4$, etc. can efficiently minimize the direct contact area between electrolyte and additional hinder the Mn break-up and the $LiMn_2O_4$ electrode [32]. ZnO had been viewed as an advantageous surface-coating material because of thermal stability and its excellent chemical [32]. Some researches of ZnO-coated $LiFePO_4$, $LiMn_{1.5}Ni_{0.50}O_4$, $LiMn_2O_4$, and $LiNi_{0.5}Co_{0.2}Mn_{0.3}O_2$, have been indicated by employing various coating methods to enhance their electrochemical performance [32, 374–378]. Via the melting impregnation technique, ZnO had been coated by Tu and others [379] on $LiMn_2O_4$ particles [32]. ZnO-coated $LiMn_2O_4$ had been indicated by Liu and others [370] by the sol-gel technique [32]. An mean capacity deterioration of 0.19% per cycle in 50 cycles under a current rate of 0.5 Zhao, C. More recently and others [380] utilized the ALD technique to deposit highly conformal and ultra-thin ZnO coatings onto $LiMn_2O_4$ cathodes had been delivered by the 2 wt% ZnO-coated $LiMn_2O_4$ [32]. There are no reports on ZnO-coated $LiMn_2O_4$ cathode materials prepared by a combustion technique till date to the optimal of our knowledge [32]. ZnO had been sampled for coating over the surface of $LiMn_2O_4$ cathodes to additional enhance cycling performance and their capacity [32]. The impacts of coating on the structure, electrochemical performance of cathode materials, and morphology, are examined in detail [32].

Layered $LiNi_{1/3}Co_{1/3}Mn_{1/3}O_2$ as cathode material has been paid extensive attention because of its high reversible capacity, low cost, and excellent systemic, thermal stability, as reasonably well [33, 223, 381]. Serious problems concerning the capacity must be circumvented for their additional application, which would consequence from the decomposition of electrolyte at the high operating voltage, hydrofluoric acid (HF) attack in $LiPF_6$-based electrolyte, and stage transition, particularly at temperature [382, 383], which is elevated, even though tremendous progress has been made in layered $LiNi_{1/3}Co_{1/3}Mn_{1/3}O_2$ as much inferior rate performances and fading [33]. Tremendous efforts have been dedicated to the amelioration of the cyclic stability and thermal stability for layered $LiNi_{1/3}Co_{1/3}Mn_{1/3}O_2$ by coating with carbon or conducting materials, doping with metal ions, and reducing the particle size [33]. Liu and others [384] have confirmed that the

surface modification of $LiNi_{1/3}Co_{1/3}Mn_{1/3}O_2$ with $FePO_4$ indicates high discharge capacity of 143 mAh g^{-1} with a retention of 87.7% at a current density of 150 mAh g^{-1} after 100 cycles [33]. The inherent semiconducting behaviour of metal oxide might consequence in the meager rate performances and increase the electrical resistance among $LiNi_{1/3}Co_{1/3}Mn_{1/3}O_2$ particles [33]. High electronic electrical conductivity of coating layer must be highly advantageous for high rate lithium batteries besides the protection from HF attack in electrolyte [33]. Owing to its injecting photocurrent behaviours by irradiates, Eu_2O_3 is regarded as a fruitful coating layer for examining the link between coating layer electrical conductivity and the enhanced performances, and even for potential application in novel notion batteries [33]. Eu_2O_3 material has excellent thermal stability, refractory properties, and chemical stability [33]. $LiNi_{1/3}Co_{1/3}Mn_{1/3}O_2@Eu_2O_3$ present enhanced thermal stability and considerably better electrochemical performances [33].

Significant attention has been paid to lithium-rich manganese-based layered structure electrode materials [usually designated as $xLi_2MnO_3{\cdot}(1-x)LiMO_2$ (M = Ni, Co, Mn, etc.)] and has been one of the most fruitful energy storage tools for large-scale applications because of their high power density, long calendar life (Yuan and others [385]; Zhou and others [386]; Jin and others [387]) and huge theoretical specific capacity ($\sim$250 mAh g^{-1}), [34]. That lithium-rich layered materials are comprised of Li_2MnO_3 element and $LiMO_2$ element to form a homogeneous solid solution structure (Lee and Manthiram [388]; Tabuchi and others [389]) is usually thought by scholars [34]. Upon the activation of the Li_2MnO_3 element which refers to an irreversible potential platform for the extraction of Li and oxygen (as Li_2O) by initially charging to 4.5 V (Nayak and others [390]; Li and others [391]), the lithium-rich layered materials display a high discharge specific capacity [34]. In the subsequent discharge/charge process, the transition metal ions occupy oxygen vacancies formed during the activation process and seem to migrate to the octahedral vacancies in the lithium layers via the adjoining tetrahedral sites, resulting in the reconstruction of the surface layer structure (Zheng and others [392]; Chen and others [393]; Zheng and others [394]), [34]. Rate performance of lithium-rich layered materials and the unsatisfactory cycle performance need to be additional enhanced [34]. The surface coating of lithium-rich layered cathodes can offer a physical protective layer to change their surface chemistry, improving the electrochemical properties of these cathode materials (Chen and others [395]; Zhao and others [396]; Li and others [397]), [34]. It is indicated that $FePO_4$-coated cathode material $Li_{1.2}Mn_{0.54}Co_{0.13}Ni_{0.13}O_2$ (Wang and others [398]) for delivering a discharge specific capacity of 202.6 mAh g^{-1} between 2.0 and 4.8 V at 0.05 C with a high coulomb efficiency of 85.1% after 100 cycles [34]. That excellent electrochemical performance had been attributable to the coating layer to electrochemical performances of Al_2O_3 coated $Li_{1.2}Mn_{0.54}Co_{0.13}Ni_{0.13}O_2$ materials and additional research the structure [34].

The capacity deterioration upon cycling at elevated temperatures (55 °C) of $LiMn_2O_4$ is still an obstacle for its practical application, which results from the synergetic effect of following possible processes [169, 399–402]: (1) Mn^{2+} break-up into the electrolyte through the disproportionation reaction of

$2Mn^{3+} \rightarrow Mn^{2+} + Mn^{4+}$, (2) irreversible systemic reconfiguration which is caused by Jahn-Teller distortion, and (3) the thermal decomposition of electrolyte at high voltages [35]. Doping with transition metal (Al [403, 404], Mg [405, 406], Ni [407], Co [408, 409], Cr [410]) is utilized to enhance its performance at temperature, which is elevated, and sustain the structure of $LiMn_2O_4$ [35]. One common strategy is coating with metal oxides including Al_2O_3 [411], Fe_2O_3 [412], TiO_2 [413], Y_2O_3 [414], and V_2O_5 [415] to lessen the electrochemically active surface area and deter undesired side reactions between cathode material and electrolyte [35]. The intercalation/de-intercalation of lithium ion will be hampered by those metal oxides, so it is required to seek for an optimal coating layer to improve the interfacial stability of $LiMn_2O_4$ electrode without influencing the Li ions' transfer between electrolyte and electrode [35]. Electrode material like $LiNi_{0.5}Mn_{0.5}O_2$ [416], $LiNi_{1/3}Co_{1/3}Mn_{1/3}O_2$ [417], $LiNi_{0.5}Mn_{1.5}O_4$ [418] as surface coating layer for $LiMn_2O_4$, and $LiNi_xMn_{2-x}O_4$ [419], has drawn the attention of persons [35]. That Li_2MnO_3 can act as a stabilized coating layer on the surface of other cathode materials to safeguard those materials from directly exposing to the electrolyte without impeding the intercalation/de-intercalation of lithium ion had been anticipated by us [35]. We report a facile technique to synthesize $LiMn_2O_4$@ Li_2MnO_3 composites with multiple coating content, then the Li_2MnO_3 stage had been coated on the surface of the spinel, which a sol-gel route $LiMn_2O_4$, and in which the pristine $LiMn_2O_4$ powder had been fabricated through a characteristic high-temperature solid-state reaction [35].

The most fruitful candidate among the 5 V cathode materials for Li-ion batteries because of its flat plateau at 4.7 V [232], a two-electron process Ni^{2+}/Ni^{4+}, and huge specific capacity (146.6 mAh g^{-1}), where the Mn^{4+} ions remain electrochemically inactive [339, 420] is the high-voltage $LiNi_{0.5}Mn_{1.5}O_4$ (LNMO) cathode [36]. LNMO had been systematically studied and extensively examined as a sort of HVLIB cathode material [36]. The advancements in the doping of LNMO cathode material for 5 V Li-ion batteries, in which the rate capability, cyclic life of multiple doped LNMO materials, and rate performance, were explained were indicated by Yi and others [36, 421]. The progress in high-voltage cathode materials and corresponding matched electrolytes, in which they introduced LNMO as high-voltage cathode materials had been presented by Hu and others [36, 291]. Zhu and others [422] emphasised the advances in the development of advanced electrolytes for enhancing the cycling stability and rate capacity of LNMO-based batteries [36]. The advantages of LNMO as the HVLIBs cathode, electrolytes, etc. or the modification techniques of doping were just outlined by these reviews [36]. It is required to compare various modification techniques based upon cyclic degradation processes of LNMO and the architectural elements and observe an efficient technique to enhance the cycle performance of LNMO [36]. Focus is given to the methodologies to enhance the cycling stability of LNMO, which is based upon the synthesis of highly purified LNMO, systemic reversibility of and cycling degradation mechanism of undesirable reactions between electrolyte and LNMO [36].

$LiCoO_2$ has been the primary cathode material in commercial lithium-ion batteries since 1992 [37]. A doping technique, which employs Mg^{2+}, Al^{3+}, Ti^{3+}, Cr^{3+} or other ions, is clear-cut considerably more and helpful to enhance the properties of lithium-ion batteries [423–427], which is because the doping technique can lower the extent of Li/Ni cation mixing and ameliorate voltage degradation [37]. That Ti-ion and Al-ion were utilized to prepare $LiNi_{0.5}Mn_{0.45}Ti_{0.05}O_2$ and $LiNi_{0.475}Al_{0.05}Mn_{0.475}O_2$, and in turn, the discharge capacity had been enhanced the extent of Li/Ni cation maxing of the $LiNi_{0.5}Mn_{0.5}O_2$ is 9.8% which lowers to 4.8 and 5.1% by Al-doping and Ti-doping, respectively; and the cycle stability had been enhanced [428] is indicated by Myung and others [37]. That Mg-ion had been replaced for Ni-ion in $LiNi_{0.5}Mn_{0.5}O_2$, which can keep the structure stable because of the greater bond of dissociation energy of Mg–O (394 kJ mol^{-1}) than that of Ni–O (391.6 kJ mol^{-1}), enhancing the cycle stability [429] is devised by Xiao and others [37]. Ca^{2+} is replaced for Ni^{2+} to produce a series of $LiNi_{0.5-x}Ca_xMn_{0.5}O_2$ ($0 \leq x \leq 0.2$) cathode materials employing a combination of coprecipitation and O a solid-state technique because of the greater bond of dissociation energy of Ca-and the effect on declining the extent of Li/Ni cation maxing in the present study [37]. The amelioration of the electrochemical properties from Ca-doping is attributable to the increasing stability of the structure, lower Li/Ni cation, which mixes, lowered polarization, which is declined enhanced the migration rate of the Li-ion and migration resistance [37].

Scholars have been attempting to synthesize materials which can operate at a potential of Zhang, greater than 4.3 V. More recently and others indicated a core-shell-structured $LiNi_{0.5}Co_{0.2}Mn_{0.3}O_2$ comprised of a shell of $(Ni_{1/3}Co_{1/3}Mn_{1/3})_{3/14}(Ni_{0.4}Co_{0.2}Mn_{0.4})_{1/2}](OH)_2$ [430] and a core of $(Ni_{0.8}Co_{0.1}Mn_{0.1})_{2/7}$ to improve the energy density of batteries [38]. At a current density of 18.5 mA g^{-1}, this material delivered a comparatively low capacity of 200 mAh g^{-1} and preserved 95% of its capacity when cycled for 40 cycles to an upper cutoff voltage of 4.5 V. Arguably, the spinel shell of $Li_{1+x}[CoNi_xMn_{2-x}]_2O_4$ enhanced its stability; even when the material had been charged to high potential of 4.5 V, it delivered just 200 mAh g^{-1} at 18 mA g^{-1} [38]. That they indicated Thackeray and others Li_2MnO_3 plays a main role in supporting the structure stability during the discharge/charge process, and preparing lithium-rich layered oxide materials (LLOs) xLi_2MnO_3–$(1-x)LiMO_2$ can consequence in high electrochemical capacity $\sim$250 mAh g^{-1} if charged to high potentials >4.6 V, had been indicated by Thackeray and others [38]. We have indicated that manganese oxide shell can substantially enhance the cyclic stability of $LiMO_2$ [431] nickel-rich layered materials, and replacing a small quantity of lithium with sodium can increase the discharge capacity of the material [38, 431, 432]. Since it is a lithium-rich material, this core-shell material delivers quite high discharge capacity, and this material is thermally stable, Li_2MnO_3 is electrochemically active at a potential greater than 4.5 V. Furthermore and could be safely cycled at a high potential of 4.7 V and delivers a considerably greater mean potential and a greater energy density than that of traditional Ni-rich materials [38].

Through the cathode materials, rechargeable lithium-ion batteries (LIB)'s performances, including voltage and capacity, are predominately dictated as one of the most fruitful energy storage tools [39]. The $xLi_2MnO_3{\cdot}(1-x)LiNi_{1/3}Co_{1/3}Mn_{1/3}O_2$ series compounds of the cathode materials in lithium-ion batteries have brought about a considerable explosion in researches because of the high capacities, low cost, and lowered toxicity [39]. The $xLi_2MnO_3{\cdot}(1-x)LiNi_{1/3}Co_{1/3}Mn_{1/3}O_2$ series compounds of the cathode materials in lithium-ion batteries are regarded as viable alternatives compared with traditional $LiCoO_2$ cathode materials [433, 434], as reasonably well [39]. Surface coating, including $AlPO_4$, CaF_2 [84], CeF_3 [435], and graphene [436] coating on the surface of the cathode materials, can restrain the undesirable reactions between cathode materials with electrolyte [39]. Metal element doping, including Al, Zr [194], Y, Mo, and Mg [437] replaced for the transitional metal elements in the oxide materials, can weaken the adverse change of crystal structure [39]. Cycling performance and systemic stability of cathode materials, which are revealed by some inquiries [262, 434] could be enhanced by these techniques [39]. We attempt to substitute traces of Al element for various transitional metal elements of $Li_{1.2}Mn_{0.54}Ni_{0.13}Co_{0.13}O_2$, in order to enhance the electrochemical performance of the Li-rich materials [39]. The structure, electrochemical performance of the pristine, and morphology, and Al-doped materials have been typified [39].

High stable reversible capacity of >250 mAh g^{-1} when it is cycled in the voltage window of 2.5–4.8 V [194, 438–443] is delivered by LMR-NMC [40]. Throughout cycling need to be tackled before it is regarded as a potential candidate for next generation cathode material for lithium-ion batteries [194, 437–443], the energy deterioration because of suppression of voltage profiles during cycling which is linked with the stage reconfiguration from a layered structure to spinel structure, capacity, and high irreversible capacity, fade [40]. That the substitution of 6 mol% of Al^{3+} ions with Ni $[Li_{1.15}(Ni_{0.275-x/2}Mn_{0.575-x/2}Al_x)O_2]$ and Mn can avoid the systemic deterioration of electrode material, which enables higher discharge capacities of 210 mAh g^{-1} at a cut off voltage of 2.5–4.6 V, whilst the undoped cathode delivers 150 mAh g^{-1} [444] had been confirmed by Park and others [40]. Through partial substituting 4% of Mg with $[Li(Li_{0.2-2x}Mg_xCo_{0.13}Ni_{0.13}Mn_{0.54})O_2]$ lithium in transitional metal layer and delivers an initial capacity of 272 mAh g^{-1} (between 2.0 and 4.8 V) and preserves 93% of capacity after 300 discharge/charge cycles [445], Wang and others stabilized the crystal structure [40]. Improvement in electrochemical performance, thermal stability, rate capability, and tap density of NMC by substituting partially oxygen with fluorine which results stabilization of the crystal lattice structure [446–453] because of smaller c-axis variability and fluorine coatings had been indicated by Kim and others [40]. Kim and others explained both magnesium and fluorine substitution in NMC $[Li(Ni_{1/3}Co_{1/3}Mn_{1/3-x}Mg_x)O_{2-y}F_y]$ and asserted decrease in cation, which mixes during amelioration in crystallinity, cycling, and tap density this density in turn impact the amelioration in thermal stability [446, 451] and capacity retention; this density in turn impact the amelioration in thermal stability [446, 451] and capacity retention [40].

$LiCoO_2$ one of the layered structure cathode material has been commonly used as cathode materials in commercial applications [41, 454]. Nevertheless; the requirements for high energy applications could be not fulfilled by this cathode material since, even though its theoretical capacity is 274 mAh/g, the practical capacity in applications roughly 150 mAh/g by charging up to 4.2 V [41, 454, 455]. Of all cathode materials NMC's ($LiNi_{1-x-y}Mn_xCo_yO_2$) are mainly researched materials because of their high discharge capacity, satisfactory systemic stability [456] and high rate capability [41]. Another of these constraints is that NMC cathode materials indicate undesireable irreversible capacity deterioration during first charge-discharge [41, 457]. That due to an overlap of the metal: 3d band with the top of the oxygen: 2p band, layered oxide cathode materials seem to loose oxygen from the lattice at consequence in a tremendous capacity deterioration [458] and deep charge had been asserted by Choi and others [41]. One restriction is that when $LiPF_6$ which is the crucial element of electrolyte decomposes in the existence of moisture, one of the product is HF; this HF gives rise to transition metal break-up in electrolytes resulting surface corrosion of cathode material [41, 459]. The reactions between electrolytes and cathode materials decreases capacity and cyclic performance of the battery [41, 455]. Surface modification can deter the reactions between cathode materials and electrolytes and can lessen the oxygen activity of the cathode at high voltages [41, 455, 460]. It is indicated that Al_2O_3 coating lowers capacity difference between discharge and cathode surface corrosion [461] and first charge [41]. The goal of the investigation is examining the effect of sonication power on alumina distribution on the $LiNi_{0.5}Mn_{0.3}Co_{0.2}O_2$ cathode materials and examining cathode performance [41].

More than 270 mAh g^{-1}, though just half of this capacity could be delivered because of the inherent systemic turbulence of the LCO material in a high delithiated state and interfacial turbulence between the electrode and electrolyte [462, 463] is the theoretical specific capacity of LCO [42]. It has been observed that surface coating had been an efficient approach to enhance electrochemical performance of cathode materials [42, 464, 465]. The surface coating indicates considerable advantages on suppressing the break-up of Co into the electrolyte and the decomposition of the electrolyte and altering the LCO surface chemistry to sustain the structure at high cut-off voltage [42]. Numerous coating materials primarily include (1) metal oxides, including ZrO_2 [466–469], and Al_2O_3, ZnO, can act as the HF scavenger and which are electrochemically inactive; (2) phosphates and silicates [357, 470], which are beneficial to enhance thermal stability of bulk materials and the overcharge safety; and (3) fluorides and other materials, including AlF_3, MgF_2, and AlW_xF_y [471–473], which is useful for enhancing the systemic stability of LCO materials at high cut-off voltage [42]. That the AZO-coated LCO electrodes delivered a greater reversible capacity of 112 mAh g^{-1} at 12 C (1680 mA g^{-1}) between 3.0 and 4.5 V versus Li^+/Li than ZnO-coated electrodes had been demonstrated by the results [42]. It means that the coating layer with electron transport or enhanced lithium-ion might be efficient to enhance the electrochemical performance of $LiCoO_2$ at high cut-off voltage [42]. Based on 0.5–4, the $LiCoO_2$ cathode materials coated with multiple quantities of $NaAlO_2$ wt [42].

High power lithium-ion rechargeable batteries and enhanced high capacity is needed by these applications [43]. A wide range of cathode materials have been devised to satisfy the expanding requirement for high power lithium-ion batteries and high capacity, though just handful of them have cycle stability and high specific capacity [43]. Due to electrochemical properties and a better cycling stability, Co and Al co-substituted material ($LiNi_{0.8}Co_{0.15}Al_{0.05}O_2$) is regarded as one of the most fruitful candidates as positive electrode materials for high-power lithium-ion batteries [43]. $LiNi_{0.8}Co_{0.15}Al_{0.05}O_2$ as a cathode material for automotive applications has been a commercial success ever since the inception of Tesla [43]. $LiNi_{0.8}Co_{0.15}Al_{0.05}O_2$ with compositionally homogenous mixing at the atomic level and micron-sized spherical particle with narrow size distribution is readily obtained by coprecipitation, and this technique has been utilized for the commercial synthesis of $LiNi_{0.8}Co_{0.15}Al_{0.05}O_2$ cathode material [43]. It is of paramount importance to build a straightforward, effective, and rapid, synthesis approach to allow large-scale synthesis of $LiNi_{0.8}Co_{0.15}Al_{0.05}O_2$ cathode material, without compromising its electrochemical performance [43]. Solid-state technique is useful for large-scale production of cathode materials for lithium-ion batteries because it is cost-efficient and straightforward [43]. That the electrochemical properties of Ni-rich cathode material, which traditional solid-state technique prepared, are not good, which is primarily attributed to the inhomogeneous distribution of transition metal ions, despite repeated mechanical ball milling before calcining is confirmed by these results [43]. The Ni–Co–Al oxide precursor based on the decomposition of oxalates displays small particle size, which is beneficial to the mixing with lithium source and a porous and loose structure [43]. Through traditional solid-state technique, the $LiNi_{0.8}Co_{0.15}Al_{0.05}O_2$ cathode material is synthesized, as reasonably well [43].

That they indicated Thackeray and others Li_2MnO_3 plays a main role in systemic stability during the charge-discharge process, and preparing lithium-rich layered oxide materials (LLOs) xLi_2MnO_3–$(1-x)LiMO_2$ can produce high electrochemical capacities of $\sim$250 mAh, which is charged g^{-1} when to high potentials of >4.6 V, had been indicated by Thackeray and others [44]. Kim and others' results revealed that the pristine material delivered a discharge capacity of $\sim$200 mAh g^{-1} at 0.5 C and preserved 85% of its capacity after 30 cycles in the potential variety 2–4.6 V, whilst the material, which is surface-modified and fluorine-doped, preserved 92% of its capacity when cycled under the identical conditions [44, 474]. The aims of the present study were (1) to enhance the thermal stability of this material by making it a core-shell structured material with a core of $LiMO_2$ and a shell of Li_2MnO_3, and (2) to increase the discharge capacity of NCM 111 by preparing NCM 111 with the formula xLi_2MnO_3–$(1-x)LiMO_2$, i.e., a lithium-rich material with a high capacity [44, 194]. Li_2MnO_3 has two advantages: this material can increase the systemic and thermal stability of the material during the charge-discharge process [474–476], and this material can partake in the electrochemical reactions at potentials >4.5 V, resulting in greater capacities, in this structure [44]. Since potentials greater than this can give rise to a rapid decline in systemic disintegration [477] and capacity, whilst the core-shell material can be

cycled to an upper cut-off potential of 4.7 V with high stability, the pristine subsample had been charged by us to an upper cut-off potential of 4.5 V [44].

Lithium intercalation compounds based upon manganese oxides are safer cheaper, and, provide an especially appealing replacement for the latter compound as a cathode material in Li-ion batteries [478–481] and less toxic than the layered compound, which is based upon cobalt or nickel oxides [45]. Of the lithium manganese oxides cathode materials researched, layered oxides ($LiMnO_2$), spinel oxides ($LiMn_2O_4$), and Li-rich Mn-based layered compounds [$Li_2MnO_3{\cdot}LiMO_2$ (M = Mn, Ni, Co)] cathodes have been devised and extensively examined [45, 97, 482–487]. Due to their high theoretical capacity (285 mAh g^{-1}), layered $LiMnO_2$ compounds have come to be of interest as cathode material, though layered $LiMnO_2$ is not thermodynamically stable, which is readily converted to a spinel-like structure during electrochemical extraction/insertion of Li ions [45, 488]. Li-rich Mn-based layered compounds have been regarded as one of the most fruitful cathode material for future Li-ion batteries due to their advantage of high reversible capacity (>200 mAh g^{-1}), which is charged when above 4.5 V [45, 476, 489–491]. Throughout the first charge, a common characteristic of Li-rich Mn-based layered compound cathode is an irreversible high voltage plateau at around 4.5 V versus Li/Li^+ [45], Preliminary discharge capacity values of this materials are usually high after activation of Li_2MnO_3 stage, though inherently inferior rate capability and cycling turbulence are detected in all reports [45, 479, 492, 493]. It might be beneficial to reinvestigate the properties of Li_2MnO_3 material to help additional understanding of the properties of Li-rich Mn-based layered compounds [45].

Owing to high-performance rechargeable batteries' high voltage, high specific capacity, excellent and other advantages, lithium-ion batteries (Li-ion batteries) are viewed as the most likely power sources for electric vehicles [46]. Great efforts have been made to maximize the cathode materials with high energy densities [182, 494, 495] because the performances of lithium-ion batteries are largely dictated by the cathode materials [46]. The primary strategy to enhance the energy density of batteries is to build cathode materials with greater operating voltages [496, 497] and high capacity [46]. A competitive candidate of the active cathode material due to its low cost, high specific capacity [498, 499], and low toxicity, is layered nickel-rich oxide $LiNi_{0.5}Co_{0.2}Mn_{0.3}O_2$ (NCM523) [46]. An efficient approach to enhance the electrochemical performance of $LiNi_xCo_yMn_{1-x-y}O_2$ is coating the powder particles with many metal oxides including CeO_2 [500], and Al_2O_3 [501], ZrO_2 [46, 502]. Lithium-containing oxides, including $LiTiO_2$ [503], Li_3VO_4 [504], Li_2SiO_3 [505], and Li_2ZrO_3 [506], have been extensively examined as the coating materials because offer 3-D paths for the migration of lithium ions during the charge and discharge process [357] though they not just provide a protective layer against side reactions on the surface [46].

The cathode material had been an essential part of lithium-ion battery [47]. Ni-rich layered oxide $LiNi_{0.8}Co_{0.1}Mn_{0.1}O_2$ is regarded as one of the most fruitful cathode materials, because $LiNi_{0.8}Co_{0.1}Mn_{0.1}O_2$ has lower cost and bigger reversible specific capacity ($\sim$200 mAh g^{-1}) and is more environment-friendly [507–512] among multiple types of the cathode materials [96, 493, 513, 514, 47].

The nickel-rich material has a highly water absorption issue, resulting in an impurity stages ($LiOH/Li_2O$) on the particle surface; this surface triggers an irregular thickness on Al foil, which coates cathode material [47]. That the coating should be thick sufficiently had been founded by scholars and can not respond with the raw material [47]. The $LiAlO_2$ as the coating material has been utilized for some cathodes, including $LiNi_{0.4}Co_{0.2}Mn_{0.2}O_2$, and the $LiAlO_2$-coated material displays better electrochemical performance, and $Li[Li_{0.2}Mn_{0.54}Co_{0.13}Ni_{0.13}]O_2$, $LiNi_{1/3}Co_{1/3}Mn_{1/3}O_2$ [47]. An excellent coating material comparable to the layered structure of $LiNi_{0.8}Co_{0.1}Mn_{0.1}O_2$ materials [515, 516] is the α-$LiAlO_2$ [47]. $LiAlO_2$ retains satisfactory lithium-ion electrical conductivity due to the material, which is inhabited partly, internal lithium ion sites [47, 517]. Thermal stability and the cycling stability at a high temperature of $LiAlO_2$-coated $LiNi_{0.8}Co_{0.1}Mn_{0.1}O_2$, which hydrolysis obtained, -hydrothermal were investigated in detail [47]. A hydrolysis-hydrothermal strategy for the successful preparation of $LiAlO_2$-coated $LiNi_{0.8}Co_{0.1}Mn_{0.1}O_2$ cathode material is indicated by us [47]. The impurity stages ($LiOH/Li_2O$) on the surface of $LiNi_{0.8}Co_{0.1}Mn_{0.1}O_2$ are discarded as raw materials to synthesize a novel $LiAlO_2$ coating layer [47]. In contrast with conventional coating materials, the $LiAlO_2$ coating layer not just inherited the advantages of Al^{3+} doping though also discarded the impurity stage on the raw materials [47].

Research in the field of Li-ion batteries is revolved around the development of systems with increased energy and longer life and power density; with the goal of employing Li-ion batteries as a power source for pure electric (EV) [435] or hybrid vehicles (HEV) [48]. In recent decades, a significant number of research groups worldwide have invested considerable effort to enhance the electrochemical properties of materials previously utilized and build novel materials for electrolytes (ionic liquids, polymeric electrolyte, inorganic solids) and separators positive electrodes (oxides, phosphates), negative (various kinds of carbon, alloys, etc.); these electrodes have better performance in terms of energy, power, cost, validity, time of life, and safety [48]. A series of fluorophosphates materials including $LiVPO_4F$ [518], $Na_3V_2(PO_4)_2F_3$ [519], $NaVPO_4F$ [520], and Li_2MPO_4F (M = Fe and Co) [251], have demonstrated tremendous promise as possible replacements for the current generation of materials [48]. Through solid-state carbothermal decrease (CTR), which employs two-stage reaction process involving VPO_4, the electrochemical properties of NASICON-type $Na_3V_2(PO_4)_2F_3$ were investigated by Gover and others [519], it had been prepared as intermediate and followed by reaction with NaF [48]. More than 90% of the specific capacity had been preserved by the material, so it might be of interest to enhance the detected electrochemical properties of this stage [48]. Another way to improve the electrochemical properties is to investigation the aliovalent doping [521], positive impacts detected, such as enhanced electric conductivity and structure stability attributed and for instance, the impacts of the vanadium substitution with other elements (Mg^{2+}, Co^{2+}, Al^{3+}) in various materials including $Li_3V_2(PO_4)_3$ have been examined [48, 522]. The effect of Al substitution on the electrochemical and systemic properties of cathode materials have been examined [48].

Owing to its high capacity, low toxicity [523, 524], and excellent thermal stability, cheap, the $LiNi_xCo_yMn_{1-x-y}O_2$ might be supposed to substitute the conventional $LiCoO_2$ cathode material in the next generation of lithium-ion battery [49]. The hydroxide precursor $Ni_xCo_yMn_{1-x-y}(OH)_2$ for the $LiNi_xCo_yMn_{1-x-y}O_2$ cathode materials are primarily synthesized through coprecipitation, which employs $NH_3{\cdot}H_2O$, as chelating actor [49, 525]. He and others [526] have indicated that the hydroxide precursor $Mn(OH)_2$ had been synthesized employing citric acid and oxalic acid as the chelating actor to control the activity of Mn^{2+} in the solution, and then the spherical spinel $LiMn_2O_4$ cathode materials with tap density as high as 1.9 g cm^{-3} and the initial discharge capacity, which reachs 116 mAh g^{-1} were obtained [49]. Zhang and others [527] and Zhao and others [528] have indicated that the sol-gel synthesis of $LiNi_{1/3}Mn_{1/3}Co_{1/3}O_2$ and $Li[Li_{0.2}Co_{0.13}Ni_{0.13}Mn_{0.54}]O_2$ had been carried out employing tartaric acid (TA), oxalic acid, and then suggested that the tartaric acid-derived cathode materials owns excellent columbic efficiency, and succinic acid (SA) as chelating actors [49]. Zhou's group [290, 529, 530] indicated that the spherical cathode materials with excellent electrochemical properties were synthesized employing oxalic acid as chelating actor [49]. The quasi-spherical hydroxide precursor $(Ni_{0.5}Co_{0.2}Mn_{0.3})(OH)_2$ has been synthesized employing sodium lactate as chelating actor through coprecipitation technique [531], and the corresponding cathode materials display stable cycleability and satisfactory rate capability [49]. The impact of lactic acid concentration on the structure and electrochemical performance of $LiNi_{0.5}Co_{0.2}Mn_{0.3}O_2$ cathode material has not yet been investigated till now [49]. Lactic acid had been utilized to synthesize the spherical $LiNi_{0.5}Co_{0.2}Mn_{0.3}O_2$ cathode materials in here [49].

Due to operating voltage and low capacity, $LiCoO_2$ cathode material in commercial lithium-ion batteries, which is utilized frequently, have confined energy density [50]. Overcharging frequently triggers significant systemic distortions (reconfiguration from hexagonal to monoclinic structures), which yield extensive defects between and within the particles, and induces potential surface reactions including Co break-up at voltages above 4.4 V [50, 223, 532]. $LiMn_{1.5}Ni_{0.5}O_4$ sometimes includes the $Li_xNi_{1-x}O$ impurity stage and it triggers huge lattice stress during cycling, which results in degradation of the electrochemical performance [50, 533–535]. Surface modification by coating with metal oxides including ZnO, Bi_2O_3, $AlPO_4$, and Al_2O_3, has been demonstrated to improve the cycleability and lessen the corrosion reaction between the cathode and the electrolyte [50, 98, 346]. The nitridation process in battery and the photocatalyst has been investigated to increase the efficiency, electrochemical property, and electric conductivity, because it can aid the formation of the nitride film on the surface [536, 537] and change the oxygen stoichiometry [50]. Above the valence band edge, the replaced N 2p states in the O-sites are situated, inducing a decline in the bandgap as a consequence in the case of nitridation of a surface, which is coated with a metal oxide [50]. That process has been utilized for surface modification of electrode materials, as reasonably well [50]. Some groups have indicated that surface nitridation of an active material can enhance electrochemical performance and the electric conductivity [50]. The as-synthesized subsample had been assessed for its suitability as a cathode

electrode material for lithium-ion batteries; it revealed satisfactory cycling performance and greater rate capability when compared to pristine $LiMn_{1.5}Ni_{0.5}O_4$ [50].

Water-based binders having high resistances to electrochemical oxidation during charging process must be devised to use these fruitful high-capacity and high-voltage cathodes in the next-generation lithium batteries prepared in ecologically compatible electrode fabrication mechanisms with a water-based binder [51]. An aqueous hybrid polymer (TRD202A, JSR) had been comprised of fluoropolymer and acrylic polymer and had been sampled as a binder for the Li-rich solid-solution layered cathode material $Li[Ni_{0.18}Li_{0.20}Co_{0.03}Mn_{0.58}]O_2$ [51]. A cathode, which is prepared with $Li[Ni_{0.18}Li_{0.20}Co_{0.03}Mn_{0.58}]O_2$ particles, conductive carbon additive, and TRD202A binder, CMC, had been evaluated and examined for charge/discharge capacity, cycle stability, rate performance, resistance of electrochemical oxidation, mechanical resistance, and transformations of the surface composition and structure after water-treatment utilized for preparing water-based slurry [51]. Wu and coworkers have not investigated the water-based binders for charge/discharge capacities, long cycle stability, rate performance, resistance of electrochemical oxidation, mechanical resistance, or transformations of the surface composition and structure after water-treatment, which is utilized for preparing the water-based slurry [51]. Li-rich solid-solution layered cathode materials' stable charge/discharge performances are accurate for the performance tests of the water-based TRD202A binder with a high-voltage Li-rich solid-solution layered cathode material; the TRD202A binder had been blamed for the performance degradation of the cathode, which is prepared with that binder [51]. The relative merits of the PVdF and TRD202A binders are outlined relating to the charge/discharge capacities, long cycling stability, rate performance, resistance of electrochemical oxidation, mechanical resistance, and transformations of the surface composition and structure after water-treatment for the preparation of a water-based slurry [51].

The main element within the Li-ion batteries, which offers significant influence on electrochemical performance and capacity is Cathode [52]. Lithium manganese phosphate ($LiMnPO_4$) is primarily centred as a useful candidates in the olivine group among LiFePO, LiNiPO and LiCoPO for cathode application [52, 538, 539]. 701 Wh kg with low electronic/ionic electrical conductivity, which affect the electrochemical property [540, 541] and meager lithium diffusion is the theoretical energy density of LiMnPO [52]. Haemoglobin-like LiMnPO microspheres were prepared for better electrochemical activity because of presence of 3-D (3D) hierarchical structures [52, 542]. That irregular flaky influenced $LiMnPO_4$ is accomplished by a hollow-sphere Li_3PO_4 precursor, which is utilized to control the particle growth of LiMnPO had been indicated by Cui et al. [52, 543]. That dry ball milling showed satisfactory electrochemical properties at high temperature and high charge/discharge rate of 2 C and the carbon-coated nanostructured LiMnPO through combination of spray pyrolysis had been indicated by Nam et al. [52, 544]. Cation, which dopes in LiMnPO, is observed to be an alternative technique to upgrade ionic electrical conductivity [52, 545]. Previous work suggested that

cesium (Ce)-doped LiMnPO contributed to easy diffusion of Li-ion in bulk materials [52, 546]. Given this fact, this work is an effort to enhance LiMnPO by partial natrium substitution on lithium sites [52]. Numerous attempts have been done to enhance electrochemical performance of cathode materials by partial natrium doping [52]. That Na substitution for Li minimizes, which mixes cation, enhances reversibility and constrains charge transfer impedance during cycling had been indicated by Chen et al. [52, 547]. Partial Na substitution for Li site has not been centred for LiMnPO-based energy storage application [52].

That novel trend in the car market suggests that requirement for Li-ion batteries will be continually expanding [53]. An increase in Li-ion batteries entails that there will be more battery waste in the near future [53]. One fact is that Li-ion battery waste includes useful metal elements including Li, Ni, Co, Cu, and Mn [53]. There have been some efforts to recycle Li-ion batteries [53, 548–551]. Lithium ion battery recyclers centred solely on cobalt as $LiCoO_2$ had been the principal cathode material in the market; the high price of cobalt motivated recycling efforts [53, 552–554]. The waste stream comprises Li-ion batteries with various cathode chemistries [53]. An effective Li-ion battery recovery process must not target a single cathode chemistry [53]. A "mixed cathode" recycling process had been first devised and devised [555, 556], by which certain quantities of Li-ion batteries with heterogeneous cathode materials could be recovered together without battery sorting [53]. Through plasma optical emission spectrometry (ICP-OES), which is coupled inductively, the concentrations of these useful metal elements could be dictated and adjusted by adding MSO_4 (M = Ni, Mn, Co) salts, cathodes with various Ni and so metal hydroxide precursors: Mn: Co molar ratios could be synthesized directly [53]. The leaching solution from the recovery stream had been employed to synthesize heterogeneous $LiNi_xMn_yCo_zO_2$ cathodes [53]. The molarities of transition metal elements were adjusted to 5:3:2 and 6:2:2 to derive $LiNi_{0.5}Mn_{0.3}Co_{0.2}O_2$ and $LiNi_{0.6}Mn_{0.2}Co_{0.2}O_2$ [53].

2.2 Cathode Materials, Samples, Spinel, Calcination, Discharge Capacity

2.2.1 *Synthesis of Spinel $LiNi_{0.5}Mn_{1.5}O_4$ as Advanced Cathode via a Modified Oxalate Co-precipitation Method [1]*

Spinel-type $LiNi_{0.5}Mn_{1.5}O_4$ (LNMO) cathode materials for Li-ion batteries have been synthesized through a modified oxalate coprecipitation technique [1]. Following one-pot reaction, the target materials could be obtained without subsequent mixing with lithium salts by virtue of the coprecipitation of Li^+ with transition metal ions [1]. The results confirm that the as-prepared material owns a cubic spinel structure with a space group of Fd-3 m, high crystallinity, excellent

electrochemical performances, and homogeneous particle size [1]. Superior rate performance and a greater initial capacity are delivered compared with that of material by traditional coprecipitation technique [1].

2.2.2 $LiNi_{0.5}Mn_{1.5}O_4$ Hollow Nano-micro Hierarchical Microspheres as Advanced Cathode for Lithium-Ion Batteries [2]

Hollow LNMO microspheres have been synthesized through coprecipitation technique, which is accompanied with high-temperature calcinations [2]. The results confirm that the microspheres combine hollow structures inward and own high crystallinity, a cubic spinel structure with space group of Fd-3m, and excellent electrochemical performances [2]. The hierarchical LNMO microspheres display 138.2 and 108.5 mAh g^{-1} at 0.5 and 10 C, respectively with the short Li^+ diffusion length and hollow structure [2].

2.2.3 Low Content Ni and Cr Co-doped $LiMn_2O_4$ with Enhanced Capacity Retention [3]

Nanoparticles of the pure and Ni–Cr codoped lithium manganese oxides Li $[Ni_xCr_yMn_{2-x-y}]O_4$ (x = y = 0.01–0.05) have been synthesized by sol-gel technique, which employs citric acid as a chelating actor [3]. That low-content Ni-Cr substitution considerably enhances the systemic stability and high rate cycling performance of $LiMn_2O_4$ had been established by impedance and electrochemical measurements [3]. 82% of the initial discharge capacity at 0.1 C is preserved at a considerably high current rate of 5 C [3]. A discharge capacity of 104 mAh g^{-1} is resumed upon reducing the current rate to 0.1 C which is 91% of the specific capacity in the first cycle after deep cycling at high rates [3]. It could be observed that the stoichiometry of all the samples is close to the nominal compositions [3]. It could be observed that the cycling performance of the Ni–Cr-substituted samples is substantially enhanced [3].

2.2.4 Effects of Lithium Excess Amount on the Microstructure and Electrochemical Properties of $LiNi_{0.5}Mn_{1.5}O_4$ Cathode Material [4]

The effect of lithium excess quantity on the microstructure, electrochemical properties of $LiNi_{0.5}Mn_{1.5}O_4$ materials, and morphology, had been systematically examined [4]. With the increase of lithium excess quantity, the cation disordering

extent (Mn^{3+} content) and stage purity first increase and then decline, whilst the cation mixing extent has the opposite trend [4]. The $LiNi_{0.5}Mn_{1.5}O_4$ material with 6% lithium excess quantity displays greater disordering lower impurity content and extent and cation mixing extent, leading to the optimal electrochemical properties, with discharge capacities of 125.0, 126.1, 124.2, and 118.9 mAh/g at 0.2-, 1-, 5-, and 10-C rates and capacity retention rate of 96.49% after 100 cycles at 1-C rate [4]. Recent reports [558, 559] indicate that the spinel $LiMn_2O_4$ with the I 311/I 400 intensity ratios between 0.96 and 1.1 normally indicates better electrochemical performances than those outside this region [4].

2.2.5 *Sn-Doped $Li_{1.2}Mn_{0.54}Ni_{0.13}Co_{0.13}O_2$ Cathode Materials for Lithium-Ion Batteries with Enhanced Electrochemical Performance [5]*

Sn-doped Li-rich layered oxides of $Li_{1.2}Mn_{0.54-x}Ni_{0.13}Co_{0.13}Sn_xO_2$ have been synthesized through a sol-gel technique, and electrochemical performance and their microstructure have been researched [5]. The electrochemical performance of $Li_{1.2}Mn_{0.54-x}Ni_{0.13}Co_{0.13}Sn_xO_2$ cathode materials is substantially enhanced after doped with an suitable quantity of Sn^{4+} [5]. The superior rate capability with discharge capacities of 239.8, 198.6, 164.4, 133.4, and 88.8 mAh g^{-1} at 0.2, 0.5, 1, 2, and 5 C, respectively, which are considerably greater than those of $Li_{1.2}Mn_{0.54}Ni_{0.13}Co_{0.13}O_2$ (196.2, 153.5, 117.5, 92.7, and 43.8 mAh g^{-1} at 0.2, 0.5, 1, 2, and 5 C, respectively) is shown by the $Li_{1.2}Mn_{0.53}Ni_{0.13}Co_{0.13}Sn_{0.01}O_2$ electrode [5]. The substitution of Sn^{4+} for Mn^{4+} widens the Li^+ diffusion channels because of its bigger ionic radius compared to Mn^{4+} and improves the systemic stability of Li-rich oxides, leading to the enhanced electrochemical performance in the Sn-doped $Li_{1.2}Mn_{0.54}Ni_{0.13}Co_{0.13}O_2$ cathode materials [5].

2.2.6 *Co-precipitation Spray-Drying Synthesis and Electrochemical Performance of Stabilized $LiNi_{0.5}Mn_{1.5}O_4$ Cathode Materials [6]*

Through a process, which spray-drys coprecipitation and calcining, the $LiNi_{0.5}Mn_{1.5}O_4$ cathode materials of lithium-ion batteries are synthesized [6]. Through a calcining treatment at the optimized temperature of 750 °C, the use of a spray-drying process to form particles, followed to generate spherical $LiNi_{0.5}Mn_{1.5}O_4$ particles with a cubic crystal structure, a specific capacity of 132.9

mAh g^{-1} at 0.1 C. and a specific surface area of 60.1 m^2 g^{-1}, a tap density of 1.15 g mL^{-1} [6]. The carbon nanofragment (CNF) additives, introduced into the spheres during the coprecipitation spray-drying period, substantially improve the rate performance and cycling stability of $LiNi_{0.5}Mn_{1.5}O_4$ [6].

2.2.7 *Synthesis and Electrochemical Performance of Spherical $LiNi_{0.8}Co_{0.15}Ti_{0.05}O_2$ Cathode Materials with High Tap Density [7]*

Through X-ray diffraction (XRD) and scanning electron microscopy (SEM), respectively, the crystal structure and particles morphology of the as-prepared powders were typified [7]. "All samples correspond to the layered α-$NaFeO_2$ structure with R-3m space group" [7]. The $LiNi_{0.8}Co_{0.15}Ti_{0.05}O_2$ prepared at 800 °C introduces better spherical particles and a better hexagonal ordering structure and retains a high tap density of 3.22 g cm^{-3} [7].

2.2.8 *A Strontium-Doped Li_2FeSiO_4/C Cathode with Enhanced Performance for the Lithium-Ion Battery [8]*

That a strontium cation occupies the Fe site in the lattice and that strontium-doped Li_2FeSiO_4 has a monoclinic $P2_{1/n}$ structure is revealed by rietveld refinement [8]. The grain size of strontium-doped Li_2FeSiO_4 is roughly 20 nm, and the nanoparticles are interlinked tightly with amorphous carbon layers [8]. Strontium-doped Li_2FeSiO_4/C delivers a high discharge capacity of 181 mAh g^{-1} at a rate of 0.5 as the cathode material of a lithium-ion battery C [8]. It could be concluded that strontium cation doping enables to increase the Li^+ diffusion capability and weakens side reactions between the electrode and electrolyte by examining the electrochemical impedance spectra [8]. Throughout charging and discharging after strontium cation doping, the amelioration of the electrochemical performance could be attributable to the undermined crystal structure stability [8]. The evident capacity degradation can not be detected and all the capacity retentions stayed above 90% for the three cathodes, as the rate ranged from 2 to 5 C [8].

2.2.9 Enhanced Electrochemical Performances of Layered $LiNi_{0.5}Mn_{0.5}O_2$ as Cathode Materials by Ru Doping for Lithium-Ion Batteries [9]

Through a moist chemical technique, which a high-temperature calcining process followed, Ru-doped $LiNi_{0.5}Mn_{0.5}O_2$ cathode materials and the pristine are synthesized [9]. The galvanostatic charge/discharge measurements highlight that the electrochemical properties of the $LiNi_{0.5}Mn_{0.5}O_2$ subsample are enhanced by Ru doping [9]. Ru doping is regarded an efficient way to improve the electrochemical performances of $LiNi_{0.5}Mn_{0.5}O_2$ cathode materials [9]. Two apparent splittings of (006)/(102) and (108)/(110) doublet peaks could be detected, which indicate a well-ordered layered structure [9, 560]. It could be observed that the lattice parameters (a and c) of $LiNi_{0.5}Mn_{0.45}Ru_{0.05}O_2$ are greater than those of $LiNi_{0.5}Mn_{0.5}O_2$ [9]. The SEM images indicate that the as-prepared samples have a polyhedral or spherical morphology in the primary particle [9]. The SAED patterns of $LiNi_{0.5}Mn_{0.45}Ru_{0.05}O_2$ show a characteristic hexagonal α-$NaFeO_2$ structure (3m) diffraction in the [03] zone, and corroborate that the primary particles are single crystalline [9].

2.2.10 Synthesis and Electrochemical Properties of $LiNi_{0.5}Mn_{1.5}O_4$ Cathode Materials with Cr^{3+} and F^- Composite Doping for Lithium-Ion Batteries [10]

Through the solid-state technique, F^- and a F^{-5} composite-doped $LiNi_{0.5}Mn_{1.5}O_4$ cathode material had been synthesized, and the impact of the doping quantity on the electrochemical and physical properties of the material had been examined [10]. The results of the charge/discharge tests, electrochemical impedance spectroscopy (EIS) test results, and cyclic voltammetry (CV), indicated that $LiCr_{0.05}Ni_{0.475}Mn_{1.475}O_{3.95}F_{0.05}$ in which the F^- and F^{-5} doping quantities were both 0.05, had the optimum electrochemical properties, with discharge rates of 0.1, 0.5, 2, 5, and 10 C and specific capacities of 134.18, 128.70, 123.62, 119.63, and 97.68 mAh g^{-1}, respectively [10]. $LiCr_{0.05}Ni_{0.475}Mn_{1.475}O_{3.95}F_{0.05}$ revealed exceedingly satisfactory cycling performance, with a capacity retention rate of 97.9% and a discharge specific capacity of 121.02 mAh g^{-1} after 50 cycles at a rate of 2 C [10].

2.2.11 *Y-Doped $Li_3V_2(PO_4)_3$/C as Cathode Material for Lithium-Ion Batteries [11]*

On the structure and electrochemical performance of $Li_3V_2(PO_4)_3$, the Y-doping quantity plays a crucial role [11]. The capacity retention had been observed to be 93.9% after 50 cycles and the capacity of $Li_3Y_{0.03}V_2(PO_4)_3$/C stayed around 100 mAh g^{-1} at a current density of 100 mA g^{-1}. the $Li_3V_2(PO_4)_3$/C samples (LVP) doped with various quantities of Y were synthesized [11]. That the Y-doping quantity plays a crucial role on the structure and electrochemical performance of $Li_3V_2(PO_4)_3$/C is demonstrated by the results [11]. The cycle performance of the samples is quite satisfactory and the reversible capacity of the as-prepared $Li_3Y_{0.03}V_2(PO_4)_3$/C is greater than the theoretical capacity (148.99 mAh g^{-1} after 50 cycles) [11]. That the aggregation of the sub-micrometer size particulates in both $Li_3Y_xV_2(PO_4)_3$/C and $Li_3V_2(PO_4)_3$/C powders, since the materials were prepared by a rheological stage reaction at high temperature with a comparatively long duration is clearly demonstrated by the SEM pictures [11]. It could be observed that porous carbon layers enmeshed the networks of aggregated particles or coated on the surface of the particles [11]. AC impedance curves of the LVP samples indicate that $Li_3Y_xV_2(PO_4)_3$/C with 3% Y-doping is the optimal material to examine the modification of Li_3V_2 $(PO_4)_3$/C [11].

2.2.12 *Nano Transition Metal Alloy Functionalized Lithium Manganese Oxide Cathodes-System for Enhanced Lithium-Ion Battery Power Densities [12]*

Manganese oxide cathode material of rechargeable lithium-ion batteries provides a distinctive blend of lower cost and toxicity, which is compared to the usually utilized cobalt, and has been shown to be safer on overcharge [12]. Alloy nanoparticles were synthesized and utilized as coating material with the aim to enhance the catalytic and microstructure activities of pristine $LiMn_2O_4$ [12]. The pristine modified and $LiMn_2O_4$ materials were investigated employing a combination of microscopic and spectroscopic methods along with in detail galvanostatic charge-discharge tests [12]. Microscopic results showed that the new composite cathode materials had high stage purity, congruent morphological structures with narrow size distributions and well-crystallized particles [12]. The systemic changes, which take place during Li^+ ion insertion with exchange current density i 0 (A cm^{-2}) of 1.83×10^{-4} and 3.18×10^{-4} for $LiMn_2O_4$. greater electrode columbic efficiency of the $LiPtAu_xMn_{2-x}O_4$ and the enhancement of the capacity retention were significant, particularly at high C rate were efficiently accommodated by the $LiPtAu_xMn_{2-x}O_4$ cathode [12].

2.2.13 Synthesis and Electrochemical Properties of $Li(Ni_{0.56}Co_{0.19}Mn_{0.24}Al_{0.01})1-yAlyO_2$ as Cathode Material for Lithium-Ion Batteries [13]

The $LiNi_{0.5376}Co_{0.1824}Mn_{0.2304}Al_{0.0496}O_2$ (y = 0.04) cathode material had the optimal electrochemical performance [13]. At 0.1 C, the reversible capacity of 174.9–115.9 mAh g^{-1} at 1 C between 2.75 and 4.4 V. had been offered by the material [13] Electrochemical impedance spectroscopy (EIS) and cyclic voltammetry (CV) were carried out to additional investigation the novel composite cathode materials, as reasonably well [13].

2.2.14 One-Step Solid-State Synthesis of Nanosized $LiMn_2O_4$ Cathode Material with Power Properties [14]

That optimum $LiMn_2O_4$ particles ($S_{0.5}$) is synthesized when the molar ratios of total Mn source and oxalic acid are 0.5:1 is revealed by the electrochemical test results [14]. The obtained subsample $S_{0.5}$ with middle size displays a high initial discharge capacity of 125.8 mAh g^{-1} at 0.2 C and 91.4% capacity retention over 100 cycles at 0.5 C, superior to any one of other samples [14]. In this work, the optimum $S_{0.5}$ can still attain a discharge capacity of 80.8 mAh g^{-1} when cycling at the high rate of 10 C [14]. That observation could be tackled to the fact that the middle size particles balance the conflicting of diffusion length in solid stage and particle agglomeration; this stage gives rise to perfect contacts with the optimum performance of $S_{0.5}$, and the conductive additive, substantial evident lithium ion diffusion rate [14]. It could be observed that among all the samples, $S_{0.5}$ acquires a minimum value of I_{222}/I_{400} ratio, suggesting that the crystal orientation in $S_{0.5}$ along the (400) direction is more influential than that in other samples [14].

2.2.15 Nanosized $0.3Li_2MnO_3 \cdot 0.7LiNi_{1/3}Mn_{1/3}Co_{1/3}O_2$ Synthesized by CNTs-Assisted Hydrothermal Method as Cathode Material for Lithium-Ion Battery [15]

Through a hydrothermal process with carbon nanotubes as template, $3Li_2MnO_3 \cdot 0.7LiNi_{1/3}Mn_{1/3}Co_{1/3}O_2$ as new cathode material had been synthesized [15]. $3Li_2MnO_3 \cdot 0.7LiNi_{1/3}Mn_{1/3}Co_{1/3}O_2$ material revealed excellent electrochemical performance, and the LR-1.0 subsample had rate capability and the optimal cycling stability [15]. Once the LR-1.0 subsample had been evaluated as a cathode

at 0.1 and 2.0 C the LR-1.0 sample's its initial discharge capacities can attain up to 267.0 and 146.6 mAh g^{-1}, respectively [15]. $3Li_2MnO_3{\cdot}0.7LiNi_{1/3}Mn_{1/3}Co_{1/3}O_2$ prepared by this technique had been a novel fruitful cathode material for Li-ion batteries [15]. To additional show the electrochemical behaviour of the 0 [15].

2.2.16 *Improvement of the Electrochemical Properties of a $LiNi_{0.5}Mn_{1.5}O_4$ Cathode Material Formed by a New Solid-State Synthesis Method [16]*

To avoid the drawbacks of huge particle size and meager homogeneity of material, which the conventional solid-state technique synthesized, straightforward amelioration of calcining process is employed (i.e., calcining-milling-recalcination) based upon the conventional solid-state synthesis to efficiently prepare a huge number of well-distributed, micrometer-sized, spherical secondary $LiNi_{0.5}Mn_{1.5}O_4$ particles [16]. Findings of the electrochemical performance tests indicate that the material displays a striking cycle performance and rate capability, which is compared with that derived from conventional synthesis technique; the spherical $LiNi_{0.5}Mn_{1.5}O_4$ particles can deliver a huge capacity of 135.8 mAh g^{-1} at a 1 C discharge rate with a high retention of 77% after 741 cycles and a satisfactory capacity of 105.9 mAh g^{-1} at 10 C. Cyclic voltammetry measurements corroborate that the substantially enhanced electrochemical properties are because of enhanced electronic electrical conductivity and lithium-ion diffusion coefficient, which results from the optimized morphology and particle size [16].

2.2.17 *Hierarchical $Li_{1.2}Mn_{0.54}Ni_{0.13}Co_{0.13}O_2$ Hollow Spherical as Cathode Material for Li-Ion Battery [17]*

High reversible capacity, excellent rate property, and satisfactory cycling stability, is shown by the as-prepared material [17]. The as-prepared material delivers a high initial discharge capacity of 305.9 mAh g^{-1} at 28 mA g^{-1} with columbic efficiency of 80% [17]. The subsample indicates a stable discharge capacity of 215 mAh g^{-1} even at high current density of 560 mA g^{-1} [17]. The enhanced electrochemical properties are attributable to the stable hierarchical hollow sphere structure and the suitable contact area between electrode and electrolyte, efficiently enhance the lithium-ion intercalation and deintercalation kinetics [17]. That the hollow structure is capable of enabling the layered lithium-rich cathode with an outstanding rate performance could be thought by us [17]. Apart from, it could be detected that the subsample HS exhibits a pair of reversible redox peaks at 3.25 V in the second cycle, in congruent with the decrease and oxidation reaction of Mn^{3+}/Mn^{4+} (Sathiya and others [557]), [17].

2.2.18 The Properties Research of Ferrum Additive on $Li[Ni_{1/3}Co_{1/3}Mn_{1/3}]O_2$ Cathode Material for Lithium-Ion Batteries [18]

Through means of cyclic voltammetry (CV), galvanostatic charge/discharge test, and electrochemical impedance spectroscopy (EIS), the electrochemical properties of $Li[Ni_{1/3}Co_{(1-x)/3}Mn_{1/3}Fe_{x/3}]O_2$ were compared [18]. Electrochemical test results suggest that $Li[Ni_{1/3}Co_{0.9/3}Mn_{1/3}Fe_{0.1/3}]O_2$ decline charge transfer resistance and improve Li^+ ion diffusion velocity and [18]. The initial discharge specific capacity of $Li[Ni_{1/3}Co_{0.9/3}Mn_{1/3}Fe_{0.1/3}]O_2$ had been 178.5 mAh/g and capacity retention had been 87.11% after 30 cycles at 0.1 C, with the battery, which indicates satisfactory cycle performance [18]. The initial columbic efficiencies and the initial discharge capacity reaches the highest value when x = 0.1 [18].

2.2.19 Comparative Study of the Electrochemical Properties of $LiNi_{0.5}Mn_{1.5}O_4$ Doped by Bivalent Ions (Cu^{2+}, Mg^{2+}, and Zn^{2+}) [19]

Scanning X-ray diffraction and electron microscopy analyses suggest that these doped $LiNi_{0.45}M_{0.05}Mn_{1.5}O_4$ samples remain the 5 V-positive electrode materials $LiNi_{0.45}M_{0.05}Mn_{1.5}O_4$ (M = Cu, Mg and Zn)'s spinel structure with an octahedral morphology [19]. The $LiNi_{0.45}Mg_{0.05}Mn_{1.5}O_4$ and $LiNi_{0.45}Cu_{0.05}Mn_{1.5}O_4$ samples display excellent rate performance with specific capacities of 98.3 and 92.4 mAh g^{-1}, respectively, at the charge-discharge rate of 10 C, whilst the $LiNi_{0.5}Mn_{1.5}O_4$ subsample delivers just 78.9 mAh g^{-1} at 10 C. Apart from, the $LiNi_{0.45}Cu_{0.05}Mn_{1.5}O_4$and $LiNi_{0.45}Mg_{0.05}Mn_{1.5}O_4$ samples indicate satisfactory capacity retention at high temperature (55 °C) with the capacities of 117.6 and 119.5 mAh g^{-1}, respectively, after 100 cycles at 1 C [19].

2.2.20 Nearly Monodispersed $LiFePO_4F$ Nanospheres as Cathode Material for Lithium-Ion Batteries [20]

Through a solid-state route, which is correlated with chemically caused precipitation technique for the first time, almost monodisperse $LiFePO_4F$ nanospheres with high purity are efficiently synthesized [20]. Approximately monodisperse nanospheres particles are summarized by the synthesized $LiFePO_4F$ with mean particle size of ~500 nm [20]. That the initial discharge capacity is 110.2 mAh g^{-1} at 0.5 C, after 200 cycles is still preserved 104.0 mAh g^{-1} with the retention rate of 94.4% is demonstrated by the results [20]. The excellent cycle performance is primarily

attributable to the homogeneous nanospheres-like morphology; this homogeneous is not just beneficial to shorten the transport distance of electrons and ions, though also enhance the interface area between electrode and electrolyte, and [20]. The excellent cycle performance could be attributable to the homogeneous nanospheres-like morphology; this homogeneous is beneficial to enhance the interface area between electrolyte and electrode, shorten the transport distance of electrons and ions and improve the power and energy densities of batteries, and enhance the kinetics of Li ions [20].

2.2.21 *Investigation of the Structural and Electrochemical Performance of $Li_{1.2}Ni_{0.2}Mn_{0.6}O_2$ with Cr-doping [21]*

Cr-doped layered oxides $Li[Li_{0.2}Ni_{0.2-x}Mn_{0.6-x}Cr_{2x}]O_2$ (x = 0, 0.02, 0.04, 0.06) were synthesized by high-temperature solid-state reaction and coprecipitation [21]. HRTEM results and XRD patterns suggest that Cr-doped $Li_{1.2}Ni_{0.2}Mn_{0.6}O_2$ and the pristine indicate the layered stage [21]. The first discharge specific capacity of $Li_{1.2}Ni_{0.16}Mn_{0.56}Cr_{0.08}O_2$ is 249.6 mAh g^{-1} at 0.1 C, whilst that of $Li_{1.2}Ni_{0.2}Mn_{0.6}O_2$ is 230.4 mAh g^{-1} [21]. The discharge capacity of $Li_{1.2}Ni_{0.16}Mn_{0.56}Cr_{0.08}O_2$ is 126.2 mAh g^{-1} at 5.0 C, whilst that of the pristine $Li_{1.2}Ni_{0.2}Mn_{0.6}O_2$ is about 94.5 mAh g^{-1} [21]. XPS results indicate that the content of Mn^{3+} in the $Li_{1.2}Ni_{0.2}Mn_{0.6}O_2$ could be restrained after Cr doping during the cycling, which results in restraining formation of better mid-point voltages and spinel-like structure [21].

2.2.22 *An Insight into the Influence of Crystallite Size on the Performances of Microsized Spherical $Li(Ni_{0.5}Co_{0.2}Mn_{0.3})O_2$ Cathode Material Composed of Aggregated Nanosized Particles [22]*

Relationships between the performance and the crystallite size of the microsized spherical $Li(Ni_{0.5}Co_{0.2}Mn_{0.3})O_2$ cathode material, which is comprised of aggregated nano-sized primary particles, have been comprehensively researched [22]. The electrochemical attributes of $Li(Ni_{0.5}Co_{0.2}Mn_{0.3})O_2$, including discharge capacity, thermal stability, and rate performance, are closely linked to the crystallite size [22]. Through that of crystallite size, the retention of discharge capacity is dictated in $Li(Ni_{0.5}Co_{0.2}Mn_{0.3})O_2$ after 100 cycles [22].

2.2.23 Synthesis and Electrochemical Performances of High-Voltage $LiNi_{0.5}Mn_{1.5}O_4$ Cathode Materials Prepared by Hydroxide Co-precipitation Method [23]

X-ray diffraction (XRD), scanning electron microscopy (SEM) and electrochemical measurements were undertaken to $LiNi_{0.5}Mn_{1.5}O_4$ cathode material, which is prepared describe [23]. Electrochemical tests at 25 °C indicate that the $LiNi_{0.5}Mn_{1.5}O_4$ cathode material, which is prepared after annealing at 600 °C, has the optimal electrochemical performances [23]. The initial discharge capacity of prepared cathode material delivers 113.5 mAh g^{-1} at 1 C rate in the variety of 3.50–4.95 V, and the subsample possesses 96.2% (1.0 C) of the initial capacity after 50 cycles [23]. The discharge capacities of obtained cathode material could be maintained at about (0.1 C) 145.0, (0.5 C) 113.5, (1.0 C) 126.8 and 112.4 (2.0 C) mAh g^{-1}, the corresponding initial coulomb efficiencies maintain above 95.2 (0.1 C)%, 95.0 (0.5 C)%, 92.5 (1.0 C)% and 94.8 (2.0 C)%, respectively under various rates with a cut-off voltage variety of 3.50–4.95 V at 25 °C [23].

2.2.24 Highly Enhanced Low-Temperature Performances of $LiFePO_4$/C Cathode Materials Prepared by Polyol Route for Lithium-Ion Batteries [24]

Based on 25 to −20 °C, the electrochemical performance of the $LiFePO_4$/C, which polyol route prepared, had been examined at a temperature variety [24]. In contrast to commercial ones, as-prepared $LiFePO_4$/C indicates a considerably better low-temperature performance with a reversible capacity of 30 mAh g^{-1} even at 5 C under −20 °C and a capacity retention of 91.1% after 100 cycles at 0.1 C under 0 °C [24].

2.2.25 Synthesis and Characterization of Nanocomposites Based on Poly(3-Hexylthiophene)-Graft-Carbon Nanotubes with $LiNi_{0.5}Mn_{1.5}O_4$ and Its Application as Potential Cathode Materials for Lithium-Ion Batteries [25]

The nanocomposite, which is premised doped spinel $LiNi_{0.5}Mn_{1.5}O_4$ (LNMO) and on P3HT-g-CNTs, have been fabricated through mixing process [25]. The structure and morphologies of LNMO/P3HT-g-CNTs nano-composites have been carried out

by SEM, TEM and XRD, as reasonably well [25]. The structure and morphology of the electrode were typified employing XRD, TEM and SEM [25]. Through electrochemical impedance spectroscopy and cyclic voltammetry, the electrochemical performance of LNMO/P3HT-g-CNTs nano-composites as cathode materials of lithium-ion batteries were examined and showed the high diffusion of lithium ions in the charge-discharge process [25]. That the electrochemical reaction of LNMO/P3HT-g-CNTs nano-composites is better than that of LNMO/VC materials as a consequence of high diffusion of lithium ions in the charge-discharge process is revealed by these results [25].

2.2.26 *Lithium-Sulphur Batteries Based on Biological 3D Structures [26]*

Enough space is offered by this 3D electrode for sulfur [26]. The electrode structure enables high sulfur loading [26]. The resultant novel cathode configuration enables reaching quite high sulfur area loading of 4.9 mg/cm^2 which is nearly four times more than in the case of a standard coated electrode [26]. Throughout cycling in comparison with a standard electrode, the electrode establishes high stability and the electrode structure reaches considerably greater square capacity, exceeded 3.0 mAh/cm^2 despite the high sulfur loading [26]. The results indicate that the 3D structured electrode establishes a stable plateau at 2.4 V including its stability [26].

2.2.27 *Carbon-Coated $LiFePO_4$–Carbon Nanotube Electrodes for High-Rate Li-Ion Battery [27]*

A fruitful cathode material for high-rated lithium-ion batteries is Olivine $LiFePO_4$ (LFP) [27]. A serious drawback of low electrical conductivity and sluggish transportation of Li^+ ions, which slows down hence the retention capacity of battery and the chemical reactions had been confronted by Olivine [27]. A mixing of carbon nanotubes (CNTs) on the composite electrode had been examined to improve the electrochemical performance of nanocomposite $LiFePO_4$/C [27]. An increase of D_{Li} had been detected with the increase of CNT quantity in electrode composite [27]. Upon 200 cycles, an excellent performance in rate capability and cycling test had been shown by the composite electrode LFP/C/10% CNTs; a retention capacity of 98% had been detected [27].

2.2.28 *Recent Advances on Fe- and Mn-Based Cathode Materials for Lithium and Sodium Ion Batteries [28]*

The ever-increasing market of electrochemical energy storage impels the advancements on environment-friendly and cost-efficient battery chemistries [28]. The development of cathode materials, which is based upon Earth's plentiful elements (Fe and Mn), largely determines the prospects of the batteries [28]. The development of a high-performance and cheap battery necessitates the advance of the anode part [28]. Prospects and issues are outlined to direct the possible development of high-performance and cost-efficient cathode materials for future rechargeable batteries [28]. Mn-based cathodes for Li-ion batteries and a critical criterion for the development of future Fe-is to attain similar or even greater energy densities [28]. That this review can inform Mn-based cathode materials and readers of the rationality and priority of Fe-as candidates for future Li-ion batteries and SIBs, and call for additional efforts to satisfy this aim is hoped by us [28]. Considering the cost's elemental relative abundance, Fe-based and Mn-cathode materials are hence preferable decisions, and the cost's sodium analogues are attracting considerably attention, as they would allow the future of Li-free SIBs, which might be optimal decisions for large-scale applications [28]. We assume better development of Fe and understanding-and Mn-based cathode materials will help to make rechargeable Na-ion and lithium batteries cheaper, better, and greener [28].

2.3 Pristine, Layered, Cathode Materials, Samples, Coating Layer

2.3.1 *$BiFeO_3$-Coated Spinel $LiNi_{0.5}Mn_{1.5}O_4$ with Improved Electrochemical Performance as Cathode Materials for Lithium-Ion Batteries [29]*

$BiFeO_3$-coated $LiNi_{0.5}Mn_{1.5}O_4$ materials were prepared through the structure, morphology and a moist chemical technique, and electrochemical performance of the materials were researched [29]. Cubic spinel structure with space group of Fd3m is shown by all $BiFeO_3$-coated $LiNi_{0.5}Mn_{1.5}O_4$ materials [29]. The coating of 1.0 wt% $BiFeO_3$ on the surface of $LiNi_{0.5}Mn_{1.5}O_4$ displays a substantial enhancement in specific capacity, rate performance, and cyclic stability [29]. The coating of $BiFeO_3$ has no apparent impact on the crystal structure of $LiNi_{0.5}Mn_{1.5}O_4$ [29]. 1.0 wt% $BiFeO_3$-coated $LiNi_{0.5}Mn_{1.5}O_4$ electrode indicates excellent rate performance with discharge capacities of 117.5, 110.2, 85.8, and 74.8

mAh g^{-1} at 1, 2, 5, and 10 C, respectively, which is greater than that of $LiNi_{0.5}Mn_{1.5}O_4$ (97.3, 90, 77.5, and 60.9 mAh g^{-1}, respectively) [29]. The surface coating of $BiFeO_3$ efficiently decreases charge transfer resistance and impedes side reactions between electrolyte and active materials and induces the enhanced electrochemical performance of $LiNi_{0.5}Mn_{1.5}O_4$ materials [29]. That the rate performance of the LNMO electrode is substantially enhanced after being coated with 1.0 wt% $BiFeO_3$ is revealed by these results [29].

2.3.2 *Li-Ion-Conductive Li_2TiO_3-Coated Li $[Li_{0.2}Mn_{0.51}Ni_{0.19}Co_{0.1}]O_2$ for High-Performance Cathode Material in Lithium-Ion Battery [30]*

Li_2TiO_3 is utilized as a new coating material to alter $Li(Li_{0.2}Mn_{0.51}Ni_{0.19}Co_{0.1})O_2$ electrode to improve the electrochemical performance of the host material [30]. The subsample coated with optimal cyclability (discharge capacity of 207.1 mAh g^{-1} at 0.5 C after 100 cycles), 3 wt% Li_2TiO_3 displays the highest rate capability (169.9 mAh g^{-1} at 2 C rate and 149.1 mAh g^{-1} at 5 C rate), and enhanced initial columbic efficiency (69.5%) in the voltage variety of 2.0–4.8 V [30]. The electrochemical impedance spectroscopy (EIS) tests confirm that the suitable Li_2TiO_3 coating layer can efficiently restrain the increased impedance of the host electrode [30]. That the efficient Li^+-conductive Li_2TiO_3 coating layer can sustain the host structure, restrain the undesirable surface side reactions on the electrode surface, which the EIS tests demonstrated, and safeguard the electrode surface from HF attack, is-confirmed by the charge discharge curves [30].

2.3.3 *Na-Doped Layered $LiNi_{0.8}Co_{0.1}Mn_{0.1}O_2$ with Improved Rate Capability and Cycling Stability [31]*

That Na-doped LNMCOs deliver a rate capability and cycling stability at high cut-off voltages of 4.3 and 4.5 V that are more efficient than those of undoped LNMCO is shown by electrochemical measurements [31]. Electrochemical impedance spectroscopy (EIS) measurement reveals that Na doping reduces both the impedance of the charge transfer and the solid electrolyte interface layer [31]. The superior electrochemical performances of Na-doped LNMCOs are attributable by us to a pillared structure; this structure simultaneously favours the amelioration of cycling stability and Li^+ mobility [31].

2.3.4 *ZnO-Coated $LiMn_2O_4$ Cathode Material for Lithium-Ion Batteries Synthesized by a Combustion Method [32]*

Through a combustion technique, which employs glucose as fuel, ZnO-coated $LiMn_2O_4$ cathode materials were prepared [32]. Through X-ray diffraction (XRD), the stage structures, size of particles, electrochemical performance of pristine, and morphology, and ZnO-coated $LiMn_2O_4$ powders are researched in detail, scanning electron microscopy (SEM), transmission electron microscopy (TEM), cyclic voltammetry (CV), electrochemical impedance spectroscopy (EIS), galvanostatic discharge/charge test, and X-ray photoelectron spectroscopy (XPS) [32]. Rate performance and galvanostatic charge/discharge test revealed that the ZnO coating can enhance the capacity and cycling performance of $LiMn_2O_4$ [32]. Upon 500 cycles at 0.5 C. Apart from, a satisfactory rate capability at various current densities from 0.5 to 5.0 C could be acquired, the 2 wt% ZnO-coated $LiMn_2O_4$ subsample showed an initial discharge capacity of 112.8 mAh g^{-1} with a capacity retention of 84.1% [32].

2.3.5 *Enhanced Electrochemical Properties and Thermal Stability of $LiNi_{1/3}Co_{1/3}Mn_{1/3}O_2$ by Surface Modification with Eu_2O_3 [33]*

The Eu_2O_3-coated subsample reveals better electrochemical performances and thermal stability than that of the pristine one [33]. The Eu_2O_3-coated $LiNi_{1/3}Co_{1/3}Mn_{1/3}O_2$ cathode reveals stable cycleability with capacity retention of 92.9%, which is greater than that (75.5%) of the pristine one in voltage variety 3.0–4.6 V. Analysis from the electrochemical measurements demonstrates that the remarkably enhanced performances of the surface-modified composites are primarily attributed to the presence of Eu_2O_3-coating layer, which can effectively restrain increased impedance and the undesired side reaction, and improve the systemic stability of active material after 100 cycles at 1 C [33]. In Ar-filled glove box, the both cells were disassembled and the electrodes were immersed into DEC solution respectively after 100 cycles [33]. The obtained results show that the presence of Eu_2O_3 on $LiNi_{1/3}Co_{1/3}Mn_{1/3}O_2$ surface plays important roles in declining the interfacial impedance, fostering kinetic behaviours of Li ions, suppressing reactivity between electrolyte and electrode and enhancing systemic stability [33].

2.3.6 Surface Modification of Cathode Material $0.5Li_2MnO_3 \cdot 0.5LiMn_{1/3}Ni_{1/3}Co_{1/3}O_2$ by Alumina for Lithium-Ion Batteries [34]

Preliminary discharge specific capacity of 211.7 mAh g^{-1} between 2.0 and 4.8 is delivered by the 2-wt% coated subsample at a rate of 1 C V with an initial columbic efficiency of 73.2% as a cathode material for lithium-ion batteries [34]. The results displays the highest discharge specific capacity of 206.2 mAh g^{-1} with 97.4% capacity retention after 100 cycles considerably elevated rate capability and at compared to uncoated material [34]. More superior rate property and the excellent cycling stability could be attributed to alumina coating layer, which has a surface stabilization effect on these cathode materials, lessening the break-up of metal ions [34]. Cyclic voltammetry researches and the electrochemical impedance suggest that coated by alumina enhanced the kinetic performance for lithium-rich layered materials, demonstrating a prospect for practical lithium battery application [34]. That lithium-rich layered materials are comprised of Li_2MnO_3 element and $LiMO_2$ element to form a homogeneous solid solution structure (Lee and Manthiram [388]; Tabuchi and others [389]) is usually thought by scholars [34]. Through hydrothermal technique, $5Li_2MnO_3 \cdot 0.5LiMn_{1/3}Ni_{1/3}Co_{1/3}O_2$ cathode material had been prepared and a thin layer of alumina had been efficiently coated on the surface of material, which is prepared, under the hydrolysis of aluminium isopropoxide which could be detected by TEM images [34].

2.3.7 Enhanced High Power and Long Life Performance of Spinel $LiMn_2O_4$ with Li_2MnO_3 Coating for Lithium-Ion Batteries [35]

In contrast with the pristine subsample, 3 wt% Li_2MnO_3-coated subsample reveals an excellent cycle performance with a capacity retention of 94.17% after 500 cycles at 25 °C and 89.75% after 200 cycles at 55 °C [35]. An excellent rate performance with a capacity of 97.6 mAh g^{-1} at 12 C, which could be primarily attributable to the stable stage interface between host $LiMn_2O_4$ material and Li_2MnO_3 coating layer is shown by the composite material [35]. An efficient way to improve the electrochemical performance of $LiMn_2O_4$ is the functionalized Li_2MnO_3 coating [35]. There is no further peak corresponding to Li_2MnO_3 that could be detected; this peak which could be attributable to its tiny amount [35]. The electrochemical results indicate that the 3 wt% Li_2MnO_3-coated subsample introduces excellent electrochemical performances compared with the pristine one, delivering a discharge capacity of 97.6 mAh g^{-1} at 12 C, with a capacity retention of 94.17% after 500 cycles at 25 °C and 89.75% after 200 cycles at 55 °C [35].

2.3.8 Research Progress in Improving the Cycling Stability of High-Voltage $LiNi_{0.5}Mn_{1.5}O_4$ Cathode in Lithium-Ion Battery [36]

High-voltage lithium-ion batteries (HVLIBs) are regarded as fruitful tools of energy storage for hybrid electric vehicle, electric vehicle, and other high-power equipment [36]. High-voltage lithium-ion batteries (HVLIBs) with moderate theoretical discharge capacity, stable high discharge platform, and high thermodynamic stability, provide novel possibilities for next batteries with high energy density [36, 513, 561, 562]. Lithium nickel manganese spinel $LiNi_{0.5}Mn_{1.5}O_4$ (LNMO) cathode is the most fruitful candidate among the 5 V cathode materials for HVLIBs because of its flat plateau at 4.7 V. Nevertheless, the degradation of cyclic performance is quite serious when LNMO cathode operates over 4.2 V [36]. We summarize many techniques for improving the cycling stability of LNMO cathodes in lithium-ion batteries, which comprises doping, electrolyte altering, cathode surface coating, and other techniques [36].

2.3.9 Improvement in the Electrochemical Performance of a $LiNi_{0.5}Mn_{0.5}O_2$ Cathode Material at High Voltage [37]

The results of XRD, Rietveld refinement, SEM and XPS measurements confirmed that Ca-doping can lower the quantity of Li/Ni cation mixing and increase the stability of the structure [37]. The results of electrochemical measurements indicate that a 3 mol% Ca-doping displays the optimal electrochemical performance, which comprises the optimal cycle stability and rate performance and the highest capacity [37]. Ca-doping had been not detected to affect the morphology or oxidation states of the $LiNi_{0.5}Mn_{0.5}O_2$ [37]. The electrochemical measurements revealed that the pristine $LiNi_{0.5}Mn_{0.5}O_2$ material has the lowest discharge capacity of 88.6 mAh g^{-1} between 4.5 V and 3 at a constant density of 0.2 C; this C had been enhanced 38% by doping with 3 mol% of Ca [37]. The capacity retention of the 3 mol% Ca-doping is 20% greater than that of the pristine $LiNi_{0.5}Mn_{0.5}O_2$ material in the voltage variety of 3.0–4.5 V. Furthermore, we examined the source of the enhancement of the electrochemical properties from Ca-doping [37].

2.3.10 High Energy Density and Lofty Thermal Stability Nickel-Rich Materials for Positive Electrode of Lithium-Ion Batteries [38]

We have prepared a core-shell material, which is comprised of a monoclinic (C2/m) Li_2MnO_3 shell and a core of NCM811 (R-3m), to circumvent this barrier [38]. That core-shell is quite various from the traditional core-shell materials [38]. The traditional core-shell materials are layered R-3 m structures which are instable at state (>4.5 V) because of the high repulsion between the two oxygen atoms facing every other across the empty Li site, which is delithiated highly, whilst our synthesized material could be safely cycled at high upper cutoff potential of 4.7 V with high capacity retention [38]. Based on 4.3–4.7 V. Differential scanning calorimetry (DSC) results indicate that the exothermic peak of the core-shell structured material seems at 360 °C with a heat evolution of 575.1 J g^{-1}, whilst that of the pristine material seems at 250 °C with a heat evolution of 239.1 J g^{-1}, the upper cutoff potential is elevated [38].

2.3.11 Effects of Doping Al on the Structure and Electrochemical Performances of Li $[Li_{0.2}Mn_{0.54}Ni_{0.13}Co_{0.13}]O_2$ Cathode Materials [39]

That all the materials revealed surface morphology and comparable XRD patterns had been confirmed by the results [39]. Nonetheless kept a discharge capacity of 135.6 mAh g^{-1}at 5.0 C. and the discharge capacity had been 265.2 mAh g^{-1} at 0.1 C [39]. The capacity retention can still be 58.2 and 66.8% after 50 cycles at 1.0 and 2.0 C, respectively [39]. Electrochemical impedance spectra results demonstrated that cycling performance and the rate capability, which is enhanced remarkably, can be attributed to enhanced reaction kinetics and the low charge transfer resistance [39].

2.3.12 Synergistic Effect of Magnesium and Fluorine Doping on the Electrochemical Performance of Lithium-Manganese Rich (LMR)-Based Ni–Mn–Co–Oxide (NMC) Cathodes for Lithium-Ion Batteries [40]

Through combustion technique, which is followed by fluorine doping by solid-state synthesis, Mg-doped-LMR-NMC ($Li_{1.2}Ni_{0.15-x}Mg_xMn_{0.55}Co_{0.1}O_2$) is synthesized [40]. Mg–F-doped LMR-NMC (Mg 0.02 mol) composite cathodes indicates

excellent discharge capacity of ~300 mAh g^{-1} at C/20 rate while pristine LMR-NMC indicates the initial capacity around 250 mAh g^{-1} in the voltage variety between 2.5 and 4.7 V. Mg–F-doped LMR-NMC indicates lesser Ohmic and charge transfer resistance, cycles reasonably well, and delivers a stable high capacity of ~280 mAh g^{-1} at C/10 rate [40]. In Mg–F-doped LMR-NMC, the voltage decay which is the main problem of LMR-NMC is mitigated compared to pristine LMR-NMC [40]. That a handful nanometer-thick Lipon film is an efficient way to enhance the interfacial stability against high voltage cycling, which gives rise to better high C-rate performance, greater usable capacity [440], and cycle life, is demonstrated by researches [40].

2.3.13 *Effect of Sonication Power on Al_2O_3 Coated $LiNi_{0.5}Mn_{0.3}Co_{0.2}O_2$ Cathode Material for LIB [41]*

In battery performance, these difficulties mainly linked with cathode materials, an amelioration in cathode materials might cause significant transformations [41]. To circumvent cycle life issue, which coates Al_2O_3 on $LiNi_{0.5}Mn_{0.3}Co_{0.2}O_2$ cathode material, which sol generated, gel technique [41]. At 600 °C, last heat treatment for Al_2O_3 crystallization had been done for 4 h. X-ray (XRD) diffraction measurements revealed that the material had a layered structure, which is ordered reasonably well-ordered layered structure and Al had been not in the $LiNi_{0.5}Mn_{0.3}Co_{0.2}O_2$ after the second gel is obtained [41]. Improved cycling performance is demonstrated by Al_2O_3 coated materials compared to the pristine material [41]. It is thought that, this amelioration is induced by the fact that Al_2O_3 layer prevents direct contact between electrolyte and reducing decomposition reactions and active material [41].

2.3.14 *Improved Electrochemical Performance of $NaAlO_2$-Coated $LiCoO_2$ for Lithium-Ion Batteries [42]*

The $NaAlO_2$ layer is coated on the $LiCoO_2$ particles efficiently [42]. The enhanced cycling stability and rate capability at a high cut-off voltage of 4.5 V versus Li^+/Li is shown by $NaAlO_2$-coated $LiCoO_2$ materials [42]. $NaAlO_2$-coating layer acts as a physical barrier; this barrier separates the LCO electrode and electrolyte, which will restrain the oxidation of solvents, the evolution of oxygen at high cut-off voltage, and break-up of cobalt ions [42]. Two-dimensional ion diffusion channel for lithium ions, which results in amelioration of electrochemical performance for $LiCoO_2$, could be offered by the $NaAlO_2$ layer [42]. It could be observed that all samples display the comparable diffraction peaks, matching reasonably well with R-3m space group (JCPDS No. 50-0653) and α-$NaFeO_2$-layered structure, and no diffraction peaks from possible impurities (e.g., $NaAlO_2$, Al_2O_3) in all samples were

observed [42]. It could be observed that the NA-coated LCO samples indicate a slight lower capacity than the pristine one; particularly, the capacity of LCO@NA-4% is 10% smaller than that of pristine LCO [42].

2.3.15 *A Ternary Oxide Precursor with Trigonal Structure for Synthesis of $LiNi_{0.80}Co_{0.15}Al_{0.05}O_2$ Cathode Material [43]*

Through calcining Ni–Co–Al composite oxalates formed by employing a facile chemical strategy, a Ni–Co–Al ternary oxide precursor with a trigonal structure, which could be utilized to synthesize $LiNi_{0.8}Co_{0.15}Al_{0.05}O_2$ cathode material, had been prepared [43]. The $LiNi_{0.8}Co_{0.15}Al_{0.05}O_2$ cathode material, which is calcined at a temperature as low as 650 °C, had satisfactory electrochemical performance with an initial discharge capacity of 183.9 mAh g^{-1} [43]. Through traditional solid-state technique, the $LiNi_{0.8}Co_{0.15}Al_{0.05}O_2$ cathode material is synthesized, as reasonably well [43]. That investigation offers a facile way to synthesize layered cathode material with satisfactory electrochemical performance at a lower calcining temperature [43]. That the electrochemical properties of Ni-rich cathode material, which traditional solid-state technique prepared, are not good, which is primarily attributed to the inhomogeneous distribution of transition metal ions, despite repeated mechanical ball milling before calcining is confirmed by these results [43].

2.3.16 *$LiMO_2@Li_2MnO_3$ Positive-Electrode Material for High Energy Density Lithium-Ion Batteries [44]*

$Li[Ni_{1/3}Co_{1/3}Mn_{1/3}]O_2$ (NCM 111)'s capacity of 155 mAh g^{-1} is fairly low, and cycling at potentials above 4.5 V gives rise to rapid capacity deterioration [44]. A successful synthesis of lithium-rich layered oxides (LLOs) with a shell of Li_2MnO_3 (C2/m) (the molar ratio of Ni, Co to Mn is the identical as that in NCM 111) and a core of $LiMO_2$ (R-3m, M = Ni, Co) is indicated by us [44]. The core-shell material $Li_{1.15}Na_{0.5}(Ni_{1/3}Co_{1/3})_{core}(Mn_{1/3})_{shell}O_2$ could be cycled to a high upper cut-off potential of 4.7 V, delivers a high discharge capacity of 218 mAh g^{-1} at 20 mA g^{-1}, and possesses 90% of its discharge capacity at 100 mA g^{-1} after 90 cycles; the use of this material in Li-ion batteries can considerably increase their energy density [44].

2.3.17 Enhanced Electrochemical Performances of Li_2MnO_3 Cathode Materials by Al Doping [45]

The Al-LMO subsample displays a considerable amelioration on the rate capability and cycling stability, which is compared to the LMO subsample [45]. The differential capacity versus voltage (dQ/dV) results show that Al doping might be to downturn the rate of reconfiguration upon cycling and deter the first charge stage reconfiguration from a layered stage to a cubic spinel-like stage [45]. Electrochemical impedance spectroscopy (EIS) results corroborate that Al doping decreases the charge-transfer resistance and enhances the electrochemical reaction kinetics [45]. Li-rich Mn-based layered compounds have been regarded as one of the most fruitful cathode material for future Li-ion batteries due to their advantage of high reversible capacity (>200 mAh g^{-1}), which is charged when above 4.5 V [45, 476, 489–491].

2.3.18 Improving the Electrochemical Performance of $LiNi_{0.5}Co_{0.2}Mn_{0.3}O_2$ by Double-Layer Coating with Li_2TiO_3 for Lithium-Ion Batteries [46]

The dual-layer Li_2TiO_3 coating of $LiNi_{0.5}Co_{0.2}Mn_{0.3}O_2$ (NCM523) compound has been efficiently synthesized by a facile technique for the first time [46]. The enhanced electrochemical performance is attributable to the stable dual-layer Li_2TiO_3; this dual-layer serves as a protective layer that prevents side reactions between electrode and electrolyte and a 3D-diffusion pathway for Li^+ ions [46]. A fruitful technique to enhance rate capability and cycle performance of NCM523 is the double-layer coating by Li_2TiO_3 [46]. The surface of the double-layer coated subsample N5@ (0.5 + 0.5)% LT is smoother than those of the single-layer and more homogeneous coated samples as could be observed from the SEM images [46].

2.3.19 Modification Research of $LiAlO_2$-Coated $LiNi_{0.8}Co_{0.1}Mn_{0.1}O_2$ as a Cathode Material for Lithium-Ion Battery [47]

Through hydrolysis-hydrothermal technique, the $LiNi_{0.8}Co_{0.1}Mn_{0.1}O_2$ with $LiAlO_2$ coating had been obtained [47]. That the $LiAlO_2$ layer had been nearly totally covered on the surface of particle had been demonstrated by the results, and the thickness of coating had been about 8–12 nm [47]. At 40 °C, side reaction between electrolyte and composite had been repressed by the $LiAlO_2$ coating; the

electrochemical performance of the $LiAlO_2$-coated $LiNi_{0.8}Co_{0.1}Mn_{0.1}O_2$ had been enhanced [47]. Upon 100 cycles at room temperature and 87.4% capacity retention after 100 cycles at 40 °C, the $LiAlO_2$-coated subsample delivered a high discharge capacity of 181.2 mAh g^{-1} (1 C) with 93.5% capacity retention [47].

2.3.20 *Aluminum Doped $Na_3V_2(PO_4)_2F_3$ via Sol-Gel Pechini Method as a Cathode Material for Lithium-Ion Batteries [48]*

The solid solution series $Na_3V_{2-x}Al_x(PO_4)_2F_3$ (where x = 0, 0.02, 0.05, and 0.1) powders have been prepared employing the Pechini technique to investigation the effect of aluminium doping on the electrochemical properties of these cathode materials for Li-ion batteries [48]. Through X-ray diffraction, differential and thermo-gravimetric analysis, specific surface area, the structure, morphology, and composition, of the compounds were examined, and pore size analysis, which employs Brunauer-Emmett-Teller-Barret-Joyner-Halenda techniques, scanning electron microscopy, elemental chemical analysis with caused coupled plasma-optical emission spectrometry, and charge/discharge galvanostatic experiments [48]. The stage with 0.05 mol of aluminium gave the optimal consequence electrochemical charge/discharge capacities of 123–101 mAh/g with a capacity retention of 82% and cell voltage of 4.4 V versus Li, compared to undoped material which gave 128–63 mAh/g, and 49% capacity retention [48]. Improved electrochemical performance maybe attributed to enhanced structure stability had been demonstrated by Al-doped samples compared to the undoped material [48].

2.3.21 *Co-precipitation Synthesis of Precursor with Lactic Acid Acting as Chelating Agent and the Electrochemical Properties of $LiNi_{0.5}Co_{0.2}Mn_{0.3}O_2$ Cathode Materials for Lithium-Ion Battery [49]*

Through coprecipitation, which employs lactic acid as the environmentally friendly chelating actor, hydroxide precursor $Ni_{0.5}Co_{0.2}Mn_{0.3}(OH)_2$ had been efficiently prepared [49]. Through sintering the mixture of Li_2CO_3 and as-prepared $Ni_{0.5}Co_{0.2}Mn_{0.3}(OH)_2$ precursor, the $LiNi_{0.5}Co_{0.2}Mn_{0.3}O_2$ cathode materials were obtained [49]. Through employing X-ray diffraction (XRD), land battery tester, and field-emission scanning electron microscopy (FE-SEM), electrochemical performances of $LiNi_{0.5}Co_{0.2}Mn_{0.3}O_2$ cathode materials, and Morphological, were

examined [49]. The results revealed that the quasi-spherical $LiNi_{0.5}Co_{0.2}Mn_{0.3}O_2$ with the size of about 5 μm showed the excellent electrochemical performance when its $Ni_{0.5}Co_{0.2}Mn_{0.3}(OH)_2$ precursor had been synthesized at the molar ratio of 1:1 between transition metal ion and lactate ion [49].

2.3.22 *Effect of Nitridation on $LiMn_{1.5}Ni_{0.5}O_4$ and Its Application as Cathode Material in Lithium-Ion Batteries [50]*

Through a solid-state reaction, which nitridation followed, Nitridated $LiMn_{1.5}Ni_{0.5}O_4$ had been prepared to examine the effect of nitrogen on the electrochemical and systemic performance of $LiMn_{1.5}Ni_{0.5}O_4$ cathode material for lithium-ion batteries [50]. Electrochemical researches on the nitridated $LiMn_{1.5}Ni_{0.5}O_4$ had been carried out employing the galvanostatic charge-electrochemical impedance spectroscopy and discharge process [50]. Rate capability and enhanced cycleability had been shown by the nitridated $LiMn_{1.5}Ni_{0.5}O_4$ compared with $LiMn_{1.5}Ni_{0.5}O_4$, which originated from the enhanced electric conductivity, which the increasing number of Mn^{3+} hopping carriers including increasing proximity between active Ni redox centres triggered [50].

2.3.23 *The Application of a Water-Based Hybrid Polymer Binder to a High-Voltage and High-Capacity Li-Rich Solid-Solution Cathode and Its Performance in Li-Ion Batteries [51]*

Uniform cathode films were prepared with a Li-rich solid-solution ($Li[Li_{0.2}Ni_{0.18}Co_{0.03}Mn_{0.58}]O_2$) cathode material and a water-based hybrid polymer binder (TRD202A, JSR, Japan), which is comprised of acrylic polymer and carboxymethylcellulose, fluoropolymer, and conducting carbon additive [51]. A cathode film, which is prepared with the water-based hybrid polymer binder, revealed long-term validity including greater electrochemical resistance when compared with a cathode film, which employs the traditional polyvinylidene difluoride binder, after 80 cycles in the chemical environment of lithium ion cells [51].

2.3.24 *Na-Doped $LiMnPO_4$ as an Electrode Material for Enhanced Lithium-Ion Batteries [52]*

Via a straightforward sol-gel technique, $Li_{1-x}Na_xMnPO_4$ with various mole ratios ($0.00 \leq x \leq 0.05$) of sodium is synthesized [52]. The discharge capacity of $Li_{1-x}Na_xMnPO_4$ differs relating to mole ratios of sodium incorporated [52]. In $Li_{0.97}Na_{0.03}MnPO_4$, which is greater than that of pristine $LiMnPO_4$ and other Na-incorporated $LiMnPO_4$, the maximal discharge capacity of 92.45 mAh g^{-1} is detected [52].

2.3.25 *Synthesis of Diverse $LiNi_xMn_yCo_zO_2$ Cathode Materials from Lithium-Ion Battery Recovery Stream [53]*

In some nations, a huge quantity of spent Li-ion batteries is being landfilled every year; in order to recover and re-use critical materials, an a high-efficiency Li-ion and cheap battery recovery process had been devised at Worcester Polytechnic Institute [53]. It had been revealed that high performance $Ni_{1/3}Mn_{1/3}Co_{1/3}(OH)_2$, $Ni_{0.5}Mn_{0.3}Co_{0.2}(OH)_2$, $LiNi_{1/3}Mn_{1/3}Co_{1/3}O_2$ and $Ni_{0.6}Mn_{0.2}Co_{0.2}(OH)_2$ precursors, $LiNi_{0.5}Mn_{0.3}Co_{0.2}O_2$, $LiNi_{0.6}Mn_{0.2}Co_{0.2}O_2$ cathode materials could be synthesized from the leaching solutions of a Li-ion battery recovery stream [53]. Electrochemical tests results shown that all cathode materials synthesized from spent Li-ion battery recovery streams carried out at a discharge capacity greater than 155 mAh/g at first cycle of 0.1 C, and after 100 cycles at 0.5 C, with over 80% of the capacity preserved [53]. An increase in Li-ion batteries signifies that there will be more battery waste in the near future [53]. That $LiNi_{1/3}Mn_{1/3}Co_{1/3}O_2$, $LiNi_{0.6}Mn_{0.2}Co_{0.2}O_2$, and $LiNi_{0.5}Mn_{0.3}Co_{0.2}O_2$, have excellent specific rate capacities is demonstrated by the electrochemical test results [53].

2.4 Conclusion

Without an further mixing process of lithium salts and retains homogeneous cation distribution, the material could be obtained with the coprecipitation of Li^+ with transition metal ions [1]. The material delivers enhanced electrochemical performances such as cycle stability and rate capability, as shown by a high reversible capacity of 104.0 mAh g^{-1} at 10 C, and more than 98.5% capacity retention after 100 cycles at 1 C. On the basis of this work, LNMO materials prepared by the present synthetic route can be a fruitful candidate cathode for high-power Li-ion batteries [1].

Hierarchical hollow $LiNi_{0.5}Mn_{1.5}O_4$ microspheres as a 5-V cathode material for Li-ion batteries has been synthesized by a coprecipitation strategy accompanied with high-temperature calcinations [2]. The obtained commodities deliver enhanced electrochemical performances with satisfactory rate capability and cycle stability; this stability makes it a fruitful cathode candidate for high-energy density Li-ion batteries [2].

Electrochemical measurements have demonstrated that Ni-Cr codoped samples display more stable cycling performance than the pure $LiMn_2O_4$ [3]. The cycling performance had been considerably better at high current rates even though the initial discharge specific capacity of the $LiNi_{0.01}Cr_{0.01}Mn_{1.98}O_4$ cell had been observed lower than the pure $LiMn_2O_4$ [3]. A discharge capacity of 91% of the initial has been regained upon reducing the current rate to 0.1 C. In contrast with the pure $LiMn_2O_4$, the enhanced capacity retention of $LiNi_{0.01}Cr_{0.01}Mn_{1.98}O_4$ had been attributable to the inhibition of the Jahn-Teller distortion effect, considerably easier Li^+ ion diffusion because of shortening of the diffusion length and formation of homogeneous smaller particle size after cycling at 5 C [3].

Spinel $LiNi_{0.5}Mn_{1.5}O_4$ cathode materials were synthesized through a facile solid-state technique and the impacts of various lithium excess quantities on the crystalline structure, particle morphology, and electrochemical performance were systematically examined [4]. The slightly inferior electrochemical performance of LNMO-10% subsample could be attributed to the greater cation, which mixes more $Li_xNi_{1-x}O$ impurity stage and extent [4]. It could be concluded that in solid-state technique, the lithium excess quantity has little impact on size and particle morphology, and the electrochemical performance is primarily dependent upon the crystalline structure, more specifically, Mn^{3+} content (disordering extent), extent, which mixes cation, and $Li_xNi_{1-x}O$ impurity quantity (stage purity) [4].

The Sn^{4+}-doped LMNC cathode materials with the enhanced electrochemical performance were synthesized employing the sol-gel technique [5]. The electrochemical performance of Sn^{4+}-doped LMNC cathode has been substantially enhanced, particularly when the doping quantity of Sn^{4+} is 0.01 [5]. A faster Li^+ diffusion process and better systemic stability, which are favourable for the electrochemical performance of the LMNC cathode material is demonstrated by these [5].

The usage of CNF and the synthetic technique offer an alternative for the synthesis of $LiNi_{0.5}Mn_{1.5}O_4$ cathode materials with greater performance and suggest their promise in practical applications [6].

The $LiNi_{0.8}Co_{0.15}Ti_{0.05}O_2$ subsample prepared at 800 °C displays a greater extent of the least cation mixing and ordering hexagonal structure and demonstrates excellent electrochemical performance with the capacity retention of 86.7% after 30 cycles at 0.2 C. and the discharge capacity of 174.2 mAh g^{-1} [7].

The integrity of the Li_2FeSiO_4 crystal structure can be enhanced by strontium cation doping because of lowered Li/Fe anti-site disorder in the lattice [8]. The 1% strontium cation-doped Li_2FeSiO_4/C delivered a high discharge capacity of 181 mAh g^{-1} at 0.5 C rate as a cathode material of a lithium-ion battery [8]. Li_2FeSiO_4/C cathode showed high specific capacity, satisfactory rate performance had been

cation-doped by the 1% strontium, and stable cycle performance, which is attributed to the enhanced Li^+ diffusion capability, undermined crystal structure stability, and restrained side reactions between the electrode and electrolyte [8].

Through XRD, SEM, TEM, XPS, galvanostatic discharge/charge test, CV, and EIS, the structure and electrochemical properties of the materials are examined [9]. That $LiNi_{0.5}Mn_{0.45}Ru_{0.05}O_2$ can deliver a preferable electrochemical performance is revealed by the electrochemical measurement [9]. The EIS and CV results corroborate that $LiNi_{0.5}Mn_{0.45}Ru_{0.05}O_2$ has a satisfactory reversibility, an enhanced diffusion coefficient to assure excellent electrochemical performance, and a low charge-transfer resistance [9].

"The specific discharge capacities of $LiCr_{0.05}Ni_{0.475}Mn_{1.475}O_{3.95}F_{0.05}$ at 0.1, 0.5, 2, 5, and 10 C were 134.18, 128.70, 123.62, 119.63, and 97.68 mAh g^{-1}, respectively" [10]. The specific discharge capacity had been 121.02 mAh g^{-1} after 50 cycles at 2 C, which is of 97.9% the initial discharge capacity [10]. The capacity retention rate of $LiCr_{0.05}Ni_{0.475}Mn_{1.475}O_{3.95}F_{0.05}$ had been the largest among the samples [10]. Cr^{3+}, F^- codoped of the materials substantially enhanced the specific discharge capacity at greater rate, enhanced the cycling stability, lowered the impedance value, and enhanced the reversibility of lithium ions [10].

$Li_3Y_xV_2(PO_4)_3$/C composites with various quantities of Y-doping were efficiently prepared by a rheological stage reaction process [11]. Y-doping and the carbon coating have considerably impact on the electrochemical properties of $Li_3V_2(PO_4)_3$ [11]. The optimal electrochemical performance with the initial discharge capacity of 158.75 mAh g^{-1} and the capacity of 148.99 mAh g^{-1} after 50 cycles at a current density of 0.1 C. Hence, carbon coating and metal ions doping are efficient ways to attain materials of greater capacity and better cycling stability is shown by $Li_3Y_{0.03}V_2(PO_4)_3$/C among all materials [11].

$LiMn_2O_4$ had been coated by new transition metal alloy (M_x = PtAu) with enhanced high rate performances have been efficiently designed and synthesized [12]. The smaller potential variations of alloy functionalized-$LiM_xMn_{2-x}O_4$ cathodes indicate smaller polarization because of faster insertion/extraction of Li^+ ions in the spinel structure [12]. The amelioration in diffusivity of Li^+ ions might be attributable to three reasons [12]. The vacancies at the octahedral sites created by M_x coating offer further diffusion pathways for lithium ions [12]. The increase in lattice parameter after M_x coating helped faster lithium diffusion [12]. Such improvements are because of enhanced lithium and electronic electrical conductivity diffusivity, which results from transition metal alloy coating [12]. That the $PtAu_{0.02}$ coating particles act as a protective layer can be a novel viable strategy for generating advanced Li-ion battery cathodes with enhanced electrochemical properties and that prevents the oxygen from outgoing which contributed to main improvements is demonstrated by the results [12].

In the compound, increased the relative content of aluminium can enhance structure stability and decline the extent of cation mixing [13]. Changing the relative content of aluminium properly is an efficient and straightforward technique to enhance the electrochemical performance of $LiNi_{0.56}Co_{0.19}Mn_{0.24}Al_{0.01}O_2$ cathode

composite materials for lithium-ion batteries [13]. Structure and rate capacities of the novel material need to be additional enhanced in later investigation [13].

The resulting $S_{0.5}$ material displays an excellent cycling performance that 91.4% of its discharge capacity can be preserved after 100 cycles [14]. $S_{0.5}$ with excellent rate performance that the discharge capacities of $S_{0.5}$ subsample are 125.7, 118.1, 111.7, and 96.6 mAh g^{-1} at 0.2, 0.5, 2, and 5 C [14]. The discharge capacities of the $S_{0.5}$ subsample are 80.8 mAh g^{-1} even at greater rate (i.e., 10 C) [14]. The middle particle size of $S_{0.5}$ subsample balances the conflicting of diffusion length in solid stage and particle agglomeration; this stage gives rise to perfect contacts with the conductive additive, substantial evident lithium ion diffusion rate, and the optimum performance [14].

The highest discharge capacity, the most excellent rate capability and the optimal cycling performance is shown by the LR-1.0 among all the samples [15]. The discharge capacity retention of 93.3% after 50 cycles and the discharge capacity of 266.6 mAh g^{-1} is shown by the LR-1.0 at 0.1 C [15]. 266.6 mAh g^{-1}'s discharge capacity can retain at 146.6 mAh g^{-1} at 2.0 C [15]. That investigation offers a novel applicable route to synthesize advanced Li-rich layered cathode materials [15].

Through utilizing an enhanced (i.e., calcining-milling-recalcination) calcining technique, which had been based upon a conventional solid-state synthesis, micrometer-sized, spherical $LiNi_{0.5}Mn_{1.5}O_4$ had been prepared [16]. The spherical particles composed a huge number of nano-and/or sub-micrometer-sized primary particles and showed striking rate capability and cycling performance than the reference material, which is formed through the conventional synthesis route [16]. A convenient and effective strategy for the solid-state synthesis of $LiNi_{0.5}Mn_{1.5}O_4$ cathode material is amelioration of the calcining process [16].

A hierarchical hollow spherical lithium-rich, which employs $Li_{1.2}Mn_{0.54}Ni_{0.13}Co_{0.13}O_2$ cathode material CTAB and sucrose as a soft template, which is combined with hydrothermal assisted homogenous precipitation technique, had been efficiently synthesized by us [17]. That this hollow spherical cathode composite displays high electrochemical performance in terms of reversible capacity and cycle stability life including rate capacity is shown, in comparison with the solid sphere subsample, by the results [17]. Especially cycled at 560 mA g^{-1}, the hollow spherical subsample indicates high discharge capacity of 215 mAh g^{-1} and can attain 143.3 mAh g^{-1} after 100 cycles [17]. That work offers an strategy to enhancing cycling ability of the layered lithium-rich cathode and the rate capacity [17].

$Li[Ni_{1/3}Co_{(1-x)/3}Mn_{1/3}Fe_{x/3}]O_2$ (x = 0.0, 0.1, 0.3, 0.5, 0.7, 0.9) cathode materials have been synthesized through hydroxide coprecipitation technique [18]. A small quantity of Fe^{3+} replaced for Co^{3+} when preparing cathode materials will give excellent electrochemical performance [18].

Both have a well-defined cubic structure, which includes the $P4_332$ space group, with Mg^{2+} and Cu^{2+} ions replacing Ni^{2+} occupying the 4b sites is randomly selected by analyses, LCNM and the LMNM [19]. Especially at a high temperature (55 °C), LMNM and the LCNM samples both display cycling stability and excellent rate performance [19].

Through a solid-state route, which is correlated with chemically caused precipitation technique for the first time, the tavorite-structured $LiFePO_4F$ nanospheres are efficiently synthesized [20]. Exhibits homogeneous almost monodisperse nanospheres-like particles with the mean particle size of 500 nm had been based on $FePO_4$ nanospheres by the $LiFePO_4F$ [20]. The Li-ion diffusion coefficient (D) of $LiFePO_4F$ is 1.0×10^{-11} cm^2 s^{-1} computed on account of EIS data [20]. The excellent cycle performance could be attributable to the homogeneous nanospheres-like morphology; this homogeneous is beneficial to enhance the interface area between electrolyte and electrode, shorten the transport distance of electrons and ions and improve the power and energy densities of batteries, and enhance the kinetics of Li ions [20].

In contrast with pristine $Li_{1.2}Ni_{0.2}Mn_{0.6}O_2$ cathode material, better cycling and rate performance and a greater coulomb efficiency is demonstrated by the Cr-doped $Li_{1.2}Ni_{0.16}Mn_{0.56}Cr_{0.08}O_2$ material [21]. The XRD and XPS results after cycling indicate that the spinel stage could be restrained after Cr doping in the layered $Li_{1.2}Ni_{0.2-x}Mn_{0.6-x}Cr_{2x}O_2$ materials [21]. Electronic electrical conductivity in the Cr-doped $Li_{1.2}Ni_{0.16}Mn_{0.56}Cr_{0.08}O_2$ material and lower transfer resistance, and greater structure stability, lithium ion, might be responsible for the better electrochemical performance of $Li_{1.2}Ni_{0.16}Mn_{0.56}Cr_{0.08}O_2$ [21].

The calcining temperature had a considerable impact on the crystallite (XS) size though had little effect on the microstructures including lattice (a, c and V) parameters, the extent of the cation mixing, and refined density, during the process of preparing $Li(Ni_{0.5}Co_{0.2}Mn_{0.3})O_2$ cathode employing a microsized spherical $(Ni_{0.5}Co_{0.2}Mn_{0.3})(OH)_2$ precursor, which a high-temperature solid-state technique in the variety of 750 to 820 °C comprised of aggregated nano-sized particles [22]. The electrochemical properties of the $Li(Ni_{0.5}Co_{0.2}Mn_{0.3})O_2$ cathode heavily rely upon its crystallite size [22]. The variability trend of the retention for the electrochemical capacity is nearly the identical as that of the retention for the crystallite size [22].

Through hydroxide coprecipitation technique, the high-voltage spherical $LiNi_{0.5}Mn_{1.5}O_4$ cathode material for lithium-ion batteries had been efficiently synthesized [23]. The discharge capacity is 109.2 mAh g^{-1} at 1.0 C with a cut-off voltage variety of 3.50–4.95 V at 25 °C and the capacity retention is 96.2% after 50 cycles [23]. Under various rates with a cut-off voltage variety of 3.50–4.95 V at 25 °C, when the obtained $LiNi_{0.5}Mn_{1.5}O_4$ cathode material discharges, the discharge capacities are maintained at about (0.1 C) 145.0, (0.5 C) 113.5, (1.0 C) 126.8 and 112.4 (2.0 C) mAh g^{-1} and the initial coulomb efficiencies maintain above 95.2 (0.1 C)%, 95.0 (0.5 C)%, 94.8 (2.0 C)%, respectively and 92.5 (1.0 C)% [23]. The results might lead to performance amelioration and industrial production of $LiNi_{0.5}Mn_{1.5}O_4$ cathode materials for 5 V lithium batteries [23].

The low-temperature properties of $LiFePO_4$/C prepared by polyol route were completely examined [24]. The as-prepared $LiFePO_4$/C summarized an excellent low-temperature electrochemical properties, delivering 146.7, 128.7, and 109.2 mAh g^{-1} at 0.1 C under 0, −10, and −20 °C, respectively [24]. That prepared $LiFePO_4$/C can maintain a specific discharge capacity of 133.7 mAh, which

is recycled g^{-1} when at 0.1 C under 0 °C, after charge/discharge measurements at lower targeted temperatures and greater rates [24].

We have efficiently prepared the cathode materials based upon LNMO/P3HT-g-CNTs through mixing process [25]. The LNMO/P3HT-g-CNTs nano-composites has been typified and demonstrated a remarkably greater efficiency of and Ni^{2+}/Ni^{4+} redox couples in comparison to conventional cathodes based upon LNMO/vulcan carbon [25]. LNMO/P3HT-g-CNTs nano-composites can act as fruitful cathode materials for the development of potential power lithium rechargeable batteries with this proof of notion [25].

It had been clearly shown that an easily accessible, environment-friendly and cheap material of the sea sponge Spongia officinalis could be utilized as a conductive matrix for electrodes of lithium-sulphur accumulators [26]. The biological material of the sea sponge had been, employing a quite straightforward technique, converted to a conductive carbon network with high concentration of nanopores on the surface [26]. In the 3D structured electrode, which is based upon the sea sponge, we attained exceedingly high loading of sulfur-nearly 5 mg/cm^2 even though the most basic possible electrode slurry, which comprises of the Super P carbon and the basic binder PVDF, had been utilized [26]. That is presumably because of the presence of nitrogen inside the 3D carbon matrix; this matrix enhances the polysulphide retention inside the electrode [26].

The current study emphasised the research issue (low electrical conductivity and sluggish transportation of Li^+ ions) on employing olivine $LiFePO_4$ (LFP) as a cathode material for high-rate lithium-ion batteries [27]. The electrochemical results revealed that electrode composite LFP/C/10% CNTs delivered a specific capacity of 190 mAh/g at C/10 rate after 200 cycles [27]. An excellent performance at rate capability had been detected with a capacity near to 200 mAh/g [27]. The generalization of this protocol on the bigger scale can improve the manufacturing of batteries with greater scored capacity; this capacity is highly desired for automotive industry applications including electric vehicles [27].

Cathode materials entail removable Li ions as charge carriers, and transition metal ions serving as redox centres, which account for most of the cost as the costliest sector of a LIB [28]. Considering the cost's elemental relative abundance, Fe-based and Mn-cathode materials are hence preferable decisions, and the cost's sodium analogues are attracting considerably attention, as they would allow the future of Li-free SIBs, which might be optimal decisions for large-scale applications [28]. That review entails the discussion of most of the Mn-based and Fe-cathode materials for SIBs and Li-ion batteries, such as polyanion compounds, oxides, and hexacyanometalates (for SIBs) [28]. It is easy to comprehend the various development stages and objectives of cathode materials for SIBs and Li-ion batteries from the clear-cut comparison [28]. In (1) the intensively examined tactics of tailoring particle size and constructing conductive composites readily cause further materials and processing expenses including inadequate volumetric and gravimetric energy densities, significant issues in this field remain: to satisfy the requirement of practical applications [28]. Some electrode materials have been indicated for cycling performance and outstanding rate capability (over 50 °C) by tailoring

particle shape and size and forming conductive composites in the case of cathodes for Li-ion batteries [28]. Regarding SIB cathodes, which are experiencing even quicker advancements with a variety of candidatures being devised, instead of merely mimicking the host structures of Li^+ during synthesis, many novel complex structures have been introduced to cope with the issues because of the distinct ionic size and electron configuration of Na^+ [28].

The cubic spinel structure with space group of Fd3 m is shown by all $LiNi_{0.5}Mn_{1.5}O_4$-based materials [29]. The 1.0 wt% $BiFeO_3$ $LiNi_{0.5}Mn_{1.5}O_4$ electrode displays the excellent cyclic stability with the capacity retention of 89.11% after 100 cycles that is greater than that of the LNMO (77.6%) [29]. The rate capability of 1.0 wt % $BiFeO_3$ $LiNi_{0.5}Mn_{1.5}O_4$ has been evidently enhanced, displaying discharge capacities of 85.8 and 74.8 mAh g^{-1} at 5 and 10 C, respectively [29]. Good cyclic stability of $BiFeO_3$-coated $LiNi_{0.5}Mn_{1.5}O_4$ electrode and the enhanced rate capability must be attributable to the surface modification of $BiFeO_3$; this modification impedes side reactions at electrolyte and reduces the charge transfer resistance and the cathode [29].

At room temperature, the significant improvements in the initial columbic efficiency, cyclic performance, and rate capability, are accomplished with proper quantity of Li_2TiO_3 coating layer [30]. The subsample coated with 3 wt% Li_2TiO_3 displays the highest rate capability, enhanced initial columbic efficiency, and optimal cyclability [30].

We utilized Na doping to Ni-rich, cycling stability of Li-ion batteries and layered LNMCO ($LiNi_{0.8}Mn_{0.1}Co_{0.1}O_2$) to enhance the rate capability [31]. The electrochemical properties of Na-LNMCOs were examined by us, and the results indicate the excellent rate capability (142 mAh g^{-1} at 7 C) and cycling stability (94.9% of capacity-retention rate after 100 cycles) of 0.2Na-LNMCO [31]. For the LNMCO along with Na doping we can derive rate capability and cycling stability that are both sound [31].

The enhanced performance of the surface-coated subsample is because the ZnO coating on the surface of $LiMn_2O_4$ can efficiently minimize electrochemical charge and polarization transfer resistance during discharge/charge cycling [32]. In the electrode material, the XRD results of the 2 wt% ZnO-coated $LiMn_2O_4$ material after 500 cycles confirmed that ZnO coating enhances the stability of the spinel structure, making lithium ions efficiently diffuse [32]. ZnO coating enhances the electrochemical performances of $LiMn_2O_4$ comparing with the pristine subsample in terms of rate capability and cycling [32].

In contrast to the bare $LiNi_{1/3}Co_{1/3}Mn_{1/3}O_2$, stability and better electrochemical performances are showed by $LiNi_{1/3}Co_{1/3}Mn_{1/3}O_2@Eu_2O_3$ [33]. Thermal safety, which is enhanced Notably, is shown by $LiNi_{1/3}Co_{1/3}Mn_{1/3}O_2@Eu_2O_3$ because of the stabilized interface [33].

Through hydrothermal technique, $5Li_2MnO_3{\cdot}0.5LiMn_{1/3}Ni_{1/3}Co_{1/3}O_2$ cathode material had been prepared and a thin layer of alumina had been efficiently coated on the surface of material, which is prepared, under the hydrolysis of aluminium isopropoxide which could be detected by TEM images [34]. Good electrochemical performance, which comprises the lowered first irreversible capacity deterioration and

the cycling stability, were accomplished for A-LMNCO materials and the reversibility of 2 wt% of A-LMNCO subsample had been the optimal [34]. The 2 wt% of A-LMNCO subsample still had a discharge specific capacity of 206.2 mAh g^{-1} after 100 cycles at 1 C rate with a high capacity retention of 97.4%, and the discharge specific capacity rebuilt to the original 95% or more assessed at low rates after cycling at high rates [34]. The alumina coating layer, which acts as a fast electron-conducting path, efficiently alleviates the side reaction between the electrolyte and the cathode material, with a low charge-transfer resistance and repress the change of surface structure [34].

An efficient approach has been introduced to improve cycle ability and rate capacity of the $LiMn_2O_4$ cathode [35]. The structures and electrochemical performances of the $LiMn_2O_4$ cathodes with various quantities of Li_2MnO_3 coating were examined [35]. The results of XPS, and SEM, TEM, highlight that Li_2MnO_3 has been efficiently coated onto the surface of $LiMn_2O_4$ cathode by the sol-gel route [35]. An efficient way to enhance the performance of $LiMn_2O_4$ cathode materials for Li-ion batteries is surface modification by Li_2MnO_3 [35].

The cycling degradation of LNMO at high voltage becomes the largest restrict in application [36]. Several types of tactics were utilized to lessen cycling degradation; this degradation can be presented as doping, electrolyte altering, cathode surface coating, and other efficient techniques [36]. Doping enhanced the cycle performance of LNMO primarily through metal ion changing structures, the crystal compositions, and parameters, including fostering the formation of structure [36]. Through employing the coating layer on the surface of LNMO, cathode surface coating can efficiently deter the undesirable side reactions, though the coated technology is complex under normal conditions [36]. Electrolyte altering is an optimal approach compared with doping and cathode surface coating; it not just prevents the undesirable side reactions between electrolyte and cathode though retains easy technology [36]. They are not able to stop the undesirable side reactions even though other techniques can enhance the cycle stable of LNMO in HVLIBs [36]. Electrolyte altering, and Doping, cathode surface coating, are able to attain the desired cycling stability in HVLIBs [36]. We outlined these methodologies to enhance the cycling stability of LNMO cathodes based upon cyclic degradation processes and its architectural elements [36]. The inquiries for high-voltage LNMO cathodes goal to ascertain the ways to enhance service and cycle performances of LNMO for the life [36]. The cycle performance of LNMO, which is based upon the synthesis of highly purified LNMO, cycling degradation mechanism of undesirable reactions between LNMO and electrolyte, and systemic reversibility of, must be enhanced by us [36]. Electrolyte additives and organic coating might be satisfactory ways to enhance the cycle performance of LNMO in multiple modification techniques [36].

The results of systemic analysis revealed that all of the materials have satisfactory crystallinity, comparable morphology and comparable size distribution [37]. The results of electrochemical measurements indicate that a 3 mol% Ca-doping displays the optimal electrochemical performance, which comprises the optimal cycle stability and rate performance and the highest capacity [37]. The charge

transfer resistance of the 3 mol% Ca-doped cathode material is substantially smaller than that of the un-doped material; this material means that it has a faster lithium-ion migration rate [37]. 3 mol% Ca-doping can lower Li/Ni cation mixing, increase the systemic stability, decline the migration resistance, lessen polarization and enhance the migration rate of the Li-ion, which, in turn, improves the electrochemical properties of $LiNi_{0.5}Mn_{0.5}O_2$ [37].

We have revealed that the materials are core-shell structured, and the core is a layered $LiMO_2$ stage (R-3 m), whilst the shell is a monoclinic Li_2MnO_3 stage (C2/m) by employing the XPS, and XRD, TEM, methods [38]. That the core-shell structures make Li^+/Ni^{+2} cation disorder less than the pristine material does, and XPS indicates that the quantity of Ni^{2+} increases along with the increase of Mn content is demonstrated by the Rietveld refinements [38]. It is thought make the composite functionally sounder and its thermal stability greater and that many Mn^{+4} in the shell and Ni^{+2} in the core interdiffuse into the counter parts [38]. The core-shell-structured materials could be safely cycled to greater upper cutoff potential of 4.7 V, in contrast to that of the pristine material, just 4.3 V; this material suggests that the Li_2MnO_3 shell has considerably enhanced the electrochemical performance of NCM811 in terms of energy density and discharge capacity [38]. The thermal analyses of the highly delithiated materials, which are prepared by charging a surface-modified material to 4.3 and 4.7 V respectively and the cells of the pristine and maintaining potential for 2 h, corroborate the greater stability of the core-shell structured materials [38]. At 360 °C, the exothermic peak of the surface-modified material seems with a heat evolution of 239.144 J g^{-1}, whilst those of the pristine material seem at 250 °C with a heat evolution 575.136 J g^{-1} [38].

FESEM and XRD results of Al-doped materials indicate surface morphology and the comparable XRD patterns to those of $Li[Li_{0.2}Mn_{0.54}Ni_{0.13}Co_{0.13}]O_2$ [39]. Electrochemical discharge and charge measurements suggest that LNCMAl1 displays better rate capability, greater discharge capacity, and better cycling performance than the other materials [39]. A high reversible capacity of 213.7 and 193.8 mAh g^{-1} at 1.0 and 2.0 C, respectively is displayed by LNCMAl1 [39]. The corresponding capacity retention ratio can still be 58.2 and 66.8% after 50 cycles at 1.0 and 2.0 C. EIS results indicate that substituting traces of Al element for Co element of $Li[Li_{0.2}Mn_{0.54}Ni_{0.13}Co_{0.13}]O_2$ can decline charge-transfer impedance and improve the reaction kinetics; these kinetics is thought to be the main reason for satisfactory rate capability of LNCMAl1 [39].

F and Mg doping does not change the crystal system of LMR-NMC which is apparent from XRD plot where no impure stage peaks are detected [40]. At C/20 rate, 10, F-doped LMR-NMC indicate excellent electrochemical performance and (1:50 wt%-LiF: LMR-NMC) doped subsample particularly 0.02 mol% of Mg, delivers capacity $\sim$300 mAh g^{-1} −15% excess capacity than pristine LMR-NMC [40]. Doped subsample indicates enhanced capacity retention, mitigated voltage decay, and high C rate performances compared to pristine LMR-NMC [40]. The enhanced electrochemical performance is attributable because of minimize stabilization of crystal structure and cation mixing during cycling [40].

$LiNi_{0.5}Mn_{0.3}Co_{0.2}O_2$ cathode material had been generated by sol-gel technique [41]. Al_2O_3 had been coated on $LiNi_{0.5}Mn_{0.3}Co_{0.2}O_2$ cathode material by employing ultrasonic stirrer and selected as a surface modifier [41]. The first discharge capacities of the samples are 99.01 178.28, 130.22 and 141.34, respectively and columbic efficiencies are observed to be 91.95 and 99.56% for pristine, NMC-45 and NMC-100 samples [41]. The first discharge capacities and charge variations of the samples are computed as 54.62, 30.94 and 31.99 for pristine, NMC-100 and NMC-45 respectively [41].

Through heating method and means of hydrolyzing, the $LiCoO_2$ cathode materials coated with multiple quantities of $NaAlO_2$ were synthesized [42]. The $NaAlO_2$ layer had been coated onto the $LiCoO_2$ particles efficiently without influencing the crystal structure of $LiCoO_2$ [42]. An effective strategy to enhance the electrochemical performance of $LiCoO_2$ at high cut-off voltage of 4.5 V versus Li^+/Li, which could be referred for other cathode material including Li-and Mn-rich and the nickel-manganese-cobalt materials layered oxide materials is the $NaAlO_2$ coating [42].

A facile approach has been devised to synthesis $LiNi_{0.8}Co_{0.15}Al_{0.05}O_2$ cathode material by chemically pretreating raw reactants to derive a ternary oxide precursor with a trigonal structure [43]. In $LiNi_{0.8}Co_{0.15}Al_{0.05}O_2$ cathode material, which traditional solid-state reaction at low-temperature prepared, a small quantity of impurity stage $LiCoO_2$ had been detected [43]. That the ternary oxide precursor with a trigonal structure is beneficial to the formation of pure stage high performance of the materials and $LiNi_{0.8}Co_{0.15}Al_{0.05}O_2$ is regarded by us [43].

The core-shell material is comprised of a core of a layered $LiMO_2$ stage (R-3 m), whilst the shell is a monoclinic Li_2MnO_3 stage (C2/m) [44]. That the core-shell structured material has less Li^+/Ni^{2+} cation disorder than the pristine material is demonstrated by rietveld refinements [44]. That stronger M * -O (M * = Mn, Co, Ni) ties are present in the core-shell material, which gives rise to high systemic stability during the charge-discharge process is confirmed by rietveld [44]. At a greater upper cut-off potential of 4.7 V than that of the pristine material (4.5 V), the core-shell material could be cycled [44]. The core-shell material exhibits a greater mean voltage, better cycling stability than those of the pristine material, and a greater energy density [44].

The electrochemical behaviour of cycled Al-LMO and LMO samples suggests the stage reconfiguration from a layered to a spinel [45]. The Al-LMO subsample showed a considerable amelioration on rate performances and cycle compared to the LMO subsample [45]. The dQ/dV results indicate that Al doping might downturn the rate of spinel stage reconfiguration of stage, which is layered, in the following cycles and deter the stage reconfiguration in the first charge process [45]. EIS results corroborate that Al doping decreases the charge-transfer resistance and enhances the electrochemical reaction kinetics [45].

It is demonstrated that both single-layer coating and double-layer coating can enhance the cycling stability and rate capability of this high-energy cathode material [46]. The double-layer Li_2TiO_3-coated subsample N5@ (0.5 + 0.5)% LT indicates the optimum properties due to its homogeneous and full coating layer,

even increases the specific capacity at all current densities, which is compared with the bare non-coated powder [46].

$LiAlO_2$-coated $LiNi_{0.8}Co_{0.1}Mn_{0.1}O_2$ material has been efficiently prepared by hydrolysis-hydrothermal technique [47]. The results indicate that the $LiAlO_2$-coated layer of 8–12 nm enhances the thermal stability of the material at 40 °C via a series of electrochemical tests, morphology, and characterization of the structure [47]. A rate capability, thermal stability compared with the pristine material, and cyclic performance, which is enhanced markedly, had been shown by $LiAlO_2$-coated material [47].

The Al-doped $Na_3V_2(PO_4)_2F_3$ with various Al concentration (x = 0, 0.02, 0.05, and 0.1) have been synthesized by Pechini technique [48]. Since ionic radius of Al^{3+} is smaller than V^{3+}, the cell parameters of the vanadium fluorophosphates lattice could be declined by aluminium doping [48]. The $Na_3V_2(PO_4)_2F_3$ with just 5% (x = 0.05 mol) of Al doping displays greater discharge capacity, capacity retention and better charge/discharge stability than the pristine $Na_3V_2(PO_4)_2F_3$ [48]. Al-doping $Na_3V_2(PO_4)_2F_3$ provides many favourable properties to be look at as a fruitful cathode material for Li-ion batteries [48]. The results of this first strategy to the investigation and preparation of this material highlight that Al-doping is a novel approach for improving the electrochemical performance of the $Na_3V_2(PO_4)_2F_3$ [48].

Through coprecipitation technique, which employs lactate ion as the chelating actor, $Ni_{0.5}Co_{0.2}Mn_{0.3}(OH)_2$ precursors were efficiently synthesized [49]. At the molar ratio of 1:1 between transition metal ion and lactate ion, when the $Ni_{0.5}Co_{0.2}Mn_{0.3}(OH)_2$ precursor had been synthesized, its $LiNi_{0.5}Co_{0.2}Mn_{0.3}O_2$ cathode revealed retention rate (93.3%) and the highest discharge capacity (194.2 mAh g^{-1}) after 100 cycles [49].

Through a solid-state reaction, which post-process nitridation and characterization by XRD, XPS, and electrochemical analysis followed, Nitridated $LiMn_{1.5}Ni_{0.5}O_4$ had been synthesized [50]. In terms of its bulk crystallographic structure, grain size, and morphology, the nitridated $LiMn_{1.5}Ni_{0.5}O_4$ had been not basically altered [50]. Excellent cycleability and high rate capability, which is attributable to the increasing number of Mn^{3+} hopping carriers including the enhanced electric conductivity, which active Ni redox centres triggered, had been shown by the nitridated $LiMn_{1.5}Ni_{0.5}O_4$ [50].

Throughout the preparation of a water-based slurry, the charge/discharge capacities, cycle stability, rate performance, mechanical resistance, resistance of electrochemical oxidation, structure and transformations of the surface composition were researched after water-treatment [51]. The TRD202A binder had been identified as a fruitful water-based binder that satisfies some required attributes for the development of environment-friendly cathodes and high-performance [51]. Some Li-rich solid-solution cathode materials having various compositions of Li, Mn, Co ions, and Ni, showed gradual decreases in the discharge capacity [51]. Especially after water-treatment of the cathode particles, the stability of the charge/discharge performance could be enhanced by the protective layers [51]. To recognize stable charge/discharge performances at all compositions, a water-stable surface layer,

including Al_2O_3 or carbon, must be formed on the cathode particles [51]. We will try to pinpoint protective surface layers for a wide range of Li-rich solid-solution cathode materials, which haves various compositions of Li, Mn, Co ions, and Ni, in our next work [51].

That work shown the effect of Na doping in LiMnPO [52]. In the LiMnPO system through the sol-gel technique, na of various concentrations had been replaced [52]. Through natrium addition (LiNaMnPO, irreversible capacity deterioration had been lowered compared with pristine LiMnPO [52]. That superior electrochemical performance could be achieved via optimizing adequate Na doping in LiMnPO towards Li-ion battery application had been demonstrated by these experimental results [52].

The following heterogeneous cathode commodities synthesized from the leaching solution were investigated: $LiNi_{1/3}Mn_{1/3}Co_{1/3}O_2$, $LiNi_{0.6}Mn_{0.2}Co_{0.2}O_2$, and $LiNi_{0.5}Mn_{0.3}Co_{0.2}O_2$ [53]. The recycling process becomes a "closed loop" process raising the possibility of scaling the recovery process up and having a viable commercial battery recovery and re-use process by synthesizing novel cathode materials that could be implemented into novel batteries [53]. The electrochemical properties of the $LiNi_xMn_yCo_zO_2$ synthesized via re-use (recycling) and recovery are satisfactory compared to those synthesized from pure commercial product [53].

2.5 Related Work

Thackeray MM, Kang SH, Johnson CS, Vaughey JT, Benedek R, Hackney SA (2007) Li_2MnO_3-stabilized $LiMO_2$ (M = Mn, Ni, Co) electrodes for lithium-ion batteries. J Mater Chem 17:3112–3125 [https://doi.org/10.1039/b702425h]

Complete extraction of Li_2O from the inactive Li_2MnO_3 element yields electrochemically active layered MnO_2 phase, improving the discharge capacity of the material [15, 194, 195]. Such lithium-rich high-capacity materials suffer from meager cycle stability and inferior rate property; this stability hinder their successful commercialization in high-energy-density lithium-ion batteries (Boulineau and others [213]; Thackeray and others [194]; Xu and others [214]), [17]. In contrast with the commonly used layered ternary or $LiCoO_2$ cathode materials with α-$NaFeO_2$ structure, layered Li-rich Mn-based ones constituted as $yLi_2MnO_3{\cdot}(1–y)LiMO_2$ (M = Co, Ni, Mn, etc.) or $Li[Li_{(1/3–2x/3)}M_xMn_{(2/3–x/3)}]O_2$ have many advantages including lower cost, safer on overcharge [194, 354, 355], and less toxic [30]. They have high capacities about 250 mAh g^{-1} at high voltage, which can play a key role in stabilizing the electrode structure [189, 194] and supply the excess lithium to the layered structure [30]. Metal element doping, including Al, Zr [194], Y, Mo, and Mg [437] replaced for the transitional metal elements in the oxide materials, can weaken the adverse change of crystal structure [39]. High stable reversible capacity of >250 mAh g^{-1} when it is cycled in the voltage window of

2.5–4.8 V [194, 438–443] is delivered by LMR-NMC [40]. Throughout cycling need to be tackled before it is regarded as a potential candidate for next generation cathode material for lithium-ion batteries [197, 437–443], the energy deterioration because of suppression of voltage profiles during cycling which is linked with the stage reconfiguration from a layered structure to spinel structure, capacity, and high irreversible capacity, fade [40]. The aims of the present study were (1) to enhance the thermal stability of this material by making it a core-shell structured material with a core of $LiMO_2$ and a shell of Li_2MnO_3, and (2) to increase the discharge capacity of NCM 111 by preparing NCM 111 with the formula xLi_2MnO_3–$(1-x)$ $LiMO_2$, i.e., a lithium-rich material with a high capacity [44, 194].

Ohzuku T, Makimura Y (2001) Chem Lett 7:642–643 [https://doi.org/10.1246/cl.2001.642**]**

$LiNi_{1/3}Co_{1/3}Mn_{1/3}O_2$ compound, which Makimura [223] and Ohzuku developed, has been regarded as a fruitful candidate of next-generation cathode materials to substitute $LiCoO_2$ for rechargeable Li-ion batteries [18]. The layered lithium transition metal oxides have been intensively examined as the cathode materials in the next generation of the rechargeable lithium-ion battery (LIB) [30, 223, 353]. Layered $LiNi_{1/3}Co_{1/3}Mn_{1/3}O_2$ as cathode material has been paid extensive attention because of its high reversible capacity, low cost, and excellent structural, thermal stability, as reasonably well [33, 223, 381]. Overcharging frequently triggers significant systemic distortions (transformation from hexagonal to monoclinic structures), which generate extensive defects between and within the particles, and induces potential surface reactions including Co break-up at voltages above 4.4 V [50, 223, 532].

References

Main Document References

1. Xiao Y, Xiang W, Zhang J et al (2016) Ionics 22:1361. https://doi.org/10.1007/s11581-016-1659-4
2. Xiao Y, Zhu Y, Gao T et al (2017) Ionics 23:27. https://doi.org/10.1007/s11581-016-1804-0
3. Iqbal A, Iqbal Y, Khan AM et al (2017) Ionics 23:1995. https://doi.org/10.1007/s11581-017-2062-5
4. Guo J, Qin X, Zong B et al (2018) Ionics 24:2241. https://doi.org/10.1007/s11581-017-2374-5
5. Zhou L, Liu J, Huang L et al (2017) J Solid State Electrochem 21:3467. https://doi.org/10.1007/s10008-017-3688-y
6. Ma Y, Wang L, Zuo X et al (2018) J Solid State Electrochem 22:1963. https://doi.org/10.1007/s10008-018-3884-4
7. Xiang M, Tao W, Wu J et al (2016) Ionics 22:1003. https://doi.org/10.1007/s11581-016-1639-8
8. Qu L, Li M, Bian L et al (2017) J Solid State Electrochem 21:3659. https://doi.org/10.1007/s10008-017-3706-0

9. Sun CF, Amruthnath N, Yu JS et al (2016) Ionics 22:1501. https://doi.org/10.1007/s11581-016-1751-9
10. Li JLS, Xu S, Huang S, Zhu J (2017) Nanoscale Res Lett 12:414. https://doi.org/10.1186/s11671-017-2172-z
11. Xu S, Lu L, Jiang X et al (2016) J Appl Electrochem 46:279. https://doi.org/10.1007/s10800-016-0929-1
12. Ross N, Iwuoha E (2018) Nano transition metal alloy functionalized lithium manganese oxide cathodes-system for enhanced lithium-ion battery power densities. In: Ramasami P, Gupta Bhowon M, Jhaumeer Laulloo S, Li Kam Wah H (eds) Emerging trends in chemical sciences. ICPAC 2016. Springer, Cham. https://doi.org/10.1007/978-3-319-60408-4_13
13. Zhang G, Han E, Zhu L et al (2017) Ionics 23:2259. https://doi.org/10.1007/s11581-017-2069-y
14. Li S, Lei D, Xue Y et al (2017) Ionics 23:1979. https://doi.org/10.1007/s11581-017-2060-7
15. Wang M, Chen Y, Luo M et al (2016) J Appl Electrochem 46:907. https://doi.org/10.1007/s10800-016-0964-y
16. Jiao C, Meng T, Lu H et al (2017) J Solid State Electrochem 21:495. https://doi.org/10.1007/s10008-016-3393-2
17. Zhang Y, Zhu T, Lin L et al (2017) J Nanopart Res 19:373. https://doi.org/10.1007/s11051-017-4033-1
18. Han E, Lu M, Zhu L et al (2016) Ionics 22:2299. https://doi.org/10.1007/s11581-016-1786-y
19. Deng MM, Zou BK, Shao Y et al (2017) J Solid State Electrochem 21:1733. https://doi.org/10.1007/s10008-017-3545-z
20. Zhang Y, Liang Q, Huang C et al (2018) J Solid State Electrochem 22:1995. https://doi.org/10.1007/s10008-018-3905-3
21. Liu Y, Liu D, Zhang Z et al (2018) Ionics 24:2251. https://doi.org/10.1007/s11581-017-2352-y
22. Fan G, Wen Y, Liu B et al (2018) J Nanopart Res 20:43. https://doi.org/10.1007/s11051-018-4147-0
23. Li S, Yang Y, Xie M et al (2017) Rare Met 36:277. https://doi.org/10.1007/s12598-016-0859-4
24. Li S, Liu X, Liu G et al (2017) Ionics 23:19. https://doi.org/10.1007/s11581-016-1818-7
25. Van Le T, Nguyen TA, Thi Nguyen NM et al (2016) Bull Mater Sci 39:1177. https://doi.org/10.1007/s12034-016-1264-1
26. Kazda T, Čudek P, Vondrák J et al (2018) J Solid State Electrochem 22:537. https://doi.org/10.1007/s10008-017-3791-0
27. Huynh LTN, Tran TTD, Nguyen HHA et al (2018) J Solid State Electrochem 22:2247. https://doi.org/10.1007/s10008-018-3934-y
28. Zhu X, Lin T, Manning E et al (2018) J Nanopart Res 20:160. https://doi.org/10.1007/s11051-018-4235-1
29. Mou J, Wu H, Deng Y et al (2017) J Solid State Electrochem 21:2849. https://doi.org/10.1007/s10008-017-3608-1
30. Kong JZ, Ren C, Jiang YX et al (2016) J Solid State Electrochem 20:1435. https://doi.org/10.1007/s10008-016-3150-6
31. Vu DL, Lee J (2018) J Solid State Electrochem 22:1165. https://doi.org/10.1007/s10008-017-3863-1
32. Li QL, Xu WQ, Bai HL et al (2016) Ionics 22:1343. https://doi.org/10.1007/s11581-016-1655-8
33. Zhu W, Zhuang Z, Lin Z et al (2016) Ionics 22:1533. https://doi.org/10.1007/s11581-016-1681-6
34. Li Y, Chang X, Xu Q et al (2018) J Nanopart Res 20:22. https://doi.org/10.1007/s11051-017-4114-1
35. Peng Z, Wang G, Cao Y et al (2016) J Solid State Electrochem 20:2865. https://doi.org/10.1007/s10008-016-3289-1

36. Xu X, Deng S, Wang H et al (2017) Nano-Micro Lett 9:22. https://doi.org/10.1007/s40820-016-0123-3
37. Li F, Yang G, Jia G et al (2017) J Appl Electrochem 47:1189. https://doi.org/10.1007/s10800-017-1118-6
38. Mezaal MA, Qu L, Li G et al (2017) J Solid State Electrochem 21:2219. https://doi.org/10.1007/s10008-017-3564-9
39. Luo M, Zhang R, Gong Y et al (2018) Ionics 24:967. https://doi.org/10.1007/s11581-017-2269-5
40. Krishna Kumar S, Ghosh S, Martha SK (2017) Ionics 23:1655. https://doi.org/10.1007/s11581-017-2018-9
41. Sivlin D, Keles O (2018) Effect of sonication power on Al_2O_3 coated $LiNi_{0.5}Mn_{0.3}Co_{0.2}O_2$ cathode material for LIB. In: Sun Z et al (eds) Energy technology 2018. TMS 2018. The minerals, metals & materials series. Springer, Cham. https://doi.org/10.1007/978-3-319-72362-4_48
42. Shen B, Zuo P, Fan P et al (2017) J Solid State Electrochem 21:1195. https://doi.org/10.1007/s10008-016-3475-1
43. Qiu Z, Zhang Y, Dong P et al (2017) J Solid State Electrochem 21:3037. https://doi.org/10.1007/s10008-017-3643-y
44. Mezaal MA, Qu L, Li G et al (2017) J Solid State Electrochem 21:145. https://doi.org/10.1007/s10008-016-3345-x
45. Xiang Y, Wu X (2018) Ionics 24:83. https://doi.org/10.1007/s11581-017-2189-4
46. Yang XQ, Tang ZF, Wang HY et al (2016) Ionics 22:2235. https://doi.org/10.1007/s11581-016-1792-0
47. Xiao Z, Hu C, Song L et al (2018) Ionics 24:91. https://doi.org/10.1007/s11581-017-2178-7
48. Pineda-Aguilar N, Gallegos-Sánchez VJ, Sánchez EM et al (2017) J Sol-Gel Sci Technol 83:405. https://doi.org/10.1007/s10971-017-4398-8
49. Zhou F, Xu L, Kong J (2018) J Solid State Electrochem 22:943. https://doi.org/10.1007/s10008-017-3837-3
50. Yoon S (2016) J Appl Electrochem 46:479. https://doi.org/10.1007/s10800-016-0919-3
51. Notake K, Gunji T, Kokubun H et al (2016) J Appl Electrochem 46:267. https://doi.org/10.1007/s10800-016-0930-8
52. Rajammal K, Sivakumar D, Duraisamy N et al (2017) Bull Mater Sci 40:171. https://doi.org/10.1007/s12034-017-1365-5
53. Sa Q, Gratz E, Heelan JA et al (2016) J Sustain Metall 2:248. https://doi.org/10.1007/s40831-016-0052-x

Other Bibliographic References

54. Zhang X, Cheng F, Yang J, Chen J (2013) $LiNi_{0.5}Mn_{1.5}O_4$ porous nanorods as high-rate and long-life cathodes for Li-ion batteries. Nano Lett 13:2822–2825
55. Wu WW, Xiang HF, Zhong GB, Su W, Tang W, Zhang Y, Yu Y, Chen CH (2014) Ordered $LiNi_{0.5}Mn_{1.5}O_4$ hollow microspheres as high-rate 5 V cathode materials for lithium ion batteries. Electrochim Acta 119:206–213
56. Wen W, Wang X, Chen S, Shu H, Yang X (2015) Design and preparation of spherical high voltage $LiNi_{0.5}Mn_{1.5}O_4$ with a novel concentration-gradient shell for lithium ion batteries. J Power Sources 281:85–93
57. Li J, Xiong S, Liu Y, Ju Z, Qian Y (2013) Uniform $LiNi_{1/3}Co_{1/3}Mn_{1/3}O_2$ hollow microspheres: designed synthesis, topotactical structural transformation and their enhanced electrochemical performance. Nano Ener 2:1249–1260
58. Zhang J, Wu Z, Hua W, Liu H, Zhong B (2015) High-performance porous spherical cathode materials based on $CaCO_3$-template synthesis of $LiNi_{1/3}Co_{1/3}Mn_{1/3}O_2$ for lithium-ion batteries. Ionics 21:3151–3158

59. Luo H, Nie P, Shen L, Li H, Deng H, Zhu Y, Zhang X (2015) Synthesis of $LiNi_{0.5}Mn_{1.5}O_4$ hollow microspheres and their lithium-storage properties. Chem Electro Chem 2:127–133
60. Luo D, Li G, Guan X, Yu C, Zheng J, Zhang X, Li L (2013) Novel synthesis of Li1.2Mn0.4Co0.4O2 with an excellent electrochemical performance from −10.4 to 45.4 °C. J Mater Chem A 1:1220–1227
61. Sun Y, Yang Y, Zhao X, Shao H (2011) Synthesis and electrochemical characterization of $LiNi_{0.5}Mn_{1.5}O_4$ by one-step precipitation method with ammonium carbonate as precipitating agent. Electrochim Acta 56:5934–5939
62. Wen W, Chen S, Fu Y, Wang X, Shu H (2015) A core–shell structure spinel cathode material with a concentration-gradient shell for high performance lithium-ion batteries. J Power Sources 274:219–228
63. Pan J, Deng J, Yao Q, Zou Y, Wang Z, Zhou H, Sun L, Rao G (2015) Novel $LiNi_{0.5}Mn_{1.5}O_4$ porous microellipsoids as high-performance cathode materials for lithium ion batteries. J Power Sources 288:353–358
64. Xue L, Liao Y, Yang L, Li X, Li W (2014) Improved rate performance of $LiNi_{0.5}Mn_{1.5}O_4$ cathode for lithium ion battery by carbon coating. Ionics 21:1269–1275
65. Boesenberg U, Falk M, Ryan CG, Kirkham R, Menzel M, Janek J, Fröba M, Falkenberg G, Fittschen UEA (2015) Correlation between chemical and morphological heterogeneities in $LiNi_{0.5}Mn_{1.5}O_4$ spinel composite electrodes for lithium-ion batteries determined by micro-X-ray fluorescence analysis. Chem Mater 27:2525–2531
66. Deng S, Mao D, Wang H, Wang B, Liu J, Ma Y, Yan H (2016) Preparation and electrochemical properties of double-shell $LiNi_{0.5}Mn_{1.5}O_4$ hollow microspheres as cathode materials for Li-ion batteries. RSC Adv 6:45369–45375
67. Zhou L, Zhao D, Lou X (2012) $LiNi_{0.5}Mn_{1.5}O_4$ hollow structures as high-performance cathodes for lithium-ion batteries. Angew Chem Int Ed 124:243–245
68. Zhou L, Zhao D, Lou X (2012) Double-shelled $CoMn_2O_4$ hollow Microcubes as high-capacity anodes for lithium-ion batteries. Adv Mater 24:745–748
69. Luo H, Nie P, Shen L, Li H, Deng H, Zhu Y, Zhang X (2015) Synthesis of $LiNi_{0.5}Mn_{1.5}O_4$ hollow microspheres and their lithium-storage properties. ChemElectro-Chem 2:127–133
70. Wang Z, Zhou L, Lou X (2012) Metal oxide hollow nanostructures for lithium-ion batteries. Adv Mater 24:1903–1911
71. Hwang BJ, Santhanam R, Hu SG (2002) Synthesis and characterization of multidoped lithium manganese oxide spinel, $Li_{1.02}Co_{0.1}Ni_{0.1}Mn_{1.8}O_4$, for rechargeable lithium batteries. J Power Sources 108:250–255. https://doi.org/10.1016/S0378-7753(02)00023-X
72. Göktepe H, Şahan H, Patat Ş, Ülgen A (2009) Enhanced cyclability of triple-metal-doped $LiMn_2O_4$ spinel as the cathode material for rechargeable lithium batteries. Ionics (Kiel) 15:233–239. https://doi.org/10.1007/s11581-008-0265-5
73. Iqbal A, Iqbal Y, Chang L, Ahmed S, Tang Z, Gao Y (2012) Enhanced electrochemical performance of La- and Zn-co-doped $LiMn_2O_4$ spinel as the cathode material for lithium-ion batteries. J Nanopart Res 14:1206. https://doi.org/10.1007/s11051-012-1206-9
74. Hernan L, Morales J, Sanchez L, Castellon ER, Aranda MAG (2002) Synthesis, characterization and comparative study of the electrochemical properties of doped lithium manganese spinels as cathodes for high voltage lithium batteries. J Mater Chem 12:734–741
75. Jayaprakash N, Kalaiselvi N, Gangulibabu Bhuvaneswari D (2011) Effect of mono- (Cr) and bication (Cr, V) substitution on $LiMn_2O_4$ spinel cathodes. J Solid State Electrochem 15:1243–1251. https://doi.org/10.1007/s10008-010-1194-6
76. Xu Y, Wan L, Liu J, Zeng L, Yang Z (2017) γ-butyrolactone and glutaronitrile as 5 V electrolyte additive and its electrochemical performance for $LiNi_{0.5}Mn_{1.5}O_4$. J Alloys Compd 698:207–214. https://doi.org/10.1016/j.jallcom.2016.11.381
77. Haridasa AK, Sharma CS, Rao TN (2016) Caterpillar-like sub-micron $LiNi_{0.5}Mn_{1.5}O_4$ structures with site disorder and excess Mn^{3+} as high performance cathode

material for lithium ion batteries. Electrochim Acta 212:500–509. https://doi.org/10.1016/j.electacta.2016.07.039
78. Yi T-F, Mei J, Zhu Y-R (2016) Key strategies for enhancing the cycling stability and rate capacity of $LiNi_{0.5}Mn_{1.5}O_4$ as high-voltage cathode materials for high power lithium-ion batteries. J Power Sources 316:85–105. https://doi.org/10.1016/j.jpowsour.2016.03.070
79. Qian Y, Deng Y, Wan L, Xu H, Qin X, Chen G (2014) Investigation of the effect of extra lithium addition and post-annealing on the electrochemical performance of high-voltage spinel $LiNi_{0.5}Mn_{1.5}O_4$ cathode material. J Phys Chem C 118(29):15581–15589. https://doi.org/10.1021/jp503584k
80. Deng Y-F, Zhao S-X, Zhai P-Y, Cao G, Nan C-W (2015) Impact of lithium excess on the structural and electrochemical properties of $LiNi_{0.5}Mn_{1.5}O_4$ high-voltage cathode material. J Mater Chem A 3(40):20103–20107. https://doi.org/10.1039/C5TA06339F
81. Liu X, Huang T, Yu A (2015) Surface phase transformation and CaF_2 coating for enhanced electrochemical performance of Li-rich Mn-based cathodes. Electrochim Acta 163:82–92
82. Lu C, Wu H, Zhang Y, Liu H, Chen B, Wu N, Wang S (2014) Cerium fluoride coated layered oxide $Li[Li_{0.2}Mn_{0.54}Ni_{0.13}Co_{0.13}]O_2$ as cathode materials with improved electrochemical performance for lithium ion batteries. J Power Sources 267:682–691
83. Kang SH, Johnson CS, Vaughey JT, Amine K, Thackeray MM (2006) The effects of acid treatment on the electrochemical properties of $0.5Li_2MnO_3{\cdot}0.5LiNi_{0.44}Co_{0.25}Mn_{0.31}O_2$ electrodes in lithium cells. J Electrochem Soc 153:A1186–A1192
84. Kang SH, Thackeray MM (2008) Stabilization of xLi_2MnO_3 $(1-x)LiMO_2$ electrode surfaces (M = Mn, Ni, Co) with mildly acidic fluorinated solutions. J Electrochem Soc 155:A269–A275
85. He W, Yuan D, Qian J, Ai X, Yang H, Cao Y (2013) Enhanced high-rate capability and cycling stability of Na-stabilized layered $Li_{1.2}[Co_{0.13}Ni_{0.13}Mn_{0.54}]O_2$ cathode material. J. Mater Chem A 1:11397–11403
86. Liu X, Liu J, Huang T, Yu A (2013) CaF_2-coated $Li[Li_{0.2}Mn_{0.54}Ni_{0.13}Co_{0.13}]O_2$ as cathode materials for Li-ion batteries. Electrochim Acta 109:52–58
87. Li Q, Li G, Fu C, Luo D, Fan J, Li L (2014) K^+-doped $Li_{1.2}Mn_{0.54}Co_{0.13}Ni_{0.13}O_2$: a novel cathode material with an enhanced cycling stability for lithium-ion batteries. ACS Appl Mater Interfaces 6:10330–10341
88. Wang D, Belharouak I, Ortega LH, Zhang X, Xu R, Zhou D, Zhou G, Amine K (2015) Synthesis of high capacity cathodes for lithium-ion batteries by morphology-tailored hydroxide co-precipitation. J Power Sources 274:451–457
89. Fu F, Deng YP, Shen CH, Xu GL, Peng XX, Wang Q, Xu YF, Fang JC, Huang L, Sun SG (2014) A hierarchical micro/nanostructured $0.5Li_2MnO_3{\cdot}0.5LiMn_{0.4}Ni_{0.3}Co_{0.3}O_2$ material synthesized by solvothermal route as high rate cathode of lithium ion battery. Electrochem Commun 44:54–58
90. Wang D, Huang Y, Huo Z, Chen L (2013) Synthesize and electrochemical characterization of Mg-doped Li-rich layered $Li[Li_{0.2}Ni_{0.2}Mn_{0.6}]O_2$ cathode material. Electrochim Acta 107:461–466
91. Zhao J, Wang Z, Guo H, Li X, He Z, Li T (2015) Synthesis and electrochemical characterization of Zn-doped Li-rich layered $Li[Li_{0.2}Mn_{0.54}Ni_{0.13}Co_{0.13}]O_2$ cathode material. Ceram Int 41(9):11396–11401
92. Zhang WH, He W, Pei F, Wu FY, Mao RJ, Ai XP, Yang HX, Cao YL (2013) Improved electrochemical properties of Al^{3+}-doped $0.5Li_2MnO_3$-$0.5LiCo_{1/3}Ni_{1/3}Mn_{1/3}O_2$ cathode for lithium ion batteries. J Inorg Mater 28:1261–1264
93. Jiao LF, Zhang M, Yuan HT, Zhao M, Guo J, Wang W, Zhou XD, Wang YM (2007) Effect of Cr doping on the structural, electrochemical properties of $Li[Li_{0.2}Ni_{0.2-x/2}Mn_{0.6-x/2}Cr_x]O_2$ (x = 0, 0.02, 0.04, 0.06, 0.08) as cathode materials for lithium secondary batteries. J Power Sources 167:178–184
94. Song B, Lai MO, Lu L (2012) Influence of Ru substitution on Li-rich $0.55Li_2MnO_3{\cdot}0.45LiNi_{1/3}Co_{1/3}Mn_{1/3}O_2$ cathode for Li-ion batteries. Electrochim Acta 80:187–195

95. Jin X, Xu Q, Liu H, Yuan X, Xia Y (2014) Excellent rate capability of Mg doped Li $[Li_{0.2}Ni_{0.13}Co_{0.13}Mn_{0.54}]O_2$ cathode material for lithium-ion battery. Electrochim Acta 136:19–26
96. He ZJ, Wang ZX, Chen H, Huang ZM (2015) Electrochemical performance of zirconium doped lithium rich layered $Li_{1.2}Mn_{0.54}Ni_{0.13}Co_{0.13}O_2$ oxide with porous hollow structure. J Power Sources 299:334–341
97. Zhao Y, Xia M, Hu X, Zhao Z, Wang Y, Lv Z (2015) Effects of Sn doping on the structural and electrochemical properties of $Li_{1.2}Ni_{0.2}Mn_{0.8}O_2$ Li-rich cathode materials. Electrochim Acta 174:1167–1174
98. Liu J, Manthiram A (2009) Understanding the improvement in the electrochemical properties of surface modified 5 V $LiMn_{1.42}Ni_{0.42}Co_{0.16}O_4$ spinel cathodes in lithium-ion cells. Chem Mater 21(8):1695–1707. https://doi.org/10.1021/cm9000043
99. Sun YK, Myung ST, Park BC, Prakash J, Belharouak I, Amine K (2009) High-energy cathode material for long-life and safe lithium batteries. Nat Mater 8(4):320–324. https://doi.org/10.1038/nmat2418
100. Sun YK, Chen ZH, Noh HJ, Lee DJ, Jung HG, Ren Y, Wang S, Yoon CS, Myung ST, Amine K (2012) Nanostructured high-energy cathode materials for advanced lithium batteries. Nat Mater 11(11):942–947. https://doi.org/10.1038/nmat3435
101. Wang DH, Choi DW, Li J, Yang ZG, Nie ZM, Kou R, Hu DH, Wang CM, Saraf LV, Zhang JG (2009) Self-assembled TiO_2-graphene hybrid nanostructures for enhanced li-ion insertion. ACS Nano 3(4):907–914. https://doi.org/10.1021/nn900150y
102. Tang X, Jan SS, Qian YY, Xia H, Ni JF, Savilov SV, Aldoshin SM (2014) Graphene wrapped ordered $LiNi_{0.5}Mn_{1.5}O_4$ nanorods as promising cathode material for lithium-ion batteries. Sci Rep 11958(5):1–10
103. Ito S, Fujiki S, Yamada T, Aihara Y, Park Y, Kim TY, Baek S-W, Lee J-M, Doo S, Machida N (2014) A rocking chair type all-solid-state lithium ion battery adopting Li_2O-ZrO_2 coated $LiNi_{0.8}Co_{0.15}Al_{0.05}O_2$ and a sulfide based electrolyte. J Power Sources 248:943–950
104. Park B-C, Kim H-B, Bang HJ, Prakash J, Sun Y-K (2008) Improvement of electrochemical performance of $Li[Ni_{0.8}Co_{0.15}Al_{0.05}]O_2$ cathode materials by AlF_3 coating at various temperatures. Ind Eng Chem Res 47:3876–3882
105. Cao D, Wu L, Sun Y (2008) Electrochemical behavior of Mg–Li, Mg–Li–Al and Mg–Li–Al–Ce in sodium chloride solution. J Power Sources 177:624–630
106. Park TJ, Lim JB, Son JT (2014) Effect of calcination temperature of size controlled microstructure of $LiNi_{0.8}Co_{0.15}Al_{0.05}O_2$ cathode for rechargeable lithium battery. Bull Kor Chem Soc 35:357–364
107. Kim J, Amine K (2001) The effect of tetravalent titanium ubstitution in $LiNi_{1-x}Ti_xO_2$ ($0.025 \leq x \leq 0.2$) system. Electrochem Commun 3:52–55
108. Kim J, Amine K (2002) A comparative study on the substitution of divalent, trivalent and tetravalent metal ions in $LiNi_{1-x}M_xO_2$ ($M = Cu^{2+}$, Al^{3+} and Ti^{4+}). J Power Sources 104:33–39
109. Myung ST, Komaba S, Hosoya K, Hirosaki N, Miura Y, Kumagai N (2005) Synthesis of $LiNi_{0.5}Mn_{0.5-x}Ti_xO_2$ by an emulsion drying method and effect of Ti on structure and electrochemical properties. Chem Mater 17:2427–2435
110. Huang H, Yin S-C, Nazar LF (2001) Approaching theoretical capacity of $LiFePO_4$ at room temperature at high rates. Electrochem Solid-State Lett 4:A170–A172
111. Yamada A, Chung SC, Hinokuma K (2001) Optimized $LiFePO_4$ for lithium battery cathodes. J Electrochem Soc 148:A224–A229
112. Nytén A, Abouimrane A, Armand M, Gustafsson T, Thomas JO (2005) Electrochemical performance of Li_2FeSiO_4 as a new Li-battery cathode material. Electrochem Commun 7:156–160

113. Gong ZL, Li YX, He GN, Li J, Yang Y (2008) Nanostructured Li_2FeSiO_4 electrode material synthesized through hydrothermal-assisted sol-gel process. Electrochem Solid-State Lett 11: A60–A63
114. Muraliganth T, Stroukoff KR, Manthiram A (2010) Microwave-solvothermal synthesis of sanostructured Li_2MSiO_4/C (M = Mn and Fe) cathodes for lithium-ion batteries. Chem Mater 22:5754–5761
115. Zhang S, Deng C, Fu BL, Yang SY, Ma L (2010) Doping effects of magnesium on the electrochemical performance of Li_2FeSiO_4 for lithium ion batteries. J Electroanal Chem 644:150–154
116. Hao H, Wang J, Liu J, Huang T, Yu A (2012) Synthesis, characterization and electrochemical performance of Li_2FeSiO_4/C cathode materials doped by vanadium at Fe/Si sites for lithium ion batteries. J Power Sources 210:397–401
117. Zhang LL, Sun H-B, Yang XL, Wen YW, Huang YH, Li M, Peng G, Tao HC, Ni SB, Liang G (2015) Study on electrochemical performance and mechanism of V-doped Li_2FeSiO_4 cathode material for Li-ion batteries. Electrochim Acta 152:496–504
118. Zhang S, Deng C, Fu BL, Yang SY, Ma L (2010) Effects of Cr doping on the electrochemical properties of Li_2FeSiO_4 cathode material for lithium-ion batteries. Electrochim Acta 55:8482–8489
119. Zhang L-L, Duan S, Yang X-L, Liang G, Huang Y-H, Cao X-Z, Yang J, Li M, Croft MC, Lewis C (2015) Insight into cobalt-doping in Li_2FeSiO_4 cathode material for lithium-ion battery. J Power Sources 274:194–202
120. Deng C, Zhang S, Yang SY, Fu BL, Ma L (2011) Synthesis and characterization of $Li_2Fe_{0.97}M_{0.03}SiO_4$ (M = Zn^{2+}, Cu^{2+}, Ni^{2+}) cathode materials for lithium ion batteries. J Power Sources 196:386–392
121. Luo W, Li X, Dahn JR (2010) Synthesis, characterization, and thermal stability of $Li[Ni_{1/3}Mn_{1/3}Co_{1/3-z}(MnMg)_{z/2}]O_2$. Chem Mater 22(17):5065–5073. https://doi.org/10.1021/cm1017163
122. Kiziltas-Yavuz N, Bhaskar A, Dixon D, Yavuz M, Nikolowski K, Lu L, Eichel R-A, Ehrenberg H (2014) Improving the rate capability of high voltage lithium-ion battery cathode material $LiNi_{0.5}Mn_{1.5}O_4$ by ruthenium doping. J Power Sources 267:533–541. https://doi.org/10.1016/j.jpowsour.2014.05.110
123. Wang H, Tan TA, Yang P, Lai MO, Lu L (2011) High-rate performances of the Ru-doped spinel $LiNi_{0.5}Mn_{1.5}O_4$: effects of doping and particle size. J Phys Chem C 115(13):6102–6110. https://doi.org/10.1021/jp110746w
124. Wang Y, Yang Y, Hu X, Yang Y, Shao H (2009) Electrochemical performance of Ru-doped $LiFePO_4$/C cathode material for lithium-ion batteries. J Alloys Compd 481(1–2):590–594. https://doi.org/10.1016/j.jallcom.2009.03.033
125. Seyyedhosseinzadeh H, Mahboubi F, Azadmehr A (2013) Diffusion mechanism of lithium ions in $LiNi_{0.5}Mn_{1.5}O_4$. Electrochim Acta 108:867–875
126. Liu YZ, Zhang MH, Xia YG, Qiu B, Liu ZP, Li X (2014) One-step hydrothermal method synthesis of core-shell $LiNi_{0.5}Mn_{1.5}O_4$ spinel cathodes for Li-ion batteries. J Power Sources 256:66–71
127. Chong J, Xun SD, Song XY, Liu G, Battaglia VS (2013) Surface stabilized $LiNi_{0.5}Mn_{1.5}O_4$ cathode materials with high-rate capability and long cycle life for lithiumion batteries. Nano Energy 2:283–293
128. Tang X, Jan SS, Qian YY, Xia H, Ni JF, Savilov SV, Aldoshin SM (2015) Graphene wrapped ordered $LiNi_{0.5}Mn_{1.5}O_4$ nanorods as promising cathode material for lithium-ion batteries. Sci Rep 5:11958
129. Leitner KW, Wolf H, Garsuch A, Chesneau F, Schulz-Dobrick M (2013) Electroactive separator for high voltage graphite/$LiNi_{0.5}Mn_{1.5}O_4$ lithium ion batteries. J Power Sources 244:548–551
130. Wang W, Liu H, Wang Y, Zhang J (2013) Effects of chromium doping on performance of $LiNi_{0.5}Mn_{1.5}O_4$ cathode material. T Nonferr Metal Soc 23:2066–2070

131. Xia H, Tang SB, Lu L, Meng YS, Ceder G (2007) The influence of preparation conditions on electrochemical properties of $LiNi_{0.5}Mn_{1.5}O_4$ thin film electrodes by PLD. Electrochim Acta 52:2822–2828
132. Wu F, Wang F, Wu C, Bai Y (2012) J Alloys Compd 513:236–241
133. Xia A, Huang JF, Tang GQ, Ren HJ (2014) Ceram Int 40:14845–14850
134. Liu S, Li S, Huang K, Chen Z (2007) Acta Phys Chim Sin 23:537–542
135. Sato M, Ohkawa H, Yoshida K, Saito M, Uematsu K, Toda K (2000) Solid State Ionics 135:137–142
136. Ren M, Zhou Z, Li Y, Gao XP, Yan J (2006) J Power Sources 162:1357–1362
137. Cho AR, Son JN, Aravindan V, Kim H, Kang KS, Yoon WS, Kim WS, Lee YS (2012) J Mater Chem 22:6556–6560
138. Goodenough JB, Kim Y (2010) Challenges for rechargeable Li batteries. Chem Mater 22:587–603
139. Barker J, Gover RKB, Burns P, Bryan A (2007) J Electrochem Soc 154:A307–A313
140. Liu HD, Gao P, Fang JH, Yang G (2011) Chem Commun 47:9110–9112
141. Chen Y, Zhao Y, An X, Liu J, Dong Y, Chen L (2009) Electrochim Acta 54:5844–5850
142. Mateyshina YG, Uvarov NF (2011) J Power Sources 196:1494–1497
143. Zhong S, Liu L, Jiang J, Li Y, Wang J, Liu J, Li Y (2009) J Rare Earths 27:134–137
144. Zhai T, Zhao M, Wang D (2011) Trans Nonferrous Met Soc China 21:523–528
145. Huang JS, Yang L, Liu KY, Tang YF (2010) J Power Sources 195:5013–5018
146. Dai C, Chen Z, Jin H, Hu X (2010) J Power Sources 195:5775–5779
147. Kuang Q, Zhao Y, An X, Liu J, Dong Y, Chen L (2010) Electrochim Acta 55:1575–1581
148. Stevenson KJ (2012) The origin, development, and future of the lithium-ion battery. J Solid State Electrochem 16:2017–2018
149. Tavassol H, Jones EMC, Sottos NR, Gewirth AA (2016) Electrochemical stiffness in lithium-ion batteries. Nat Mater 15:1182–1187
150. Julien CM, Mauger A, Zaghib K, Groult H (2014) Comparative issues of cathode materials for Li-ion batteries. Inorganics 2:132–154
151. Nitta N, Wu F, Tae Lee J, Yushin G (2015) Li-ion battery materials: present and future. Mater Today 18:252–264
152. Arico AS, Scrosati B, Tarascon JM, Van Schalkwijk W (2005) Nanostructured materials for advanced energy conversion and storage devices. Nat Mater 4:366–377
153. Li X, Cheng F, Guo B, Chen J (2005) Template-synthesized $LiCoO_2$, $LiMn_2O_4$, and $LiNi_{0.8}Co_{0.2}O_2$ nanotubes as the cathode materials of lithium ion batteries. J Phys Chem B 109:14017–14024
154. Meng X, Han B, Wang Y, Nan J (2016) Effects of samarium doping on the electrochemical performance of $LiFePO_4$/C cathode material for lithium-ion batteries. Ceram Int 42:2599–2604
155. Dahn JR, Sacken U, Michal CA (1990) Structure and electrochemistry of $Li_{1\pm y}NiO_2$ and a new Li_2NiO_2 phase with the $Ni(OH)_2$ structure. Solid State Ionics 44:87–97
156. Kim JM, Chung HT (2004) Role of transition metals in layered Li[Ni Co, Mn]O_2 under electrochemical operation. Electrochim Acta 49:3573–3580
157. Tsai YW, Lee JF, Liu DG, Hwang BJ (2004) In-situ X-ray absorption spectroscopy investigations of a layered $LiNi_{0.65}Co_{0.25}Mn_{0.1}O_2$ cathode material for rechargeable lithium batteries. J Mater Chem 14:958–965
158. Lee SW, Kim H, Kim MS et al (2016) Improved electrochemical performance of $LiNi_{0.6}Co_{0.2}Mn_{0.2}O_2$ cathode material synthesized by citric acid assisted sol-gel method for lithium ion batteries. J Power Sources 315:261–268
159. Ruan Z, Zhu Y, Teng X (2016) Effect of pre-thermal treatment on the lithium storage performance of $LiNi_{0.8}Co_{0.15}Al_{0.05}O_2$. J Mater Sci 51:1400–1408
160. Liu XH, Kou LQ, Shi T, Liu K, Chen L (2014) Excellent high rate capability and high voltage cycling stability of Y_2O_3-coated $LiNi_{0.5}Co_{0.2}Mn_{0.3}O_2$. J Power Sources 267:874–880

161. Kang S, Qin H, Fang Y, Li X, Wang Y (2014) Preparation and electrochemical performance of yttrium-doped $Li[Li_{0.20}Mn_{0.534}Ni_{0.133}Co_{0.133}]O_2$ as cathode material for lithium-ion batteries. Electrochim Acta 144:22–30
162. Valanarasu S, Chandramohan R, Somasundaram RM, Srikumar RS (2011) Structural and electrochemical properties of Eu-doped $LiCoO_2$. J Mater Sci Mater Electron 22:151–157
163. Zhou F, Qiu K, Peng G, Li X (2015) Silver/carbon nanotube hybrids: a novel conductive network for high-rate lithium ion batteries. Electrochim Acta 151:16–20
164. Liu T, Zhao SX, Wang K, Nan CW (2012) CuO-coated $Li[Ni_{0.5}Co_{0.2}Mn_{0.3}]O_2$ cathode material with improved cycling performance at high rates. Electrochim Acta 85:605–611
165. Park CW, Kim SH, Nahm KS, Chung HT, Lee YS, Lee JH, Boo S, Kim J (2008) Structural and electrochemical study of $Li[Cr_xLi_{(1-x)/3}Mn_{2(1-x)/3}]O_2$ ($0 \leq x \leq 0.328$) cathode materials. J Alloy Compd 449:343–348
166. Woo SW, Myung ST, Bang H, Kim DW, Sun YK (2009) Improvement of electro chemical and thermal properties of $Li[Ni_{0.8}Co_{0.1}Mn_{0.1}]O_2$ positive electrode materials by multiple metal(Al, Mg) substitution. Electrochim Acta 54:3851–3856
167. Huang YH, Chou HL, Wang FM et al (2013) Synergy between experiment and simulation in describing the electrochemical performance of Mg-doped$LiNi_xCo_yMn_zO_2$ cathode material of lithium ion battery. J Electrochem Sci 8:8005–8009
168. Zhu X, Doan TNL, Yu Y, Tian Y, Sun KEK, Zhao H et al (2015) Ionics 22:1–6
169. Lee MJ, Lee S, Oh P, Kim Y, Cho J (2014) Nano Lett 14:993–999
170. Ragavendran KR, Xia H, Yang G, Vasudevan D, Emmanuel B, Sherwood D et al (2014) Phys Chem Chem Phys 16:2553–2560
171. Arico AS, Bruce P, Scrosati B, Tarascon JM, Schalkwijk WV. Nat Mater
172. Jiang J, Liu Q, Xu L, Xu J, Du J, He X et al (2016) J Nanosci Nanotechnol 16:12640–12643
173. Bruck AM, Cama CA, Gannett CN, Marschilok AC, Takeuchi ES, Takeuchi KJ (2015) ChemInform 47:26–40
174. Thirunakaran R, Kim T, Yoon WS (2015) J Sol-Gel Sci Technol 73:62–71
175. Jiang Q, Wang X, Zhang H (2016) J Electron Mater 45:4350–4356
176. Jiang Q, Xu L, Ma Z, Zhang H (2015) Appl Phys A 119:1069–1074
177. Christiansen TL, Bojesen E, Søndergaard M, Birgisson S, Becker-Christensen J, Bo BI (2016) CrystEngComm 18:1996–2004
178. Yu W, Cao C, Zhang J, Lin W, Ma X, Xu X (2016) ACS Appl Mater Interfaces 8
179. Luo W, Wang X, Meyers C, Wannenmacher N, Sirisaksoontorn W, Lerner MM, Ji X (2013) Sci Rep
180. Huang Y, Li J, Jia D (2013) J Nanopart Res 6:533–538
181. Caballero A, Cruz M, Hernán L, Melero M, Morales J, Castellón ER (2005) J Power Sources 150:192–201
182. Armand M, Tarascon JM (2008) Building better batteries. Nature 451:652–657
183. Jo YN, Prasanna K, Park SJ, Lee CW (2013) Characterization of Li-rich $xLi_2MnO_3{\cdot}(1-x)Li$ [MnyNizCo1−y−z]O2 as cathode active materials for Li-ion batteries. Electrochim Acta 108:32–38
184. Koyama Y, Tanaka I, Nagao M, Kanno R (2009) First-principles study on lithium removal form Li_2MnO_3. J Power Sources 189:798–801
185. Tabuchi M, Nabeshima Y, Takeuchi T, Tatsumi K, Imaizumi J, Nitta Y (2010) Fe content effects on electrochemical properties of Fe-substituted Li_2MnO_3 positive electrode material. J Power Sources 195:834–844
186. Wu Y, Manthiram A (2008) Structural stability of chemically delithiated layered $(1-z)Li[Li_{1/3}Mn_{2/3}]O_{2-z}Li[Mn_{0.5-y}Ni_{0.5-y}Co_{2y}]O_2$ solid solution cathodes. J Power Sources 183:749–754
187. Lee CW, Sun YK, Prakash J (2004) A novel layered $Li[Li_{0.12}Ni_2Mg_{0.32-z}Mn_{0.56}]O_2$ cathode material for lithium-ion batteries. Electrochim Acta 49:4425–4432
188. Ito A, Li D, Sato Y, Arao M, Watanabe M, Hatano M, Horie H, Ohsawa Y (2010) Cyclic deterioration and its improvement for Li-rich layered cathode material $Li[Ni_{0.17}Li_{0.2}Co_{0.07}Mn_{0.56}]O_2$. J Power Sources 195:567–573

189. Thackeray MM, Johnson CS, Vaughey JT, Li N, Hackney SA (2005) J Mater Chem 15:2257–2267
190. Liu YJ, Li SB (2013) Effect of cooling method on the electrochemical performance of $0.5Li_2MnO_3{\cdot}0.5LiNi_{0.5}Mn_{0.5}O_2$ cathodes. Ionics 19:477–481
191. Lin J, Mu DB, Jin Y, Wu B, Ma Y, Wu F (2013) Li-rich layered composite Li $[Li_{0.2}Ni_{0.2}Mn_{0.6}]O_2$ synthesized by a novel approach as cathode material for lithium ion battery. J Power Sources 230:76–80
192. Xiang XD, Li XQ, Li WS (2013) Preparation and characterization of size-uniform Li $[Li_{0.131}Ni_{0.304}Mn_{0.565}]O_2$ particles as cathode materials for high energy lithium ion battery. J Power Sources 230:89–95
193. Johnson CS, Li N, Lefief C, Thackeray MM (2007) Anomalous capacity and cycling stability of xLi2MnO3·(1–x)LiMO2 electrodes (M = Mn, Ni, Co) in lithium batteries at 50 ° C. Electrochem Commun 9:787–795
194. Thackeray MM, Kang S-H, Johnson CS, Vaughey JT, Benedek R, Hackney SA (2007) Li_2MnO_3-stabilized $LiMO_2$ (M = Mn, Ni, Co) electrodes for lithium-ion batteries. J Mater Chem 17(30):3112–3125
195. Johnson CS, Li N, Lefief C, Vaughey JT, Thackeray MM (2008) Synthesis, characterization and electrochemistry of lithium battery electrodes: $xLi_2MnO_3{\cdot}(1–x)$ $LiMn_{0.333}Ni_{0.333}Co_{0.333}O_2$ ($0 \leq x \leq 0.7$). Chem Mater 20:6095–6106
196. Li L, Zhang X, Chen R, Zhao T, Lu J, Wu F, Amine K (2014) Synthesis and electrochemical performance of cathode material $Li_{1.2}Co_{0.13}Ni_{0.13}Mn_{0.54}O_2$ from spent lithium-ion batteries. J Power Sources 249:28–34
197. Ryu WH, Lim SJ, Kim WK, Kwon H (2014) 3-D dumbbell-like $LiNi_{1/3}Mn_{1/3}Co_{1/3}O_2$ cathode materials assembled with nano-building blocks for lithium-ion batteries. J Power Sources 257:186–191
198. Zhang L, Borong W, Ning L, Feng W (2014) Hierarchically porous micro-rod lithium-rich cathode material $Li_{1.2}Ni_{0.13}Mn_{0.54}Co_{0.13}O_2$ for high performance lithium-ion batteries. Electrochim Acta 118:67–74
199. Ohzuku T, Takeda S, Iwanaga M (1999) Solid-state redox potentials for $Li[Me_{1/2}Mn_{3/2}]$ O_4 (me: 3d-transition metal) having spinel-framework structures: a series of 5 volt materials for advanced lithium-ion batteries. J Power Sources 81–82:90–94
200. Liu D, Zhu W, Trottier J, Gagnon C, Barray F, Guerfi A, Mauger A, Groult H, Julien CM, Goodenoughd JB, Zaghib K (2014) Spinel materials for high-voltage cathodes in Li-ion batteries. RSC Adv 4:154–167
201. Julien CM, Mauger A (2013) Review of 5 V electrodes for Li-ion batteries: status and trends. Ionics 19:951–988
202. Cao A, Manthiram A (2012) Shape-controlled synthesis of high tap density cathode oxides for lithium ion batteries. Phys Chem Chem Phys 14:6724–6728
203. Zhu HL, Chen ZY, Ji S, Linkov V (2008) Influence of different morphologies on electrochemical performance of spinel $LiMn_2O_4$. Solid State Ionics 179:1788–1793
204. Kim MG, Cho J (2009) Reversible and high-capacity nanostructured electrode materials for Li-ion batteries. Adv Funct Mater 19:1497–1514
205. Song MK, Park SJ, Alamgir FM, Cho J, Liu M (2011) Nanostructured electrodes for lithium-ion and lithium-air batteries: the latest developments, challenges, and perspectives. Mat Sci Eng R 72:203–252
206. Huang B, Zheng XD, Jia DM, Lu M (2010) Design and synthesis of high-rate micron-sized, spherical $LiFePO_4$/C composites containing clusters of nano/microspheres. Electrochim Acta 55:1227–1231
207. Park SH, Oh SW, Myung ST, Kang YC, Sun YK (2005) Effects of synthesis condition on $LiNi_{1/2}Mn_{3/2}O_4$ cathode material prepared by ultrasonic spray pyrolysis method. Solid State Ionics 176:481–486
208. Cao SS, Huang JF, Ouyang HB, Cao LY, Li JY, Wu JP (2014) A simple method to prepare $NH_4V_3O_8$ nanorods as cathode material for Li-ion batteries. Mater Lett 126:20–23

209. Xia L, Wang H, Lu Z, Yang S, Ma R, Deng J, Chung CY (2012) Facile synthesis of porous $LiMn_2O_4$ spheres as positive electrode for high-power lithium ion batteries. J Power Sources 198:251–257
210. Habtom DA, Matthew RR, Tai CW, Reza Y, Mario V (2014) Nanosized $LiFePO_4$-decorated emulsion-templated carbon foam for 3D micro batteries: a study of structure and electrochemical performance. Nanoscale 6:8804–8813
211. Yang K, Su J, Zhang L, Long Y, Lv X, Wen Y (2012) Urea combustion synthesis of $LiNi_{0.5}Mn_{1.5}O_4$ as a cathode material for lithium ion batteries. Particuology 10:765–770
212. Tarascon JM, Armand M (2001) Issues and challenges facing rechargeable lithium batteries. Nature 414:359–367
213. Boulineau A, Simonin L, Colin JF, Bourbon C, Patoux P (2013) First evidence of manganese-nickel segregation and densification upon cycling in Li-rich layered oxides for lithium batteries. Nano Lett 13:3857–3863
214. Xu B, Fell CR, Chi MF, Meng YS (2011) Identifying surface structural changes in layered Li-excess nickel manganese oxides in high voltage lithium ion batteries: a joint experimental and theoretical study. Energy Environ Sci 4:2223–2233
215. Guo YG, JS H, Wan LJ (2008) Nanostructured materials for electrochemical energy conversion and storage devices. Adv Mater 20:2878–2887
216. Li S, Ma G, Guo B, Yang ZH, Fan XM, Chen ZX, Zhang WX (2016) Kinetically controlled synthesis of $LiNi_{0.5}Mn_{1.5}O_4$Micro- and nanostructured hollow spheres as high-rate cathode materials for lithium ion batteries. Ind Eng Chem Res 55:9352–9361
217. Li Y, Wu C, Bai Y, Liu L, Wang H, Wu F, Zhang N, Zou YF (2016) Hierarchical mesoporous lithium-rich $Li[Li_{0.2}Ni_{0.2}Mn_{0.6}]O_2$ cathode material synthesized via ice templating for lithium-ion battery. ACS Appl Mater Interfaces 8:18832–18840
218. Wu F, Wang Z, Yf S, Guan YB, Jin Y, Yan N, Tian J, Bao LY, Chen S (2014) Synthesis and characterization of hollow spherical cathode $Li_{1.2}Mn_{0.54}Ni_{0.13}Co_{0.13}O_2$ assembled with nanostructured particles via homogeneous precipitation-hydrothermal synthesis. J Power Sources 267:337–346
219. Lin B, Li QF, Liu BD, Zhang S, Deng C (2016) Biochemistry-directed hollow porous microspheres: bottom-up self-assembled polyanion-based cathodes for sodium ion batteries. NANO 8:8178–8188
220. He X, Wang J, Kloepsch R, Krueger S, Jia HP, Liu HD, Vortmann B, Li J (2013) Enhanced electrochemical performance in lithium ion batteries of a hollow spherical lithium-rich cathode material synthesized by a molten salt method. Nano Res 7:110–118
221. Abdelaal HM, Harbrecht B (2015) Fabrication of hollow spheres of metal oxide using fructose-derived carbonaceous spheres as sacrificial templates. CR Chim 18:379–384
222. Makimura Y, Ohzuku T (2003) Crystal and electronic structures of superstructural $Li_{1-x}[Co_{1/3}Ni_{1/3}Mn_{1/3}]O_2$ ($0 \leq x \leq 1$). J Power Sources 156:119–123
223. Ohzuku T, Makimura Y (2001) Chem Lett 7:642–643
224. Li H, Chen G, Zhang B, Xu J (2008) Advanced electrochemical performance of $Li[Ni_{(1/3-x)}Fe_xCo_{1/3}Mn_{1/3}]O_2$ as cathode materials for lithium-ion battery. Solid State Commun 146:115–120
225. Zhao T, Li L, Chen S, Amine K (2014) The effect of chromium substitution on improving electrochemical performance of low-cost Fe-Mn based Li-rich layered oxide as cathode material for lithium-ion batteries. J Power Sources 245:898–907
226. Hwang BJ, Tsai YW, Carlier D, Ceder G (2003) A combined computational/ experimental study on $LiNi_{1/3}Co_{1/3}Mn_{1/3}O_2$. Chem Mater 15(19):3676–3682
227. Tang T, Zhang HL (2016) Synthesis and electrochemical performance of lithium-rich cathode material $Li[Li_{0.2}Ni_{0.15}Mn_{0.55}Co_{0.1-x}Al_x]O_2$. Electrochim Acta 191:263–269
228. Samarasingha PB, Wijayasinghe A, Behm M, Dissanayake L, Lindbergh G (2014) Development of cathode materials for lithium ion rechargeable batteries based on the system $Li(Ni_{1/3}Mn_{1/3}Co_{(1/3-x)}M_x)O_2$, (M = Mg, Fe, Al and x = 0.00 to 0.33). Solid State Ionics 268:226–230

229. Wu Q, Liu Y, Johnson CS (2014) Insight into the structural evolution of a high-voltage spinel for lithium-ion batteries. Chem Mater 26(16):4750–4756
230. Lin M, Ben L, Sun Y (2015) Insight into the atomic structure of high-voltage spinel $LiNi_{0.5}Mn_{1.5}O_4$ cathode material in the first cycle. Chem Mater 27(1):292–303
231. Moorhead-Rosenberg Z, Huq A (2015) Electronic and electrochemical properties of $Li_{1-x}Mn_{1.5}Ni_{0.5}O_4$ spinel cathodes as a function of lithium content and cation ordering. Chem Mater 27(20):6934–6945
232. Ma J, Hu P, Cui GL, Chen LQ (2016) Surface and interface issues in spinel $LiNi_{0.5}Mn_{1.5}O_4$: insights into a potential cathode material for high energy density lithium ion batteries. Chem Mater 28:3578–3606. https://doi.org/10.1021/acs.chemmater.6b00948
233. Deng YF, Zhao SX, Xu YH, Gao K, Nan C-W (2015) Impact of P doped in spinel $LiNi_{0.5}Mn_{1.5}O_4$ on degree of disorder, grain morphology, and electrochemical performance. Chem Mater 27(22):7734–7742
234. Zhu YR, Yi TF, Zhu RS, Zhou AN (2013) Increased cycling stability of $Li_4Ti_5O_{12}$ -coated $LiMn_{1.5}Ni_{0.5}O_4$ as cathode material for lithium-ion batteries. Ceram Int 39(3):3087–3094
235. Konishi H, Suzuki K, Taminato S, Kim K, Zheng Y, Kim S, Lim J, Hirayama M, Son J-Y, Cui Y, Kanno R (2014) Effect of surface Li_3PO_4 coating on $LiNi_{0.5}Mn_{1.5}O_4$ epitaxial thin film electrodes synthesized by pulsed laser deposition. J Power Sources 269:293–298
236. Huang B, Li X, Wang Z, Guo H, Xiong X, Wang J (2014) A novel carbamide-assistant hydrothermal process for coating Al_2O_3 onto $LiMn_{1.5}Ni_{0.5}O_4$ particles used for cathode material of lithium-ion batteries. J Alloys Comp 583:313–319
237. Niketic S, Couillard M, MacNeil D, Abu-Lebdeh Y (2014) Improving the performance of high voltage $LiMn_{1.5}Ni_{0.5}O_4$ cathode material by carbon coating. J Power Sources 271:285–290
238. Wang H, Shi Z, Li J, Yang S, Ren R, Cui J, Xiao J, Zhang B (2015) Direct carbon coating at high temperature on $LiNi_{0.5}Mn_{1.5}O_4$ cathode: unexpected influence on crystal structure and electrochemical performances. J Power Sources 288:206–213
239. Fang X, Shen C, Ge M, Rong J, Liu Y, Zhang A, Wei F, Zhou C (2015) High-power lithium ion batteries based on flexible and light-weight cathode of $LiNi_{0.5}Mn_{1.5}O_4$/carbon nanotube film. Nano Energy 12:43–51
240. Arrebola JC, Caballero A, Hernán L, Morales J (2010) Re-examining the effect of ZnO on nanosized 5 V $LiNi_{0.5}Mn_{1.5}O_4$ spinel: an effective procedure for enhancing its rate capability at room and high temperatures. J Power Sources 195(13):4278–4284
241. Zhong GB, Wang YY, Zhang ZC, Chen CH (2011) Effects of Al substitution for Ni and Mn on the electrochemical properties of $LiNi_{0.5}Mn_{1.5}O_4$. Electrochim Acta 56(18):6554–6561
242. Zhong GB, Wang YY, Yu YQ, Chen CH (2012) Electrochemical investigations of the $LiNi_{0.45}M_{0.10}Mn_{1.45}O_4$ (M = Fe Co, Cr) 5 V cathode materials for lithium ion batteries. J Power Sources 205:385–393
243. Fedotov SS, Khasanova NR, Samarin AS, Drozhzhin OA, Batuk D, Karakulina OM, Hadermann J, Abakumov AM, Antipov EV (2016) $AVPO_4F$ (A = Li, K): a 4 V cathode material for high-power rechargeable batteries. Chem Mater 28:411–415
244. Barker J, Saidi MY, Swoyer JL (2005) Lithium metal fluorophosphate materials and preparation thereof. US Pat 7:462–855
245. Khasanova NR, Drozhzhin OA, Storozhilova DA, Delmas C, Antipov EV (2012) New form of Li_2FePO_4F as cathode material for Li-ion batteries. Chem Mater 24(22):4271–4273. https://doi.org/10.1021/cm302724a
246. Ramesh T, Lee KT, Ellis B, Nazar L (2010) Tavorite lithium iron fluorophosphate cathode materials: phase transition and electrochemistry of $LiFePO_4F$-Li_2FePO_4F. Electrochem Solid-State Lett 13:43–47
247. Yang Y, Zhang Y, Hua Z, Wang X, Peng H, Bakenov Z (2016) Effect of VO_4^{3-} substitution for PO_4^{3-} on electrochemical properties of the $Li_3Fe_2(PO_4)_3$ cathode materials. Electrochim Acta 219:547–552. https://doi.org/10.1016/j.electacta.2016.10.044
248. Wang C, Wang S, Tang L, He YB, Gan L, Du J, Li H, Li B, Lin Z, Kang F (2016) A robust strategy for crafting monodisperse $Li_4Ti_5O_{12}$ nanospheres as superior rate anode for lithium ion batteries. Nano Energy 21:133–144. https://doi.org/10.1016/j.nanoen.2016.01.005

249. Huang B, Liu S, Li H, Zhuang S, Fang D (2012) Comparative study and electrochemical properties of $LiFePO_4F$ synthesized by different routes. Bull Kor Chem Soc 33(7):2315–2319. https://doi.org/10.5012/bkcs.2012.33.7.2315
250. Recham N, Chotard JN, Jumas JC, Laffont L, Armand M, Tarascon JM (2010) Ionothermal synthesis of Li-based fluorophosphates electrodes. Chem Mater 22(3):1142–1148. https://doi.org/10.1021/cm9021497
251. Ellis BL, Ramesh TN, Rowan-Weetaluktuk WN, Ryan DH, Nazar LF (2012) Solvothermal synthesis of electroactive lithium iron tavorites and structure of Li_2FePO_4F. J Mater Chem 22(11):4759–4766. https://doi.org/10.1039/c2jm15273h
252. Devaraju M, Honma I (2013) One-pot synthesis of Li_2FePO_4F nanoparticles via a supercritical fluid process and characterization for application in lithium-ion batteries. RSC Adv 3(43):19849–19852. https://doi.org/10.1039/c3ra42686f
253. Asl HY, Choudhury A (2014) Phosphorous acid route synthesis of iron tavorite phases, $LiFePO_4(OH)_xF_{1-x}$ [$0 \leq x \leq 1$] and comparative study of their electrochemical activities. RSC Adv 4:37691–37700
254. Choi M, Ham G, Jin BS (2014) Ultra-thin Al_2O_3, coating on the acid-treated $0.3Li_2MnO_3{\cdot}0.7LiMn_{0.60}Ni_{0.25}Co_{0.15}O_2$, electrode for Li-ion batteries. J Alloys Compd 608:110–117
255. Numata K, Yamanaka S (1997) Synthesis of solid solutions in a system of $LiCoO_2$-Li_2MnO_3 for cathode materials of secondary lithium batteries. Chem Lett 8:725–726
256. Kim DH, Kang SH, Balasubramanian M (2010) High-energy and high-power Li-rich nickel manganese oxide electrode materials. Electrochem Commun 12(8):1618–1621
257. Croy JR, Kang SH, Balasubramanian M, Thackeray MM (2011) Li_2MnO_3-based composite cathodes for lithium batteries: a novel synthesis approach and new structures. Electrochem Commun 13:1063–1066
258. Gallagher KG, Kang SH, Park SU (2011) $xLi_2MnO_3{\cdot}(1–x)LiMO_2$ blended with $LiFePO_4$ to achieve high energy density and pulse power capability. J Power Sources 196:9702–9707
259. West WC, Staniewicz RJ, Ma C (2011) Implications of the first cycle irreversible capacity on cell balancing for Li_2MnO_3-$LiMO_2$ (M = Ni, Mn, Co) Li-ion cathodes. J Power Sources 196:9696–9701
260. Kang YJ, Kim JH, Lee SW (2005) The effect of $Al(OH)_3$ coating on the $Li[Li_{0.2}Ni_{0.2}Mn_{0.6}]O_2$ cathode material for lithium secondary battery. Electrochim Acta 50(24):4784–4791
261. Yan Z, Hu Q, Yan G et al (2017) Co_3O_4/Co nanoparticles enclosed graphitic carbon as anode material for high performance Li-ion batteries. Chem Eng J 321:495–501
262. Wu Y, Murugan VA, Manthiram A (2008) Surface modification of high capacity layered $Li[Li_{0.2}Mn_{0.54}Ni_{0.13}Co_{0.13}]O_2$ cathode by $AlPO_4$. J Electrochem Soc 155(9):635–641
263. Wang WD, Qiu WH, Ding QQ (2015) Nickel cobalt manganese based cathode materials for Li-ion batteries technology production and application. Chemical Industry Press, M. Beijing, pp 030–035
264. Lee E, Park JS, Wu T (2015) Role of Cr^{3+}/Cr^{6+} redox in chromium-substituted $Li_2MnO_3{\cdot}LiNi_{1/2}Mn_{1/2}O_2$ layered composite cathodes: electrochemistry and voltage fade. J Mater Chem A 3(18):9915–9924
265. Lu C, Yang SQ, Wu H, Zhang Y (2016) Enhanced electrochemical performance of Li-rich $Li_{1.2}Mn_{0.52}Co_{0.08}Ni_{0.2}O_2$ cathode materials for Li-ion batteries by vanadium doping. Electrochim Acta 209:448–455
266. Huang ZM, Li XH, Liang YH, He ZJ (2015) Structural and electrochemical characterization of Mg-doped $Li_{1.2}[Mn_{0.54}Ni_{0.13}Co_{0.13}]O_2$ cathode material for lithium ion batteries. Solid State Ionics 282:88–94
267. Dianat A, Seriani N, Bobeth M, Cuniberti G (2013) Effects of Al-doping on the properties of Li–Mn–Ni–O cathode materials for Li-ion batteries: an ab initio study. J Mater Chem A 1:9273–9280
268. Wang D, Liu MH, Wang XY, Yu RZ (2016) Facile synthesis and performance of Na-doped porous lithium-rich cathodes for lithium ion batteries. RSC Adv 6:57310–57319

269. Song BH, Zhou CF, Wang HL (2014) Advances in sustain stable voltage of Cr-Doped Li-rich layered cathodes for lithium ion batteries. J Electrochem Soc 161(10):A1723–A1730
270. Song BH, Day SJ, Sui T (2016) Mitigated phase transition during first cycle of a Li-rich layered cathode studied by in operan do synchrotron X-ray powder diffraction. Phys Chem Chem Phys 18(6):4745–4752
271. Singh G, Thomas R, Kumar A, Katiyar RS (2012) Electrochemical behavior of Cr-doped composite Li_2MnO_3-$LiMn_{0.5}Ni_{0.5}O_2$ cathode materials. J Electrochem Soc 159:A410–A420
272. Zhu WX, Li XH, Wang ZX (2013) Synthesis and modification of Li-rich cathode Li $[Li_{0.2}Ni_{0.2}Mn_{0.6}]O_2$ for Li-ion batteries. Chin J Nonferrous Metals 23(4):1047–1052
273. Ding Y, Mu D, Wu B, Wang R, Zhao Z, Wu F (2017) Recent progresses on nickel-rich layered oxide positive electrode materials used in lithium-ion batteries for electric vehicles. Appl Energy 195:586–599. https://doi.org/10.1016/j.apenergy.2017.03.074
274. Pampal ES, Stojanovska E, Simon B, Kilic A (2015) A review of nanofibrous structures in lithium ion batteries. J Power Sources 300:199–215. https://doi.org/10.1016/j.jpowsour.2015.09.059
275. Kuriyama H, Saruwatari H, Satake H, Shima A, Uesugi F, Tanaka H, Ushirogouchi T (2015) Observation of anisotropic microstructural changes during cycling in $LiNi_{0.5}Co_{0.2}Mn_{0.3}O_2$ cathode material. J Power Sources 275:99–105. https://doi.org/10.1016/j.jpowsour.2014.10.197
276. Yuan J, Wen J, Zhang J, Chen D, Zhang D (2017) Influence of calcination atmosphere on structure and electrochemical behavior of $LiNi_{0.6}Co_{0.2}Mn_{0.2}O_2$ cathode material for lithium-ion batteries. Electrochim Acta 230:116–122
277. Waje SB, Hashim M, Yusoff WDW, Abbas Z (2010) X-ray diffraction studies on crystallite size evolution of $CoFe_2O_4$ nanoparticles prepared using mechanical alloying and sintering. Appl Surf Sci 256(10):3122–3127. https://doi.org/10.1016/j.apsusc.2009.11.084
278. Pukazhselvan D (2012) Effect of crystallite size of Al on the reversible hydrogenstorage of $NaAlH_4$ and few aspects of catalysts and catalysis. Int J Hydrog Energy 37(12):9696–9705. https://doi.org/10.1016/j.ijhydene.2012.03.098
279. Mguni LL, Mukenga M, Jalama K, Meijboom R (2013) Effect of calcination temperature and MgO crystallite size on MgO/TiO_2 catalyst system for soybean oil transesterification. Catal Commun 34:52–57. https://doi.org/10.1016/j.catcom.2013.01.009
280. Iqbal MJ, Yaqub N, Sepiol B, Ismail B (2011) A study of the influence of crystallite size on the electrical and magnetic properties of $CuFe_2O_4$. Mater Res Bull 46(11):1837–1842. https://doi.org/10.1016/j.materresbull.2011.07.036
281. Upadhyay S, Parekh K, Pandey B (2016) Influence of crystallite size on the magnetic properties of Fe_3O_4 nanoparticles. J Alloys Compd 678:478–485
282. Zhao S, Ka O, Xian XC, Sun LM, Wang J (2016) Effect of primary crystallite size on the high-rate performance of $Li_4Ti_5O_{12}$ microspheres. Electrochim Acta 206:17–25
283. Tlili R, Bejar M, Dhahri E, Zaoui A, Hlil EK, Bessais L (2017) Influence of crystallite size reduction on the magnetic and magnetocaloric properties of $La_{0.6}Sr_{0.35}Ca_{0.05}CoO_3$ nanoparticles. Polyhedron 121:19–24. https://doi.org/10.1016/j.poly.2016.09.044
284. Burton AW, Ong K, Rea T, Chan IY (2009) On the estimation of average crystallite size of zeolites from the Scherrer equation: a critical evaluation of its application to zeolites with one-dimensional pore systems. Microporous Mesoporous Mater 117(1–2):75–90. https://doi.org/10.1016/j.micromeso.2008.06.010
285. Uvarov V, Popov I (2007) Metrological characterization of X-ray diffraction methods for determination of crystallite size in nano-scale materials. Mater Charact 58(10):883–889. https://doi.org/10.1016/j.matchar.2006.09.002
286. Uvarov V, Popov I (2013) Metrological characterization of X-ray diffraction methods at different acquisition geometries for determination of crystallite size in nano-scale materials. Mater Charact 85:111–123. https://doi.org/10.1016/j.matchar.2013.09.002
287. Yashpal V, Sharma BV, Kumar M (2015) Issues in determining size of nano-crystalline ceramic particles by X-ray diffraction. Mater Today 2(4–5):3534–3538. https://doi.org/10.1016/j.matpr.2015.07.330

288. Sikora MS, Rosario AV, Pereira EC, Paiva-Aantos CO (2011) Influence of the morphology and microstructure on the photocatalytic properties of titanium oxide films obtained by sparking anodization in H_3PO_4. Electrochim Acta 56(9):3122–3127. https://doi.org/10.1016/j.electacta.2011.01.068
289. Kong J-Z, Zhai H-F, Ren C, Gao M-Y, Zhang X, Li H, Li J-X, Tang Z, Zhou F (2013) Synthesis and electrochemical performance of macroporous $LiNi_{0.5}Co_{0.2}Mn_{0.3}O_2$ by a modified sol–gel method. J Alloys Compd 577:507–510. https://doi.org/10.1016/j.jallcom.2013.07.007
290. Kong J-Z, Zhou F, Wang C-B, Yang X-Y, Zhai H-F, Hui L, Li J-X, Tang Z, Zhang S-Q (2013) Effects of Li source and calcination temperature on the electrochemical properties of $LiNi_{0.5}Co_{0.2}Mn_{0.3}O_2$ lithium-ion cathode materials. J Alloys Compd 554:216–221. https://doi.org/10.1016/j.jallcom.2012.11.090
291. Hu M, Pang XL, Zhou Z (2013) Recent progress in high-voltage lithium ion batteries. J Power Sources 237:229–242. https://doi.org/10.1016/j.jpowsour.2013.03.024
292. Yun FL, Tang L, Li WC, Jin WR, Pang J, Lu SG (2016) Thermal behavior analysis of a pouch type $Li[Ni_{0.7}Co_{0.15}Mn_{0.15}]O_2$-based lithium-ion battery. Rare Met 35(4):309
293. Ren L, Li XE, Wang FF, Han Y (2015) Spindle $LiFePO_4$ particles as cathode of lithium-ion batteries synthesized by solvothermal method with glucose as auxiliary reductant. Rare Met 34(10):731
294. Liu DL, Du LC, Liu YF, Chen YB (2014) Effects of Mn-precursor on performances of $LiMn_2O_4$ cathode material for lithium ion battery. Rare Met Mater Eng 43(11):2584
295. Hu M, Tian Y, Su LW, Wei JP, Zhou Z (2013) Preparation and Ni-doping effect of nanosized truncated octahedral $LiCoMnO_4$ as cathode materials for 5 V Li-ion batteries. ACS Appl Mater Interfaces 5(22):12185
296. Wang HL, Xia H, Lai MO, Lu L (2009) Enhancements of rate capability and cyclic performance of spinel $LiNi_{0.5}Mn_{1.5}O_4$ by trace Ru-dopping. Electrochem Commun 11(7):1539
297. Wu P, Zheng XL, Zhou C, Gu GF, Tong DG (2013) Improved electrochemical performance of $LiNi_{0.5-x}$ $Rh_xMn_{1.5}O_4$ cathode materials for 5 V lithium ion batteries via Rh-doping. Mater Chem Phys 138(2–3):716
298. Yang Z, Jiang Y, Kim JH, Wu Y, Li GL, Huang YH (2014) The $LiZn_xNi_{0.5-x}Mn_{1.5}O_4$ spinel with improved high voltage stability for Li-ion batteries. Electrochim Acta. 117(4):76
299. Hu M, Tian Y, Wei JP, Wang DG, Zhou Z (2014) Porous hollow $LiCoMnO_4$ microspheres as cathode materials for 5 V lithium ion batteries. J Power Sources 247(2):794
300. Zhan GC, Tang XC, Wang ZM (2012) Preparation of $LiCo_{1/3}Ni_{1/3}Mn_{1/3}O_2$ cathode material by improved co-precipitation method. J Cent South Univ 43(10):3780
301. Yang Y, Xu SM, Weng YQ, Huang GY, Li LY. (2013) Preparation and characterization of $xLi_2MnO_3{\cdot}(1-x)$ $Li(Ni_{1/3}Co_{1/3}Mn_{1/3})O_2$ (x = 0.2, 0.4, 0.6) cathode materials synthesized by hydroxide co-precipitation method. J Funct Mater. 44(19):2878
302. Jeon HJ, Monim SA, Kang CS, Son JT. (2013) Synthesis of $Li_x[Ni_{0.225}Co_{0.125}Mn_{0.65}]O_2$ as a positive electrode for lithium-ion batteries by optimizing its synthesis conditions via a hydroxide co-precipitation method. J Phys Chem Solids 74(9):1185
303. Lou X-M, Zhang Y-X (2011) Synthesis of $LiFePO_4$/C cathode materials with both high-rate capacity and high tap density for lithium-ion batteries. J Mater Chem 21:4156–4160
304. Fan J-M, Chen J-J, Chen Y-X, Huang H-H, Wei Z-K, Zheng M-S, Dong Q-F (2014) Hierarchical structure $LiFePO_4$@C synthesized by doleylamine-mediated method for low temperature applications. J Mater Chem A 2:4870–4873
305. Wu X-L, Guo Y-G, Su J, Xiong J-W, Zhang Y-L, Wan L-J (2013) Carbon-nanotube-decorated nano-$LiFePO_4$@C cathode materials with superior high-rate and low-temperature performance for lithium-ion batteries. Adv Energy Mater 3:1155–1160
306. Li S-M, Liu XC, Mi R, Liu H, Li YC, Lau W-M, Mei J (2014) A facile route to modify ferrous phosphate and its use as an iron-containing resource for $LiFePO_4$ via a polyol process. ACS Appl Mater Interfaces 6:9449–9457

307. Tasis D, Tagmatarchis N, Bianco A, Prato M (2006) Chem Rev 106:1105
308. Andrews R, Jacques D, Qian D, Rantell T (2002) Acc Chem Res 35:1008
309. Li G, Shrotriya V, Huang J, Yao Y, Moriarity T, Emery K, Yang Y (2005) Nat Mater 4:864
310. McCullough RD (1998) Adv Mater 10:93
311. Iijima S (1991) Nature 354:56
312. Shao QG, Chen WM, Wang ZH, Qie L, Yuan LX, Zhang WX et al (2011) Electrochem Commun 13:1431
313. Zhao Y, Li J, Wang N, Wu C, Dong G, Guan L (2012) J Phys Chem C 116:18612
314. Kim J, Lee D, Jung H, Sun Y, Hassoun J, Scrosati B (2013) An advanced lithium-sulfur battery. Adv Funct Mater 23:1076–1080
315. Yoo H, Markevich E, Salitra G, Sharon D, Aurbach D (2014) On the challenge of developing advanced technologies for electrochemical energy storage and conversion. Mater Today 17:110–121
316. Brodd R (2013) Batteries for sustainability: selected entries from the encyclopedia of sustainability science and technology. Springer New York, New York
317. Fedorková A, Oriňáková R, Čech O, Sedlaříková M (2013) New composite cathode materials for Li/S batteries: a review. Int J Electrochem Sci 8
318. Fedorková A, Nacher-Alejos A, Gómez-Romero P, Oriňáková R, Kaniansky D (2010) Structural and electrochemical studies of PPy/PEG-$LiFePO_4$ cathode material for Li-ion batteries. Electrochim Acta 55:943–947
319. Assary R, Curtiss L, Moore J (2014) Toward a molecular understanding of energetics in Li–S batteries using nonaqueous electrolytes: a high-level quantum chemical study. J Phys Chem 118:11545–11558
320. Choi Y, Kim K, Ahn H, Ahn J (2008) Improvement of cycle property of sulfur electrode for lithium/sulfur battery. J Alloys Compd 449:313–316
321. Cao Z, Ma C, Jia Y, Sun Z, Yue H, Yin Y, Yang S (2015) Activated clay of nest structure encapsulated sulfur cathodes for lithium–sulfur batteries. RSC Adv 36:28349–28353
322. Zhao X, Tu J, Lu Y, Cai J, Zhang Y, Wang X, Gu C (2013) Graphene-coated mesoporous carbon/sulfur cathode with enhanced cycling stability. Electrochim Acta 113:256–262
323. Wang X, Zhang Z, Yan X, Qu Y, Lai Y, Li J (2015) Interface polymerization synthesis of conductive polymer/graphite oxide@sulfur composites for high-rate lithium-sulfur batteries. Electrochim Acta 155:54–60
324. Cheng H, Wang S (2014) Recent progress in polymer/sulphur composites as cathodes for rechargeable lithium–sulphur batteries. J Mater Chem A 2:13783
325. Babu G, Ababtain K, Ng K, Arava L (2015) Electrocatalysis of lithium polysulfides: current collectors as electrodes in Li/S battery configuration. Sci Rep 5:8763
326. He J, Chen Y, Li P, Fu F, Wang Z, Zhang W (2015) Three-dimensional CNT/graphene–sulfur hybrid sponges with high sulfur loading as superior-capacity cathodes for lithium–sulfur batteries. J Mater Chem A 3:18605–18610
327. Zhou G, Paek E, Hwang G, Manthiram A (2015) Long-life Li/polysulphide batteries with high sulphur loading enabled by lightweight three-dimensional nitrogen/sulphur-codoped graphene sponge. Nat Commun 6:7760–7771
328. Alves A, Bergman CP, Berutti FA (2013) Novel synthesis and characterization of nanostructured materials, engineering materials. Springer, Berlin, Heidelberg. https://doi.org/10.1007/978-3-642-41275-2-1
329. Li Z, Zhang D, Yang F (2009) Developments of lithium-ion batteries and challenges of $LiFePO_4$ as one promising cathode material. J Mater Sci 44(10):2435–2443
330. Chang H-H, Chang C-C, Wu H-C, Guo ZZ, Yang MH, Chiang YP, Sheu HS, Wu NL (2006) Kinetic study on low-temperature synthesis of $LiFePO_4$ via solid-state reaction. J Power Sources 158(1):550–556
331. Amin R, Maier J, Balaya P, Chen DP, Lin CT (2008) Ionic and electronic transport in single crystalline $LiFePO_4$ grown by optical floating zone technique. Solid State Ionics 179(27–32):1683–1687

332. Lung-Hao HuB, Wu F-Y, Lin C-T, Khlobystov AN, Li LJ (2013) Graphene-modified $LiFePO_4$ cathode for lithium ion battery beyond theoretical capacity. Nat Commun 4:1687
333. Zhou X, Wang F, Zhu Y, Liu Z (2011) Graphene modified $LiFePO_4$ cathode materials for high power lithium ion batteries. J Mater Chem 21(10):3353–3358
334. Yang J, Wang J, Tang Y, Wang D, Li X, Hu Y, Li R, Liang G, Sham TK, Sun X (2013) $LiFePO_4$–graphene as a superior cathode material for rechargeable lithium batteries: impact of stacked graphene and unfolded graphene. Energy Environ Sci 6(5):1521–1528
335. Rui X, Zhao X, Lu Z, Tan H, Sim D, Hng HH, Yazami R, Lim TM, Yan Q (2013) Olivine-type nanosheets for lithium ion battery cathodes. ACS Nano 7(6):5637–5646
336. Larcher D, Tarascon JM (2015) Towards greener and more sustainable batteries for electrical energy storage. Nat Chem 7:19–29. https://doi.org/10.1038/nchem.2085
337. Thackeray MM, Wolverton C, Isaacs ED (2012) Electrical energy storage for transportation-approaching the limits of, and going beyond, lithium-ion batteries. Energ Environ Sci 5:7854–7863. https://doi.org/10.1039/C2EE21892E
338. Palomares V, Serras P, Villaluenga I, Hueso KB, Carretero-Gonzalez J, Rojo T (2012) Na-ion batteries, recent advances and present challenges to become low cost energy storage systems. Energy Environ Sci 5:5884–5901. https://doi.org/10.1039/c2ee02781j
339. Santhanam R, Rambabu B (2010) J Power Sources 195:5442–5451
340. Eftekhari A (2004) J Power Sources 132:240–243
341. Lu DS, Xu MQ, Zhou L, Garsuch A, Lucht BL (2013) J Electrochem Soc 160:A3138–A3143
342. Yang L, Ravdel B, Lucht BL (2010) Electrochem Solid-State Lett 13:A95–A97
343. Wu HM, Belharouak I, Abouimrane A, Sun Y-K, Amine K (2010) J Power Sources 195:2909–2913
344. Liu D, Trottier J, Charest P, Fréchette J, Guerfi A, Mauger A, Julien CM, Zaghib K (2012) J Power Sources 204:127–132
345. Sun Y-K, Lee Y-S, Yoshio M, Amine K (2003) J Electrochem Soc 150:L11–L11
346. Liu J, Manthiram A (2009) Kinetics study of the 5 V spinel cathode $LiMn_{1.5}Ni_{0.5}O_4$ before and after surface modifications. J Electrochem Soc 156:A833–A838
347. Liu D, Bai Y, Zhao S, Zhang W (2012) J Power Sources 219:333–338
348. Li J, Zhang Y, Li J, Wang L, He X, Gao J (2011) Ionics 17:671–675
349. Kraytsberg A, Drezner H, Auinat M, Shapira A, Solomatin N, Axmann P, Margret W-M, Yair E-E (2015) ChemNanoMat 1:577–585
350. Lee K-S, Myung S-T, Amine K, Yashiro H, Sun Y-K (2009) J Mater Chem 19:1995–2005
351. Luo SH, Gao M, Chen J, Xing XR, Li Z, Zhou XT, Wen W (2011) J New Mater Electrochem Syst 14:141–146
352. Xia H, Yan F, Lai MO, Lu L, Song WD (2009) Funct Mater Lett 02:163–167
353. Ménétrier M, Saadoune I, Levasseur S, Delmas C (1999) J Mater Chem 9:1135–1140
354. Lu Z, Dahn JR (2002) J Electrochem Soc 149:A815–A822
355. Liu JL, Chen L, Hou MY, Wang F, Che RC, Xia YY (2012) J Mater Chem 22:25380–25387
356. Kong JZ, Wang CL, Xu Q, Tai GA, Li AD, Wu D, Li H, Zhou F, Yu C, Sun Y, Jia D, Tang WP (2015) Electrochim Acta 174:542–550
357. Lu J, Peng Q, Wang W, Nan C, Li L, Li Y (2013) J Am Chem Soc 135:1649–1652
358. Padhy R, Rao AN, Parashar SKS, Parashar K, Chaudhuri P (2014) Solid State Ionics 256:29–37
359. Yu C, Wang H, Guan XF, Zheng J, Li LP (2013) J Alloys Compd 546:239–245
360. Wang Y, Zhou AJ, Dai XY, Feng LD, Li JW, Li JZ (2014) J Power Sources 266:114–120
361. Shi SJ, Tu JP, Tang YY, Yu YX, Zhang YQ, Wang XL, Gu CD (2013) J Power Sources 228:14–23
362. Miao XW, Ni H, Zhang H, Wang CG, Fang JH, Yang G (2014) J Power Sources 264: 147–154

363. Vijayakumar M, Kerisit S, Yang ZG, Graff GL, Liu J, Sears JA, Burton SD, Rosso KM, Hu JZ (2009) J Phys Chem C 113:20108–20116
364. Luo D, Li G, Fu C, Chao Z, Jing F, Jian M, Li Q (2015) $LiMO_2$ (M = Mn, Co, Ni) hexagonal sheets with (101) facets for ultrafast charging–discharging lithium ion batteries. J Power Sources 276:238–246. https://doi.org/10.1016/j.jpowsour.2014.11.122
365. Lee KS, Myung ST, Amine K, Lee KS, Myung ST, Amine K, Yashiro H, Sun YK (2007) Structural and electrochemical properties of layered Li[Ni[sub 1−2x]Co[sub x]Mn[sub x]]O [sub 2] (x = 0.1–0.3) positive electrode materials for Li-ion batteries. J Electrochem Soc 154 (10):A971–A977. https://doi.org/10.1149/1.2769831
366. Eom J, Kim MG, Cho J (2008) Storage characteristics of LiNi[sub 0.8]Co[sub 0.1+x]Mn [sub 0.1−x]O[sub 2] (x = 0, 0.03, and 0.06) cathode materials for lithium batteries. J Electrochem Soc 155(3):A239–A245. https://doi.org/10.1149/1.2830946
367. Bang H, Kim DH, Bae YC, Sun YK (2008) Effects of metal ions on the structural and thermal stabilities of Li[Ni[sub 1−x−y]Co[sub x]Mn[sub y]]O[sub 2] (x+y $\leq$ 0.5) studied by in situ high temperature XRD. J Electrochem Soc 155(12):A952–A958. https://doi.org/10.1149/1.2988729
368. Fey GT, Shiu R, Subramanian V, Chen JG, Chen CL (2002) $LiNi_{0.8}Co_{0.2}O_2$ cathode materials synthesized by the maleic acid assisted sol–gel method for lithium batteries. J Power Sources 103(2):265–272. https://doi.org/10.1016/S0378-7753(01)00859-X
369. Yao JH, Shen CQ, Zhang PJ, Gregory DH, Wang LB (2013) Surface coating of $LiMn_2O_4$ spinel via in situ hydrolysis route: effect of the solution. Ionics 19:739–745
370. Liu DQ, Liu XQ, He ZZ (2007) Surface modification by ZnO coating for improving the elevated temperature performance of $LiMn_2O_4$. J Alloys Compd 436:387–391
371. Ha HW, Yun NJ, Kim K (2007) Improvement of electrochemical stability of $LiMn_2O_4$ by CeO_2 coating for lithium-ion batteries. Electrochim Acta 52:3236–3241
372. Zhao S, Chang QJ, Jiang K, Bai Y, Yang YQ, Zhang WF (2013) Performance improvement of spinel $LiMn_2O_4$ cathode material by LaF_3 surface modification. Solid State Ionics 253:1–7
373. Shang YS, Liu JL, Huang T, Yu AS (2013) Effect of heat treatment on the structure and electrochemical performance of $FePO_4$ coated spinel $LiMn_2O_4$. Electrochim Acta 113:248–255
374. Hu YM, Yao J, Zhao Z, Zhu MY, Li Y, Jin HM, Zhao HJ, Wang JZ (2013) ZnO-doped $LiFePO_4$ cathode material for lithium-ion battery fabricated by hydrothermal method. Mater Chem Phys 141:835–841
375. Singhala R, Tomarb MS, Burgos JG, Katiyara RS (2008) Electrochemical performance of ZnO-coated $LiMn_{1.5}Ni_{0.5}O_4$ cathode material. J Power Sources 183:334–338
376. Kong JZ, Ren C, Tai GA, Zhang X, Li AD, Wu D, Li H, Zhou F (2014) Ultrathin ZnO coating for improved electrochemical performance of $LiNi_{0.5}Co_{0.2}Mn_{0.3}O_2$ cathode material. J Power Sources 266:433–439
377. Tu J, Zhao XB, Xie J, Cao GS, Zhung DG, Zhu TJ, Tu JP (2007) Enhanced low voltage cycling stability of $LiMn_2O_4$ cathode by ZnO coating for lithium ion batteries. J Alloys Compd 432:313–317
378. Liu HW, Cheng CX, Hu ZQ, Zhang KL (2007) The effect of ZnO coating on $LiMn_2O_4$ cycle life in high temperature for lithium secondary batteries. Mater Chem Phys 101:276–279
379. Tu J, Zhao XB, Cao GS, Zhu TJ, Zhung DG, Tu JP (2006) Electrochemical performance of surface-modified $LiMn_2O_4$ prepared by a melting impregnation method. J Mater Sci Technol 22:433–436
380. Zhao JQ, Wang Y (2012) Ultrathin surface coatings for improved electrochemical performance of lithium ion battery electrodes at elevated temperature. J Phys Chem C 116:11867–11876
381. Yabuuchi N, Ohzuku T (2003) J Power Sources 119–121:171–174
382. Amine K, Chen Z, Zhang Z, Liu J, Lu W, Qin Y, Lu J, Curtis L, Sun Y (2011) J MaterChem 21:17754–17759
383. Kim G-H, Kim M-H, Myung S-T, Sun YK (2005) J Power Sources 146:602–605

384. Liu XZ, Li HQ, Yoo E, Ishida M, Zhou HS (2012) Electrochim Acta 83:253–258
385. Yuan X, Xu QJ, Liu X, Liu H, Min Y, Xia Y (2016) Layered cathode material with improved cycle performance and capacity by surface anchoring of TiO_2 nanoparticles for Li-ion batteries. Electrochim Acta 213:648–654. https://doi.org/10.1016/j.electacta.2016.07.157
386. Zhou LZ, Xu QJ, Liu MS, Jin X (2013) Novel solid-state preparation and electrochemical properties of $Li_{1.13}[Ni_{0.2}Co_{0.2}Mn_{0.47}]O_2$ material with a high capacity by acetate precursor for Li-ion batteries. Solid State Ionics 249–250:134–138. https://doi.org/10.1016/j.ssi.2013.07.024
387. Jin X, Xu Q, Yuan X, Zhou L, Xia Y (2013) Synthesis, characterization and electrochemical performance of $Li[Li_{0.2}Mn_{0.54}Ni_{0.13}Co_{0.13}]O_2$ cathode materials for lithium-ion batteries. Electrochim Acta 114:605–610. https://doi.org/10.1016/j.electacta.2013.10.091
388. Lee ES, Manthiram A (2014) Smart design of lithium-rich layered oxide cathode compositions with suppressed voltage decay. J Mater Chem A 2(11):3932. https://doi.org/10.1039/c3ta14975g
389. Tabuchi M, Nabeshima Y, Takeuchi T, Kageyama H, Tatsumi K, Akimoto J, Shibuya H, Imaizumi J (2011) Synthesis and electrochemical characterization of Fe and Ni substituted Li_2MnO_3—an effective means to use Fe for constructing "Co-free" Li_2MnO_3 based positive electrode material. J Power Sources 196(7):3611–3622. https://doi.org/10.1016/j.jpowsour.2010.12.060
390. Nayak PK, Grinblat J, Levi M, Levi E, Kim S, Choi JW, Aurbach D (2016) Al doping for mitigating the capacity fading and voltage decay of layered Li and Mn-rich cathodes for Li-ion batteries. Adv Energy Mater 6(8):1502398. https://doi.org/10.1002/aenm.201502398
391. Li B, Li C, Cai J, Zhao J (2015) Retracted article: in situ nano-coating on $Li_{1.2}Mn_{0.52}Ni_{0.13}Co_{0.13}O_2$ with a layered@spinel@coating layer heterostructure for lithium-ion batteries. J Mater Chem A 3(42):21290–21297. https://doi.org/10.1039/c5ta06387f
392. Zheng J, Gu M, Genc A, Xiao J, Xu P, Chen X, Zhu Z, Zhao W, Pullan L, Wang C, Zhang JG (2014) Mitigating voltage fade in cathode materials by improving the atomic level uniformity of elemental distribution. Nano Lett 14(5):2628–2635. https://doi.org/10.1021/nl500486y
393. Chen CJ, Pang WK, Mori T, Peterson VK, Sharma N, Lee PH, Wu SH, Wang CC, Song YF, Liu RS (2016) The origin of capacity fade in the $Li_2MnO_3{\cdot}LiMO_2$ (M = Li, Ni, Co, Mn) microsphere positive electrode: an operando neutron diffraction and transmission X-ray microscopy study. J Am Chem Soc 138(28):8824–8833. https://doi.org/10.1021/jacs.6b03932
394. Zheng J, Xu P, Gu M, Xiao J, Browning ND, Yan P, Wang C, Zhang JG (2015) Structural and chemical evolution of Li- and Mn-rich layered cathode material. Chem Mater 27(4):1381–1390. https://doi.org/10.1021/cm5045978
395. Chen Y, Xie K, Zheng C, Ma Z, Chen Z (2014) Enhanced Li storage performance of $LiNi_{0.5}Mn_{1.5}O_4$-coated $0.4Li_2MnO_3{\cdot}0.6LiNi_{1/3}Co_{1/3}Mn_{1/3}O_2$ cathode materials for Li-ion batteries. ACS Appl Mater Interfaces 6(19):16888–16894. https://doi.org/10.1021/am504412n
396. Zhao E, Liu X, Hu Z, Sun L, Xiao X (2015) Facile synthesis and enhanced electrochemical performances of Li_2TiO_3-coated lithium-rich layered $Li_{1.13}Ni_{0.30}Mn_{0.57}O_2$ cathode materials for lithium-ion batteries. J Power Sources 294:141–149. https://doi.org/10.1016/j.jpowsour.2015.06.059
397. Li J, Zhan C, Lu J, Yuan Y, Shahbazian Yassar R, Qiu X, Amine K (2015) Improve first-cycle efficiency and rate performance of layered-layered $Li_{1.2}Mn_{0.6}Ni_{0.2}O_2$ using oxygen stabilizing dopant. ACS Appl Mater Interfaces 7(29):16040–16045. https://doi.org/10.1021/acsami.5b04343
398. Wang Z, Liu E, He C, Shi C, Li J, Zhao N (2013) Effect of amorphous $FePO_4$ coating on structure and electrochemical performance of $Li_{1.2}Ni_{0.13}Co_{0.13}Mn_{0.54}O_2$ as cathode material for Li-ion batteries. J Power Sources 236:25–32. https://doi.org/10.1016/j.jpowsour.2013.02.022
399. Xu G, Liu Z, Zhang C, Cui G, Chen L (2015) Strategies for improving the cyclability and thermo-stability of $LiMn_2O_4$-based batteries at elevated temperatures. J Mater Chem A 3(8):4092–4123

400. Yang L, Takahashi M, Wang B (2006) A study on capacity fading of lithium-ion battery with manganese spinel positive electrode during cycling. Electrochim Acta 51(16):3228–3234
401. Amatucci G, Du Pasquier A, Blyr A, Zheng T, Tarascon J-M (1999) The elevated temperature performance of the $LiMn_2O_4$/C system: failure and solutions. Electrochim Acta 45(1):255–271
402. Quinlan FT, Sano K, Willey T, Vidu R, Tasaki K, Stroeve P (2001) Surface characterization of the spinel $Li_xMn_2O_4$ cathode before and after storage at elevated temperatures. Chem Mater 13(11):4207–4212
403. Amine K, Liu J, Kang S, Belharouak I, Hyung Y, Vissers D, Henriksen G (2004) Improved lithium manganese oxide spinel/graphite Li-ion cells for high-power applications. J Power Sources 129(1):14–19
404. Xiao L, Zhao Y, Yang Y, Cao Y, Ai X, Yang H (2008) Enhanced electrochemical stability of Al-doped $LiMn_2O_4$ synthesized by a polymer-pyrolysis method. Electrochim Acta 54 (2):545–550
405. Wang X, Tanaike O, Kodama M, Hatori H (2007) High rate capability of the Mg-doped Li–Mn–O spinel prepared via coprecipitated precursor. J Power Sources 168(1):282–287
406. Huang J, Yang F, Guo Y, Peng C, Bai H, Peng J, Guo J (2015) $LiMg_xMn_{2-x}O_4$ ($x \leq 0.10$) cathode materials with high rate performance prepared by molten-salt combustion at low temperature. Ceram Int 41(8):9662–9667
407. Zhong Q, Bonakdarpour A, Zhang M, Gao Y, Dahn J (1997) Synthesis and electrochemistry of $LiNi_xMn_{2-x}O_4$. J Electrochem Soc 144(1):205–213
408. Amarilla J, Petrov K, Pico F, Avdeev G, Rojo J, Rojas R (2009) Sucrose-aided combustion synthesis of nanosized $LiMn_{1.99-y}Li_yM_{0.01}O_4$ (M = Al^{3+}, Ni^{2+}, Cr^{3+}, Co^{3+}, y = 0.01 and 0.06) spinels: characterization and electrochemical behavior at 25 and at 55 °C in rechargeable lithium cells. J Power Sources 191(2):591–600
409. Zhang L-X, Wang Y-Z, Jiu H-F, Wang Y-L, Sun Y-X, Li Z (2014) Controllable synthesis of Co-doped spinel $LiMn_2O_4$ nanotubes as cathodes for Li-ion batteries. Electron Mater Lett 10 (2):439–444
410. Uludag AA, Erdaş A, Ozcan S, Nalci D, Güler MO, Cetinkaya T, Uysal M, Akbulut H (2015) Cr-and V-substituted $LiMn_2O_4$ cathode electrode materials for high-rate battery applications. In: Progress in clean energy, vol 2. Springer, pp 41–56
411. Luan X, Guan D, Wang Y (2012) Enhancing high-rate and elevated-temperature performances of nano-sized and micron-sized $LiMn_2O_4$ in lithium-ion batteries with ultrathin surface coatings. J Nanosci Nanotechnol 12(9):7113–7120
412. Şahan H, Dokan FK, Ülgen A, Patat Ş (2014) Improvement of cycling stability of $LiMn_2O_4$ cathode by Fe_2O_3 surface modification for Li-ion battery. Ionics 20(3):323–333
413. Lai C, Ye W, Liu H, Wang W (2009) Preparation of TiO_2-coated $LiMn_2O_4$ by carrier transfer method. Ionics 15(3):389–392
414. Ju B, Wang X, Wu C, Wei Q, Yang X, Shu H, Bai Y (2014) Excellent cycling stability of spherical spinel $LiMn_2O_4$ by Y_2O_3 coating for lithium-ion batteries. J Solid State Electrochem 18(1):115–123
415. Ming H, Yan Y, Ming J, Adkins J, Li X, Zhou Q, Zheng J (2014) Gradient V_2O_5 surface-coated $LiMn_2O_4$ cathode towards enhanced performance in Li-ion battery applications. Electrochim Acta 120:390–397
416. Lee J-W, Park S-M, Kim H-J (2009) Effect of $LiNi_{1/2}Mn_{1/2}O_2$ coating on the electrochemical performance of Li–Mn spinel. Electrochem Commun 11(6):1101–1104
417. Yan J, Liu H, Wang Y, Zhao X, Mi Y, Xia B (2015) Enhanced high-temperature cycling stability of $LiNi_{1/3}Co_{1/3}Mn_{1/3}O_2$-coated $LiMn_2O_4$ as cathode material for lithium ion batteries. Ionics 21(7):1835–1842
418. Qiu T, Wang J, Lu Y, Yang W (2014) Improved elevated temperature performance of commercial $LiMn_2O_4$ coated with $LiNi_{0.5}Mn_{1.5}O_4$. Electrochim Acta 147:626–635
419. Li X, Xu Y, Wang C (2009) Novel approach to preparation of $LiMn_2O_4$ core/$LiNi_xMn_{2-x}O_4$ shell composite. Appl Surf Sci 255(11):5651–5655

420. Lin GQ, Wen L, Liu YM (2010) Spinel $LiNi_{0.5}Mn_{1.5}O_4$ and its derivatives as cathodes for high-voltage Li-ion batteries. J Solid State Electrochem 14(12):2191–2202. https://doi.org/10.1007/s10008-010-1061-5
421. Yi TF, Xie Y, Ye MF, Jiang LJ, Zhu RS, Zhu YR (2011) Recent developments in the doping of $LiNi_{0.5}Mn_{1.5}O_4$ cathode material for 5 V lithium-ion batteries. Ionics 17:383–389. https://doi.org/10.1007/s11581-011-0550-6
422. Zhu YR, Yi TF (2016) Recent progress in the electrolytes for improving the cycling stability of $LiNi_{0.5}Mn_{1.5}O_4$ high-voltage cathode. Ionics 22:1759–1774. https://doi.org/10.1007/s11581-016-1788-9
423. Mao J, Ma MZ, Liu PP, Hu JH, Shao GS, Battaglia V, Dai KH, Liu G (2016) The effect of cobalt doping on the morphology and electrochemical performance of high-voltage spinel $LiNi_{0.5}Mn_{1.5}O_4$cathode material. Solid State Ionics 292:70–74. https://doi.org/10.1016/j.ssi.2016.05.008
424. Lu M, Han ES, Zhu LZ, Chen S, Zhang GQ (2016) The effects of Ti^{4+}–Fe^{3+} co-doping on Li $Ni_{1/3}Co_{1/3}Mn_{1/3}$ O_2. Solid State Ionics 298:9–14. https://doi.org/10.1016/j.ssi.2016.10.014
425. Kou YJ, Han ES, Zhu LZ, Liu LL, Zhang ZA (2016) The effect of Ti doping on electrochemical properties of $Li_{1.167}Ni_{0.4}Mn_{0.383}Co_{0.05}O_2$ for lithium-ion batteries. Solid State Ionics 296:154–157. https://doi.org/10.1016/j.ssi.2016.09.020
426. Svegl F, Orel B, Grabec-Svegl I, Kaucic V (2000) Characterization of spinel Co_3O_4 and Li-doped Co_3O_4 thin film electrocatalysts prepared by the sol-gel route. Electrochim Acta 45 (25–26):4359–4371
427. Saadoune I, Delmas C (1996) $LiNi_{1-y}Co_yO_2$ positive electrode materials: relationships between the structure, physical properties and electrochemical behaviour. J Mater Chem 6 (2):193–199. https://doi.org/10.1039/jm9960600193
428. Myung S-T, Komaba S, Hirosaki N, Hosoya K, Kumagai N (2005) Improvement of structural integrity and battery performance of $LiNi_{0.5}Mn_{0.5}O_2$ by Al and Ti doping. J Power Sources 146(1–2):645–649. https://doi.org/10.1016/j.jpowsour.2005.03.083
429. Yang G, Zhao E, Chen M, Cheng Y, Xue L, Hu Z, Xiao X, Li F (2017) Mg doping improving the cycle stability of $LiNi_{0.5}Mn_{0.5}O_2$ at high voltage. J Solid State Electr. https://doi.org/10.1007/s10008-017-3666-4
430. Song D, Hou P, Wang X, Shi X, Zhang L (2015) Understanding the origin of enhanced performances in core-shell and concentration-gradient layered oxide cathode materials. ACS Appl Mater Interfaces 7(23):12864–12872
431. Mezaal MA, Qu L, Li G, Zhang R, Xuejiao J, Zhang K, Liu W, Lei L (2015) Promoting the cyclic and rate performance of lithium-rich ternary materials via surface modification and lattice expansion. RSC Adv 5(113):93048–93056
432. Gong C, Lv W, Qu L, Bankole OE, Li G, Zhang R, Hu M, Lei L (2014) Syntheses and electrochemical properties of layered $Li_{0.95}Na_{0.05}Ni_{1/3}Co_{1/3}Mn_{1/3}O_2$ and $LiNi_{1/3}Co_{1/3}Mn_{1/3}O_2$. J Power Sources 247:151–155
433. Islam MS, Fisher CA (2014) Lithium and sodium battery cathode materials: computational insights into voltage, diffusion and nanostructural properties. Chem Soc Rev 43:185–204
434. Yu XZ, Lu BA, Xu Z (2014) Super long-life supercapacitors based on the construction of nanohoneycomb-like strongly coupled CoMoO-3D graphene hybrid electrodes. Adv Mater 26:1044–1051
435. Whittingham MS (2004) Lithium batteries and cathode materials. Chem Rev 104(10):4271–4302. https://doi.org/10.1021/cr020731c
436. Yu H, Kim H, Wang Y, He P, Asakura D, Nakamura Y, Zhou H (2012) High energy 'composite' layered manganese-rich cathode materials via controlling Li_2MnO_3 phase activation for lithium-ion batteries. Phys Chem 14:6584–6595

437. Armstrong AR, Holzapfel M, Novàk P, Johnson CS, Kang S-H, Thackeray MM, Bruce PG (2006) Demonstrating oxygen loss and associated structural reorganization in the lithium battery cathode $Li[Ni_{0.2}Li_{0.2}Mn_{0.6}]O_2$. J Am Chem Soc 128:8694–8698
438. Martha SK, Nanda J, Veith GM, Dudney NJ (2012) Electrochemical and rate performance study of high-voltage lithium-rich composition: $Li_{1.2}Mn_{0.525}Ni_{0.175}Co_{0.1}O_2$. J Power Sources 199:220–226
439. Mohanty D, Sefat AS, Kalnaus S, Li J, Meisner RA, Payzant EA, Abraham DP, Wood DL, Daniel C (2013) Investigating phase transformation in the$Li_{1.2}Co_{0.1}Mn_{0.55}Ni_{0.15}O_2$ lithium-ion battery cathode during high-voltage hold (4.5 V) via magnetic, X-ray diffraction and electron microscopy studies. J Mater Chem A 1:6249–6261
440. Martha SK, Nanda J, Kim Y, Unocic RR, Pannala S, Dudney NJ (2013) Solid electrolyte coated high voltage layered–layered lithium-rich composite cathode: $Li_{1.2}Mn_{0.525}Ni_{0.175}Co_{0.1}O_2$. J Mater Chem A 1:5587–5595
441. Martha SK, Nanda J, Veith GM, Dudney NJ (2012) Surface studies of high voltage lithium rich composition: $Li_{1.2}Mn_{0.525}Ni_{0.175}Co_{0.1}O_2$. J Power Sources 216:179–186
442. Bettge M, Li Y, Gallagher K, Zhu Y, Wu Q, Lu W, Bloom I, Abraham DP (2013) Voltage fade of layered oxides: its measurement and impact on energy density. J Electrochem Soc 160(11):A2046–A2055
443. Nayak PK, Grinblat J, Levi E, Penki Ti R, Levi M, Sun Y-K, Markovsky B, Aurbach D (2016) Remarkably improved electrochemical performance of Li- and Mn-rich cathodes upon substitution of Mn with Ni. ACS Appl Mater Interfaces. https://doi.org/10.1021/acsami.6b07959
444. Park SH, Sun Y-K (2003) Synthesis and electrochemical properties of layered $Li[Li_{0.15}Ni_{(0.275-x/2)}Al_xMn_{(0.575-x/2)}]O_2$ materials prepared by sol–gel method. J Power Sources 119–121:161–165
445. Wang YX, Shang KH, He W, Ai XP, Cao YL, Yang HX (2015) Magnesium-doped $Li_{1.2}$ $[Co_{0.13}Ni_{0.13}Mn_{0.54}]$ O_2 for lithium-ion battery cathode with enhanced cycling stability and rate capability. ACS Appl Mater Interfaces 7:13014–13021
446. Robert R, Villevieille C, Novák P (2014) Enhancement of the high potential specific charge in layered electrode materials for lithium-ion batteries. J Mater Chem A 2:8589–8598
447. Kim G-H, Kim J-H, Myung S-T, Yoon CS, Sun Y-K (2005) Improvement of high-voltage cycling behavior of surface-modified $Li[Ni_{1/3}Co_{1/3}Mn_{1/3}]O_2$ cathodes by fluorine substitution for Li-ion batteries. J Electrochem Soc 152:A1707–A1713
448. Shin HS, Park SH, Yoon CS, Sun YK (2005) Effect of fluorine on the electrochemical properties of layered $LiNi_{0.43}Co_{0.22}Mn_{0.35}O_2$ cathode materials via a carbonate process. Electrochem Solid-State Lett 8:A559
449. Woo SU, Park BC, Yoon CS, Myung ST, Prakash J, Sun YK (2007) Improvement of electrochemical performances of $LiNi_{0.8}Co_{0.1}Mn_{0.1}O_2$ cathode materials by fluorine substitution. J Electrochem Soc 154:A649
450. Shin HS, Shin D, Sun YK (2006) Improvement of electrochemical properties of Li $[Ni_{0.4}Co_{0.2}Mn_{(0.4-x)}Mg_x]O_{2-y}F_y$ cathode materials at high voltage region. Electrochim Acta 52:1477
451. Kim G-H, Myung S-T, Bang HJ, Prakash J, Sun Y-K (2004) Synthesis and electrochemical properties of $Li[Ni_{1/3}Co_{1/3}Mn_{(1/3-x)}Mg_x]O_{2-y}F_y$ via coprecipitation. Electrochem Solid-State Lett 7(12):A477–A480
452. Axelbaum RL, Lengyel M (2015) Doped lithium-rich layered composite cathode materials. United States Patent, US2015/0270545A1
453. Luo W, Zhou F, Zhao X, Lu Z, Li X, Dahn JR (2010) Synthesis, characterization, and thermal stability o $LiNi_{1/3}Mn_{1/3}Co_{1/3-z}Mg_zO_2$, $LiNi_{1/3-z}Mn_{1/3}Co_{1/3}Mg_zO_2$, and $LiNi_{1/3}Mn_{1/3-z}Co_{1/3}Mg_zO_2$. Chem Mater 22:1164–1172
454. Kim Y, Kim HS, Martin SW (2006) Synthesis and electrochemical characteristics of Al_2O_3-coated $LiNi_{1/3}Co_{1/3}Mn_{1/3}O_2$ cathode materials for lithium ion batteries. Electrochim Acta 52 (3):1316–1322

455. Chen Y, Zhang Y, Wang F, Wang Z, Zhang Q (2014) Improve the structure and electrochemical performance of $LiNiCoMnO_2$ cathode material by nano Al_2O_3 ultrasonic coating. J Alloys Compd 611:135–141
456. Li D, Kato Y, Kobayakawa K, Noguchi H, Sato Y (2006) Preparation and electrochemical characteristics of $LiNi_{1/3}Mn_{1/3}Co_{1/3}O_2$ coated with metal oxides coating. J Power Sources 160(2):1342–1348
457. Wu Y, Manthiram A (2006) High capacity, surface-modified layered LiLi, 1–x…/3Mn, 2–x…/3Nix/3Cox/3O2 cathodes with low irreversible capacity loss. Electrochem Solid State Lett 9(5):A221–A224
458. Choi J, Manthiram A (2005) Investigation of the irreversible capacity loss in the layered $LiNi_{1/3}Mn_{1/3}Co_{1/3}O_2$ cathodes. Electrochem Solid State Lett 8(8):C102–C105
459. Chen Z, Qin Y, Amine K, Sun YK (2010) Role of surface coating on cathode materials for lithium-ion batteries. J Mater Chem 20:7606–7612
460. Huang Y, Chen J, Cheng F, Wan W, Liu W, Zhou H, Zhang X (2010) A modified Al_2O_3 coating process to enhance the electrochemical performance of $Li(Ni_{1/3}Co_{1/3}Mn_{1/3})O_2$ and its comparison with traditional Al_2O_3 coating process. J Power Sources 195(24):8267–8274
461. Wu Y, Manthiram A (2007) Effect of Al^{3+} and F^{-} doping on the irreversible oxygen loss from layered $Li[Li_{0.17}Mn_{0.58}Ni_{0.25}]O_2$ cathodes. Electrochem Solid-State Lett 10(8):A151–A154
462. Shu J, Shui M, Huang F, Ren Y, Wang Q, Xu D, Hou L (2010) J Phys Chem C 114:3323–3328
463. Wang ZG, Wang ZX, Peng WJ, Guo HJ, Li XH, Wang JX, Qi A (2014) Ionics 20:1525–1534
464. Luo W, Li X, Dahn JR (2010) J Electrochem Soc 157:A782–A789
465. Scott ID, Jung YS, Cavanagh AS, Yan Y, Dillon AC, George SM, Lee SH (2011) Nano Lett 11:414–418
466. Jung YS, Lu P, Cavanagh AS, Ban C, Kim GH, Lee SH, George SM, Harris SJ, Dillon AC (2013) Adv Energy Mater 3:213–219
467. Dai X, Zhou A, Xu J, Yang B, Wang L, Li J (2015) J Power Sources 298:114–122
468. Shim J, Lee S, Park S (2014) Chem Mater 26:2537–2543
469. Cho J, Kim Y, Kim T, Park B (2001) Angew Chem Int Ed Engl 18:3367–3369
470. Lee J, Kim B, Cho J, Kim Y, Park B (2004) J Electrochem Soc 151:A801–A805
471. Sun Y, Yoon C, Myung S, Belharouak I, Amine K (2009) J Electrochem Soc 156:A1005–A1010
472. Lee H, Park Y (2013) Solid State Ionics 230:86–91
473. Park JS, Mane AU, Elam JW, Croy JR (2015) Chem Mater 27:1917–1920
474. Kim S-M, Jin B-S, Lee S-M, Kim H-S (2015) Effects of the fluorine-substitution and acid treatment on the electrochemical performances of $0.3Li_2MnO_3{\cdot}0.7LiMn_{0.60}Ni_{0.25}Co_{0.15}O_2$ cathode material for Li-ion battery. Electrochim Acta 171:35–41
475. Li J, Xu Y, Li X, Zhang Z (2013) Li_2MnO_3 stabilized $LiNi_{1/3}Co_{1/3}Mn_{1/3}O_2$ cathode with improved performance for lithium ion batteries. Appl Surf Sci 285:235–240
476. Yu H, Zhou H (2013) High-energy cathode materials (Li_2MnO_3-$LiMO_2$) for lithium-ion batteries. J Phys Chem Lett 4(8):1268–1280
477. Yano A, Aoyama S, Shikano M, Sakaebe H, Tatsumi K, Ogumi Z (2015) Surface structure and high-voltage charge/discharge characteristics of Al-oxide coated $LiNi_{1/3}Co_{1/3}Mn_{1/3}O_2$ cathodes. J Electrochem Soc 162(2):A3137–A3144
478. Wang D, Wang X, Yu R, Bai Y, Wang G, Liu M, Yang X (2016) The control and performance of $Li_4Mn_5O_{12}$ and Li_2MnO_3 phase ratios in the lithium-rich cathode materials. Electrochim Acta 190:1142–1149
479. Yan J, Liu X, Li B (2014) Recent progress in Li-rich layered oxides as cathode materials for Li-ion batteries. RSC Adv 4:63268–63284
480. Zhong S, Hu P, Luo X, Zhang X, Wu L (2016) Preparation of $LiNi_{0.5}Mn_{1.5}O_4$ cathode materials by electrospinning. Ionics 22:2037–2044

481. Wu L, Lu J, Wei G, Wang P, Ding H, Zheng J, Li X, Zhong S (2014) Synthesis and electrochemical properties of $xLiMn_{0.9}Fe_{0.1}PO_4 \cdot yLi_3V_2(PO_4)_3$/C composite cathode materials for lithium-ion batteries. Electrochim Acta 146:288–294
482. Wang Z, Wang Z, Guo H, Peng W, Li X (2015) Synthesis of Li_2MnO_3-stabilized $LiCoO_2$ cathode material by spray-drying method and its high-voltage performance. J Alloy Compd 626:228–233
483. Liu Y, Zhang Z, Fu Y, Wang Q, Pan J, Su M, Battaglia VS (2016) Investigation the electrochemical performance of $Li_{1.2}Ni_{0.2}Mn_{0.6}O_2$ cathode material with $ZnAl_2O_4$ coating for lithium ion batteries. J Alloy Compd 685:523–532
484. Chen M, Chen D, Liao Y, Zhong X, Li W, Zhang Y (2016) Layered lithium-rich oxide nanoparticles doped with spinel phase: acidic sucrose-assistant synthesis and excellent performance as cathode of lithium ion battery. ACS Appl Mater Inter 8:4575–4584
485. Johnson CS, Korte SD, Vaughey JT, Thackeray MM, Bofinger TE, Shao-Horn Y, Hackney SA (1999) Structural and electrochemical analysis of layered compounds from Li_2MnO_3. J Power Sources 81–82:491–495
486. He L, Xu J, Han T, Han H, Wang Y, Yang J, Wang J, Zhu W, Zhang C, Zhang Y (2017) $SmPO_4$-coated $Li_{1.2}Mn_{0.54}Ni_{0.13}Co_{0.13}O_2$ as a cathode material with enhanced cycling stability for lithium ion batteries. Ceram Int 43:5267–5273
487. Wang R, Li X, Wang Z, Guo H, Wang J (2015) Electrochemical analysis for cycle performance and capacity fading of lithium manganese oxide spinel cathode at elevated temperature using p-toluenesulfonyl isocyanate as electrolyte additive. Electrochim Acta 180:815–823
488. Armstrong AR, Bruce PG (1996) Synthesis of layered $LiMnO_2$ as an electrode for rechargeable lithium batteries. Nature 381:499–500
489. Zheng F, Ou X, Pan Q, Xiong X, Yang C, Liu M (2017) The effect of composite organic acid (citric acid & tartaric acid) on microstructure and electrochemical properties of $Li_{1.2}Mn_{0.54}Ni_{0.13}Co_{0.13}O_2$ Li-rich layered oxides. J Power Sources 346:31–39
490. Xiang Y, Sun Z, Li J, Wu X, Liu Z, Xiong L, He Z, Long B, Yang C, Yin Z (2017) Improved electrochemical performance of $Li_{1.2}Ni_{0.2}Mn_{0.6}O_2$ cathode material for lithium ion batteries synthesized by the polyvinyl alcohol assisted sol-gel method. Ceram Int 43:2320–2324
491. Song L, Tang Z, Chen Y, Xiao Z, Li L, Zheng H, Li B, Liu Z (2016) Structural analysis of layered Li_2MnO_3-$LiMO_2$ (M = $Ni_{1/3}Mn_{1/3}Co_{1/3}$, $Ni_{1/2}Mn_{1/2}$) cathode materials by Rietveld refinement and first-principles calculations. Ceram Int 42:8537–8544
492. Oishi M, Yogi C, Watanabe I, Ohta T, Orikasa Y, Uchimoto Y, Ogumi Z (2015) Direct observation of reversible charge compensation by oxygen ion in Li-rich manganese layered oxide positive electrode material, $Li_{1.16}Ni_{0.15}Co_{0.19}Mn_{0.50}O_2$. J Power Sources 276:89–94
493. He Z, Wang Z, Huang Z, Chen H, Li X, Guo H (2015) A novel architecture designed for lithium rich layered $Li[Li_{0.2}Mn_{0.54}Ni_{0.13}Co_{0.13}]O_2$ oxides for lithium-ion batteries. J Mater Chem A 3:16817–16823
494. Lu LG, Han XB, Li JQ et al (2013) J Power Sources 226:272–288
495. Hassoun J, Lee KS, Sun YK et al (2011) J Am Chem Soc 133:3139–3143
496. Xiong X, Wang Z, Guo H, Zhang Q et al (2013) J Mater Chem A 1:1284–1288
497. Jo M, Noh M, Oh P et al (2014) Adv Energy Mater 4:1301583
498. Hou PY, Wang XQ, Song DW (2014) J Power Sources 265:174–181
499. Wu KC, Wang F, Gao LL et al (2012) Electrochim Acta 75:393–398
500. Wu F, Wang M, Su Y et al (2009) Electrochim Acta 54:6803–6807
501. Xu M, Chen ZY, Zhu HL et al (2015) J Mater Chem A 3:13933–13945
502. Chen Z, Dahn JR (2002) Electrochem Solid-State Lett 5:A213–A216
503. Li L, Chen Z, Song L et al (2015) J Alloy Compd 638:77–82
504. Huang Y, Jin F-M, Chen F-J et al (2014) J Power Sources 256:1–7
505. Zhao EY, Xiao XL, Hu ZB et al (2015) Chem Commun 51:9093–9096
506. Wang D, Li XH, Wang WL et al (2015) Ceram Int 41:6663–6667

507. Weaving JS, Coowar F, Teagle DA, Cullen J, Dass V, Bindin P, Green R, Macklin WJ (2001) Development of high energy density Li-ion batteries based on $LiNi_{1-x-y}Co_xAl_yO_2$. J Power Sources 97:733–735
508. Lee KK, Yoon WS, Kim KB, Lee KY, Hong ST (2001) Characterization of $LiNi_{0.85}Co_{0.10}M_{0.05}O_2$ (M = Al, Fe) as a cathode material for lithium secondary batteries. J Power Sources 97:308–312
509. Cao H, Xia BJ, Xu NX, Zhang CF (2004) Structural and electrochemical characteristics of Co and Al co-doped lithium nickelate cathode materials for lithium-ion batteries. J Alloys Compd 376(1):282–286
510. Yabuuchi N, Ohzuku T (2006) Lithium insertion material of $LiCo_{1/3}Ni_{1/3}Mn_{1/3}O_2$ for advanced lithium-ion batteries. Electrochem Soc 4:107–107
511. Wang Y, Jiang J, Dahn JR (2007) The reactivity of delithiated $Li(Ni_{1/3}Co_{1/3}Mn_{1/3})O_2$, $Li(Ni_{0.8}Co_{0.15}Al_{0.05})O_2$ or $LiCoO_2$ with non-aqueous electrolyte. Electrochem Commun 9 (10):2534–2540
512. Li T, Li X, Wang Z, Guo H (2017) A short process for the efficient utilization of transition-metal chlorides in lithium-ion batteries: a case of $Ni_{0.8}Co_{0.1}Mn_{0.1}O_{1.1}$ and $LiNi_{0.8}Co_{0.1}Mn_{0.1}O_2$. J Power Sources 342:495–503
513. Wang D, Li X, Wang Z, Guo H, Xu Y, Fan Y, Ru J (2016) Role of zirconium dopant on the structure and high voltage electrochemical performances of $LiNi_{0.5}Co_{0.2}Mn_{0.3}O_2$ cathode materials for lithium ion batteries. Electrochim Acta 188:48–56
514. Wang J, Liu Z, Yan G, Li H, Peng W, Li X, Shih K (2016) Improving the electrochemical performance of lithium vanadium fluorophosphate cathode material: focus on interfacial stability. J Power Sources 329:553–557
515. Marezio M, Remeika JP (1966) High-pressure synthesis and crystal structure of α-$LiAlO_2$. J Chem Phys 44(8):3143–3144
516. Hu L, Tang Z, Zhang Z (2008) Hydrothermal synthesis of single crystal mesoporous $LiAlO_2$ nanobelts. Mater Lett 62(12):2039–2042
517. Robertson AD, West AR, Ritchie AG (1997) Review of crystalline lithium-ion conductors suitable for high temperature battery applications. Solid State Ionics 104(1):1–11
518. Barker J, Saidi MY, Gover RKB, Burns P, Bryan A (2007) The effect of Al substitution on the lithium insertion properties of lithium vanadium fluorophosphate, $LiVPO_4F$. J Power Sources 174(2):927–931. https://doi.org/10.1016/j.jpowsour.2007.06.079
519. Gover RKB, Bryan A, Burns P, Barker J (2006) The electrochemical insertion properties of sodium vanadium fluorophosphate, $Na_3V_2(PO_4)_2F_3$. Solid State Ionics 177(17–18):1495–1500. https://doi.org/10.1016/j.ssi.2006.07.028
520. Barker J, Saidi MY, Swoyer JL (2003) A sodium-ion cell based on the fluorophosphate compound NaVPO4 F. Electrochem Solid-State Lett 6(1):A1–A4. https://doi.org/10.1149/1.1523691
521. Wang J, Li X, Wang Z, Guo H, Li Y, He Z, Huang B (2013) Enhancement of electrochemical performance of Al-doped $LiVPO_4F$ using AlF_3 as aluminum source. J Alloys Compd 581:836–842. https://doi.org/10.1016/j.jallcom.2013.07.147
522. Bai G, Yang Y, Shao H (2013) Synthesis and electrochemical properties of polyhedron-shaped $Li_3V_{2-x}Sn_x(PO_4)_3$ as cathode material for lithium-ion batteries. J Electroanal Chem 688:98–102. https://doi.org/10.1016/j.jelechem.2012.08.018
523. Wang HY, Tang AD, Huang KL (2011) Thermal behavior investigation of $LiNi_{1/3}Co_{1/3}Mn_{1/3}O_2$-based Li-ion battery under overcharged test. Chin J Chem 29(1):27–32. https://doi.org/10.1002/cjoc.201190056
524. Lin CH, Zhang YZ, Chen L, Lei Y, Junker O, Guo Y, Yuan HY, Xiao D (2015) Hydrogen peroxide assisted synthesis of $LiNi_{1/3}Co_{1/3}Mn_{1/3}O_2$ as high-performance cathode for lithium-ion batteries. J Power Sources 280:263–271. https://doi.org/10.1016/j.jpowsour.2015.01.084
525. Noh HJ, Youn S, Yoon CS, Sun YK (2013) Comparison of the structural and electrochemical properties of layered $Li[Ni_xCo_yMn_z]O_2$ (x = 1/3, 0.5, 0.6, 0.7, 0.8 and 0.85) cathode materials for lithium-ion batteries. J Power Sources 233:121–130. https://doi.org/10.1016/j.jpowsour.2013.01.063

526. He XM, Li JJ, Cai Y, Jiang CY, Wan CR (2006) Preparation of spherical spinel $LiMn_2O_4$ cathode material for Li-ion batteries. Mater Chem Phys 95(1):105–108. https://doi.org/10.1016/j.matchemphys.2005.06.006
527. Zhang XY, Mauger A, Lu Q, Groult H, Perrigaud L, Gendron F, Julien CM (2010) Synthesis and characterization of $LiNi_{1/3}Mn_{1/3}Co_{1/3}O_2$ by wet-chemical method. Electrochim Acta 55 (22):6440–6449. https://doi.org/10.1016/j.electacta.2010.06.040
528. Zhao T, Chen S, Li L, Zhang X, Chen R, Belharouak I, Wu F, Amine K (2013) Synthesis, characterization, and electrochemistry of cathode materials Li $Li[Li_{0.2}Co_{0.13}Ni_{0.13}Mn_{0.54}]O_2$ using organic chelating agents for lithium-ion batteries. J Power Sources 228:206–213. https://doi.org/10.1016/j.jpowsour.2012.11.099
529. Kong JZ, Yang XY, Zhai HF, Ren C, Li H, Li JX, Tang Z, Zhou F (2013) Synthesis and electrochemical properties of Li-excess $Li_{1+x}[Ni_{0.5}Co_{0.2}Mn_{0.3}]O_2$ cathode materials using ammonia-free chelating agent. J Alloys Compd 580:491–496. https://doi.org/10.1016/j.jallcom.2013.06.149
530. Wang CL, Zhou F, Ren C, Wang YF, Kong JZ, Jiang YX, Yan GZ, Li JX (2015) Influences of carbonate co-precipitation temperature and stirring time on the microstructure and electrochemical properties of $Li_{1.2}[Mn_{0.52}Ni_{0.2}Co_{0.08}]O_2$ positive electrode for lithium ion battery. Solid State Ionics 281:96–104. https://doi.org/10.1016/j.ssi.2015.09.016
531. Kong JZ, Zhai HF, Ren C, Tai GA, Yang XY, Zhou F, Li H, Li JX, Tang Z (2014) High-capacity $Li(Ni_{0.5}Co_{0.2}Mn_{0.3})O_2$ lithium-ion battery cathode synthesized using a green chelating agent. J Solid State Electrochem 18(1):181–188. https://doi.org/10.1007/s10008-013-2240-y
532. Gabrisch H, Yazami R, Fultz B (2004) Hexagonal to cubic spinel transformation in lithiated cobalt oxide TEM investigation. J Electrochem Soc 151:A891–A897
533. Kim JH, Myung ST, Yoon CS, Kang SG, Sun YK (2004) Comparative study of $LiNi_{0.5}Mn_{1.5}O_4$-δ and $LiNi_{0.5}Mn_{1.5}O_4$ cathodes having two crystallographic structures: Fd3m and P4332. Chem Mater 16:906–914
534. Jafta CJ, Mathe MK, Manyala N, Roos WD, Ozoemena KI (2013) Microwave-assisted synthesis of high-voltage nanostructured $LiMn_{1.5}Ni_{0.5}O_4$ spinel: tuning the Mn^{3+} content and electrochemical performance. ACS Appl Mater Interfaces 5:7592–7598
535. Manthiram A, Chemelewski K, Lee ES (2014) A perspective on the high-voltage $LiMn_{1.5}Ni_{0.5}O_4$ spinel cathode for lithium-ion batteries. Energy Environ Sci 7:1339–1350
536. Yoon S, Bridges CA, Unocic RR, Paranthaman MP (2013) Mesoporous TiO_2 spheres with a nitridated conducting layer for lithium-ion batteries. J Mater Sci 48:5125–5131
537. Zhang HZ, Qiao QQ, Li GR, Ye SH, Gao XP (2012) Surface nitridation of Li-rich layered Li $(Li_{0.17}Ni_{0.25}Mn_{0.58})O_2$ oxide as cathode material for lithium-ion battery. J Mater Chem 22:13104–13109
538. Koleva V, Zhecheva E, Stoyanova R (2011) Dalton Trans 40:7385
539. Zhang W, Shan Z, Zhu K, Liu S, Liu X, Tian J (2015) Electrochim Acta 153:385
540. Aono S, Urita K, Yamada H, Moriguchi I (2012) Solid State Ion 225:556
541. Dong Y, Wang L, Zhang S et al (2012) J Power Sources 215:116
542. Gu Y, Wang H, Zhu Y, Wang L, Qian Y, Chu Y (2015) Solid State Ion 274:106
543. Cui Y-T, Xu N, Kou L-Q, Wu M-T, Chen L (2014) J Power Sources 249:42
544. Nam T, Doan L, Bakenov Z, Taniguchi I (2010) Adv Powder Technol 21:187
545. Jo M, Yoo H, Jung YS, Cho J (2012) J Power Sources 216:162
546. Kou L, Chen F, Tao F, Dong Y, Chen L (2015) Electrochim Acta 173:721
547. Chen Z, Xie T, Li L, Xu M (2014) Ionics 20:629
548. Lain MJ (2001) Recycling of lithium ion cells and batteries. J Power Sources 97–98:736–738
549. Xu J, Thomas HR, Francis RW, Lum KR, Wang J, Liang B (2008) A review of processes and technologies for the recycling of lithium-ion secondary batteries. J Power Sources 177:512–527

550. Paulino JF, Busnardo NG, Afonso JC (2008) Recovery of valuable elements from spent Li-batteries. J Hazard Mater 150:843–849
551. Zhang P, Yokoyama T, Itabashi O, Suzuki TM, Inoue K (1998) Hydrometallurgical process for recovery of metal values from spent lithium-ion secondary batteries. Hydrometallurgy 47:259–271
552. Contestabile M, Panero S, Scrosati B (2001) A laboratory-scale lithium-ion battery recycling process. J Power Sources 92:65–69
553. Shin SM, Kim NH, Sohn JS, Young DH, Kim YH (2005) Development of a metal recovery process from Li-ion battery wastes. Hydrometallurgy 79:172–181
554. Dorella G, Mansur MB (2007) A study of the separation of cobalt from spent Li-ion battery residues. J Power Sources 170:210–215
555. Zou H, Gratz E, Apelian D, Wang Y (2013) A novel method to recycle mixed cathode materials for lithium ion batteries. Green Chem 15:1183–1191
556. Gratz E, Sa Q, Apelian D, Wang Y (2014) A closed loop process for recycling spent lithium ion batteries. J Power Sources 262:255–262
557. Sathiya M, Rousse G, Ramesha K, Laisa CP, Vezin H, Sougrati MT, Doublet ML, Foix D, Gonbeau D, Walker W, Prakash AS, Ben Hassine M, Dupont L, Tarascon JM (2013) Reversible anionic redox chemistry in high-capacity layered-oxide electrodes. Nat Mater 12:827–835
558. Wei YJ, Nam KW, Kim KB, Chen G (2006) Spectroscopic studies of the structural properties of Ni substituted spinel $LiMn_2O_4$. Solid State Ionics 177(1–2):29–35. https://doi.org/10.1016/j.ssi.2005.10.015
559. Lee YS, Kumada N, Yoshio M (2001) Synthesis and characterization of lithium aluminum-doped spinel ($LiAl_xMn_{2-x}O_4$) for lithium secondary battery. J Power Sources 96(2):376–384. https://doi.org/10.1016/S0378-7753(00)00652-2
560. Liao L, Wang X, Luo X, Wang X, Gamboa S, Sebastian PJ (2006) Synthesis and electrochemical properties of layered $Li[Ni_{0.333}Co_{0.333}Mn_{0.293}Al_{0.04}]O_{2-z}F_z$ cathode materials prepared by the sol–gel method. J Power Sources 160(1):657–661. https://doi.org/10.1016/j.jpowsour.2005.12.095
561. Wang J, Yao SZ, Lin WQ, Wu BH, He XY, Li JY, Zhao JB (2015) Improving the electrochemical properties of high-voltage lithium nickel manganese oxide by surface coating with vanadium oxides for lithium ion batteries. J Power Sources 280(15):114–124. https://doi.org/10.1016/j.jpowsour.2015.01.087
562. Zhao D, Wang Y, Zhang Y (2011) High-performance Li-ion batteries and supercapacitors base on 1-D nanomaterials in prospect. Nano-Micro Lett. 3(1):62–71. https://doi.org/10.3786/nml.v3i1.p62-71

Chapter 3
Ionic Conductivity, Polymer Electrolyte, Membranes, Electrochemical Stability, Separators

3.1 Introduction

The most commonly used separators in Li-ion batteries are the polyolefin membranes due to their satisfactory electrochemical stability, useful thickness and advantageous mechanical strength [1]. The most commonly used separators in LIBs' low porosity, inferior thermal dimensional turbulence and inadequate electrolyte wettability might give rise to high cell resistance or an internal short circuit; this circuit seriously hinders the electrochemical and safety performance of Li-ion batteries (Lee and others [20]; Yanilmaz and others [21]), [1]. Some attempts have been devoted to the development of new separators with excellent thermal stability and satisfactory electrolyte wettability [1]. Cellulose-based materials have been examined as separators in Li-ion batteries due to their outstanding properties, such as excellent thermal stability (Chun and others [22]; Jabbour and others [23]; Kim and others [24]; Xu and others [25]; Zhang and others [26, 27]; Jiang and others [28]; Weng and others [29]; Liao and others [30]) and the desired electrochemical stability in recent decades [1]. Via an electrospinning method, co-workers (Zhang and others [26]) and Cui have prepared a superior and renewable thermal-resistant cellulose/poly(vinylidene fluoride-co-hexafluoropropylene) composite non-woven separator for high-performance Li-ion batteries [1]. Through a force-spinning method, Alcoutlabi and others (Weng and others [29]) have mass-produced fibrous cellulose membranes as a fruitful alternative to commercial polyolefin separators [1]. The BC nanofibrous membrane has been devised as a separator for Li-ion batteries through a facile hot-pressing fabrication approach by co-workers (Jiang and others [28]) and Zhang [1]. The tensile strength of the devised BC separator is meager as compared to the commercial Celgard membrane [1]. Hydrophilic inorganic Al_2O_3 powders are normally utilized as supports to alter the surface of the separators due to their chemical inertness, excellent thermal stability (Deng and

This book was machine-generated

Beta Writer, *Lithium-Ion Batteries*,
https://doi.org/10.1007/978-3-030-16800-1_3

others [31]; Jeon and others [32]) and satisfactory wettability [1]. A BC/Al_2O_3 nanofibrous composite membrane as an LIB separator had been appropriately prepared by coating Al_2O_3 on BC nanofibres via a straightforward in situ thermal decomposition technique [1]. The porosity, thermal shrinkage, tensile strength, ionic electrical conductivity and electrolyte wettability of the devised BC/Al_2O_3 membrane were typified [1].

The separator does not entail directly in any cell reactions, though properties and its structure play important roles in determining the battery performance, which comprises cycle life, safety, power density [33], and energy density, in Li-ion batteries [2]. Some modification methodologies, including polymer coatings [34], electrospinning technique [35], and polydopamine treatment [36], have been examined to circumvent the shortcomings of polyolefin-based separators [2]. A ZrO_2-added composite separator had been devised by Scrosati and others [2, 37]. A new silica tube-coated PE composite separator had been devised by Zhang and others [2, 38]. It could be concluded that multiple kinds of ceramic-coated composite separators have been demonstrated, resulting in enhanced separator, which wets thermal shrinkage and ability, at high temperature [2]. That incorporation of pottery particles into the separators is an appealing technique to derive high-performance separators is demonstrated by some reports [2]. The nanosized pottery particles including TiO_2, and Al_2O_3, SiO_2, can substantially enhance thermal stability the mechanical strength, including their thermal resistance [33] and ionic electrical conductivity of separators because of their high hydrophilicity and high surface area [2]. It could be surmised that the new composite separator retains superior performances compared with traditional separators if the traditional pottery oxides were substituted by zeolites or molecular sieves [2]. In terms of morphology, structure, thermal stability, the electrochemical performances, and electrolyte wettability, the attributes of the separator are assessed [2].

Porous polyolefin separators including polyethylene (PE), PP/PE/PP, and polypropylene (PP), are the most popular separators for Li-ion batteries due to advantages including high mechanical strength, low cost [39–41], and satisfactory electrochemical stability [3]. In high-performance Li-ion batteries [42], low porosity and their meager thermal stability restrict their application [3]. Developing an optimum separator to ameliorate the shortcomings of traditional polyolefin separators is required to satisfy the increased performance and safety demands of Li-ion batteries to this effect [3]. Some recent research initiatives have been carried out in effort to circumvent the drawbacks of the polyolefin separator to satisfy the requirements of high-performance Li-ion batteries [3, 43]. Zhu and others devised a new, ceramic-grafted PE separator, which is fabricated with electron beam irradiation; the ceramic-grafted PE separator showed highly enhanced dimensional thermal stability without any deviation from its original primitive thickness and pore structure [3, 44]. That a PE-coated PI nonwoven composite membrane not just indicates excellent thermal shutdown function though displays considerably greater thermal stability, lower internal resistance than the PP/PE/PP separator [45], and better wettability with the polar electrolyte, had been shown by Shi and others, [3]. The incorporation of pottery particles and nonwoven fabrics has been shown that

nanosized inorganic fillers can substantially enhance the mechanical strength, ionic electrical conductivity of composite separators [46], and thermal stability [3]. Various basic properties of the composite separator, which comprises its surface morphology, porosity, thermal stability, ionic electrical conductivity, and electrolyte wettability, were assessed and compared to those of the commercial Celgard 2500 separator [3].

All of the above exploit of the special properties of Li-ion batteries: no memory effect, high energy density, high operation voltages, and long cycle life (Fang and others [47]; Liang and others [48]; Kumar and others [49]), which self-discharges low [4]. A critical element of a LIB is the separator membrane [4]. Architecture and the separator membrane's property play a crucial role in affecting the cell performance, which comprises energy density, power density, service life, and safety, even though the separator does not take part directly in electrochemical reaction of a LIB cell [4]. Lots of contextual factors should to be regarded whilst choosing useful separators for Li-ion batteries [4].

The pore structure and thickness of the separator should be carefully controlled, as a satisfactory balance between mechanical strength and ionic electrical conductivity should be kept (Arora and Zhang [40]; Lee and others [33]; Zhang [50]) in order to satisfy these two functions [5]. The pore structure and porosity of the material are clearly quite crucial to the performance of the separator in a battery in addition to the separator material [5]. To enhance systematic researches of the impact of these properties on the performance of Li-ion batteries there is hence a need for clear-cut techniques by which the pore structure and porosity of a specific material could be varied conveniently [5]. We are, however, not cognizant of any researches on cellulose premised LIB separators revolved around the thickness reliance of the pore structure, porosity and i.e. the pore size distribution [5]. A clear-cut paper-making filtration process by which CC separators with pore structures and various thicknesses could be manufactured simply by differing the quantity of cellulose utilized is explained by us [5]. CC separators with pore structures and various thicknesses are permitted by this strategy to be manufactured without various drying methods or utilizing external pressure [5]. It is demonstrated that thinner separators display a less compact structure with greater porosities and bigger pores and that this leads to Li-ion batteries with lower cell resistances [5].

Lithium-ion battery with light weight, long cycle life, and huge capacity, has demonstrated to be an optimal choice for electric vehicles [51] under the nervous circumstance in the energy resources [6]. The safety problem of high-power lithium-ion battery has aroused more and more attention [52] with the rapid development of lithium ion battery industry [6]. High temperature running of battery systems normally triggers the shrinkage of conversional battery separator, leading to quite fast internal shorting of the battery [6]. Due to the high-power charge and discharge, violent oscillation, long time, and collision, which might give rise to the contraction of the conventional separators [53, 54], which works, overcharge, the normal working temperature can be surpassed by the local temperature inside battery, as reasonably well [6]. The amelioration of thermodynamic stability for the separators of lithium batteries is problematic [55–58] and crucial

[6]. It is urgently required to build heatproof and anti-shrink separators for a safer lithium-ion battery [6]. Through porous polyethylene (PE), polypropylene (PP), and/or PP/PE/PP membrane because of their satisfactory electrochemical performance [46], the separators for commercial lithium-ion batteries are normally comprised [6]. Some researches focus on the amelioration of the safety and stability of lithium-ion battery [6]. It is pointed out that electrospun is a convenient technique to prepare lithium-ion battery separator with some excellent performances, including small holes, high porosity, distribution homogeneity [57, 59], and huge specific surface area [6].

Safety problem is still a largest obstacle for the large-scale applications [60] in spite of the widespread application of lithium-ion batteries [7]. The safety concern of lithium-ion batteries is a serious obstacle in the technology development [7]. Since the state-of-art electrolytes of lithium-ion batteries use highly flammable carbonate-based organic electrolytes; these electrolytes may be ignited and then presumably cause serious hazards of firing and upsurge under abused conditions (heat, overcharge, short circuit, etc.) [7]. A novel sort of multi-component (MC) additive is summarized by us for lithium-ion battery electrolyte (1.0 mol/L $LiPF_6$/ethylene carbonate (EC) + diethyl carbonate (DEC) (1:1 wt.%)) [7]. The impacts of MC additive in enhancing the cell performance of the lithium-ion cell and the thermal stability of the electrolyte were investigated [7]. How the MC additive might behave on the surface of electrodes needs additional research, and its possibility as the flame retardant for commercial lithium-ion battery needs to assess [7].

Electrolyte cum separator Beside electrodes, the separator cum electrolyte is an indispensable element of the battery, as it plays a significant role in the transportation of ions during charging and discharging mechanisms, so it should be in stable form during battery operation [8]. Lithium batteries is superior to all existing systems because of its safety, high energy density, light weight, cost effective, and shape flexibility, among these [8]. Mostly fast ionic conductors are based upon inorganic materials with excellent transport properties, though inferior electrolyte stability limits their use as electrolyte cum electrode separator [8]. Through Michael Faraday, the phenomena of ionic conduction had been identified in the 1800s on solid electrolytes PbF_2; later in 1964, first-time polymer electrolytes came in existence which had been based upon $CdCl_2$ and multivalent salts $HgCl_2$ [8]. The presence of both crystalline stage and amorphous stage makes attempting to investigation the properties of polymer electrolytes correctly [61, 62] as multivalent cations are easier to deal with and cheap than widely used alkali metal salts [8]. The electrolyte along with a separator serves as a medium to keep electrodes individually when liquid electrolytes are utilized and for transportation of ions in any battery system [8]. The polymer electrolyte is utilized as a thin-film membrane which can function for both ion conduction and separation of electrodes for the solid-state Li-ion batteries [8]. Polymer electrolytes formed by dissolving Li salt in a high molecular weight polymer host including PEO are dual ionic conductors [8]. In the electrolyte, polymers with low T g are preferred for excellent flexibility and fast ion transport [8].

In a matrix of organic solvent display, lithium batteries based upon liquid electrolytes consisting of a lithium salt dissolved a low flash point and are

susceptible to leakage (Tasaki and others [63]), [9]. Suitable electrochemical stability, satisfactory mechanical strength, tremendous lithium ion transference number, high ionic electrical conductivity, advantageous compatibility with electrode materials (He and others [64]; Li and others [65]; Isken and others [66]) and thermal stability must be possessed by polymer electrolytes as separator in lithium batteries [9]. The most often investigated polymer electrolytes for Lithium-ion batteries (Sil and others [67]) is the complexes of Li salts with high molecular weight PEO [9]. To combine the benefits of SPEs and liquid electrolytes gel polymer electrolytes have been introduced (Deka and Kumar [68]) that display high ionic electrical conductivity at ambient temperature by retaining huge quantity of liquid electrolyte in the polymer host (Sil and others [67]), [9]. While the electrolyte introduces high mechanical stability for application as separator in lithium batteries (Ramesh and others [69]), high ionic conductivities could be accomplished [9]. $LiClO_4$ retains huge size anions, low dissociation energy and is exceedingly soluble in most organic solvents, offering so high ionic electrical conductivity (Park [70]) and a high concentration of free ions [9]. EC and PC solvents are normally utilized as high dielectric constant of 66 and 89 [71], respectively and high-permittivity element in fabrication of lithium batteries because of their low-viscosity [9]. Applying low concentrations of PMMA caused in formation of GPEs, which constitutes high ionic conductivities comparable to liquid electrolytes [9]. At high concentration of PMMA the ionic electrical conductivity of GPEs had been declined which had been attributed to greater relationships between the electrolyte and the polymer matrix [9]. That the kind of utilized polymer, Li salt and plasticizer play crucial role in determining electrochemical performances of the prepared GPEs [70] and the ionic electrical conductivity is revealed by these studies [9].

An polymer system with a polymer as separator/electrolyte, which conducts ionically, is of extreme interest because of their various applications, such as super capacitors, fuel cells, solar cells, Li ion batteries, and electro chromic windows [10]. The advantageous electrolyte for any application in energy storage/conversion tools should have (a) high ionic electrical conductivity, (b) an electrochemical stability window (>4 V), (c) a low melting point, (d) a high boiling point, (e) high chemical stability, (f) low cost and satisfactory compatibility with electrodes [40, 72–74], and (g) non-toxicity [10]. The majority of of the tools are based upon liquid/gel polymer electrolytes because of compatibility with electrodes and their high ionic electrical conductivity (10^{-3} to 10^{-2} S cm^{-1}) [10]. That elicits the scholars toward replacement of the traditional liquid polymer electrolyte with a solvent-free polymer electrolyte, which haves high ionic electrical conductivity, leak proofing, better flexibility, a wide electrochemical window, satisfactory mechanical strength, ease of preparation [75–77], and light weight [10]. Polyethylene oxide (PEO) is undoubtedly the optimal host polymer utilized as SPEs with strong, unstrained C–O, C, and C–C, –H ties and it has a SPEs dielectric constant, easy availability, high ionic electrical conductivity in the amorphous stage, low glass transition temperature, satisfactory dimensional and chemical stability, and high flexibility, out of the aforesaid host polymers [10]. Incorporation of the nanofiller enables in impeding the recrystallization tendency of the polymer chain and decreases the glass

transition temperature of the composite polymer electrolyte; this electrolyte suggests enhancement in ionic electrical conductivity [10, 78] The nanofiller supports ion dissociation and strengthens the ion migration by offering further conducting paths for the cation within the host polymer matrix [10, 79, 80].

Given the practical applications, the SPEs must owns the properties of high ionic conductivities (exceeded 10^{-4} S cm^{-1} at operator temperature), huge Li^+ transference number (close to unity), wide electrochemical stability window (4–5 V vs. Li/Li^+), excellent mechanical strength, low interfacial resistance between the electrolyte and the electrode [81–85], and satisfactory thermal stability [11]. A block copolymer, which is comprised which of soft and hard segment, is polyurethane [11]. A polyurethane-based gel polymer electrolyte for Li-ion batteries had been synthesized by Liu and others [11, 86]. A single-ion electrolyte, which is based upon polyurethane and the $LiFePO_4$/Li cell, which employs, this electrolyte that revealed outstanding rate performance, had been indicated by Porcarelli and others [11, 87]. At least a handful works have focus on the SPEs based upon polyurethane, Liu and others [88] indicated series of cationic PU for SPEs; this PU revealed high ionic electrical conductivity at room temperature [11]. The performance of all-solid-state Li-ion batteries employing these PU-based SPEs have not been evaluated even though these polyurethane-based SPEs have been confirmed to owns excellent mechanical properties and high ionic conductivities [11]. Through changing the composition of the hard and soft segment [89], the properties of polyurethane could be readily tailored [11]. The polyether-based soft segment in polyurethane with $(-CH_2–CH_2–O)$ n unit can offer the transport path way for the Li^+ ions [90] and dissolve the cations [11]. Isophorone diisocyanate (IPDI) [91] and 4, 4′-methylenediphenyl diisocyanate (MDI) [88, 92, 93] had been utilized by the earlier literatures for the hard segment, and the rigidity alicyclic and aromatic structure with strong hydrogen bonding between the hard and soft segment confined the segmental movements of give rise to low ionic electrical conductivity and the polyurethane [11]. Given that the high ionic electrical conductivity depends upon the rapid segmental movements of the polymer matrix [94], both hard segment and soft segment are flexible will useful [11].

Such difficulties have been resolved by replacing liquid electrolyte with solid polymer electrolyte in the batteries [12, 73]. Due to their distinctive properties, including leakage proof, flexibility and satisfactory toughness, and easy fabrication into shapes [95, 96] and advantageous sizes, polymer electrolyte films attract an increased interest [12]. Some shortcomings of the polymer electrolyte films, including electrochemical stability and comparatively low ionic electrical conductivity, still deter their practical application in batteries [12, 97]. Confronted with these limitations, gel polymer electrolyte films have attracted considerable attention as they owns the enhanced ionic electrical conductivity and improve the interfacial property substantially [12, 98, 99]. In organic solvents, this sort of salt could be dissolved totally, so that the Li-ions could be transferred in polymer electrolyte films [12]. A 85PVdF–HFP: 15$LiBF_4$ complexed polymer electrolyte had been devised, displaying ionic electrical conductivity [100] and comparatively high amorphicity [12]. The 85PVdF–HFP: 15$LiBF_4$ polymer electrolyte had been

selected to be the host system for preparing gel polymer electrolyte films in the present study [12]. Ion pairing could be lowered by the plasticizer, improve the flexibility of polymer chains, increase ionic electrical conductivity and lithium-ion battery property, and enhance the stability of electrode/electrolyte interface [12]. Firstly, the gel polymer electrolyte films were prepared based upon the 85PVdF–HFP: 15$LiBF_4$ system along with plasticizers PC and EC in a weight ratio of 1:1 [12]. The 2032 coin cells were assembled employing their charge-discharge cycling performance had been assessed employing a computerized battery cycling unit and the self-made gel polymer electrolyte films [12].

Polymer electrolytes are the crucial class of materials for the applications in clean energy tools including batteries, sensors [101–103] because of its flexibility and safety, and fuel cells, and it is non-corrosive [13]. Ion transport mechanism, mechanical stability in polymer electrolyte and improving electrical conductivity, is critically crucial in the past century [13]. Through the incorporation of inert fillers including TiO_2, SiO_3, Al_2O_3, etc. [104, 105], nanocomposite polymer electrolyte is prepared in order to attain the greater ionic electrical conductivity at ambient temperature [13]. To attain the hybrid polymer electrolyte for the fabrication of Li-ion polymer battery, electrochemical and electrical performance has been examined in the present work [13]. The principal aim of the current study is to prepare lithium-ion: PVdF, which is incorporated with TiO_2 nanofiller by solution casting method, which conducts hybrid polymer electrolyte based upon PVA [13]. Structural, vibrational, electrical conductivity, mechanical, thermal, electrochemical behaviour of the prepared samples, and morphological, have been examined employing XRD, FTIR, AC impedance spectroscopic method, stress-strain measurement, DSC, TGA, SEM, cyclic voltammetry (CV), respectively, and linear sweep voltammetry (LSV) [13].

There are many fatal shortcomings such as leakage, blast [106] in the liquid Li-ion batteries, and flame, even though lower cost of organic liquid electrolyte and the high ion electrical conductivity can preferably derive economical battery and the high energy density [14]. Upon Fenton and others observed the polymer electrolyte with ionic electrical conductivity; this electrical conductivity is composed of poly (ethylene oxide) (PEO) and alkali metal salt in 1973 [107], polymer electrolyte has been extensively researched due to ease of processing, satisfactory plasticity, and efficient prevention of electrolyte leakage [14, 108]. Solid macromolecule, which limits the migration of lithium ions to a certain extent and additional gives rise to a decline in the ionic electrical conductivity of the electrolyte is the matrix of polymer electrolyte [14]. That issue has been demonstrated to be solved by gel polymer electrolyte (GPE) because it comprises of polymer matrix, plasticizer, and lithium [14]. There are handful applications for commercial Li-ion batteries with cellulose as the GPE matrix due to transfer number [109–111] and low ionic electrical conductivity even though cellulose is the most plentiful biopolymer resources on the earth [14]. The second plentiful biopolymer on the earth [112], a novel kind of biopolymer of lignin and extensively exists in the cell wall of plants, as the GPE matrix, which not just can dramatically lessen the cost, though can derive high ionic

electrical conductivity, lithium-ion transference number, wide electrochemical stability window, and stable cycling performance had been founded by us [14].

The $LiFePO_4$ (LFP) is one of the most useful cathode materials for LIB because of its environmental compatibility, low cost, high theoretical capacity (170 mAh g^{-1}), non-toxicity [113, 114], and excellent thermal stability [15]. That cathode material usually suffers from many shortcomings including deterioration of capacity, inferior stability, rate performance, and Li^+ ion diffusivity ($\sim 10^{-14}$ cm^2 s^{-1}), at high discharge/charge current density [15, 115, 116]. That inferior performance, which is correlated with defects in side reaction between cathode material and electrolyte decreases or olivine structure of LFP, Li^+ electronic electrical conductivity and ion diffusion rate [15]. That graphitic and carbon carbon coating is an effective strategy for enhancing electronic electrical conductivity and electrochemical performance of the cathode material in a LIB [117] is revealed by the most recent report [15]. Since a blocking layer is formed between electrolyte and active material particles, carbon coating method has concentrated on enhancing the electrochemical performance of LFP [15]. The carbon-coated active material particle is not an effective way to enhance discharge and charge performance at high current rate because most of the carbon is amorphous [118] and the contact area between LFP particles is quite less [15]. Salt LiTFSI has been selected because it could be readily disassociated into anions and cations [119] and it indicates low lattice energy, and IL EMIMFSI is utilized because it indicates low viscosity, satisfactory electrochemical/thermal stability, high ionic electrical conductivity, and satisfactory plasticizer effect including a supplier of free charge carriers [15, 120]. We have examined thermal stability, electrochemical performance of the prepared ILGPE, and ionic electrical conductivity, and assembled coin cell by employing 80 wt% IL containing GPE with lithium metal foil as anode with a standard GO@LFP and LFP (i.e., without coating) cathode [15].

Ionic liquid electrolyte has devised into entire solid polymer electrolyte [121, 122] and gel polymer electrolyte [16]. Gel polymer electrolyte with better security and greater electrical conductivity has aroused more attention [16, 123–125]. Ionic liquids recognize environment protection, the cleaner generate, and cycle economics because of its advantages such as non-flammable and non-toxic property, low vapour pressure, high electrical conductivity, high ion transference number, wide electrochemistry window, and satisfactory stability performance [16, 126–128]. Ionic liquids are one of main elements in the ionic liquid polymer electrolyte (IL-PE) membrane since it is one of principal carry out mediums [16]. The gel polymer electrolyte is prepared by Jae-Kwang Kim with N-methyl-N-butyl pyrrolidinium bis (trifluoromethanesulfonyl) imide ($Py_{14}TFSI$), which the electrostatic spinning technique this technique indicates the electrical conductivity of 1.1×10^{-4} S cm^{-1} at 0 °C [129] based upon poly(vinylidene fluoride-co-hexafluoropropylene) (P (VdF–HFP)); this technique indicates the electrical conductivity of 1.1×10^{-4} S cm^{-1} at 0 °C [16, 129]. Polymer matrix is one of the essential materials as supporting conceptual framework of gel polymer electrolytes [16, 130]. There are primarily four systems as polymer matrix for polymer lithium-ion battery, such as polyvinylidene fluoride (PVDF) system [131], polyether (PEO) system [132–134],

polyacrylonictrile (PAN) system [135], and polymethyl methacrylate (PMMA) [16, 136]. BF_4/PVDF–HFP/PMMA gel polymer electrolyte by the stage inversion technique which has the electrochemistry stability window of 4.5 V and the electrical conductivity of 1.4×10^{-3} S cm^{-1} is prepared by Wei Zhai [16]. Light-sensitive urethane acrylate (PUA) and the polymethyl methacrylate (PMMA) is contained by the IL-PE membrane as the electrolyte matrix, the lithium bis (trifluoromethanesulfonyl) imide (LiTFSI) as the lithium salt and the N-methyl-N-propyl pyrrolidinium bis (trifluoromethanesulfonyl) imide (Py_{13}TFSI) ionic liquid as enhancing actor of the electrical conductivity [16].

Lithium ion batteries have been enhanced employing polymer nanofibrous electrolyte membrane with its highly porous structure, ionic electrical conductivity and high electrolyte uptake to transport as considerably as lithium ions via it [17]. Scholars in this field are more involved to prepare polymer electrolyte membranes by blending or forming composites employing metal oxides or various polymers to increase ionic electrical conductivity, electrochemical stability than that of pure polymer electrolytes [137–141], and electrolyte uptake [17]. Some various synthesis techniques are utilized to prepare polymer electrolyte membrane by stage inversion [142], solution casting [139, 143] and electrospinning [17, 144]. A straightforward technique for preparation of nanofibrous membranes with high porosity because of tunable fiber diameter, which is controlled by differing utilized electric field, distance between grounded collector and syringe needle, flow rate of viscous polymer solution, and polymer solution concentration, is Electrospinning [17]. Porosity is the size-dependent property; hence, electrospun nanofibres of blended polymers synthesized by electrospinning owns high porosity which is responsible for high ionic electrical conductivity at room temperature [145, 146] and increase in electrolyte uptake [17]. Attempts have been made to maximize the composition of PMMA and PVdF to fabricate their composites nanofibrous membrane by electrospinning so as to increase the ionic electrical conductivity [17]. The fabrication of polymer nanofibrous electrolyte membranes of PVdF–PMMA composites in various percentage (PVdF: PMMA = 100:0, 80:20 and 50:50) by electrospinning is indicated to examine the impact of PMMA on Li-ion battery performance [17].

Ionic liquids (ILs) are comprised of completely charged species and owns high ionic electrical conductivity, wide electrochemical window, excellent thermal stability, non-volatility, nonflammability [147–149] and ecologically benignity [18]. Solubility of Li salt is high in BF_4- and $TFSI^-$ ions, and in particular, $TFSI^-$ anion-based ionic liquids indicate greater electrochemical and thermal stability than the other counter anions of the IL [18, 150]. It is reluctant to generate effective solid and stable electrolyte interface (SEI) [151, 152] even if the ILs owns wide electrochemical window and high ionic electrical conductivity [18]. Menne and others has researched the combination of LiTFSI salt with an organic solvent, which is dissolved in N-butyl, N-methylpyrrolidinium bis (trifluoromethylsulfonyl) imide (Pyr_{14}-TFSI) (50:50 wt%) as an electrolyte for Li battery, and the results show better thermal stability including greater performance than the pristine ILs [18, 153]. Of the various kinds of the ILs examined till date, quaternary

ammonium-based acyclic and cyclic cations including pyrrolidinium, tetraalkylammonium and piperidinium high cathodic stability towards lithium metal [154] and display wide electrochemical window [18]. LiTFSI mixed with alkyl carbonate, which includes $Pyr_{24}TFSI$ indicates nonflammability, enhanced electrical conductivity and electrochemical stability window, which is compared when to traditional alkylcarbonate-based electrolyte, as pointed out by Lombardo and others [18, 155]. The symmetric salts owns high thermal including wide electrochemical window and cathodic stability [18]. Olivine structured transition metal phosphates, including $LiFePO_4$ (LFP), have gained considerably attention because of its cost efficacy this IL's high theoretical capacity, nontoxicity, thermal, chemical including high cycling stability, electrochemical stability and flat voltage plateau [156, 157] among the various cathode materials [18].

Binder, as a required functional material of electrode in Li-ion battery, has a crucial impact on the electrochemical performance [19]. Polyvinylidene fluoride (PVDF), which is costly, difficult to recycle [158] is the most frequent binder, which is utilized in the Li-ion battery [19]. He and others [159] have utilized the cyanoethylated carboxymethyl chitoan (CN–CCTS) as the binder for cathode $LiFePO_4$ and it displayed better resistance to the organic electrolyte solvents than that with sodium carboxymethylcellulose (CMC) and PVDF [19]. Qiu and others [160] have indicated the carboxymethylcellulose derivative (CMC–Li) as the binder for $LiFePO_4$ electrode [19]. In contrast with the PVDF, these water-soluble binders are environment-friendly and carry out excellent electrochemical performance [19]. Very few studies have been carried out on humics as the binder for $LiFePO_4$ cathode till now [19]. The electrochemical performance could be considerably enhanced with many reasonable regulation with the humics as the principal binder [19].

3.2 Separators, Porosity, Shrinkage, Uptake, Ionic Conductivity, Thermal Stability, Membranes

3.2.1 A Bacterial Cellulose/Al_2O_3 Nanofibrous Composite Membrane for a Lithium-Ion Battery Separator [1]

The bacterial cellulose (BC)/Al_2O_3 nanofibrous composite membrane as a lithium-ion battery separator has been efficiently prepared by coating Al_2O_3 on the BC nanofibres via a straightforward in situ thermal decomposition of $Al(NO_3)_3{\cdot}9H_2O$ [1]. The half lithium-ion battery, which is assembled with the BC/Al_2O_3 separator, reveals satisfactory cycling performance and huge discharge capacity, implying that the BC/Al_2O_3 membrane could be utilized as a lithium-ion battery separator [1]. That the tensile strength of the BC membrane is considerably lower than that of the PP-PE-PP membrane, whilst the value of the BC–Al_2O_3 membrane substantially increasing, similar to that of the PP-PE-PP membrane is revealed by the results [1].

3.2.2 Hollow Mesoporous Silica Sphere-Embedded Composite Separator for High-Performance Lithium-Ion Battery [2]

A high-performance composite separator based upon hollow mesoporous silica spheres, poly(vinylidene fluoride-co-hexafluoropropylene) (PVdF–HFP), and poly (ethylene terephthalate) non-woven had been examined as lithium-ion battery separator through a dip coating method, which a stage separation moist process followed [2]. Due to comparatively polar components and the preferable microstructure, the composite separator displays greater porosity, outstanding thermal stability, and superior electrolyte wettability [2]. A straightforward strategy to prepare high-performance separator, which is shown to be a satisfactory candidate for lithium-ion batteries is summarized by this research [2].

3.2.3 Al_2O_3/Poly(Ethylene Terephthalate) Composite Separator for High-Safety Lithium-Ion Batteries [3]

Separators have garnered considerable attention from developers and scholars in respect to their important role in the safety of lithium-ion batteries [3]. Through scanning electron microscopy and other specific measurements in regard to a composite separator's morphology, electrolyte wettability, porosity, and a composite separator's application in lithium-ion batteries including thermal shrinkage, the basic properties of the Al_2O_3-coated PET nonwoven composite separator were typified [3]. The lithium-ion battery assembled with this composite separator indicates better electrochemical performance (e.g., cycling and discharge C-rate capability) compared to that with the Celgard 2500 separator [3]. The results of the present study constitute a straightforward strategy to preparing high-performance separators; these separators could be utilized to improve the safety of lithium-ion batteries [3].

3.2.4 Recent Developments of Cellulose Materials for Lithium-Ion Battery Separators [4]

The recent advancements of cellulose materials for lithium-ion battery separators are studied [4].

3.2.5 *Thickness Difference Induced Pore Structure Variations in Cellulosic Separators for Lithium-Ion Batteries [5]*

The pore structure of the separator is important to the performance of a lithium-battery as it affects the cell resistance [5]. It is shown that the pore size and porosity of the CC separator could be increasing simply by declining the thickness of the CC separator by employing less CC in the manufacturing of the separator [5]. It is clear that the various pore structure of the separators had been an crucial factor, which affects the battery performance in addition to the separator thickness, as the results revealed that a greater ionic electrical conductivity had been obtained for the 10 μm thick CC separator than for the 20 and 40 μm thick CC separators [5]. The present clear-cut, yet effective, approach for modifying the pore structure consequently holds significant promise for the manufacturing of separators with performance, which is enhanced, including for fundamental researches of the impact of the properties of the separator on the performance of lithium-ion cells [5]. Contemporary LIB separators usually are made from polyolefin-based polymer materials and usually suffer from low thermal stabilities and electrolyte wettabilities (Chun and others [22]; Prasanna and others [161]; Ryou and others [36]; Weng and others [29]; Xu and others [25, 162]; Zhang and others [46, 163]; Zhou and others [164]); these wettabilities has caused in a search for alternative separator materials [5]. That CC is a fruitful separator material that is worth additional researches especially as such separators most most likely could be manufactured employing up-scalable paper-making mechanisms is demonstrated by these results [5]. A $LiFePO_4$/Li battery, which includes a 10 μm CC separator, displaying the largest pores and the highest porosity, is demonstrated to characteristic a specific capacity of about 100 mAh g^{-1} at a rate of 2 C. Ionic electrical conductivity data, clearly indicate that the cell resistance for a thinner separator had been substantially declined as a consequence of its more open pore structure [5]. The SEM images indicate that the CC-25 separator featured bigger pores and a less compact structure than the CC-50 and CC-100 separators, despite the fact that the fiber morphology and overall structure (entangled CC fibres with a thickness of around 30 nm) were the identical in all three instances [5].

3.2.6 *A Heatproof Separator for Lithium-Ion Battery Based on Nylon66 Nanofibers [6]*

Membrane is utilized as lithium-ion battery separator, demonstrating satisfactory thermodynamics properties through thermo-gravimetric analysis (TG), tension test, and thermal shrinkage experiment, had been nanofiber-based by Electrospun nylon66 (PA66) [6]. Electrospun nylon66 separator premised battery displays better safety than the battery, which applys Celgard commerce separator under the

condition of serious vibration and high temperature [6]. Such facts confirm that the electrospun nylon66 separator is an optimal separator candidate for power lithium-ion battery of electric vehicles [6].

3.2.7 *The Effect of Multicomponent Electrolyte Additive on $LiFePO_4$-Based Lithium-Ion Batteries [7]*

In a $LiPF_6$ baseline electrolyte, which is called flame-retarding electrolyte, one multi-component (MC) additive is utilized to enhance the safety of lithium-ion battery [7]. The electrochemical performances of $LiFePO_4$/Li half cells with flame-retarding electrolytes and baseline were assessed, respectively [7]. The MC additive enhances the thermal stability and does not deteriorate the battery electrochemical performance with $LiFePO_4$ cathode, hence, the combination is a fruitful additive for the safer lithium-ion battery with the MC additive, the cycling performances of $LiFePO_4$/Li half cells were enhanced efficiently at the rate of 0.1 C. Therefore, and the resistance of flame-retarding electrolyte didn't increase [7]. It could be observed that the rest mass of both electrolytes are equal (both are 0.316 g), though compared to the extinguishing time (60 s) of baseline electrolyte, flame-retarding electrolyte employs more time (66.8 s) [7]. It could be observed that the electrical conductivity of flame-retarding electrolyte is 9.42 mS/cm, which is greater than that of baseline electrolyte (7.80 mS/cm), suggesting better electrical conductivity [7]. It could be observed that there are two principal exothermic peaks at 244.2 °C and 220.3 °C, respectively, with the total heat generation of −158.5 J/g [7].

3.3 Ionic Conductivity, Electrochemical Stability, Polymer Electrolytes, Salt

3.3.1 *Polymer Electrolytes for Lithium-Ion Batteries: A Critical Study [8]*

The present review essay on a brief history, polymer electrolytes (PEs)'s brief application of polymer electrolyte systems, and advantage [8]. The essay began with a brief introduction of polymer electrolytes followed by extreme employs and their varieties [8]. The role of host polymer matrix by taking several examples of polymer electrolyte, which the various renowned group of the preoccupied field published, has been examined [8]. The criteria for selection of suitable host polymer, salt, aprotic solvents to be utilized in polymer electrolyte, and inorganic filler/clay, have been outlined in detail [8]. That essay includes various methods for the preparation of polymer electrolyte films [8]. The various self-proposed processes

(like VTF, WLF, free volume theory, dispersed/intercalated processes, etc.) have been outlined in order to elucidate the Li-ion conduction in polymer electrolyte systems [8].

3.3.2 *Electrochemical Investigation of Gel Polymer Electrolytes Based on Poly(Methyl Methacrylate) and Dimethylacetamide for Application in Li-Ion Batteries [9]*

Solution-casting method had been utilized to fabricate GPEs containing various weight proportion of PMMA [9]. Spectroscopy had been utilized to investigation the level of relationships between PMMA and lithium salt in the prepared GPEs had been infra-red by fourier reshape [9]. Through estimating the bulk resistance of polymer electrolytes from Nyquist plot, Li-ion electrical conductivity of GPEs had been dictated [9]. Increased PMMA content of GPEs caused in an amelioration in the electrochemical potential window from 4.2 to 4.5 V [9]. Moreover the optimal electrochemical properties and the highest lithium transference number (0.42) were obtained for GPE containing 10 wt% PMMA and 0.75 M $LiClO_4$ [9]. Optimized electrochemical properties and the highest lithium transfer number (0.42) were obtained for GPEs containing 10 wt% of PMMA [9].

3.3.3 *Effect of Variation of Different Nanofillers on Structural, Electrical, Dielectric, and Transport Properties of Blend Polymer Nanocomposites [10]*

The effect of multiple nano-fillers with various particle sizes and dielectric constants ($BaTiO_3$, Er_2O_3, CeO_2, or TiO_2) on blend solid polymer electrolyte, which includes PVC and PEO, complexed with bulky $LiPF_6$ has been examined [10]. Evidence of interaction among the functional groups of the nanofiller in terms of shifting and change of the peak profile and the polymer with the ions is offered by FTIR [10]. The particle size and the dielectric constant indicate an abnormal trend with various nano-fillers [10]. "The particle size of the pristine nanofiller follows the trend $Er_2O_3 \cong BaTiO_3 > CeO_2 > TiO_2$" [10]. The particle size of CeO_2 is greater than that of TiO_2, though the dielectric constant of the polymer nanocomposite, which is dispersed with TiO_2, is greater than that of the CeO_2 [10]. The AC electrical conductivity follows the universal Jonscher power law, and an efficient mechanism has been devised to comprehend the nanofiller interaction with cation co-ordinated polymer [10]. The high-frequency dispersion region corresponding to bulk relaxation phenomena falls outside the assessed frequency variety and can not be detected for the high-conductivity system [10]. That dielectric constant and the

particle size have an crucial effect on systemic, microstructural, dielectric, and electric, properties is shown by the results [10]. The ion transference number (∼0.99) results suggest the SPE films to be predominately ionic with a broad voltage stability window (∼3.5 V) [10].

3.3.4 *Effect of the Soft and Hard Segment Composition on the Properties of Waterborne Polyurethane-Based Solid Polymer Electrolyte for Lithium-Ion Batteries [11]*

An increase in hard segment content declined the crystallinity and thermal stability of WPU [11]. The ionic electrical conductivity increasing first with the increased of the hard segment content and declined [11]. The ionic electrical conductivity against the temperature of WPU10–25% Li is linear, suggesting that the ionic electrical conductivity of this electrolyte showed Arrhenius-like behaviour [11, 92]. Through the hard segment content, the compatibility of WPU-based SPEs with lithium electrode had been shaped [11]. The compatibility of WPU-based SPEs with lithium electrode were examined conducting the AC impedance spectra of Li/SPE/Li cell [11]. All-solid-state $LiFePO_4$/SPE/Li battery, which is based upon WPU12–20% Li electrolyte, delivered discharge specific capacities of 159 and 162 mAh g^{-1} under 60 and 80 °C at 0.1 C, respectively [11]. All-solid-state $LiFePO_4$/SPE/Li battery, which is based upon WPU12–20% Li electrolyte delivered the discharge capacities of 159 mAh g^{-1} at 60 °C and 162 mAh g^{-1} at 80 °C at 0.1 C [11]. Tuning the suitable soft and hard segment composition of WPU might eventually give rise to the successful use of WPU-based SPEs for all-solid-state Li-ion batteries [11]. The LSV results indicate that the WPU-based SPEs showed an electrochemical stability up to 5.0 V and offer feasibility for the application in Li-ion batteries [11]. The consequence suggests that the battery can deliver a comparatively high specific capacity at high temperature and low rates [11]. The consequence suggests that the WPU-based battery can deliver similar capacities at low rates to that of PEO one [11]. The uncontrolled passivation, which gives rise to the continuous impedance growth [165], is revealed by this consequence [11].

3.3.5 *Preparation, Properties, and Li-Ion Battery Application of EC + PC-Modified PVdF–HFP Gel Polymer Electrolyte Films [12]*

Following poly(vinylidene fluoride-co-hexafluoropropylene) (PVdF–HFP) and lithium tetrafluoroborate ($LiBF_4$) salt along with blending plasticizers, propylene carbonate (PC) and ethylene carbonate (EC), high Li-ion-conducting gel polymer

electrolyte films are devised [12]. Lithium-ion batteries based upon the gel polymer electrolyte film display striking charge-cycling and discharge performances [12]. The initial discharge capacity of this battery is as high as 165.1 mAh g^{-1} at 0.1 C and indicates a small capacity fading of 4.8% after 120 cycles, suggesting that the 85PVdF–HFP: 15$LiBF_4$ + 150 (EC + PC) system is an excellent electrolyte candidate for lithium-ion battery applications [12]. The charge-discharge performance of the lithium ion cell, which is fabricated with this gel polymer electrolyte film, is apparently better than that of the previously indicated lithium ion cells fabricated with other PVdF–HFP-based gel polymer electrolyte films [12]. Performances of the button cells fabricated with the present gel polymer electrolyte films were assessed at ambient temperature are-discharged by the charge [12].

3.3.6 *Influences of $LiCF_3SO_3$ and TiO_2 Nanofiller on Ionic Conductivity and Mechanical Properties of PVA: PVdF Blend Polymer Electrolyte [13]*

Solid polymer electrolytes have been intensively studied because of its flexibility, safety, electrochemical stability, and long life for its applications in multiple electrochemical tools in recent decades [13]. Interaction of $LiCF_3SO_3$ and TiO_2 nanofiller in the optimized composition of PVA:PVdF (80:20-system-A possessing $\sim 2.8 \times 10^{-7}$ S cm^{-1} at 303 K) blend polymer electrolyte have been examined in the current study [13]. The effect of various concentration of TiO_2 in system-B has been examined and the optimized system is regarded as system-C ($\sim 3.7 \times 10^{-3}$ S cm^{-1} at 303 K) [13]. Vibrational, systemic, mechanical, electrical conductivity, electrochemical properties, and thermal, have been investigated employing FTIR, DSC, XRD, stress-strain, AC impedance spectroscopic method and TGA, LSV, and CV respectively to ascertain the optimized system [13].

3.3.7 *A High-Performance and Environment-Friendly Gel Polymer Electrolyte for Lithium-Ion Battery Based on Composited Lignin Membrane [14]*

Mechanical property, the morphology, and thermal stability of the composite lignin-PVP membrane and the electrochemical properties of LP-GPE are examined [14]. A high ionic electrical conductivity of 2.52×10^{-3} S cm^{-1} at room temperature, outstanding electrochemical stability of LP-GPE, and excellent lithium-ion transference number of 0.56, are revealed for electrochemical properties [14]. That LP-GPE could be utilized as a new electrolyte for Li-ion battery with high-performance, environmentally friendly properties, and cheap, is shown by all these results [14].

3.3.8 Electrochemical Characterization of Ionic Liquid Based Gel Polymer Electrolyte for Lithium Battery Application [15]

The 80 wt% IL containing GPE indicates satisfactory thermal stability (∼200 °C), ionic electrical conductivity (6.42×10^{-4} S cm^{-1}), wide electrochemical stability window (∼4.10 V versus Li/Li^+ at 30 °C), and Li-ion electrical conductivity (1.40×10^{-4} S cm^{-1} at 30 °C) [15]. $LiFePO_4$ cathode indicates enhanced electrochemical performance with cyclic stability up to 50 cycles and a satisfactory discharge/charge capacity at 1 C rate, as compared with the without coated $LiFePO_4$ had been oxide-coated by the graphene [15]. The discharge capacity reaches a maximal value of 104.50 and 95.0 mAh g^{-1} for graphene oxide-coated $LiFePO_4$ and without coated $LiFePO_4$ at 1 C rate respectively at 30 °C [15]. $LiFePO_4$ cathode after coating with graphene oxide, these results revealed enhanced electrochemical performance of pristine [15]. That the GO@LFP cathode indicates electronic electrical conductivity and satisfactory electrochemical reactivity is revealed by this consequence [15]. Complex impedance spectroscopic researches indicate that the 80 wt% IL containing GPE has ionic electrical conductivity of 6.42×10^{-4} S cm^{-1} at 30 °C [15].

3.3.9 A Novel and Shortcut Method to Prepare Ionic Liquid Gel Polymer Electrolyte Membranes for Lithium-Ion Battery [16]

The ionic liquid polymer electrolyte (IL-PE) membrane is prepared by ultraviolet (UV) cross-linking technology with polyurethane acrylate (PUA), methylmethacrylate (MMA), ionic liquid ($Py_{13}TFSI$), lithium salt (LiTFSI), benzoyl peroxide (BPO), and ethylene glycol dimethacrylate (EGDMA) [16]. The room temperature the lithium ions transference number of 0.22 and ionic electrical conductivity of 1.37×10^{-3} S cm^{-1} is displayed by the resultant electrolyte membranes [16]. The interfacial resistances between the electrodes and the IL-PE have the less change after 10 cycles than before 10 cycles [16]. Upon 10 cycles, IL-PE has better compatibility with the Li electrode and the $LiFePO_4$ electrode [16]. 131.9 mAh g^{-1} with 95.5% columbic efficiency after 80 cycles is the discharge capacity [16]. The battery, which employs the IL-PE, displays a satisfactory rate and cycle performance [16].

3.3.10 *Poly(Methyl Methacrylate) Reinforced Poly (Vinylidene Fluoride) Composites Electrospun Nanofibrous Polymer Electrolytes as Potential Separator for Lithium-Ion Batteries [17]*

Fabrication of nanofibrous polymer electrolyte membranes in various percentage (PVdF: PMMA = 100:0, 80:20 and 50:50) by electrospinning and poly(methylmethacrylate) (PMMA) of poly(vinylidene fluoride) (PVdF) is indicated to examine the impact of PMMA on Li-ion battery performance of PVdF membrane as separator [17]. At room temperature, PVdF–PMMA (50:50) polymer electrolyte membrane revealed ionic electrical conductivity 0.15 S/cm and electrolyte uptake 290% [17]. Nanofibrous PVdF–PMMA (50:50) polymer electrolyte membrane had been observed to be a potential separator for Li-ion batteries [17]. That the PVdF–PMMA membrane has a satisfactory thermal stability with minimum weight% deterioration is revealed by these results [17].

3.3.11 *Asymmetric Tetraalkyl Ammonium Cation-Based Ionic Liquid as an Electrolyte for Lithium-Ion Battery Applications [18]*

Performance of N-butyl N,N,N-triethylammonium bis (trifluoromethanesulfonyl)-imide (N_{2224}TFSI) as a room temperature ionic liquid (RTIL), which includes ethylene carbonate (EC)/diethylcarbonate (DEC) and lithium salt has been examined as an electrolyte for lithium-ion battery [18]. The electrolyte is highly susceptible to fire during direct exposure to the flame, suggesting an electrolyte for lithium-ion battery's non-flammable character [18]. The performance of the IL electrolyte has been evaluated with lithium-ion half cells employing mesocarbon and $LiFePO_4$ microbead (MCMB) electrodes, demonstrating satisfactory galvanostatic cycling with high capacity retention of about 84 and 90%, respectively [18]. The impedance plots show that when the lithium metal is in contact with IL electrolyte, the impedance notably increases with time [18].

3.3.12 *The Investigation of Humics as a Binder for $LiFePO_4$ Cathode in Lithium-Ion Battery [19]*

Binder, as a required functional material of electrode in Li-ion battery, has a crucial impact on the electrochemical performance [19]. The methods of galvanostatic discharge/charge and cyclic voltammetry (CV) were carried out to assess the performance of humics binder in LFP electrode [19].

3.4 Conclusion

Through coating Al_2O_3 on the BC nanofibres via a straightforward in situ thermal decomposition technique, we have efficiently prepared a BC–Al_2O_3 nanofibrous composite membrane as an LIB separator [1]. Smaller interfacial resistance, superior thermal dimensional stability and better electrochemical stability as compared to the PP-PE-PP and BC separators is shown by the BC–Al_2O_3 membrane [1]. The BC–Al_2O_3 composite membrane must be a quite fruitful candidate separator for high-power Li-ion batteries [1].

Hollow mesoporous SiO_2 spheres/PVdF–HFP-coated PET non-woven composite separators had been devised by us as an advanced separator for lithium-ion battery [2]. With greater porosity, greater ionic electrical conductivity which have significant affects on the cell performances, and superior electrolyte wettability, the incorporation of the distinctive SiO_2 spheres allows the composite separator [2].

Higher porosity, enhanced electrolyte wettability, greater ionic electrical conductivity, which is compared to the commercial Celgard 2500 separator, and greater electrolyte uptake, had been shown by the Al_2O_3/PET separator [3]. The Al_2O_3/PET separator displayed superior dimensional thermal stability, implying that it can be utilized to noticeably improve the safety of Li-ion batteries [3]. The cell, which includes the Al_2O_3/PET separator, showed superior electrochemical performance (e.g., cycling and C-rate capability) compared to the cell containing the Celgard 2500 [3]. Electrochemical performance and nonwoven PET's excellent thermal makes the Al_2O_3/PET composite separator a fruitful candidate as the next-generation separator for high-safety Li-ion batteries [3].

In the application of LIB separators, Cellulose has received considerably attention due to thermal stabilities and its satisfactory chemical [4]. Cellulose can not play a role as a supporter, a gelator in LIB separators, and an enhancer, though also be endowed new functions by modification [4]. The preparation techniques for cellulose LIB separators include traditional coating, casting, electrospinning, papermaking, including ISISA and stage inversion and forcespinning [4]. The use of cellulose materials for LIB separators is supposed to be more extensive with diversified applications of Li-ion batteries and the increasingly restrictive environmental requirements [4]. The preparation technique for cellulose LIB separators needs to be enhanced to lessen the environmental influence and decline the production cost [4]. Structural design of cellulose-based LIB separators and functional modification are satisfactory directions for the next generation of high-performance/high-safety batteries [4].

A surprisingly facile paper-making strategy has been explained for the manufacturing of stratified Cladophora cellulose (CC) separators with pore structures and various thicknesses [5]. Through differing the quantity of CC, which is utilized in the manufacturing process, as an increasing thickness leads to a declined peak and porosity pore size in the paper-making process, the pore size distribution and porosity of the separators could be controlled simply [5]. The technique enables the manufacturing of CC separators with thicknesses down to 10 μm and fosters the

manufacturing of separators premised with various pore structures and consequently ionic conductivities though on the identical material [5]. It has been demonstrated that a decline in the CC separator thickness from 40 to 10 μm results in an increase in the peak pore size from 12 to 21 nm including an increase in the porosity from 33 to 44%, resulting in an increase in the ionic electrical conductivity of the electrolyte soaked separators from 0.69 to 0.82 mS cm^{-1} [5].

Electrospun nylon66 nanofiber separator displays excellent mechanical and thermal properties [6].

The MC additive had been added into the baseline electrolyte as the flame retardant, and the impacts of the flame-retarding electrolyte were examined in this work [7]. The flame-retarding electrolyte, which includes MC, additive indicates the better nonflammability and electrical conductivity than that of baseline electrolyte [7]. The specific capacity of flame-retarding electrolyte indicates more excellent cycling performance than that of baseline one at 0.1 in the electrochemical cycling tests C [7]. Following nonflammability, electrochemical performance, and thermal stability, it could be concluded that the MC additive enhances the thermal stability substantially and indicates better electrochemical performance in the $LiFePO_4$/Li half cells; hence, the MC additive is a possible excellent choice of electrolyte additive [7].

A thorough critical review of the PEs (published over the last three decades) utilized in electrochemical tools has been outlined and examined appropriately [8]. A thorough ion transport processes for Li-ion transport like VTF, WLF, free volume theory, dispersed/intercalated processes, etc., in polymer electrolysis are examined and studied [8]. The fillers/clays have been utilized for improving the properties like ionic electrical conductivity, surface structure/microstructure, electrochemical, stability, etc. [8]. A thin/safe/flexible/cheap electrolyte cum separator is asserted for electrochemical tools, and it could be achieved by employing solid polymer electrolytes cum separators [8].

The PMMA-based gel polymer electrolytes were efficiently prepared employing solution-casting method with differing polymer content from 2 to 10 wt% [9]. The PMMA-based gel polymer electrolytes has been demonstrated that the ionic electrical conductivity of the GPEs increases with decline in polymer content displays a maximal value of 2.3×10^{-3} S cm^{-1} at ambient condition from AC impedance spectroscopy [9]. Electron transfer and lithium transfer number number enhanced substantially which is requirement for Li ion batteries whilst in increasing polymer content [9]. Through estimating the bulk resistance of polymer electrolytes from Nyquist plot, Li-ion electrical conductivity of GPEs had been dictated [9]. Based on 4.2–4.5 V, the electrochemical potential window had been enhanced by increased PMMA content in GPEs [9]. Optimized electrochemical properties and the highest lithium transfer number (0.42) were obtained for GPEs containing 10 wt% of PMMA [9].

Free-standing polymer nanocomposite films consisting of (PEO–PVC) + $LiPF_6$ with 10 wt% nanofiller, which haves dielectric constant ($BaTiO_3$ and a various particle size, CeO_2, TiO_2), and Er_2O_3, have been prepared via the solution cast method [10]. That dielectric constant and the particle size have an crucial effect on

systemic, microstructural, dielectric, and electric, properties is shown by the results [10]. X-ray diffraction results confirmed the polymer nanocomposite formation [10]. The FTIR investigation revealed clear empirical evidence for polymer-ion, ion-ion, and polymer-ion-nanofiller interaction [10]. The dielectric spectroscopy offers important information of the increase in three to four orders of the dielectric constant as compared to the nanofiller free polymer salt matrix [10]. The supremacy of the erbium oxide nanofiller as compared to other nano-fillers for enhancing the energy-storage performance of nano-composites is revealed by the present study [10].

Solid polymer electrolytes (SPEs) based upon LiTFSI and WPU were fabricated through an organic solvent free process [11]. The crystallinity of WPU declined and the surface of WPU membrane became homogenous and smooth with the increase of hard segment content [11]. The ionic electrical conductivity increasing first with the increased hard segment content and declined [11]. The WPU12–20% Li electrolyte (55 wt% soft segment content) revealed an ion electrical conductivity of 5.14×10^{-5} S cm^{-1} at 25 °C and 1.26×10^{-3} S cm^{-1}at 60 °C with the electrochemical stability window reached around (vs. Li^+/Li) 5.0 V [11]. All-solid-state $LiFePO_4$/SPE/Li battery, which is based upon WPU12–20% Li electrolyte delivered the discharge capacities of 159 mAh g^{-1} at 60 °C and 162 mAh g^{-1} at 80 °C at 0.1 C [11].

"The 85PVdF–HFP: 15$LiBF_4$ + x (EC + PC) (x = 0, 50, 100, 150, and 200 wt %) gel polymer electrolyte films are prepared" [12]. The 85PVdF–HFP: 15$LiBF_4$ + 150 (EC + PC) film displays the optimal properties, whose crystallinity, ionic electrical conductivity, melting temperature, and electrochemical stability window are 9.5%, 115 °C, 4.6 V, respectively, and 8.1×10^{-4} S cm^{-1} [12]. The performance of the present cell is in the optimal position in comparison to the indicated lithium ion cells fabricated with PVdF–HFP-based gel polymer electrolyte films [12]. The 85PVdF–HFP: 15$LiBF_4$ + 150 (EC + PC) gel polymer electrolyte film can be an excellent electrolyte candidate for lithium-ion batteries [12].

Influence of nanoTiO_2 and $LiCF_3SO_3$ with the polymer blend PVA: PVdF (system-A) have been investigated [13]. XRD pattern demonstrates that the interaction of nanoTiO_2 and $LiCF_3SO_3$ with the host polymer by the inference of greater width of peak and change in peak intensity [13]. The incorporation of TiO_2 improves the properties of polymer electrolyte and it has been assessed its electrochemical performance and configured as the cell [13].

The prepared lignin-PVP composite membrane displays satisfactory mechanical property and advantageous thermal stability [14]. A high liquid electrolyte uptake of lignin-PVP composite membrane gives rise to good electrochemical performances of the corresponding LP-GPE, such as excellent ionic electrical conductivity, high Li-ion transference number, better compatibility with active electrode, and wide electrochemical stability window [14]. The exploration of the LP-GPE will be a brand-new candidate to satisfy zero environmental influence Li-ion batteries and high-performance [14].

Free-standing 80 wt% IL, which includes GPE membrane based upon polymer PVdF–HFP, salt LiTFSI, and the electrochemical properties of membrane, which is prepared, were examined and IL EMIMFSI had been prepared for lithium battery application [15]. Complex impedance spectroscopic researches indicate that the 80 wt% IL containing GPE has ionic electrical conductivity of 6.42×10^{-4} S cm^{-1} at 30 °C [15]. We have computed electrochemical stability window ($\sim$4.10 V vs. Li/Li^+) for 80 wt% IL, which includes GPE membrane which is useful for lithium battery application, and the Li-ion electrical conductivity ($Li^+ = 1.40 \times 10^{-4}$ S cm^{-1}) [15]. The surface of $LiFePO_4$ cathode particle had been modified with coating of graphene oxide [15]. The graphene oxide coating not just offers as a protective layer though also enhanced the electronic electrical conductivity of cathode [15]. Upon surface coating with graphene oxide, electrochemical performance of pristine LFP cathode material enhances [15].

A series of tests on the Py_{13}TFSI/LiTFSI/PUA/PMMA ionic liquid polymer the Li/IL-PE/$LiFePO_4$ half-cell and electrolyte membrane were undertaken and examined [16]. An electrochemical stabilization window of about 4.8 V had been obtained, and the electrolyte membrane had sufficient electrochemical stability to act as an electrolyte material in the Li/IL-PE/$LiFePO_4$ half-cell [16]. The ionic liquid polymer electrolyte membrane had a satisfactory compatibility with Li electrode and $LiFePO_4$ electrode; the discharge and charge performance of lithium ion battery had been investigated [16]. In lithium-ion battery, the Py_{13}TFSI/LiTFSI/PUA/PMMA kind ionic liquid polymer electrolyte membranes were fruitful [16].

PVdF–PMMA composite fibres with diameter in nano-scale membranes were efficiently prepared by electrospinning [17]. The increase in proportion of PMMA improves electrolyte uptake and ionic electrical conductivity of PVdF–PMMA composites membranes [17]. That the preparation approach for PVdF/PMMA composites membranes by electrospinning with PVdF/PMMA (50:50) nanofibrous polymer electrolyte membrane had been observed to be fruitful and potential separator for Li-ion batteries than that of PVdF and pure PVdF–PMMA (80:20) had been demonstrated by these results [17].

The addition of EC/DEC solvent mixture to the IL improves the efficient SEI layer formation and prevents the graphitic disorder of MCMB during discharge/charge cycling [18]. An initial high irreversible capacity in the variety of 557 mAh g^{-1} at 0.1 C rate is demonstrated by the MCMB half cell [18]. High reversible capacity and satisfactory rate capability are obtained, where the capacity retention (94%) is kept up to 75 cycles due to the presence of high content of graphitic behaviour and microspores [18]. Preliminary capacity of 132 mAh g^{-1} at 0.1 C rate after the formation cycle with more than 85% capacity retention for 50 cycles is demonstrated by the LFP [18].

The way raw materials are mixed is an crucial factor for the quality of electrode and can substantially affect the electrochemical performance [19].

3.5 Related Work

Lee H, Yanilmaz M, Toprakci O, Fu K, Zhang XW (2014) A review of recent developments in membrane separators for rechargeable lithium-ion batteries. Energy Environ Sci 7:3857–3886 [https://doi.org/10.1039/c4ee01432d]

The separator does not entail directly in any cell reactions, though properties and its structure play important roles in determining the battery performance, which comprises cycle life, safety, power density [33], and energy density, in LIBs [2]. The nanosized pottery particles including TiO_2, and Al_2O_3, SiO_2, can substantially enhance thermal stability the mechanical strength, including their thermal resistance [33] and ionic electrical conductivity of separators because of their high hydrophilicity and high surface area [2]. The pore structure and thickness of the separator should be carefully controlled, as a satisfactory balance between mechanical strength and ionic electrical conductivity should be kept (Arora and Zhang [40]; Lee and others [33]; Zhang [50]) in order to satisfy these two functions [5].

References

Main Document References

1. Xu Q, Wei C, Fan L et al (2017) Cellulose 24:1889. https://doi.org/10.1007/s10570-017-1225-x
2. Xiao, W., Wang, J., Wang, H et al (2016) J Solid State Electrochem 20:2847. https://doi.org/10.1007/s10008-016-3268-6
3. Li W, Li X, Yuan A et al (2016) Ionics 22:2143. https://doi.org/10.1007/s11581-016-1752-8
4. Sheng J, Tong S, He Z et al (2017) Cellulose 24:4103. https://doi.org/10.1007/s10570-017-1421-8
5. Pan R, Wang Z, Sun R et al (2017) Cellulose 24:2903. https://doi.org/10.1007/s10570-017-1312-z
6. Wang H, Wang N, Liu T et al (2016) Ionics 22:731. https://doi.org/10.1007/s11581-016-1698-x
7. Feng L, Wang Q, Ai C, Sun J (2017) The effect of multicomponent electrolyte additive on $LiFePO_4$-based lithium ion batteries. In: Harada K, Matsuyama K, Himoto K, Nakamura Y, Wakatsuki K (eds) Fire science and technology 2015. Springer, Singapore. https://doi.org/10.1007/978-981-10-0376-9_16
8. Arya A, Sharma AL (2017) Ionics 23:497. https://doi.org/10.1007/s11581-016-1908-6
9. Faridi M, Naji L, Kazemifard S et al (2018) Chem Pap 72:2289. https://doi.org/10.1007/s11696-018-0458-y
10. Arya A, Sadiq M, Sharma AL (2018) Ionics 24:2295. https://doi.org/10.1007/s11581-017-2364-7
11. Ren N, Song Y, Tao C et al (2018) J Solid State Electrochem 22:1109. https://doi.org/10.1007/s10008-017-3855-1
12. Song S, Wang J, Tang J et al (2017) Ionics 23:3365. https://doi.org/10.1007/s11581-017-2130-x

13. Hema M, Tamilselvi P, Hirankumar G (2017) Ionics 23:2707. https://doi.org/10.1007/s11581-016-1925-5
14. Liu B, Huang Y, Cao H et al (2018) J Solid State Electrochem 22:807. https://doi.org/10.1007/s10008-017-3814-x
15. Singh SK, Gupta H, Balo L et al (2018) Ionics 24:1895. https://doi.org/10.1007/s11581-018-2458-x
16. Li L, Yang X, Li J et al (2018) Ionics 24:735. https://doi.org/10.1007/s11581-017-2254-z
17. Mahant YP, Kondawar SB, Nandanwar DV et al (2018) Mater Renew Sustain Energy 7:5. https://doi.org/10.1007/s40243-018-0115-y
18. Selvamani V, Suryanarayanan V, Velayutham D et al (2016) J Solid State Electrochem 20:2283. https://doi.org/10.1007/s10008-016-3248-x
19. Han G, Yang S, Liu J, Huang Y (2018) The investigation of humics as a binder for $LiFePO_4$ cathode in lithium ion battery. In: Li B et al (eds) Characterization of minerals, metals, and materials 2018. TMS 2018, The minerals, metals & materials series. Springer, Cham. https://doi.org/10.1007/978-3-319-72484-3_4

Other Bibliographic References

20. Lee J, Lee CL, Park K, Kim ID (2014) Synthesis of an Al_2O_3-coated polyimide nanofiber mat and its electrochemical characteristics as a separator for lithium ion batteries. J Power Sources 248:1211–1217
21. Yanilmaz M, Lu Y, Dirican M, Fu K, Zhang X (2014) Nanoparticle-on-nanofiber hybrid membrane separators for lithium-ion batteries via combining electrospraying and electrospinning techniques. J Membrane Sci 456:57–65
22. Chun SJ, Choi ES, Lee EH, Kim JH, Lee SY, Lee SY (2012) Eco-friendly cellulose nanofiber paper-derived separator membranes featuring tunable nanoporous network channels for lithium-ion batteries. J Mater Chem 22:16618–16626
23. Jabbour L, Bongiovanni R, Chaussy D, Gerbaldi C, Beneventi D (2013) Cellulose-based Li-ion batteries: a review. Cellulose 20:1523–1545
24. Kim JH, Kim JH, Choi ES, Yu HK, Kim JH, Wu Q, Chun SJ, Lee SY, Lee SY (2013) Colloidal silica nanoparticle-assisted structural control of cellulose nanofiber paper separators for lithium-ion batteries. J Power Sources 242:533–540
25. Xu Q, Kong Q, Liu Z, Zhang J, Wang X, Liu R, Yue L, Cui G (2013) Polydopamine-coated cellulose microfibrillated membrane as high performance lithium-ion battery separator. RSC Adv 4:7845–7850
26. Zhang J, Liu Z, Kong Q, Zhang C, Pang S, Yue L, Wang X, Yao J, Cui G (2013) Renewable and superior thermal-resistant cellulose-based composite nonwoven as lithium-ion battery separator. ACS Appl Mater Interfaces 5:128–134
27. Zhang J, Yue L, Kong Q, Liu Z, Zhou X, Zhang C, Xu Q, Zhang B, Ding G, Qin B, Duan Y, Wang Q, Yao J, Cui G, Chen L (2014) Sustainable, heat-resistant and flame-retardant cellulose-based composite separator for high-performance lithium ion battery. Sci Rep 4:3935
28. Jiang F, Yin L, Yu Q, Zhong C, Zhang J (2015) Bacterial cellulose nanofibrous membrane as thermal stable separator for lithium-ion batteries. J Power Sources 279:21–27
29. Weng B, Xu F, Alcoutlabi M, Mao Y, Lozano K (2015) Fibrous cellulose membrane mass produced via forcespinning® for lithium-ion battery separators. Cellulose 22:1311–1320
30. Liao H, Hong H, Zhang H, Li Z (2016) Preparation of hydrophilic polyethylene/methylcellulose blend microporous membranes for separator of lithium-ion batteries. J Membrane Sci 498:147–157
31. Deng Y, Song X, Ma Z, Zhang X, Shu D, Nan J (2016) Al_2O_3/PVdF–HFP–CMC/PE separator prepared using aqueous slurry and post-hot-pressing method for polymer lithium-ion batteries with enhanced safety. Electrochem Acta 212:416–425

32. Jeon H, Yeon D, Lee T, Park J, Ryou MH, Yong ML (2016) A water-based Al_2O_3 ceramic coating for polyethylene-based microporous separators for lithium-ion batteries. J Power Sources 315:161–168
33. Lee H, Yanilmaz M, Toprakci O, Fu K, Zhang X (2014) A review of recent developments in membrane separators for rechargeable lithium-ion batteries. Energy Environ Sci 7:3857–3886. https://doi.org/10.1039/C4EE01432D
34. Jeong YB, Kim DW (2004) Effect of thickness of coating layer on polymer-coated separator on cycling performance of lithium-ion polymer cells. J Power Sources 128:256–262
35. Hwang K, Kwon B, Byun H (2011) Preparation of PVdF nanofiber membranes by electrospinning and their use as secondary battery separators. J Membr Sci 378:111–116
36. Ryou MH, Lee YM, Park JK, Choi JW (2011) Mussel-inspired polydopamine treated polyethylene separators for high-power Li-ion batteries. Adv Mater 23:3066–3070
37. Croce F, Settimi L, Scrosati B (2006) Superacid ZrO_2-added, composite polymer electrolytes with improved transport properties. Electrochem Commun 8:364–368
38. Zhang P, Chen LX, Shi C, Yang PT, Zhao JB (2015) Development and characterization of silica tube-coated separator for lithium ion batteries. J Power Sources 284:10–15
39. Shi JL, Fang LF, Li H, Zhang H, Zhu BK, Zhu LP (2013) Improved thermal and electrochemical performances of PMMA modified PE separator skeleton prepared via dopamine-initiated ATRP for lithium ion batteries. J Membr Sci 437:160–168
40. Arora P, Zhang ZJ (2004) Battery separators. Chem Rev 104:4419–4462. https://doi.org/10.1021/cr020738u
41. Huang X (2011) Separator technologies for lithium-ion batteries. J Solid State Electrochem 15:649–662
42. He MN, Zhang XJ, Yang K, Wang J, Wang Y (2015) Pure inorganic separator for lithium ion batteries. ACS Appl Mater Interfaces 7:738–742
43. Xiao W, Gong YQ, Wang H, Zhao LN, Liu JG, Yan CW (2015) Preparation and electrochemical performance of ZrO_2 nanoparticle embedded nonwoven composite separator for lithium-ion batteries. Ceram Int 41:14223–14229
44. Zhu XM, Jiang XY, Ai XP, Yang HX, Cao YL (2015) A highly thermostable ceramic-grafted microporous polyethylene separator for safer lithium-ion batteries. ACS Appl Mater Interfaces 7:24119–24126
45. Shi C, Zhang P, Huang SH, He XY, Yang PT, Wu DZ, Sun DH, Zhao JB (2015) Functional separator consisted of polyimide nonwoven fabrics and polyethylene coating layer for lithium-ion batteries. J Power Sources 298:158–165
46. Zhang SS (2007) A review on the separators of liquid electrolyte Li-ion batteries. J Power Sources 164(1):351–364
47. Fang M, Ho T, Yen J, Lin Y, Hong J, Wu S, Jow J (2015) Preparation of advanced carbon anode materials from mesocarbon microbeads for use in high C-rate lithium ion batteries. Mater 8:3550–3561. https://doi.org/10.3390/ma8063550
48. Liang Z, Zheng G, Liu C, Liu N, Li W, Yan K, Yao H, Hsu P, Chu S, Cui Y (2015) Polymer nanofiber-guided uniform lithium deposition for battery electrodes. Nano Lett 15:2910–2916. https://doi.org/10.1021/nl5046318
49. Kumar J, Kichambare P, Rai AK, Bhattacharya R, Rodrigues S (2016) A high performance ceramic-polymer separator for lithium batteries. J Power Sources 301:194–198. https://doi.org/10.1016/j.jpowsour.2015.09.117
50. Zhang J, Yue L, Kong Q et al (2014) Sustainable, heat-resistant and flame-retardant cellulose-based composite separator for high-performance lithium ion battery. Sci Rep 4:3935. https://doi.org/10.1038/srep03935
51. Jansen AN, Kahaian AJ, Kepler KD et al (1999) Development of a high-power lithium-ion battery. J Power Sources 81:902–905
52. Wu H, Zhuo D, Kong D et al (2014) Improving battery safety by early detection of internal shorting with a bifunctional separator. Nat Commun 5(1):5193
53. Balakrishnan PG, Ramesh R, Kumar TP (2006) Safety mechanisms in lithium-ion batteries. J Power Sources 155(2):401–414

54. Tingfeng Y, Caibo Y, Yanrong Z et al (2009) A review of research on cathode materials for power lithium ion batteries. Rare Metal Mater Eng 38(9):1687–1692
55. Wen J, Yu Y, Chen C (2012) A review on lithium-ion batteries safety issues: existing problems and possible solutions. Mater Express 2(3):197–212
56. Qian J, Henderson WA, Xu W et al (2015) High rate and stable cycling of lithium metal anode. Nat Commun 6:6362–6370
57. Lee H, Alcoutlabi M, Toprakci O et al (2014) Preparation and characterization of electrospun nanofiber-coated membrane separators for lithium-ion batteries. J Solid State Electrochem 18(9):2451–2458
58. Yang M, Hou J (2012) Membranes in lithium ion batteries. Membrane 2(3):367–383
59. Wang YS, Li SM, Hsiao ST et al (2014) Integration of tailored reduced graphene oxide nanosheets and electrospun polyamide-66 nanofabrics for a flexible supercapacitor with high-volume-and high-area-specific capacitance. Carbon 73:87–98
60. Zeng Z, Jiang X, Wu B, Xiao L, Ai X, Yang H, Cao Y (2014) Bis(2,2,2-trifluoroethyl) methylphosphonate: an novel flame-retardant additive for safe lithium-ion battery. Electrochim Acta 129:300–304
61. Dunn B, Kamath H, Tarascon JM (2011) Electrical energy storage for the grid: a battery of choices. Science 334(6058):928–935
62. Sequeira C, Santos D (eds) (2010) Polymer electrolytes: fundamentals and applications. Elsevier
63. Tasaki K, Goldberg A, Winter M (2011) On the difference in cycling behaviors of lithium-ion battery cell between the ethylene carbonate- and propylene carbonate-based electrolytes. Electrochim Acta 56:10424–10435
64. He T, Zhou Z, Xu W et al (2009) Preparation and photocatalysis of TiO_2-fluoropolymer electrospun fiber nanocomposites. Polymer (Guildf) 50:3031–3036. https://doi.org/10.1016/j.polymer.2009.04.015
65. Li W-L, Gao Y-M, Wang S-M (2012) Gel polymer electrolyte with semi-IPN fabric for polymer lithium-ion battery. J Appl Polym Sci 125:1027–1032. https://doi.org/10.1002/app.33963
66. Isken P, Winter M, Passerini S, Lex-Balducci A (2013) Methacrylate based gel polymer electrolyte for lithium-ion batteries. J Power Sources 225:157–162. https://doi.org/10.1016/j.jpowsour.2012.09.098
67. Sil A, Sharma R, Ray S (2015) Mechanical and thermal characteristics of PMMA-based nanocomposite gel polymer electrolytes with CNFs dispersion. Surf Coatings Technol 271:201–206. https://doi.org/10.1016/j.surfcoat.2014.12.036
68. Deka M, Kumar A (2010) Enhanced electrical and electrochemical properties of PMMA-clay nanocomposite gel polymer electrolytes. Electrochim Acta 55:1836–1842. https://doi.org/10.1016/j.electacta.2009.10.076
69. Ramesh S, Liew C-W, Ramesh K (2011) Evaluation and investigation on the effect of ionic liquid onto PMMA–PVC gel polymer blend electrolytes. J Non Cryst Solids 357:2132–2138. https://doi.org/10.1016/j.jnoncrysol.2011.03.004
70. Park J-K (ed) (2012) Principles and applications of lithium secondary batteries. Wiley-VCH, Weinheim
71. Orbakh D (1999) Nonaqueous electrochemistry. CRC Press, Boca Raton
72. Goren A, Costa CM, Machiavello MT, Cintora-Juarez D, Nunes-Pereira J, Tirado JL, Silva MM, Ribelles JG, Lanceros-Mendez S (2015) Effect of the degree of porosity on the performance of poly(vinylidene fluoride-trifluoroethylene)/poly(ethylene oxide) blend membranes for lithium-ion battery separators. Solid State Ion 280:1–9. https://doi.org/10.1016/j.ssi.2015.08.003
73. Armand M, Tarascon JM (2008) Building better batteries. Nature 451:652–657
74. Sadiq M, Sharma AL, Arya A (2016) Optimization of free standing polymer electrolytes films for lithium ion batteries application. Integr Res Adv 3(1):16–20
75. Stephan AM (2006) Review on gel polymer electrolytes for lithium batteries. Eur Polym J 42(1):21–42. https://doi.org/10.1016/j.eurpolymj.2005.09.017

76. Sharma AL, Thakur AK (2013) Plastic separators with improved properties for portable power device applications. Ionics 19(5):795–809. https://doi.org/10.1007/s11581-012-0760-6
77. Ngai KS, Ramesh S, Ramesh K, Juan JC (2016) A review of polymer electrolytes: fundamental, approaches and applications. Ionics 22(8):1259–1279. https://doi.org/10.1007/s11581-016-1756-4
78. Yap YL, You AH, Teo LL, Hanapei H (2013) Inorganic filler sizes effect on ionic conductivity in polyethylene oxide (PEO) composite polymer electrolyte. Int J Electrochem Sci 8:2154–2163
79. Marcinek M, Bac A, Lipka P, Zaleska A, Zukowska G, Borkowska R, Wieczorek W (2000) Effect of filler surface group on ionic interactions in PEG–$LiClO_4$–Al_2O_3 composite polyether electrolytes. J Phys Chem B 104:11088–11093
80. Wieczorek W, Florjanczyk Z, Stevens JR (1995) Composite polyether based solid electrolytes. Electrochim Acta 40(13–14):2251–2258. https://doi.org/10.1016/0013-4686(95)00172-B
81. Long L, Wang S, Xiao M, Meng Y (2016) Polymer electrolytes for lithium polymer batteries. J Mater Chem A 4(26):10038–10069. https://doi.org/10.1039/C6TA02621D
82. Yan X, Li Z, Wen Z, Han W (2017) Li/Li7La3Zr2O12/LiFePO4 all-solid-state battery with ultrathin nanoscale solid electrolyte. J Phys Chem C 121(3):1431–1435. https://doi.org/10.1021/acs.jpcc.6b10268
83. He D, Cho SY, Kim DW, Lee C, Kang Y (2012) Enhanced ionic conductivity of semi-IPN solid polymer electrolytes based on star-shaped oligo(ethyleneoxy)cyclotriphosphazenes. Macromolecules 45(19):7931–7938. https://doi.org/10.1021/ma3016745
84. Ma T, Yu X, Cheng X, Li H, Zhu W, Qiu X (2017) Confined solid electrolyte interphase growth space with solid polymer electrolyte in hollow structured silicon anode for Li-Ion batteries. ACS Appl Mater Interfaces 9(15):13247–13254. https://doi.org/10.1021/acsami.7b03046
85. Zhai H, Xu P, Ning M, Cheng Q, Mandal J, Yang Y (2017) A flexible solid composite electrolyte with vertically aligned and connected ion-conducting nanoparticles for lithium batteries. Nano Lett 17(5):3182–3187. https://doi.org/10.1021/acs.nanolett.7b00715
86. Liu K, Liu M, Cheng J, Dong S, Wang C, Wang Q, Zhou X, Sun H, Chen X, Cui G (2016) Novel cellulose/polyurethane composite gel polymer electrolyte for high performance lithium batteries. Electrochim Acta 215:261–266. https://doi.org/10.1016/j.electacta.2016.08.076
87. Porcarelli L, Manojkumar K, Sardon H, Llorente O, Shaplov AS, Vijayakrishna K, Gerbaldi C, Mecerreyes M (2017) Single ion conducting polymer electrolytes based on versatile polyurethanes. Electrochim Acta 241:526–534. https://doi.org/10.1016/j.electacta.2017.04.132
88. Liu L, Wu X, Li T (2014) Novel polymer electrolytes based on cationic polyurethane with different alkyl chain length. J Power Sources 249:397–404. https://doi.org/10.1016/j.jpowsour.2013.10.116
89. Chang Z, Zhang M, Hudson AG, Orler EB, Moore RB, Wilkes GL, Turner SR (2013) Synthesis and properties of segmented polyurethanes with triptycene units in the hard segment. Polymer 54(26):6910–6917. https://doi.org/10.1016/j.polymer.2013.10.028
90. Wang S, Jeung S, Min K (2010) The effects of anion structure of lithium salts on the properties of in-situ polymerized thermoplastic polyurethane electrolytes. Polymer 51(13):2864–2871. https://doi.org/10.1016/j.polymer.2010.04.022
91. Bao J, Tao C, Yu R, Gao M, Huang Y, Chen CH (2017) Solid polymer electrolyte based on waterborne polyurethane for all-solid-state lithium ion batteries. J Appl Polym Sci 134(48):45554. https://doi.org/10.1002/app.45554
92. Mustapa SR, Aung MM, Ahmad A, Mansor A, TianKhoon L (2016) Preparation and characterization of jatropha oil-based polyurethane as non-aqueous solid polymer electrolyte for electrochemical devices. Electrochim Acta 222:293–302. https://doi.org/10.1016/j.electacta.2016.10.173

93. Wang S, Min K (2010) Solid polymer electrolytes of blends of polyurethane and polyether modified polysiloxane and their ionic conductivity. Polymer 51(12):2621–2628. https://doi.org/10.1016/j.polymer.2010.04.038
94. Tan R, Gao R, Zhao Y, Zhang M, Xu J, Yang J, Pan F (2016) Novel organic–inorganic hybrid electrolyte to enable $LiFePO_4$ quasi-solid-state Li-ion batteries performed highly around room temperature. ACS Appl Mater Interfaces 8(45):31273–31280. https://doi.org/10.1021/acsami.6b09008
95. Meyer W (1998) Polymer electrolytes for lithium-ion batteries. Adv Mater 10:439–448
96. Scrosati B, Garche J (2010) Lithium batteries: status, prospects and future. J Power Sources 195:2419–2430
97. Wu CG, Lu MI, Tsai CC, Chuang HJ (2006) PVdF–HFP/metal oxide nanocomposites: the matrices for high-conducting, low-leakage porous polymer electrolytes. J Power Sources 159:295–300
98. Tian Z, He XM, Pu WH, Wan CR, Jiang CY (2006) Preparation of poly(acrylonitrile–butyl acrylate) gel electrolyte for lithium-ion batteries. Electrochim Acta 52:688–693
99. Pu WH, He XM, Wang L, Tian Z, Jiang CY, Wan CR (2008) Preparation of P(AN–MMA) gel electrolyte for Li-ion batteries. Ionics 14:27–31
100. Tang JW, Muchakayala R, Song SH, Wang M, Kumar KN (2016) Effect of $EMIMBF_4$ ionic liquid addition on the structure and ionic conductivity of $LiBF_4$-complexed PVdF–HFP polymer electrolyte films. Polym Test 50:247–254
101. Zhang Y, Zhao Y, Gosselink D, Chen P (2015) Synthesis of poly(ethylene-oxide)/nanoclay solid polymer electrolyte for all solid-state lithium/sulfur battery. Ionics 21:381–385
102. Nath AK, Kumar A (2014) Scaling of AC conductivity, electrochemical and thermal properties of ionic liquid based polymer nanocomposite electrolytes. Electrochim Acta 129:177–186
103. Ramkumar R, Sundaram MM (2016) A biopolymer gel-decorated cobalt molybdate nanowafer: effective graft polymer cross-linked with an organic acid for better energy storage. New J Chem 40:2863–2877
104. Ashrafi R, Sahu DK, Kesharwani P, Ganjir M, Agrawal RC (2014) Ag+-ion conducting nano-composite polymer electrolytes (NCPEs): synthesis, characterization and all-solid-battery studies. J Non-Cryst Solids 391:91–95
105. Verma ML, Minakshi M, Singh NK (2014) Synthesis and characterization of solid polymer electrolyte based on activated carbon for solid state capacitor. Electrochim Acta 137:497–503
106. Yang P, Liu L, Li L, Hou J, Xu Y, Ren X, An M, Li N (2014) Gel polymer electrolyte based on polyvinylidenefluoride-co-hexafluoropropylene and ionic liquid for lithium ion battery. Electrochim Acta 115:454–460
107. Fenton DE, Parker JM, Wright PV (1973) Complexes of alkali metal ions with poly(ethylene oxide). Polymer 14:589
108. Yue L, Ma J, Zhang J, Zhao J, Dong S, Liu Z, Cui G, Chen L (2016) All solid-state polymer electrolytes for high-performance lithium ion batteries. Energy Storage Mater 5:139–164
109. Xiao S, Wang F, Yang Y, Chang Z, Wu Y (2013) An environmentally friendly and economic membrane based on cellulose as a gel polymer electrolyte for lithium ion batteries. RSC Adv 4:76–81
110. Xiao SY, Yang YQ, Li MX, Wang FX, Chang Z, YP W, Liu X (2014) A composite membrane based on a biocompatible cellulose as a host of gel polymer electrolyte for lithium ion batteries. J Power Sources 270:53–58
111. Wen H, Zhang J, Chai J, Ma J, Yue L, Dong T, Zang X, Liu Z, Zhang B, Cui G (2017) Sustainable and superior heat-resistant alginate nonwoven separator of $LiNi_{0.5}Mn_{1.5}O_4$/li batteries operated at 55 °C. ACS Appl Mater Interfaces 9:3694–3701
112. Ge Y, Xiao D, Li Z, Cui X (2014) Dithiocarbamate functionalized lignin for efficient removal of metallic ions and the usage of the metal-loaded bio-sorbents as potential free radical scavengers. J Mater Chem A 2:2136–2145

113. Appetecchi GB, Hassoun J, Scrosati B, Croce F, Cassel F, Salomon M (2003) Hot-pressed, solvent-free, nanocomposite, PEO-based electrolyte membranes: II. All solid-state Li/$LiFePO_4$ polymer batteries. J Power Sources 124(1):246–253. https://doi.org/10.1016/S0378-7753(03)00611-6
114. Zaghib K, Striebel K, Guerfi A, Shim J, Armand M, Gauthier M (2004) $LiFePO_4$/polymer/natural graphite: low cost Li-ion batteries. Electrochim Acta 50(2–3):263–270. https://doi.org/10.1016/j.electacta.2004.02.073
115. Manthiram A (2011) Materials challenges and opportunities of lithium ion batteries. J Phys Chem Lett 2(3):176–184. https://doi.org/10.1021/jz1015422
116. Croce F, d'Epifanio A, Hassoun J, Deptula A, Olczac T, Scrosati B (2002) A novel concept for the synthesis of an improved $LiFePO_4$ lithium battery cathode. Electrochem Solid State Lett 5(3):A47–A50. https://doi.org/10.1149/1.1449302
117. Wang J, Sun X (2012) Understanding and recent development of carbon coating on $LiFePO_4$ cathode materials for lithium-ion batteries. Energy Environ Sci 5(1):5163–5185. https://doi.org/10.1039/C1EE01263K
118. Doeff MM, Hu Y, McLarnon F, Kostecki R (2003) Effect of surface carbon structure on the electrochemical performance of $LiFePO_4$. Electrochem Solid State Lett 6(10):A207. https://doi.org/10.1149/1.1601372
119. Costa LT, Sun B, Jeschull F, Brandell D (2015) Polymer-ionic liquids ternary systems for electrolytes: molecular dynamics studies of LiTFSI in an EMIm-TFSI and PEO blend. J Chem Phys 143(1–9):024904. https://doi.org/10.1063/1.4926470
120. Matsumoto K, Endo T (2011) Preparation and properties of ionic-liquid-containing poly (ethylene glycol)-based networked polymer films having lithium salt structures. J Polym Sci Part A Polym Chem 49(16):3582–3587. https://doi.org/10.1002/pola.24795
121. Kovalska E, Kocabas C (2016) Organic electrolytes for graphene-based supercapacitor: liquid, gel or solid. Mater Today Comm 7:155–160
122. Fasciani C, Panero S, Hassoun J, Scrosati B (2015) Novel configuration of poly (vinylidenedifluoride)-based gel polymer electrolyte for application in lithium-ion batteries. J Power Sources 294:180–186
123. Zhu YS, Xiao SY, Li MX, Chang Z, Wang FX, Gao J, Wu YP (2015) Natural macromolecule based carboxymethyl cellulose as a gel polymer electrolyte with adjustable porosity for lithium ion batteries. J Power Sources 288:368–375
124. Choi JA, Yoo JH, Yoon WY, Kim DW (2014) Cycling characteristics of lithium powder polymer cells assembled with cross-linked gel polymer electrolyte. Electrochim Acta 132:1–6
125. Lim DH, Manuel J, Ahn JH, Kim JK, Jacobsson P, Matic A, Ha JK, Cho KK, Kim KW (2012) Polymer electrolytes based on poly(vinylidene fluoride-co-hexafluoropropylene) nanofibrous membranes containing polymer plasticizers for lithium batteries. Solid State Ion 225:631–635
126. Kuo PL, Tsao CH, Hsu CH, Chen ST, Hsu HM (2016) A new strategy for preparing oligomeric ionic liquid gel polymer electrolytes for high-performance and nonflammable lithium ion batteries. J Membrane Sci 499:462–469
127. Nunes-Pereira J, Lopes AC, Costa CM, Leones R, Silva MM, Lanceros-Méndez S (2012) Porous membrane of montmorillonite/poly(vinylidene fluoride-trifluorethylene) for Li-ion battery separators. Electroanalysis 24:2147–2156
128. Padmaraj O, Venkateswarlu M, Satyanarayana N (2014) Characterization and electrochemical properties of p(VdF-co-HFP) based electrospun nanocomposite fibrous polymer electrolyte membrane for Lithium battery applications. Electroanalysis 26:2373–2379
129. Kim JK, Niedzicki L, Scheers J, Shin CR, Lim DH, Wieczorek W, Johansson P, Ahn JH, Matic A, Jacobsson P (2013) Characterization of N-butyl-N-methyl-pyrrolidinium bis (trifluoromethanesulfonyl) imide-based polymer electrolytes for high safety lithium batteries. J Power Sources 224:93–98

130. Kimura K, Matsumoto H, Hassoun J, Panero S, Scrosati B, Tominaga Y (2015) A Quaternary poly(ethylene carbonate)-lithium bis(trifluoromethanesulfonyl) imide-ionic liquid-silica fiber composite polymer electrolyte for lithium batteries. Electrochim Acta 175:134–140
131. Arof AK, Aziz MF, Noor MM, Careem MA, Bandara LRAK, Thotawatthage CA, Rupasinghe WNS, Dissanayake MAKL (2014) Efficiency enhancement by mixed cation effect in dye-sensitized solar cells with a PVdF based gel polymer electrolyte. Int J Hydrogen Energ 39:2929–2935
132. Kang Y, Cho N, Noh KA, Kim J, Lee C (2005) Improvement on cycling efficiency of lithium by PEO-based surfactants in cross-linked gel polymer electrolyte. J Power Sources 146:171–175
133. Samad YA, Asghar A, Hashaikeh R (2013) Electrospun cellulose/PEO fiber mats as a solid polymer electrolytes for Li ion batteries. Renew Energy 56:90–95
134. Polu AR, Rhee HW (2017) Ionic liquid doped PEO-based solid polymer electrolytes for lithium-ion polymer batteries. Int J Hydrogen Energ 42:7212–7219
135. Krishna Jyothi N, Ratnam KKV, Murthy PN, Kumar KV (2016) Electrical studies of gel polymer electrolyte based on PAN for electrochemical cell applications. Mater Today Proc 3:21–30
136. Osman Z, Ghazali MIM, Othman L, Md Isa KB (2012) AC ionic conductivity and DC polarization method of lithium ion transport in PMMA–$LiBF_4$ gel polymerelectrolytes. Results Phys 2:1–4
137. Choi ES, Lee SY (2011) Particle size-dependent, tunable porous structure of a SiO_2/poly (vinylidene fluoride-hexafluoropropylene)-coated poly(ethylene terephthalate) nonwoven composite separator for a lithium-ion battery. Mater Chem 21:14747–14753
138. Kim YJ, Ahn CH, Lee MB, Choi MS (2011) Characteristics of electrospun PVDF/SiO_2 composite nanofiber membranes as polymer electrolyte. Mater Chem Phys 127:137–142
139. Masoud EM (2016) Nano lithium aluminate filler incorporating gel lithium triflate polymer composite: preparation, characterization and application as an electrolyte in lithium ion batteries. Polym Test 56:65–73
140. Rhoo HJ, Kim H, Park J, Hwang T (1997) Ionic conduction in plasticized PVC/PMMA blend polymer electrolytes. Electrochim Acta 42:1557–1579
141. Ma X, Huang X, Gao J, Zhang S, Deng Z, Suo J (2014) Compliant gel polymer electrolyte based on poly(methyl acrylate-co-acrylonitrile)/poly(vinyl alcohol) for flexible lithium-ion batteries. Electrochim Acta 115:216–222
142. He X, Shi Q, Zhou Q, Wan C, Jiang C (2005) In situ composite of nano SiO_2–P(VDF–HFP) porous polymer electrolytes for Li-ion batteries. Electrochim Acta 51:1069–1075
143. Li Z, Zhang H, Zhang P, Li GC, Wu Y, Zhou XD (2008) Effects of the porous structure on conductivity of nanocomposite polymer electrolyte for lithium ion batteries. J Membr Sci 322:416–422
144. Cui WW, Tang DY, Gong ZL (2013) Electrospun poly(vinylidene fluoride)/poly(methyl methacrylate) grafted TiO_2 composite nanofibrous membrane as polymer electrolyte for lithium-ion batteries. J Power Sources 223:206–214
145. Xiao QZ, Li ZH, Gao DS, Zhang HL (2009) A noval sandwiched membranes as polymer electrolyte for application in lithium ion battery. J Membr Sci 326:260–264
146. Li X, Cao Q, Wang X, Jiang S, Deng H, Wu N (2011) Preparation of poly(vinylidene fluoride)/poly(methyl methacrylate) membranes by novel electrospinning system for lithium ion batteries. J Appl Polym Sci 122:2616–2620
147. Wongittharom N, Lee TC, Hsu CH, Fey GTK, Huang KP, Chang JK (2013) Electrochemical performance of rechargeable Li/LiFePO4 cells with ionic liquid electrolyte: effects of Li salt at 25 °C and 50 °C. J Power Sources 240:676–682
148. Galiński M, Lewandowski A, Stepniak I (2006) Ionic liquids as electrolytes. Electrochim Acta 51:5567–5580
149. Lewandowski A, Swiderska-mocek A (2009) Ionic liquids as electrolytes for Li-ion batteries —an overview of electrochemical studies. J Power Sources 194:601–609

150. Madria N, Arunkumar TA, Nair NG, Vadapalli A, Huang YW, Jones SC, Prakash Reddy V (2013) Ionic liquid electrolytes for lithium batteries: synthesis, electrochemical, and cytotoxicity studies. J Power Sources 234:277–284
151. Xu K (2004) Nonaqueous liquid electrolytes for lithium-based rechargeable batteries. Chem Rev 104:4303–4417
152. Kim K, Cho YH, Shin HC (2013) 1-Ethyl-1-methyl piperidinium bis(trifluoromethanesulfonyl)imide as a co-solvent in Li-ion batteries. J Power Sources 225:113–118
153. Menne S, Kühnel RS, Balducci A (2013) The influence of the electrochemical and thermal stability of mixtures of ionic liquid and organic carbonate on the performance of high power lithium-ion batteries. Electrochim Acta 90:641–648
154. Zheng H, Jiang K, Abe T, Ogumi Z (2006) Electrochemical intercalation of lithium into a natural graphite anode in quaternary ammonium-based ionic liquid electrolytes. Carbon 44:203–210
155. Lombardo L, Brutti S, Navarra MA, Panero S, Reale P (2013) Mixtures of ionic liquid-alkylcarbonates as electrolytes for safe lithium-ion batteries. J Power Sources 227:8–14
156. Guerfi A, Duchesne S, Kobayashi Y, Vijh A, Zaghib K (2008) $LiFePO_4$ and graphite electrodes with ionic liquids based on bis(fluorosulfonyl)imide (FSI)- for Li-ion batteries. J Power Sources 175:866–873
157. Lewandowski A, Acznik I, Swiderska-Mocek A (2010) $LiFePO_4$ cathode in N-methyl-N-propylpiperidinium and N-methyl-N-propylpyrrolidinium bis(trifluoromethanesulfonyl)imide. J Appl Electrochem 40:1619–1624
158. Courtemanche RJM, Pinter T, Hof F (2011) Just add tetrazole: 5-(2-Pyrrolo) tetrazoles are simple, highly potent anion recognition elements. Chem Commun 47(47):12688–12690
159. He J, Wang J, Zhong H, Ding J, Zhang L (2015) Cyanoethylated carboxymethyl chitosan as water soluble binder with enhanced adhesion capability and electrochemical performances for LiFePO4 cathode. Electrochim Acta 182:900–907. https://doi.org/10.1016/j.electacta.2015.10.006
160. Qiu L, Shao Z, Wang D, Wang F, Wang W, Wang J (2014) Novel polymer Li-ion binder carboxymethyl cellulose derivative enhanced electrochemical performance for Li-ion batteries. Carbohydr Polym 112:532–538. https://doi.org/10.1016/j.carbpol.2014.06.034
161. Prasanna K, Kim C-S, Lee CW (2014) Effect of SiO_2 coating on polyethylene separator with different stretching ratios for application in lithium ion batteries. Mater Chem Phys 146:545–550. https://doi.org/10.1016/j.matchemphys.2014.04.014
162. Xu Q, Kong QS, Liu ZH et al (2014) Cellulose/polysulfonamide composite membrane as a high performance lithium-ion battery separator. ACS Sustain Chem Eng 2:194–199. https://doi.org/10.1021/sc400370h
163. Zhang J, Yue L, Kong Q et al (2013) A heat-resistant silica nanoparticle enhanced polysulfonamide nonwoven separator for high-performance lithium ion battery. J Electrochem Soc 160:A769–A774. https://doi.org/10.1149/2.043306jes
164. Zhou X, Yue L, Zhang J, Kong Q, Liu Z, Yao J, Cui G (2013) A core-shell structured polysulfonamide-based composite nonwoven towards high power lithium ion battery separator. J Electrochem Soc 160:A1341–A1347. https://doi.org/10.1149/2.003309jes
165. He W, Cui Z, Liu X, Cui Y, Chai J, Zhou X, Liu Z, Cui G (2017) Carbonate-linked poly (ethylene oxide) polymer electrolytes towards high performance solid state lithium batteries. Electrochim Acta 225:151–159. https://doi.org/10.1016/j.electacta.2016.12.113

Chapter 4
Models, SOC, Maximum, Time, Cell, Data, Parameters

4.1 Introduction

Previous studies on the hazards and incidents correlated with thermal runaway in lithium-ion batteries have been studied by numerous scholars [1, 39–41]. The suspected processes which cause the thermal runaway in lithium-ion batteries are obscure even now and required to be researched thoroughly [1]. To seek the physics or chemistry in relation to such uncontrollable reactions and to elucidate the phenomenon of the tremendous self-heat rate when a lithium-ion battery displays thermal runaway necessitate extensive efforts [1]. The plot of pressure versus absolute temperature is capable of verifying whether decomposition or the runaway reaction is a vapour, gassy or hybrid system within lithium-ion battery [1]. Our earlier works on thermal runaway of multiple 14,500 lithium-ion batteries, electrode materials and reaction chemistry between the elements of electrolytes have been investigated step by step by employing DSC and the restricted instrument to examine the obscure thermochemistry inside lithium-ion batteries [1, 42–46]. Four kinds of commercial E-One Moli 18,650 lithium-ion batteries were dynamically screened to thermal runaway under external heating in restricted settings in view of the tolerance limits of thermal abuses [1]. In every sampled E-One Moli 18,650 lithium-ion battery, goals of safety-concerned elements in conjunction with the following points: (1) exothermic onset temperature, (2) adiabatic temperature rise, (3) enthalpy change, (4) maximal temperature, (5) maximal pressure, (6) maximal self-heat rate, respectively, could be corroborated under the abusive circumstances of thermal runaway [1]. Through taking into account important temperature, maximal pressure, maximal self-heat rate in these lithium-ion batteries and maximal temperature, repercussions inferred from credible worst scenarios will be validated [1].

Li-ion batteries consist a positive and negative electrode capable of Li^+ ion insertion/de-insertion, and a separator; this separator is soaked with a lithium salt,

This book was machine-generated

Beta Writer, *Lithium-Ion Batteries*,
https://doi.org/10.1007/978-3-030-16800-1_4

which includes mixture of liquid organic solvents, to assure the rapid transfer of Li^+ ions within the cell [2, 47, 48]. The electrode active materials, enmeshed in a mixture of binder [49] and conductive additive [50, 51], are coated on current collectors, where Cu foil (8–18 μm) is preferably utilized for Al foil (12–20 μm) for the positive electrode [47–51, 52–55, 56–60] and the negative electrode [2, 56]. The negative electrode is forced to accommodate electrons from the positive electrode; these electrons flow via the external current circuit [2]. Li^+ ions, which are retrieved at the positive electrode side into the solution stage and migrate and diffuse via the bulk electrolyte to the negative electrode side, to assure the charge balance are inserted by the negative electrode [2]. The negative electrode acts as the positive electrode as cathode and anode during the discharge process [2]. Throughout charge and discharge of the LIB, the active Li^+ ions are shuttled between two insertion host electrodes in the overall reaction of the LIB portrayed in Scheme [2]. The positive electrode is named as the negative electrode as the anode and the cathode in the remainder of this manuscript and throughout the scientific literature [2].

The groundbreaking cathode material of $LiCoO_2$ where Li-ion can be lithiated and delithiated between cathode [61, 62] and anode had been created by Mizushima and Goodenough [3]. Respectively, safety issue is apparently challengeable till now even after the first commercialization of lithium-ion battery, which employs, which SONY Co. announced, petroleum coke and $LiCoO_2$ as anode [63] and cathode [3]. Lithium transition metal oxides of $LiNiO_2$, $LiCoO_2$, $LiMn_2O_4$, $LiFePO_4$ and $LiNi_xMn_yCo_zO_2$ have been most devised as cathode materials for commercial lithium-ion batteries [3, 64, 65]. The majority of the organic solvents in electrolytes responded with the released O_2 or broken down on the surface of cathode materials to ignite exothermic runaway; this runaway might cause leakage, upsurge, or catch fire or rupture in case of thermal abuses [3]. Trends of thermal stabilities in cathode materials utilized in commercial lithium-ion batteries need to be proclaimed or ranked in entire from the perspective of safety [3]. Reactions of EC with eight cathode materials including Li_xCoO_2, NiO_2, Li_xNiO_2, $Li_xNi_{0.8}Co_{0.2}O_2$, Mn_2O_4, $Li_x\ Mn_2O_4$, $FePO_4$ and Co_3O_4, lithiated transition metal oxides traditionally utilized in lithium-ion batteries, are going to be implemented by confinement tests [3]. Thermal runaway in a lithium-ion battery is always attributable to the most exothermic reaction, which cathode materials with electrolytes led [3]. Phenomena or results on thermal runaway in EC and these delithiated cathode materials are validated to divulge the conflicts emphasised on the thermal runaway in lithium-ion batteries above 200 °C; these batteries are suspected from either anode or cathode apartment [3].

Between the two electrodes, ions shuttle back-and-forth through liquid electrolyte (this electrolyte is made up of a useful lithium salt, including, dissolved in an suitable organic electrolyte) during operation [4]. Porous separator sandwiched between two porous electrodes is contained by the cell [4]. “Consider the discharge operation of this cell” [4]. The ions produced at anode-electrolyte interface because of deintercalation will move toward cathode because of a combined impact of electric field-induced migration and concentration gradient-driven diffusion [4]. Efficient operation of a lithium-ion cell rests on proper functioning of every of these transport mechanisms [4]. The cell performance varies from its theoretical

(thermodynamic) behaviour, which is given various geometrical configurations of operating conditions including multiple stages [4, 66, 67]. Mathematical modelling has demonstrated to be an appealing tool in governing Li-ion batteries examining the physics and helping us understand the behaviour of these cells [4]. Established mathematical models for performance inferences of these cells, with useful instance simulations are described by the present chapter [4]. Thermodynamic, transport, and kinetic, attributes of LIB constituent materials, the building blocks for performance analyses, are thorough first [4]. In the above-mentioned model to clarify the non-isothermal operation of the cell, thermal impacts are integrated, as reasonably well [4]. Deterioration of battery health could be attributable to two sets of events: (a) mechanical impacts-repeated intercalation/deintercalation gives rise to strain lowered effectiveness of the intercalation process and cycling of the electrode materials inducing damage, and (b) chemical impacts-highly reactive lithium metal responds with electrolyte to yield insoluble and/or gaseous commodities, inducing decrease in cyclable inventory [4]. Cell failure can consequence from anomalous operation, i.e., under misuse conditions like thermal misuse [39, 68, 69], and overcharge, external short [4].

Previous studies on the hazards correlated with thermal runaway happened in lithium-ion batteries were studied [5, 39–41]. The suspected processes which cause the thermal runaway in lithium-ion batteries are obscure even now and required to be investigated thoroughly [5]. Explanations among the elements of cells or on the phenomena or results of thermal runaway in lithium-ion batteries are needed more discriminative studies [5]. A entire cell is often introduced in an adiabatic calorimeter to examine the phenomena of thermal potential or runaway hazards in an 18,650 lithium-ion battery [5]. Pressure in relation to absolute temperature is capable of verifying whether decomposition or the runaway reaction is a vapour, gassy or hybrid system in lithium-ion battery [5]. Through restricted instrument to examine the misty thermochemistry inside lithium-ion batteries [42–46]. Thermal runaway of multiple 14,500 lithium-ion batteries, cathode materials responded with organic carbonates and lithium responded with electrolytes, had been efficiently carried out [5]. Runaway under restricted settings, seven kinds of commercial 18,650 lithium-ion batteries are dynamically screened to excessive temperature in pursuit of thermal [5]. Objectives of safety-concerned elements are aiming at the following points: (1) the important temperature in which the temperature will be accelerating or not returnable (2) average value of adiabatic temperature rise (3) enthalpy change in an 18,650 lithium-ion battery (4) maximal temperature could be reached under thermal runaway (5) maximal pressure (6) maximal self-heat rate [5]. Through combining exothermic onset temperature, important temperature, maximal self-heat rate, maximal pressure in these lithium-ion batteries and maximal temperature, repercussions caused from credible worst scenarios will be validated [5].

Lithium-ion batteries are compact, effective, rechargeable [70] and high energy [6]. Under abnormal environmental conditions, the chemical contents of lithium-ion batteries might go via thermal runaway reactions [6]. Such reactions are differing depending upon the kind of electrochemistry inside the lithium-ion battery [6]. Upon the rupture of battery, fire or upsurge is subsequently triggered by the thermal

runaway reactions [6]. Little data exist concerning with upsurge response recommendations and battery fire since the rapid exploitation of high-power lithium-ion batteries into industrial and commercial applications [6]. Use Evaluation and the Lithium-Ion Batteries Hazard had been published by the National Fire Protection Association to offer many research data of lithium-ion batteries fires [6, 71]. Some other scholars have carried out a set of fire experiments about single lithium-ion battery, and the state of charge (SOC) is regarded to be the principal factor of influencing the fires in these studies [6, 72–76]. Parallel and series connection is dangerous cause if one battery undergoes thermal runaway reactions and the other battery intends to balance the voltage or current, the system, which is destroyed maybe [6]. When fire had been caught by one battery, it generates sufficiently heat to cause adjoining batteries to become thermally unstable as reasonably well [6]. Heat propagation and the heating will also be various if the batteries pack is heated in various ways [6]. The 18,650 lithium-ion batteries configurations inside the laptops maybe have a direct relationship with the fire accidents based upon the realistic consideration [6]. This work carried out many experiments in Lhasa in order to investigation the burning variations of various configurations batteries fires [6].

Lithium transition metal oxides ($Li_{1+x}Ni_yCo_zMn_wO_2$, NCM with y + z + w = 1) of various composition frequently substitute the "classic" $LiCoO_2$ (LCO) cathode material in nowadays's lithium-ion batteries (Li-ion batteries) [7, 77]. The NCM stages, frequently denoted as next-generation cathode materials, indicate greater specific capacities because of the addition of nickel and have a lower price than LCO thanks to the content of manganese, whilst still maintaining satisfactory cycleability [7, 78]. A non-negligible contribution to capacity degradation results from gassing, i.e., from the decomposition of electrolyte elements into gaseous compounds, particularly at elevated temperatures [7]. A thorough and systematic examination of these gassing mechanisms is unavoidable in order to observe an approach for the development of enhanced complete cells employing NCM cathodes [7]. It is the result of electrolyte and/or electrode material oxidation at the cathode side due to the requirement for high terminal voltages [7]. That the in situ identification of CO through quadrupole mass spectrometry in a gas mixture is not clear-cut, since CO_2 modes molecular pieces that superimpose the CO spectrum is pointed out by us [7]. The Ni-rich NCM523 stage is one of the main marketed NCM materials [7]. In NCM523-based complete cells, we present a comprehensive analysis of the gassing phenomena [7]. We indicate the longer-term cycling tests, the details of the first cycle, the gassing during a characteristic battery formation cycle, and the gases because of SEI formation [7].

It is required to carry out an additional investigation on the thermal attributes of Li-ion batteries to have a better understanding of LIB safety [8]. Under outer radiation, Wang and others [79] and Huang and others [80] examined the combustion behaviours of large-scale lithium-ion battery by assessing flame/surface temperature, flame topography and mass deterioration rate, heat release rate [8]. Some experiments have been carried out to examine the effect of state of charge (SOC) on the fire behaviours of Li-ion batteries [8, 73, 75, 76, 81]. Under the help

of cone calorimeter, Fu and others [75] and Chen and others [76] had taken experiments of Li-ion batteries with various SOCs (0–100%) and observed that LIB with greater SOC might owns greater fire hazards [8]. Ye and others [82] evaluated the thermal behaviours of Li-ion batteries under power cycling with the help of accelerating rate calorimeter (ARC) and the charge/discharge cycle instrument under adiabatic condition [8]. That the temperature rise or temperature rise rate increasing with the growth of circulation rate and the temperature of Li-ion batteries had been greater under discharge condition had been founded by Ye and others, [8]. Scarce work examines the thermal runway of Li-ion batteries with various SOCs under discharging condition, particularly for the overcharge condition, and variations in the thermal fire and runaway behaviours of Li-ion batteries without discharging and with had not been examined [8]. Cone calorimeter, as an crucial apparatus in the evaluation of combustible materials, has not been utilized to analyze the fire behaviours of Li-ion batteries under discharging condition [8]. This work aims to examine the thermal behaviours of Li-ion batteries with and without discharge employing the cone calorimeter in order to fill in the disparity [8].

Up to their full destruction, overdischarge, i.e., overreaching certain minimum allowable voltage region upon discharge of a lithium battery is regarded to consequence in the irreversible degradation of cathode materials [9]. Overdischarge phenomena have been researched for batteries with $LiCoO_2$ [83], $LiFePO_4$, $LiMn_2O_4$ cathodes [84], and $LiNiO_2$ [9]. Say, a conclusion, which is drawn for cells with $LiCoO_2$, cathodes [85] states that declining voltage to below than 1.5 V triggers no significant capacity losses [9]. In the composition ranges of $0 \leq x \leq 0.5$ and $0.5 \leq x \leq 1.0$. In the composition ranges of $0 \leq x \leq 0.5$ and $0.5 \leq x \leq 1.0$, the reaction occurs in two phases the electrochemical intercalation/deintercalation of lithium-ions into/from the lattice happens at about 4 V, if the lithium manganese spinel $LiMn_2O_4$ is utilized as a cathode. though the spinel keeps its cubic structure (space group Fd3m, Z = 8) [86–88] with the lattice parameter a = 8.248 Å and the unit call volume V = 539.75 $Å^3$ [9]. That upon longer-term cycling, particularly at small overdischarge, the surface of $LiMn_2O_4$ particles enriches with lithium is emphasised by coworkers and Thackeray [9]. That implies tetragonal $Li_2Mn_2O_4$ arises, the Jahn-Teller reconfiguration, and finally Li_2MnO_3 and soluble MnO are forming via the disproportionation reaction [89, 90] as That means that upon longer-term cycling, a combined overdischarge and break-up impacts reshape the better part of electrode material from $LiMn_2O_4$ to Li_2MnO_3 reasonably well detectable in XRD researches [9]. Another can conclude that overdischarge substantially increases the probability of its occurrence, and the formation of $Li_{1+x}Mn_2O_4$ in modern Li-ion batteries is a negative phenomenon [9].

A crucial dimension in the application of Li-ion batteries (Li-ion batteries) with liquid, flammable and volatile organic solvent-based electrolytes [91–95] is safety [10]. The analysis of organic electrolyte additives in LIB and organic carbonate solvents electrolytes through GC is reasonably well established [10]. The majority of researches, revolved around the identification through utilized GC-FID or GC-MS for quantification and utilized organic solvents for the dilution of samples prior to liquid injection [10, 96–99]. They, diluted their samples with the organic

solvent acetonitrile whilst the organic carbonates dimethyl carbonate (DMC), diethyl carbonate (DEC), ethyl methyl carbonate (EMC) and propylene carbonate (PC) with limits of detection (LODs) in the variety of 11.7–31.7 mg/kg had been efficiently quantifyed by Grützke and others [10, 100]. Sloop and others [101, 102] firstly diluted LIB electrolyte solutions with water in contrast to most researches [10]. The focus of this work had been the development of a quantification technique for the organic carbonates EMC, DEC, ethylene carbonate (EC) and vinylene carbonate (VC) in aqueous solutions of cell culture medium and cell pellet solutions incubated with commercial LIB electrolytes based upon a liquid-liquid extraction and subsequent analysis through GC-MS [10]. The technique had been validated and utilized for the transfer across the blood-cerebrospinal fluid (CSF) barrier in a porcine cell culture model to gain more insights into the toxic impacts of these compounds and the analysis of the cellular uptake of organic carbonates in human lung adenocarcinoma cells [10].

The transition metal intercalation oxides have induced the main research interests as the LIB cathodes since layered $LiCoO_2$ had been firstly utilized as a cathode material for Li-ion batteries in 1991 [11]. The traditional cathode materials include layered $LiMO_2$ (M = Co, Ni, Mn) compounds [103–105], Li-rich materials [106], spinel $LiMn_2O_4$ [107], orthorhombic structure Li_2MSiO_4 (M = Fe, Co, Mn, Ni) compounds [108, 109], olivine $LiMPO_4$ (M = Fe, Co, Mn, Ni) compounds [110, 111], and tavorite $LiMSO_4F$ (M = Fe, Mn, Co) [11, 112, 113]. The layered $LiMO_2$ (M = Co, Ni, Mn) compounds have been the most intensively utilized and examined cathodes, though they suffer from greater cost ($LiCoO_2$), toxicity ($LiCoO_2$), thermal turbulence ($LiNiO_2$), serious voltage decay (Li-rich material), systemic turbulence ($LiNiO_2$), and serious security ramifications ($LiNiO_2$) and ($LiCoO_2$) [11]. Several non-toxic polyanionic compounds including $LiMSO_4F$, and $LiMPO_4$, Li_2MSiO_4, have aroused interest for use as possible cathode materials in Li-ion batteries, though the inherent inferior electronic electrical conductivity and low ionic diffusivity, including the systemic turbulence because of Jahn-Teller distortion Li_2MnSiO_4, ($LiMnPO_4$, and $LiMnSO_4F$) restrict the practical application [11]. Spinel $LiMn_2O_4$ is one of the most sought-after cathode due to low toxicity, its safety, and high thermal stability, though the meager high-temperature performance restrict its additional application because of the Jahn-Teller distortion of the structure [11]. $LiNi_{0.5}Mn_{1.5}O_4$ has been viewed as one of the most fruitful high-voltage candidate for lithium-ion batteries [11]. It is required to observe suitable electrolyte systems to then exert the perfect electrochemical performance of $LiNi_{0.5}Mn_{1.5}O_4$ material, and increase the stabilization of a $LiNi_{0.5}Mn_{1.5}O_4$ cathode/electrolyte interface [11]. "The stability of electrolytes at high voltages become a constraining factor for the development of $LiNi_{0.5}Mn_{1.5}O_4$ electrode" [11].

That becomes a primary concern for battery users, and consequently a non-destructive technique is needed to access the harmful effect of the overcharging in order to decide if one must change the cell from the safety and validity viewpoint [12]. Whether one can pinpoint the internal elements in a cell that are most susceptible to excessive cut-off voltage COV, they can enhance their cells so as to make the cell more reliable against this misuse from battery manufacturers point of

view [12]. The degradation of every individual elements inside a cell could be dictated via its discharging curve (i.e., terminal voltage versus time during discharging) alone with the recent development of electrochemistry-based electrical (ECBE) model (Leng and others [114]), [12]. The ECBE technique is utilized by us to analyze the effect of excessive COV on the degradation of every element experimentally [12].

Gases formed in the sealed cells give rise to the buildup of internal pressure and swelling of the cell, de-contacting of the active material and hence present safety difficulties [115] and de-lamination of the electrodes [13]. In an LIB that can sometimes be detected after the battery has been utilized for many time or after electrical misuse tests, a characteristic instance is the swelling [13]. The swelling normally results from the reductive decomposition of the electrolyte on the negative electrode; this electrode gives rise to excess pressure within the cell [13, 116]. Gas bubbles on the graphite electrodes in LIB cells employing in situ neutron image analysis [117] were detected by Goers and others [13]. Such authors did not carry out experiments to examine the traces of gas bubbles generated in the process of disassembling the cell or inside the disassembled cell [13]. In dry rooms, Commercial LIB manufacturers usually assemble batteries to lessen the moisture within the cells [13]. The wound cell is positioned in a foil pouch or an aluminium body case, and linkages are made between the external battery terminals and the electrodes [13]. The link between the swelling of those batteries during their cycle life and the generation of gas bubbles in prismatic batteries during longer-term storage has not been indicated yet [13]. Throughout longer-term storage, which employs cell disassembly analysis and CT, the electrode deformation phenomena of cells and the initial generation of gas bubbles had been examined by us, and we carried out a failure analysis on the swelling that happens during the lifecycle of the battery such as longer-term storage [13].

Due to its well-established advantages, i.e., high theoretical capacity (roughly 170 mAh g^{-1}), low cost, useful lithium-ion insertion/extraction potential (roughly 3.45 V vs. Li^+/Li) [111, 118, 119], and low toxicity, olivine-type lithium iron phosphate ($LiFePO_4$) electrode has extensively aroused attention [14]. The well-established combination of the positive electrode of $LiFePO_4$ in lithium-ion battery and negative electrode of graphite are one of the most fruitful candidate power sources for electric vehicle [14, 120, 121]. A complex set of interacting mechanisms is Lithium-ion battery ageing [14]. A variety of various ageing processes for lithium-ion batteries have been devised, such as deterioration of electrolyte, separator, active materials, and composite electrode structure, including evolution of solid electrolyte interphase (SEI) [14, 122–124]. Post mortem analysis confirmed the break-up of Fe^{2+} from the $LiFePO_4$ electrode and its subsequent deposition on the carbon anode; this anode acts as a catalyst that accelerates the formation of SEI layer and continually consumes active lithium [14]. Through employing multiple methods, such as destructive analyses on internal materials [125–127] and nondestructive electrochemical techniques, taking into account the wide range of processes contributing to the ageing of lithium-ion batteries, we diagnosed battery ageing [14]. Electrochemical methods, including galvanostatic

cycling at differential capacity and differential voltage analyses [128–135] and various rates [136, 137], offer an evaluation of kinetic deterioration, which results from increase in resistance, and low-rate capacity deterioration [14]. Destructive techniques, such as half-cell test, scanning electron microscopy (SEM), and X-ray diffraction (XRD), were carried out to additional clarify capacity fading [14].

Spent LIB are rich source of useful metals like lithium, cobalt, manganese, nickel, aluminium, copper, etc. [15]. Several chemical and physical mechanisms have been indicated which comprises crushing, dismantling, sieving, electrochemical techniques and chemical precipitation to effectively recover the useful metals [15]. Through employing separation and chemical precipitation, alkaline or acidic leaching is undertaken for extraction of useful metals in hydrometallurgical process [15]. In the scientific literature, it is indicated that the leaching efficiency of the useful metals employing the strong acids lies in the variety of 85–99% [138, 139] while for weak acids lies in the variety of 70–99% [15, 140, 141]. Leaching efficiency comprises of efficiencies of all the steps incurred in extraction of the useful metals [15]. Extractions of useful metals from the spent lithium-ion battery comprise of three principal steps, viz. (1) peeling of active cathode materials from the cathode (2) electrode break-up of active materials into the acid (3) and extraction of useful metals from the dissolved active materials employing chemical precipitation [15]. The high efficiency of these steps eventually results in high recovery of useful metals [15]. Whether high purity of retrieved metals is accomplished then those metals in the form of oxalates or carbonates could be combined to form the active cathode material for consequently overexploitation rate from global reservoir of these metals could be lowered to many extent and manufacturing of cathode of the lithium-ion battery [15]. The cobalt oxalate is retrieved employing precipitation technique at the optimum operating condition with effective technique with high purity [15].

An experimental parametric investigation to evaluate the thermal attributes of heat pipe cold plates (HPCPs) for lithium-ion cell/pack with numerous cooling methodologies and various charge rates had been carryed out by Ye and others [16, 142]. The excellent thermal performance of heat pipe, which is premised BTMSs primarily on the cooling effect at constant charge/discharge rate with various configurations, had been shown by the above pertinent studies [16]. Given the miniaturization and compaction of the cooling/heating device to satisfy the requirements on arrangement and optimum structure in EVs, the advantage of heat pipes' bi-directional feature must be completely employed for high-efficient heat pipe BTMS and a well-design to offer not just satisfactory cooling effect at high temperatures though also excellent preheating performance under low temperatures [16]. The principal contributions of this work are developing such a small sized heat pipe and presenting its application to a BTMS with both cooling and heating, and then the experimental temperature attributes of UMHPs could be carried out to guide thermal analysis and optimization of heat pipe BTMSs [16]. This chapter explains an UMHP BTMS for a lithium-ion battery pack, which is utilized in EVs; and introduce an experimental setup established for thermal assessment of the UMHP pack; then the cooling performance of the UMHP pack is assessed under

constant discharging conditions and transient heat inputs on the federal urban driving timetable (FUDS) highway condition, and two preheating techniques by sticking (1) on the surface of cells, heating films and, (2) on the fins of UMHPs are compared to evaluate the heating efficiency under subzero temperatures in this chapter; finally, numerous conclusions are drawn [16].

That well-established statistical techniques, e.g. the log-linear model [143], characterize satisfactorily the link between the design parameters [144–147] and the battery life-time had been demonstrated by some researches [17]. Owing to the huge number of contextual factors engaged, some problems persist to solve the issue of the battery size optimization over a prefixed time horizon of interest [17]. Cycle life (CL, as assessed by the charge-discharge cycles), or battery life-time, depends upon some parameters, including design maximal specific power, operating environment, depth-of-discharge, etc. [17, 148]. In real operating conditions, the randomness of the above parameters, reliable techniques to examine these dependences are required, since these uncertainties might cause significant differences in cycle-life estimation, so that huge variations are detected between the battery CL, which is supposed experienced and, as exhaustively demonstrated in a number of experimental works [149–151] by taking into consideration [17]. A number of researches, which is based upon stochastic technique for calculating the likelihood distributions of the battery life-time, have been lately dedicated to observe accurate solutions to such an issue [17]. With a proper stochastic input, had been devised for deducing the battery life-time, adopting a probabilistic strategy, based on an extension of the (deterministic) Virudhula and Rakhmatov battery model [152, 153] in [154] an advanced battery model [17]. In [155] the devised probabilistic technique has been utilized to the design of lead-acid battery modules [17]. The technique enable to conceptualize battery module parameters that assure, with a high extent of likelihood, that the CL is greater than a prefixed value by stemming the time-to-failure probabilistic density function from a statistical analysis of experimental data [17].

Battery models are a crucial element of a dynamic electric vehicle simulator [18, 156]. It is hence required to build battery models; these models precisely imitate real battery attributes [18]. The models should be fast, highly reliable, straightforward, should imitate the attributes that conceptualize a battery and less memory intensive [18]. Battery models that are included in EVs/HEVs should be capable of reliably predicting SOH and the SOC to enhance the validity of the vehicle [18]. In considerable detail, electrochemical models [157–159] characterize the battery chemistry making these models highly reliable [18]. Such models seem to become too complex as a set of partial differential equations describing diffusion phenomena and the ion transport, mass and charge balance, temperature and ion distribution impacts have to be resolved to observe the behaviour of battery [18]. Both models depend on the high-level representation of battery with analytical expressions based upon physical regulations [18]. Such models are useful and computationally complex for predicting just individual behavioral facets of the battery [18]. Complex impedance network is utilized by these models to match the battery ac response [18]. The ability of these models to match the complex transient attributes

of the battery is restricted, as reasonably well [18]. Such models are misleading and considerably complex in predicting battery attributes [18]. The focus of this work is modelling the steady-state and transient behaviour of battery, which employs Thevenin-based circuit model [18]. The transient I-V and steady-state performance of battery is persuasively replicated with the model [18]. Battery internal voltage, which is constituted as CVS, is experimentally demonstrated to be various from OCV and it is modelled as a function of SOC [18].

Commonly utilized battery models include electrochemical models [160] and equivalent circuit models [19]. Following the dynamic attributes and working principles of batteries, the equivalent circuit model is devised employing resistors, voltage sources, and capacitors, to form a circuit network [19, 161, 162]. A straightforward model is normally reluctant to reflect all the dynamic impacts of a battery, which might consequence in errors in the identification of parameters; hence, the precision of the equivalent circuit model must be enhanced [19, 163]. The electrochemical model of a lithium-ion battery, which Newman (the DFN model), and Doyle, Fuller, devised, is based upon porous electrode theory and concentrated solution theory [19, 164]. An electrochemical model can be an accurate and reliable candidate for the model-based design of battery management system (BMS) [19, 165]. A single-particle model (SPM) is set up following [166] to generate an reliable and straightforward electrochemical model of a battery [19]. The model captures most of the electrochemical reaction inside the battery, is more reliable than the equivalent circuit models, and has a simpler structure than the DFN model [19]. The single-particle model of a lithium-ion battery includes fewer parameters than the DFN model, though it is time, which consumes and complex to pinpoint all the parameters in the model [19]. Initially, a single-particle model, which explains the electrochemical attributes of a lithium-ion battery, is set up based upon the electrochemical reaction mechanism [19]. The single-particle model is simplified employing the volume-average integration technique and the three-parameter polynomial approximation technique [19]. Through the BFOA, the parameters characterizing the electrochemical attributes of the single-particle model are identified [19].

Dynamical models of the battery pack could be a useful tool to design these estimators [20]. In the scientific literature for this sort of batteries including purely electric models [167] or fuzzy models [168], or electrochemical models [169–171], some models exist [20]. An extensive analysis on Li-ion batteries modelling is devised in [20, 172]. Fractional order models, models that could be explained by fractional differential equations [173, 174], are devised [20]. These an strategy makes it possible to convey the parameters of the simplified model as a function of the electrochemical and dimensional constants of the lithium-ion cell [20]. That model has an crucial physical meaning, unlike purely electric models devised in the scientific literature [20]. The introduction of fractional differentiation that enables to characterize many parts of the model with a small number of parameters again directly linked to the electrochemical parameters of the battery is another interest [20]. That last model is utilized to design a State of an aging estimator and Charge (SOC) [20]. A solution is devised to conceptualize if the model parameters adjustment is needed as because of aging model and cell behaviour discrepancy [20].

There are also various explanations for disagreements among discussed models [175]: the specific experimental conditions and the dependency of delithiation/lithiation kinetics and stage compositions on the morphology, the particle size, and physical properties of the $LiFePO_4$ material, which is researched to name a handful [21]. The "many-particle" model had been introduced by Dreyer and others [176, 177], which posits that equilibrium potential of LFP material is a non-monotonic function of lithium concentration and lithiation/delithiation of particles happens randomly [21]. Farkhondeh and others devised a mesoscopic model [178] to circumvent this limitation of quasistatic operation of the LFP electrode and to incorporate a mechanism for mass transfer/phase transition within individual particles [21]. In Safari and Delacourt [179]'s RR model introduced to emulate LFP, Delacourt [179] and Safari presumed four spherical particle groups with various electronic connectivities to the conductive matrix though with the identical particle size [21]. They are still not ideally suited to performing tedious researches including ageing and battery pack level simulation and examine the cycling conditions even though VSSD and RR models appear satisfactory methodologies to emulate the inferior electronic electrical conductivity of LFP and the slow solid-state Li ion transport [21]. Aiming at introducing a straightforward model to take into consideration the resistive reactant characteristic of LFP, Marcicki [180] combined his simplified lithium-ion battery model with a resistance; this resistance differs linearly with the depth of discharge (DOD) [21]. His modelling results indicate a satisfactory concordance when compared to experimental data derived from a cylindrical graphite/iron phosphate cell for a variety of galvanostatic discharge experiments from C/3 to 4.8 C. Nevertheless, there is also a need to investigation the resistive reactant effect of LFP in the entire fraction of discharge/charge curves of a Li/LFP cell [21].

The microstructure of the optimized electrode gives rise to increasing surface area, shorter lithium-ion transport pathways, collectively resulting in a significant enhancement of the battery performance [181–183], and enhanced inter-particle active material relationships [22]. LIB models that characterize electrode structures are grouped into four distinct groups: (1) models that characterize electrodes comprising of homogeneous single-sized spherical particles [164, 184, 185]; (2) models that characterize electrodes consisting of multi-sized spherical particles [186–188]; (3) models that employ sophisticated mathematical techniques to emulate electrode structures [189–191]; (4) models that reconstitute real electrode microstructures employing two imaging techniques of X-ray tomography (XCT), which is computed, and focused ion beam-Scanning electron microscopy (FIB-SEM) in the scientific literature [22]. The group (4) model which employs reconstruction of real electrode morphologies has been made possible with recent advancements in 3D imaging technologies [22]. Several groups have devised models to predict LIB performance, which is based upon real 3D electrode microstructures [22]. That the distribution of lithium-ion concentrations, global polarization, which XCT-based electrode model obtained, and current density, were substantially various from those of 1D single-sized spherical models had been demonstrated by Yan and others [22, 192, 193]. The 3D electrode morphology,

which employs nano-XCT, had been reconstructed by us, whilst for macro-scale, the galvanostatic discharge behaviour had been simulated by utilizing Newman psedudo-2D model [157, 158] and the homogenization theory for the micro-scale model [22]. The multiscale model included the real 3D morphology of the electrode and had been an amelioration over the Newman pseudo-2D model, while the present RVE model is an advancement over the single-particle model [194, 195]; this model enables the formation of a computationally effective conceptual framework for such as reconstructed 3-D morphology of the electrode [22].

There are some useful research works on prognostics and the battery degradation modelling for battery SOH estimation [196, 197] in recent decades [23]. In the SOH estimation of battery, in which the empirical degradation models are frequently utilized to develop the dynamical system equation, Stochastic filtering methodologies including Kalman filtering [198], extended Kalman filtering [199, 200], Bayesian filtering [201] and unscented filtering are extensively devised [23]. Some methodologies have been devised including the Dempster-Shafer theory for battery SOH estimation and RUL prediction [202] and a prognostic algorithm, which is based upon a Bayesian Monte Carlo technique [23]. Liu and others [203] utilized the Gaussian process regression (GPR) to carry out SOH prediction for lithium-ion battery, where the degradation trends are learnt from battery data sets with the combination of Gaussian process functions [23]. A new strategy to lithium-ion battery SOH estimation is summarized via the integration of particle filtering and the MGP model learning [23]. The devised technique comprises of two stages, and the first is the MGP is utilized to learn the statistical properties of the degradation model parameter, which integrates training data sets from unclear battery conditions [23]. Following the parameter distribution information for the degradation process, particle filtering is exploited to derive the battery SOH estimation [23]. In two points, the contributions of the present study could be presented: the first is a fusion prognostics conceptual framework for the lithium-ion battery SOH estimation is devised by combining the degradation conditions from various batteries, the second is the devised algorithm implements distribution, which learns for the multimode process under uncertainty [23].

The lithium-ion and NiMH batteries have a considerable potential for a greater efficiency HEVs [24]. A big advancement in HEVs necessitates to generate novel designs capable to incorporate the lithium-ion battery technologies with vehicles engines of high efficiency, as is noted in [24, 204]. The lithium batteries design must be congruent in conformity with the international standards specs for “vibration, shocks, temperature effects, acceleration, crush impact, heat, overcharge and over-discharge cycles, and short circuit”, as is discussed in [24, 204, 205]. A lithium-ion battery cell has a short term life because of the inside presence of physical transformations that affect significant its electrical performance [205] or the undesired irreversible chemical [24]. The Li-Ion battery SOC remains one of the main operational condition battery parameter, which BMS monitored tightly, though it can not be assessed directly [24]. The reason for this model selection is to profit of its simplicity and its ability to uncover reliably the whole dynamics of Li-Ion battery, and to be implemented readily in real time with satisfactory variety

of performance [24]. Extensive simulations undertaken in MATLAB R2017a simulation environment demonstrated that this electrical circuit model is comparatively reliable to uncover the principal dynamic circuit attributes of a Li-Ion battery cell, including the open-circuit voltage, transient response, and terminal voltage [24]. The NREL Li-Ion battery model, which is integrated in ADVISOR MATLAB platform, is a Li-Ion battery model 6 Ah and nominal voltage of 3.6 V generated by the corporation SAFT America, as is discussed in [24, 205, 206].

Batteries are the prototypical easily accessible storage device, and Li-ion batteries are among the most helpful because of low rate of self-discharge [207] and their high energy density [25]. In tools ranging from cell phones to electric vehicles, Li-ion batteries are observed and will continue to remain crucial for these and other energy storage applications in the future [25]. That work examines how Li-ion batteries could be utilized to transform mechanical work into electrical energy, a property; this property has not been examined in detail [25]. Previous work on battery electrode mechanics has examined how strains and utilized emphasizes can affect electrochemistry for multiple systems, such as lithium-silicon, sulfuric acid-graphite [208–214], and lithium-graphite [25]. The results of this earlier research were extended to graphite electrodes, and a straightforward conservation of energy model finds a comparable linear correlation between a corresponding increase in voltage [208] and utilized strain on a battery [25]. In energy harvesting applications, the coupling between electrochemistry and mechanical strain could be employed [25]. Battery intercalation materials, or "piezoelectrochemical" materials, exploit of the stress-voltage coupling in intercalation materials and harvest energy at exceedingly low frequencies (less than 1 MHz) [25]. Two antiparallel Li-ion batteries linked via an external load were utilized by us to highlight how to harvest small quantities of energy by squeezing one battery [25, 215]. We build a model to then use this model to describe the harvesting system and specify its maximal theoretical efficiency and investigation the process with Li-ion batteries, which harvests piezoelectrochemical [25]. Our model leverages the fundamental coupling between electrochemistry in battery materials and mechanics and could be utilized to other intercalation materials to predict their efficacy for energy harvesting applications [25].

The mechanical integrity of Li-ion batteries has captured the interest of technicians and scientists from the fields of electrochemistry, mechanics, and material science, thereby becoming a hot research topic [26]. Several loading conditions, including indentation [216, 217], radial compression [216, 218, 219], and bending [216, 220], on completely drained Li-ion batteries with low state of charge (SOC), were utilized to imitate real-life loadings to comprehend mechanical-electrochemical behaviours [26, 216, 218, 219, 221]. The qualitative onset of short-circuit criteria had been dictated on the basis of the mechanical behaviours of Li-ion batteries to aid mechanical integrity [26, 216]. Owing to the continuous charge/discharge cycles of batteries, state of health (SOH) of Li-ion batteries and the SOC continually differ, which gives rise to various strain statuses within the cell [26, 222, 223]. That the mechanical properties [224, 225] and volumes [226] of the active particles change due to differing SOC values had been shown by recent evidences [26]. The qualitative relationship between mechanical behaviours and SOC status were dictated via

experiments [227] to additional reliably characterize and predict the electrochemically reliant mechanical behaviours of Li-ion batteries exposed to abusive mechanical loadings [26]. The coupling effect that induced SOC and SOH and the lifecycle of Li-ion batteries were not regarded [26]. Through choosing 18,650 Li-ion batteries as target cells, the present study analyzes the mechanical integrity behaviour of Li-ion batteries under various SOC and SOH values to bridge this disparity [26]. Governing parameters that describe the mechanical integrity of Li-ion batteries are presented, compared, and examined at various SOCs and SOHs and among various kinds of Li-ion batteries [26]. The experimental results on the three kinds of batteries are outlined by forth this chapter [26].

The majority of the capacity deterioration, which is detected in the first lithiation/delithiation cycle of secondary lithium-ion batteries, is because of this SEI layer formation [27]. Previous studies [37, 228–230] have demonstrated that surface coatings including SiO_2 on nanotubes and nanoparticles can enhance the cyclic performance of high energy density electrode materials by stabilizing the SEI layers and minimizing the mechanical degradation [27]. In SiO_2 samples, depending upon the subsample configuration (nanoparticle, nanotube, or thin film); electrochemical conditions (charge rates, potentials, or potential sweep rate); and kind of materials in contact (electrolyte and components of composite electrode), a combination of two concurrent reactions, either one reaction, or all possible reaction processes take place simultaneously during lithiation/delithiation [27]. Through numerous other researches [228, 231, 232], they were able to cycle the films reversibly with stable capacities of $\sim$500 mAh/g, implying that the $Li_2Si_2O_5$ reaction is reversible; this had been revealed [27]. Some crucial questions relating to their mechanical behaviour remain unanswered even though the characterization researches [231–236] enabled in understanding electrochemical and systemic change behaviour of lithiated SiO_2 commodities and the material design efforts [37, 228, 229, 230] caused in innovative core-shell microstructures [27]. That the mechanical properties of electrode materials (both anodes and cathodes) change during electrochemical cycling had been indicated by numerous researches [213, 237–241]; and similarly, the properties of SiO_2 might change continually during the lithiation/delithiation process because of the formation and decomposition of reaction commodities in (Eqs. 1–3), [27]. The primary aim of the present study is to measure the magnitude of emphasizes produced in SiO_2 material, additional, comprehend how the variability of mechanical properties affect the mechanics of core-shell kind of particles, and comprehend how these emphasizes differ during electrochemical cycling [27].

Mechanical failure, which emerges from the insertion/extraction of lithium-ions, is one of the principal reasons for capacity deterioration of electrodes [242] as is well-established [28]. Plenty of scientific literature clarified the mechanism of electrode failure based upon the diffusion-induced strain [28, 243–249]. Verbrugge and Chen devised analytic expressions of strain within a spherical electrode particle under either potentiostatic or galvanostatic operation [28, 247]. The quantitative trends for isotropic electrode particles could be given by this analysis, though might be an over-simplification for anisotropic electrodes and can not elucidate many experimental results of anisotropic electrode; this electrode encourages us to investigation

the impacts of anisotropy and to shed light on something various though significant for battery design or battery application [28]. Regrettably, researches of anisotropic electrodes are still restricted, and the specific impacts of anisotropic properties on the diffusion-induced strain for spherical electrodes have not been indicated [28]. The researched electrodes are posited to be spherically isotropic (i.e., the special case of anisotropy) [28]. The first one is that no experimental data ascertain that spherical electrode particles are all isotropic [28]. The second is the existence of spherically isotropic complete and medium anisotropic electrodes [28, 250, 251]. We, based upon this premise, focus considerably attention on the impacts of anisotropic properties on the diffusion-induced strain inside spherically isotropic electrodes; these electrodes might show many positive signals for anisotropic electrodes in practical application [28]. Our findings indicate that more depth of delithiation (or lower depth of lithiation), which lithiation (or delithiation) followed, is a satisfactory approach to minimize strain and improve battery performance for anisotropic elastic electrodes [28]. It is plausible that the principal results in the present study are instructive for complete anisotropic electrodes [28].

The volumetric change for the silicon electrode is considerably bigger than the carbonaceous anode [29]. That might consequence in substantially high emphasizes and henceforth cracking or delamination of the electrodes [29, 252]. Patterned silicon islands are fabricated as active material [253], which might avoid the in-plane cracking [29, 254]. The delamination in the interface between current collector and active material still exists [29, 252, 253]. In thin film electrodes, the delamination had been tackled by numerous experimental and theoretical works [29]. The shear-lag model had been utilized by Haftbaradaran and others [255] to predict the critical size, in which the energy release rate is utilized as the delamination criteria in both 2D and axisymmetric structure [29]. Following the cohesive model Pal and others [256] revolved around the influence of elasto-plastic deformation in the current collector on interfacial delamination [29]. The evolution of the interfacial delamination has been researched by utilizing the cohesive model under the axisymmetric condition [29]. Plane strain and plane stress are two extreme instances for the 3-D issue of the rectangular plate to many extent [29]. The edge surface of the rectangular plate is in accord with the plane strain condition [29]. The stress/strain conditions in the rest region of the rectangular plate are in many measure between plane strain and plane stress [29]. The plane analysis will be utilized to assess the delamination for the rectangular island electrode as two extreme instances [29].

The volume change of anode electrode active materials can trigger huge emphasizes; these emphasizes can cause damages of the electrode including delamination and crack when the solute atoms migrate to the anode in Li-ion batteries [30, 253, 257, 258]. The stable crack growth in hollow nanoparticles had been studyed by Aifantis and others [259] spherical electrode [30]. Some literatures have investigated the strain fields of hollow spherical electrode theoretically and experimentally [30]. Yao and others [260] researched the interlinked silicon hollow nanospheres and indicated that the emphasizes of the hollow electrodes are smaller than that of solid ones [30]. Liu and others [261, 262] established a theoretical conceptual framework to investigation the strain fields in hollow core-shell spherical electrodes, and offered explicit

formulations for the emphasizes [30]. The coupling effect between electrochemical reactions and DIS in lithium-ion battery electrodes has not been studied systematically [30]. The process of electrochemical reaction will simultaneously take place when lithium-ions are inserted into the electrode [30]. That relative low rate of diffusion and reaction and the high displacement density can profit stability of solid spherical electrodes and the cycling capacity had been studied by Liu and others [30, 263]. In cylindrical electrodes with the effect of reversible electrochemical reaction, strain and the diffusion had been studyed by Zhang and others [30, 264]. A novel model is established to examine the DIS with the effect of electrochemical reaction-induced strain and investigation the coupling effect from the following three facets: (1) which computes reaction-induced strain in various spherical electrode on potentiostatic charging operation, (2) comparing the coupling effect of DIS the DIS and electrochemical and electrochemical reaction-induced strain in hollow and solid sphere, and (3) examining the DIS and electrochemical reaction-induced strain with the various thickness in the hollow spherical electrode [30].

Lithium-ion batteries have been commonly used as rechargeable power for electric vehicles for the big advantages of light-weight and its high energy density [31]. More and more electric vehicle fire accidents induced by lithium-ion batteries have been indicated, and the safety performance of lithium-ion battery has aroused considerable attention as the explosive growth of electric vehicle, which is equipped with lithium-ion batteries [31]. The serious damage of a lithium-ion battery can consequence in an internal short circuit condition, which follows a thermal runaway [31]. It is required to investigation the response of the lithium-ion battery under mechanical loading in order to lessen the risk of catching fires in electric vehicle crash accidents [31]. Sahraei and others [217, 218, 220, 221, 265] carried out a set of loading test on various kinds of lithium-ion cells and devised homogenized model which captured the short-circuit point reasonably well [31]. Choi and others [266] undertaken various types of mechanical tests to investigation the response of lithium-ion pouch cells, examined its mechanical behaviour toward stress rate, temperature, and anisotropy [31]. All of those literatures discussed before are primarily concentrated on the examination of mechanical properties on lithium-ion battery cell level, and most of these test conditions are quasistatic [31].

Ceramic materials are one of the principal groups in the Materials Science by reason of their applications in modern life [32]. There are numerous techniques of preparation including chemical technique, which comprises sol-gel and hydrothermal process, and mechanical technique, which comprises solid-state reaction [32]. Ceramic materials, alkaline-earth-metal pyrophosphates, with the general formula $A_2MP_2O_7$ (A = Li, K, Na, Ag.; M = Ba, Ni, Cu, Zn.) [267–269], are well established for their potential applications as magnetic and luminescent materials [32, 270]. The theoretical methodologies of transport phenomena at the microscopic level could be undertaken taking into consideration two principal contextual factors: the structure of the compound and the concentration of the ionic species responsible for the transport which could be typified by its ionic radius, its charge, and polarizability [32]. Compound, which is Titled, has been previously investigated magnetic and systemic viewpoint whilst the electrical properties were not indicated [32]. Structural

co-ordination of the prepared materials and thermal behaviour were examined, respectively, employing FT-IR and DTA/TGA measurements [32]. The DTA/TGA results yielded two endothermic peaks: An endothermic peak at 571 K is attributable because of the chemical decomposition and releasing of ligands and a peak at 721 K is because of the irreversible stage transition of the compound [32]. Here, we have the interest to present and explore for the first time the dielectric and electrical properties of the Li-ion pyrophosphate compound $Li_2CuP_2O_7$ as function of temperature, which employs impedance spectroscopy, and frequency for that [32].

Sony Corporation first marketed Li-ion batteries in 1991, employing a carbon-based anode, organic liquid electrolytes solvents (Blomgren [271]), and lithium cobalt oxide cathode [33]. Specific combinations of nickel, cobalt ($Ni_xMn_yCo_{(1-x-y)}$), and manganese, are utilized as Li-ion battery cathodes to combine their inherent properties of high capacity, huge electronic electrical conductivity, and enhanced electrochemical stability, respectively (Myung and others [272]), [33]. A transition in the anode material, from traditional graphite to lithium metal, is of paramount importance for increased the energy density of present-day electric vehicles [33]. The majority of the above methods for increased energy density entail lithium metal as an anode, as it retains an exceedingly low electrochemical potential of −3.04 V relating to hydrogen reference electrode, and theoretical specific capacity of 3870 mAh/g, which is nearly an order-of-magnitude greater than the traditional graphite premised anodes (375 mAh/g) (Xu and others [273]; Lin and others [274]), [33]. In the second half of the last few decades for usage in Li-ion batteries, lithium metal anodes were actively studied, though did not see commercial success because of numerous problems (Blomgren [271]; Cheng and others [275]): (a) Loss of electrolyte because of reaction with the anode surface and formation of a solid electrolyte interface; this interface gives rise to significant capacity fade (b) Formation of dead lithium that does not partake in the electrochemical reaction and can potentially give rise to capacity fade if Growth of dendritic protrusions that can penetrate via the separator and short is excess lithium not utilized (c) the cell (d) Thermal runaway because of internal shorting and subsequent upsurge of the cell Nucleation and propagation of dendritic protrusions during lithium deposition are linked to all of these difficulties [33].

At ca 1 V versus Li^+/Li^0, utilized electrolytes, based upon mixtures of organic carbonates, undergo decrease mechanisms with the formation of a passivation layer-the solid electrolyte interphase (SEI) [34]. The SEI layer limits additional decrease of the electrolyte and affects some crucial battery parameters including power density and the capacity fade [34]. A spontaneously formed SEI triggers a significant decrease in battery capacity, which is additional deteriorated by subsequent charge-discharge cycles, so the application of a "functional" electrolyte is recommended [34, 276]. These an electrolyte comprises of salt (s), solvent (s), and special functional additives; whereof SEI-forming additives are responsible for rapid creation of an SEI layer and the controlled [34]. Some such researches have concentrated on explaining the decrease processes correlated with SEI formation, primarily for carbonate compounds including VC [277–284], through a homolytic

ring-opening mechanism, and EC, DMC [34]. A greater μ gives rise to a stronger nonbonding interaction with Li^+, while weak binding between the lithium cation and the additive fosters mechanisms on the anode and assures rapid formation of the SEI [34, 285]. Han evaluated numerous various DFT functionals with the goal of assessing additive performance by describing the decrease of VC [282] and EC [34].

4.2 Electrolytes, Cathode, Thermal Runaway, Cell, Case, Organic, Point

4.2.1 Thermal Runaway on 18,650 Lithium-Ion Batteries Containing Cathode Materials with and Without the Coating of Self-terminated Oligomers with Hyper-Branched Architecture (STOBA) Used in Electric Vehicles [1]

The mean exothermic onset temperature had been assessed to be (159.1 ± 8.3) °C [1]. Lithium-ion batteries comprised of cathode materials made of $LiNi_xMn_yCo_zO_2$ have been shown to display the calamitous attributes of thermal runaway if they rise above the important temperature of (204.8 ± 16.5) °C [1]. Surface coating of self-terminated oligomers with hyper-branched architecture (STOBA) upon cathode materials had been reluctant to deter the uncontrollable thermal runaway under external heating in these lithium-ion batteries [1]. The results of the present study must foster the pursuit of safer lithium-ion battery chemistries; these chemistries display less response to thermal misuse [1].

4.2.2 Interfaces and Materials in Lithium-Ion Batteries: Challenges for Theoretical Electrochemistry [2]

That review explores the Li-ion battery as the leading electrochemical storage technology, examining its principal elements, namely electrode (s) as active and electrolyte as inactive materials [2]. State-of-the-art (SOTA) anode and cathode materials are studied, stressing viable methodologies towards validity of Li-ion batteries and advancement of the overall performance; existing issues are not overlooked [2]. Liquid aprotic electrolytes for Li-ion batteries constitute a Li-ion, which conducts salt, a mixture of multiple additives and solvents [2]. Owing to its role in a given cell chemistry and its complexity, the most fruitful, element for additional amelioration of Li-ion batteries, including electrolyte, besides the cathode materials, is identified as most prone [2]. The advantages and shortcomings of SOTA lithium battery systems are emphasised by this overview, aimed to motivate scholars to carry forward and bolster the research towards advanced Li-ion batteries, tailored for specific applications [2].

4.2.3 Thermal Stability of Ethylene Carbonate Reacted with Delithiated Cathode Materials in Lithium-Ion Batteries [3]

Confinement tests are implemented for assessing exothermic behaviours of eight non-lithiated or delithiated cathode materials mixed with ethylene carbonate (EC); these materials are widely used in lithium-ion batteries [3]. Eight delithiated and non-lithiated cathode materials, namely lithium cobalt oxide (Li_xCoO_2), nickel oxide (NiO_2), lithium nickel oxide (Li_xNiO_2), lithium nickel cobalt oxide ($Li_xNi_{0.8}Co_{0.2}O_2$), manganese oxide (Mn_2O_4), cobalt oxide (Co_3O_4), lithium manganese oxide ($Li_xMn_2O_4$) and iron phosphate ($FePO_4$) are mixed with EC under a programmed rate of heating, respectively [3]. The ranking of thermal stabilities of delithiated cathode and non-lithiated materials with EC is compared and outlined [3]. Safety problem, which regards lithium-ion battery, remains to be a fight even in the near future [3]. At least quite small exothermic peaks can be detected by DSC [43, 44] for both $LiFePO_4$ and $FePO_4$ with electrolytes [3]. Not just the stability of the structures themselves though also the complex reaction processes between electrolytes responded with lithiated cathode materials caused in the exothermic behaviours [3].

4.2.4 Porous Media Applications: Electrochemical Systems [4]

Through heat and mass transport in the porous electrodes, electrochemical phenomena including thermal management of Li-ion batteries are substantially shaped [4]. Direct numerical simulation (DNS) is utilized by present chapter to assess the species transport via the composite electrodes of Li-ion batteries [4].

4.2.5 Characterization on the Thermal Runaway of Commercial 18,650 Lithium-Ion Batteries Used in Electric Vehicle [5]

Through confinement tests, 18650A Panasonic and 18650B lithium-ion batteries at full-charged state are carried out to run via thermal runaway [5]. The majority of the maximal temperatures within the batteries under thermal runaway surpass both 800 auto-ignition and °C temperature of organic carbonates to ignite the flammable vapors of the electrolytes in the air [5]. Under thermal runaway, the calamitous attributes must be carryed by Panasonic 18650A and 18650B lithium-ion batteries if they rise above the important temperature of (188.0 ± 4.4) °C [5]. Averaged enthalpy change, which thermal runaway of a Panasonic 18,650 lithium-ion battery induced, is similar to the equivalence of heat released by 0.71 g of gasoline under combustion [5].

4.2.6 An Experimental Study About the Effect of Arrangement on the Fire Behaviors of Lithium-Ion Batteries [6]

The knowledge on the battery combustion behaviour is restricted [6]. The fire hazard of lithium-ion batteries must be regarded to increase the safety margin [6]. An experimental investigation of various configurations: horizontal 4 × 1, horizontal 2 × 2 and vertical 2 × 2 lithium-ion batteries fire behaviours had been carried out [6]. The mass deterioration rate, heat flux and heat release rate were utilized to examine the combustion behaviour, which is thorough more [6]. The mass deterioration, heat flux and heat release rate were assessed [6]. Lithium-ion batteries are burning with potentially deadly explosions and volatile [6].

4.2.7 On the Gassing Behavior of Lithium-Ion Batteries with NCM523 Cathodes [7]

For the first time, the gassing behaviour of one of the main marketed cathode materials, namely Ni-rich $Li_{1+x}Ni_{0.5}Co_{0.2}Mn_{0.3}O_2$ (NCM523 with $0.01 < x < 0.05$), is indicated [7]. The generation pattern of the most characteristic gases CO_2, H_2, C_2H_4, and CO during 30 cycles by means of differential electrochemical mass spectrometry, which is combined with Fourier reshape infra-red spectroscopy, is examined by us [7]. We monitor its gas, which is potential-resolved, evolution and assess the total quantity of gas from cycle to cycle in a longer-term test of an NCM523/graphite cell [7]. Through combining total and the spectrometric gas pressure data, an explanation on the feature elements of pressure versus time curves during cycling is given [7].

4.2.8 Experimental Study on the Thermal Behaviors of Lithium-Ion Batteries Under Discharge and Overcharge Conditions [8]

Through a cone calorimeter, many tests were carried out to have a better understanding of the thermal behaviours of lithium-ion batteries (Li-ion batteries) under overcharge and discharge conditions [8]. Various parameters were assessed including the battery surface temperature, voltage, the time to thermal runaway, the time to maximal temperature, total heat released and heat release rate [8]. The current treatment (discharge) can accelerate the warming up, lessen the heat released, and consequence in previous thermal runaway [8].

4.2.9 *Effect of Overdischarge (Overlithiation) on Electrochemical Properties of $LiMn_2O_4$ Samples of Different Origin [9]*

Overdischarge (overlithiation) effect on electrochemical parameters of lithium manganese spinels of various origin is researched [9]. In reduced and recommended potential ranges, charge/discharge tests for 240 cycles are carried out [9]. Insertion of lithium-ions into spinels by declining potential to +2.4 or +1.5 V against Li/Li^+ is observed to give rise to the formation of the overlithiated Li_{2-x} Mn_2O_4 spinel stage [9]. Repeated cycling, which entails the low-potential areas, deteriorates electrochemical parameters: specific capacity decreases and cell resistance increases [9]. The microsized BE-30 (NEI) subsample better tolerates cycling at reduced potentials [9]. That might connote that at least half of the gram equivalent of extra lithium-ions could be electrochemically inserted into the 16c voids in the spinel structure, which results in the $Li_{1.5}Mn_2O_4$ compound this compound is able to reversibly work within the 2.4–4.6 V potential variety; this compound is able to reversibly work within the 2.4–4.6 V potential variety [9]. Manganese ions share these identical oxygens, so that a subsequent increase in Mn–O ionicity must be detected [9]. That even small overdischarge is completely unacceptable for the MTI and JDEES samples is shown by comparisons [9].

4.2.10 *Towards Quantification of Toxicity of Lithium-Ion Battery Electrolytes—Development and Validation of a Liquid-Liquid Extraction GC-MS Method for the Determination of Organic Carbonates in Cell Culture Materials [10]*

A new technique, which is based upon mass spectrometric detection (GC-MS) for the quantification of organic carbonates in cell culture materials and liquid-liquid extraction with subsequent gas chromatography separation, is summarized [10]. The approach had been utilized to cell culture models incubated with commercial Li-ion battery (LIB) electrolytes to gain more insights into the potential toxic impacts of these compounds [10]. The stability of the organic carbonates in cell culture medium after incubation had been investigated [10]. The stability of EC and EMC in cell culture medium had been examined, and the transfer of EMC, EC and DEC across the blood-CSF barrier had been examined [10]. It can be demonstrated that a transfer of organic carbonates into the compartment, which faces brain, took place in a porcine model of the blood-cerebrospinal fluid (CSF) barrier [10]. The character of the subsample matrices might have a significant impact on the outcome [286] in qualitative analytical analysis [10].

4.2.11 Recent Progress in the Electrolytes for Improving the Cycling Stability of $LiNi_{0.5}Mn_{1.5}O_4$ High-Voltage Cathode [11]

The main aim of this review is to underscore the recent advances in the development of advanced electrolytes for enhancing the cycling stability and rate capacity of $LiNi_{0.5}Mn_{1.5}O_4$-based batteries [11]. An insights into the future research and additional development of advanced electrolytes for $LiNi_{0.5}Mn_{1.5}O_4$-based batteries is outlined [11].

4.2.12 Quality Decision for Overcharged Li-Ion Battery from Reliability and Safety Perspective [12]

The effect of excessive COV on the discharging ability of cell, and the use of a new non-destructive technique to assess if the damage, which the excessive COV made in the cell, is rendering the cell from additional safe usage or it is still satisfactory with minor degradation in validity and safety, offering a basis for quality consideration of the cell is demonstrated by this work [12]. The technique allows battery manufacturers to pinpoint the internal elements for their cells that are most susceptible to the excessive COV so that quality amelioration of their batteries could be generated and designed [12]. That technique alerts electric vehicles user on the hidden safety problems of battery manufacturers' battery pack, and allows battery management system to carry out validity balancing, a novel patented method to assure the accurate and safe operation of battery pack [12].

4.2.13 Failure Analysis of Swelling in Prismatic Lithium-Ion Batteries During Their Cycle Life After Long-Term Storage [13]

Upon longer-term storage, the first cell is investigated, traces of side reactants are observed around the centre of the anode electrode, and in which case a void space, probably a gas bubble, is detected around the Ni tap in the cell [13]. That cell is compared with a swollen cell, in which, according to the CT results before and after gas removal, gas is observed inside the space between the can body and the jelly roll and inside the jelly roll, which is investigated after undergoing numerous cycles after longer-term storage [13]. The gas bubbles are demonstrated by the results and side reactants produced as a consequence of longer-term storage are dictated to be responsible for the swelling in the cell because of prolonged cycling [13].

4.2.14 *Cycle-Life and Degradation Mechanism of $LiFePO_4$-Based Lithium-Ion Batteries at Room and Elevated Temperatures [14]*

At elevated temperatures and room, cycle-life tests of commercial 22,650-type olivine-type lithium iron phosphate ($LiFePO_4$)/graphite lithium-ion batteries were carried out [14]. A number of nondestructive electrochemical methods, i.e., capacity recovery, which employs a small current density, differential voltage and differential capacity analyses, and electrochemical impedance spectroscopy, were carried out to infer the degradation mechanism of these batteries [14]. We disassembled the batteries, and material analyses were carried out to additional describe these batteries' internal materials [14].

4.2.15 *Manufacturing of Lithium Cobalt Oxide from Spent Lithium-Ion Batteries: A Cathode Material [15]*

Disposal of huge quantity of spent lithium-ion batteries will cause will generate waste management issue including adverse environment influence [15]. Use of Extracted metals from recycling for manufacturing of cathode active material, i.e., lithium cobalt oxide will help in reducing the rate of overexploitation of these useful metals [15]. Recycling process comprises of peeling, extraction steps, and break-up [15]. Variations of parameters for improving the peeling and the break-up steps along with extraction of cobalt oxalate and manufacturing of lithium cobalt oxide have been researched here [15]. The extraction efficiency of cobalt oxalate is observed to be 91% with purity of 90% [15]. The purity of manufactured lithium cobalt oxide is observed to be 91% [15].

4.2.16 *Experimental Investigation on Cooling/Heating Characteristics of Ultra-thin Micro Heat Pipe for Electric Vehicle Battery Thermal Management [16]*

Owing to the heat pipes' transient conduction, fluid dynamics and stage change during cooling/heating with high frequency charging/discharging of batteries, it is important to examine in depth the experimental dynamic thermal attributes in such complex heat transfer mechanisms for design of a BTMS and more reliable thermal analysis [16]. The use of ultrathin micro heat pipe (UMHP) for thermal management of a lithium-ion battery pack in EVs is examined by experiments to show the cooling/heating attributes of the UMHP pack [16]. That heating films stuck on the

fins of UMHPs brought about adequate high heating efficiency comparing with that stuck on the surface of cells under the identical heating power is revealed by experimental data, though has less cost for the BTMS and more convenient maintenance [16]. The experimental dynamic temperature attributes of UMHP which is observed to be a low-energy and high-efficient consumption, which cooling/heates technique for BTMSs, could be carried out to guide thermal analysis and optimization of heat pipe BTMSs [16].

4.3 SOC, Models, Stress, Parameters, Function, Conditions, Estimation

4.3.1 Probabilistic Battery Design Based upon Accelerated Life Tests [17]

A probabilistic battery design technique is outlined, with reference to lithium-ion batteries, based on linked economical facets and battery life-time [17]. The reliance of battery life-time on various parameters, including operating environment and design maximal specific power is taken into consideration by the technique [17]. A probabilistic technique for battery design is devised which assures the minimization of a useful cost function which has the supposed life-time as a basic input after a detailed statistical data analysis [17]. The technique enables to assure the needed robustness design against the random differences in specific power experienced by a Li-ion battery, which is designed for a small electric bus (public transport service) [17].

4.3.2 A Novel Approach for Electrical Circuit Modeling of Li-Ion Battery for Predicting the Steady-State and Dynamic I-V Characteristics [18]

The dynamic and steady-state behaviour of battery is mimiced by the model [18]. Internal charge distribution of the battery is modelled employing two RC circuits [18]. Self-discharge feature of the battery is modelled employing a leakage resistance [18]. The internal voltage source of the battery model differs dynamically with SOC to replicate the experimental terminal voltage attributes of battery [18]. The internal voltage CVS is accomplished as a second-order polynomial function of SOC to retain the simplicity of model including to reliably portray the terminal attributes [18].

4.3.3 *Electrochemical Modeling and Parameter Identification Based on Bacterial Foraging Optimization Algorithm for Lithium-Ion Batteries [19]*

This chapter aims to characterize a single-particle model of a lithium-ion battery that has a straightforward structure, could be enmeshed in simulation computer program for on-line applications, and offers a high-accuracy characterization of the dynamics [19]. A simplified electrochemical model that underlies the dynamic voltage response is the single-particle model; this model is explained by a set of partial differential equations [19]. The single-particle model is simplified employing the volume-average integration technique and the three-parameter polynomial approximation technique [19]. A protocol for reducing the model, which is based upon the volume-average integration technique and the three-parameter polynomial approximation, is devised to simplify the partial differential equations of the single-particle model [19]. The single-particle model of a lithium-ion battery is set up in Simulink and MATLAB [19]. Comparing the terminal voltages of the model and the battery, the accuracy of the single-particle model is ascertained [19]. That the single-particle model of a lithium-ion battery is straightforward and quite reliable, verifying the validity of the parameter identification process is demonstrated by the results [19].

4.3.4 *Fractional Models of Lithium-Ion Batteries with Application to State of Charge and Ageing Estimation [20]*

In the pack, the BMS employs models of every cell to undertake an reliable battery diagnosis [20]. A two fractional models of lithium-ion cell are devised [20]. The quite low number of parameters in the simpler devised model allows a two fractional models of lithium-ion cell's adjustment with a quite straightforward protocol [20]. A solution is devised to conceptualize if the model parameters adjustment is needed as because of aging model and cell behaviour discrepancy [20].

4.3.5 *Lithium Iron Phosphate Electrode Semi-empirical Performance Model [21]*

Following the meager inherent electronic electrical conductivity elements of LFP, an empirical variable resistance strategy is devised for the single particle model (SPM) [21]. Through the increasing ohmic resistance, a resistive-reactant characteristic of LFP as the positive electrode active materials, the increased resistance

behaviour, which is detected at the end of discharge process of LFP batteries, could be justified [21]. "Schematic of the coated LFP active material particles in (a) beginning of discharge with well-connected particles, (b) end of discharge with poor-connected particles" [21].

4.3.6 *Representative Volume Element Model of Lithium-Ion Battery Electrodes Based on X-Ray Nano-tomography [22]*

A novel model that keeps all main advantages of the single-particle model of lithium-ion batteries (Li-ion batteries) and comprises 3-D structure of the electrode had been devised [22]. A small volume element of an electrode, called the representative volume element (RVE), which constitutes the real electrode structure is regarded by this model unlike the single spherical particle [22]. The advantages of employing RVE as the model geometry were shown for a characteristic LIB electrode, which comprises of nano-particle $LiFePO_4$ (LFP) active material [22]. The simulation results revealed that the distribution of lithium inside the electrode microstructure is quite various from the results obtained based upon the single-particle model [22]. The simulation results are in satisfactory concordance with the discharge profile of LFP cathode at multiple discharge rates; these rates have been validated with experimental data [22].

4.3.7 *Prognostics of Lithium-Ion Batteries Under Uncertainty Using Multiple Capacity Degradation Information [23]*

Under unclear conditions, where the degradation process parameters distribution could be learnt from the various readily available capacity measurements, a new integrated strategy, which is based upon a mixture of Gaussian process (MGP) model, is summarized for lithium-ion battery SOH estimation [23]. Through fusing the training data from various battery conditions with the MGP model, the distribution information of the degradation model parameter is retrieved to uncover the time-varying degradation behaviour [23]. The PF algorithm is utilized to predict the battery SOH by exploiting the degradation model parameter distribution information [23].

4.3.8 An Adaptive Observer State-of-Charge Estimator of Hybrid Electric Vehicle Li-Ion Battery—A Case Study [24]

The efficacy of the examiner state estimator design is demonstrated via intensive simulations carried out to calculate the state-of-charge of a lithium-ion rechargeable battery, which is integrated in a hybrid electric vehicle Battery Management System structure for a particular Honda Insight Japanese car [24]. The state-of-charge is an indispensable internal parameter of the lithium-ion battery, though not directly measureable, hence an reliable estimation of battery state-of-charge becomes a crucial operation for the Battery Management System [24].

4.3.9 Characterization and Model of Piezoelectrochemical Energy Harvesting Using Lithium-Ion Batteries [25]

Lithium-ion intercalation materials are also mechanically active even though Li-ion battery research frequently examines electrochemical properties [25]. We build a model to investigation and predict the efficacy of intercalation materials as mechanical energy harvesters [25]. We indicate that a Li-ion battery harvester could be modeled as a straightforward circuit and that we can make both quantitative and qualitative inferences about the efficacy of a battery material, which is given its inherent mechanical and electrochemical properties [25].

4.3.10 Coupling Effect of State-of-Health and State-of-Charge on the Mechanical Integrity of Lithium-Ion Batteries [26]

Two governing contextual factors that impact the electrochemical behaviours of lithium-ion batteries (Li-ion batteries), state of charge (SOC) and state of health (SOH), are continually swapped, hence impeding the understanding of the mechanical integrity of Li-ion batteries [26]. The electrochemical failure of Li-ion batteries with multiple SOHs and SOCs exposed to abusive mechanical loading is examined by the present study [26]. Comprehensive experiments on $LiNi_{0.8}CoO_{15}Al_{0.05}O_2$ (NCA) LIB indicate that the change trend differs with SOC value and that SOH decrease gives rise to systemic stiffness [26]. Electrochemical failure stress at short circuit has no relationship with SOH or SOC, while failure strain increases with the increase of SOC value [26].

4.3.11 Real-Time Stress Measurement in SiO_2 Thin Films During Electrochemical Lithiation/Delithiation Cycling [27]

Through monitoring the substrate curvature, which employs a multi-beam optical sensing technique, strain evolution in the SiO_2 thin film electrodes during electrochemical lithiation/delithiation is assessed in situ [27]. A straightforward plane stress finite element model of Si nanotube coated with SiO_2 shell had been devised to comprehend the mechanical response of the core-shell kind microstructures under electrochemical cycling; assessed strain response had been utilized in the model to constitute SiO_2 constitutive behaviour whilst Si had been treated as an elasto-plastic material with concentration reliant mechanical properties derived from the scientific literature [27]. The results indicated here offer insights and qualitative understanding as to why the highly brittle SiO_2 coatings are able to improve cyclic performance of Si indicated in the scientific literature and stabilize significant volume expansion (300%) of Si core without fracture [27]. The basic mechanical properties summarized here are required first step for future design and development of SiO_2-based electrodes or durable Si/SiO_2 core shell structures [27]. The energy density and capacity of current lithium-ion batteries is restricted by electric vehicle and non-conventional energy production technologies' electrode materials and are not adequate to satisfy the future energy demands [27]. It could be detected that when SiO_2 coating is presumed as a pure mechanical clamping layer with elasto-plastic properties [232], the hoop strain in SiO_2 reaches as high as 2.9 GPa, which is substantially greater tensile strain than the fracture strength of SiO_2; this strength can give rise to cracking [27].

4.3.12 Diffusion-Induced Stress of Electrode Particles with Spherically Isotropic Elastic Properties in Lithium-Ion Batteries [28]

Mechanical degradation, which pulverization and crack nucleation produced, can give rise to the capacity fade in lithium-ion batteries; this fade has been attributable to diffusion-induced strain inside battery electrodes in recent decades [28]. Not considerably attention has been directly taken to the models of diffusion-induced strain for anisotropic electrodes [28]. An analytical model of diffusion-induced strain for spherically isotropic elastic electrodes under galvanostatic and potentiostatic operation is devised by us [28].

4.3.13 Two-Dimensional Analysis of Progressive Delamination in Thin Film Electrodes [29]

A semi-analytical technique is devised to examine the interfacial delamination in electrodes by utilizing the 2D analysis, i.e., plane strain and plane stress [29]. It is observed that the delamination in the plane stress condition happens easier, suggesting that the constraint is damaging to retain the structure stability [29]. With regard to the obtained governing equations, a formula of the dimensionless critical size for delamination is offered, which is a function of the Poisson's ratio of the active layer and the maximal volumetric stress [29].

4.3.14 Effect of Electrochemical Reaction on Diffusion-Induced Stress in Hollow Spherical Lithium-Ion Battery Electrode [30]

Stress (DIS), which is Diffusion-induced, has been examined in hollow and solid spherical electrode [30]. In a hollow spherical electrode, a novel coupled model is established to examine the DIS with electrochemical reaction [30]. In contrast to strain evolution in hollow and solid sphere electrode, electrochemical-induced strain in solid electrode is considerably smaller than that in hollow electrode [30]. A novel approach is put forth to maximize the reaction-induced strain and the electrode thickness; this strain might eventually expand the overall battery life [30].

4.3.15 Mechanical Performance Study of Lithium-Ion Battery Module Under Dynamic Impact Test [31]

Vehicle crashes are one of the leading triggers of catching fires in electrical vehicle accidents, whilst the mechanical intrusion triggered failure of battery which is the most frequent cause of these fires [31]. To lessen the risk of catching fires in electrical vehicle accidents, the crash failure threshold of battery module, which can be provided as an crucial design parameter in CAE analysis of battery systems' safety, is required to be reasonably well investigated [31]. That influence directions have considerable affects on mechanical attributes, crash failure threshold of battery module, and electric voltage, had been demonstrated by results [31]. Failure stress of separator has been researched that separator under greater stress rate caused in a satisfactory elongation feature of separator and smaller elongation ratio can enhance safety performance of pouch cell under mechanical loadings [31, 287, 288].

4.3.16 *Phase Transition and Electrical Investigation in Lithium Copper Pyrophosphate Compound $Li_2CuP_2O_7$ Using Impedance Spectroscopy [32]*

XRD and FTIR results, accomplished at room temperature, suggest respectively a pure monoclinic stage with I2/a space group and the hegemonic characteristic of pyrophosphate anion $(P_2O_7)^{4-}$ [32]. Dielectric and electrical properties have been researched employing impedance spectroscopy complex over a wide frequency (209 Hz–1 MHz) and temperature (576–710 K) variety [32]. The frequency-dependent AC electrical conductivity obeys Jonscher's universal power law $\sigma_{AC} \sim A\omega^s$ [32].

4.3.17 *Computational Modeling of Morphology Evolution in Metal-Based Battery Electrodes [33]*

Superior energy and low toxicity, power density, and enhanced shelf life have led to the popularity of Li-ion batteries as energy storage tools in the automotive and electronics sectors [33]. Especially greater energy densities will be needed by next-generation Li-ion batteries to satisfy ever-growing demands for longer battery life [33]. Due to low electrochemical decrease potential (−3.04 V relating to H/H^+ reference electrode) and superior's exceedingly high theoretical specific capacity (roughly ten times bigger than that of traditional anode materials), lithium metal is a highly appealing candidate as an anode material for next-generation Li-ion batteries [33]. Stabilization of lithium deposition will be needed by successful commercialization [33].

4.3.18 *SEI-Forming Electrolyte Additives for Lithium-Ion Batteries: Development and Benchmarking of Computational Approaches [34]*

SEI-forming additives play important roles in lithium-ion batteries, and the crucial to enhancing battery functionality is to specify if, how, and when these additives are lowered [34]. A number of computational methodologies and techniques to specify the optimal way to predict and characterize the properties of the additives had been evaluated by us [34].

4.4 Conclusion

A risk concluded to be satisfactory or not is judged from the severity of temperature and pressure under runaway of an 18,650 lithium-ion battery [1]. Maximum temperature above 450° (exceeded the auto-ignition temperature (AIT) C of organic carbonates at the values between 430 and 465 °C) (exceeded 4 times of maximal allowable working pressure, MAWP) and pressure will cause fire and upsurge when a lithium-ion battery goes via an uncontrollable runaway [1]. The following overpressure, which is caused from thermal runaway, is too huge to be tempered or relieved from a rupture disk equipped with lithium-ion battery under such excessive self-heat rate (dT/dt), which accompanys a pressure-rising wave [1]. When under a presumably thermal misuse, when the temperature of the battery surpasses an exothermic onset temperature, thermal runaway is too violent to be stopped by either inhibitor, a pressure relief device, which is installed oligomer for thermal shutdown inside the battery, or by a pressure relief device installed inside the battery [1]. Lithium-ion batteries with the cathode materials made of $LiNi_xMn_yCo_zO_2$ have been devised to owns the high-rate ability, acquire better thermal stability than that of $LiNiO_2$ or $LiCoO_2$ and maintain the excellent capacity near that of $LiNiO_2$ [1]. Such four kinds of lithium-ion batteries correlated with the cathode materials of $LiNi_xMn_yCo_zO_2$ pose the highly unacceptable risk of thermal runaway when these batteries are in full-charged states and under external heating with the temperature, which surpasses 160 °C, in the present study [1]. Investigation of the suppression or thermal shutdown of thermal runaway in an 18,650 lithium-ion battery, which is designed with cathode coated by STOBA and made of $LiNi_xMn_yCo_zO_2$, had been demonstrated to be unclear, not successful in preventing thermal runaway or not good [1].

Research into novel electrode materials to additional increase energy density, power density, safety at affordable cost and cycle life tends [2]. The design and development of novel electrode materials and electrolyte elements based upon understanding of operation and failure processes of the battery, also at the electrolyte/electrode interfaces is crucial to additional advance the limits of cycle life in the LIB and safety, power [2]. The physicochemical properties and attributes of the electrolyte/electrode interfaces formed safety and substantially specify power despite the fact that electrolyte belongs to the group of inactive materials in the LIB [2].

Lithium-ion batteries are not immune to incidents triggered by possible abuses or thermal turbulence [3]. Calorimetry combined with confinement test possessed overwhelming supremacy for evaluating thermal reactive or runaway hazards submerged in lithium-ion battery [3]. A risk is satisfactory or not is judged from the pressure and temperature runaway of lithium-ion battery [3]. Pressure (exceeded 4 times of maximal allowable working pressure, MAWP) and maximal temperature (exceeded auto ignition temperature, AIT) will cause upsurge and fire in batteries, and their assemblies are both unacceptable risks when lithium-ion batteries go to uncontrollable runaway [3]. Through confinement test, ignoring the affects of lithium salt and binder, which is equipped in lithium-ion batteries in the present

study, simplified reactive systems between EC with transition metal oxides can be clearly examined [3]. $FePO_4$ is the candidate for large-sized lithium-ion battery based upon the perspective of most reactive inertness, which is demonstrated most, from the relationships of cathode materials with EC [3].

State-of-the-art Li-ion batteries are comprised of porous electrodes in order to increase surface area-to-volume ratio and lead to batteries with better volume-specific and weight-specific energy and power densities [4]. Description, which is Theory-based, enables elucidate some dynamic elements of cell performance had been electroded by Porous [4]. Various solid stages are contained by the electrodes for such batteries, and reliable quantification of electrode properties becomes a quite crucial topic [4].

Confinement test is shown to be an influential method for characterizing the thermal runaway of commercial Panasonic 18,650 lithium-ion batteries [5]. A risk concluded to be satisfactory or not is judged from the temperature and pressure runaway of 18,650 lithium-ion battery [5]. Maximum temperature above 450° (exceeded the auto-ignition temperature (AIT) C of organic carbonates at about 430-pressure and 465 °C) (exceeded four times of maximal allowable working pressure, MAWP) will cause fire and upsurge in batteries, and their assemblies were drawn when a lithium-ion battery went to uncontrollable runaway [5]. Prevention in the induction of thermal runaway from thermal misuse, overcharge, internal short, LiC_6 responded with electrolytes below 60 °C is the optimal stratagem in employing lithium-ion battery safely from the runaway processes devised from low to high temperature [5]. The caused repercussions of thermal runaway in lithium-ion battery are unacceptable risks by judging from the maximal temperature, maximal self-heat rate or maximal pressure [5].

An experimental investigation of various configurations: horizontal 4×1, horizontal 2×2 and vertical 2×2 batteries fire behaviours had been summarized [6]. The thorough analysis of the ignition time, mass deterioration, heat release rate, heat flux and released heat offers a comprehensive understanding of the complex fire hazard, which batteries with various configurations induced [6]. Experimental results indicate that the configurations have considerable affects on the burning behaviours of lithium-ion batteries [6]. The batteries of various configurations experienced resemble mass deterioration mechanisms, and the total mass deterioration is comparable, whilst HRR, heat flux and combustion heat are fairly various [6].

H_2, C_2H_4, and CO, are the most characteristic gases in the initial cycles; CO_2 is dominating if the terminal cell voltage is increasing [7]. The origin of the SEI forming gases has been identified with separate measurements carried out on graphite/Li cells [7]. In a rather stable fashion, these could be cycled without reconstruction of the SEI when the potential of the graphite anode remains between 0.01 and 0.40 V [7]. Throughout a characteristic battery formation cycle, the gas generation had been examined, as reasonably well [7].

Under overcharge and discharge conditions by means of a cone calorimeter, the thermal behaviours of Li-ion batteries are summarized [8]. Detailed analysis on the surface temperature, voltage, the time to thermal runaway, the time to maximal

temperature increased rate, released heat and HRR offers a comprehensive understanding of the thermal behaviours of Li-ion batteries fire [8]. LIB has apparent warming up during discharge due to irreversible heat and reversible heat [8]. The batteries under discharging owns greater heating rates which make them obtain into thermal runaway previous [8]. Discharging will make LIB harder to control and riskier [8]. Apart from, it is observed that overcharge is damaging to the LIB safety that it will make LIB easier to behave considerably more violent when catching fires and obtain into thermal runaway [8].

Four lithium-manganese spinels of various origin, viz., nano-sized stoichiometric homemade (JDEES) material, microsized commercial aluminum-doped (Toda) spinel and two microsized commercial stoichiometric (MTI and NEI) spinels have been exposed to cyclic galvanostatic and voltammetric overdischarge researches for 240 cycles [9]. Intercalation of lithium-ions into lithium-manganese spinels by declining potential to +2.4 or +1.5 V against Li/Li^+ gives rise to the formation of the overlithiated $Li_{2-x}Mn_2O_4$ spinel stage detectable by a feature Li^+ insertion/deinsertion peak in the 2.9 V region [9]. No notable transformations of this peak with scan number denotes no changes of the spinel structure, and materials investigated maintain their electrochemical activity in the working region of spinel electrodes, i.e., >3.5 V [9]. An ability to intercalate extra lithium-ions at low potentials substantially depends upon material [9]. Through no more than half gram equivalent, uptake/release of extra Li^+ is restricted for other (microsized) samples [9]. Through declining potential to +2.4 V, being electrochemically overlithiated, all samples uptake/release half of the gram-equivalent of extra Li^+ [9]. Repeated cycling, which entails the low-potential areas, deteriorates electrochemical parameters: specific capacity decreases and cell resistance increases [9]. That might connote that at least half of the gram equivalent of extra lithium-ions could be electrochemically inserted into the 16c voids in the spinel structure, which results in the $Li_{1.5}Mn_2O_4$ compound this compound is able to reversibly work within the 2.4–4.6 V potential variety; this compound is able to reversibly work within the 2.4–4.6 V potential variety [9].

The development of a quantification technique for EMC, DEC, VC and EC in aqueous solutions of cell culture cell pellet and medium solutions had been indicated and organic carbonates as elements of LIB electrolytes were examined in the context of cell culture experiments [10]. The combination of extraction with subsequent GC-MS analysis and an organic solvent demonstrated to be able to pinpoint all feature individual mass traces of the organic carbonates [10]. The stability of EC and EMC in cell culture medium had been examined, and the transfer of EMC, EC and DEC across the blood-CSF barrier had been examined [10]. Organic carbonate solvents were observed to pass is supposed to enter the brain this way in all three examined concentrations and the simulated in vitro blood-CSF barrier [10].

Spinel $LiNi_{0.5}Mn_{1.5}O_4$ material has been regarded as one of the most fruitful cathode material in practical energy application because of its eco-friendliness, low synthesis cost, satisfactory practical capacity of about 135 mAh g^{-1}, and high power

capability with an operating voltage of 4.7 V [11]. With regard to the discussion, the fruitful electrolyte additives utilized in high-voltage $LiNi_{0.5}Mn_{1.5}O_4$ cathode ought have the following attributes: (1) the additive can scavenge HF molecules from the electrolyte and form a stable protective film on the surface of $LiNi_{0.5}Mn_{1.5}O_4$, then enhance cell performance a high charge potential without side reactions at the anode surface; (2) high-voltage electrolytes put forward with the solvents must have superior anodic stability [11]. Much feasible solutions must be devised and examined, such as the development of high-voltage solvents (including sulfones, ionic liquids, etc.), novel lithium salts with high thermostability (including LiBOB), and the creation of carbonate derivatives (including fluorinated carbonates) [11].

Through having it to charge with high COV, we have efficiently identified the seeming gain of Li-Ion cell, and confirmed the hidden problems correlated with charging the cell with high COV, with the use of ECBE battery model, which is devised lately [12]. We are able to offer real-time on-line non-destructive evaluation of the internal elements in a Li-Ion cell to assess its validity and safety relating to this overcharging misuse with our technique [12]. Our technique could be incorporated into existing battery management system so that a more advanced safety technology to assure safe operation of the battery pack with enhanced system validity could be possible [12].

Details of the failure analysis of swelling in prismatic Li-ion batteries after a cycle life and primarily via non-destructive analysis techniques including CT, after longer-term storage and cell disassembly were summarized [13]. The CT disassembly and scans analysis confirmed a void space; this space had been believed to be triggered by gas bubbles, near the Ni tap and exposed to longer-term storage near the edges of the cell, and there were wrinkle-like stripes on the corresponding separators [13]. The CT scans recorded after gas removal revealed between the can body and jelly roll and that gas accumulated between the jelly rolls in the swollen cell that underwent a number of cycles after longer-term storage [13]. The gas bubbles and side reactants produced as a consequence of longer-term storage were dictated to be responsible for the swelling in the cell because of prolonged cycling [13].

The mechanism of capacity degradation in $LiFePO_4$/graphite lithium-ion batteries cycled at 25 and 55 °C had been examined by this work [14]. A series of destructive materials, which underlies nondestructive electrochemical analysis and methods, suggested that deterioration of active lithium had been the principal reason for cell degradation both at 25 and 55 °C, and a greater discharge rate and the evident increase in impedance must be responsible for the sudden capacity fall down at 25 °C [14]. Primarily in the anode, active material downturn at 55 °C happened, even though this phenomenon did not directly give rise to capacity degradation of cylindrical battery [14]. Novel characterization methods should be examined to additional investigation the capacity degradation mechanism of $LiFePO_4$ Li-ion batteries [14].

Recycling of smartphone's lithium-ion secondary batteries is undertaken employing sulfuric acid as the leachate [15]. The break-up efficiency of the

recycling process is enhanced employing multiple optimum operating conditions [15]. 91% with 90% purity of cobalt oxalate is the extraction efficiency of cobalt [15]. The battery grade lithium cobalt oxide is procured lithium carbonate (Loba Chemicals, India) and manufactured from the retrieved cobalt oxalate [15]. The battery grade cathode material must have the purity of 99.5% and consequently additional research is going to enhance the purity of cobalt oxalate and also to extract lithium carbonate from the spent lithium-ion batteries, so that cathode active material could be purely manufactured from metals retrieved from spent lithium-ion batteries [15].

The former is considerably more cost-effective for BTMS with heating films by more convenient maintenance and smaller size [16]. The cost of heat pipe limits its wide application in BTMS due to the use of copper as the wall and wick material and the complicated fabrication process [16]. Given feasibility [35, 36] and the aluminium heat pipe manufacturing, the examination on employing aluminium heat pipe in BTMS could be shown as accurate and efficient way to lessen the cost and weight of EV [16].

A novel technique is exemplified for the optimum design of battery [17]. The statistical elements of life-time and other random variables characterizing the operating conditions, in order to derive an effective estimation of the above life-time distribution are taken appropriately into consideration by the technique [17]. Through the proper combination of a probabilistic strategy for stemming the optimum size of a battery and the statistical analysis of the accelerated test, the core of the technique is constituted [17]. Monte Carlo protocol has been carried out, allowing to derive the statistical elements of the interest variables [17]. That approach could be utilized to the characterization of battery life-time, which incorporates in a proper way the multiple uncertainties engaged in the design [17]. That a full protocol for the design optimization dealt with necessitates the solution of a parameter identification problem for the battery modelling is remarked by the authors [17]. The devised optimum design of battery, by a novel technique which takes appropriately into consideration the statistical elements of the battery parameters, is just a first step towards a deeper series of researches employing non-linear programming methods, including non-linear Kalman Filtering or non-linear least squares [17]. The use the Particle filter technique is worth being devised for probabilistic modeling of batteries: hence it is not bound on prior knowledge about likelihood distributions describing the model of the battery and the technique has the advantage that it is a non-parametric one [17].

The devised lithium-ion battery model employs the elements of both electrical circuit and analytical modelling methods [18]. The model is based upon assessed impedance and BTV attributes [18]. The internal voltage CVS is accomplished as a second-order polynomial function of SOC to retain the simplicity of model including to reliably portray the terminal attributes [18]. To keep the model straightforward mean values of impedance parameters are incorporated [18]. The dynamic attributes of battery are mimiced by the model, with precision [18]. In determining the battery performance, the series internal resistance R S plays a crucial role [18]. It could be utilized as a parameter to assess the health of the

battery [18]. Estimating the state of health (SOH) of the battery is important to enhance validity of the vehicle and it is considerably simpler if it is based upon the value of R S [18]. The terminal attributes of battery rely on temperature, as reasonably well [18]. The battery model is demonstrated to match the assessed battery attributes for pulse and constant loading conditions [18]. Through modelling the series resistance R S as a function of battery ageing, future work will entail the battery SOH estimation [18]. "State of charge State of health Open-circuit voltage Battery terminal voltage Controllable voltage source Depth of discharge Internal series resistance of the battery Transient response parameters of the battery Self-discharge resistor of the battery Equivalent or base resistance of the battery Equivalent or base capacitance of the battery Nominal voltage of the battery Cut-off voltage of the battery Nominal capacity of the battery" [18].

An SPM that adequately constitutes the principal dynamics of a battery is established [19]. A BFOA is devised to pinpoint the unknown parameters in the SPM [19]. The results of the parameter identification process are inserted into the SPM, which is set up and simulated in Simulink and MATLAB with LiFePO as an instance [19]. It is ascertained that the results of the parameter identification process are accurate [19]. The single-particle model will be packaged and enmeshed into AMESim to ascertain the effect of the battery on vehicle performance in a future investigation [19].

Fractional models and fractional differentiation are now commonly used to model systems that displays long systems or memory behaviours in which diffusion phenomena occur [20]. Two models for a lithium-ion cell in which fractional transfer functions are utilized and that are inferred from an electrochemical model after numerous presumptions are devised [20]. Owing to the strategy utilized, numerous internal variables in the first model (the most complex), are real electrochemical variable and its parameters are directly associated to the electrochemical and dimensional constants of the lithium-ion cell [20]. A non-linear law (to model the cell open circuit voltage) and the tuning of three parameters is just needed by the second model (the simpler one) [20].

An empirical variable resistance has been added inside a SPM to constitute the increased overpotential specifically observed at the end of the charge/discharge process of a Li/LFP cell [21]. Through taking into consideration the increased ohmic resistance from the resistive-reactant characteristic of LFP, this enhanced the predictability of the SPM model [21]. The electrolyte overpotential can also be a part of this increased resistance; this resistance makes the model ideally suited for charge/discharge rates greater than 1C [21].

A computationally effective 3-D RVE model has been efficiently devised and validated to reliably predict LIB electrode performance at various operating conditions [22]. The model takes advantage of computational efficiency of the single-particle model, whilst simultaneously employing 3D electrode microstructure as the real geometry [22]. A computationally effective 3-D RVE model's advantages and the demonstration of the model are outlined for a common LIB electrode, which comprises of nano-particle LFP active material [22]. That value is observed to be 1.2×, which is premised 10^{-14} m^2/s on the current model, which is

congruent with lately indicated experimental data ranging from 10^{-13} to 10^{-15} m^2/s, unlike widely used lithium-ion diffusion coefficient that are in the order of 10^{-19} in spherical particle models [22]. The distribution of the lithium-ions in RVE is shown to be broader than that of the single-spherical-particle model because of the inherent diverse microstructure [22].

A novel model for the battery SOH estimation is summarized based upon the MGP model; this model had been exploited to learn the distribution parameters from various training sets on the various degradation conditions [23]. The initialized distribution parameters could be updated recursively via MGP learning from the current capacity measurements of battery to constitute the density of the degradation model parameters under unclear conditions [23]. Our technique is based upon distribution, which learns from training data, and does not presume any certain state model of degradation parameter, which is normally hard to be obtained in advance [23]. The prognostics for battery SOH estimation under unclear conditions have some issues, as various capacity degradation models with multiple degradation elements can not be obtained in advance [23].

The MATLAB SIMULINK simulation results of the devised AOSE real time implementation in terms of SOC estimation precision, robustness and convergence speed, are fruitful [24].

We examined Li-ion battery materials as mechanical energy harvesters and shown that Li-ion batteries can efficiently be utilized to transform from mechanical to electrochemical energy in addition to storing energy [25]. We typified this process, which employs basic circuit elements, and offered a model and conceptual framework to predict the pertinent energy harvesting parameters including efficiency and peak voltage from basic electrochemical and mechanical data [25]. They serve reasonably well as a prototype for our model and highlight how our model can take raw voltage and expansion data from intercalation materials and predict energy production whilst our commercial Li-ion batteries are not optimal energy harvesters [25]. We dictated that the maximal theoretical efficiency for energy harvesting employing these battery materials is $2.9 \pm 0.5\%$ from our model [25].

Real-time strain evolution in planar SiO_2 thin film electrodes were assessed whilst cycling against Li foil counter/reference electrodes under galvanostatic lithiation/delithiation cycling [27]. It had been detected that upon lithiation the SiO_2 film undergoes compressive strain which increases linearly at low Li concentrations, below 0.4 GPa of strain and 70 mAh/g capacity, presumably representing a linear elastic response of the film [27]. A straightforward finite element model of SiO_2-coated Si nanotube (core-shell kind microstructure) had been devised; the SiO_2 coating had been modelled employing electrochemical response and strain to be able to offer mechanistic explanation as to how highly brittle SiO_2 coatings on Si were able enhance the cyclic performance of Si [37, 38] by sustaining 300% volume expansion for numerous hundred cycles assessed [27]. It had been detected that the maximal strain in the SiO_2 coating during electrochemical cycling (i.e., under 300% volume change of Si) is roughly 0.41 GPa, which is less than the fracture strength of pure SiO_2 films, offering a plausible explanation as to why oxide coatings survived numerous hundreds of cycles

without failure [27]. That observation along with the strain measurements indicates that makes the SiO_2 film ductile so that the SiO_2 film can maintain huge deformation without fracture, though the addition of Li to SiO_2 film not just enhances the film, as they are able to stabilize strain values as high as 3.1 GPa [27]. Insights, observations made in the present study and the results are also helpful (i) to design and build next generation SiO_2 coating-based core-shell kind of microstructures for electrodes that are mechanically and chemically stable and (ii) to build a comprehensive electro-chemo-mechanics models of SiO_2 films [27].

We have examined the impacts of spherical isotropy on diffusion-induced strain inside electrode particles under potentiostatic and galvanostatic operations and devised the theoretical model of diffusion-induced strain for elastic electrodes with spherical isotropy [28]. The elastic modulus ratio and the lithiation expansion coefficient ratio, which are the feature parameters of the extent of departure from isotropy, have the significant impacts on the diffusion-induced strain [28]. Highlighting the effect of initial condition, we observe that the tangential and radial emphasizes increase with bigger initial concentration; this concentration suggests that extracting more lithium before lithiation (or inserting lower lithium before delithiation) is beneficial to lessen the strain and mitigate the electrochemical properties [28]. It is notable that the strain, because of the initial condition, can not strategy zero even though the concentration is almost homogeneous under potentiostatic operation [28].

Through plane analysis, delamination of the active layer bonded on the substrate had been examined [29]. In both the evolution of the critical time and delamination, the influence of seven crucial parameters, i.e., the length of the active layer, the thickness of the active layer, the electrochemical load factor, the Poisson's ratio of the substrate and the active layer, the Young's modulus ratio, and the cohesive strength were assessed [29]. Poisson's ratio of substrate, cohesive strength, and elastic modulus ratio, have statistically insignificant effect on both the critical time and the delamination process [29].

DIS evolution in the hollow sphere electrode and the solute concentration is examined [30]. In hollow sphere, when compared the DIS in the hollow spherical electrode with that in solid, it is detected that the DIS is smaller [30]. By comparing the DIS in various thickness of hollow sphere, the DIS in hollow sphere is observed that the wall thickness of the bigger hollow sphere, the lesser the influence on the electrochemical reaction-induced strain [30]. Will grow bigger because more surfaces in the hollow sphere; this sphere will bring on the solute concentration and greater changing/exchanging rate [30]. The consequence demonstrates that the electrochemical reaction-induced strain is compressive all the time and grows larger with time increasing [30]. What's more, the strain in the hollow spherical electrode is considerably larger than that in solid [30]. The reaction radial strain is compressive in the hollow spherical electrode and in the thinner hollow sphere, the strain is larger under the impact of electrochemical reaction [30]. The tangential strain with the effect of electrochemical reaction is considerably smaller than in the

solid electrode [30]. The tangential strain with the effect of electrochemical reaction will be smaller with the increasing thickness of the hollow electrode [30].

On lithium-ion battery modules, numerous dynamic influence tests were carried out under various influence directions [31]. That influence directions have considerable affects on mechanical attributes, crash failure threshold of battery module, and electric voltage, had been demonstrated by results [31].

The temperature reliance of s, which is dictated from the fitting of AC electrical conductivity as a function of frequency at various temperatures, is examined in order to comprehend the conduction mechanism in the various stages [32]. CBH model observed to be the OLPT model for the rest of temperature variety ($T > 622$ K) and the most useful conduction mechanism in the low temperature variety ($T < 622$ K) [32]. The activation energy, which is computed from modulus formalism spectra and AC electrical conductivity, is congruent with the estimated value from the impedance spectra, suggesting that ion transport is presumably because of the hopping of lithium (Li^+) ions [32]. For the first time, an experimental investigation of the ionic electrical conductivity of $Li_2CuP_2O_7$ had been demonstrated [32].

Following the analysis of ten SEI-forming compounds, we were able to observe the most effective protocol to predict their decrease behaviour [34]. Comparison of basis sets and various techniques revealed that functionals from the Minnesota family, particularly M06-2X, were the optimal devices to characterize the decrease potential [34]. Analysis of popular descriptors confirmed that it is impossible to evaluate the decrease potential, which is based upon straightforward parameters including the LUMO energy in a wide variety of chemical compounds; such screening is just helpful when taking into account compounds; these compounds indicate just small variations in structure [34]. The chemical hardness had been, however, observed to be an helpful property for predicting transformations during the electrode process, even for quite various chemistries [34].

4.5 Related Work

Lisbona D, Snee T. A review of hazards associated with primary lithium and lithium-ion batteries. Process Saf Environ Prot. 2011;89:434–42. [https://doi.org/10.1016/j.psep.2011.06.022**]**

Previous studies on the hazards and incidents correlated with thermal runaway in lithium-ion batteries have been studied by numerous scholars [1, 39–41]. Previous studies on the hazards correlated with thermal runaway happened in lithium-ion batteries were studied [5, 39–41].

References

Main Document References

1. Duh YS, Tsai MT, Kao CS (2017) J Therm Anal Calorim 129:1935. https://doi.org/10.1007/s10973-017-6356-7
2. Kasnatscheew J, Wagner R, Winter M et al (2018) Top Curr Chem (Z) 376:16. https://doi.org/10.1007/s41061-018-0196-1
3. Duh YS, Chen YL, Kao CS (2017) J Therm Anal Calorim 127:995. https://doi.org/10.1007/s10973-016-5794-y
4. Das MK, Mukherjee PP, Muralidhar K (2018) Porous media applications: electrochemical systems. In: Modeling transport phenomena in porous media with applications. Mechanical engineering series. Springer, Cham. https://doi.org/10.1007/978-3-319-69866-3_4
5. Duh YS, Tsai MT, Kao CS (2017) J Therm Anal Calorim 127:983. https://doi.org/10.1007/s10973-016-5767-1
6. Chen M, Yuen R, Wang J (2017) J Therm Anal Calorim 129:181. https://doi.org/10.1007/s10973-017-6158-y
7. Berkes BB, Schiele A, Sommer H et al (2016) J Solid State Electrochem 20:2961. https://doi.org/10.1007/s10008-016-3362-9
8. Ouyang D, He Y, Chen M et al (2018) J Therm Anal Calorim 132:65. https://doi.org/10.1007/s10973-017-6888-x
9. Kosilov VV, Potapenko AV, Kirillov SA (2017) J Solid State Electrochem 21:3269. https://doi.org/10.1007/s10008-017-3671-7
10. Strehlau J, Weber T, Lürenbaum C et al (2017) Anal Bioanal Chem 409:6123. https://doi.org/10.1007/s00216-017-0549-6
11. Zhu YR, Yi TF (2016) Ionics 22:1759. https://doi.org/10.1007/s11581-016-1788-9
12. Leng F, Tan CM, Yazami R, Maher K, Wang R (2017) Quality decision for overcharged Li-Ion battery from reliability and safety perspective. In: Tan C, Goh T (eds) Theory and practice of quality and reliability engineering in Asia industry. Springer, Singapore. https://doi.org/10.1007/978-981-10-3290-5_20
13. Lee SH, Ko IH (2018) J Fail Anal Preven 18:554. https://doi.org/10.1007/s11668-018-0440-6
14. Cao W, Li J, Wu Z (2016) Ionics 22:1791. https://doi.org/10.1007/s11581-016-1703-4
15. Methekar R, Anwani S (2019) Manufacturing of lithium cobalt oxide from spent lithium-ion batteries: a cathode material. In: Deb D, Balas V, Dey R (eds) Innovations in infrastructure. Advances in intelligent systems and computing, vol 757. Springer, Singapore. https://doi.org/10.1007/978-981-13-1966-2_20
16. Liu FF, Lan FC, Chen JQ et al (2018) Chin J Mech Eng 31:53. https://doi.org/10.1186/s10033-018-0255-0
17. Chiodo E, Lauria D, Andrenacci N et al (2016) Intell Ind Syst 2:243. https://doi.org/10.1007/s40903-016-0054-9
18. Saxena S, Raman SR, Saritha B et al (2016) Sādhanā 41:479. https://doi.org/10.1007/s12046-016-0486-7
19. Ma Y, Ru J, Yin M et al (2016) J Appl Electrochem 46:1119. https://doi.org/10.1007/s10800-016-0998-1
20. Sabatier J, Guillemard F, Lavigne L, Noury A, Merveillaut M, Francico JM (2018) Fractional models of lithium-ion batteries with application to state of charge and ageing estimation. In: Madani K, Peaucelle D, Gusikhin O (eds) Informatics in control, automation and robotics. Lecture notes in electrical engineering, vol 430. Springer, Cham. https://doi.org/10.1007/978-3-319-55011-4_3
21. Rajabloo B, Jokar A, Wakem W et al (2018) J Appl Electrochem 48:663. https://doi.org/10.1007/s10800-018-1189-z

22. Kashkooli AG, Amirfazli A, Farhad S et al (2017) J Appl Electrochem 47:281. https://doi.org/10.1007/s10800-016-1037-y
23. Li F, Wang Y (2018) Prognostics of lithium-ion batteries under uncertainty using multiple capacity degradation information. In: Xu J, Gen M, Hajiyev A, Cooke F (eds) Proceedings of the eleventh international conference on management science and engineering management. ICMSEM 2017. Lecture notes on multidisciplinary industrial engineering. Springer, Cham. https://doi.org/10.1007/978-3-319-59280-0_109
24. Tudoroiu RE, Zaheeruddin M, Tudoroiu N (2019) An adaptive observer state-of-charge estimator of hybrid electric vehicle li-ion battery—a case study. In: Świątek J, Borzemski L, Wilimowska Z (eds) Information systems architecture and technology: proceedings of 39th international conference on information systems architecture and technology—ISAT 2018. ISAT 2018. Advances in intelligent systems and Computing, vol 853. Springer, Cham. https://doi.org/10.1007/978-3-319-99996-8_4
25. Schiffer ZJ, Arnold CB (2018) Exp Mech 58:605. https://doi.org/10.1007/s11340-017-0291-1
26. Xu J, Jia Y, Liu B et al (2018) Exp Mech 58:633. https://doi.org/10.1007/s11340-018-0380-9
27. Rakshit S, Tripuraneni R, Nadimpalli SPV (2018) Exp Mech 58:537. https://doi.org/10.1007/s11340-017-0371-2
28. Zhang X, Chen H, Fang D (2016) J Solid State Electrochem 20:2835. https://doi.org/10.1007/s10008-016-3292-6
29. Liu M, Lu B, Shi DL et al (2018) Acta Mech Sin 34:359. https://doi.org/10.1007/s10409-017-0692-5
30. Liu Z, Cai R, Chen B et al (2017) Ionics 23:617. https://doi.org/10.1007/s11581-016-1848-1
31. Shi F, Yu H, Chen X, Cui T, Zhao H, Shi X (2019) Mechanical performance study of lithium-ion battery module under dynamic impact test. In: (SAE-China) S (eds) Proceedings of the 19th Asia Pacific automotive engineering conference & SAE-China Congress 2017: selected papers. SAE-China 2017. Lecture notes in electrical engineering, vol 486. Springer, Singapore. https://doi.org/10.1007/978-981-10-8506-2_1
32. Krichen M, Gargouri M, Guidara K et al (2017) Ionics 23:3309. https://doi.org/10.1007/s11581-017-2161-3
33. Srinivasan V, Higa K, Barai P, Xie Y (2018) Computational modeling of morphology evolution in metal-based battery electrodes. In: Andreoni W, Yip S (eds) Handbook of materials modeling. Springer, Cham. https://doi.org/10.1007/978-3-319-42913-7_87-1
34. Jankowski P, Wieczorek W, Johansson P (2017) J Mol Model 23:6. https://doi.org/10.1007/s00894-016-3180-0

Other Bibliographic References

35. Chen YT, Kang SW, Hung YH et al (2013) Feasibility study of an aluminum vapor chamber with radial grooved and sintered powders wick structures. Appl Therm Eng 51:864–870
36. Ameli M, Agnewa B, Leung PS et al (2013) A novel method for manufacturing sintered aluminium heat pipes (SAHP). Appl Therm Eng 52:498–504
37. Wu H, Chan G, Choi JW, Ryu I, Yao Y, McDowell MT, Lee SW, Jackson A, Yang Y, Hu L, Cui Y (2012) Stable cycling of double-walled silicon nanotube battery anodes through solid–electrolyte interphase control. Nat Nanotechnol 7:310
38. Tu J, Yuan Y, Zhan P, Jiao H, Wang X, Zhu H, Jiao S (2014) Straightforward approach toward SiO_2 Nanospheres and their superior lithium storage performance. J Phys Chem C 118:7357–7362
39. Spotnitz R, Franklin J (2003) Abuse behavior of high-power, lithium-ion cells. J Power Sources 113:81–100
40. Lisbona D, Snee T (2011) A review of hazards associated with primary lithium and lithium-ion batteries. Process Saf Environ Prot 89:434–442

41. Wang Q, Ping P, Zhao X, Chu G, Sun J, Chen C (2012) Thermal runaway caused fire and explosion of lithium ion battery. J Power Sources 208:210–224
42. Hsieh TY, Duh YS, Kao CS (2014) Evaluation of thermal hazard for commercial 14500 lithium-ion batteries. J Therm Anal Calorim 116:1491–1495
43. Ou WJ, Duh YS, Kao CS, Hsu JM (2014) Thermal instabilities of organic carbonates with discharged cathode materials in lithium-ion batteries. J Therm Anal Calorim 116:1111–1116
44. Duh YS, Ou WJ, Kao CS, Hsu JM (2014) Thermal instabilities of organic carbonates with charged cathode materials in lithium-ion batteries. J Therm Anal Calorim 116:1105–1110
45. Li YC, Duh YS, Hsu JM, Kao CS (2014) Thermal instability of organic esters and ethers with deposited lithium in lithium-ion battery. J Therm Anal Calorim 116:1219–1226
46. Sun YY, Hsieh TY, Duh YS, Kao CS (2014) Thermal behaviors of electrolytes in lithium-ion batteries determined by differential scanning calorimeter. J Therm Anal Calorim 116:1175–1179
47. Besenhard JO, Winter M (1998) Pure Appl Chem 70:603
48. Winter M, Besenhard JO, Spahr ME, Novak P (1998) Adv Mater 10:725
49. Lux SF, Schappacher F, Balducci A, Passerini S, Winter M (2010) J Electrochem Soc 157: A320. https://doi.org/10.1149/1.3291976
50. Qi X, Blizanac B, DuPasquier A, Oljaca M, Li J, Winter M (2013) Carbon 64:334. https://doi.org/10.1016/j.carbon.2013.07.083
51. Qi X, Blizanac B, DuPasquier A, Meister P, Placke T, Oljaca M, Li J, Winter M (2014) Phys Chem Chem Phys 16:25306
52. Speer ME, Kolek M, Jassoy JJ, Heine J, Winter M, Bieker PM, Esser B (2015) Chem Commun 51:15261. https://doi.org/10.1039/c5cc04932f
53. Bieker P, Winter M (2016) Chem Unserer Zeit 50:172. https://doi.org/10.1002/ciuz.201600745
54. Winter M, Placke T, Rothermel S, Meister P, Bar A, von Wedel W (2017) Elektromobilität—Was uns jetzt und künftig antreibt. BINE-Themeninfo I/2017. https://www.bine.info/fileadmin/content/Publikationen/Themen-Infos/I2017/themen0117internetx.pdf
55. Andre D, Kim S-J, Lamp P, Lux SF, Maglia F, Paschos O, Stiaszny B (2015) J Mater Chem A 3:6709. https://doi.org/10.1039/c5ta00361j
56. Kasnatscheew J, Börner M, Streipert B, Meister P, Wagner R, Cekic Laskovic I, Winter M (2017) J Power Sources 362:278. https://doi.org/10.1016/j.jpowsour.2017.07.044
57. Krämer E, Schedlbauer T, Hoffmann B, Terborg L, Nowak S, Gores HJ, Passerini S, Winter M (2013) J Electrochem Soc 160:A356. https://doi.org/10.1149/2.081302jes
58. Wagner R, Preschitschek N, Passerini S, Leker J, Winter M (2013) J Appl Electrochem 43:481. https://doi.org/10.1007/s10800-013-0533-6
59. Meister P, Qi X, Kloepsch R, Krämer E, Streipert B, Winter M, Placke T (2017) Chemsuschem 10:804. https://doi.org/10.1002/cssc.201601636
60. Streipert B, Roser S, Kasnatscheew J, Janssen P, Cao X, Wagner R, Cekic-Laskovic I, Winter M (2017) J Electrochem Soc 164:A1474. https://doi.org/10.1149/2.0671707jes
61. Mizushima K, Jones PC, Wiseman PJ, Goodenough JB (1980) Li_xCoO_2 ($0 < x < 1$): a new cathode material for batteries of high energy density. Mater Res Bull 15:783–789
62. Goodenough JB (2007) Cathode materials: a personal perspective. J Power Sources 174:996–1000
63. Nagaura T (1991) Development of rechargeable lithium batteries. JEC Battery Newsletter 2:17–5
64. Wittingham MS (2004) Lithium batteries and cathode materials. Chem Rev 104:4271–4301
65. Koksbang R, Barker J, Shi H, Saidi MY (1996) Cathode materials for lithium rocking batteries. Solid State Ion 84:1–21
66. Arthur TS et al (2011) Three-dimensional electrodes and battery architectures. MRS Bull 36(07):523–531
67. Stein M, Mistry A, Mukherjee PP (2017) Mechanistic understanding of the role of evaporation in electrode processing. J Electrochem Soc 164(7):A1616–A1627

68. Doughty D, Roth EP (2012) A general discussion of Li ion battery safety. Electrochem Soc Interface 21(2):37–44
69. Mikolajczak C et al (2012) Lithium-ion batteries hazard and use assessment. Springer, Berlin
70. Thackeray MM, Wolverton C, Isaacs ED (2012) Electrical energy storage for transportation —approaching the limits of, and going beyond, lithium-ion batteries. Energy Environ Sci 5(7):7854–7863
71. Mikolajczak C, Kahn M, White K, Long RT (2012) Lithium-ion batteries hazard and use assessment. Springer, Berlin
72. Webster H (2013) Lithium battery update: full scale fire tests. Washington: Federal Aviation Administration
73. Webster H (2010) Fire protection for the shipment of lithium batteries in aircraft cargo compartments. Washington: Federal Aviation Administration
74. Ribière P, Grugeon S, Morcrette M, Boyanov S, Laruelle S, Marlair G (2012) Investigation on the fire-induced hazards of Li-ion battery cells by fire calorimetry. Energy Environ Sci 5(1):5271–5280
75. Fu Y, Lu S, Li K, Liu C, Cheng X, Zhang H (2015) An experimental study on burning behaviors of 18650 lithium ion batteries using a cone calorimeter. J Power Sources 273:216–222
76. Chen M, Zhou D, Chen X, Zhang W, Liu J, Yuen R, Wang J (2015) Investigation on the thermal hazards of 18650 lithium ion batteries by fire calorimeter. J Therm Anal Calorim 122(2):755–763
77. Ohzuku T, Brodd RJ (2007) An overview of positive-electrode materials for advanced lithium-ion batteries. J Power Sources 174:449–456
78. Nitta N, Wu F, Lee JT, Yushin G (2015) Li-ion battery materials: present and future. Mater Today 18:252–264
79. Wang Q, Huang P, Ping P et al (2017) Combustion behavior of lithium iron phosphate battery induced by external heat radiation. J Loss Prev Process Ind 49:961–969
80. Huang P, Wang Q, Li K et al (2015) The combustion behavior of large scale lithium titanate battery. Sci Rep 5:7788
81. Chen WC, Shu CM, Wang YW (2015) Effects of thermal hazard on 18650 lithium-ion battery under different states of charge. J Therm Anal Calorim 121(1):525–531
82. Ye J, Chen H, Wang Q et al (2016) Thermal behavior and failure mechanism of lithium ion cells during overcharge under adiabatic conditions. Appl Energy 182:464–474
83. Li HF, Gao JK, Zhang SL (2008) Effect of overdischarge on swelling and recharge performance of lithium ion cells. Chin J Chem 26:1585–1588
84. Shu J, Shui M, Xu D, Wang D, Ren Y, Gao S (2012) A comparative study of overdischarge behaviors of cathode materials for lithium-ion batteries. J Solid State Electrochem 16:819–824
85. Maleki H, Howard JN (2006) Effects of overdischarge on performance and thermal stability of a li-ion cell. J Power Sources 160:1395–1402
86. Jeevarajan JA, Winchester CS (2012) Battery safety qualifications for human rating. Electrochem Soc Interface 21:51–55
87. Rossouw MH, de Kock A, de Piciotto LA, Thackeray MM, David WIF, Ibberson RM (1990) Structural aspects of lithium-manganese-oxide electrodes for rechargeable lithium. Mater Res Bull 25:173–182
88. Ohzuku T, Kitagawa M, Hirai T (1990) Electrochemistry of manganese dioxide in lithium nonaqueous cell. J Electrochem Soc 137:769–775
89. Thackeray MM, Yang S, Kahaian AJ, Kepler KD, Skinner E, Vaughey JT, Hackney SA (1998) Structural fatigue in spinel electrodes in high voltage (4 V) $Li/Li_xMn_2O_4$ cells. Electrochem Solid-State Lett 1:7–9
90. Cho J, Thackeray MM (1999) Structural changes of $LiMn_2O_4$ spinel electrodes during electrochemical cycling. J Electrochem Soc 146:3577–3581
91. Kalhoff J, Eshetu GG, Bresser D, Passerini S (2015) Safer electrolytes for lithium-ion batteries: state of the art and perspectives. Chemsuschem 8:2154–2175

92. Besenhard JO, Werner K, Winter M (1996) Fluorhaltige Lösungsmittel für Lithiumbatterien mit erhöhter Sicherheit. German Patent DE196191233A1
93. Schmitz RW, Murmann P, Schmitz R, Müller R, Krämer L, Kasnatscheew J et al (2014) Investigations on novel electrolytes, solvents and SEI additives for use in lithium-ion batteries: systematic electrochemical characterization and detailed analysis by spectroscopic methods. Prog Solid State Chem 42:65–84
94. Brox S, Roeser S, Husch T, Hildebrand S, Fromm O, Korth M et al (2016) Alternative single-solvent electrolytes based on cyanoesters for safer lithium-ion batteries. Chemsuschem 13:1704–1711
95. Möller KC, Hodal T, Appel WK, Winter M, Besenhard JO (2001) Fluorinated organic solvents in electrolytes for lithium ion cells. J Power Sources 97–98:595–597
96. Gachot G, Grugeon S, Eshetu GG, Mathiron D, Ribière P, Armand M et al (2012) Thermal behaviour of the lithiated-graphite/electrolyte interface through GC/MS analysis. Electrochim Acta 83:402–409
97. Terborg L, Weber S, Passerini S, Winter M, Karst U, Nowak S (2014) Development of gas chromatographic methods for the analyses of organic carbonate-based electrolytes. J Power Sources 245:836–840
98. Grützke M, Kraft V, Hofmann B, Klamor S, Diekmann J, Kwade A et al (2015) Aging investigations of a lithium-ion battery electrolyte from a field-tested hybrid electric vehicle. J Power Sources 273:83–88
99. Grützke M, Kraft V, Weber W, Wendt C, Friesen A, Klamor S et al (2014) Supercritical carbon dioxide extraction of lithium-ion battery electrolytes. J Supercrit Fluids 94:216–222
100. Grützke M, Mönninghoff X, Horsthemke F, Kraft V, Winter M, Nowak S (2015) Extraction of lithium-ion battery electrolytes with liquid and supercritical carbon dioxide and additional solvents. RSC Adv 5:43209–43217
101. Sloop SE, Pugh JK, Wang S, Kerr JB, Kinoshita K (2001) Chemical reactivity of PF_5 and $LiPF_6$ in ethylene carbonate dimethyl carbonate solutions. Electrochem Solid-State Lett 4: A42–A44
102. Sloop SE, Kerr JB, Kinoshita K (2003) The role of Li-ion battery electrolyte reactivity in performance decline and self-discharge. J Power Sources 119–121:330–337
103. Wu LM, Zhang Y, Jung YG, Zhang J (2015) Three-dimensional phase field based finite element study on Li intercalation-induced stress in polycrystalline $LiCoO_2$. J Power Sources 299:57–65
104. Kwon SN, Song JH, Mumm DR (2011) Effects of cathode fabrication conditions and cycling on the electrochemical performance of $LiNiO_2$ synthesized by combustion and calcination. Ceram Int 37:1543–1548
105. He Y, Li RH, Ding XK, Jiang LL, Wei MD (2010) Hydrothermal synthesis and electrochemical properties of orthorhombic $LiMnO_2$ nanoplates. J Alloys Compd 492:601–604
106. Zheng Z, Liao S-X, Xu B-B, Zhong B-H (2015) The roles of nickel/manganese in electrochemical cycling of lithium-rich Mn-based nickel cathode materials. Ionics 21:3295–3300
107. Dou S (2015) Review and prospects of Mn-based spinel compounds as cathode materials for lithium-ion batteries. Ionics 21:3001–3030
108. Arroyo-de Dompablo ME, Armand M, Tarascon JM, Amador U (2006) On-demand design of polyoxianionic cathode materials based on electronegativity correlations: an exploration of the Li_2MSiO_4system (M = Fe, Mn Co, Ni). Electrochem Commun 8:1292–1298
109. Wu SQ, Zhu ZZ, Yang Y, Hou ZF (2009) Structural stabilities, electronic structures and lithium deintercalation in $LixMSiO_4$ (M = Mn, Fe Co, Ni): a GGA and GGA + U study. Comput Mater Sci 44:1243–1251
110. Recham N, Oró-Solé J, Djellab K, Palacín MR, Masquelier C, Tarascon JM (2012) Hydrothermal synthesis, silver decoration and electrochemistry of $LiMPO_4$ (M = Fe, Mn, and Co) single crystals. Solid State Ionics 220:47–52

111. Zhang H, Chen Y, Zheng C, Zhang D, He C (2015) Enhancement of the electrochemical performance of $LiFePO_4$/carbon nanotubes composite electrode for Li-ion batteries. Ionics 21:1813–1818
112. Barpanda P, Ati M, Melot BC, Rousse G, Chotard JN, Doublet ML, Sougrati MT, Corr SA, Jumas JC, Tarascon JM (2011) A 3.90 V iron-based fluorosulphate material for lithium-ion batteries crystallizing in the triplite structure. Nat Mater 10:772–779
113. Ati M, Walker WT, Djellab K, Armand M, Recham N, Tarasconz JM (2010) Fluorosulfate positive electrode materials made with polymers as reacting media. Electrochem Solid-State Lett 13:A150–A153
114. Leng F, Tan CM, Yazami R, Le MD (2014) A practical framework of electrical based online state-of-charge estimation of lithium ion batteries. J Power Sources 255:423–430
115. Holzapfel M, Würsig A, Scheifele W, Vetter J, Novák P (2007) J Power Sources 174:1156
116. Zhang N, Tang H (2012) J Power Sources 218:52
117. Goers D, Holzapfel M, Scheifele W, Lehmann E, Vontobel P, Novák P (2004) J Power Sources 130:221
118. Zhu YM, Ruan ZW, Tang SZ, Thangadurai V (2014) Research status in preparation of $FePO_4$: a review. Ionics 20(11):1501–1510. https://doi.org/10.1007/s11581-014-1241-x
119. Sehrawat R, Sil A (2015) Polymer gel combustion synthesis of $LiFePO_4$/C composite as cathode material for Li-ion battery. Ionics 21(3):673–685. https://doi.org/10.1007/s11581-014-1229-6
120. Barré A, Deguilhem B, Grolleau S, Gérard M, Suard F, Riu D (2013) A review on lithium-ion battery ageing mechanisms and estimations for automotive applications. J Power Sources 241:680–689. https://doi.org/10.1016/j.jpowsour.2013.05.040
121. Yu F, Zhang LL, Li YC, An YX, Zhu MY, Dai B (2014) Mechanism studies of $LiFePO_4$ cathode material: lithiation/delithiation process, electrochemical modification and synthetic reaction. RSC Adv 4(97):54576–54602. https://doi.org/10.1039/c4ra10899j
122. Zaghib K, Guerfi A, Hovington P, Vijh A, Trudeau M, Mauger A, Goodenough JB, Julien CM (2013) Review and analysis of nanostructured olivine-based lithium rechargeable batteries: status and trends. J Power Sources 232:357–369. https://doi.org/10.1016/j.jpowsour.2012.12.095
123. Zhong K, Cui Y, Xia XD, Xue JJ, Liu P, Tong YX (2014) Study on the stability of the $LiFePO_4$ Li-ion battery via an electrochemical method. J Power Sources 250:296–305. https://doi.org/10.1016/j.jpowsour.2013.11.019
124. Waldmann T, Wilka M, Kasper M, Fleischhammer M, Wohlfahrt-Mehrens M (2014) Temperature dependent ageing mechanisms in lithium-ion batteries—a post-mortem study. J Power Sources 262:129–135. https://doi.org/10.1016/j.jpowsour.2014.03.112
125. Liu P, Wang J, Hicks-Garner J, Sherman E, Soukiazian S, Verbrugge M, Tataria H, Musser J, Finamore P (2010) Aging mechanisms of $LiFePO_4$ batteries deduced by electrochemical and structural analyses. J Electrochem Soc 157(4):A499–A507. https://doi.org/10.1149/1.3294790
126. Song H, Cao Z, Chen X, Lu H, Jia M, Zhang Z, Lai Y, Li J, Liu Y (2013) Capacity fade of $LiFePO_4$/graphite cell at elevated temperature. J Solid State Electrochem 17(3):599–605. https://doi.org/10.1007/s10008-012-1893-2
127. Harks PPRML, Mulder FM, Notten PHL (2015) In situ methods for Li-ion battery research: a review of recent developments. J Power Sources 288:92–105. https://doi.org/10.1016/j.jpowsour.2015.04.084
128. Aurbach D, Markovsky B, Weissman I, Levi E, Ein-Eli Y (1999) On the correlation between surface chemistry and performance of graphite negative electrodes for Li ion batteries. Electrochim Acta 45(1–2):67–86. https://doi.org/10.1016/S0013-4686(99)00194-2
129. Dubarry M, Liaw BY (2009) Identify capacity fading mechanism in a commercial $LiFePO_4$ cell. J Power Sources 194(1):541–549. https://doi.org/10.1016/j.jpowsour.2009.05.036
130. Safari M, Delacourt C (2011) Aging of a commercial graphite/$LiFePO_4$ cell. J Electrochem Soc 158(10):A1123–A1135. https://doi.org/10.1149/1.3614529

131. Eddahech A, Briat O, Vinassa JM (2015) Performance comparison of four lithium-ion battery technologies under calendar aging. Energy 84:542–550. https://doi.org/10.1016/j.energy.2015.03.019
132. Petzl M, Kasper M, Danzer MA (2015) Lithium plating in a commercial lithium-ion battery—a low-temperature aging study. J Power Sources 275:799–807. https://doi.org/10.1016/j.jpowsour.2014.11.065
133. Ouyang MG, Chu ZY, Lu LG, Li JQ, Han XB, Feng XN, Liu GM (2015) Low temperature aging mechanism identification and lithium deposition in a large format lithium iron phosphate battery for different charge profiles. J Power Sources 286:309–320. https://doi.org/10.1016/j.jpowsour.2015.03.178
134. Bloom I, Jansen AN, Abraham DP, Knuth J, Jones SA, Battaglia VS, Henriksen GL (2005) Differential voltage analyses of high-power, lithium-ion cells: 1. Technique and application. J Power Sources 139(1–2):295–303. https://doi.org/10.1016/j.jpowsour.2004.07.021
135. Bloom I, Christophersen J, Gering K (2005) Differential voltage analyses of high-power lithium-ion cells: 2. App J Power Sources 139(1–2):304–313. https://doi.org/10.1016/j.jpowsour.2004.07.022
136. Dubarry M, Liaw BY, Chen MS, Chyan SS, Han KC, Sie WT, Wu SH (2011) Identifying battery aging mechanisms in large format Li ion cells. J Power Sources 196(7):3420–3425. https://doi.org/10.1016/j.jpowsour.2010.07.029
137. Dubarry M, Truchot C, Liaw BY (2014) Cell degradation in commercial $LiFePO_4$ cells with high-power and high-energy designs. J Power Sources 258:408–419. https://doi.org/10.1016/j.jpowsour.2014.02.052
138. Aktas S, Fray DJ, Burheim O, Fenstad J, Acma E (2006) Recovery of metallic values from spent lithium ion secondary batteries. Miner Process Ext Metal 115(2):95–100
139. Swain B, Jeong J, Lee JC, Lee GH, Sohn JS (2007) Hydrometallurgical process for recovery of cobalt from waste cathodic active material generated during manufacturing of lithium ion batteries. J Power Sources 167:536–544
140. Li L, Jing G, Renjie C, Feng W, Shi C, Xiaoxiao Z (2010) Environmental friendly leaching reagent for cobalt and lithium recovery from spent lithium ion batteries. Waste Mange 30:2615–2621
141. Chen L, Tang X, Zhang Y, Li L (2011) Process for recovery of cobalt oxalate from spent lithium ion batteries. Hydrometallurgy 108:80–86
142. Ye Y-H, Shi Y-X, Liphuat S et al (2016) Performance assessment and optimization of a heat pipe thermal management system for fast charging lithium ion battery packs. Int J Heat Mass Transf 92:893–903
143. Kalbfleisch JD, Prentice RL (2002) The statistical analysis of failure time data. Wiley, New York
144. Burke AF (1995) Cycle life consideration for batteries in electric and hybrid vehicles, SAE World Congress 1995, SP-1105
145. Schmidt P, Bitzer M, Guzzella ÁW (2010) Model-based distinction and quantification of capacity loss and rate capability fade in Li-ion batteries. J Power Sources 195:7634–7638
146. Chiodo E, Lauria D, Pagano M, Pede G, Vellucci F (2013) Experimental performances and life cycle estimation of hybrid electric storage systems. In: Proceedings of IEEE international conference on clean electrical power renewable energy resources impact (ICCEP 2013), Alghero, 11–13 June 2013
147. Burke AF, Miller M (2013) Life cycle testing of lithium batteries for fast charging and second-use applications. In: Electric vehicle symposium & exhibition, vol 27, Barcelona, 17–20 Nov 2013
148. Wenzl H, Baring-Gould I, Kaiser R, Liaw BY, Lundsager P, Manwell J et al (2005) Life prediction of batteries for selecting the technically most suitable and cost effective battery. J Power Sources 144:373–384
149. Arunachala R, Jossen A, Garche J, Makinejad K, Athlekar S (2013) Cycle life characterization of large format lithium-ion cells. In: Electric vehicle symposium & exhibition, vol 27, Barcelona, 17–20 Nov 2013

150. Schmalstieg J, Käbitz S, Ecker M, Sauer DU (2013) From accelerated ageing tests to a lifetime prediction model: analyzing lithium-ion batteries. In: Electric vehicle symposium & exhibition, vol 27, Barcelona, 17–20 Nov 2013
151. Sarasketa Zabala E, Laresgoiti I, Alava I, Rivas M, Villareal I, Blanco F (2013) Validation of the methodology for lithium-ion batteries lifetime prognosis. In: Electric vehicle symposium & exhibition, vol 27, Barcelona, 17–20 Nov 2013
152. Rakhmatov D, Vrudhula S, Wallach DA (2003) A model for battery lifetime analysis for organizing applications on a pocket computer. IEEE Trans Very Large Scale Integr (VLSI) Syst 11(6):1019–1030
153. Rakhmatov D, Vrudhula S (2001) An analytical high-level battery model for use in energy management of portable electronic systems. In: Proceedings of international conference on computer aided design (IC-CAD01), pp 488–493
154. Chiodo E, Del Pizzo A, Di Noia LP, Lauria D (2013) Modeling and Bayes estimation of battery lifetime for smart grids under an inverse Gaussian model. Int Rev Electr Eng 8(4):1253–1266
155. Chiodo E, Lauria D, Fabrizi V, Ortenzi F, Sglavo V (2014) Battery design based upon life cycle statistics. In: Proceedings of 3rd renewable power generation conference (RPG 2014), Napoli, 24–26 Sep 2014
156. Wipke KB, Cuddy MR, Burch SD (1999) ADVISOR 2.1: a user-friendly advanced powertrain simulation using a combined backward/forward approach. IEEE Trans Veh Technol 48(6):1751–1761
157. Doyle M, Fuller TF, Newman J (1993) Modeling of galvanostatic charge and discharge of the lithium/polymer/insertion cell. J Electrochem Soc 140(6):1526–1533
158. Doyle M, Newman J (1995) The use of mathematical modeling in the design of lithium/polymer battery systems. Electrochim Acta 40(13–14):2191–2196
159. Fuller TF, Doyle M, Newman J (1994) Simulation and optimization of the dual lithium-ion insertion cell. J Electrochem Soc 141(1):1–10
160. Sung W, Shin C (2015) Electrochemical model of a lithium-ion battery implemented into an automotive battery management system. Comput Chem Eng 76:87–97
161. He H, Xiong R, Fan J (2011) Evaluation of lithium-ion battery equivalent circuit models for state of charge estimation by an experimental approach. Energies 4(4):582–598
162. Thele M, Bohlen O, Sauer D, Karden E (2008) Development of a voltage-behavior model for NiMH batteries using an impedance-based modeling concept. J Power Sources 175(1):635–643
163. Seaman A, Dao T, McPhee J (2014) A survey of mathematics-based equivalent-circuit and electrochemical battery models for hybrid and electric vehicle simulation. J Power Sources 256:410–423
164. Zarrin H, Farhad S, Hamdullahpur F, Chabot V, Yu A, Fowler M (2014) Effects of diffusive charge transfer and salt concentration gradient in electrolyte on li-ion battery energy and power densities. Electrochim Acta 125:117–123
165. Tanim T, Rahn C, Wang C (2014) A reduced order electrolyte enhanced single particle lithium ion cell model for hybrid vehicle applications. In: American control conference (ACC), pp 141–146
166. Tatsukawa E, Tamura K (2014) Activity correction on electrochemical reaction and diffusion in lithium intercalation electrodes for discharge/charge simulation by single particle model. Electrochim Acta 115:75–85
167. Buller S, Thele M, De Doncker RWAA, Karden E (2005) Impedance-based simulation models of supercapacitors and Li-ion batteries for power electronic applications. IEEE Trans Ind Appl 11(3):742–747
168. Singh P, Vinjamuri R, Wang X, Reisner D (2006) Design and implementation of a fuzzy logic-based state-of-charge meter for Li-ion batteries in portable defibrillators. J Power Sources 162:829–836

169. Kandler AS, Rahn DC, Wang C (2010) Model-based electrochemical estimation and constraint management for pulse operation of lithium ion batteries. IEEE Trans Control Syst Technol 18(N 3):654–663
170. Kandler AS (2006) Electrochemical modeling, estimation and control of lithium-ion batteries. Pennsylvania University PhD thesis
171. Newman J, Thomas-Alyea KE (2004) Electrochemical systems, 3rd edn. Wiley
172. Sikha G, White RE, Popov BN (2005) A mathematical model for lithium-ion battery/electrochemical Capacitor hybrid System. J Electrochem Soc, A1682–A1693
173. Agrawal OP, Machado JAT, Sabatier J (2004) Nonlinear dynamics: introduction. Nonlinear Dyn 38(N 1–4):1–2
174. Podlubny I (1999) Fractional differential equations. In: Mathematics in sciences and engineering. Academic Press
175. Wang J, Sun X (2015) Olivine $LiFePO_4$: the remaining challenges for future energy storage. Energy Environ Sci 8(4):1110–1138
176. Dreyer W, Jamnik J, Guhlke C, Huth R, Moškon J, Gaberšček M (2010) The thermodynamic origin of hysteresis in insertion batteries. Nat Mater 9(5):448–453
177. Dreyer W, Guhlke C, Herrmann M (2011) Hysteresis and phase transition in many-particle storage systems. Continuum Mech Thermodyn 23(3):211–231
178. Farkhondeh M, Pritzker M, Fowler M, Delacourt C (2017) Mesoscopic modeling of a $LiFePO_4$ electrode: experimental validation under continuous and intermittent operating conditions. J Electrochem Soc 164(11):E3040–E3053
179. Safari M, Delacourt C (2011) Modeling of a commercial graphite/LiFePO[sub 4] Cell. J Electrochem Soc 158:A562–A571
180. Marcicki J (2012) Modeling, parametrization, and diagnostics for lithium-ion batteries with automotive applications. Dissertation, The Ohio State University
181. Komini Babu S, Mohamed AI, Whitacre JF, Litster S (2015) Multiple imaging mode X-ray computed tomography for distinguishing active and inactive phases in lithium-ion battery cathodes. J Power Sources 283:314–319. https://doi.org/10.1016/j.jpowsour.2015.02.086
182. Bruce PG, Scrosati B, Tarascon J-M (2008) Nanomaterials for rechargeable lithium batteries. Angew Chemie Int Ed 47:2930–2946. https://doi.org/10.1002/anie.200702505
183. Feng K, Ahn W, Lui G et al (2016) Implementing an in-situ carbon network in Si/reduced graphene oxide for high performance lithium-ion battery anodes. Nano Energy 19:187–197. https://doi.org/10.1016/j.nanoen.2015.10.025
184. Yu S, Chung Y, Song MS et al (2012) Investigation of design parameter effects on high current performance of lithium-ion cells with $LiFePO_4$/graphite electrodes. J Appl Electrochem 42:443–453. https://doi.org/10.1007/s10800-012-0418-0
185. Kashkooli AG, Lui G, Farhad S et al (2016) Nano-particle size effect on the performance of $Li_4Ti_5O_{12}$ spinel. Electrochim Acta 196:33–40. https://doi.org/10.1016/j.electacta.2016.02.153
186. Farkhondeh M, Safari M, Pritzker M et al (2013) Full-range simulation of a commercial $LiFePO_4$ electrode accounting for bulk and surface effects: a comparative analysis. J Electrochem Soc 161:A201–A212. https://doi.org/10.1149/2.094401jes
187. Mastali Majdabadi M, Farhad S, Farkhondeh M et al (2015) Simplified electrochemical multi-particle model for $LiFePO_4$ cathodes in lithium-ion batteries. J Power Sources 275:633–643. https://doi.org/10.1016/j.jpowsour.2014.11.066
188. Jung S (2016) Computational study about the effect of electrode morphology on the performance of lithium-ion batteries. Int J Energy Res 40:1073–1084. https://doi.org/10.1002/er.3501
189. Martin MA, Chen C-F, Mukherjee PP et al (2015) Morphological influence in lithium-ion battery 3D electrode architectures. J Electrochem Soc 162:A991–A1002. https://doi.org/10.1149/2.0631506jes
190. Chung D-WD-WD-W, Shearing PR, Brandon NP et al (2014) Particle size polydispersity in Li-ion batteries. J Electrochem Soc 161:A422–A430. https://doi.org/10.1149/2.097403jes

191. Liu Z, Mukherjee PP (2014) Microstructure evolution in lithium-ion battery electrode processing. J Electrochem Soc 161:E3248–E3258. https://doi.org/10.1149/2.026408jes
192. Yan B, Lim C, Yin L, Zhu L (2012) Three dimensional simulation of galvanostatic discharge of $LiCoO_2$ cathode based on X-ray nano-CT images. J Electrochem Soc 159:A1604–A1614. https://doi.org/10.1149/2.024210jes
193. Yan B, Lim C, Song Z, Zhu L (2015) Analysis of polarization in realistic Li ion battery electrode microstructure using numerical simulation. Electrochim Acta 185:125–141. https://doi.org/10.1016/j.electacta.2015.10.086
194. Guo M, Sikha G, White RE (2011) Single-particle model for a lithium-ion cell: thermal behavior. J Electrochem Soc 158:A122. https://doi.org/10.1149/1.3521314
195. Ma Y, Ru J, Yin M et al (2016) Electrochemical modeling and parameter identification based on bacterial foraging optimization algorithm for lithium-ion batteries. J Appl Electrochem. https://doi.org/10.1007/s10800-016-0998-1
196. Piller S, Perrin M, Jossen A (2001) Methods for state-of-charge determination and their applications. J Power Sources 96(1):113–120
197. Williard N, He W, Pecht M (2012) Model based battery management system for condition based maintenance. In: Proceedings of the MFPT, vol 2012
198. Burgess WL (2009) Valve regulated lead acid battery float service life estimation using a kalman filter. J Power Sources 191(1):16–21
199. Hu C, Youn BD, Chung J (2012) A multiscale framework with extended kalman filter for lithium-ion battery soc and capacity estimation. Appl Energy 92(4):694–704
200. Plett GL (2004) Extended kalman filtering for battery management systems of lipb-based hev battery packs: part 3. state and parameter estimation. J Power Sources 134(2):277–292
201. Cui H, Miao Q et al (2012) Application of unscented particle filter in remaining useful life prediction of lithium-ion batteries 2012:1–6
202. He W, Williard N et al (2011) Prognostics of lithium-ion batteries based on dempster-shafer theory and the bayesian monte carlo method. J Power Sources 196(23):10314–10321
203. Liu D, Pang J et al (2013) Prognostics for state of health estimation of lithium-ion batteries based on combination gaussian process functional regression. Microelectron Reliab 53(6):832–839
204. Jayam AP, Ferdowsi M (2008) Comparison of NiMH and Li-Ion batteries in automotive applications. In: Proceedings of the IEEE vehicle power and propulsion conference, pp 1–6. IEEE Xplore Digital Library
205. Tudoroiu R-E, Zaheeruddin M, Radu M-S, Tudoroiu N (2018) Real-time implementation of an extended kalman filter and a pi observer for state estimation of rechargeable li-ion batteries in hybrid electric vehicle applications—a case study. J Batteries 4(2):19. https://doi.org/10.3390/batteries4020019
206. Farag M (2013) Lithium-Ion batteries, modeling and state of charge estimation. Master's thesis. McMaster University of Hamilton, Hamilton, ON, Canada
207. Ramadesigan V, Northrop PWC, De S et al (2012) Modeling and simulation of lithium-ion batteries from a systems engineering perspective. J Electrochem Soc 159:R31. https://doi.org/10.1149/2.018203jes
208. Cannarella J, Leng CZ, Arnold CB (2014) On the coupling between stress and voltage in lithium-ion pouch cells 9115:91150K. https://doi.org/10.1117/12.2055152
209. Muralidharan N, Carter R, Oakes L et al (2016) Strain engineering to modify the electrochemistry of energy storage electrodes. Sci Rep 6:27542. https://doi.org/10.1038/srep27542
210. Jacques E, Lindbergh G, Zenkert D et al (2015) Piezo-electrochemical energy harvesting with lithium-intercalating carbon fibers. ACS Appl Mater Interfaces 7:13898–13904. https://doi.org/10.1021/acsami.5b02585
211. Sheldon BW, Soni SK, Xiao X, Qi Y (2012) Stress contributions to solution thermodynamics in li-Si alloys. Electrochem Solid-State Lett 15:A9. https://doi.org/10.1149/2.016201esl

212. Sethuraman VA, Srinivasan V, Bower AF, Guduru PR (2010) In situ measurements of stress-potential coupling in Lithiated silicon. J Electrochem Soc 157:A1253–A1261. https://doi.org/10.1149/1.3489378
213. Sethuraman VA, Chon MJ, Shimshak M, Srinivasan V, Guduru PR (2010) In situ measurements of stress evolution in silicon thin films during electrochemical Lithiation and Delithiation. J Power Sources 195(15):5062
214. Massey C, McKnight G, Barvosa-Carter W, Liu P (2005) Reversible work by electrochemical intercalation of graphitic materials 5759:322–330. https://doi.org/10.1117/12.601491
215. Cannarella J, Arnold CB (2015) Toward low-frequency mechanical energy harvesting using energy-dense Piezoelectrochemical materials. Adv Mater n/a-n/a. https://doi.org/10.1002/adma.201502974
216. Greve L, Fehrenbach C (2012) Mechanical testing and macro-mechanical finite element simulation of the deformation, fracture, and short circuit initiation of cylindrical Lithium ion battery cells. J Power Sources 214:377–385
217. Sahraei E, Campbell J, Wierzbicki T (2012) Modeling and short circuit detection of 18650 Li-ion cells under mechanical abuse conditions. J Power Sources 220:360–372
218. Sahraei E, Meier J, Wierzbicki T (2014) Characterizing and modeling mechanical properties and onset of short circuit for three types of lithium-ion pouch cells. J Power Sources 247:503–516
219. Lai W-J, Ali MY, Pan J (2014) Mechanical behavior of representative volume elements of lithium-ion battery cells under compressive loading conditions. J Power Sources 245:609–623
220. Sahraei E, Hill R, Wierzbicki T (2012) Calibration and finite element simulation of pouch lithium-ion batteries for mechanical integrity. J Power Sources 201:307–321
221. Wierzbicki T, Sahraei E (2013) Homogenized mechanical properties for the jellyroll of cylindrical Lithium-ion cells. J Power Sources 241:467–476
222. Cannarella J, Arnold CB (2014) State of health and charge measurements in lithium-ion batteries using mechanical stress. J Power Sources 269:7–14
223. Cannarella J, Leng CZ, Arnold CB (2014) On the coupling between stress and voltage in lithium-ion pouch cells. Proc SPIE 9115:91150K
224. Sethuraman VA, Chon MJ, Shimshak M, Van Winkle N, Guduru PR (2010) In situ measurement of biaxial modulus of Si anode for Li-ion batteries. Electrochem Commun 12(11):1614–1617
225. Amanieu H-Y, Aramfard M, Rosato D, Batista L, Rabe U, Lupascu DC (2015) Mechanical properties of commercial Mn_2O_4 cathode under different states of charge. Acta Mater 89:153–162
226. Tao X, Du J, Sun Y, Zhou S, Xia Y, Huang H, Gan Y, Zhang W, Li X (2013) Exploring the energy storage mechanism of high performance MnO_2 electrochemical capacitor electrodes: an in situ atomic force microscopy study in aqueous electrolyte. Adv Funct Mater 23(37):4745–4751
227. Xu J, Liu BH, Hu DY (2016) State of charge dependent mechanical integrity behavior of 18650 Lithium-ion batteries. Sci Rep 6:11
228. McDowell MT, Lee SW, Ryu I, Wu H, Nix WD, Choi JW, Cui Y (2011) Novel size and surface oxide effects in silicon nanowires as lithium battery anodes. Nano Lett 11(9):4018
229. Wu H, Cui Y (2012) Designing nanostructured Si anodes for high energy lithium ion batteries. Nano Today 7:414
230. Wu H, Yu G, Pan L, Liu N, McDowell MT, Bao Z, Cui Y (2013) Stable Li-ion battery anodes by in-situ polymerization of conducting hydrogel to conformally coat silicon nanoparticles. Nat Commun 4:1943
231. Chang W-S, Park C-M, Kim J-H, Kim Y-U, Jeong G, Sohn H-J (2012) Quartz (SiO_2): a new energy storage anode material for li-ion batteries. Energy Environ Sci 5:6895–6899

232. Yan N, Wang F, Zhong H, Liu Y, Wang Y, Hu L, Chen Q (2013) Hollow porous SiO_2 Nanocubes towards high-performance anodes for Lithium-ion batteries. Sci Rep 3:1568
233. Sun Q, Zhang B, Fu Z-W (2008) Lithium electrochemisty of SiO_2 thin film electrode for lithium-ion batteries. Appl Surf Sci 254:3774–3779
234. Miyachi M, Yamamoto H, Kawai H, Ohta T, Shirakata M (2005) Analysis of SiO anodes for lithium-ion batteries. J Electrochem Soc 152(10):A2089–A2091
235. Favors Z, Wang W, Bay HH, George A, Ozkan M, Ozkan CS (2014) Stable cycling of SiO_2 nanotubes as high-performance anodes for Lithium-ion batteries. Sci Rep 4:4605
236. Guo B, Shu J, Wang Z, Yang H, Shi L, Liu Y, Chen L (2008) Electrochemical reduction of Nano-SiO_2 in hard carbon as anode material for Lithium ion batteries. Electrochem Commun 10:1876–1878
237. Nadimpalli SPV, Tripuraneni R, Sethuraman VA (2015) Real-time stress measurements in germanium thin film electrodes during electrochemical Lithiation/Delithiation cycling. J Electrochem Soc 162(4):A2840–A2846
238. Zhao K, Wang WL, Gregoire J, Pharr M, Suo Z, Vlassak JJ, Kaxiras E (2011) Lithium-assisted plastic deformation of silicon electrodes in lithium-ion batteries: a first-principles theoretical study. Nano Lett 11(7):2962
239. Al-Obeidi A, Kramer D, Thompson CV, Monig R (2015) Mechanical stresses and morphology evolution in germanium thin film electrodes during Lithiation and Delithiation. J Power Sources 297:472–480
240. Boles ST, Sedlmayr A, Kraft O, Monig R (2012) In situ cycling and mechanical testing of silicon nanowire anodes for Lithium-ion battery applications. Appl Phys Lett 100:243901
241. Sheth J, Karan NK, Abraham DP, Nguyen CC, Lucht BL, Sheldon BW, Guduru PR (2016) In situ stress evolution in $Li_{1+x}Mn_2O_4$ thin films during electrochemical cycling in li-ion cells. J Electrochem Soc 163(13):A2524–A2530
242. Mukhopadhyay A, Sheldon BW (2014) Prog Mater Sci 63:58–116
243. Bhandakkar TK, Gao H (2010) Int J Solids Struct 47:1424–1434
244. Bhandakkar TK, Gao H (2011) Int J Solids Struct 48:2304–2309
245. Haftbaradaran H, Xiao XC, Gao HJ (2013) Model Simul Mater Sci Eng 21:9
246. Zhao K, Pharr M, Hartle L, Vlassak JJ, Suo Z (2012) J Power Sources 218:6–14
247. Cheng Y, Verbrugge MW (2009) J Power Sources 190:453–460
248. Cheng Y, Verbrugge MW (2008) J Appl Phys 104:083521
249. Christensen J, Newman J (2006) J Solid State Electrochem 10:293–319
250. ChiuHuang C, Huang HS (2015) J Solid State Electrochem 19:2245–2253
251. Tungyand C (1993) Mech Mater 14:257–268
252. Maranchi JP, Hepp AF, Evans AG et al (2006) Interfacial properties of the a-Si/Cu: active-inactive thin-film anode system for lithium-ion batteries. J Electrochem Soc 153: A1246–A1253
253. Xiao X, Liu P, Verbrugge MW, Haftbaradaran H, Gao H (2011) Improved cycling stability of silicon thin film electrodes through patterning for high energy density lithium batteries. J Power Sources 196:1409–1416
254. Maranchi JP, Hepp AF, Kumta PN (2003) High capacity, reversible silicon thin-film anodes for lithium-ion batteries. Electrochem Solid State 6:A198–A201
255. Haftbaradaran H, Xiao X, Verbrugge MW et al (2012) Method to deduce the critical size for interfacial delamination of patterned electrode structures and application to lithiation of thin-film silicon islands. J Power Sources 206:357–366
256. Pal S, Damle SS, Patel SH et al (2014) Modeling the delamination of amorphous-silicon thin film anode for lithium-ion battery. J Power Sources 246:149–159
257. Birchenall CE (1984) Topics in metallurgical thermodynamics-Devereux. Am Sci 72:412–413
258. Baggetto L, Niessen RAH, Roozeboom F, Notten PHL (2008) High energy density all-solid-state batteries: a challenging concept towards 3D integration. Adv Funct Mater 18:1057–1066

259. Aifantis KE, Hackney SA, Kumar RV (2010) High energy density lithium batteries: materials, engineering, applications. John 2010:53–80
260. Yao Y, Mcdowell MT, Ryu I, Wu H, Liu N, Hu L, Nix WD, Cui Y (2011) Interconnected silicon hollow nanospheres for lithium-ion battery anodes with long cycle life. Nano Lett 11:2949–2954
261. Liu Y, Duan H (2016) Stress analysis of electrode particles in lithium-ion batteries, alkali-ion batteries
262. Liu Y, Lv P, Ma J, Bai R, Duan HL (2014) Stress fields in hollow core-shell spherical electrodes of lithium ion batteries. Proc R Soc A 470
263. Liu Z, Zhou J, Chen B, Zhu J (2015) Interaction between dislocation mechanics on diffusion induced stress and electrochemical reaction in a spherical lithium ion battery electrode. RSC Adv 5:74835–74843
264. Zhang T, Guo Z, Wang Y, Zhu J (2014) Effect of reversible electrochemical reaction on Li diffusion and stresses in cylindrical Li-ion battery electrodes. J Appl Phys 115:083504–083512
265. Xia Y, Wierzbicki T, Sahraei E, Zhang X (2014) Damage of cells and battery packs due to ground impact. J Power Sources 267:78–97
266. Choi HY, Lee I, Lee JS, Kim YM, Kim H (2013) A study on mechanical characteristics of lithium-polymer pouch cell battery for electric vehicle. In: Paper No. 13-0115, Proceedings of 23rd international technical conference on the enhanced safety of vehicles (ESV 2013)
267. Rasiman MSA, Badrudin W, Kudin TIT, Yaakob MK, Taib MFM, Yahya MZA, Hassan OH (2014) Determination of Electronic Structure and Band Gap of $Li_2MnP_2O_7$ via First-Principle Study. Integr Ferroelectr 155:71–79
268. Barpanda P, Ye T, Lu J, Yamada Y, Chung SC, Nishimura S, Okubo M, Zhou H, Yamad A (2013) Splash combustion synthesis and exploration of alkali metal pyrophosphate ($A_2MP_2O_7$, A = Li, Na) cathodes. ECS Trans 50:71–77
269. Lapshin AE, Petrova MA (2012) Mixed alkali-zinc diphosphates: synthesis, structure, and properties. Glas Phys Chem 38:491–503
270. Baitahe R, Yakorn NV (2016) Dielectric properties and characterizations of binary $Cu_{(2-x)}$ $Mg_xP_2O_7$ pyrophosphates. Ferroelectrics 490:174–183
271. Blomgren GE (2017) The development and future of lithium ion batteries. J Electrochem Soc 164(1):A5019–A5025
272. Myung ST, Maglia F, Park KJ, Yoon CS, Lamp P, Kim SJ, Sun YK (2017) Nickel-rich layered cathode materials for automotive lithium-ion batteries: achievements and perspectives. ACS Energy Lett 2(1):196–223
273. Xu W, Wang JL, Ding F, Chen XL, Nasybutin E, Zhang YH, Zhang JG (2014) Lithium metal anodes for rechargeable batteries. Energy Environ Sci 7(2):513–537
274. Lin DC, Liu YY, Cui Y (2017) Reviving the lithium metal anode for high-energy batteries. Nat Nanotechnol 12(3):194–206
275. Cheng XB, Zhang R, Zhao CZ, Zhang Q (2017) Toward safe lithium metal anode in rechargeable batteries: a review. Chem Rev 117(15):10403–10473
276. Haregewoin AM, Wotangoa AS, Hwang BJ (2016) Energy Environ Sci 9:1955–1988
277. Leung K (2013) Chem Phys Lett 568–569:1–8
278. Endo E, Ata M, Tanaka K, Sekai K (1998) J Electrochem Soc 145:3757–3764
279. Li T, Balbuena PB (2000) Chem Phys Lett 317:421–429
280. Wang Y, Balbuena PB (2002) J Phys Chem B 106:4486–4495
281. Wang Y, Nakamura S, Ue M, Balbuena PB (2001) J Am Chem Soc 123:11708–11718
282. Han YK, Lee SU (2004) Theor Chem Acc 112:106–112
283. Wang Y, Nakamura S, Tasaki K, Balbuena PB (2002) J Am Chem Soc 124:4408–4421
284. Vollmer JM, Curtiss LA, Vissers DR, Amine K (2004) J Electrochem Soc 151:A178–A183
285. Park MH, Lee YS, Lee H, Han YK (2011) J Power Sources 196:5109–5114
286. Cammann K (2001) Instrumentelle analytische chemie. Spektrum Akademischer Verlag, Heidelberg

287. Luo H, Jiang X, Xia Y, Zhou Q (2015) Fracture mode analysis of lithium-ion battery under mechanical loading. In: Proceedings of the ASME 2015 international mechanical engineering congress and exposition (IMECE 2015)
288. Xu J, Wang L, Guan J, Yin S (2016) Coupled effect of strain rate and solvent on dynamic mechanical behaviors of separators in lithium ion batteries. Mater Des 95:319–328